Transactions of the ASME

TRANSACTIONS OF THE AMERICAN SOCIETY OF MECHANICAL ENGINEERS

VOLUME 78 JULY 1956 NUMBER 5

Transactions

of The American Society of Mechanical Engineers

Published on the tenth of every month, except March, June, September, and December

Published monthly by The American Society of Mechanical Engineers. Publication office at 20th and Northampton Streets, Easton, Pa. The editorial department is located at the headquarters of the Society, 29 West Thirty-Ninth Street, New York 18, N. Y. Cable address, "Dynamic," New York. Price $1.50 a copy, $12.00 annually for Transactions and the *Journal of Applied Mechanics* to members, $1.00 a copy, $6.00 annually. Add $1.50 for postage to all countries outside the United States, Canada, and Pan American Union. Changes of address must be received at Society headquarters seven weeks before they are to be effective on the mailing list. Please send old as well as new address.... By-Law: The Society shall not be responsible for statements or opinions advanced in papers or...printed in its publications (B13, Par. 4).... Entered as second-class matter March 2, 1928, at the Post Office at Easton, Pa., under the Act of August 24, 1912....

Behavior of Air in the Hydrostatic Lubrication of Loaded Spherical Bearings

By T. L. COREY,[1] C. M. TYLER, JR.,[2] H. H. ROWAND, JR.,[1] AND E. M. KIPP[1]

Some experimental data have been obtained relating the load-bearing capacity of air films of various thicknesses and operating at different pressures and rates of flow for 2, 4, and 6-in. spherical-type bearings. Semi-empirical equations have been developed for calculation of (a) minimum air pressure as a function of load; (b) minimum flow of air as a function of pressure; (c) bearing lift as a function of air pressure.

Introduction

THE basic principle of hydrostatic lubrication is not new, one of the earliest public demonstrations of the principle having been made at the Paris Industrial Exposition in 1878.[3] As is often the case, applications of the principle did not immediately follow. Recently, interest in this subject has developed rapidly and the principles of hydrostatic lubrication are finding increasing application in the improved lubrication of bearing elements operating under conditions unfavorable to hydrodynamic lubrication.

With reference to hydrostatically lubricated spherical bearings, reference may be made to U. S. Patent 2,346,281 granted to R. L. Templin[4] in 1944, and to the Sperry Gyroscope Company who built a spherical bearing to explore the possibilities of air as the lift medium.[3]

Hydrostatic lubrication finds its optimum usefulness in bearing elements operating under high unit loads and at low speeds. One of the most notable applications of hydrostatic principles is to be found in the lubrication of the bearings for the Mount Palomar telescope.[3] Numerous theoretical and practical studies have developed theoretical relationships upon which satisfactory design of hydrostatically lubricated bearing elements can be based.[3] There are occasions, however, when it is undesirable or difficult to use fluids such as oils or other liquids as the hydrostatic lubricant fluids. In such instances, it is of interest to consider the possibility of employing gases as lubricating media. Unfortunately, the theoretical relationships governing the use of liquids as hydrostatic lubricants do not apply to gases. Furthermore, the literature on this subject as applied to gases is very limited. For this reason, it is of interest to develop, for gases, corresponding theoretical relationships upon which effective practical design of air or gas-lubricated hydrostatic bearings can be based.

Preliminary experiments were undertaken utilizing loaded steel balls of 2, 4, and 6 in. diam, operating with a 140-deg angle of contact in a spherical seat and hydrostatically lubricated with air. The data obtained and discussion of results are here presented.

Experimental Procedure

A schematic outline of the experimental arrangement is given in Fig. 1. Three spheres were employed of 2, 4, and 6 in. diam. The details of the hemispherical seats and of the hydrostatic pads are indicated in Fig. 2. The following is a typical sequence of events during an experimental run.

After the apparatus is assembled and checked carefully, an initial load is applied to the top of the hinged loading platform (Fig. 1) and the system thoroughly bled of air in order to assure contact between the ball and its seat. This is important because the position of the ball under these conditions is that from which the measurements are made to determine the height to which the ball is lifted when air pressure is applied. Air is then supplied to the bearing assembly in increments of 5-psi pressure until a lift of the sphere is obtained as indicated on the dial gages. At this point the values of the air flow and air pressure are recorded. The air pressure is then increased by another increment of 5 psi, and the air flow, air pressure, and lift are again recorded. This procedure is continued until no further lifting of the ball can be obtained or until the maximum volume of air supply available is used. Each run is repeated in duplicate. Also, checks are made at the end of each test to make certain that the dial-gage readings return to their initial zero-point values whenever the entire system is bled of air.

The experimental data obtained are presented in Figs. 3 to 8. On the basis of these data, the following relationships have been derived by the methods shown in the Appendix.

Nomenclature

N = load on sphere, lb
P = line pressure, psig
P_0 = minimum lifting P for given N
R = radius of sphere, in.
F = flow rate, cfm
F_m = maximum flow rate, cfm
l = lift, in.

Minimum Pressure as a Function of Load

$$P_0 = \frac{N}{2.0\,R^2} \qquad [1]$$

Flow Rate as a Function of Pressure

$$\left.\begin{aligned} F &= \\ &F_m \sqrt{1 - \left(\frac{P - 18 - 1.5P_0}{18 + 0.5P_0}\right)^2}\ ;\quad P \le 18 + 1.5P_0 \\ F &= F_m;\ P \ge 18 + 1.5P_0 \end{aligned}\right\} \qquad [2]$$

[1] Aluminum Research Laboratories, Aluminum Company of America, New Kensington, Pa.

[2] Associate Professor of Mechanical Engineering, Carnegie Institute of Technology, Pittsburgh, Pa. Mem. ASME.

[3] "Hydrostatic Lubrication," by D. D. Fuller, *Machine Design*, vol. 19, 1947, June, pp. 110–116; July, pp. 117–122; August, pp. 115–120; September, pp. 127–131, 188, and 190.

[4] Assistant Director of Research, Aluminum Research Laboratories, New Kensington, Pa.

Contributed by the Research Committee on Lubrication under the auspices of the Lubrication Activity of The American Society of Mechanical Engineers, and presented at the First Annual ASME-ASLE Lubrication Conference, Baltimore, Md., October 18–20, 1954.

Note: Statements and opinions advanced in papers are to be understood as individual expressions of their authors and not those of the Society. Manuscript received at ASME Headquarters, December 16, 1953. Paper No. 54—LUB-8.

Lift as a Function of Pressure

$$\left.\begin{aligned} l &= \frac{P + 25R - 5}{5000\left[(0.37 + 0.025\,R^3)\sqrt{P_0}\right]}; \qquad P \geq P_0 + 25 \\ l &= \frac{P_0 + 20 + 25R}{5000\left[(0.37 + 0.025\,R^3)\sqrt{P_0}\right]}\sqrt[3]{\frac{P - P_0}{25}}; \qquad P \leq P_0 + 25 \end{aligned}\right\} \quad \ldots [3]$$

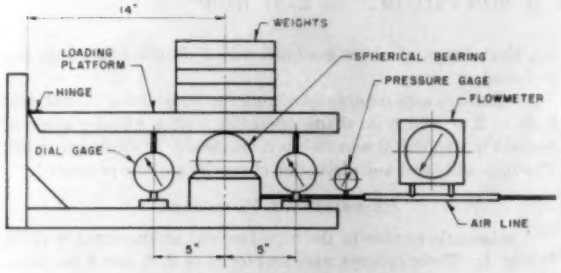

FIG. 1 TEST ARRANGEMENT

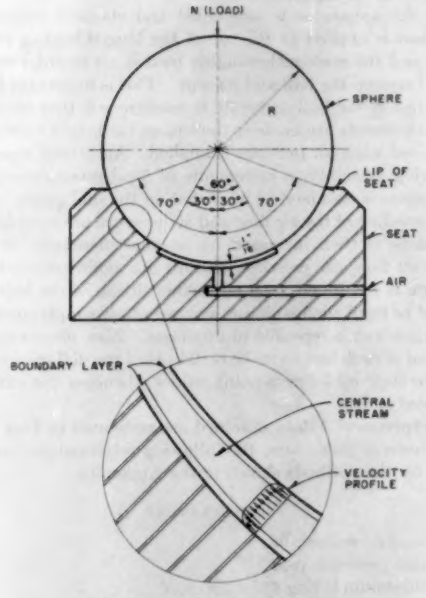

FIG. 2 TYPE OF TEST SPHERES

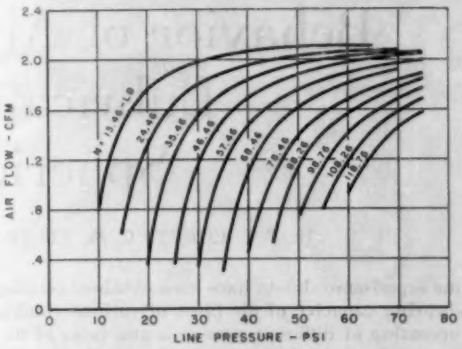

FIG. 3 AIR FLOW VERSUS PRESSURE—2-IN-DIAM SPHERE

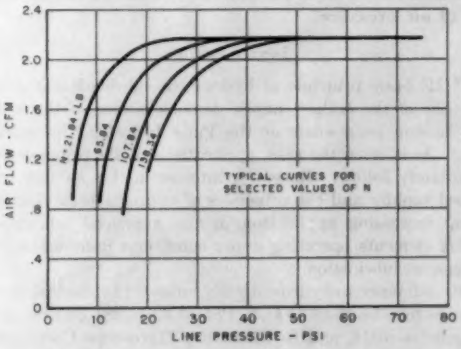

FIG. 4 AIR FLOW VERSUS PRESSURE—4-IN-DIAM SPHERE

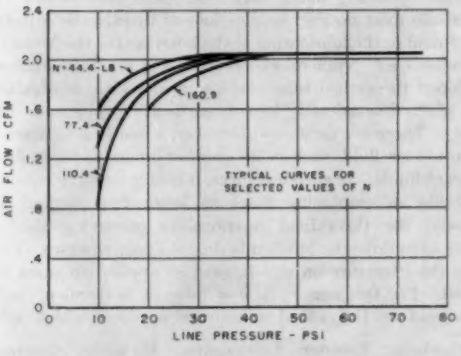

FIG. 5 AIR FLOW VERSUS PRESSURE—6-IN-DIAM SPHERE

It is interesting to note the surprisingly high load-carrying capacities of loaded spherical bearings floated on a film of air at line pressures available in most plants. The following table will serve to illustrate this point:

Size, in. diam	Line pressure, psi	Seat pressure, psi	Load, lb	Lift, in.	Flow, cfm
2	80	70	140	0.00515	1.23
4	80	70	560	0.0043	1.26
6	80	70	1260	0.0027	1.19

The validity of extrapolating Equations [2] and [3] beyond the range of diameters for which the data were obtained has not been determined. Computation of the range of Reynolds numbers involved in these experiments indicates values as high as 80,000, showing that turbulent flow exists. Under conditions of turbulent flow, the variable of boundary-layer thickness in the variable-velocity air-flow channels becomes a factor of considerable concern. At the present time, the magnitude of the boundary-layer thickness effects has not been established.

Equation [1], relating the minimum pressure P_0 as a function of load and radius, has a theoretical basis and should be applicable to spheres of diameters beyond the ranges tested.

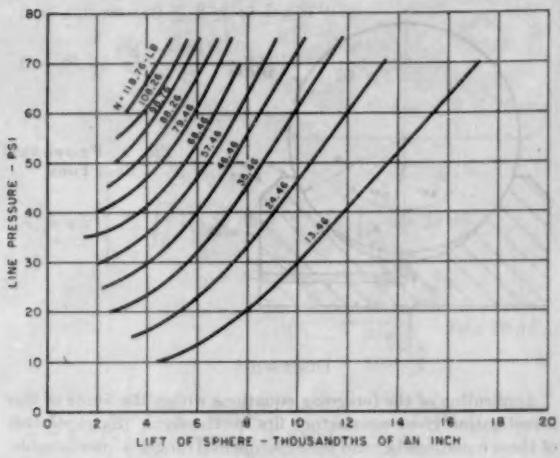

FIG. 6 LIFT VERSUS PRESSURE—2-IN-DIAM SPHERE

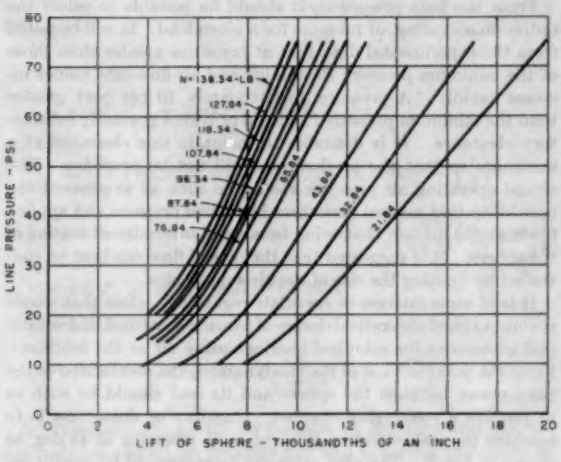

FIG. 7 LIFT VERSUS PRESSURE—4-IN-DIAM SPHERE

THEORY

The mechanics of a loaded sphere floated on a spherical seat by a stream of high-pressure air are drastically different from those of conventional bearing geometries. In this instance, the operation is more analogous to flow of gases through turbine nozzles and cannot be handled by the usual theories associated with hydrostatic lubrication. Ordinarily, using liquid lubricants, viscosity is the property of primary interest. When utilizing a gas such as air, the viscosity is of lesser importance and then only in connection with the effects of the boundary layers adjacent to the surfaces of the sphere and its seat. Unfortunately, no experimental data are available upon which to predict the properties and extent of the boundary layers in the current investigation. Consequently, treatment of the present data cannot necessarily be generally extrapolated to conditions beyond those employed in these investigations.

Subject to the foregoing limitations, semi-empirical relationships have been developed with regard to several of the factors associated with the performance of these air hydrostatically lubricated spherical bearings.

Calculation of Minimum Pressure Required to Raise a Given Load. In the Appendix, Section (*a*), the equation for the area of the passageway is derived as

$$A = \pi R l \sin 2\theta$$

where

R = radius of sphere, in.
l = lift of sphere, in.
θ = angle measured from center of sphere; 0° is at bottom

This equation can be seen to have a maximum value when $\theta = 45$ deg, and then converging to the lip of the seat.

A lower bound for the pressure required to lift a given load N may be calculated by assuming that the pressure remains constant up to 45 deg and then drops uniformly to atmospheric at the lip. From Appendix, Section (*b*), this is found to be

$$P_0 = \frac{N}{2.21R^2}$$

A reasonable upper bound for the value of P_0 may be found by assuming that the pressure drops uniformly from the edge of the high-pressure pad to the lip of the seat. In the Appendix, Section (*c*), this is found to be

$$P_0 = \frac{N}{1.83R^2}$$

Experimental data indicate that a value about halfway between the lower and upper values of P_0 is correct, that is

$$P_0 = \frac{N}{2R^2}$$

for a 60-deg included angle high-pressure pad, Fig. 2.

In the Appendix, Section (*d*), similar expressions have been derived for 30 and 90-deg high-pressure pads, as follows

$$P_0 = \frac{N}{1.80R^2}$$

$$P_0 = \frac{N}{2.21R^2}$$

Air Flow Versus Air Pressure. The assemblies tested were geometrically proportionate, except that the same air-supply pipe was used in each case. This pipe limited the maximum

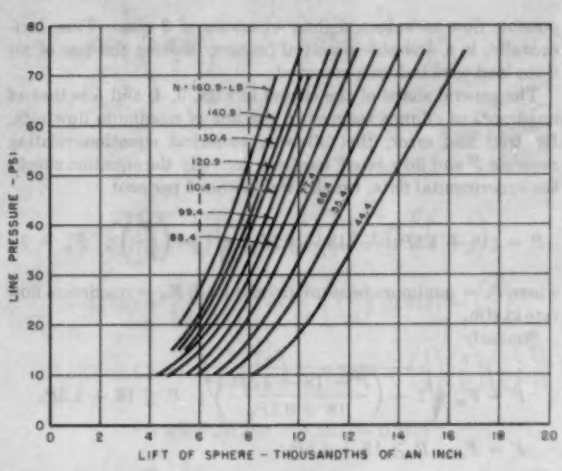

FIG. 8 LIFT VERSUS PRESSURE—6-IN-DIAM SPHERE

possible flow to values slightly in excess of 2 cfm. This, incidentally, is a desirable practical feature, limiting the loss of air if the load were suddenly removed.

The general shape of the curves in Figs. 3, 4, and 5 is that of quadrants of ellipses tangent to the line of maximum flow rate. By trial and error, the following empirical equation relating pressure P and flow rate F has been derived; the equation checks the experimental data, usually well within 5 per cent

$$P = (18 + 1.5P_0) - (18 + 0.5P_0)\sqrt{1 - \left(\frac{F}{F_m}\right)^3}; \quad F_m \approx 2$$

where P_0 = minimum pressure to raise load, F_m = maximum flow rate in cfm.

Similarly

$$F = F_m\sqrt{1 - \left(\frac{P - 18 - 1.5P_0}{18 + 0.5P_0}\right)^3}; \quad P \leq 18 + 1.5P_0$$

$$F = F_m; \quad P \geq 18 + 1.5P_0$$

Air Pressure Versus Lift. The experimental form of these curves is that of straight lines radiating from a point below the origin connected to P_0 by a cubic parabola tangent at a pressure about 25 psi above P_0.

An empirical expression for the straight-line portion of the curves is

$$P = (5 - 25R) + 5000[(0.37 + 0.025R^3)\sqrt{P_0}]l; \quad P \geq P_0 + 25$$

or

$$l = \frac{P + 25R - 5}{5000[(0.37 + 0.025R^3)\sqrt{P_0}]}; \quad P \geq P_0 + 25$$

The accompanying expression for the curved portions is

$$P = P_0 + 25\left(\frac{5000[(0.37 + 0.025R^3)\sqrt{P_0}]l}{P_0 + 20 + 25R}\right)^3; \quad P \leq P_0 + 25$$

or

$$l = \frac{P_0 + 20 + 25R}{5000[(0.37 + 0.025R^3)\sqrt{P_0}]}\sqrt[3]{\frac{P - P_0}{25}}; \quad P \leq P_0 + 25$$

Again, agreement with the experimental data is usually well within 5 per cent.

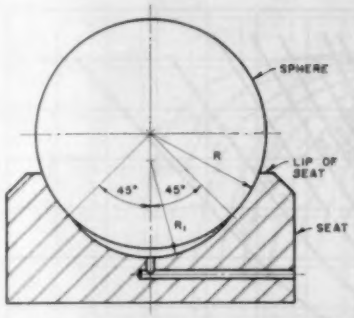

FIG. 9 PROPOSED SEAT FORM

DISCUSSION

Application of the foregoing equations within the limits of this investigation gives satisfactory fits for the data. Extrapolation of these equations beyond the experimental ranges is questionable, with the possible exception of the equations relating minimum pressure for a given load.

From the data presented, it should be possible to select the optimum operating air pressure for a given load. It will be noted from the experimental data that at pressures greater than those of the minimum pressure P_0, the lift and air-flow-rate values increase rapidly. A pressure approximately 10 per cent greater than the minimum pressure P_0 should provide a generally satisfactory clearance. It is desirable to maintain this clearance at a minimum so that the air-flow rate will not be excessive. The actual operating air pressure should be such as to prevent the possibility that normal variations in air-line pressure and applied loads would initiate chattering because of intermittent seating of the sphere. It is suggested that the rate of flow can best be controlled by limiting the size of the air-supply pipe.

It is of some interest to speculate regarding factors that would pertain to ideal theoretical design of bearing seats and hydrostatic pad geometries for spherical bearings using air as the lubricant. From the point of view of thermodynamics, the ideal shape of the passageway between the sphere and its seat should be such as to provide a converging channel. One way of doing this is to machine the seat with two different radii, changing at 45 deg, as shown in Fig. 9. The area ratio can be controlled by modifying the angle of the lip of the seat and the depth of machining of the inner radius. This type of design should provide maximum load-bearing capacity for the air with minimum flow requirements.

Appendix

(*a*) Area of passageway, Fig. 10. Neglecting the higher powers of lift

$$\begin{aligned} A &= l\cos\theta[2\pi R\sin\theta] \\ &= \pi Rl[2\sin\theta\cos\theta] \\ &= \pi Rl\sin 2\theta \end{aligned}$$

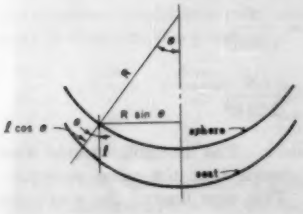

FIG. 10

(*b*) Calculation of load N for pressure P_0 constant for $0 \leq \theta \leq 45$ deg and dropping uniformly to atmospheric at $\theta = 70$ deg:

$$\begin{aligned} \text{Area of circular strip} &= \text{length} \times \text{width} \\ &= 2\pi R\sin\theta \times R\,d\theta \\ \text{Vertical component of pressure} &= P\cos\theta \\ \text{Force on circular strip} &= 2\pi R^2 P\sin\theta\cos\theta\,d\theta \\ &= \pi R^2 P\sin 2\theta\,d\theta \end{aligned}$$

Integrating the force

$$N = \pi R^2\int_0^{\frac{7\pi}{18}} P\sin 2\theta\,d\theta$$

where

$$P = P_0; \text{ when } 0 \leq \theta \leq 45 \text{ deg}$$

$$P = P_0 - \frac{P_0(\theta - 45)}{70 - 45} = 2.80P_0 - \frac{P_0\theta}{25};$$

$$\text{when } 45 \text{ deg} \leq \theta \leq 70 \text{ deg}$$

Then

$$N = \pi R^2 \left[P_0 \int_0^{\frac{\pi}{4}} \sin 2\theta \, d\theta + 2.80P_0 \int_{\frac{\pi}{4}}^{\frac{7\pi}{18}} \sin 2\theta \, d\theta - \frac{P_0}{\frac{25\pi}{180}} \int_{\frac{\pi}{4}}^{\frac{7\pi}{18}} \theta \sin 2\theta \, d\theta \right]$$

$$= \pi R^2 P_0 \left[\left(-\frac{\cos 2\theta}{2} \right)_0^{\frac{\pi}{4}} + 2.80 \left(-\frac{\cos 2\theta}{2} \right)_{\frac{\pi}{4}}^{\frac{7\pi}{18}} - \frac{180}{25\pi} \left(\frac{\sin 2\theta}{4} - \frac{\theta \cos 2\theta}{2} \right)_{\frac{\pi}{4}}^{\frac{7\pi}{18}} \right]$$

$$= \pi R^2 P_0 \left\{ \frac{1}{2} + 2.80 \left[-\frac{1}{2} - (-0.766) \right] - \frac{180}{25\pi} \left[(0.25 \times 0.642) - (0.25 \times 1.00) - \left(\frac{1}{2} \right) \left(\frac{7\pi}{18} \right) (-0.766) \right] \right\}$$

$$= \pi R^2 P_0 \, [0.500 + 1.071 - 0.868]$$

$$= 2.21 P_0 R^2$$

$$P_0 = \frac{N}{2.21R^2}$$

(*c*) Calculation of load N for pressure P_0 constant over the 60-deg included-angle high-pressure pad and dropping uniformly to atmospheric at $\theta = 70$ deg. As before

$$N = \pi R^2 \int_0^{\frac{7\pi}{18}} P \sin 2\theta \, d\theta$$

where

$$P = P_0; \text{ when } 0 \leq \theta \leq 30 \text{ deg}$$

$$P = P_0 - \frac{P_0(\theta - 30)}{70 - 30} = 1.75P_0 - \frac{P_0\theta}{40};$$

$$\text{when } 30 \text{ deg} \leq \theta \leq 70 \text{ deg}$$

then

$$N = \pi R^2 \left[P_0 \int_0^{\frac{\pi}{6}} \sin 2\theta \, d\theta + 1.75P_0 \int_{\frac{\pi}{6}}^{\frac{7\pi}{18}} \sin 2\theta \, d\theta - \frac{P_0}{\frac{4\pi}{18}} \int_{\frac{\pi}{6}}^{\frac{7\pi}{18}} \theta \sin 2\theta \, d\theta \right]$$

$$= \pi R^2 P_0 \left[\left(\frac{\cos 2\theta}{2} \right)_0^{\frac{\pi}{6}} + 1.75 \left(\frac{\cos 2\theta}{2} \right)_{\frac{\pi}{6}}^{\frac{7\pi}{18}} - \frac{18}{4\pi} \left(\frac{\sin 2\theta}{4} - \frac{\theta \cos 2\theta}{2} \right)_{\frac{\pi}{6}}^{\frac{7\pi}{18}} \right]$$

$$= \pi R^2 P_0 \left\{ \left[\left(-\frac{1}{2} \right) \left(\frac{1}{2} \right) + \left(\frac{1}{2} \right) \right] + 1.75 \left[\left(-\frac{1}{2} \right) (-0.766) + \left(\frac{1}{2} \right) \left(\frac{1}{2} \right) \right] - \frac{18}{4\pi} \left[\left(\frac{1}{4} \right) (0.642) - \left(\frac{1}{4} \right) (0.866) - \left(\frac{1}{2} \right) \left(\frac{7\pi}{18} \right) (-0.766) + \left(\frac{1}{2} \right) \left(\frac{\pi}{6} \right) \left(\frac{1}{2} \right) \right] \right\}$$

$$= \pi R^2 P_0 [0.250 + 1.107 - 0.777]$$

$$= 1.83 P_0 R^2$$

$$P_0 = \frac{N}{1.83R^2}$$

(*d*) Formulas for 30 and 90-deg included-angle high-pressure pads for the 90-deg pad configuration; the previous upper and lower bounds coincide so that

$$P_0 = \frac{N}{2.21R^2}$$

For the 30-deg pad the lower bound is the same; the upper bound is calculated as before

$$N = \pi R^2 \int_0^{\frac{7\pi}{18}} P \sin 2\theta \, d\theta$$

where

$$P = P_0; \text{ when } 0 \leq \theta \leq 15 \text{ deg}$$

$$P = P_0 - \frac{P_0(\theta - 15)}{70 - 15} = 1.273P_0 - \frac{P_0\theta}{55};$$

$$\text{when } 15 \text{ deg} \leq \theta \leq 70 \text{ deg}$$

Then

$$N = \pi R^2 \left[P_0 \int_0^{\frac{\pi}{12}} \sin 2\theta \, d\theta + 1.273P_0 \int_{\frac{\pi}{12}}^{\frac{7\pi}{18}} \sin 2\theta \, d\theta - \frac{P_0}{\frac{55\pi}{180}} \int_{\frac{\pi}{12}}^{\frac{7\pi}{18}} \theta \sin 2\theta \, d\theta \right]$$

$$= \pi R^2 P_0 \left[\left(-\frac{\cos 2\theta}{2} \right)_0^{\frac{\pi}{12}} + 1.273 \left(\frac{\cos 2\theta}{2} \right)_{\frac{\pi}{12}}^{\frac{7\pi}{18}} - \frac{180}{55\pi} \left(\frac{\sin 2\theta}{4} - \frac{\theta \cos 2\theta}{2} \right)_{\frac{\pi}{12}}^{\frac{7\pi}{18}} \right]$$

$$= \pi R^3 P_0 \left\{ \left[\left(-\frac{1}{2} \right)(0.866) + \frac{1}{2} \right] + 1.273 \left[\left(-\frac{1}{2} \right)(-0.766) + \left(\frac{1}{2} \right)(0.866) \right] - \frac{180}{55\pi} \left[\left(\frac{1}{4} \right)(0.642) - \left(\frac{1}{4} \right)\left(\frac{1}{2} \right) \right.\right.$$

$$\left.\left. - \left(\frac{1}{2} \right)\left(\frac{7\pi}{18} \right)(-0.766) + \left(\frac{1}{2} \right)\left(\frac{\pi}{12} \right)(0.866) \right] \right\} = \pi R^3 P_0 \, [0.067 + 1.040 - 0.642] = 1.46 \, P_0 R^3$$

$$P_0 = \frac{N}{1.46 R^3}$$

An average value that may be used for calculations would be $P_0 = \frac{N}{1.80 R^3}$.

Power Loss in Elliptical and 3-Lobe Bearings

By OSCAR PINKUS,[1] W. LYNN, MASS.

The power losses for elliptical and three-lobe bearings, both symmetrical and asymmetrical, were derived as functions of the customary bearing parameters and bearing ellipticity. Expressions are given for two cases; one assuming a complete oil film, and one taking into account the incompleteness of the oil film in the diverging sections of the bearing. All equations are for a concentric shaft position, this being a plausible assumption as noncylindrical bearings are mostly used in low load, high-speed applications. For convenience the power losses for the noncylindrical bearings are plotted in comparison with those for cylindrical bearings of clearance c as given by Petroff's equation. Excellent agreement was found between the theoretical power losses and experimental results in bearings.

Nomenclature

The following nomenclature is used in the paper:

B = width of oil film, in.
D = diameter of bearing, in.
H = power loss, hp
H_c = power loss in cylindrical bearings, hp
L = length of bearing, in.
N = speed, rpm
R_l = radius of lobe, in.
U = linear velocity, ipm
W_c = power loss in cylindrical bearings, in-lb/min
W = power loss, in-lb/min
Z = oil viscosity, lb-min/sq in.
c = $2(R + \epsilon - r)$, in.
c_r = $c/2$, in.
e = shaft eccentricity, in.
h = oil-film thickness, in.
j = power-loss factor due to ellipticity and incomplete oil film, dimensionless
j_0 = power-loss factor from incomplete oil-film portion of one lobe, dimensionless
k = power-loss factor due to ellipticity, dimensionless
m = $2\epsilon/c$, ellipticity ratio, dimensionless
r = radius of shaft, in.
ϵ = ellipticity of bearing, $R_l - R$, in.
μ = oil viscosity, centipoises
θ_2 = angle at point of minimum film thickness, radians

Introduction

Present-day technology is, among other things, characterized by the advent of high-speed machinery. Hydrodynamic bearings called upon to operate under these conditions are confronted with some new problems, among which instability, known as oil whip, is one of the most prevalent and the most troublesome. Also power losses and subsequently bearing temperatures become excessive at high speeds and new designs are required to cope with these difficulties. The existing high-speed bearings are characterized by their noncylindrical bores among which the elliptical and the 3-lobe bearings are the most popular.

In practice the elliptical bearing is made up of two cylindrical halves brought together so that their centers are displaced from the bearing center. This kind of bearing is manufactured conveniently by placing shims at the horizontal split and machining a cylindrical bore. The shims are later removed and the two halves brought together to produce the elliptical bearing, as shown in Fig. 1. The 3-lobe bearing comes in two variations,

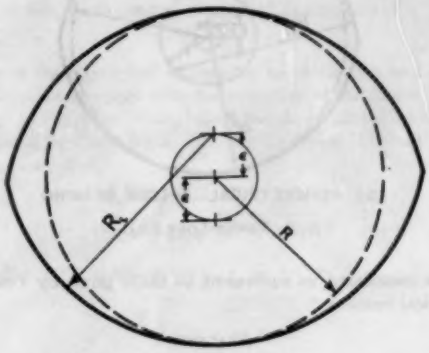

Fig. 1 Elliptical Bearing

symmetrical and asymmetrical. The symmetrical 3-lobe bearing is made up of three 120-deg arcs, their centers being displaced from the bearing center. The asymmetrical 3-lobe bearing is commonly made up of a 180-deg portion on the bottom and two 90-deg sections on top. The geometry of both of these bearings is shown in Fig. 2.

In all these designs convergent clearance regions exist even at a concentric shaft position. This convergence creates high-pressure regions which, in effect, put an additional load on the bearing—a factor known to enhance shaft stability. The extra clearance space, as compared with a cylindrical bearing having a diameter equal to the inscribed circle increases the oil flow, and also often reduces the power losses, resulting in lower temperature rises. For these reasons the elliptical and 3-lobe bearings are widely used in industry.

Unfortunately, studies of the various noncylindrical bearings have not kept pace with their popularity. This paper deals with power losses in these types of bearings. It provides expressions for power losses as a function of the customary bearing parameters as well as a newly defined variable, ellipticity. The analysis is carried out both assuming a full oil film as well as with an allowance for the incomplete oil film which surely exists in the diverging portions of the bearing. The method of including the effect of

[1] Bearing Development Engineer, Thomson Laboratory, General Electric Company. Assoc. Mem. ASME.

Contributed by the Research Committee on Lubrication under the auspices of the Lubrication Activity of The American Society of Mechanical Engineers, and presented at the First Annual ASME-ASLE Lubrication Conference, Baltimore, Md., October 18–20, 1954.

Note: Statements and opinions advanced in papers are to be understood as individual expressions of their authors and not those of the Society. Manuscript received at ASME Headquarters, April 29, 1954. Paper No. 54—LUB-9.

an incomplete oil film is that previously used by Rosenblatt and Wilcock[2] in their analysis of cylindrical bearings. The expressions are derived for a concentric shaft position and thus they

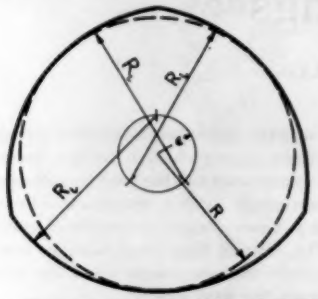

a) SYMMETRICAL 3-LOBE BEARING

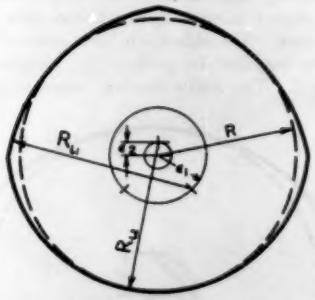

b) ASYMMETRICAL 3-LOBE BEARING

FIG. 2 THREE-LOBE BEARING

may be considered as equivalent to those given by Petroff for cylindrical bearings.[3]

ANALYSIS

Petroff's equation as obtained from the basic relationship

$$W = (\text{shear stress} \times \text{area}) \times (\text{linear velocity})$$

$$= \left(Z \frac{U}{h} L 2\pi R\right) U = \frac{2\pi Z U^2 R L}{h} \quad [1]$$

can be written in differential form

$$dW = \frac{Z U^2 R L d\theta}{h} \quad [2]$$

For a circular bearing h is constant and Equation [1] gives the power loss. For noncircular bearings the clearance is not constant and an appropriate expression for h as a function of θ must be used. Following is the derivation of power-loss expressions for three types of noncircular bearings; elliptical, 3-lobe symmetrical, and 3-lobe asymmetrical. Like Petroff's equation, they are all based on a concentric shaft position.

FULL OIL FILM

The derivation of the expressions for power loss in this section assumes the existence of a complete oil film all around the bearing. This should yield power losses higher than those encountered in actual cases.

Elliptical Bearings. In Fig. 1 the diameter of the inscribed circle of the elliptical bearing is $2R$, while the radius of curvature of both arcs is $R + \epsilon$, ϵ being here called the ellipticity of the bearing. When a shaft runs eccentrically in a cylindrical bearing the thickness of the oil film at any point is given by

$$h = c_r + e \cos \theta \quad [3]$$

From an observation of Fig. 3 it is apparent that a shaft running concentrically in an elliptical bearing creates a situation similar

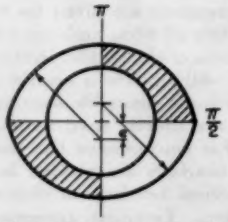

CONCENTRIC POSITION OF SHAFT IN ELLIPTICAL BEARING

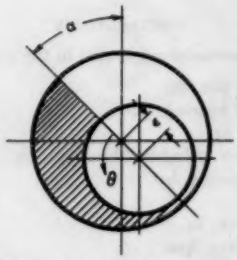

ECCENTRIC POSITION OF SHAFT IN CYLINDRICAL BEARING

FIG. 3 RELATION BETWEEN CYLINDRICAL AND ELLIPTICAL BEARINGS

to Fig. 3 with ϵ, the ellipticity, taking the place of e, the eccentricity. This applies to both halves of the bearing. Thus the oil-film thickness in each half of an elliptical bearing can be expressed as

$$h = c_r + \epsilon \cos \theta \quad [4]$$

with θ going from $\pi/2$ to $3\pi/2$.

For a circular bearing Equation [1] gives the power loss. For an elliptical bearing where $h = c_r + \epsilon \cos \theta$ we have

$$dW = \frac{Z U^2 R L d\theta}{c_r + \epsilon \cos \theta} \quad [5]$$

$$W = 4 \int_{\pi/2}^{\pi} \frac{Z U^2 R L d\theta}{c_r + \epsilon \cos \theta} \quad [6]$$

where the integral is evaluated for one quarter of the bearing. This integrates[4] to

$$W = \frac{4 Z U^2 R L}{\sqrt{c_r^2 - \epsilon^2}} \arctan \frac{\sin \theta \sqrt{c_r^2 - \epsilon^2}}{c_r \cos \theta + \epsilon} \Bigg|_{\pi/2}^{\pi} \quad [7]$$

Evaluating the limits, we obtain

[2] "Oil Flow, Key Factor in Sleeve-Bearing Performance," by D. F. Wilcock and M. Rosenblatt, Trans. ASME, vol. 74, 1952, pp. 849–866.

[3] "Friction in Machines and the Effect of the Lubricant," by N. Petroff, *Engineering Journal*, St. Petersburg, 1883, Nos. 1, 2, and 4.

[4] "Mathematical Tables and Formulas," by R. H. Burington Handbook Publishers, Inc., Sandusky, Ohio, 1949, p. 74.

$$W = \frac{4ZU^2RL}{\sqrt{c_r^2 - \epsilon^2}} \left[\pi - \arctan \frac{\sqrt{c_r^2 - \epsilon^2}}{\epsilon} \right] \quad [8]$$

Rearranging the values

$$W = \frac{8ZU^2RL}{c\sqrt{1 - m^2}} \left[\pi - \arctan \frac{\sqrt{1 - m^2}}{m} \right] \quad [9]$$

When $\epsilon = 0$, which means that the bearing is circular, the value of arctan ∞ is $\pi/2$ and Equation [9] reduces to [1], Petroff's equation for a circular bearing. When $\epsilon = c_r$, the shaft is rubbing against the bearing surface and Equation [9] gives an infinite power loss.

In practical terms of horsepower, Equation [9] can be written as

$$H = \frac{2.4\mu N^2D^3L \times 10^{-12}}{c\sqrt{1 - m^2}} \left[\pi - \arctan \frac{\sqrt{1 - m^2}}{m} \right] \quad [10]$$

Symmetrical 3-Lobe Bearings. From an observation of Fig. 2 it is apparent that as far as each individual lobe is concerned, a shaft running concentrically in a 3-lobe bearing creates a situation similar to a shaft running eccentrically in a cylindrical bearing. In the 3-lobe bearing ϵ, the ellipticity, takes the place of e, the eccentricity. The oil-film thickness for each lobe can be expressed as

$$h = c_r + \epsilon \cos \theta$$

with θ going from $2\pi/3$ to $4\pi/3$ as shown in Fig. 4. We have then

$$W = 3 \int_{2\pi/3}^{\pi} \frac{2ZU^2RL}{c_r + \epsilon \cos \theta} d\theta \quad [11]$$

where the integration is performed over one half of one lobe which is the symmetrical element of the bearing.

The integral of Equation [11] evaluated between the limits π and $2\pi/3$ yields

$$W = \frac{8ZU^2RL}{\sqrt{c_r^2 - \epsilon^2}} \left[\pi - \arctan \frac{\sqrt{3}/2 \sqrt{c_r^2 - \epsilon^2}}{\epsilon - 1/2c_r} \right]$$

Dividing out by c_r and rearranging, the final form is obtained

$$W = \frac{8ZU^2RL}{c\sqrt{1 - m^2}} \frac{3}{2} \left[\pi - \arctan \frac{\sqrt{3(1 - m^2)}}{2m - 1} \right] \quad [12]$$

When $\epsilon = 0$, the value of Equation [12] reduces to

$$W = \frac{8ZU^2RL}{c} \frac{3}{2} \left[\pi - \arctan \left(-\sqrt{3} \right) \right]$$

$$= \frac{8ZU^2RL}{c} \frac{3}{2} \frac{\pi}{3} = \frac{4\pi ZU^2RL}{c}$$

which is Petroff's equation for circular bearings. When $\epsilon = c_r$, Equation [12] gives an infinite power loss.

In practical terms of horsepower, Equation [12] can be written as

$$H = \frac{3.6\mu N^2D^3L \times 10^{-12}}{c\sqrt{1 - m^2}} \left[\pi - \arctan \frac{\sqrt{3(1 - m^2)}}{2m - 1} \right] \quad [13]$$

For any given operating conditions and ellipticity ratio, the expected power losses in 3-lobe symmetrical bearings can be computed from Equation [13].

Asymmetrical 3-Lobe Bearing. An asymmetrical 3-lobe bearing consists of an elliptical lower half and of two 90-deg lobes for the upper half, as shown in Fig. 2. The power losses in the lower half can be obtained by using the formula for elliptical bearings. The

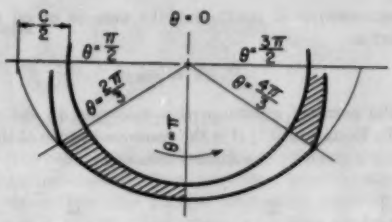

a) 120° LOBE OF SYMMETRICAL 3-LOBE BEARING

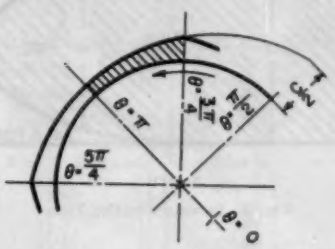

b) 90° LOBE OF ASYMMETRICAL 3-LOBE BEARING

FIG. 4 ELEMENTS OF THREE-LOBE BEARINGS

analysis of the upper half follows the same pattern as for symmetrical 3-lobe bearings with the exception of the limits of integration. In Fig. 4 the 90-deg lobe is seen to be contained between the limits of $3\pi/4$ and $5\pi/4$. Writing Equation [11] only for the upper half we obtain

$$W = 2 \int_{3\pi/4}^{5\pi/4} \frac{ZU^2RL}{c_r + \epsilon \cos \theta} d\theta$$

or since π is a line of symmetry

$$W = 2 \int_{3\pi/4}^{\pi} \frac{2ZU^2RL}{c_r + \epsilon \cos \theta} d\theta \quad [14]$$

Evaluated between these limits, the power losses in the upper half are then given by

$$W = \frac{8ZU^2RL}{c\sqrt{1 - m^2}} \left[\pi - \arctan \frac{\sqrt{1 - m^2}}{\sqrt{2}\, m - 1} \right] \quad [15]$$

For $m = 0$ this equation reduces to half the value of Petroff's equation for circular bearings. In terms of practical units Equation [15] becomes

$$H = \frac{2.4\mu N^2D^3L \times 10^{-12}}{c\sqrt{1 - m^2}} \left[\pi - \arctan \frac{\sqrt{1 - m^2}}{\sqrt{2}\, m - 1} \right] \quad [16]$$

INCOMPLETE OIL FILM

As pointed out previously, the dimension h in noncircular bearings is a variable even for a concentric shaft position. Most of these bearings are built with oil-inlet slots at the ends of the lobes and a full oil film exists in the clearance space only where it decreases in the direction of rotation since there is not enough oil to fill in the ever-increasing clearance space. From the point of minimum film thickness on, the oil film is incomplete throughout the divergent region. The oil film can be considered to break up into streamlets,[2] air and foam replacing the oil in the exposed regions. Presumably no more side leakage occurs and to satisfy

the requirements of continuity the volume of oil must remain constant or

$$Bh = \text{const} \quad [17]$$

from the point of minimum film thickness to the next oil-inlet slot. In Equation [17] B is the combined width of the oil streamlets, and is given by the shaded area of Fig. 5.

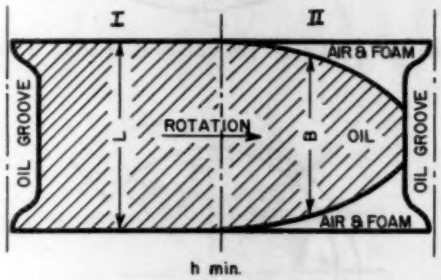

FIG. 5 INCOMPLETE OIL FILM

In section I of Fig. 5 a complete oil film exists and the power losses are given by the formulas derived in the previous section. In part II we have

$$Bh = Lh_{\min} \quad [18]$$

Defining j as the ratio of power loss with incompleteness of the oil film taken into account to that obtained from Petroff's expression we have

$$j = \frac{H}{H_c} = \frac{\int_0^{2\pi} \frac{ZU^2RBd\theta}{h}}{\frac{4\pi ZU^2RL}{c}} = \frac{1}{2\pi}\int_0^{2\pi}\left(\frac{B}{L}\right)\left(\frac{c}{\frac{2}{h}}\right)d\theta \quad [19]$$

From Equation [18]

$$B = L\frac{h_{\min}}{h} = L\frac{\frac{c}{2}(1-m)}{h}$$

Using this in Equation [19] and defining j_0 as the power-loss ratio over that portion of a lobe where the oil film is incomplete

$$j_0 = \frac{1}{2\pi}\int_{\pi}^{\theta_2}\frac{Lc(1-m)\frac{c}{2}}{L2h\,h}d\theta = \frac{1-m}{2\pi}\int_{\pi}^{\theta_2}\frac{d\theta}{(1+m\cos\theta)^2} \quad [20]$$

Using the substitution

$$\gamma = \arccos\left(\frac{\cos\theta + m}{1 + m\cos\theta}\right)$$

Equation [20] integrates into

$$j_0 = \frac{(1-m)}{2m(1-m^2)^{3/2}}\left[\arccos\left(\frac{\cos\theta+m}{1+m\cos\theta}\right) - m\sin\arccos\left(\frac{\cos\theta+m}{1+m\cos\theta}\right)\right]\Bigg|_{\pi}^{\theta_2} \quad [21]$$

For elliptical bearings $\theta_2 = 3\pi/2$ and Equation [21] becomes

$$j_0 = \frac{(1-m)}{2\pi(1-m^2)^{3/2}}(\arccos m - m\sin\arccos m - \pi) \quad [22]$$

For symmetrical 3-lobe bearings $\theta_2 = 5\pi/4$ and Equation [21] becomes

$$j_0 = \frac{(1-m)}{2\pi(1-m^2)^{3/2}}\left(\arccos\frac{2m-1}{2-m} - m\sin\arccos\frac{2m-1}{2-m} - \pi\right) \quad [23]$$

For asymmetrical 3-lobe bearings $\theta_2 = 5\pi/4$ and Equation [21] becomes

$$j_0 = \frac{(1-m)}{2\pi(1-m^2)^{3/2}}\left(\arccos\frac{\sqrt{2}m-1}{\sqrt{2}-m} - m\sin\arccos\frac{\sqrt{2}m-1}{\sqrt{2}-m} - \pi\right) \quad [24]$$

To obtain the power losses in the portion of the bearing where the oil film is incomplete, Equation [22] has to be multiplied by 2; Equation [23] by 3; and for the asymmetrical 3-lobe bearing Equation [24] has to be multiplied by 2 and added to Equation [22]. For the half where the oil film is complete, the losses are given by one half of Equations [9], [12], and [15].

In Table 1 and Fig. 6 the power losses in elliptical and 3-lobe bearings, assuming a complete oil film, are presented as a function of the ellipticity ratio m. The values represent the ratio of the power losses in the noncircular bearings to the cylindrical type having a diametral clearance c. To compute then the power losses

TABLE 1 POWER-LOSS RATIO k WITH COMPLETE OIL FILM

Ellipticity ratio	Type of bearing: Elliptical	Symm. 3-lobe	Symm. 4-lobe
0.2	1.15	1.20	1.23
0.4	1.38	1.51	1.58
0.6	1.77	2.04	2.24
0.8	2.65	3.34	3.82

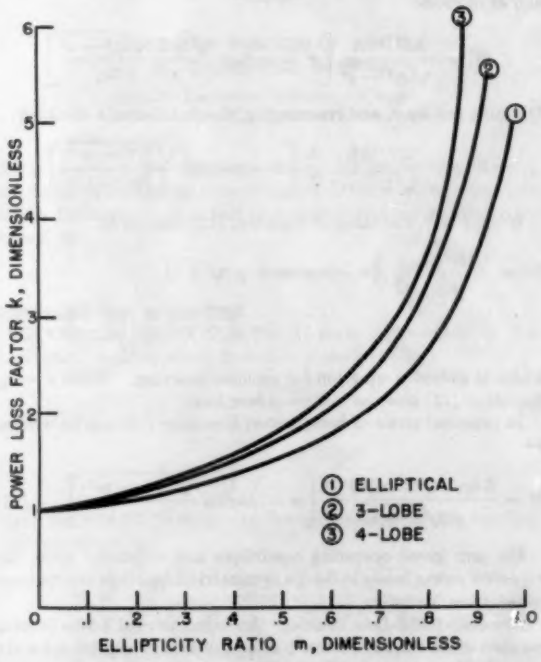

FIG. 6 RATIO OF POWER LOSSES OF NONCYLINDER TO CYLINDER BEARINGS VERSUS ELLIPTICITY RATIO WITH COMPLETE OIL FILM

in elliptical and 3-lobe bearings, it suffices to compute the losses for a circular bearing of clearance c (the major clearance) using Petroff's Equation [1] and multiply it by the proper factor k from Fig. 6, or

$$H = kH_c \quad \ldots\ldots [25]$$

Table 2 and Fig. 7 give the same results for the assumption of an incomplete oil film. In this case

$$H = jH_c \quad \ldots\ldots [26]$$

where j is taken from Fig. 7. The column denoted Symm. 4-lobe can be used to calculate losses in an actual 4-lobe bearing. In our case it applies to the upper half of asymmetrical 3-lobe bearings.

TABLE 2 POWER-LOSS RATIO j WITH INCOMPLETE OIL FILM

Ellipticity ratio m	Type of bearing: Elliptical	Symm. 3-lobe	Symm. 4-lobe
0.2	1.11	1.18	1.21
0.4	1.28	1.45	1.54
0.6	1.55	1.88	2.11
0.8	2.19	2.90	3.42

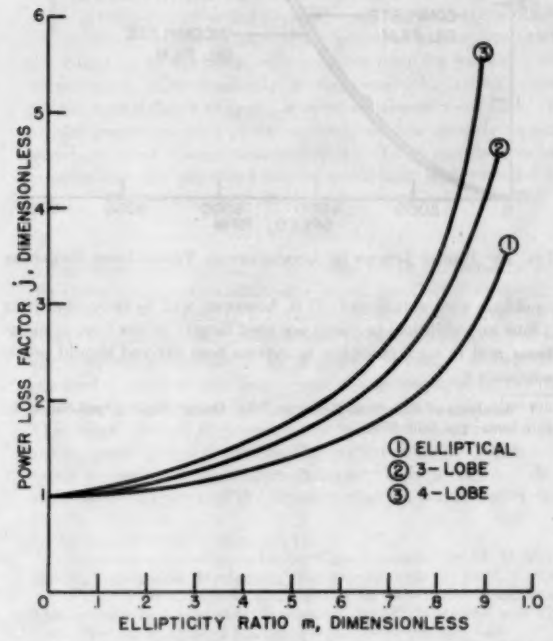

FIG. 7 RATIO OF POWER LOSSES OF NONCYLINDER TO CYLINDER BEARINGS VERSUS ELLIPTICITY RATIO WITH INCOMPLETE OIL FILM

Since the value of m in asymmetrical 3-lobe bearings is usually not the same for the upper and lower half no composite value of k and j can be given for it. To compute the power losses in an asymmetrical 3-lobe bearing the upper half is treated as a symmetrical 4-lobe bearing and the lower half as an elliptical bearing

$$H = \frac{1}{2}(k_1 H_{c1} + k_2 H_{c2})$$

or

$$H = \frac{1}{2}(j_1 H_{c1} + j_2 H_{c2}) \quad \ldots\ldots [27]$$

where, in general

$$k_1 \neq k_2,\ j_1 \neq j_2, \quad \text{and} \quad H_{c1} \neq H_{c2}$$

COMPARISON WITH TEST RESULTS

In Table 3 a comparison is made of the power losses obtained from direct experiments with those calculated from the appropriate equation derived in this paper. The same information is plotted in Figs. 8, 9, and 10. The experiments were conducted on a large journal test-stand with a dynamometer housing that enables direct torque measurements. Considering the numerous

TABLE 3 COMPARISON OF CALCULATED AND EXPERIMENTAL POWER LOSSES

Speed, rpm	Viscosity at outlet oil temp, cps	Power losses, hp: Tests	Calculated complete oil film[a]	Calculated incomplete oil film[b]
ELLIPTICAL BEARING $D = 8$ in. $L = 4$ in. $c = 0.024$ in. $m = 1/2$				
1000	23.0	1.5	1.2	1.1
2000	22.2	4.6	4.1	3.7
3000	20.5	10.5	9.4	8.5
4000	18.0	11.5	14.7	13.3
5000	17.5	25.3	22.5	20.3
7000	12.0	28.8	30.0	27.1
9000	10.0	47.7	41.5	37.5
SYMMETRICAL 3-LOBE BEARING $D = 2\ 5/8$ in. $L = 5/4$ in. $c = 0.016$ in. $m = 1/2$				
6000	53.0	0.71	0.57	0.55
12000	44.4	1.92	1.90	1.82
18000	37.8	3.25	3.67	3.52
24000	31.8	4.75	5.50	5.28
ASYMMETRICAL 3-LOBE BEARING $D = 4$ in. $L = 3$ in. $c_1 = 0.0118$ in. $c_2 = 0.0166$ in. $m_1 = 0.17$ $m_2 = 0.4$				
3000	13.3	0.97	.87	0.84
5000	13.8	2.24	2.44	2.35
6000	13.3	3.08	3.40	3.26
7000	11.4	3.94	4.20	4.05
9000	11.3	6.86	6.40	6.15

[a] Equations [10], [13], [16].
[b] Equations [22], [23], [24].

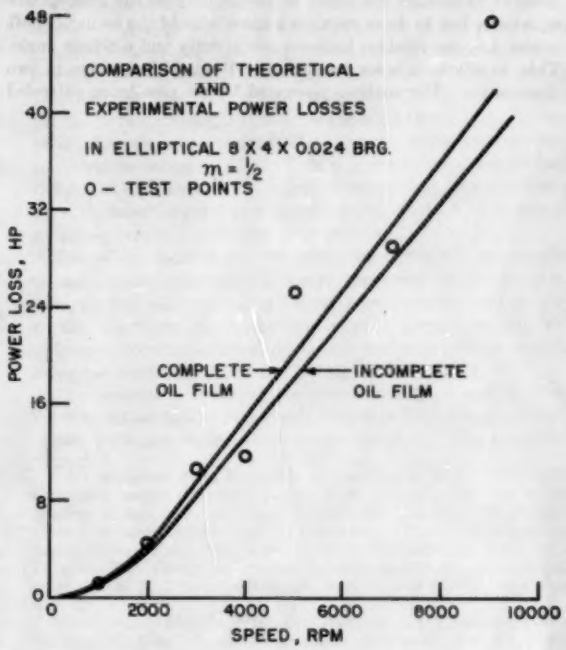

FIG. 8 POWER LOSSES IN ELLIPTICAL BEARINGS

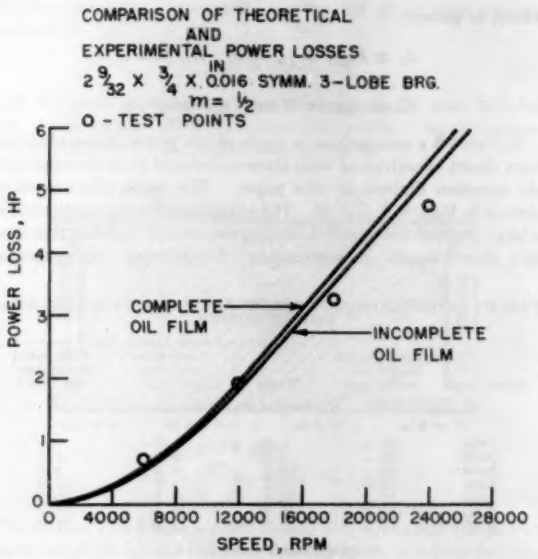

FIG. 9 POWER LOSSES IN SYMMETRICAL THREE-LOBE BEARINGS

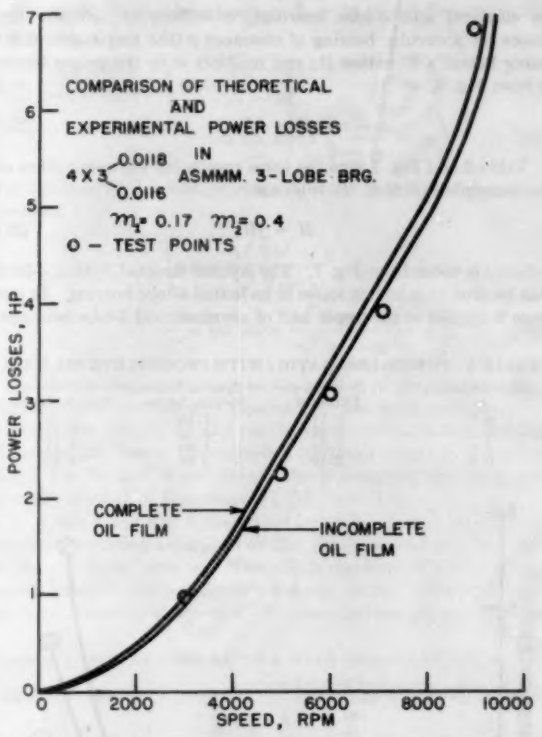

FIG. 10 POWER LOSSES IN ASYMMETRICAL THREE-LOBE BEARINGS

variables involved in testing bearing performance and the difficulty in obtaining reliable measurements of elliptical and 3-lobe bearings, the agreement between the experimental and theoretical results is very good. The calculated results are not much affected by considerations of an incomplete oil film. At low ellipticities this effect is almost negligible.

In closing, it should be mentioned that the power losses will be higher when the shaft is running at some eccentricity. It is possible to include the effect of eccentricity in the appropriate equations, but to do so requires a knowledge of the locus of shaft center, i.e., the relation between eccentricity and attitude angle. This, in effect, calls for a solution of Reynolds' equation in two dimensions. The analysis presented here is now being extended to obtain such solutions.[5] It is, however, well to remember that 3-lobe and elliptical bearings are used largely in low load applications and in such cases the equations here derived should prove adequate.

[5] "Analysis of Elliptical Bearings," by Oscar Pinkus, published in this issue, pp. 965–973.

Prediction of Lubricating-Oil Viscosities at High Pressures

By O. H. CLARK,[1] PAULSBORO, N. J.

Data from the ASME project on high-pressure viscosity have been applied to test the feasibility of predicting viscosity at high pressures from room-pressure measurements at 100 and 210 F. For ASME test oils graphical relations were developed to predict viscosities up to about 50,000 psi at 100 and 210 F. Two scales were used, according as oils were classified as paraffinic or naphthenic. Discrepancies between measured and predicted values are noted and discussed.

Introduction

THERE exists a degree of correlation between the effects of temperature and of pressure upon the viscosity of oils.[2,3,4] This correlation makes it attractive to attempt to predict the variation of viscosity with pressure from its variation with temperature. The feasibility of such prediction on lubricating oils has been difficult to appraise because of insufficient data. The ASME project on high pressure viscosities has recently reported an extensive set of such measurements.[5] These results have been used to test the practicability of predicting high pressure viscosity. The ASME oils studied are described in Table 1.

Method

The basic assumption is that the effect of pressure upon the viscosity of an oil is established when the effect of temperature is known.[6] Specifically, a certain change of viscosity from a given temperature and pressure may be effected either by changing temperature alone or by changing pressure alone. It is assumed that for all oils the pressure change required to duplicate the effect of any specified temperature change is the same. Then measurement of pressure and temperature variations upon one reference oil will determine the pressure changes which correspond to various temperature changes. This in turn will determine for an unknown oil the pressure changes which would correspond to viscosity changes effected by varying its temperature alone.

To devise a simple graphical procedure to test this assumption, use was made of the ASTM Kinematic Viscosity Chart. This chart provides a scale on which the kinematic viscosities of oils at various temperatures (and room pressure) give straight-line plots, which may be established by measurement at 100 and 210 F. Such a scale would apply equally generally to plotting viscosities at various pressures, provided the correspondence between temperature variation and pressure variation were good enough. The same straight line could be used merely by replacing each temperature value on the scale with its equivalent pressure value. The proper equivalent pressures would be obtained from actual measurements on a reference oil over the required pressure range. These pressures would apply at the temperature at which the scale started.

For the oils of Table 1, it was found that a single pressure scale showed obvious differences between paraffinic and naphthenic oils.[7] Therefore the oils were grouped into paraffinic and naphthenic categories and separate calibrations worked out for the two categories. In each group a reference oil was chosen, selected to be near the middle of the group as regards viscosity-temperature coefficient. Calibrated pressure scales were then established from these arbitrary reference oils at two temperatures 100 and 210 F.

Results

Comparison of measured and predicted viscosities is shown in tables. These give the per cent deviations of the predicted or graphical viscosities from the measured viscosities at pressure intervals of 5000 psi over the range covered by ASME results. Interpolation was used where necessary. Table 2 lists results for the paraffinic oils, Table 3 for the naphthenic oils. In each table the oils are arranged according to increasing viscosity-temperature-rating (VTR). This is a simplified viscosity index developed by Ramser.[8] It is defined as per cent viscosity change per Fahrenheit degree, averaged from 100 to 210 F; i.e., it is the mean temperature coefficient over this range.

The tables show that, even after classifying oils as paraffinic or naphthenic, considerable errors can occur in the predicted values. For oils possessing viscosity-temperature ratings close to the reference oil, prediction is quite good. As the VTR difference becomes greater, deviations increase, predicted values being too low for low VTR and too high for high VTR.

The pressure scales used are shown in Figs. 1 and 2. They are entered on ASTM Kinematic Viscosity High Range, Chart E paper, replacing temperature as the abscissa. The ordinate is

---

[1] Socony Mobil Oil Company, Inc.

[2] "Viscosity of Lubricants Under High Pressure," by M. D. Hersey and R. F. Hopkins, *Mechanical Engineering*, vol. 67, 1945, p. 820.

[3] "Velocity of Compressional Waves in Petroleum Fractions at Atmospheric and Elevated Pressures," by R. Matteson and C. J. Vogt, *Journal of Applied Physics*, vol. 11, 1940, pp. 658–665.

[4] "A Correlation of Viscosity, Temperature, and Pressure," by R. T. Sanderson, *Mechanical Engineering*, vol. 71, 1949, p. 349; also, "Viscosity, Temperature, and Pressure of Lubricating Oils," by R. T. Sanderson, *Industrial and Engineering Chemistry*, vol. 41, 1949, pp. 2059–2061.

[5] "Viscosity and Density of Over 40 Lubricating Fluids of Known Composition at Pressures to 150,000 Psi and Temperatures to 425° F," published by The American Society of Mechanical Engineers, 1953.

[6] This assumption is not new. The form in which it is expressed here was used by Sanderson, loc. cit.

Contributed by the Special Research Committee on Lubrication and presented at a joint session of the Lubrication Activity and Applied Mechanics and Machine Design Divisions at the Semi-Annual Meeting, Pittsburgh, Pa., June 20–24, 1954, of The American Society of Mechanical Engineers.

Note: Statements and opinions advanced in papers are to be understood as individual expressions of their authors and not those of the Society. Manuscript received at ASME Headquarters, September 24, 1953. Paper No. 54—SA-39.

[7] A convenient index for degree of paraffinicity is the UOP characterization factor. Defined in terms of boiling point and specific gravity, it has been correlated to viscosity and may be estimated from kinematic viscosity and API gravity. Curves for this purpose are reproduced in "Petroleum Refinery Engineering," by W. L. Nelson. In Table 1 the characterization factors are given, ranging from 12.3 to 12.5 for paraffinic oils, from 11.4 to 12.0 for naphthenic oils.

[8] "Representation of Viscosity-Temperature Characteristics of Lubricating Oils," by J. H. Ramser, *Industrial and Engineering Chemistry*, vol. 41, 1949, pp. 2053–2059.

TABLE 1 ASME OILS USED FOR PRESSURE-VISCOSITY STUDY

A. Paraffinic Oils

A.S.M.E. Number	Description	c.s. at 100°	c.s. at 210°	V.I.	Characterization Factor
24 E	A.P.I. High Shear Test Oil, Mineral Oil	33.1	5.32	102	12.3
31 G	250 SSU at 100°F., Cut 100 F at 1 mm.	55.3	7.17	96	12.3
30 F	Navy Symbol 9250 Diesel Engine Lube Oil	115.8	12.17	102.9	12.3
41 G	32 G Dearomatized	150.9	14.7	104	12.5
32 G	700 SSU at 100°F., Cut 100 F at 1 mm.	165.3	15.12	99	12.4
35 G	700 SSU at 100°F., 31 G plus Bright Stock	155	14.08	95	12.3
13 D	C.R.C. Gear Oil, Aircraft Engine Oil	352.6	25	99	12.5
33 G	2500 SSU at 100°F., Cut 100 F at 1 mm.	586.1	32.3	91	12.4

B. Naphthenic Oils

A.S.M.E. Number	Description	c.s. at 100°	c.s. at 210°	V.I.	Characterization Factor
25 E	A.P.I. High Shear Test Oil, Mineral Oil	8.75	2.24	60	11.7
17 D	C.R.C. Gear Oil, Mil-O-6081	10.3	2.47	52	11.8
36 G	250 SSU at 100°F., Cut 100 F at 1 mm.	55.1	5.87	23	11.7
42 G	37 G Dearomatized	73.1	7.54	62	12.0
29 F	Naval Boiler and Turbine Lab Gear Test Oil	94.5	9.08	72	11.9
37 G	700 SSU at 100°F., Cut 100 F at 1 mm.	143.1	9.48	8	11.7
38 G	2500 SSU at 100°F., Cut 100 F at 1 mm.	514.3	17.21	-42	11.4

C. Miscellaneous Oils

A.S.M.E. Number	Description	c.s. at 100°	c.s. at 210°	V.I.	Characterization Factor
45 G	31 G plus Acryloid 710	153.3	21.8	136	12.6
52 G	Aromatic Extract from 37 G	53.7	13.62	-187	10.9

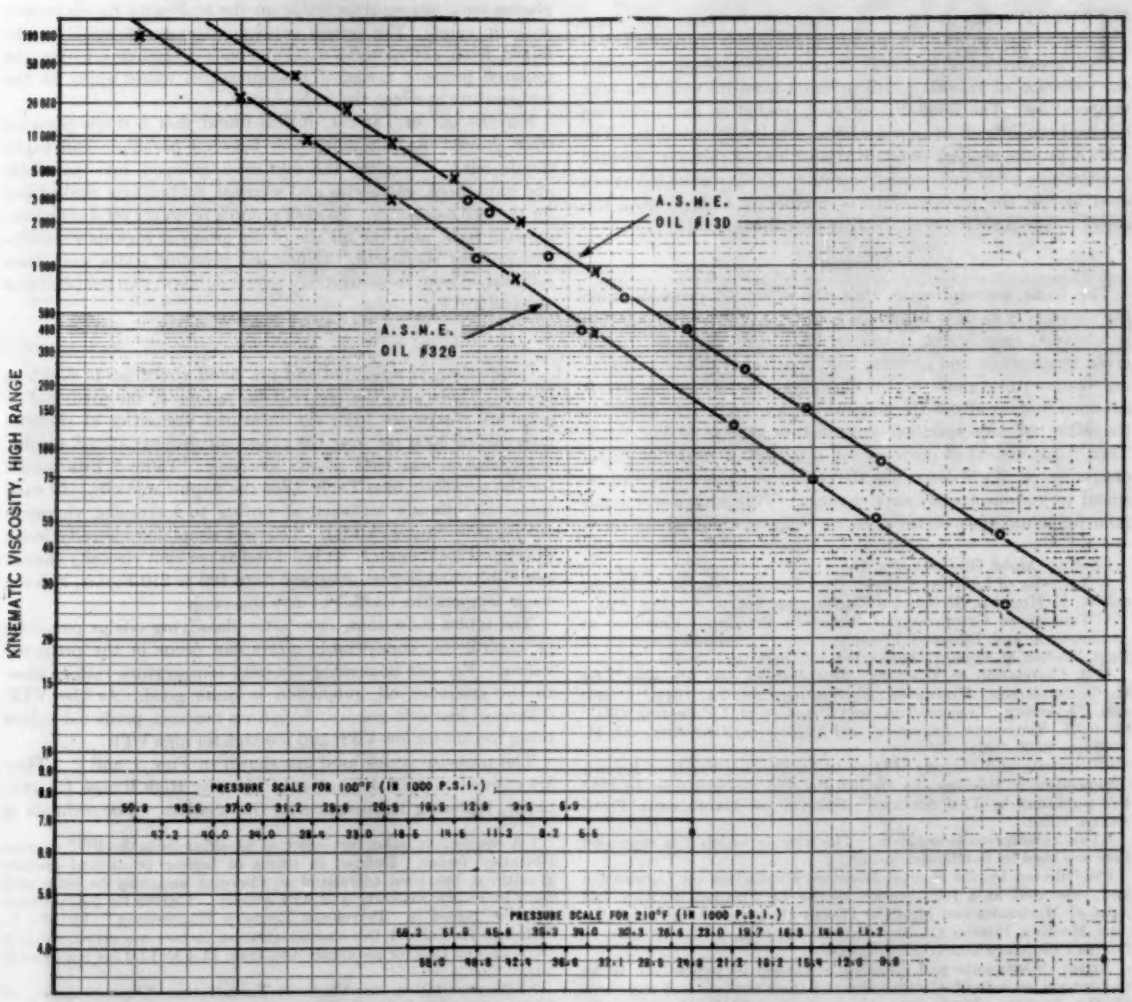

FIG 1 PRESSURE VARIATION OF VISCOSITY PARAFFINIC OILS
(Points are measured values. x = 100 deg F; 0 = 210 deg F.)

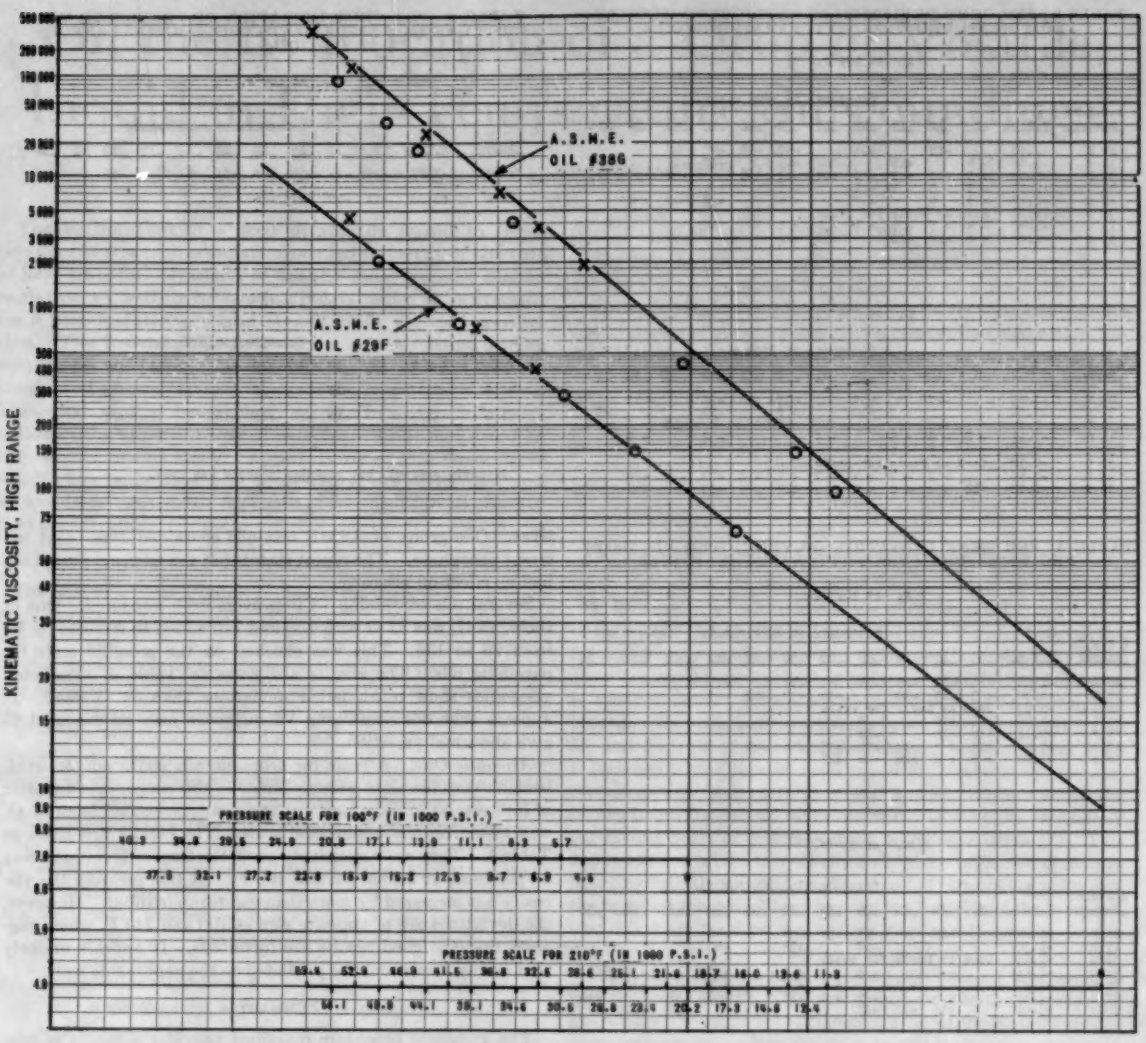

FIG. 2 PRESSURE VARIATION OF VISCOSITY NAPHTHENIC OILS
(Points are measured values. x = 100 deg F; 0 = 210 deg F.)

centistokes. On each figure a pair of sample oils is plotted to illustrate the method. The customary straight line on ASTM Chart E paper is drawn through the two points marking room-pressure viscosity at 100 and 210 F. The abscissa is labeled with the pressure scale given by pressure measurements on the reference oil. ASME measurements at various pressures are entered as points for comparison with the predicted graphical values.

APPRAISAL AND DISCUSSION

It is evident the correlation between viscosity-pressure relationship and viscosity-temperature relationship shows considerable variation, even after classifying oils as paraffinic, etc.[9] Use of a single conversion scale for each class of oil, as here tried, would apparently give results usually reliable to ±50 per cent. However, greater errors could occur, as illustrated by oil 38 G at 210 F.

It should be noted that very large viscosity increases are in question, factors of several hundred to a thousand or more. Over so wide a range, such approximate results may be useful for many purposes. For example, oil 38 G at 35,000 psi and 210 F was predicted as 6200 centistokes instead of 3550. This difference would often be of little importance. However, it is apparent that this simple method could not be relied upon for better than such semiquantitative answers.

More reliable predictions of high-pressure viscosity probably would be obtained by using reference oils specially selected for similarity to the test oils, or by using available data to develop scale correction factors based upon VTR. J. H. Ramser has suggested (private communication) that correction factors could be obtained by smoothing the per cent deviations in the tables with a family of curves using VTR as parameter. This possi-

[9] The deviations found could not be appreciably reduced by a different choice of reference oil. This is indicated by the regular trend from low values to high values as the VTR of test oils increase.

TABLE 2 PER CENT DEVIATION OF PREDICTED VISCOSITY FROM MEASURED VISCOSITY, PARAFFINIC OILS

A. At 100°F.

A.S.M.E. Number	V.T.R.	Pressure, in 1000 p.s.i. 5	10	15	20	25	30	35	40	45	50	55
24 E	-1.66		-25		-24		-40	-38	-40	-48		
31 G	-1.86	- 4		+18			-13		-17	-17		
30 F	-2.04	+ 5	-11	- 9	- 6	+10	-13	- 8		- 8		
41 G	-2.11	- 9	- 3	- 4	- 1		- 5		+ 4			
32 G	-2.17	+ 3	0		+ 7		+ 4		+ 9		+40	
35 G	-2.18	Used as basis for scale										
13 D	-2.40	- 4	- 5	- 5	+ 4	- 1	- 1					
33 G	-2.63	+ 6	+18	+16		+18	+20					

B. At 210°F.

A.S.M.E. Number	V.T.R.	Pressure, in 1000 p.s.i. 5	10	15	20	25	30	35	40	45	50	55
24 E	-1.66		-25		-31		-35		-37		-45	
31 G	-1.86				-10		- 8		-10			- 5
30 F	-2.04		+ 5				-15			-15		
41 G	-2.11	- 8	- 6	- 9		- 9			- 2		+ 9	
32 G	-2.17	- 6	- 5	- 5	- 5			+12			+10	
35 G	-2.18	Used as basis for scale										
13 D	-2.40	0	+ 2	- 5	- 4	- 7	+ 4	+18	+13	+14	+20	
33 G	-2.63	-12	+ 3	+ 2	+ 2		+24		+33		+42	

TABLE 3 PER CENT DEVIATION OF PREDICTED VISCOSITY FROM MEASURED VISCOSITY, NAPHTHENIC OILS

A. At 100°F.

A.S.M.E. Number	V.T.R.	Pressure, in 1000 p.s.i. 5	10	15	20	25	30	35	40	45	50	55
25 E	-1.24		-21	-29	-34		-44		-45			
17 D	-1.30	- 3	-15	-19		-35	-37	-42	-45			
36 G	-2.03	Used as basis for scale										
42 G	-2.06	- 2	-10		0							
29 F	-2.12	-10	-10		-12							
37 G	-2.46	+24	+ 2	+30	+30	+35	+46	+44				
38 G	-3.08	+ 6	+ 8	+26	+26	+27						

B. At 210°F.

A.S.M.E. Number	V.T.R.	Pressure, in 1000 p.s.i. 5	10	15	20	25	30	35	40	45	50	55
25 E	-1.24		-15		-25	-30	-34		-40		-46	
17 D	-1.30				-28		-34		-43			
36 G	-2.03	Used as basis for scale										
42 G	-2.06		- 3		- 3		+ 2		+12		+33	
29 F	-2.12			+ 1		- 1	- 2		+ 7		+10	
37 G	-2.46		+ 6		+ 9	+ 9	+15		+38	+38		+36
38 G	-3.08		+16	+22	+27			+74		+114	+119	

bility is indicated by the consistent way the deviations in Tables 2 and 3 follow the VTR differences. The consistent trend from low predictions at low VTR values to high predictions at high VTR values suggests that corrections based on VTR would have general validity for lubricating oils. However, a great many more data than are now available would be required to evaluate properly the reliability and limitations of such a procedure.

Miscellaneous Observations

Additives. Very few data are available on the effect of additives. One group of ASME test oils contained 1 per cent tricresyl phosphate. The report states that the tricresyl phosphate had no effect on viscosity.

Several oils containing VI improvers were measured. One of these, 45 G, was 31 G with acryloid 710 added to increase its VI from 96 to 136. This was checked on the pressure scale for paraffinic oils. The results are given in Table 4. Predicted viscosities show much larger deviations than 31 G itself. It appears that oils containing VI improver may be expected to give abnormal variation.

Aromatic Oils. A scale for aromatic oils could not be tried, because very few data were available in this range. As a matter of interest, oil 52 G, which was the aromatic extract from 37 G, was tested on the naphthenic scale. The results are given in Table 4. They are surprisingly good, the largest deviation being 36 per cent, at 20,000 psi and 100 F. At this pressure the viscosity has increased by more than eight-hundredfold. However, the deviations are of opposite sign at 100 and 210 F, which suggests that the good results are fortuitous. It appears unlikely that aromatic oils could be predicted on the naphthenic scale.

TABLE 4 PER CENT DEVIATION OF PREDICTED VISCOSITY FROM MEASURED VISCOSITY, MISCELLANEOUS OILS

A. At 100°F.

A.S.M.E. Number	V.T.R.	Pressure, in 1000 p.s.i. 5	10	15	20	25	30	35	40	45	50
45 G	-1.77	-16	-24	-36	-45	-53	-61		-65		
52 G*	-3.33	-11	-19	-27	-36						

B. At 210°F.

A.S.M.E. Number	V.T.R.	Pressure, in 1000 p.s.i. 5	10	15	20	25	30	35	40	45	50
45 G	-1.77		-15		-28		-36		-43		-51
52 G*	-3.33		+10	+20	+20	+18		+26	+21		- 5

*Aromatic extract, but naphthenic scale was used.

Summary

The graphical procedure described provides a means of predicting high-pressure viscosities of lubricating oils from measurements at atmospheric pressure and two temperatures. Predictions are quite good for moderate viscosity increases. For viscosity increases by factors of hundreds, as may be found at pressures in the neighborhood of 40,000 psi and higher, errors of the order of 100 per cent may occur.

The results indicate that introducing correction factors for the mean temperature coefficient would improve the accuracy of prediction. However, there are insufficient data to evaluate the improvement which could be obtained by such means.

On the Evaporation of a Drop of Volatile Liquid in High-Temperature Surroundings

By W. E. RANZ,[1] UNIVERSITY PARK, PA.

The evaporation of a drop of volatile liquid in high-temperature surroundings is analyzed in terms of the rate of heat transfer. Transfer of heat by mass transfer and by radiation as well as by conduction is taken into account for a pseudostationary and steady state without convection. The flow of cold vapor to the surroundings during evaporation requires that a considerable amount of heat conducted inward be used to warm vapor moving outward. This waylaying of heat energy results in a significant decrease in the apparent rate of heat transfer as measured by the rate of evaporation. Applications of the theoretical results to evaporation and combustion are discussed, and an empirical treatment for cases of free and forced convection is indicated.

Nomenclature

The following nomenclature is used in the paper:

C_{pA} = average heat capacity of vapor molecules in transfer region
F_A = angle factor in radiation equation (see reference 5)
F_E = emissivity factor in radiation equation (see reference 5)
k_{avg} = average thermal conductivity in transfer region
k_1 = thermal conductivity of gas and vapor at r_1
N = $R_A C_{pA}/k_{avg} r_1$
N_{Gr} = Grashof number = $8r_1^3\rho^2 g_L \beta(T_2 - T_1)/\mu^2$ where ρ = gas density, g_L = local acceleration of gravity, β = coefficient of thermal expansion of gas, and μ = gas viscosity
N_{Nu} = Nusselt number for heat transfer (c.f. Equations [10], [15], and [16])
N_{Pr} = Prandtl number = $C_p\mu/k$ where C_p = gas heat capacity, μ = gas viscosity, and k = gas thermal conductivity
N_{Re} = Reynolds number = $2r_1\rho v/\mu$ where ρ = gas density, v = gas velocity, and μ = gas viscosity
r = radial position
r_1 = radius of drop
r_2 = outer radius of transfer region
$\bar{r}$ = r/r_1
$\bar{r}_2$ = r_2/r_1
R_A = evaporation rate
$t_{l.0}$ = lifetime of an evaporating drop
T = absolute temperature
T_1 = temperature at r_1
T_2 = temperature at r_2
λ_1 = latent heat of vaporization at temperature T_1
θ = $(T_2 - T)/(T_2 - T_1)$
σ = radiation constant (1.365×10^{-12} cal/sec cm^2 deg K^4)
ρ_l = density of liquid

[1] Associate Professor of Engineering Research, The Pennsylvania State University.

Contributed by the Heat Transfer Division and presented at the Annual Meeting, New York, N. Y., November 28–December 3, 1954, of The American Society of Mechanical Engineers.

Note: Statements and opinions advanced in papers are to be understood as individual expressions of their authors and not those of the Society. Manuscript received at ASME Headquarters, August 26, 1954. Paper No. 54—A-143.

Introduction

Because the general phenomenon is one of heat and mass transfer for a spherical shape, the evaporation of a single drop is of considerable engineering interest and has a direct relationship with the processes of spray cooling, drying, absorption, desorption, humidification, and combustion. It is the purpose here to add to the extensive literature on the subject (2, 4, 6, 7)[2] a statement of the effect of simultaneous mass transfer on the rate of heat transfer, clarifying a point which in the past has led to many errors in interpreting data and in estimating the rate of evaporation under extreme conditions. The effect is illustrated by taking an example of the evaporation of a drop of volatile liquid in high-temperature surroundings.

Calculating Rate of Evaporation From Rate of Heat Transfer

It is desirable to calculate the rate of evaporation from the rate of heat transfer rather than the rate of mass transfer because the former is better understood and values of thermal conductivity are more readily available than values of diffusivity. However, to use this method the surface temperature must be known, and because a dynamic balance exists between the rate of heat transfer and the rate of mass transfer, its calculation requires some knowledge of the rate of mass transfer. Fortunately, for surroundings with temperatures several hundred degrees above the boiling point, the surface temperature can be taken as very nearly the boiling point or estimated by a crude calculation (7). This happy state of affairs is a consequence of the rapid rise of saturation concentrations in the neighborhood of the boiling point and the fact that the rate of heat transfer is a function of the temperature difference between the surroundings and the surface and is not sensitive to the exact surface temperature.

When drop diameters are less than 100 microns, the terminal velocity under gravity of a drop with respect to the surrounding gas stream is so small as to make negligible its effect on the rate of drop evaporation. Thus the more tractable situation of no convection is a case of great technical importance. Indeed, when forced or free convection is important, the problem becomes so complex that the only solutions possible are empirical ones based on experimental data.

When a drop is injected into a hot gas stream and evaporates, the rate of evaporation is certainly changing with time, and steady-state conditions are realized only in part. Usually the drop is cold and must be warmed to an equilibrium temperature. In the meantime it evaporates at an increasing rate. Stable temperature and concentration gradients do not exist at first, and during their formation the evaporation rate is faster than it otherwise would be. The drop size shrinks during evaporation, and the radius of the surface is not a constant boundary condition. The drop may be surrounded by other drops, and the heat available may be insufficient for keeping constant the outer boundary conditions or for complete evaporation. All these factors could be included in the basic equations; but only in special cases, most of which are impractical, can solution be obtained.

[2] Numbers in parentheses refer to the Bibliography at the end of the paper.

The problem treated here pretends to be only the solution for a pseudostationary and steady state without convection, a state which is believed to be a fair approximation of the actual situation.

Mass Transfer and Radiation

When such a drop evaporates, heat is transferred to the surface by conduction where it is used to transform the liquid into vapor which in turn is transferred away from the surface by diffusion. There is a temperature gradient from the surroundings to the surface and a concentration gradient from the surface to the surroundings. When the surroundings are at a relatively high temperature, however, two other forms of heat transfer should be taken into account, heat transfer by mass transfer and radiation:

1 A large mass flow of cold vapor to the surroundings carries with it coldness and acts exactly like a convective velocity in the positive r-direction. Another way of looking at the situation is to visualize some of the heat transferred inward by conduction to be used in warming up the vapor moving outward. An over-all mass and energy balance will show that the heat required to warm the vapor may be considerably higher than the heat required for evaporation, particularly when the liquid is one of low latent heat.

2 In high-temperature surroundings a drop receives a significant amount of heat by radiation. Normally, this radiation can be treated as coming directly from the surroundings to the surface without intermediate absorptions and radiations and can be incorporated into the heat-transfer equations in an approximate manner as it is done in the following. When intermediate absorptions and radiations are important, as they may be in combustion, a term representing generation of heat must be introduced into the differential equation which then becomes nonlinear and unsolvable, a complication far beyond the scope of the present problem.

Heat-Balance Equation

Without further discussion we write the differential equation for a heat balance on a differential volume in the transfer region, assuming a steady state and no convection with heat being transferred in this region only by conduction and mass transfer

$$k_{avg}\left[\frac{d^2T}{dr^2}+\frac{2}{r}\frac{dT}{dr}\right]=\frac{R_A C_{pA}}{4\pi r^2}\frac{dT}{dr} \quad \ldots\ldots [1]$$

Terms on the left-hand side of the equation represent heat transfer by conduction. Although the thermal conductivity may vary severalfold over a large temperature range, it is necessary to choose an unspecified average conductivity to avoid nonlinearity. The term on the right-hand side represents the mass flow of heat where R_A is the rate of evaporation or mass transfer and C_{pA} is an average heat capacity of the vapor molecules under the conditions specified. For a pseudostationary state the following boundary conditions are chosen

$$T = T_1 \text{ at } r = r_1$$
$$T = T_2 \text{ at } r = r_2$$

and the special case where $T = T_2$ as $r = r_2 \to \infty$.

In terms of heat transfer the rate of evaporation or mass transfer is given by

$$R_A = 4\pi r_1^2\,[k_1(dT/dr)_{r=r_1} + \sigma(T_2^4 - T_1^4)F_A F_E]/\lambda_1 \ldots [2]$$

where the effect of radiation is taken into account in an approximate manner by the second term in the bracket (5). The numerator of Equation [2] is the rate at which heat is transferred to the surface and used for evaporation.

With the problem stated in this manner we reduce it to compact form by the following substitutions

$$\theta = (T_2 - T)/(T_2 - T_1) \quad \ldots\ldots [3]$$

$$\rho = r/r_1 \quad \ldots\ldots [4]$$

$$N = R_A C_{pA}/4\pi k_{avg} r_1 \quad \ldots\ldots [5]$$

whence Equation [1] becomes

$$\frac{d^2\theta}{d\rho^2}+\left[\frac{2}{\rho}-\frac{N}{\rho^2}\right]\frac{d\theta}{d\rho}=0 \quad \ldots\ldots [6]$$

with boundary conditions

$$\theta = 1 \text{ at } \rho = 1$$
$$\theta = 0 \text{ at } \rho = \rho_2$$

The solution of Equation [6] is

$$\theta = \frac{\exp(-N/\rho_2) - \exp(-N/\rho)}{\exp(-N/\rho_2) - \exp(-N)} \quad \ldots\ldots [7]$$

which in combination with Equation [2] gives

$$R_A = \frac{4\pi r_1 k_1 (T_2 - T_1)}{\lambda_1}\left[\frac{N}{\exp(N-(N/\rho_2))-1} + \frac{r_1\sigma(T_2^4 - T_1^4)F_A F_E}{k_1(T_2 - T_1)}\right] \quad \ldots\ldots [8]$$

By combining Equation [8] with the definition of N, Equation [5], an equation is obtained for the implicit solution of N in terms of known quantities

$$N = \frac{k_1 C_{pA}(T_2 - T_1)}{k_{avg}\lambda_1}\left[\frac{N}{\exp(N-(N/\rho_2))-1} + \frac{r_1\sigma(T_2^4 - T_1^4)F_A F_E}{k_1(T_2 - T_1)}\right] \quad \ldots\ldots [9]$$

N calculated implicitly from Equation [9] is now substituted in Equation [5] or Equation [8] to give the rate of evaporation in terms of known quantities.

The expression for Nusselt number is also of interest

$$\left.\begin{aligned} N_{Nu} &= (k_1(dT/dr)_{r=r_1})(2r_1)/(T_2 - T_1)k_1 \\ &= \frac{2N}{\exp(N-(N/\rho_2))-1} \\ &= \frac{2}{(1-(1/\rho_2))\left[1+\frac{(N-(N/\rho_2))}{2!}+\frac{(N-(N/\rho_2))^2}{3!}+\ldots\right]} \end{aligned}\right\} \ldots [10]$$

N_{Nu} is dependent on its definition which in this case is one based on the rate of heat transfer to the surface by conduction only. However, Equation [10] includes the effect of radiation in so far as its effect on the temperature gradients is concerned. The expanded form shows that decreasing ρ_2 increases N_{Nu} and increasing N decreases N_{Nu} from a value of 2 which holds for negligible mass transfer of heat, a small temperature difference, and a distant outer boundary.

The lifetime, $t_{1,0}$, of a drop evaporating under the general conditions is obtained by numerically integrating the expression

$$t_{1,0} = \int_0^{r_1} 4\pi\rho_l(r_1^2/R_A)dr_1 \quad \ldots\ldots\ldots\ldots [11]$$

where R_A is a function of r_1 given by Equations [5] or [8] and [9]. Simple forms and analytical solutions are possible in special cases.

Example

An example serves to illustrate the use of these equations. Consider the rate of evaporation of a water drop in air at 500 F (260 C) and 1 atm when it is 100 microns in diameter. The known quantities in cgs cal units are as follows:

$r_1 = 0.5 \times 10^{-2}$ cm; $T_1 = 327$ K (estimated as wet-bulb temperature)

$r_2 = \infty$; $T_2 = 533$ K

$\lambda_1 = 566$ cal/gm mass (heat of evaporation of water at 327 K)

$k_{avg} = 8.25 \times 10^{-5}$ cal/sec cm K (average thermal conductivity of air for the temperature range. For the estimated drop temperature the saturated volume ratio of water vapor to air is only $^{16}/_{360}$ which falls off rapidly with increasing r)

$k_1 = 6.30 \times 10^{-4}$ cal/sec cm K (volumetric average conductivity of water vapor and air at estimated surface conditions)

$C_{pA} = 0.48$ cal/gm mass K (heat capacity of water vapor at average temperature)

$\sigma = 1.365 \times 10^{-12}$ cal/sec cm^2 K^4 (constant in radiation equation)

$F_A F_E = 0.95$ (emissivity of water surface, reference 5)

Equation [9] then becomes $N = 0.1332\ [(N/(\exp N - 1) + 0.035]$ which gives $N = 0.129$. The evaporation rate from Equation [5] is

$$R_A = 0.129 \times 4\pi \times 8.25 \times 10^{-5} \times 0.5 \times 10^{-2}/0.48 = 1.39 \times 10^{-6} \text{ gm mass/sec}$$

For liquids other than water the major numerical difference in such a calculation is the result of λ_1 being about one sixth that of water. N then becomes of the order of 0.5–0.7 for similar conditions. It is evident that radiation plays only a minor role in the evaporation of drops less than 100 microns in diameter even at higher temperatures. The effect often warrants the calculation of its order of magnitude, but rarely does it gain first place in importance.

Case of Negligible Radiation

The special case of negligible radiation with $\mathfrak{r}_2 = \infty$ is of interest because it always allows an approximate calculation of N which in many situations turns out to be accurate enough for the problem at hand. When radiation is negligible and $\mathfrak{r}_2 = \infty$, Equation [9] reduces to

$$N = \ln\left[1 + \frac{k_1 C_{pA}(T_2 - T_1)}{k_{avg}\lambda_1}\right] \quad \ldots\ldots\ldots [12]$$

Equations [5] and [8] give

$$R_A = \frac{k_{avg} r_1}{C_{pA}} \ln\left[1 + \frac{k_1 C_{pA}(T_2 - T_1)}{k_{avg}\lambda_1}\right] \quad \ldots\ldots [13]$$

or

$$= \frac{4\pi r_1 k_1 (T_2 - T_1)}{\lambda_1} \frac{N}{(\exp N - 1)}$$

$$= \frac{4\pi r_1 k_1 (T_2 - T_1)}{\lambda_1(1 + (N/2!) + (N^2/3!) + \ldots\ldots)}$$

and for constant ambient conditions Equation [11] gives

$$t_{1,0} = \frac{\rho_l \lambda_1 r_1^2}{2k_1(T_2 - T_1)} \frac{(\exp N - 1)}{N}$$

$$= \frac{\rho_l \lambda_1 r_1^2 (1 + (N/2!) + (N^2/3!) + \ldots.)}{2k_1(T_2 - T_1)} \quad \ldots\ldots [14]$$

Thus, when the mass transfer of heat is the only significant heat effect other than conduction, the evaporation rate is decreased and the lifetime is increased by a factor equal to $(\exp N - 1)/N = (1 + (N/2!) + (N^2/3!) + (N^3/4!) + \ldots\ldots\ldots)$.

Application to Combustion of Liquid Fuel Drop

The application of these results to the combustion of a liquid fuel drop has been handled adequately by Godsave (3) who considers the combustion to be controlled by evaporation to a flame front at r_2 which is at the flame temperature T_2. Godsave shows that the experimental burning rate can be estimated theoretically when the flame front distance r_2 is measured. As an addition to his treatment, it is interesting to note that an r_2 can be calculated for a known flame velocity and a known maximum vapor concentration for combustion if it is assumed that the vapor velocity balances the flame velocity at the flame front. Certainly the process is more complicated than the one visualized, but the assumption that evaporation controls the rate of combustion is a reasonable one and an r_2 so calculated is probably accurate enough for purposes of estimating the burning rate.

Forced Convection

For forced convection the rate of evaporation of a drop in high-temperature surroundings can only be approximated. Probably the best method of attacking the problem is to consider that the so-called "effective film thickness" as specified by the Reynolds and Prandtl numbers remains unchanged for the same convective conditions (1). Here the effective thickness is interpreted as $r_2 - r_1$ which can be calculated from heat-transfer correlations obtained under normal conditions

$$2/(\mathfrak{r}_2 - 1) = \lim_{(T_2 - T_1)\to 0} N_{Nu}(N_{Re}, N_{Pr}) \text{ for forced convection} \quad [15]$$

$$2/(\mathfrak{r}_2 - 1) = \lim_{(T_2 - T_1)\to 0} N_{Nu}(N_{Gr}, N_{Pr}) \text{ for free convection} \quad [16]$$

As examples of the use of empirical correlations (7)

$$2/(\mathfrak{r}_2 - 1) = 2 + 0.60\, N_{Pr}^{1/3} N_{Re}^{1/2} \text{ for forced convection} \quad [17]$$

$$2/(\mathfrak{r}_2 - 1) = 2 + 0.60\, N_{Pr}^{1/4} N_{Gr}^{1/4} \text{ for free convection} \quad [18]$$

As before, approximations for special conditions can be made, especially when $\mathfrak{r}_2$ is nearly unity and the film can be treated as a lamina.

BIBLIOGRAPHY

1 "The Condensation of Mixed Vapors," by A. P. Colburn and T. B. Drew, Trans. of the American Institute of Chemical Engineers, vol. 33, 1937, p. 197; "General Theory of Diffusional Operations," by A. P. Colburn and R. L. Pigford, Chemical Engineers' Handbook

by J. H. Perry, McGraw-Hill Book Company, Inc., New York, N. Y., third edition, 1950, p. 559.

2 "On the Evaporation of Falling Drops," by N. Frössling, *Gerlands Beitr. Geophys.*, vol. 52, 1938, p. 170.

3 "Studies of the Combustion of Droplets in a Fuel Spray—The Burning of Single Drops of Fuel," by G. A. E. Godsave, collected papers of the Fourth International Symposium on Combustion, Cambridge, Mass., September 1–5, 1952, The Williams and Wilkins Company, Baltimore, Md., 1953, p. 818.

4 "Vaporization Rates and Heat-Transfer Coefficients for Pure Liquid Drops," by R. D. Ingebo, *Chemical Engineering Progress*, vol. 48, 1952, p. 403.

5 "Heat Transmission," by W. H. McAdams, McGraw-Hill Book Company, Inc., New York, N. Y., second edition, 1950; Chapter III, by H. C. Hottell and Appendix Table XIII, p. 396.

6 "Mass Transfer" (containing a critical review of references on "drop evaporation"), by R. L. Pigford, *Industrial and Engineering Chemistry*, vol. 45, 1953, p. 957.

7 "Evaporation From Drops," by W. E. Ranz and W. R. Marshall, Jr., *Chemical Engineering Progress*, vol. 48, 1952, pp. 141–173.

Discussion

O. A. Uyehara[3] and P. S. Myers.[4] The author is to be congratulated for his reminder that mass transfer affects heat transfer and for his thoughts on this matter after he has had time for reflection on his data as presented in reference (7) of the text.

In considering the evaporation of a drop of volatile liquid in high-temperature surroundings it must be remembered that the temperature of this liquid does not instantly rise from its initial temperature to its vaporizing or wet-bulb temperature. This situation is illustrated in Fig. 1 of this discussion where an experimental temperature-time history of a drop of fuel is presented. The data were obtained as described in the references[5,6] and are intended to be representative of the history of a drop suddenly introduced into hot air. It can be clearly seen in Fig. 1 that the time required for the drop to reach its wet-bulb temperature is an appreciable portion of the lifetime of the drop. It should be clear that the equations and concepts expressed by the author are applicable only to the steady-state portion of the curve.

As a matter of interest the accompanying references[5,6] also consider the effect of mass transfer on heat transfer. Although they were derived in a slightly different fashion the resulting equations are the same as those presented by the author. In this connection the N-factor of the author or the Z-factor of these references[5,6] are also plotted in Fig. 1. It can be seen that under these circumstances only a small fraction of the Q entering the film surrounding the drop reaches the liquid. Thus there is ample justification for the author's insistence of recognition of the effects of mass transfer on heat transfer. As a matter of interest, Equations [17] and [18] of the text were used in the computations and the computed results were in reasonable agreement with the experimental data.

Inasmuch as some of the peculiarities of heat transfer in the presence of mass transfer are being discussed, it might be well to mention the discrepancies in the definitions of the Nusselt number under these circumstances.

The Nusselt number is customarily defined as $h2r/k$; the symbols are as defined in the text. However, as is clearly pointed out in the text (and Fig. 1) the heat that is transferred to the edge of the film surrounding the drop and the heat that actually reaches the liquid surface may differ by a factor of 4 or more. This effect does not show up in the Nusselt number when it is defined as in the foregoing. If however, the Nusselt number is defined as

$$(dT^*/dr^*)_{r=r_1}$$

as in Equation [10] of the text where

$$dT^* = \frac{dt}{(T_2 - T_1)} \quad \text{and} \quad dr^* = \frac{dr}{2r_1}$$

then clearly the temperature gradient

$$\left(\frac{dT^*}{dr^*}\right)_{r=r_1}$$

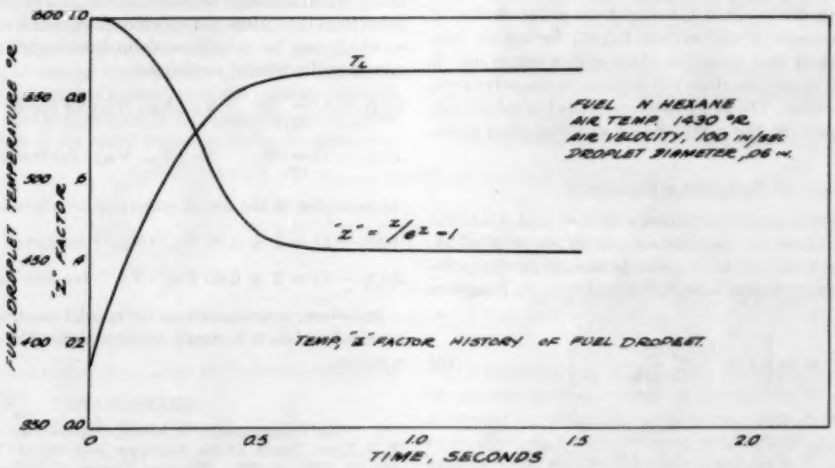

FIG. 1 EXPERIMENTAL TEMPERATURE-TIME HISTORY OF A DROP OF FUEL

[3] Associate Professor of Mechanical Engineering, University of Wisconsin, Madison, Wis. Assoc. Mem. ASME.

[4] Professor of Mechanical Engineering, University of Wisconsin, Madison, Wis. Mem. ASME.

[5] "A Theoretical Investigation of the Heating-Up Period of Injected Fuel Droplets Vaporizing in Air," by M. M. El Wakil, O. A. Uyehara, and P. S. Myers, NACA TN 3179, May, 1954.

[6] "Experimental and Calculated Temperature and Mass Histories of Vaporizing Fuel Droplets," by M. M. El Wakil, R. J. Priem, H. J. Brikowski, P. S. Myers, and O. A. Uyehara, NACA TN 3490.

will be different with and without mass transfer. Using this definition of the Nusselt number does take into account the effect of mass transfer on heat transfer. This definition also makes it clear (Equation [10]) that the thermal conductivity is to be evaluated at the surface and not at an average temperature somewhere between the air and liquid temperatures.

Equation [15] of the text presents another definition of the Nusselt number in terms of the "effective film thickness." If, as is suggested by the author, we assume that the effective film thickness remains unchanged for the same convective conditions then this definition also says that the Nusselt number is independent of mass transfer. Perhaps a discussion as to exactly what is meant by the Nusselt number would be helpful.

In conclusion it might be mentioned that Williams[7] has shown that internal reflection inside the drop can cause an appreciable increase in the absorptivity of the drop.

Author's Closure

The only rules that one should follow in defining the Nusselt number are that it be composed entirely of quantities which are known or wanted and that it be clearly defined. To restrict the definition may spoil the fun of authors and discussers. Indeed, the definition should not be restricted since the Nusselt number can be a generalized dimensionless heat-transfer rate which is related to the boundary conditions and finds many uses and definitions in many different types of problems.

Equation [10] of the text is not a definition of the Nusselt number but a consequence of the definition which is given in the sentence which follows the equation. In this case the Nusselt number is the average rate of heat transfer by conduction per unit area of interface (symbol q_{ai}) multiplied by a characteristic linear dimension (chosen as the drop diameter) and divided by the temperature difference across the transfer path and the thermal conductivity (chosen as the gas-phase thermal conductivity at the interface). Thus

$$N_{Nu} \equiv q_{ai}(2r_1)/(T_2 - T_1)k_1$$

Because of radial symmetry q_{ai} does not have to be found by integrating and averaging local values of the surface temperature gradients; and the defined dependent quantity can be represented in terms of the known independent quantities of Equation [10].

Another interesting way to look at the problem of heat transfer with mass transfer is from the standpoint of dimensional analysis. No longer can $h \equiv q_{ai}/(T_2 - T_1)$ be treated as a single quantity. q_{ai} and $(T_2 - T_1)$ are now independent of each other; and one new dimensionless group, N, must appear in the final correlation. A wide temperature variation in k also introduces a complication. Such a variation can be treated by another dimensionless group, e.g., the power on T in a $k - T$ correlation; but the experimental and theoretical problem becomes much more complicated, in most cases impossible of solution. The present paper tries to avoid the issue by employing an unspecified average conductivity. What this average should be, what its limits of use are, and whether its use is the most practical way of handling such problems are matters which must eventually be considered by those who would understand heat transfer.

---

[7] "The Combustion of Droplets of Heavy Liquid Fuels," by H. C. Hottel, G. C. Williams, and H. C. Simpson, presented at the Fifth Symposium on Combustion, Pittsburgh, Pa., September, 1954.

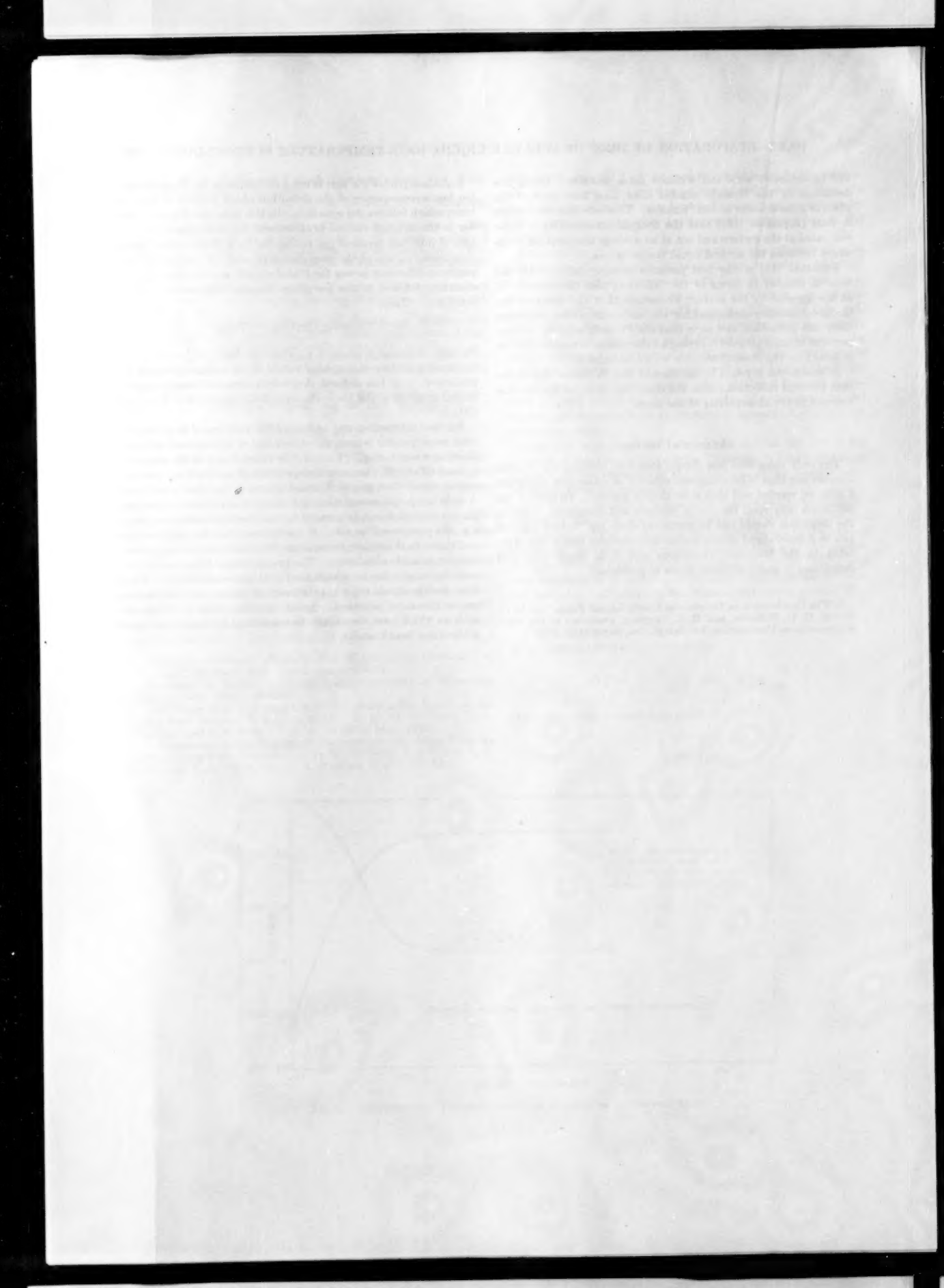

Turbulent Flow in the Entrance Region of a Pipe[1]

By DONALD ROSS,[2] WHIPPANY, N. J.

This paper presents an analytical solution for the turbulent boundary-layer flow in the entrance region of a pipe. The equations yield the relative momentum thickness at any station within ten diameters of the entrance, and from this the pressure drop and head loss are calculated. The ratio of these quantities to the corresponding values for fully developed pipe flow are found to be practically independent of Reynolds number. Comparison of the theoretical expressions with the few data that are available shows good agreement, confirming the formulas for design applications.

Introduction

THE solution of the problem of turbulent flow in the entrance region of a pipe is of special importance for the design of closed-jet working sections for wind and water tunnels, as well as for the design of tubular heat exchangers and hydraulic-pipe systems.

It is assumed that the fluid enters the pipe through a well-rounded entrance from a large reservoir and that a uniform velocity distribution occurs at the start of the pipe. Through the action of wall friction, a boundary layer is created at the wall, which gradually encroaches on the uniform stream as the flow proceeds down the pipe. As the total flux remains constant, the flow in the undisturbed central core must accelerate to compensate for this retardation of the flow near the wall. This change of the stream velocity causes a greater reduction of the static pressure than for the corresponding pipe flow. The wall friction is also greater than that for the fully developed pipe, giving a larger gradient of the energy head. There are many applications for which it is necessary to take into account these differences between the flow in the entrance region and that in a normal pipe. These differences are only appreciable while the boundary layer is quite thin, and the analysis in the present paper is limited to that portion of the entrance region about ten pipe diameters in length.

Fig. 1 illustrates the growth of the boundary layer and serves to define several of the pertinent quantities. In general, the boundary layer will be laminar up to the transition point and then become turbulent. As the present analysis is limited to turbulent boundary layers it is desirable that transition take place close to the entrance. For this the pipe Reynolds number should be greater than about 10^5. With this restriction, we may assume that the boundary layer acts as though it had been turbulent from the start, the effective point of zero thickness being at a distance x_0 from the start of the straight pipe. At high Reynolds numbers, or with gradual approaches, this distance may be negative.

The entrance-region problem has been solved for laminar boundary layers by Schiller (1),[3] following a method of analysis suggested by Prandtl that involved writing the relation between the change in momentum, the pressure drop, and the friction force acting on an element of a boundary layer. A later, more exact analysis was made by Langhaar (2) starting from the Navier-Stokes equations. An approximate analysis of the flow with a turbulent boundary layer was first made by Latzko (3) using the one seventh-power velocity-distribution law. A similar analysis for closed-jet wind tunnels was later given by Glauert (4). The one seventh-power law is only valid over a limited Reynolds-number range, so that Latzko's and Glauert's analyses are not reliable for large flows.

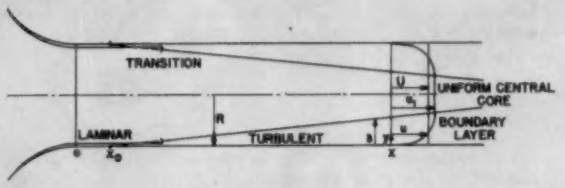

Fig. 1 Growth of Turbulent Boundary Layer in Entrance Region of Pipe

In the analysis that follows, the continuity, momentum, and energy equations for a pipe are combined to yield expressions for the growth of the boundary layer and for the pressure and energy gradients. These approximate expressions are in a simple form made possible by the assumption that the boundary layer is turbulent. Integration of these equations requires an analytical expression for the wall-shear-stress coefficient, which is found in terms of the momentum-thickness Reynolds number from published data on flat plates and pipes. Similar data are used to establish a curve for the shape parameter also as a function of the momentum-thickness Reynolds number.

In the section on experimental confirmation, the theoretical results are compared with data from two model water-tunnel studies and with the high Reynolds-number data obtained recently in the working section of the 48-in. water tunnel at The Pennsylvania State College.

Theoretical Relations

In analyzing boundary-layer flow in axisymmetric conduits, the appropriate definition of the displacement thickness is

$$\delta^* = \int_0^R \left(1 - \frac{u}{u_i}\right)\left(1 - \frac{y}{R}\right) dy \quad [1]$$

and that of the momentum thickness is

[1] Work done at the Ordnance Research Laboratory under Navy Contract NOrd 7958, in connection with the working section flow studies for the 48-in. water tunnel at The Pennsylvania State College. Reported in detail in O.R.L. Report NOrd 7958-283, "Flow in Closed-Jet Working Sections."

[2] Bell Telephone Laboratories, Inc.

Contributed by the Hydraulic Division and presented at the Annual Meeting, New York, N. Y., November 28–December 3, 1954, of The American Society of Mechanical Engineers.

Note: Statements and opinions advanced in papers are to be understood as individual expressions of their authors and not those of the Society. Manuscript received at ASME Headquarters, March 25, 1954. Paper No. 54—A-89.

[3] Numbers in parentheses refer to the Bibliography at the end of the paper.

$$\theta = \int_0^R \left(1 - \frac{u}{u_1}\right) \frac{u}{u_1} \left(1 - \frac{y}{R}\right) dy \quad [2]$$

where u, u_1, R, and y are defined in Fig. 1. These three-dimensional definitions reduce to the usual two-dimensional values when the boundary layer is thin relative to the pipe radius. In terms of these definitions, the continuity equation may be expressed

$$\frac{d}{dx}(u_1 R^2 - 2u_1 R\delta^*) = 0 \quad [3]$$

and the integral momentum equation is

$$\frac{1}{R}\frac{d(R\theta)}{dx} = \frac{c_f}{2} - \frac{(2\theta + \delta^*)}{u_1}\frac{du_1}{dx} \quad [4]$$

where c_f is the wall-shear-stress coefficient. This equation is valid provided only that there exist a uniform central core in which the shear stress is zero. In this central core, the Bernoulli head is constant along each streamline, and the static pressure gradient is related to the velocity gradient by

$$\frac{1}{\rho u_1^2}\frac{dp}{dx} = -\frac{1}{u_1}\frac{du_1}{dx} \quad [5]$$

These equations for conduit flows are derived in detail in reference (5).

In a straight pipe the radius is constant and the momentum equation becomes formally identical to that for a two-dimensional boundary layer

$$\frac{d\theta}{dx} = \frac{c_f}{2} - (2 + H)\frac{\theta}{u_1}\frac{du_1}{dx} \quad [6]$$

where H is the shape parameter, defined as the ratio of the displacement to the momentum thickness. The continuity relation for a straight pipe may be written

$$\frac{R}{u_1}\frac{du_1}{dx} = \frac{2\left(H\frac{d\theta}{dx} + \theta\frac{dH}{dx}\right)}{\left(1 - 2H\frac{\theta}{R}\right)} \quad [7]$$

where the denominator is the ratio of the average velocity to the maximum core value. If this expression for the velocity gradient is substituted in Equation [6] there results a general differential equation for the growth of the momentum thickness as a function of the wall-shear-stress coefficient, the shape parameter, and its derivative.

The usefulness of the general equation is limited by its dependence on the derivative of the shape parameter, which stems from Equation [7]. When the problem is restricted to turbulent flows, this term, significant in the analysis of laminar flows, becomes negligible. Neglecting higher powers of (θ/r), the resultant approximate equation for the growth of the momentum thickness is

$$\frac{d\theta}{dx} \cong \frac{\frac{c_f}{2}}{1 + (2 + H)\left(2H\frac{\theta}{R}\right)} \quad [8]$$

This equation is accurate to about one to two per cent in the first ten diameters of the entrance region. It shows that the rate of growth of the momentum thickness for very thin boundary layers is the same as that for a flat plate at the same local Reynolds number. As the boundary layer grows, the rate decreases, becoming less than that of the corresponding flat plate and approaching the zero value that it must have for fully developed pipe flow. If one were to analyze the entrance region by assuming that the pressure gradient does not affect the growth of the boundary layer, then an exaggerated rate of growth would be predicted.

By a similar analysis, a simple equation for the pressure gradient can be derived which is accurate for turbulent flows

$$\frac{R}{\frac{1}{2}\rho U^2}\frac{dp}{dx} \cong -2H c_f \quad [9]$$

This equation shows that the pressure gradient is relatively high in the entrance region only because H and c_f are higher at the low Reynolds numbers that prevail there.

The loss of energy head h is given simply by the rate at which work is done on the fluid by the wall-friction forces

$$\frac{R}{\frac{1}{2}\rho U^2}\frac{dh}{dx} = \frac{-2\tau_w}{\frac{1}{2}\rho U^2} = \frac{-2c_f}{\left(1 - 2H\frac{\theta}{R}\right)^2} \quad [10]$$

where τ_w is the wall shear stress. This may be expressed in terms of the loss of specific energy head per unit change in the momentum thickness. The resultant equation is

$$\frac{R}{\frac{1}{2}\rho U^2}\frac{dh}{d\theta} = \frac{-2c_f}{\left(1 - 2H\frac{\theta}{R}\right)^2}\left(\frac{d\theta}{dx}\right)^{-1} \cong -4\left[1 + (4 + H)2H\frac{\theta}{R}\right] \quad [11]$$

where the approximate expression is, of course, restricted to turbulent flows. When this equation is used for the head loss, Equation [8] for the momentum thickness must be solved simultaneously.

Empirical Relations

To integrate the various differential equations derived in the preceding section, relations are needed for the wall-shear-stress coefficient and the shape parameter as functions of the momentum-thickness Reynolds number. These relations should be valid in the region where the boundary layer is an appreciable fraction of the radius, as well as in the region where it is very thin. In a recent analysis of pipe flow, Ross (6) has shown that both c_f and H are practically unique functions of R_θ for plate and pipe flows, provided only that the proper three-dimensional momentum thickness, Equation [2], is used in calculating the Reynolds number. As the slight negative pressure gradient in the entrance region has only a small influence on the shape of the velocity profile, it seems reasonable to assume that these universal pipe and plate relations may be used to analyze the flow in the entrance region of a pipe.

The relation for the wall-shear-stress coefficient, which differs only slightly from that of Squire and Young (7), may be written

$$c_f = (4.4 + 3.8 \log_{10} R_\theta)^{-2} \quad [12]$$

This equation has been developed directly from Nikuradse's (8) data for smooth pipes. It is shown in Fig. 2.

Experimental data for pipe and flat-plate flows yield a single curve for the shape parameter H as a function of R_θ (Fig. 3). A formula that fits these data reasonably well is

$$H = 1 + \frac{1}{1.05 \log_{10} R_\theta - 1.0} \quad [13]$$

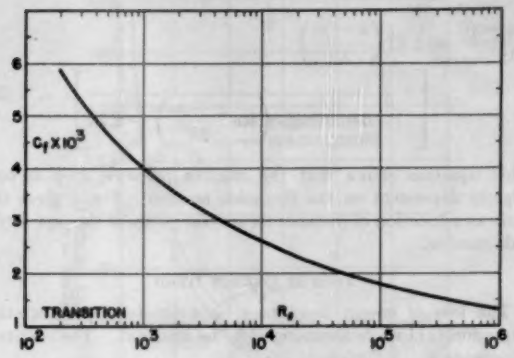

FIG. 2 WALL-SHEAR-STRESS COEFFICIENT AS FUNCTION OF MOMENTUM-THICKNESS REYNOLDS NUMBER

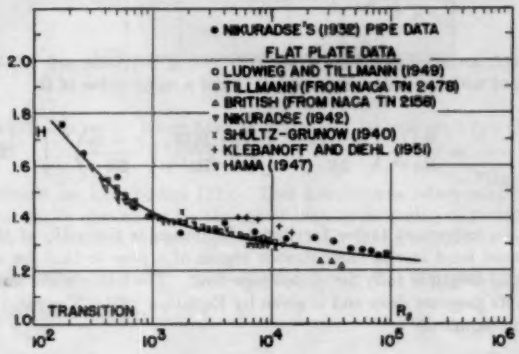

FIG. 3 EXPERIMENTAL VALUES OF FLAT-PLATE SHAPE PARAMETER H, AS FUNCTION OF MOMENTUM-THICKNESS REYNOLDS NUMBER

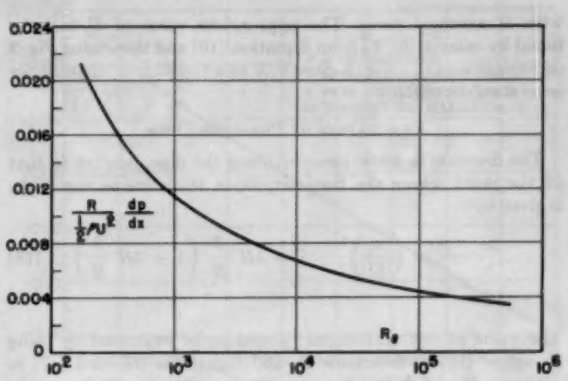

FIG. 4 PRESSURE GRADIENT AS FUNCTION OF MOMENTUM-THICKNESS REYNOLDS NUMBER

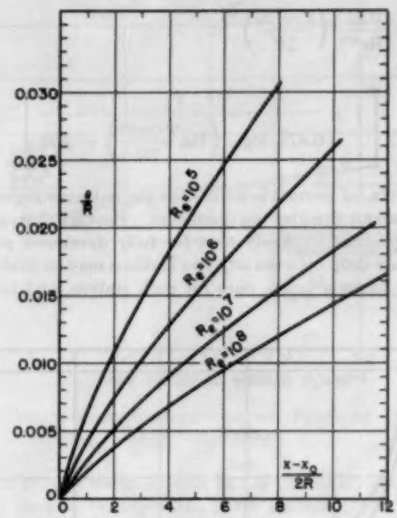

FIG. 5 θ/R AS FUNCTION OF DISTANCE FOR SEVERAL VALUES OF REYNOLDS NUMBER

As this formula is based on more data, it should be more reliable than the equation for H as a function of R_θ that was proposed previously by Tetervin and Lin (9).

Equation [9] for the pressure gradient is also a function of the momentum-thickness Reynolds number. The curves of Figs. 2 and 3 may be used to derive the relation for the pressure gradient shown in Fig. 4.

INTEGRATION OF EQUATION FOR MOMENTUM THICKNESS

Approximate integration of the momentum equation to determine the momentum thickness as a function of distance is made possible by using Equation [12] for the wall-shear-stress coefficient and assuming H to be approximately constant. Discarding certain terms that are negligible, the result of the integration is

$$\frac{\theta}{R} \cong \frac{c_f}{2}\left(\frac{x-x_0}{R}\right)\left(\frac{1-[2+H]H\,\frac{\theta}{R}}{1-3\sqrt{c_f}}\right) \quad \ldots\ldots [14]$$

where x_0 is the effective start of the turbulent boundary layer, as indicated in Fig. 1, and c_f and H are evaluated at the point being calculated. Both c_f and H are functions of the momentum-thickness Reynolds number R_θ, while what is really needed is an expression for the momentum thickness in terms of the pipe Reynolds number Re and the distance from the effective start of the turbulent boundary layer.

An approximate formula for the momentum thickness may be derived empirically by plotting the terms involving c_f in Equation [14] as a function of the momentum-thickness Reynolds number. The approximate expression which fits this curve closely is

$$\frac{\frac{c_f}{2}}{1-3\sqrt{c_f}} \approx 0.010\ R_\theta^{-\frac{1}{5}} \quad \ldots\ldots\ldots [15]$$

The momentum-thickness Reynolds number then follows as a function of the pipe Reynolds number

$$R_\theta \equiv \frac{\theta u_1}{\nu} = \frac{1}{2}\left(\frac{u_1}{U}\right)\left(\frac{\theta}{R}\right)\mathrm{Re} \approx 0.215\left(\mathrm{Re}\,\frac{x-x_0}{2R}\right)^{\frac{5}{6}} \quad [16]$$

and finally, the momentum thickness itself is given by

$$\frac{\theta}{R} \approx \frac{0.043}{\mathrm{Re}^{1/4}}\left(\frac{x-x_0}{2R}\right)^{\frac{5}{6}}\left(1-[2+H]H\,\frac{\theta}{R}\right) \quad \ldots [17]$$

This expression is sufficiently accurate for most entrance-region calculations provided one iteration is made. The value of θ/R to be used in the correction term is found by first using the equation

with H assumed zero. The appropriate value of H may be found by calculating R_θ from Equation [16] and then using Fig. 3 or Equation [13]. Fig. 5 gives θ/R as a function of distance for several values of Re.

Evaluation of Pressure Drop

The decrease in static pressure along the pipe, relative to that at the point where the boundary-layer thickness is negligible, is given by

$$\frac{p_0 - p}{\frac{1}{2}\rho U^2} = \left(\frac{u_1}{U}\right)^2 - 1 \approx 4H\frac{\theta}{R}\left(1 + 3H\frac{\theta}{R}\right) \quad [18]$$

The value at any station may therefore be evaluated by using Equation [16] to determine R_θ and Equations [13] and [17] to evaluate H and θ/R. An approximate relation which may be used for most engineering purposes is

$$\frac{p_0 - p}{\frac{1}{2}\rho U^2} \approx \frac{0.17}{\mathrm{Re}^{1/6}}\left(\frac{x - x_0}{2R}\right)^{\frac{5}{6}} \left[1 + \frac{1}{0.875\ \log_{10}\left(\mathrm{Re}\frac{x - x_0}{2R}\right) - 2.75}\right] \quad [19]$$

This formula, of course, is limited to the entrance region of the pipe, i.e., about the first ten diameters. Beyond that point the pressure gradient is closely that for fully developed pipe flow. The pressure drop between any two stations may be evaluated by using this formula twice, once for each station, and taking the difference.

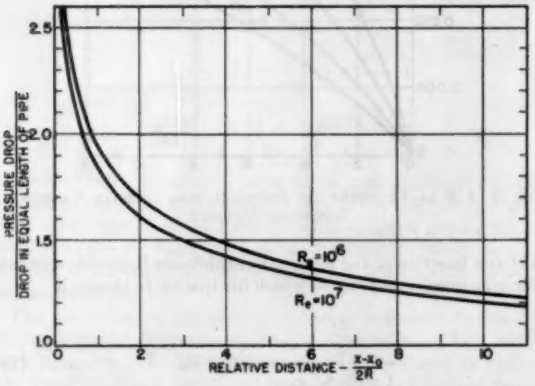

Fig. 6 Ratio of Pressure Drop in Entrance Region to That for Equivalent Length of Fully Developed Pipe Flow

An interesting way of expressing this quantity is in relation to the pressure drop in an equivalent length of pipe having fully developed turbulent flow. For the Reynolds-number range of 10^5 to 10^8, which covers the entire practical application, the pressure drop in a smooth pipe is given closely by the interpolation formula

$$\left(\frac{\Delta p}{\frac{1}{2}\rho U^2}\right)_{\text{pipe}} \cong \frac{0.120}{\mathrm{Re}^{1/4}}\left(\frac{x - x_0}{2R}\right) \quad [20]$$

Dividing Equation [19] by Equation [20] yields

$$\frac{p_0 - p}{(\Delta p)_{\text{pipe}}} \approx 1.42\left(\frac{x - x_0}{2R}\right)^{-\frac{1}{6}} \left[1 + \frac{1}{0.875\ \log_{10}\left(\mathrm{Re}\frac{x - x_0}{2R}\right) - 2.75}\right] \quad [21]$$

This equation shows that the relative pressure drop is only slightly dependent on the Reynolds number. Fig. 6 gives this ratio as a function of distance for several values of the pipe Reynolds number.

Loss of Energy Head

The loss of energy head may be evaluated by integrating Equation [11] while assuming H to be constant. The resultant expression is

$$\frac{h_0 - h}{\frac{1}{2}\rho U^2} \approx 4\frac{\theta}{R}\left[1 + (4H + H^2)\frac{\theta}{R}\right] \quad [22]$$

Here, an adequate answer for engineering purposes can be derived with the aid of Equation [17] and a mean value of H

$$\frac{h_0 - h}{\frac{1}{2}\rho U^2} \approx \frac{0.17}{\mathrm{Re}^{1/6}}\left(\frac{x - x_0}{2R}\right)^{\frac{5}{6}}\left[1 + \frac{0.12}{\mathrm{Re}^{1/6}}\left(\frac{x - x_0}{2R}\right)^{\frac{5}{6}}\right] \quad [23]$$

An important factor for hydraulic design is the ratio of the actual head loss in the entrance region of a pipe to that for an equal length of fully developed pipe flow. The latter is the same as its pressure drop and is given by Equation [20]. The ratio is approximately

$$\frac{h_0 - h}{(\Delta h)_{\text{pipe}}} \approx 1.42\frac{1 + \frac{0.12}{\mathrm{Re}^{1/6}}\left(\frac{x - x_0}{2R}\right)^{\frac{5}{6}}}{\left(\frac{x - x_0}{2R}\right)^{\frac{1}{6}}} \quad [24]$$

In a recent investigation of this subject, using laborious step-by-step solutions, Holdhusen (10) found the head-loss ratio to be practically independent of the pipe Reynolds number. The explanation for this constancy is found in the fact that the pipe Reynolds number has only a small influence in the numerator of Equation [24]. Fig. 7 shows this ratio as a function of distance for several pipe Reynolds numbers. The formula is only accurate for lengths up to about six diameters; but, as Holdhusen (10) has found, the region in which the head-loss gradient is greater than in fully developed pipe flow is less than this length. The calculations show a small, consistent trend with Reynolds number, which Holdhusen was unable to distinguish. His average curve is also shown in Fig. 7 and is seen to be in good agreement with the present calculations. Both analyses agree that, after the first few diameters, the total head loss is given approximately by that of fully developed pipe flow with an additional "entrance-length" of 0.7 diameter.

Elimination of the Pressure Gradient

Before comparing the equations developed in the previous sections with experimental data, we may digress here to consider the practical problem of elimination of the pressure gradient by the use of a slightly diverging pipe. The pressure gradient in a closed-jet working section of a wind or water tunnel causes a buoyancy effect which makes drag measurements rather

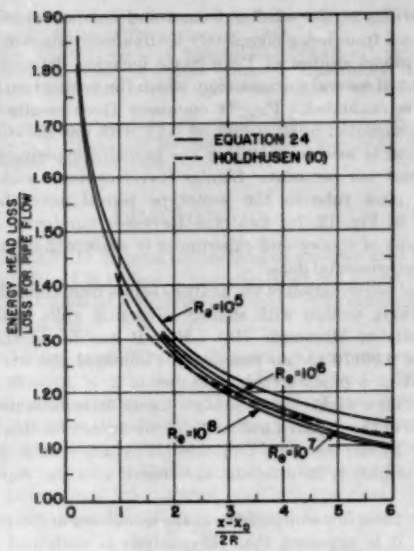

FIG. 7 RATIO OF HEAD LOSS IN ENTRANCE REGION TO THAT FOR FULLY DEVELOPED PIPE

difficult on long bodies (11). This interference effect may be practically eliminated by the use of slightly diverging walls (12). For this analysis, we use Equations [3] and [4] for continuity and momentum but set $\frac{du_1}{dx} = 0$ instead of $\frac{dR}{dx} = 0$. The continuity equation then gives

$$\frac{dR}{dx} = \frac{H\frac{d\theta}{dx} + \theta\frac{dH}{dx}}{\left(1 - H\frac{\theta}{R}\right)} \quad \ldots\ldots\ldots\ldots [25]$$

while the momentum equation becomes

$$\frac{d\theta}{dx} + \frac{\theta}{R}\frac{dR}{dx} = \frac{c_f}{2} \quad \ldots\ldots\ldots\ldots [26]$$

Eliminating $(d\theta)/(dx)$ between these two equations gives for the required half-angle simply

$$\alpha_0 = \left(\frac{dR}{dx}\right)_{\frac{dp}{dx}=0} = H\frac{c_f}{2} + \theta\frac{dH}{dx} \quad \ldots\ldots [27]$$

which is valid for laminar or turbulent flows. For turbulent flows, the second term is usually negligible, and it is seen that the pressure gradient can be strictly eliminated for only a single value of the Reynolds number. The required half angle will usually be of the order of 0.002 radian, or about 0.1 deg. In radians, it is equal to one fourth of the pressure gradient that would exist for a straight pipe at the same local Reynolds number.

COMPARISON WITH EXPERIMENTAL DATA

Very few accurate experimental data are available on turbulent flow in the entrance region of a pipe. Measurements reported by Shapiro and Smith (13) tend to confirm the trends of the analytic formulas, but the scatter of the data is too great to define clearly any regions of agreement or disagreement. Measurements have been made in connection with model studies for

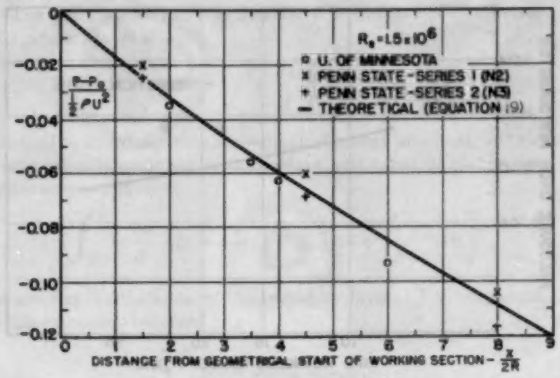

FIG. 8 PRESSURE DROP FOR MODEL WATER-TUNNEL WORKING SECTIONS

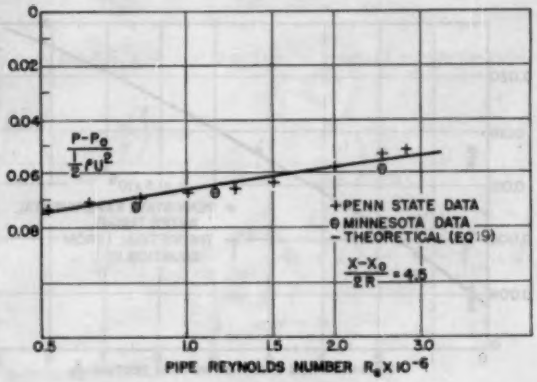

FIG. 9 VARIATION OF WORKING-SECTION PRESSURE DROP WITH REYNOLDS NUMBER

the design of large water tunnels, at the University of Minnesota (14) and at The Pennsylvania State College (15). Recently, measurements also have been made in the test section of the 48-in. water tunnel at Penn State. These water-tunnel data are the best available for confirmation of the analysis.

The Minnesota and Penn State model studies covered the same range of Reynolds numbers and so may be treated together. Fig. 8 shows the theoretical and measured wall-pressure distributions at a single Reynolds number; while Fig. 9 compares the data at a single station with theory, the Reynolds number being variable. In both cases the agreement between the calculated and experimental values is within the scatter of the data. The major difficulty in making the comparison is the choice of the effective start of the turbulent boundary layer. In computing the theoretical curve it was assumed that this occurred $^3/_4$ diameter upstream of the start of the straight section, a value based on boundary-layer measurements. Although this may not be the same for both tunnels the choice of x_0 does not affect the pressure curve seriously and the comparison is valid.

Tests at higher Reynolds numbers in the working section of the 48-in. water tunnel are compared with theoretical values in Fig. 10. In this case, it is the average gradients which are compared, as the data did not disclose any variation of the slope with distance. The experimental values are seen to be about ten per cent too high; but this may not be a discrepancy in the theory as it is more likely that the difference is attributable to

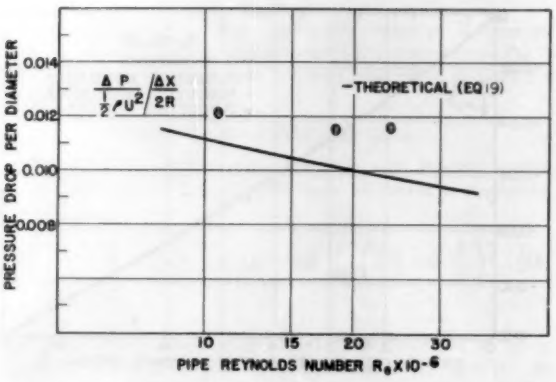

FIG. 10 PRESSURE GRADIENT IN WORKING SECTION OF 48-IN. WATER TUNNEL

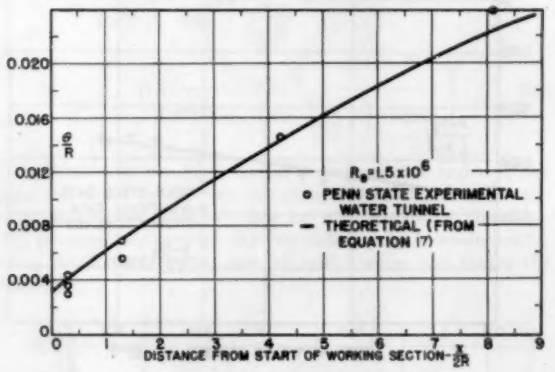

FIG. 11 COMPARISON OF THEORY AND EXPERIMENT FOR GROWTH OF BOUNDARY-LAYER MOMENTUM THICKNESS

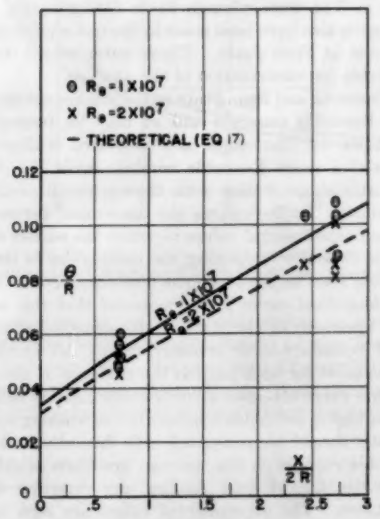

FIG. 12 MOMENTUM THICKNESS IN WORKING SECTION OF 48-IN. WATER TUNNEL

irregularities at the window frames and hatches which prevent the tunnel from being completely hydraulically smooth.

The model studies at Penn State included detailed velocity traverses at several stations, from which the momentum thickness could be evaluated. Fig. 11 compares these results with the values calculated using Equation [17], with one iteration. The agreement is seen to be within the probable experimental error of at least ten per cent. Similar traverses made with a hypodermic pitot tube in the prototype tunnel gave the results plotted in Fig. 12, for two pipe Reynolds numbers. Here the agreement of theory and experiment is again within the scatter of the experimental data.

A final confirmation of the analysis comes from tests of a closed-jet working section with slightly diverging walls made at the University of Minnesota (16). Here it was found that a half angle of 0.00170 radian practically eliminated the wall-pressure gradient at a pipe Reynolds number of 2×10^6. It was estimated that a slightly greater angle should have been used. Calculation of the required half angle of divergence for this Reynolds number by the complete Equation [27] yields a value of 0.00178 radian, which is in excellent agreement with the experimental results.

From these few comparisons of the calculated and experimental results, it is apparent that the analysis is confirmed and that the various approximations are justified. The formulas which have been given may all be used with confidence for design and analysis purposes.

BIBLIOGRAPHY

1 "Investigations of Laminar and Turbulent Flow," by L. Schiller, *Forschungsarbeiten Verein deutscher Ingenieure*, 1922, p. 248; also, *Zeitschrift für angewandte Mathematik und Mechanik*, vol. 2, 1922, p. 96.

2 "Steady Flow in the Transition Length of a Straight Tube," by H. L. Langhaar, *Journal of Applied Mechanics*, Trans. ASME, vol. 64, 1942, p. A-55.

3 "Heat Transmission to a Turbulent Flow of Liquid or Gas," by H. Latzko, Abhandlungen aus dem Aerodynamischen Institut an der Technischen Hochschule Aachen vol 1, 1921—translated in National Advisory Committee for Aeronautics Technical Memorandum 1068, 1944.

4 "A Theoretical Estimate of the Pressure Gradient in a Wind Tunnel," by H. Glauert, Aeronautical Research Council R & M 1159, 1928.

5 "Equations of Motion for Three-Dimensional Boundary Layer Flow," by Frank Lane, Donald Ross, and J. M. Robertson, Ordnance Research Laboratory, Report NOrd 7958-154, September, 1949.

6 "A New Analysis of Nikuradse's Experiments on Turbulent Flow in Smooth Pipes," by Donald Ross, Proceedings of the Third Midwestern Conference on Fluid Mechanics, 1953, pp. 651–667.

7 "The Calculation of the Profile Drag of Air Foils," by H. B. Squire and A. D. Young, British Aeronautical Research Council R & M 1838, 1938.

8 "Gesetzmässigkeiten der turbulenten Strömung in glatten Rohren," by J. Nikuradse, *Forschungsheft Verein deutscher Ingenieure*, 1932, p. 356.

9 "A General Integral Form of the Boundary Layer Equation," by N. Tetervin and C. C. Lin, National Advisory Committee for Aeronautics Technical Note 2158, 1950.

10 "The Turbulent Boundary Layer in the Inlet Region of Smooth Pipes," by J. S. Holdhusen, PhD thesis, University of Minnesota, February, 1952.

11 "The Effect of the Static Pressure Gradient on the Drag of a Body Tested in a Wind Tunnel," by H. Glauert, Aeronautical Research Council R & M 1158, 1928.

12 "Elimination of the Static Pressure Gradient Along Wind Tunnels of the N.P.L. Type," by L. F. G. Simmons and E. Ower, Aeronautical Research Council R & M 873, 1923.

13 "Friction Coefficients in the Inlet Length of Smooth Round Tubes," by A. H. Shapiro and R. D. Smith, National Advisory Committee for Aeronautics Technical Note 1785, 1948.

14 "Model Experiments for the Design of a Sixty-Inch Water Tunnel, Part III—Test Section and Cavitation Index Studies," by

J. S. Holdhusen, University of Minnesota, Project Report 12, Bureau of Ships Contract NObs-34208, September, 1948.

15 "Water Tunnel Working Section Flow Studies," by J. M. Robertson and D. Ross, Ordnance Research Laboratory, Report NOrd 7958-97, June, 1948. (The theoretical section of this report is obsolete.)

16 "A Diverging Closed-Jet Test Section for a Water Tunnel," by R. M. Olson, University of Minnesota, Project Report 32, Bureau of Ships Contract N600s-s-11459, June, 1952.

Discussion

N. TETERVIN.[4] In general the method of analysis used in the paper is sound. It is believed, however, that the paper can be improved by changes at a number of points. The detailed comments are as follows:

1 It is stated that "at high Reynolds numbers, or with gradual approaches the distance x_0 may be negative." The distance x_0 will be negative only when the turbulent boundary layer at a point is thicker than it would be for a boundary layer that is turbulent from the beginning of the flow. This can result if the surface is rough or if the laminar boundary layer has separated in passing from the entrance cone into the pipe.

2 To obtain Equation [8], it is assumed that

$$\frac{2(H+2)\left(\theta\frac{dH}{dx}\right)\frac{\theta}{R}}{c_f/2}$$

is negligible. While this assumption is probably true in general, it may not be true in the region where the boundary layer changes from laminar to turbulent. In this region $\theta(dH/dx)$ can become large. The statement that the equation is accurate to 1 or 2 per cent should be moved to the section of the paper in which theory is compared with experiment.

3 It is believed that the quantity U in Equations [9], [10], [11] should be U_1.

4 The statement that the loss of energy head is equa' to the rate at which work is done on the fluid by the wall-friction forces is only an approximation. The wall-friction forces do no work on the fluid because the wall does not move. The correct expression for the loss of head is obtained by multiplying the equation of motion in cylindrical co-ordinates

$$u\frac{\partial u}{\partial x}+v\frac{\partial u}{\partial r}=-\frac{1}{\rho}\frac{dp}{dx}+\frac{\nu}{r}\frac{\partial}{\partial r}\left(r\frac{\partial u}{\partial r}\right)$$

by ru and integrating from $r=0$ to $r=R$ and using the equation of continuity

$$r\frac{\partial u}{\partial x}+\frac{\partial rv}{\partial r}=0$$

where v is velocity along r
ν is kinematic viscosity
r is measured from center of pipe

(The other symbols are the same as in the paper.)
The result is

$$\frac{d\int_0^R\left(p+\frac{\rho u^2}{2}\right)urdr}{dx}=-\mu\int_0^R\left(\frac{\partial u}{\partial r}\right)^2rdr=\int_0^{\delta R}\tau\frac{\partial u}{\partial r}rdr$$

where τ is shear stress, μ is viscosity, and $\tau=-\mu(\partial u/\partial r)$.

[4] Langley Aeronautical Laboratory, Langley Field, Va.

The result states that the derivative of the rate of flow across the pipe of the total head

$$\left(p+\frac{\rho u^2}{2}\right)$$

is equal to the dissipation of mechanical energy into heat. If the assumption is made that τ is constant and equal to the surface shear stress τ_0, then

$$\int_0^R\tau\frac{\partial u}{\partial r}rdr=-\tau_0\left[U(R-\delta)+\int_{R-\delta}^R udr\right]$$

where δ is the thickness of the boundary layer. For very small δ this expression becomes

$$\int_0^R\tau\frac{\partial u}{\partial r}rdr=-\tau_0UR$$

or

$$\frac{d\int_0^R\left(p+\frac{\rho u^2}{2}\right)urdr}{dx}=-\tau_0UR$$

For very small δ, $p+\rho u^2/2$ is close to constant across the pipe, then

$$\frac{d\int_0^R\left(p+\rho\frac{u^2}{2}\right)urdr}{dx}=\frac{d}{dx}\left(p+\rho\frac{u^2}{2}\right)\int_0^R urdr$$

$$=\left(p+\frac{\rho u^2}{2}\right)\frac{d}{dx}\int_0^R urdr+d\frac{\left(p+\frac{\rho u^2}{2}\right)}{dx}\int_0^R urdr$$

but

$$\frac{d}{dx}\int_0^R urdr=0$$

by continuity. Thus

$$\frac{d\left(p+\frac{\rho u^2}{2}\right)\int_0^R urdr}{dx}=-\tau_0UR$$

Now, putting $\int_0^R urdr=\frac{UR^2}{2}$ for $u\approx U$

$$\frac{UR^2}{2}\frac{d\left(p+\frac{\rho U^2}{2}\right)}{dx}=-\tau_0UR$$

or

$$Rd\frac{\left(p+\frac{\rho U^2}{2}\right)}{dx}=-2\tau_0$$

This expression is Equation [10]. It thus appears that Equation [10] is based on an assumption that is true only for very small boundary-layer thicknesses.

If the "head" is to be based on average quantities, when δ is not very small, it appears that the equation of continuity and the momentum equation can be used to find the static pressure p and the average velocity across a section and the "total head" then calculated.

5 The shape parameter H should be determined only by the velocity distribution across the boundary layer. If, however, Equations [1] and [2] are used to calculate H the factor $(1-y/R)$ will make H depend on the ratio of the boundary-layer thickness to the pipe radius as well as on the velocity distribution. Thus

H cannot really be a shape parameter if δ^* and θ are calculated from Equations [1] and [2].

6 Referring to Equation [17], it is believed that an equation for θ/R can be obtained directly from Equation [6], and the assumptions that H is constant and that

$$\frac{c_f}{2} = \frac{k}{R_\theta^n}$$

where n and k can be chosen to fit any friction curve over part of the range of R_θ. Such an equation requires no iteration to get θ/R and does not need to neglect powers of θ/R to obtain Equation [8]. The development is as follows

$$\frac{d\theta}{dx} = \frac{c_f}{2} - \frac{\theta}{R}\left(\frac{R}{U_1}\frac{dU_1}{dx}\right)(H+2) \quad \text{momentum equation}$$

$$\frac{R}{U_1}\frac{dU_1}{dx} = \frac{2\left(H\frac{d\theta}{dx} + \theta\frac{dH}{dx}\right)}{1 - 2H\frac{\theta}{R}} \quad \text{from continuity}$$

$$\frac{c_f}{2} = \frac{k}{R_\theta^n} = \frac{k\nu^n}{U_1^n\theta^n} \quad \text{(assumed that } c_f \text{ can be based on } \theta \text{ from Equation [2]}$$

Then

$$\frac{d\theta}{dx} = \frac{k\nu^n}{U_1^n\theta^n} - \frac{\theta}{R}(H+2)\frac{2\left(H\frac{d\theta}{dx} + \theta\frac{dH}{dx}\right)}{1 - 2H\frac{\theta}{R}}$$

Now

$$\int_0^R urdr = -U_1R\,\delta^* + \frac{U_1R^2}{2} = K_\theta \quad \text{definition of } K_\theta$$

Then

$$U_1 = \frac{2K_\theta}{R^2\left(1 - 2H\frac{\theta}{R}\right)}$$

Then

$$\frac{d\theta}{dx}\left[1 + \frac{\theta}{R}(H+2)\frac{2H}{1 - 2H\frac{\theta}{R}}\right] = \frac{k\nu^nR^{2n}\left(1 - 2H\frac{\theta}{R}\right)^n}{\theta^n(2K_\theta)^n} - \frac{\theta}{R}(H+2)\frac{\theta\frac{dH}{dx}}{1 - 2H\frac{R}{\theta}}$$

Now if $\frac{dH}{dx} = 0$

$$\frac{\left[1 + \frac{\theta}{R}(H+2)\frac{2H}{1 - 2H\frac{\theta}{R}}\right]\theta^n}{\left(1 - 2H\frac{\theta}{R}\right)^n}d\theta = \frac{k\nu^nR^{2n}}{(2k_\theta)^n}dx$$

or

$$\int_{\frac{\theta_0}{R}}^{\frac{\theta}{R}}\left[\frac{\frac{\theta}{R}}{1 - 2H\frac{\theta}{R}}\right]^n\left[1 + \frac{\theta}{R}(H+2)\frac{2H}{1 - 2H\frac{\theta}{R}}\right]d\frac{\theta}{R} = k\left(\frac{\nu R}{2K_\theta}\right)^n\left(\frac{X}{R} - \frac{X_0}{R}\right)$$

This equation gives X/R as a function of θ/R or what is the same thing, θ/R as a function of x/R.

7 It is not clear why it is necessary to use the approximate equation (Equation [18]) rather than the exact equation

$$\frac{p_0 - p}{\rho/2U_0^2} = \frac{1}{\left(1 - 2H\frac{\theta}{R}\right)^2} - 1$$

8 It is believed that a nomenclature containing all the symbols and their definitions would make the paper easier to read.

Author's Closure

In writing this closure the author wishes first to comment on Mr. Tetervin's discussion and then to show that the present analysis is not restricted to turbulent flows, as stated in the paper. Mr. Tetervin's detailed comments are numbered and may be answered similarly:

1 When a straight pipe is preceded by a gradual approach section, the boundary layer may develop before the start of the straight section. In this case, x_0 as defined by Fig. 1 will be negative.

2 In making his statements concerning the relative magnitude of terms involving the gradient of H, the author was quite conscious of the changes occurring near transition. The transition region is not important as long as transition takes place within a few pipe diameters of the entrance, as assumed throughout the paper.

3 The quantity U in Equations [9], [10], and [11] is the flow-average velocity, as correctly implied in the paper.

4 The author believes that the calculation of hydraulic head loss in the paper is more nearly correct than the approximate analysis given by the discusser.

5 The definition of the quantity H as the ratio of the appropriate displacement thickness to the momentum thickness has made possible the correlation of flat-plate and pipe boundary-layer data. It would seem that this should far outweigh the disadvantage that H is not uniquely related to the shape of the velocity distribution. As no unique relation exists between H and the velocity profiles even for flat plates, the concept of H as a "shape parameter" has only limited value in any case.

6 The analysis given by Mr. Tetervin leaves the engineer with an integral to evaluate in terms of two coefficients that vary with Reynolds number. The analysis presented in the paper gives him algebraic equations requiring merely simple computations.

7 The calculation using the exact equation would be no more accurate as the quantities in it are approximations.

8 Most of the nomenclature is explained by Fig. 1 and the first two equations.

The author was chagrined to find that through his concentration on turbulent flows he failed to appreciate the possible application of the present analysis to laminar flows. Through a simple error he had incorrectly estimated the importance of the gradient of H for the laminar case. It is actually as unimportant for this case as for the turbulent one. The entire first section of the paper is thus equally applicable to laminar and turbulent flows.

In the section on empirical relations, equations for c_f and H were found that are valid both for flat plates and fully developed pipe flow. In laminar flows the corresponding step is to note that

$$c_fH^2 = 3R_\theta^{-1}$$

for both plates and pipes. As $H = 2.6$ for a plate and 3.0 for a

pipe, the assumption that $H \approx 2.7$ should give excellent results for the entrance region of a pipe. In terms of the dimensionless distance

$$\sigma \equiv \frac{x}{2R} \mathrm{Re}^{-1} = \mathrm{Re}_x \mathrm{Re}^{-2}$$

the solution for the momentum thickness is

$$\frac{\theta}{R} \approx \frac{1.28\sqrt{\sigma}}{1 + 11\sqrt{\sigma}}$$

while that for the pressure drop is simply

$$\frac{p_0 - p}{\frac{1}{2}\rho U^2} \approx 13.85\sqrt{\sigma}$$

These equations are valid only so long as an essentially lossless central core exists, but otherwise they are unrestricted.

In a recent paper on laminar entry flows,[1] Shapiro and his co-workers have shown experimentally that

$$\frac{p_0 - p}{\frac{1}{2}\rho U^2} = 13.74\sqrt{\sigma}$$

which is within 1 per cent of the value calculated here. This result applies only for $\sigma < 5 \times 10^{-2}$, indicating that the assumption of a lossless central core may not be valid for thicker boundary layers. The present simple calculation agrees better with the experimental coefficient than do those of four of the five calculations that they compare with the experiments.

It would seem then that the key to the solution of laminar as well as turbulent entrance flows lies in the finding of relations for c_f and H that are equally valid for pipe and plate flows.

[1] "Friction Factor in the Laminar Entry Region of a Smooth Tube," by A. H. Shapiro, R. Siegel, and S. J. Kline, Proceedings of the Second U. S. National Congress of Applied Mechanics, 1954, pp. 733–741. Also, National Advisory Committee for Aeronautics Technical Note 3048, 1953.

An Experimental and Analytical Investigation of a Differential Surge-Tank Installation

By W. L. GIBSON[1] and W. SHELSON,[1] TORONTO, ONTARIO, CANADA

The performance of a differential surge tank was measured experimentally for various acceleration and retardation conditions, and the results were compared with those obtained analytically. In the experimental investigation, the dynamic pressures at several places in the hydraulic system, together with the turbine-gate positions, were recorded simultaneously on a multichannel oscillograph. For comparison, the corresponding water-hammer pressures and mass flows in the system were calculated by recognized step-by-step processes, adequate numbers of steps being made practicable by the use of high-speed digital computers. The calculated results agreed closely with those determined experimentally.

General Problem and Objectives of Investigation

THE differential surge tank was developed by R. D. Johnson (1)[2] as an economical means of reducing and damping the flow and pressure oscillations resulting from moderate changes in the gate opening controlling the flow through a long hydraulic system.

The solution to the general proportions for the tank can be initiated from the basic mathematical treatment given in R. D. Johnson's paper; then step-by-step arithmetic methods should be used to check the regulation characteristics of proposed designs. The water-hammer pressures in the conduits also should be determined, either by step-by-step arithmetic methods (2), or by a graphical interpretation of the arithmetic solution (3, 4), or, if sufficient simplification is permissible, by reference to Allievi's Charts (5) for water hammer in simple conduits. The large numbers of steps often necessary in practical examples can make the analysis tedious, and in the case of water hammer, the precise analysis by either arithmetical or graphical methods can become almost impracticable. There are few published precise data from operational tests on actual surge-tank installations to support the analytical results and to assess the effects of the usual approximations.

The general problem then is:

1 To obtain from operating tests on actual surge-tank installations, experimental data to add to the store of experience.

2 For a given surge-tank application, to assess the performance with the full precision of the recognized theoretical analyses and to assess the effects of approximations.

When the Aguasabon Generating Station was built in 1947–1948 the opportunity arose to obtain further experimental data on surge-tank performance. During the construction period, instrumentation was installed in the hydraulic conduit system so that the tests described later in this paper could be performed when the plant was put into operation. The precise calculation of the theoretical performance was simplified when automatic high-speed digital computers became available to the authors several years after the plant had been designed and constructed.

Objectives of the Investigation. To provide specific information about the plant, and to contribute data applicable to the general problem, the objectives of this investigation were as follows:

1 For various rates of turbine-gate operation, to determine the water-hammer pressures together with the surge-tank and riser water-level changes, caused by various selected changes in the generating-station load.

2 On the basis of the foregoing, to modify the area of the surge-tank port and the adjustment of the turbine governors if the tests indicated the need.

3 To compare the experimental results with the corresponding analytical results, and with results calculated by approximate methods.

4 To improve the practicable analytical approach if warranted and possible.

The Aguasabon Generating Station

The Aguasabon Generating Station consists of two 22,500-kw vertical-shaft generators driven by Francis turbines operating under 300 ft head. It forms part of a 240,000-kw system, most of the generation being from larger plants on the Nipigon river about 70 miles west of the station. The plant is located on the north shore of Lake Superior about 130 miles east of Port Arthur and Fort William. A concrete gravity dam and sluiceway structure located about 2 miles from the mouth of the Aguasabon River retains a forebay water-storage area at an elevation about 300 ft above Lake Superior and approaching within 3500 ft of the shore line at one place. The generating station is located on the shore line and is supplied with water through a 15-ft-diam circular concrete-lined tunnel from the storage area.

Fig. 1 shows diagrammatically a cross section on a vertical plane through the plant and its hydraulic supply system. The tunnel rises from the generating station with a slope of 1 in 200 from horizontal and turns upward in a smooth bend to join the vertical shaft from the intake structure. A differential surge tank located with its vertical axis 461 ft from the plant is connected to the tunnel by a 15-ft-diam vertical riser. The tank main dimensions are diameter 32 ft, inside riser diameter $13\frac{1}{2}$ ft, port area 8.4 sq ft, inside riser height above forebay level 39 ft, tank-top height above forebay level 44 ft, tank-bottom depth below forebay level 49 ft.

Fig. 2 shows the tank with the generating station in the background. The tunnel and surge-riser excavations are lined with concrete about 3 ft thick. The part of the tunnel within 476 ft of the powerhouse, and the surge riser up to ground level, are lined with steel inside the concrete. The conduit divides into two $10\frac{1}{2}$-ft-diam branches just outside the powerhouse structure to feed the two turbines. The 79-ft length of the conduit between the tunnel portal and the powerhouse is encased in a massive concrete envelope. The surge riser above ground is a continuation of the steel lining of the shaft, and the tank and

---

[1] Applied Mechanics Section, Research Division, Hydro-Electric Power Commission of Ontario.

[2] Numbers in parentheses refer to the Bibliography at the end of the paper.

Contributed by the Hydraulic Division and presented at the Annual Meeting, New York, N. Y., November 28–December 3, 1954, of The American Society of Mechanical Engineers.

Note: Statements and opinions advanced in papers are to be understood as individual expressions of their authors and not those of the Society. Manuscript received at ASME Headquarters, August 26, 1954. Paper No. 54—A-138.

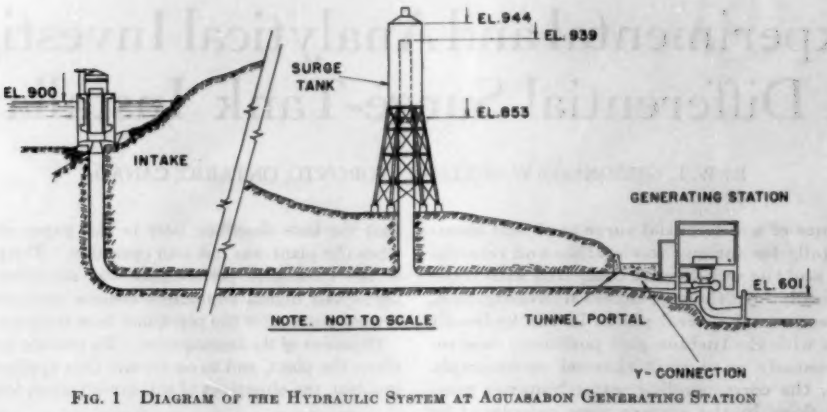

FIG. 1 DIAGRAM OF THE HYDRAULIC SYSTEM AT AGUASABON GENERATING STATION

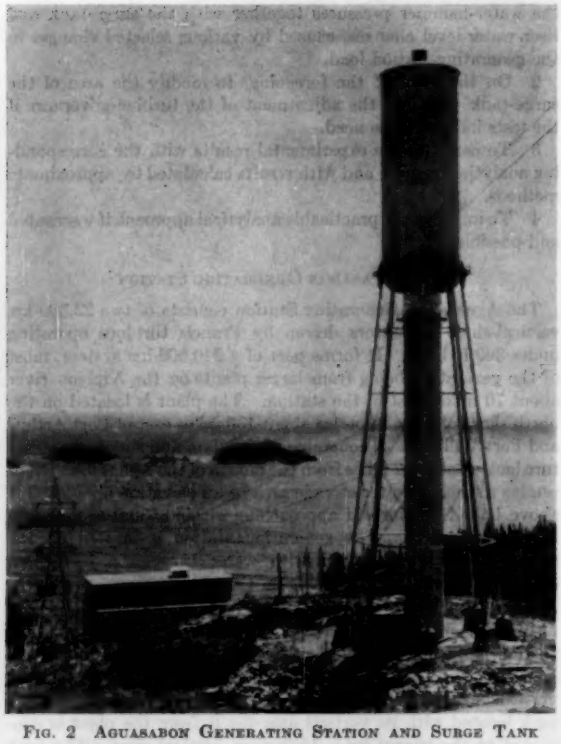

FIG. 2 AGUASABON GENERATING STATION AND SURGE TANK

inner riser are of steel. The required port area was adjusted by blanking off part of the annulus between the vertical pipe and the inside riser. The water enters the tunnel through an intake structure housing a cylindrical-type headgate.

TEST INSTRUMENTATION

The important data required from the experimental work were as follows:

1 Dynamic water pressures at various locations in the hydraulic system.

2 Continuous water levels in the tank and in the internal riser.

3 Continuous values of turbine-gate opening during the operating period of each test.

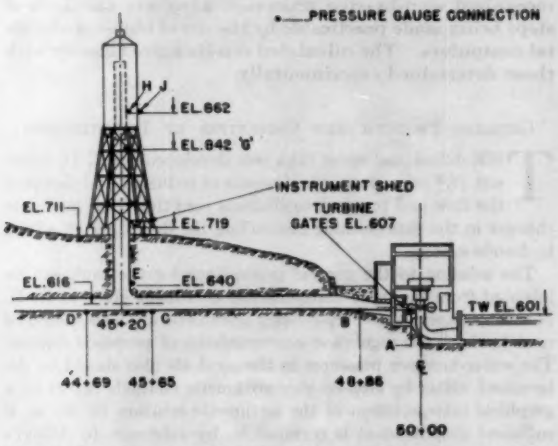

FIG. 3 LOCATIONS OF PRESSURE GAGES; DIAGRAMMATIC ONLY (Elevations from sea level; horizontal stations from arbitrary datum with turbines at 50 + 00 and intake at 14 + 03.)

4 The initial rate of water flow in the conduit at the commencement of each test and, in some cases, the rate of flow at the end of the test.

The water levels in the tank and riser were determined from pressure measurements. The water flow at any instant during turbine-gate movement was found from a calibration of flow against turbine-gate opening, corrected for head on the turbine. Thus the instrumentation used during the tests consisted of electrically operated remote-reading fluid pressure gages installed at the selected stations, electrically operated remote-reading turbine-gate position indicators, a multichannel oscillograph for recording the pressures and gate positions, and a differential manometer for measuring turbine discharge.

Pressure and Water-Level Measurements. The locations of the pressure stations selected for the investigation are indicated in the cross section of the part of the hydraulic system shown in Fig. 3. The pressure gage J at EL 862 was connected directly to the outer tank, and the pressure gage H was mounted on the outside of the tank but was connected to the inside of the inner riser by a horizontal pipe bridging the tank annulus. Bourdon-tube type pressure gages were installed at the turbine scroll-case entries. All the other gages were electrically operated and were made specially for the investigation. They are described later. The gages at the buried stations were installed while the tunnel

was being constructed and at the same time piezometer connections with shutoff valves were installed at the other stations. All the buried gages were connected by electric cables to terminals and jacks on a panel board located where the riser emerges from the rock. The board was mounted in a sheet-steel box cast into a concrete casing for protection, and a heater was included in the box to prevent water condensation. The panel casing projected into a shed erected to house the oscillograph and other test instruments.

Remote-Reading Pressure Gages. The remote-reading pressure gages were designed around the bonded resistance-wire strain gages that were used as sensing elements. Fig. 4 shows a photo-

FIG. 4 REMOTE-READING FLUID PRESSURE GAGE

graph and Fig. 5 shows a cross section of the gage used at the buried stations. In operation, the applied water pressure distends the metallic bellows A, which in turn bends the cantilever B. Strain gages cemented to both sides of the cantilever, near the root, respond to the surface compressive and tensile strains. The resulting electrical resistance changes cause signal-voltage changes across a Wheatstone bridge in which the gages are connected as two of the arms.

The somewhat massive proportions of the remote-reading pressure gage result largely from the wish to use only one casing joint for easy sealing. This feature resulted in a long access passage between the pressure connection and the bellows that is usually not desirable because of the effect on frequency response. In this case, however, it was considered unimportant as only low-frequency operation was anticipated. The cable entry was sealed with a straightforward compression gland using a piece of rubber tubing C as the sealing element. The cable was secured mechanically in a slit boss on the gland nut encircled by a worm-drive hose clamp.

Turbine-Gate Position Indicators. A voltage divider was used as the turbine-gate position indicator. A contact brush traversed along the length of a cylinder on which a resistance wire was wound in closely spaced insulated coils. The brush was moved along its guide bar by a mechanical linkage from the gate-operating piston rod, tapping off a voltage corresponding to its position. This voltage was connected across an oscillograph galvanometer

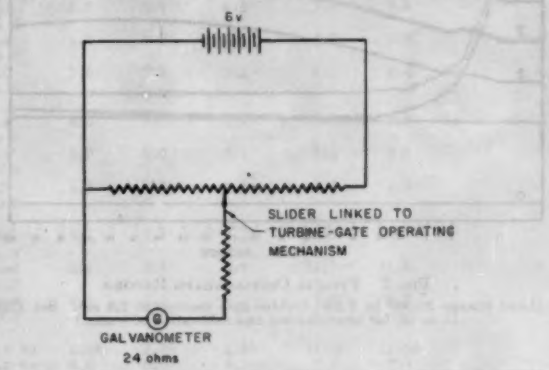

FIG. 6 TURBINE-GATE SERVOMOTOR POSITION-INDICATOR CIRCUIT

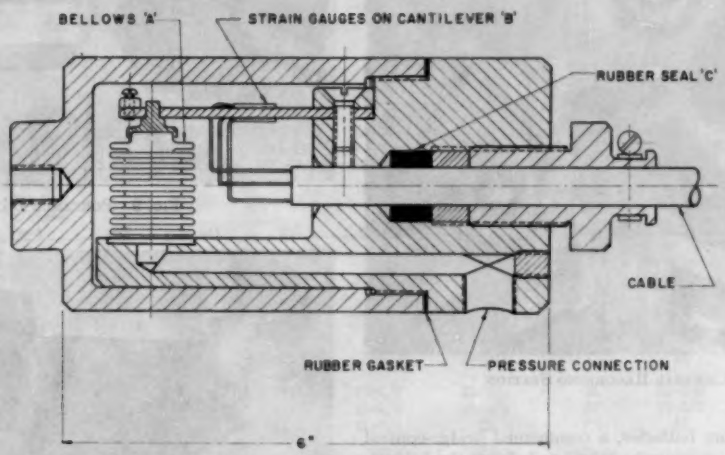

FIG. 5 CROSS SECTION OF REMOTE-READING FLUID PRESSURE GAGE

in series with a resistance used to limit the galvanometer current. Fig. 6 shows the circuit diagram.

Water Flow Rate. The flow versus turbine-gate-position calibration under steady load conditions was determined by the Gibson time-pressure method (6), using differential piezometers. The water flow rate at any instant during turbine-gate movement was found by determining the gate position at that instant and referring it to the calibration, adjusted for changes in head. The flows for the initial steady gate positions were determined also from previously calibrated piezometer readings in the scroll cases.

Recording Equipment. The recording equipment consisted of a commercial multichannel oscillograph equipped with electromagnetic suspended-mirror-type galvanometers. The records were made on photographic paper 7 in. wide. A typical record is shown in Fig. 7.

The strain-gage bridges in the pressure gages were supplied

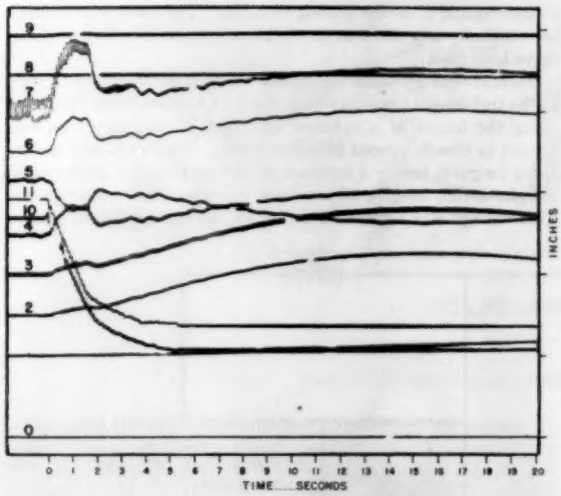

FIG. 7 TYPICAL OSCILLOGRAPH RECORD
(Load change 20,000 to 0 kw; turbine-gate movement 2.3 sec. See Figs. 11 to 15, for identification and calibration of traces.)

FIG. 8 CENTRAL RECORDING STATION

with direct current from batteries, a commercial bridge-control unit being used to adjust the voltage and to balance the bridges. The bridge-output signals were fed directly to the galvanometers without amplification. The pressure-gage calibrations were about 20 to 30 psi per in. of oscillograph-trace deflection and the traces could be measured to about 0.01 in. The precise calibration figures are listed in Figs. 11 to 15. The galvanometer frequency response was flat up to 100 cycles per second (cps).

The gate-position indicators were connected to the galvanometers through resistance boxes that were adjusted to give trace deflections of about 3.3 in. for full gate travel.

Fig. 8 shows the recording station with the instrumentation installed. The two bridge amplifiers on the right were used to amplify the signals from resistance-wire strain gages mounted on the outside surface of the steel lining of the conduit.

SURGE TESTS

The surge tests were carried out with all the generating plants on the system alerted. At the beginning of each test the Aguasabon station turbine governors were adjusted to give approximately the desired rate of gate operation and the plant was operated at the selected initial steady-state power output. The water flow rate was measured and the selected load-change operation was initiated. During the tests the units remained on the line at all times. Load rejections were made by operating the turbine governors manually, and load was picked up by operating the governors manually up to the preset load-limit stop. Fourteen effective test operations were carried out as listed in Table 1.

During the progress of the tests, the photographic records were processed immediately after each test operation so that the water pressures and surge-tank water levels could be determined before proceeding to the next scheduled operation. A small portable "darkroom" of rubberized waterproof twill was used.

Fig. 9 shows a photograph of a darkroom packed for carrying and of the internal arrangement when erected, and Fig. 10 shows the equipment in use. The required approximate measurements were made on the record after it had been in the fixing bath a

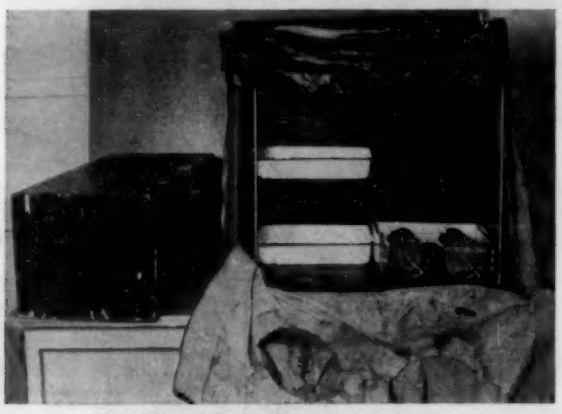

FIG. 9 PORTABLE DARKROOM

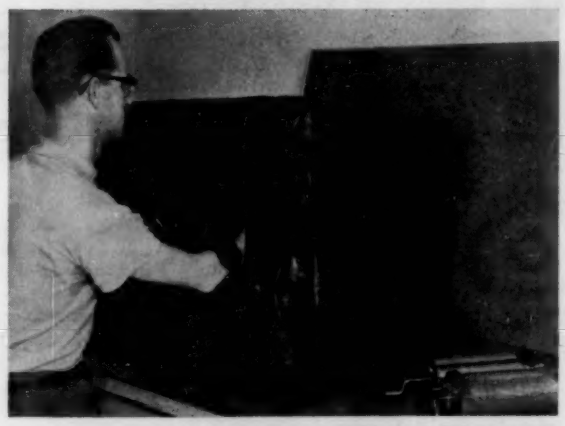

FIG. 10 DARKROOM IN USE

few minutes, then the fixing process was completed while the next test operation was in progress. The most important results of each test were available for discussion in less than 10 min. This factor was extremely valuable as it avoided loss of time between tests and permitted each following test to be approached with confidence.

TABLE 1 HYDRAULIC SURGE TESTS AT AGUASABON GENERATING STATION

Load Changes (Two Generators) kw	Discharge cfs Unit 1	Discharge cfs Unit 2	Discharge cfs Total	Gate-Opening Per Cent Full Gate Unit 1	Gate-Opening Per Cent Full Gate Unit 2	Time For Gate Movement Seconds Unit 1	Time For Gate Movement Seconds Unit 2	Time For Gate Movement Seconds Average	Equivalent Full Stroke of the Gates Seconds Unit 1	Equivalent Full Stroke of the Gates Seconds Unit 2
20000 to 0	499	465	964	45.9 to 0	41.3 to 0	3.8	3.3	3.6	8.3	7.9
20000 to 0	500	476	976	46.8 to 0	42.1 to 0	2.4	2.2	2.3	5.1	5.2
30000 to 0	687	662	1349	62.1 to 0	57.6 to 0	5.1	4.5	4.8	8.2	7.8
40000 to 0	902	897	1799	85.0 to 0	78.4 to 0	6.7	5.9	6.3	7.9	7.5
40000 to 0	904	895	1799	84.3 to 0	78.4 to 0	4.2	3.9	4.1	5.0	5.0
40000 to 0	900	889	1789	84.8 to 0	78.0 to 0	3.5	3.2	3.4	4.2	4.2
46300 to 0	1035	1075	2110	100.0 to 0	99.8 to 0	8.0	7.5	7.8	8.0	7.5
46300 to 0	1035	1067	2102	100.0 to 0	99.8 to 0	5.2	5.0	5.1	5.2	5.0
46300 to 0	1039	1078	2117	100.0 to 0	100.0 to 0	4.3	4.3	4.3	4.3	4.3
0 to 20000	509	502	1011	0 to 47.1	0 to 44.2	5.1	5.6	5.4	10.7	12.7
20000 to 40000	488 to 897	474 to 902	962 to 1799	opened 38.9	opened 37.6	4.4	5.3	4.9	11.3	14.0
20000 to 40000	497 to 909	477 to 879	974 to 1788	opened 38.6	opened 35.0	2.3	2.4	2.4	5.9	6.8
20000 to 40000 to 0*	489 to 874	467 to 865	956 to 1739	43.0 to 84.0 to 0	41.6 to 78.0 to 0	4.6& 6.6	5.0& 6.0	4.8& 6.3	11.7& 7.8	13.6& 7.7
20000 to 40000 to 0**	498 to 870	477 to 860	975 to 1730	46.4 to 84.1 to 0	42.6 to 77.7 to 0	4.3& 6.6	4.8& 5.6	4.6& 6.1	11.3& 7.8	13.7& 7.2

*Forty seconds delay between start of gate opening and closure.
**Thirty seconds delay between start of gate opening and closure.

TABLE 2 MAXIMUM PRESSURE CHANGES DURING TESTS

Load Changes (Two Generators) kw	Time For Gate Movement. Average Of The Two Turbines sec	Outer Tank EL.862 I* psi	Inner Riser EL. 862 H psi	Main Riser EL. 842 G psi	Main Riser EL. 640 E psi	Conduit STN.44+69 D psi	Conduit STN.45+65 C psi	Conduit STN.48+86 B psi	Scroll Case Entry STN.49+50 A psi
20000 to 0	3.6	5	17	17	17	16-1/4	17	-	17-1/4
20000 to 0	2.3	5-1/4	16-3/4	16-3/4	17-1/4	16	17	25	29-3/4
30000 to 0	4.8	7-3/4	19	19	19	18	19-3/4	-	21-1/2
40000 to 0	6.3	12-1/2	20-1/4	20-1/4	21	19-1/4	20-1/4	20	26
40000 to 0	4.1	12-1/2	20-1/4	20-1/2	21	19-1/2	21-1/4	27-1/4	35
40000 to 0	3.4	12-1/2	20-1/4	20-1/2	21	19-3/4	21-1/2	31	40
46300 to 0	7.8	16	21-1/2	21-1/2	22-1/2	21-3/4	24	24-1/2	31
46300 to 0	5.1	16-1/4	21-1/2	21-3/4	21-1/2	20-3/4	23	27-1/2	38
46300 to 0	4.3	16-1/4	21-1/2	21-1/2	21-3/4	21	23	33	44
0 to 20000	5.4	- 5-3/4	- 16-1/4	- 16-1/4	- 15	- 14-1/2	- 15-1/2	- 13-1/2	- 16
20000 to 40000	4.9	- 4-3/4	- 12-1/4	- 12-1/2	- 11-3/4	- 10-3/4	- 12-1/2	-	- 13-1/2
20000 to 40000	2.4	- 4-1/2	- 11-3/4	- 12	- 11-1/2	- 10-1/4	- 11-1/2	- 19-3/4	- 20-1/2
20000 to 40000	4.8&	- 4-3/4&	- 12&	- 12-1/4&	-11-1/2&	- 10-3/4&	- 12&	- 10-3/4&	
to 0	6.3	+10-1/2	+18-1/2	+18-3/4	+18-1/4	+17-3/4	+19-1/4	+19-3/4	-
20000 to 40000	4.6&	- 4-1/2&	- 12&	- 12&	- 10-3/4&	- 10-1/4&	- 11-3/4&	- 10-3/4&	-
to 0	6.1	+ 9-1/2	+18-1/2	+18-1/2	+18-1/4	+17-3/4	+ 19	+17-1/2	

* The letters refer to the pressure station identification used in Figure 3.

The values in Column D are believed to be slightly less accurate than the remaining figures which are estimated to be correct within 5 per cent.

Experimental Results

The maximum and minimum pressures measured at the various places in the hydraulic system during each test are listed in Table 2. Figs. 11 to 15, inclusive, show tracings of the oscillograph records for the tests indicated in Table 3.

TABLE 3 TEST DATA

Plant output, kw	Turbine-gate time, sec
(1) 46,300 to 0	7.8
(2) 46,300 to 0	5.1
(3) 46,300 to 0	4.3
(4) 20,000 to 0	2.3 (equivalent full stroke 5.2 sec)
(5) 20,000 to 40,000	2.4 (equivalent full stroke 6.4 sec)

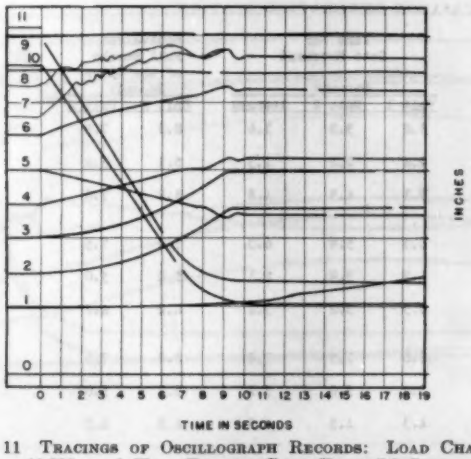

FIG. 11 TRACINGS OF OSCILLOGRAPH RECORDS: LOAD CHANGE, 46,300 TO 0 KW; TURBINE-GATE TIME, 7.8 SEC

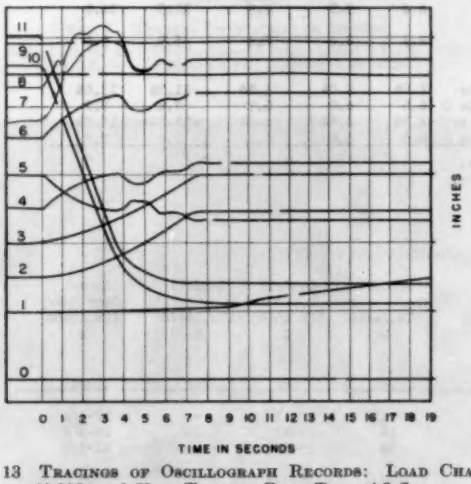

FIG. 13 TRACINGS OF OSCILLOGRAPH RECORDS: LOAD CHANGE, 46,300 TO 0 KW; TURBINE-GATE TIME, 4.3 SEC

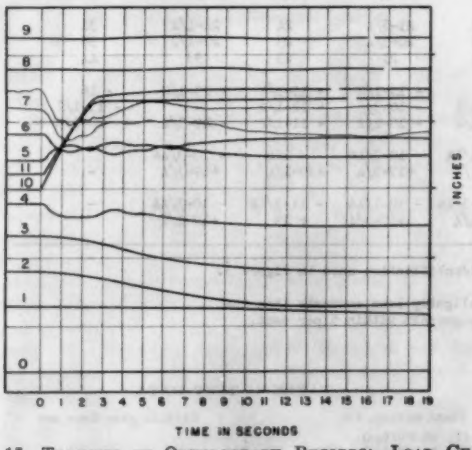

FIG. 15 TRACINGS OF OSCILLOGRAPH RECORDS: LOAD CHANGE 20,000 TO 40,000 KW; TURBINE-GATE TIME, 2.4 SEC; EQUIVALENT FULL STROKE, 6.4 SEC

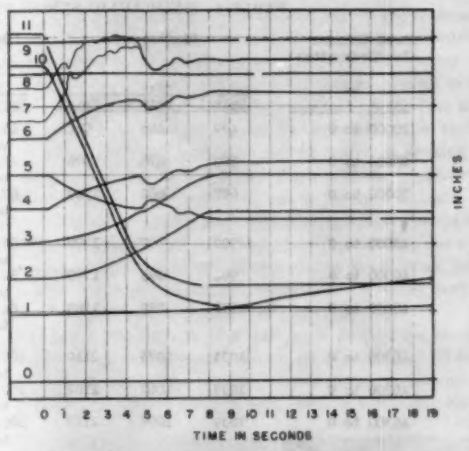

FIG. 12 TRACINGS OF OSCILLOGRAPH RECORDS: LOAD CHANGE, 46,300 TO 0 KW; TURBINE-GATE TIME, 5.1 SEC

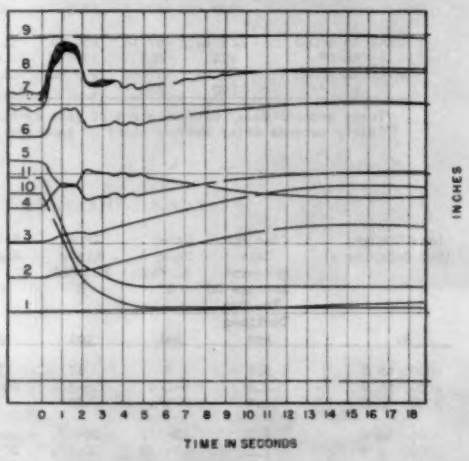

FIG. 14 TRACINGS OF OSCILLOGRAPH RECORDS: LOAD CHANGE 20,000 TO 0 KW; TURBINE-GATE TIME, 2.3 SEC; EQUIVALENT FULL STROKE, 5.2 SEC

KEY TO TRACES, FIGS. 11 TO 15

0, Datum line	
1, Pressure in outer tank (EL 862), psi/in	21.8
2, Pressure in riser (EL 862), psi/in	21.9
3, Pressure in riser (EL 842), psi/in	21.0
4, Pressure in riser (EL 640), psi/in	31.1
5, Pressure in conduit (44 + 69), psi/in	−30.1
6, Pressure in penstock (45 + 65), psi/in	32.8
7, Pressure in penstock (48 + 86), psi/in	31.4
8, Steel strain in penstock (45 + 49), microinches/in/in	183
9, Steel strain in penstock (46 + 05), microinches/in/in	211
10, Gate position	Unit No. 1
11, Gate position	Unit No. 2

NOTE: The wide band formed by Trace 7 occurred because the pressure-gage natural frequency almost coincided with the 81 cps frequency of a turbine vibration induced by the movement of the runner blades past the guide vanes.

The foregoing turbine-gate times are equivalent times for linear closure of the gates without including the cushioning part of the stroke. The average for the two turbines was used.

These representative test conditions were selected for comparisons between results obtained experimentally and results calculated analytically. Later in the paper the comparisons are presented in graphical form.

Theoretical Analysis of Water Hammer in System

Suitable methods, described in the literature, are available for the calculation of water hammer both in simple and complex hydraulic systems, and for the calculation of mass water flow in differential surge tanks. In order to compare the experimental and corresponding analytical results, these methods were applied to the test conditions listed previously. Some refinements and variations in the analyses, described later, were introduced either because they were found necessary to improve the accuracy of the calculated results or to assess the precision of the methods generally.

The present bases for the calculation of water-hammer pressures are due to Joukovski (7) and Allievi (8) although many others have served to interpret and extend their work. While the equations they developed can be applied in a relatively straightforward way to the problem of water hammer in simple conduits, the treatment of any complex system tends to become much more involved and lengthy owing to the subdivision and interaction of pressure waves at junctions and discontinuities in the network. As a result, in the analysis of hydraulic systems, as in the analysis of any complex physical phenomenon, approximations and simplifications are often introduced. For example, in calculating the water-hammer pressure in a hydraulic conduit with a surge tank, it is common practice to consider only the water-hammer effect that would occur in a simple pipe composed of the penstock and surge riser (9).

In the present instance, however, the calculations were based on an equivalent system more closely resembling the actual installation. This was done in order to obtain a better understanding of the extent to which the performance of a full-scale installation could be predicted using the best means available, but without excessive refinements.

The hydraulic system used for the calculations is shown in Fig. 16. It consists of a uniform conduit from the forebay to the junction at the base of the surge riser, the vertical surge riser, and a uniform penstock from the junction to the turbine gates. The gate movement was assumed to take place in a series of small steps, each movement creating a water-hammer shock wave which travels up the penstock to the junction, where it undergoes a triple division, partly up the riser, partly into the conduit, and partly reflected back along the penstock. The respective waves are reflected on reaching the ends of the pipes and the effects of the reflected waves are superposed on the existing pressures.

Although this problem can be handled either graphically (3, 4) or algebraically, the latter approach was chosen because both methods applied to the particular problem appeared to be too lengthy for manual solution, and only the algebraic computation could be handled directly by the available automatic digital computer. The algebraic method employed was similar in principle to the tabular methods which have been evolved by Glover (2) and Thomas (10). In this method, several tables specifying the algebraic operations are prepared, each representing the hydraulic conditions in separate elements of the hydraulic system. Thus, in the system described here, four tables in all were used representing, respectively, the penstock, the junction at the base of the riser, the riser, and the conduit.

In carrying out the computations, the pressure increment

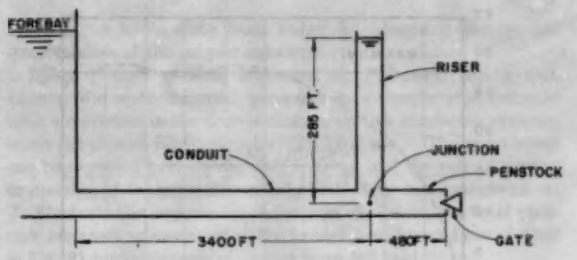

PIPE ELEMENT	AREA	WAVE VELOCITY
PENSTOCK	177 SQ FT	3897 FT/SEC
RISER	143 SQ FT	3471 FT/SEC
CONDUIT	177 SQ FT	4601 FT/SEC

Fig. 16 Schematic Diagram of Hydraulic System Used for Water-Hammer Calculations

(Wave velocities shown are approximate and values shown were chosen for convenience in computation.)

resulting from one step of gate movement is calculated in the table for the penstock. This result is transferred to the operations table for the junction in which the pressures and flows at the junction are found. The results are then transferred to the tables for the three pipe elements and the flow conditions in each element calculated. This sequence of calculations is repeated, results being transferred from table to table in sequence and calculations done in a semiautomatic way in accordance with the routine instructions for each table. The various tables are synchronized by choosing as the step time common to all of them, a period that is the highest common factor of the reflection times of the pipes. The pipe reflection time is the time required for a pressure wave to travel from the point where it is initiated to the point where it is reflected and back to its starting point, and is $2L/c$, twice the pipe length divided by the velocity of sound in the pipe.

In the present example, using the pipe lengths and pressure-wave velocities shown in Fig. 16, the highest common factor was 0.04105 sec and the gate was assumed to move in a series of steps separated by this time. The number of steps required for a representative closure time of 5.2 sec was 127, which indicates the excessive length of time required for the calculations by manual methods. Since the detailed procedures for this form of solution are adequately described in the references mentioned, a full description will not be repeated here. Of course the solution of this problem in the automatic digital computer required a revision of the method as outlined, but the mode of solution followed the sequence noted here.

Comparison of Theoretical and Measured Pressures

The results for a gate-closure operation and for an opening operation are shown in Figs. 17 and 18, as representative examples of the theoretical solutions obtained. The measured water-hammer pressures for the three locations shown on each chart are plotted for comparison.

The measured pressures were obtained from the measurements of total pressure change minus the change in riser level, the latter being obtained from a pressure gage near the top of the riser. The actual water hammer at the scroll cases, based on the maximum reading of a Bourdon gage, was adjusted both for change in riser level and decrease in friction loss in the penstock.

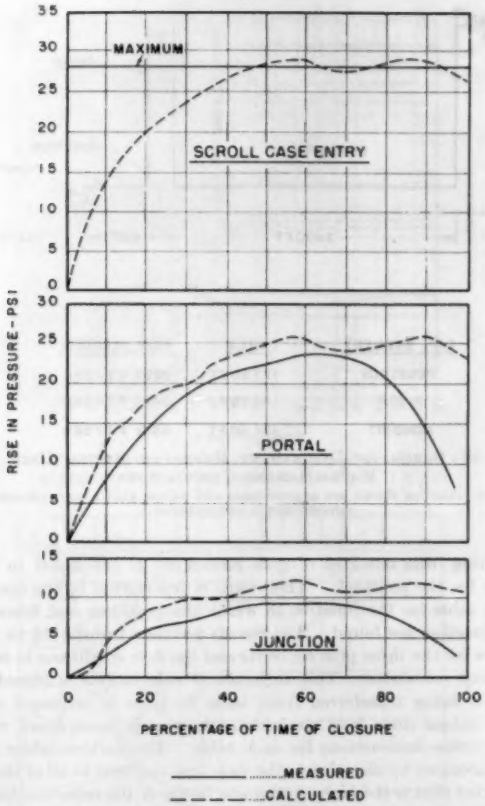

FIG. 17 PRESSURE CHANGE DUE TO WATER HAMMER
(Load change, 46,300 to 0 kw; turbine-gate movement, 5.1 sec.)

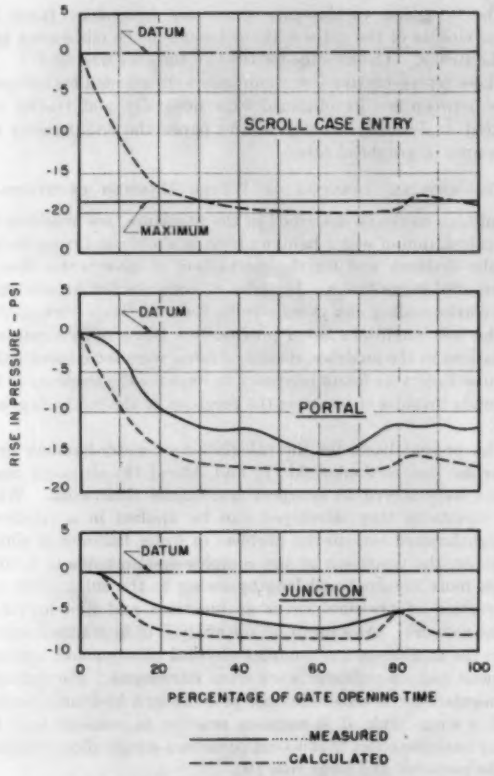

FIG. 18 PRESSURE CHANGE DUE TO WATER HAMMER
(Load change, 20,000 to 40,000 kw; turbine-gate movement, 2.4 sec.

In obtaining the theoretical curves, the following assumptions were made to simplify the computational procedure:

(*a*) The rate of gate movement was assumed to be linear. The oscillograph records show that the rate is not linear over the whole stroke but, in the particular cases considered, the linearity assumption is realistic as the maximum water-hammer pressure occurred before departure from linearity took place. The assumption is usual in design procedures.

(*b*) The curve of flow against gate opening at constant head was assumed to be comprised essentially of two straight lines. Using this assumption together with assumption (*a*), the graph illustrated in Fig. 19 was constructed for use in the subsequent calculations of flow at any instant. The instantaneous flow was based on the percentage "effective" gate opening corresponding to the percentage of the gate-closure time. The effect of the change in head was included in the calculations.

(*c*) The performance and operation of both turbine gates were assumed to be identical. As a result no account was taken of the Y-junction where the penstock divides to supply the two turbines.

(*d*) The water-hammer pressure was assumed to vary linearly between the scroll case and the base of the vertical riser. This assumption was used in plotting the theoretical curve for the water-hammer pressures at the portal.

These assumptions serve to explain some of the differences between the experimental and theoretical curves. Nevertheless,

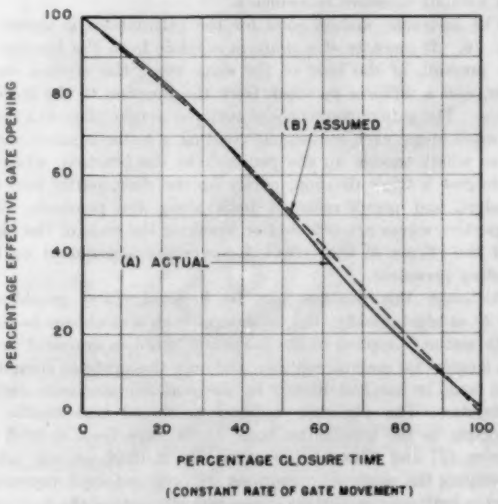

FIG. 19 EFFECTIVE GATE OPENING VERSUS PERCENTAGE CLOSURE TIME

(A) Actual: actual gate operation based on calibration of flow versus gate position at constant head;

(B) Assumed: assumed gate operation for water-hammer calculations.

the agreement is reasonably good considering that the behavior of the plant was deduced from a somewhat simplified mathematical equivalent.

Two Approximate Calculations of Water Hammer. One of the objectives of the investigation was to compare the experimental results with the fairly precise analytical results and also with the results calculated by approximate design methods. Two approximate methods were used, both being based on very much simplified conduit systems instead of the more accurate system used for the analytical method described earlier:

(*a*) In the first approximate method the conduit upstream of the surge-riser junction is considered to be so long that gate closure is complete before the return of the reflected wave, e.g., the conduit length is infinite. There is, nevertheless, a subdivision of pressures at the riser junction.

(*b*) In the second approximate method the conduit length upstream of the surge-riser junction is considered to be zero. Thus the hydraulic system is replaced by a single pipe with length equivalent to the combined length of the penstock and the initial height of the water in the riser.

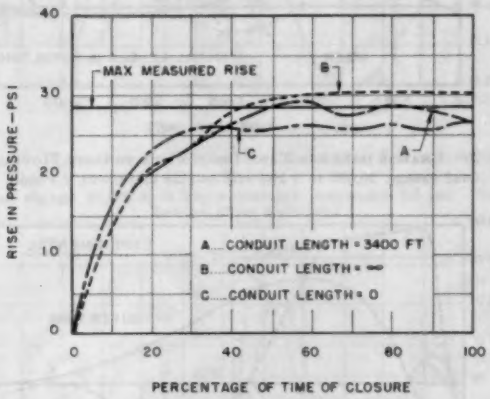

FIG. 20 COMPARISON OF CALCULATED WATER-HAMMER PRESSURES AND MAXIMUM MEASURED PRESSURE AT SCROLL-CASE ENTRY
(Load change, 46,300 to 0 kw; turbine-gate movement, 5.2 sec.)

The results of these calculations are given in Fig. 20. As expected, the highest water-hammer pressure is obtained with the infinite conduit since the mitigating effect of the reflected wave is lost. Also, the long conduit in itself tends toward higher pressures as the gate-closure time then is within the critical $2L/c$ time. Of course the presence of the riser means that the influence of this latter consideration is greatly reduced, but is not likely absent. As the length of the conduit is reduced, the calculated pressures decrease.

For the particular hydraulic system analyzed here, the maximum difference between calculated values is of the order of 20 per cent, although in absolute terms the difference is not sufficient to single out any particular method for design use. The best correlation between measured and calculated pressures was obtained by using the most accurate of the chosen analytical methods. It is considered that, although for this plant the water-hammer pressures are only a fraction of the total pressures and therefore the variation in results between the different methods is not important, there may be installations in which a difference of 20 per cent in calculated water-hammer pressures may be economically important and the most accurate method should be employed. Also, since the more complex solutions can be handled quite easily with the aid of modern digital computers, there seems to be little basis today for accepting the greater uncertainties of the simpler solutions.

Effect of Rate of Gate Movement on Pressures. As is well known, the water-hammer pressures in a simple pipe increase with a reduction in the time of closure, up to a maximum pressure when the closure is completed within $2L/c$ sec. The same trend can be expected in more complex systems, and the rate of closure or opening of the gates is normally limited by this consideration. To illustrate the importance of the rate of closure, the total pressure increases as measured at the tunnel portal have been plotted in Fig. 21 for three rates of closure from full load.

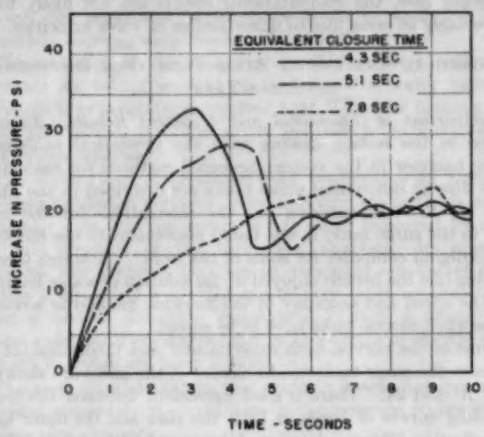

FIG. 21 TOTAL MEASURED PRESSURE INCREASE AT TUNNEL PORTAL FOR DIFFERENT RATES OF TURBINE-GATE CLOSURE
(Load change, 46,300 to 0 kw.)

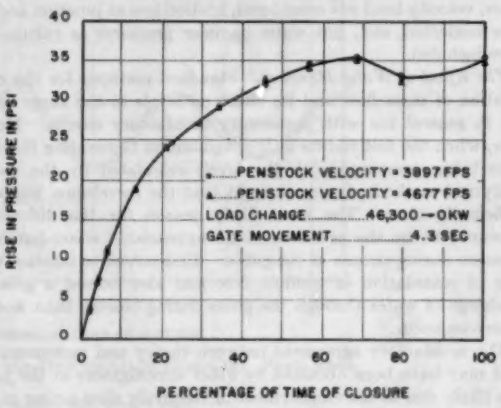

FIG. 22 EFFECT OF DIFFERENT WAVE VELOCITIES ON CALCULATED WATER-HAMMER PRESSURES AT TURBINE GATES

Effect of Changes in Velocity of Pressure Wave. The velocity of a pressure wave in a pipe filled with fluid can be determined knowing the diameter, thickness, and modulus of elasticity of the pipe, and the density and bulk modulus of compression of the fluid. In practice, however, the accurate calculation of the velocity may not be practicable; therefore the effects of approximations were investigated for the present example.

In the case of the simple pipe and within the normal range of velocities, the accepted opinion (11) is that for relatively slow closures, the value of wave velocity need not be known precisely. In this case where the problem is more complex and the wave

velocities difficult to evaluate precisely, the importance of the accuracy of the chosen velocities was unknown. Hence two solutions using different wave velocities were computed for one of the test conditions with relatively quick closure. The wave velocities chosen for these computations were 3897 and 4677 fps in the penstock, the other velocities remaining as before. These particular values for the penstock were selected because they were convenient for computation. The results are plotted in Fig. 22 and for the two selected velocities they are almost coincident. Since the wave velocities used in the computations generally are unlikely to be in error as much as the limits in the foregoing case, the computational results are not likely to be appreciably in error due to uncertainties in wave velocities.

Theoretical Analysis of Mass Flow in a Differential Surge Tank

Comparison of Theoretical and Measured Results. As mentioned in the section dealing with the theoretical analysis of water hammer in the system, accepted methods for calculating mass flow in differential surge tanks are described in the literature (1, 12). In carrying out the calculations for the mass flow in the surge tank, it was found convenient to use the automatic digital computer for some of the work. Although there is nothing like the benefit enjoyed in the solution of water hammer, yet the speed and economy of the machine method is advantageous when several cases have to be solved.

Some of the curves, both experimental and theoretical, of the levels in the surge tank due to closure of the gates are shown in Figs. 23 and 24. There is good agreement between the corresponding curves of levels in both the riser and the outer tank. The effective differential action of the surge tank is clearly evident in the curves, from the rapid decrease in amplitude of the water fluctuations in the riser and outer tank. In the calculations, the usual assumptions were made including linear closure of the gates, velocity head not considered, friction loss at junction and in riser neglected, etc., but water-hammer pressures as calculated were included.

The Effect of Water Hammer. Standard methods for the calculation of mass flow and its effect on levels in the surge tank are in general use with apparently satisfactory results. However, when the test results at the Agusabon Generating Station were being compared with the levels calculated by the usual analytical methods, it was thought that the correlation was not sufficiently close. The most likely reason for the difference appeared to be the presence of an appreciable water-hammer pressure during closure of the gates. This served to increase the rate of retardation of conduit flow and also caused a greater discharge of water through the gates during closure than would otherwise occur.

The satisfactory agreement between theory and measurement that may have been obtained by other investigators in the past was likely due to the employment of relatively slow-acting gates which created negligible water-hammer pressures or to the existence of a relatively long conduit less sensitive to transient pressures. However, when considering more responsive and rapid adjustment of turbine output, the water-hammer effect should not be overlooked as an important factor in surge-tank design and as an aid to regulation.

Both the experimental and the analytical results for surge-tank levels shown in Fig. 24 may also be compared with the calculated levels given in the lower half of Fig. 25. Fig. 25 was derived from the usual design procedure which neglects the influence of water-hammer pressures on mass flow. These results demonstrate the greater accuracy obtained by including the effect of water hammer. The simpler solution predicts a maximum level in the outer tank of 33 ft above forebay level, whereas

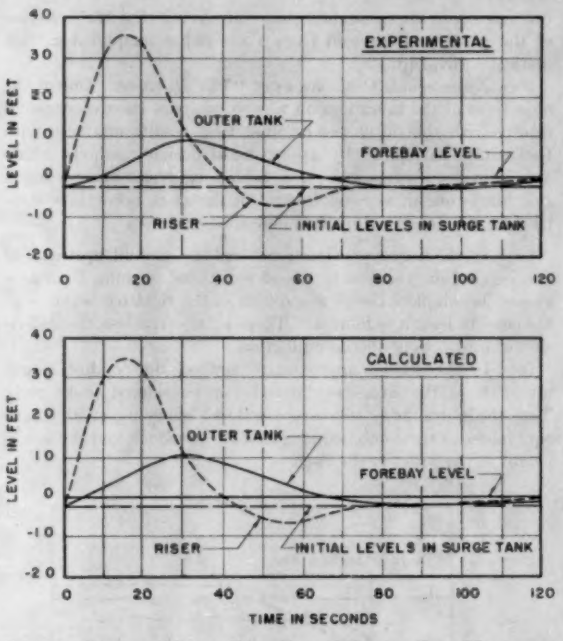

Fig. 23 Change in Surge-Tank Levels Due to Gate Movement (Load change, 20,000 to 0 kw; turbine-gate movement, 2.3 sec.)

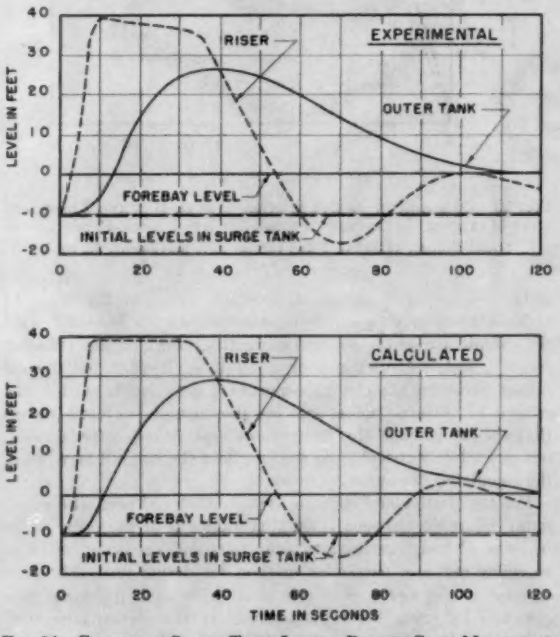

Fig. 24 Change in Surge-Tank Levels Due to Gate Movement (Load change, 46,300 to 0 kw; turbine-gate movement, 5.1 sec.)

the addition of water hammer reduces this figure to 29 ft. Actually the measured maximum was about 26 ft. The equivalent minimum-level figures for the riser are: —20 ft, —16 ft, and —17 ft, respectively. Thus consideration of the influence of the modest water-hammer pressures has provided more accurate

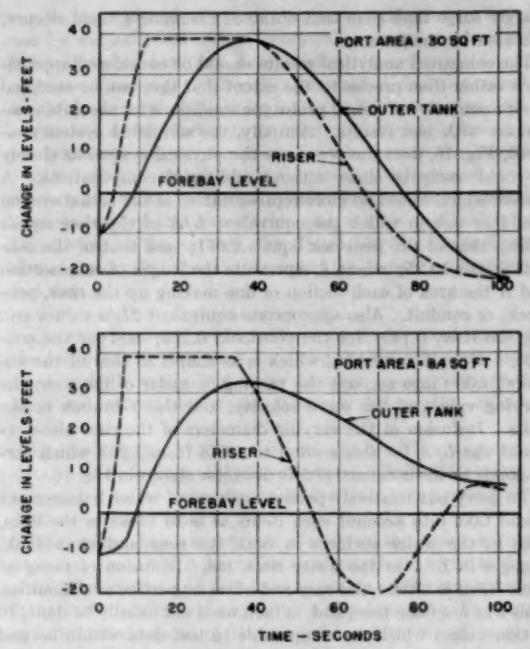

FIG. 25 EFFECT OF PORT AREA ON CALCULATED LEVELS IN SURGE TANK

(Load change, 46,300 to 0 kw; turbine-gate movement, 5.0 sec. Water-hammer effect neglected.)

former shows the comparative results for port areas of 30 sq ft and 8.4 sq ft, calculated using the usual design assumptions. The latter figure, Fig. 26, shows experimental results for the Aguasabon surge tank with the port area enlarged to 30 sq ft. With the large port area, the oscillations tend to approximate those of a simple surge tank with inevitably slow damping, although the differential action is in evidence during the first quarter-cycle. The curve for an 8.4-sq-ft port area shows that the surge tank is highly effective in damping out the mass oscillations.

CONCLUSIONS

The investigation showed that, for the hydraulic system investigated, the surge-tank performance could be analyzed quite accurately by recognized theoretical methods.

The accuracy of the mass-flow predictions were noticeably increased by taking account of the effects of water hammer. Although it is generally recognized that the water hammer will affect the results, it is frequently omitted in ordinary surge-tank design analyses.

The water-hammer pressures were predicted with sufficient accuracy for design purposes, using approximate methods in this particular case, but the accuracy was much improved by using the full precision of the theoretical analyses. In practical problems this precision involves an enormous amount of fairly routine arithmetical work that can be very much accelerated by using a modern automatic computer. In fact, a computer is almost essential if several designs or the effects of several small changes in design are being studied.

The tests showed that in this example it was not important to know accurately the velocities of the pressure waves in the various pipe elements.

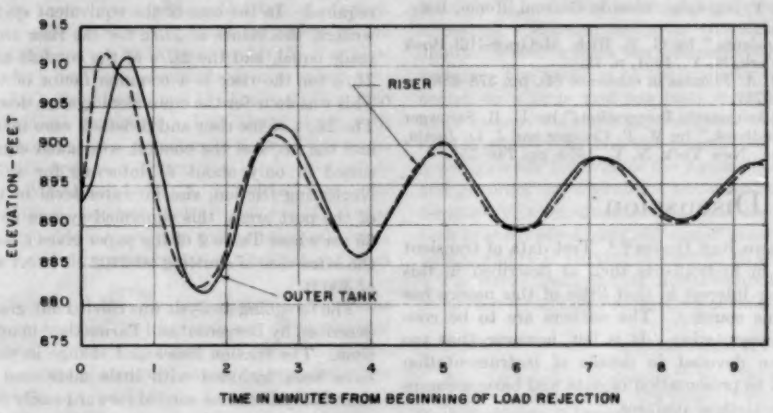

FIG. 26 MEASURED CHANGES IN SURGE-TANK LEVELS DUE TO GATE CLOSURE: PORT AREA = 30 SQ FT

(Load change, 40,000 to 0 kw; total turbine-gate time, 9 sec.)

NOTE: These curves are presented to show the approach toward simple tank characteristics when the differential tank has relatively large ports.

Discrepancies occur in the relationship between the two curves because (a) the levels were not the same when the surge was initiated and (b) because of measuring accuracy limitations imposed by the particular instrumentation used for this test.

results. This can be used to design more economical tanks. Of course designs must be checked for slower closures which result in lower water-hammer pressures but which may require a larger surge tank than is occasioned by rapid closure.

Effect of Port Area. Much of the effectiveness of the differential surge tank is dependent on the selection of a suitable port area. The importance of this factor is well demonstrated by comparing the three curves shown in Figs. 25 and 26. The

The importance of the port area in the differential surge tank was well demonstrated, and the tests showed that the Aguasabon Generating Station surge-tank port area of 8.4 sq ft was very effective as originally designed.

The tests had a direct effect on the plant in showing that fast turbine-gate operation of 5 to 7 sec equivalent full gate time was permissible, with improved system regulation; and that the surge-tank regulation was entirely adequate to permit both machines

to be operated at full gate with the possibility of full-load rejection.

In closing it should be pointed out that it is only in the past decade or so that measurements of the type described in this paper have become practicable as a result of new instruments and measuring techniques having been developed for other purposes.

Acknowledgments

The authors wish to express their thanks to the Hydro-Electric Power Commission of Ontario for permission to publish this paper, and to acknowledge the co-operative effort of many associates who helped to initiate and carry out the investigation, notably Mr. E. G. Tallman and Mr. A. E. Aeberli.

Bibliography

1 "The Differential Surge Tank," by R. D. Johnson, Trans. ASCE, vol. 78, 1915, p. 760.

2 "Computation of Water Hammer Pressures in Compound Pipes," by R. E. Glover, Symposium on Water Hammer, The American Society of Mechanical Engineers, 1933, pp. 64–71.

3 "Étude des variations de régime dans les conduites d'eau; solution graphique générale," by L. Bergeron, *Revue Générale de l'Hydraulique*, vol. 1, 1935, p.12.

4 "Water-Hammer Pressures in Compound and Branched Pipes," by R. W. Angus, Trans. ASCE, vol. 104, 1939, pp. 340–401.

5 "Water Hammer," by E. B. Strowger, in "Hydro-Electric Handbook," by W. P. Creager and J. D. Justin, John Wiley & Sons, Inc., New York, N. Y., 1950, pp. 713–719.

6 "The Gibson Method and Apparatus for Measuring the Flow of Water in Closed Conduits," by N. R. Gibson, Trans. ASME, vol. 45, 1923, p. 343.

7 "Water Hammer," by N. Joukovski, English translation by O. Simin in Proceedings of the American Water Works Association, vol. 24, 1904, p. 341.

8 "Theory of Water Hammer," by L. Allievi, English translation by E. E. Halmos, Typography, Ricardo Garroni, Rome, Italy, 1925.

9 "Hydraulic Transients," by G. R. Rich, McGraw-Hill Book Company, Inc., New York, N. Y., 1951, p. 11.

10 Discussion by H. A. Thomas in reference (4), pp. 378–388.

11 Reference (5), p. 717.

12 "Surge Tanks; Arithmetic Integration," by E. B. Strowger in "Hydro-Electric Handbook," by W. P. Creager and J. D. Justin, John Wiley & Sons, Inc., New York, N. Y., 1950, pp. 746–751.

Discussion

F. E. Cornwell[8] and Ben Donsky.[8] Test data of transient hydraulic conditions in hydroplants such as described in this paper are of particular interest in that little of this nature has been published in this country. The authors are to be congratulated on their presentation. It is felt, however, that too much space has been devoted to details of instrumentation and testing compared to presentation of data and basic assumptions made in their analytical analyses.

Although the details of water-hammer and surge computations, both numerically and graphically, are well covered in the literature, basic assumptions vary widely in making the necessary simplifications prior to solution. In the present case a true evaluation of the comparisons between test and computed values is difficult. For instance, it would be of interest to know the nature of the revisions required in adapting the method to the digital computer. Also some details on the manner in which water-hammer effects were included in computing surge heights are desirable as we believe this could well explain why the authors differ with previous investigators in their conclusions on the importance of water-hammer effects on surge height. The writers do not feel that a slower gate closure could result in the need for a larger surge tank than that obtained assuming a rapid closure, as stated by the authors.

The computed analytical results should be considered approximate rather than precise to the extent that they can be accepted as representative of actual prototype conditions for absolute comparison with test results. Actually, the simplified system analyzed, Fig. 16, does not represent the physical system as closely as could easily be done without additional complications. A system which would be more representative of the actual system would be one in which the equivalent L/A of the riser equals 1.678; that of the penstock equals 2.671; and that of the conduit equals 19.25; where L represents the length of each section and A the area of each section of line making up the riser, penstock, or conduit. Also appropriate equivalent $2L/a$ values are: For the riser, 0.149; for the penstock, 0.225; and for the conduit, 1.478. This system, which is as simple as that of the authors', takes into account the varying diameter of the riser, the varying values of the wave velocity, and the Y-branch to the units. Inclusion of the varying diameters of the riser alone reduced the L/A for this section to 1.678 from 1.993 which corresponds to the constant 13.5-ft diameter shown in Fig. 16.

To carry out relatively precise analyses of water hammer one would take into account such items as head losses in the lines, rises in the water surfaces in both the riser and main tank, changes in L/A as the water rises, etc. Inclusion of many of these items is often quite easy and offers no particular difficulties. This was not done here, and, in fact, need not usually be done, to obtain values which are comparable to test data within normal tolerances.

The authors point out that the wave velocity is of secondary importance. We have made use of this property for many years to adjust $2L/a$ values to reduce the number of analytical steps required. In the case of the equivalent system described by the writers, the values of $2L/a$ for the riser and penstock could be made equal, and the $2L/a$ of the conduit adjusted to where the $2L/a$ for the riser is a common factor of that for the conduit. This was done for the equivalent system described by the writers. The $2L/a$ of the riser and penstock were taken equal to 0.19, and and the $2L/a$ of the conduit was taken equal to 1.52. This resulted in only about 27 intervals for a 5.1-sec gate closure. Neglecting friction, rise in water level in the riser, and effects of the port areas, this simplified system gave a pressure rise of 35 psi where Table 2 of the paper gives a test value of 38 psi for the same case of shutting off 2102 cfs in 5.1 sec with a static head of 300 ft.

The foregoing analysis was carried out graphically by methods described by Bergeron[4] and Parmakian[5] in approximately 3 hours' time. The friction losses and change in riser water level could have been included with little additional effort. The surge-tank analysis can be carried forward easily from this point by extension of Bergeron's water-hammer methods or by the graphical methods, developed specifically for this problem, of Schoklitsch[6] as modified by Bouvard and Molbert.[7] The latter article presents a typical graphical solution for a differential surge tank.

The writers feel that, in general, graphical methods are far superior to numerical ones for handling both water-hammer and surge problems. Irregularly shaped tanks, multiple lines and tanks, friction, throttling orifices, and other complex features

[8] Engineers, Design and Construction, Bureau of Reclamation, U. S. Department of the Interior, Denver, Colo.

[4] "Du Coup de Bélier en Hydraulique au Coup de Foudre en Électricité," by L. Bergeron, Dunod, Paris, France, 1950.

[5] "Waterhammer Analysis," by John Parmakian, Prentice-Hall, Inc., New York, N. Y., 1955.

[6] "Spiegelbewegung in Wasserschlössern," by A. Schoklitsch, *Schweizerische Bauzeitung*, vol. 79, 1923/I, pp. 129-146.

[7] "Méthode Graphique pour le Calcul des Cheminées d'Équilibre," by M. Bouvard and J. Molbert, *La Houille Blanche*, vol. 5, September-October, 1950, pp. 535-554.

can be incorporated without excessive complications. We made use for several years of the numerical procedures referenced by the authors but have found them inflexible and unwieldy as well as time-consuming. Although a high-speed digital computer is available, we have no plans for its use in this connection. Should a situation arise where a large number of similar solutions were needed, it might prove feasible to process them in this manner.

Although the writers have disagreed with some of the conclusions stated and prefer other simplifications and methods of analysis, we feel this paper deals with a subject of real interest. In addition to the authors, the Hydro-Electric Power Commission of Ontario is to be complimented for its part in obtaining the test data.

CHARLES JAEGER.[8] The authors are to be congratulated on the originality of their work involving the simultaneous measurement of both surges and water hammer on a prototype surge tank and comparison of the measured values with calculated results.

In their paper the two authors say that few experimental data on existing surge tanks have been published. This adds more importance to the very comprehensive study they submit on the Aguasabon surge tank.

The writer has summarized elsewhere the more important practical data, which have been published on surge tanks, including laboratory and field tests on surges and on water hammer (1)[9] and the failures and accidents to pipe lines (2). These publications include some of the material published previously by Billings (3). Since these three publications, several important publications by L. Escande (4) which cover much ground on the design and calculation of surge tanks and water hammer also should be mentioned.

More recently two theses have been submitted at English universities and one in Belgium on a subject very close to the one dealt with by the authors. A PhD thesis by Mr. P. Hawkins, (Edinburgh University) has been summarized in a paper submitted by Messrs. O. C. Zienkiewicz and P. Hawkins (5) to The Institution of Mechanical Engineers. This thesis deals with the distribution of water-hammer pressures in hydraulic systems with surge tanks, with special consideration of the restricted-orifice surge tank. A MSc thesis by Mr. I. S. Pearsall (Professor Evans, University College, London) and a thesis by M. Moons (Prof. A. Schlag, Liege) dealing with the computation of surges, the first one with extensive laboratory tests, have not yet been published.

A close examination of all these papers leads to conclusions quite similar to those reached by the authors. The classical methods for surge and for water-hammer analysis give reliable results within such margins of accuracy as can be expected when dealing with these difficult problems. Not one author has proved anything to the contrary.

These detailed bibliographical references may be useful to English-speaking engineers as they refer to data published in many foreign countries.

A recent paper by the writer also may be referred to (6) where the "Present Trends in Surge Tank Design" are analyzed on a somewhat wider basis than in the paper by the authors. The written discussion by about 15 contributors brought to light many important aspects of modern research work and the paper with discussion may be recommended to those who want to compare their knowledge with the theories of their opposite numbers in France, Italy, and other European countries.

A detailed analytical theory of the water hammer in hydraulic systems with surge tank was developed many years ago (7), quite independently of the publications by Schnyder and Bergeron. This method leads to approximate formulas for the estimate of water hammer at the turbine end and at the junction of the surge tank. A short calculation taking a few minutes shows that for the "turbine gates fully closing in 5.2 sec" condition, the pressure at the junction is 41 per cent of the pressure at the scroll-case entry as against 36 per cent found on the diagram, Fig. 17, by the authors' detailed calculation on the digital computer. The approximate formulas also give good values for the pressure at the turbine gate, compared with the results in Fig. 20. At a discussion meeting of the Societé des Ingenieurs Civils de France (July 6, 1934) Professor Bergeron agreed with the writer that the analytical developments were identical with the graphical methods. In his thesis Mr. Hawkins said that the theory of the water hammer in restricted surge tanks, published in 1933, was in good agreement with tests made in 1953 at Edinburgh. This analytical theory was extended to problems of resonance in a paper submitted to The American Society of Mechanical Engineers in 1939 (8) and is summarized in the writer's paper (1).

The authors mention that all the tests for switching the load on and off were made with hand operation, and no governor. A rapid calculation shows that the area of the main tank is approximately that given by the formula of Thoma with a "safety factor" of 1. The Aguasabon surge tank, however, has an additional safety margin because of the energy head $V^2/2g$ which should be added to the friction losses for stability calculations. Most of the tests were for $\delta\eta/\delta t \geq 0$ (where η = turbine efficiency). The writer believes that the losses in the T-junction of the vertical differential riser and the tunnel have additional stabilizing effect. Two recent papers (9, 10) deal with the problem of the stability of restricted orifice and differential tanks. The most important stabilizing factor for the Aguasabon surge tank undoubtedly results from the interconnection with the 240,000-kw system. The problem of the stability of a power station connected to a large grid has been mentioned in paper (6). By hand maneuvering the turbine gates, the stability problem has been eliminated for the test period. It would be of interest to investigate the behavior of the Aguasabon tank when the turbine and governor are operated when connected to the grid and, alternatively, when disconnected from the grid. The Aguasabon tank is obviously a marginal case of great interest and additional data would be of striking interest to all specialists.

The writer confirms that digital computers also have been used in Britain for detailed surge-tank calculation.

[8] The English Electric Company Ltd., Rugby, England.

[9] Numbers in parentheses refer to the Bibliography at the end of this discussion.

BIBLIOGRAPHY

1 "Technische Hydraulik," by Charles Jaeger, Birkhäuser, Basle, Switzerland, 1949, 464 pages; French translation "Hydraulique Technique," Dunod, Paris, France, 1953; English translation by P. O. Wolf, Blackie and Son, Glasgow, Scotland, 1956.

2 "Water Hammer Effects in Power Conduits," by Charles Jaeger, *Civil Engineering and Public Works Review*, February- May, 1948.

3 "High Head Penstock Design," by A. W. K. Billings, O. M. Dodkin, F. Knapp, and A. Santos, ASME and ASCE Symposium on Water Hammer, 1933.

4 "Methodes nouvelles pour le calcul des chambres d'équilibre," by L. Escande, Dunod, Paris, France, 1953; "Complements D'Hydraulique," by L. Escande, Dunod, Paris, France, vols. 1 and 2, 1947–1951.

5 "Transmission of Water Hammer Through Surge Tank," by O. C. Zienkiewicz and P. Hawkins, The Institution of Mechanical Engineers, advance copy (no number), February 1, 1954.

6 "Present Trends in Surge Tank Design," by Charles Jaeger, Proceedings of The Institution of Mechanical Engineers, vol. 168, no. 2, 1954, pp. 91–124.

7 "Théorie générale du coup de Bélier," by Charles Jaeger, Dunod, Paris, France, 1933, 268 pages.

8 "Theory of Resonance in Pressure Conduits," by Charles Jaeger, Trans. ASME, vol. 61, 1939, pp. 109–115.
9 "Stability of Restricted Orifice Tanks," by L. Escande, *Water Power*, vol. 4, 1952, p. 221.
10 "Surge Tank Stability," by Charles Jaeger, *Water Power*, vol. 4, 1952, p. 334.

M. G. SALZMAN.[10] Surge tanks have been designed for many years on the basis of well-known principles. It is in the application of these principles to actual layouts that simplifying assumptions are necessary to avoid an inordinate amount of computational work. In view of these assumptions and the importance of surge tanks in terms of plant operation and cost, it is surprising how little verification has been made of their actual behavior to that determined by calculation. The authors in presenting their paper have made a valuable contribution in a field where there is a paucity of confirming data.

In the proper design of differential surge tanks, one of the most important considerations is the value of the port coefficient. Usually, analyses are made by assuming various net port areas and adopting that area which gives the best over-all surge-tank performance. This is fine from a theoretical standpoint, but in converting from the net port area of the analysis to the gross port area of the actual surge tank, it is necessary to assume or determine theoretically a port coefficient. In some installations, the difference between actual and assumed port coefficients may cause a wide divergence between calculated and actual surge-tank hydraulic behavior. The authors have shown the comparative effect of two port areas in their Fig. 25. In many designs, this uncertainty about port coefficients has been resolved by means of model studies. While such a method is an excellent solution to the problem, nevertheless it would be extremely desirable to learn the port coefficients of prototype installations to confirm their actual value. At the Aguasabon Generating Station, data are presently available to evaluate the actual port coefficients (load-on and load-off conditions). Perhaps the authors have already determined these. If so, such data added to the information already furnished would be desirable.

The authors' comments on the effects of penstock water hammer on surge-tank behavior are very interesting and confirm what the writer's organization has discovered as a result of many surge-tank analyses. The practice, therefore, is to determine first, surge tank-dimensions and hydraulic characteristics by formulas and experience curves and then check the design by means of step-by-step computations. Simultaneously, a water-hammer analysis of the penstock is made so that mutual effects are incorporated into the analysis. In this way a more correct analysis of the hydraulic system is developed.

It should be mentioned that in certain cases, usually where governor timing is relatively long, it may be necessary to use turbine characteristics including speed rise during shutdowns rather than wicket-gate characteristics as the downstream control in the penstock water-hammer analysis. In these cases the control inevitably shifts from turbine control to gate control. This is mentioned because this speed-rise characteristic sometimes results in higher calculated water-hammer pressures than application of gate movement alone and should not be overlooked in the analytical investigation of the surge tank and/or the penstock.

The authors are to be complimented for the simple and clear manner in which they have presented a complicated problem.

E. B. STROWGER.[11] There have been very few reports on tests covering water hammer on complex installations including surge tanks, and the present paper therefore is timely. It also answers several questions which have been in need of investigation. The writer was particularly pleased to see the authors' results regarding the effect of an error in assuming the value of wave velocity shown by Fig. 22, which supports the following statement published by the writer in connection with the extended Allievi chart in Creager and Justin's "Hydroelectric Handbook" (page 717):

"It should be noted that 'a' appears in the expression for each coordinate of the Allievi chart and that θ and ρ each vary directly with 'a'. Since for all values of θ greater than about 5, the lines on the chart for equal pressure rise are approximately straight, and when extended very nearly pass through the zero of coordinates, it is evident that, for problems involving more than about 5 intervals, a considerable error can be made in the value of 'a' without affecting the result appreciably."

It might be of interest to check the experimental surge curve in Fig. 24 by comparing the total foot-seconds of momentum in the conduit before closure with the area in foot-seconds in the surge diagram. For this purpose the area of the diagram would be determined by the riser level, the line representing the gradient of the water in the conduit at the tank and the vertical line representing the time when the conduit velocity becomes zero. From the data given by the authors, the momentum in the conduit to the surge tank when the total station load is 46,300 kw is

$$\frac{LV}{g} = \frac{3400 \times 11.9}{32.2} = 1255 \text{ ft sec}$$

where

$$V = \frac{2102}{177} = 11.9 \text{ fps}$$

The time when the energy gradient as recorded by the riser level begins to take the form of a damped harmonic curve, i.e., at the point where the velocity of the conduit becomes zero, is estimated from Fig. 24 at 35 sec. The area in the diagram above the initial level out to $t = 35$ is 1450 ft sec. The ft sec of impulse due to the recovery of friction and velocity head included in this area is $\frac{2}{3} \times 10 \times 35 = 234$. The net diagram area is $1450 - 234 = 1216$ ft sec which represents the impulse used to destroy the initial momentum of 1255 ft sec. The diagram, therefore, seems to check the theoretical amount within about 3 per cent.

There do not seem to be many data published on the coefficient of discharge for the ports of a differential tank. It would be of interest to know the shape of ports and corresponding discharge coefficient for the Aguasabon tank.

AUTHORS' CLOSURE

The authors thank the discussers for contributing, from their own experience, additional information on surge-tank analysis.

Messrs. F. E. Cornwell and Ben Donsky comment that too much space has been devoted to the instrumentation and testing aspect of the investigation. The authors dealt with this part of the work in some detail because so little such information has been published previously. Messrs. Cornwell and Donsky have expressed a preference for the graphical method and emphasize its versatility. Since the basic relationships underlying the graphical and analytical calculations are identical, the solutions are equivalent. The choice of method is then a simple one of deciding on the degree of approximation acceptable, then using the most economical procedure. An element favoring electronic computer methods is the preference of engineers for creative work rather than routine tedious computation, graphical or numerical. In the examples used by the authors, the revisions required in

[10] Hydraulic Engineer, Ebasco Services, Inc., New York, N. Y.
[11] Chief Hydraulic Engineer, Niagara Mohawk Power Corporation, Buffalo, N. Y. Mem. ASME.

adapting the method to the digital computer refer only to the process of setting up the problem in a form suitable for manipulation by the computer. The results were identical with those obtainable manually.

Water-hammer effects were included in the surge calculations as follows: The calculated water-hammer pressure at the gates was added to the head at the gates (i.e., level in the riser less friction loss.) This combined value of head was then used to calculate the discharge through the gates for the interval considered. The calculated water-hammer pressure at the riser junction was added to the retarding head at the junction, and the combined value of retarding head thus obtained was used to calculate the change in velocity for the interval considered. Since water hammer results in a more rapid retardation of flow in the conduit, and also increases the discharge, it seems reasonable that surge tanks designed with this in mind could possibly be smaller than tanks not so designed. Further, it seems feasible that in some designs slower gate closure, producing little water hammer with its accompanying retarding effect, could result in the need for a larger surge tank. Detailed calculations are of course needed to confirm this matter.

Messrs. Cornwell and Donsky have also proposed an approximately equivalent computational model of the Aguasabon installation which they claim is simpler and more accurate. They have also mentioned additional factors which can be included to make the analysis more precise and stress that the wave velocity is of secondary importance. It will be noted that using their simplified computational model, they have calculated a water-hammer pressure of 35 psi for rejecting 46,300 kw in 5.1 sec, and have compared this, incorrectly, with the measured test pressure of 38 psi given in Table 2. The latter value, however, represents the maximum pressure change during the test and includes changes in friction loss, changes in riser level and water-hammer pressure. In Fig. 17 of our paper we gave the water-hammer pressure figures calculated as outlined under the heading Theoretical Analysis of Water Hammer in System, and for comparison we showed the corresponding water-hammer pressure obtained from the pressure rise measured at the scroll-case entry. The pressure rise measured at the scroll-case entry was the water-hammer pressure at the scroll case plus the increase in riser pressure plus the change in friction head between the riser and the scroll case due to the change in flow rate. The pressure rise at the scroll case is given in Table 2 as 38 psi. The oscillograph record shows that the increase in the riser pressure at the same instant was 6 psi. The change in friction head was 4 psi, determined from a series of tests made on the plant to measure the various friction losses for different flow rates. The water-hammer pressure based entirely on experimental data was therefore $38 - (6 + 4)$ psi $= 28$ psi which agrees very closely with our calculated value. The discussers' calculated value neglecting friction and increase in riser level is thus in error by 25 per cent. It would have been interesting if Messrs. Cornwell and Donsky had carried out a complete graphical analysis to permit a comparison of the times required for different methods of solution. The question of the importance of wave velocity was covered in the paper.

Dr. Charles Jaeger's references, both to his own work and that of others, will be found extremely useful to readers wishing to obtain a comprehensive and up-to-date picture of the state of surge-tank analysis. With regard to the method of changing load during the Aguasabon G. S. tests, it should be noted that the governor was operative during the tests but the speed-sensitive components were, in effect, rendered inoperative since the turbine output was controlled with the load-limit device on the Woodward type "A" actuator. Thus "hand-operation" refers to the method of setting the governor mechanism in motion either to

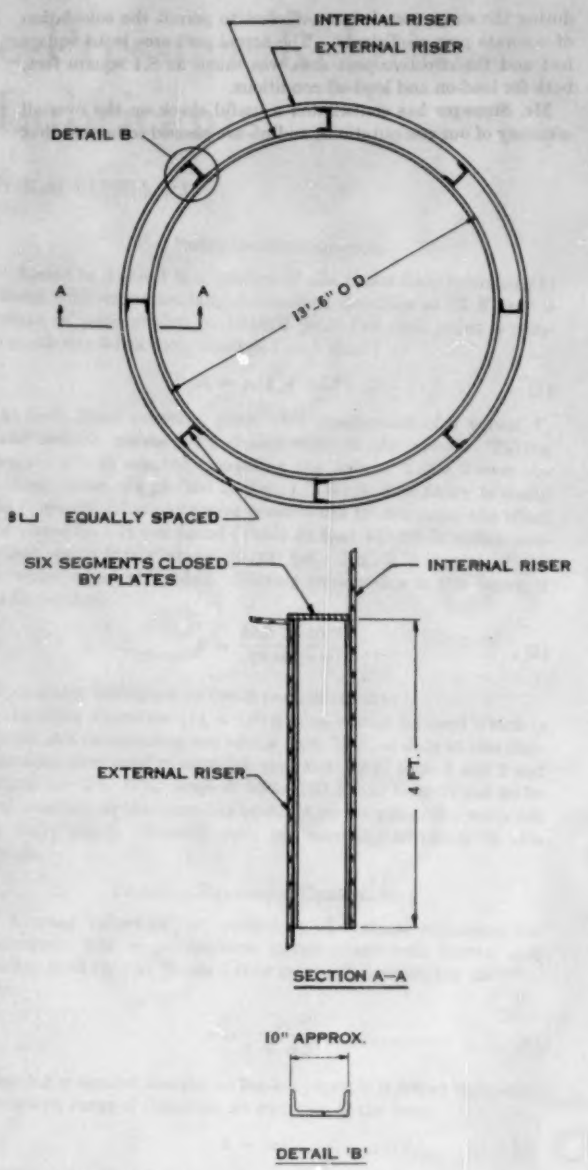

FIG. 27 SURGE-TANK PORT DETAILS
(Six annular segments were closed off and two were left open in the completed structure.)

reject or accept load. The rate of closure was entirely determined by the governor mechanism and its setting. Dr. Jaeger has calculated that the area of the main tank is approximately that given by the formula of Thoma, with a "safety factor" of 1. Using the Thoma criterion, our own calculations show that the tank diameter is about 25 per cent larger than the minimum permissible for stability. As this is in accordance with recommended practice based on past experience (reference 9 in the paper, page 116), the tank is conventional rather than marginal.

Mr. Salzman's question on the effective port area is a pertinent one. Unfortunately, the precision of the measurements recorded

during the surge tests is not sufficient to permit the calculation of accurate port coefficients. The actual port area is 9.4 square feet and the effective port area was taken as 8.4 square feet, both for load-on and load-off conditions.

Mr. Strowger has contributed a useful check on the over-all accuracy of our computations, and we are pleased to be told that the comparison of momentum of the water in the conduit is closely equivalent to the impulse represented by the experimental surge curve. The theoretical surge curve would give similar results.

As noted above, the measurements made did not permit us to obtain a reliable coefficient of discharge. Fig. 27 has been added to show the shape and dimensions of the ports.

Density-Temperature-Pressure Relations for Liquid Lubricants

By H. A. HARTUNG,[1] PHILADELPHIA, PA.

Recently published data on the density of lubricating fluids have been treated to separate the effects of temperature and pressure. Correlations are developed which reproduce the original data within less than 1 per cent in most cases for petroleum fractions, pure hydrocarbons, polymer blended oils, and commercial lubricants. It is expected that the relations found will apply to all liquid lubricants which are principally petroleum hydrocarbons. Density at any temperature up to 425 F and at pressures up to 80,000 psi can be found from the density at room temperature and atmospheric pressure and the viscosity at 100 F.

Nomenclature

The following nomenclature is used in the paper:

ρ = density, g/cc, at temperature t and pressure P
ρ_0 = density, g/cc, at room temperature, atmospheric pressure
ρ_1 = density, g/cc, at room temperature, pressure P
t = temperature at which density ρ is desired, deg F
t_0 = temperature at which ρ_0 is known (50 to 100 F)
$\Delta t = t - t_0$, deg F
P = pressure at which density ρ is desired, psia
P_0 = atmospheric pressure
$\Delta P = P - P_0$
V = viscosity, centistokes, at 100 F
$b = \frac{1}{\rho}\frac{\Delta\rho}{\Delta P}$, incremental compressibility
$\alpha = \frac{1}{\rho}\frac{\Delta\rho}{\Delta t}$, incremental coefficient of thermal expansion
$k = \alpha\rho^2$
v = volume

Introduction

Extensive data on the density of a number of liquid lubricants at various temperatures and pressures have recently been reported (1).[2] The present work seeks to enhance the utility of these data by suitable correlation.

Starting with the density ρ_0, at room temperature t_0, and atmospheric pressure P_0, and the viscosity V, at 100 F, a correction for the effect of pressure is made, giving density ρ_1, at room temperature and the desired pressure P. The effect of temperature is then taken into account, giving the density ρ, at the desired temperature t, and pressure P. Equations fitted to the various correlation plots have been combined into a single equation, permitting direct calculation of the density.

[1] The Atlantic Refining Company.

[2] Numbers in parentheses refer to the Bibliography at the end of the paper.

Contributed by the Research Committee on Lubrication under the auspices of the Lubrication Activity of The American Society of Mechanical Engineers, and presented at the Second Annual ASME-ASLE Lubrication Conference, Indianapolis, Ind., October 10–12, 1955.

Note: Statements and opinions advanced in papers are to be understood as individual expressions of their authors and not those of the Society. Manuscript received at ASME Headquarters, July 20, 1955. Paper No. 55—LUB-7.

Pressure Correlation

Listed in Table 1 is a number of oils taken from reference (1) along with experimentally determined densities at 77 F over a range of pressures up to 100,000 psi. For each point a compressibility b has been calculated such that

$$\rho_1 = \rho_0(1 + b\Delta P) \quad [1]$$

At each listed pressure, plots were constructed of b versus V, and smooth curves were drawn through the points. Taking values of b at selected viscosities, the data of Table 2 were obtained; these are plotted in Fig. 1. While this figure is useful as it stands, cross plots were constructed to determine the effect of viscosity. It was found (Table 3) that $bV^{0.333}$ is rather constant, particularly above 10,000 psi. Fig. 2 is a plot of the average values of Table 3. Fitting an equation to this curve, it is found that

$$b = \frac{42.8 \times 10^{-6}}{V^{0.333}P^{0.25}} \quad [2]$$

from about 10,000 psi up (solid portion of curve).

In using Equation [1], a value of ρ_0 should be used which is taken at a temperature not too far from 77 F, as data at this temperature were used to establish the relations of Figs. 1 and 2 and Equation [2]. The range of 50 to 100 F has been found to be satisfactory, as the temperature effect on the pressure correlation is fairly small. Density data are normally available in this range.

Thermal-Expansion Correlation

Average values of the coefficient of thermal expansion for petroleum oils at atmospheric pressure are well known and widely used (2, 3). Table 4 lists values of α satisfying the relation

$$\rho = \frac{\rho_1}{1 + \alpha\Delta t} \quad [3]$$

Plotting α against density on log-log paper, it is found that, over the whole range of densities, an equation of the form

$$k = \alpha\rho^2 \quad [4]$$

applies, where $k = 3.43 \times 10^{-4}$. A slightly better fit is obtained in the lubricating-oil range from

$$k = \alpha\rho^{1.5} = 3.60 \times 10^{-4} \quad [5]$$

However, computation would be somewhat more difficult, the added accuracy would be small, and the relation would be seriously in error for light hydrocarbon liquids. Table 5 and Fig. 3 show values of k to be used in the equation

$$\rho = \frac{\rho_1}{1 + k\frac{\Delta t}{\rho_1^2}} \quad [6]$$

Table 6 shows the results of some check calculations on a number of oils of different types. Agreement is quite good, with the possible exception of oil 36-G. This oil showed the greatest

TABLE 1 COMPRESSIBILITY OF OILS AT 77 F

Oil	ρ_0, g/cc	ρ @ 10,000 psi, g/cc	$b \times 10^6$ [b]	ρ @ 20,000 psi, g/cc	$b \times 10^6$	ρ @ 30,000 psi, g/cc	$b \times 10^6$	ρ @ 40,000 psi, g/cc	$b \times 10^6$	ρ @ 50,000 psi, g/cc	$b \times 10^6$	ρ @ 60,000 psi, g/cc	$b \times 10^6$	ρ @ 80,000 psi, g/cc	$b \times 10^6$	ρ @ 100,000 psi, g/cc	$b \times 10^6$	Vis @ 100 F, CS
S[a] 1-A	0.913	0.947	3.72	0.974	3.34	0.995	2.99	1.015	2.79	1.030	2.56	1.044	2.39	1.069	2.13	1.093	1.97	12.61
13-D	0.887	0.917	3.38	0.937	2.82	...		...		...		...		...		...		352.6
15-D	0.875	0.907	3.66	0.929	3.09	...		...		...		...		...		...		102.5
17-D	0.868	0.902	3.92	0.926	3.34	0.948	3.07	0.965	2.79	0.979	2.56	0.993	2.41	1.017	2.15	...		10.32
23-D	0.856	0.890	3.97	0.915	3.41	0.937	3.15	0.954	2.87	0.969	2.64	0.982	2.45	1.006	2.19	1.026	1.99	4.61
24-E	0.864	0.896	3.70	0.920	3.24	0.940	2.93	0.956	2.66	...		...		...		...		33.1
25-E	0.872	0.906	3.90	0.932	3.44	0.953	3.09	0.971	2.83	0.985	2.59	0.999	2.43	1.024	2.18	...		8.75
26-E	0.881	0.916	3.97	0.940	3.35	0.962	3.07	0.978	2.75	0.994	2.57	1.008	2.41	1.033	2.16	...		33.0
27-E	0.877	0.910	3.76	0.935	3.31	0.955	2.97	0.973	2.74	0.988	2.53	1.002	2.38	...		...		33.3
30-F	0.878	0.909	3.53	0.932	3.08	0.950	2.73	0.967	2.53	...		...		...		...		115.8
31-G	0.875	0.908	3.77	0.930	3.15	0.949	2.82	0.967	2.63	0.981	2.43	...		...		...		55.3
32-G	0.880	0.911	3.53	0.933	3.01	0.952	2.73	0.968	2.50	0.983	2.34	...		...		...		105.3
33-G	0.899	0.929	3.34	0.951	2.89	0.971	2.67	...		...		...		...		...		586.1
34-G	0.878	0.909	3.53	0.932	3.07	0.952	2.81	0.968	2.53	0.982	2.37	...		...		...		177.2
35-G	0.886	0.916	3.39	0.938	2.93	0.958	2.71	0.974	2.48	0.988	2.30	...		...		...		155.0
36-G	0.911	0.942	3.40	0.964	2.91	0.984	2.67	1.001	2.44	...		...		...		...		55.1
37-G	0.922	0.952	3.25	0.976	2.93	0.997	2.71	...		...		...		...		...		143.1
38-G	0.940	0.970	3.19	0.992	2.77	...		...		...		...		...		...		514.3
39-G	0.930	0.960	3.23	0.983	2.85	1.003	2.62	...		...		...		...		...		146.9
40-G	0.928	0.958	3.23	0.982	2.91	1.001	2.62	...		...		...		...		...		142.3
41-G	0.876	0.907	3.54	0.929	3.03	0.949	2.78	0.963	2.49	0.979	2.35	...		...		...		150.9
42-G	0.887	0.918	3.50	0.942	3.10	...		...		...		...		...		...		73.1
45-G	0.880	0.912	3.64	0.934	3.07	0.953	2.77	0.971	2.59	...		...		...		...		153.3
S 46-G	0.838	0.871	3.94	0.895	3.40	0.914	3.02	0.931	2.77	...		...		...		...		53.3
S 47-G	0.843	0.875	3.80	0.898	3.32	0.918	2.97	...		...		...		...		...		150.5
S 48-G	0.854	0.887	3.86	0.909	3.22	...		...		...		...		...		...		536.1
49-G	0.873	0.905	3.67	...		...		...		...		...		...		...		53.1
52-G	0.980	1.009	2.96	...		...		...		...		...		...		...		536.7
S 53-H	1.070	1.111	3.83	1.140	3.27	1.164	2.93	1.184	2.57	...		...		...		...		116
S 54-H	1.952	2.032	4.09	2.090	3.53	...		...		...		...		...		...		86.9
S 55-H	0.970	1.030	6.18	1.069	5.11	1.100	4.47	1.125	4.00	1.147	3.65	1.165	3.35	1.200	2.97	...		70
S 56-H	0.980	1.017	3.76	1.042	3.17	1.063	2.83	1.082	2.60	1.098	2.41	1.112	2.25	1.138	2.02	..		30.1

[a] *S* = synthetics.

[b] Defined by $\rho = \rho_0(1 + b\Delta P)$.

Source of density data: ASME Pressure Viscosity Report, ASME, NYC, 1954.

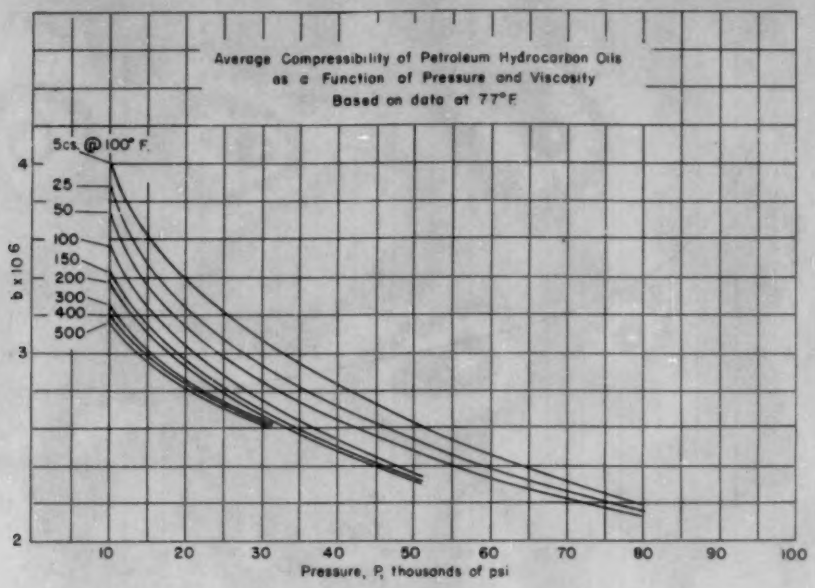

FIG. 1

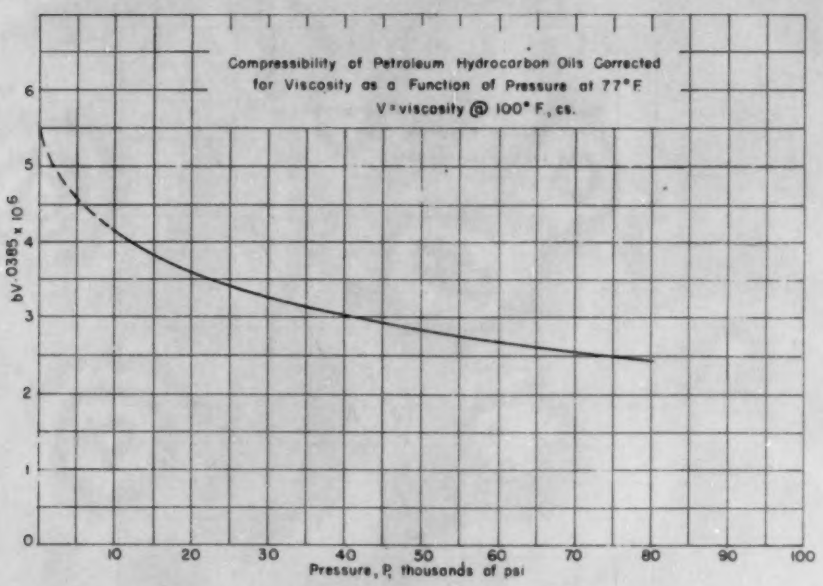

FIG. 2

TABLE 2 COMPRESSIBILITY OF OILS AT 77 F AS FUNCTION OF VISCOSITY AND PRESSURE

Vis at 100 F, CS	Value of $b \times 10^6$ at pressure P in 10^3 psi						
	10	20	30	40	50	60	80
5.....	4.00	3.42	3.15	2.87	2.64	2.45	2.19
25.....	3.87	3.26	2.97	2.72	2.53	2.40	2.15
50.....	3.75	3.16	2.86	2.64	2.46	2.39	2.13
100.....	3.56	3.04	2.75	2.56	2.38		
150.....	3.44	2.96	2.70	2.52	2.35		
200.....	3.36	2.92	2.67	2.50	2.32		
300.....	3.27	2.87	2.65				
400.....	3.21	2.84	2.64				
500.....	3.16	2.83	2.63				

TABLE 3 COMPRESSIBILITY OF OILS AT 77 F AS FUNCTION OF VISCOSITY AND PRESSURE

Vis at 100 F, CS	Value of $bV^{0.385} \times 10^6$ at pressure P in 10^3 psi						
	10	20	30	40	50	60	80
5.....	4.27	3.65	3.36	3.06	2.81	2.61	2.34
25.....	4.37	3.69	3.36	3.07	2.86	2.71	2.43
50.....	4.36	3.67	3.32	3.07	2.85	2.77	2.47
100.....	4.27	3.64	3.29	3.06	2.85		
150.....	4.17	3.59	3.27	3.05	2.85		
200.....	4.14	3.60	3.29	3.08	2.86		
300.....	4.09	3.59	3.32				
400.....	4.05	3.58	3.33				
500.....	4.02	3.60	3.34				
Average...	4.19	3.62	3.32	3.07	2.85	2.70	2.41

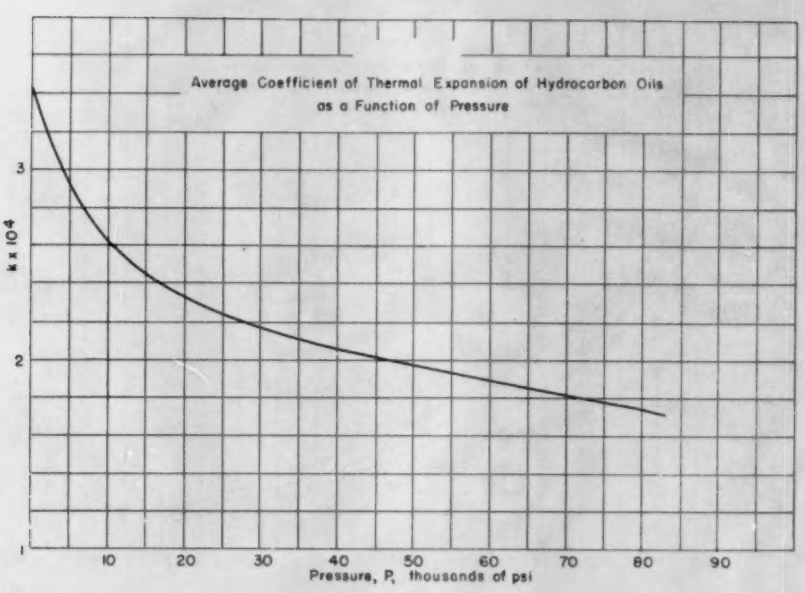
Average Coefficient of Thermal Expansion of Hydrocarbon Oils
as a Function of Pressure
k x 10⁴
3
2
1
10
20
30
40
50
60
70
80
90
Pressure, P, thousands of psi

FIG. 3

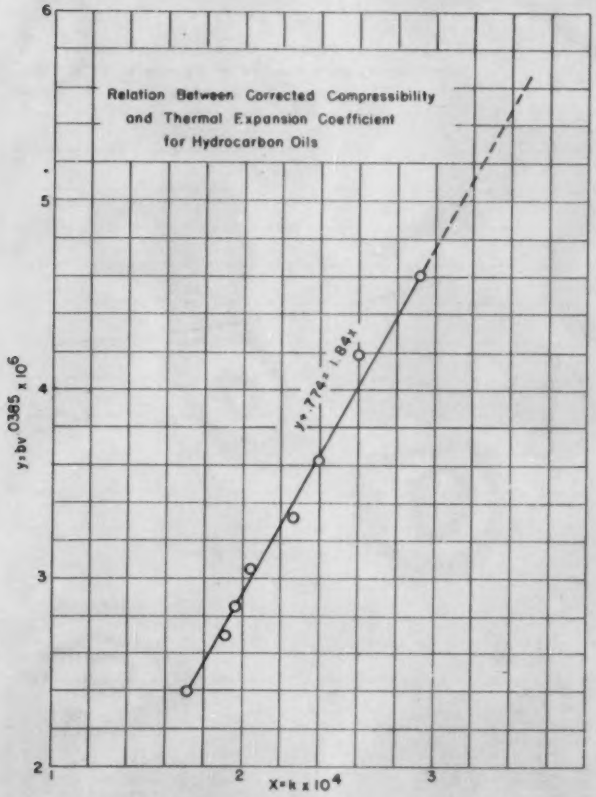
Relation Between Corrected Compressibility
and Thermal Expansion Coefficient
for Hydrocarbon Oils
y = bv 0385 x 10⁶
6
5
4
3
2
1
2
3
X = k x 10⁴
y = 774 x - 1.841

FIG. 4

TABLE 4 COEFFICIENT OF THERMAL EXPANSION OF LIQUID HYDROCARBONS AT ATMOSPHERIC PRESSURE

α^a	Gravity, deg API	Sp gr 60/60 F, ρ_0	$\frac{1}{\rho_0^2}$	$k = \alpha\rho_0^2$	$k = \alpha\rho_0^{1.8}$
3.5×10^{-4}	6	1.0291	0.940	3.72×10^{-4}	3.65×10^{-4}
4	22	0.9218	1.176	3.40	3.55
5	44	0.8063	1.532	3.26	3.62
6	58	0.7467	1.784	3.36	3.86
7	72	0.6953	2.06	3.40	4.05
8	86	0.6506	2.35	3.40	4.19
8.5	91	0.6306	2.47	3.44	4.25
9	97	0.6193	2.59	3.47	4.37

[a] Defined by $v = v_0(1 + \alpha t)$ or $\rho = \frac{\rho_0}{1 + \alpha\Delta t}$

[b] For the purpose of this correlation, ρ = sp gr 60/60 F.

Using Equations [1], [2], [6], and [7], it is possible to calculate ρ without the use of any of the plots

$$\rho = \frac{\rho_0\left(1 + \frac{42.8 \times 10^{-6}\,\Delta P}{P^{0.25}\,V^{0.0325}}\right)}{1 + \frac{\left(\frac{23.2}{P^{0.25}} + 0.421\right)10^{-4}\,\Delta t}{\rho_0^2\left(1 + \frac{42.8 \times 10^{-6}\Delta P}{P^{0.25}\,V^{0.0325}}\right)^2}} \quad (P \geq 10{,}000) \ldots [8]$$

TABLE 5 THERMAL EXPANSION OF OILS AT VARIOUS PRESSURES

Oil	$k^a \times 10^4$ @ various pressures, 77 to 425 F except as noted: Atmospheric	5000 psi	10,000 psi	20,000 psi	40,000 psi	60,000 psi	80,000 psi
8-C				2.34[c]			1.58[d]
9-C					1.93[c]		
10-C							1.79[d]
17-D						1.90	1.78[b]
23-D						1.96	1.72
24-E		2.88	2.60				
25-E						1.96	1.78
26-E						1.93	
31-G	3.45	2.98		2.36			
32-G						1.78[b]	
35-G					2.10		
36-G					2.10		
38-G	3.56			2.46		1.86[d]	
Average	3.50	2.93	2.60	2.39	2.05	1.90	1.73

[a] Defined by $\rho = \frac{\rho_1}{1 + \frac{k\Delta t}{\rho_1^2}} = \frac{\rho_1^3}{\rho_1^2 + k\Delta t}$

[b] Temperature range, 68–400 F.
[b] Temperature range, 100–425 F.
[c] Temperature range, 100–400 F.
[d] Temperature range, 210–425 F.
[e] Temperature range, 210–400 F.

TABLE 6 COMPARISON OF CALCULATED AND OBSERVED DENSITIES AT HIGH PRESSURE AND TEMPERATURE

Oil	Density @ 40,000 psi 210 F, g/cc: Calculated[a]	Observed	Density @ 80,000 psi 425 F, g/cc: Calculated[a]	Observed
9-C	0.867	0.867	0.801[b]	0.895[b]
12-C	0.928	0.928	0.957[b]	0.955[b]
15-D	0.935	0.938		
27-E	0.942	0.944	0.968	0.970
30-F	0.938	0.941		
34-G	0.937	0.941		
36-G	0.980	0.972	1.012	0.995
39-G	0.996	0.991		

[a] Using Figs. 2 and 3.
[b] 400 F.

divergence in all attempts at correlation. It is interesting to note that Dow and Fenske (4) found similar anomalies with two cuts (out of 34) prepared by vacuum fractionation of a petroleum oil.

Pressure-Temperature Correlation

One disadvantage of this method of correlation is the difficulty of obtaining values of b at atmospheric pressure. A plot of b versus k, Fig. 4, however, showed that these two quantities are related linearly by

$$10^4 k = \frac{10^6 b V^{0.0325} + 0.774}{1.84} = \frac{23.2}{P^{0.25}} + 0.421 \quad (P \geq 10{,}000) \ldots [7]$$

Extrapolating this line to the atmospheric value of k, a value for b can be read. The dotted section of Fig. 2 was obtained in this way. As a check on this section of Fig. 2, it was used to reproduce some data given by Dow and Fenske (4). Table 7 shows the agreement obtained, which is quite satisfactory.

TABLE 7

P, psi	Measured relative volume @ 40 C[a]	Calculated relative volume	Per Cent Error
Atm	1.0000	...	
700	0.9967	0.9967	0
1400	0.9936	0.9937	0.01
3550	0.9847	0.9853	0.06
7100	0.9723	0.9733	0.1
10650	0.9615	0.9626	0.1
28360	0.9219	0.9231	0.1

[a] Dow and Fenske (4).

Synthetics. These correlations apply within about 1 to 2 per cent for the diesters and polybutenes listed in Table 1. Dow and Fink (5) report that animal and vegetable oils behave like hydrocarbons as far as density-temperature-pressure relations are concerned. The only serious deviations noted in this work occur with oil 54-H (fluorolube) where the temperature-density correlation is in error by as much as 15 per cent, and with oil 55-H (silicone), where the pressure-density correlation is off about 6 per cent.

Scope. With the exceptions noted herein, the correlations predict density of liquid lubricants over the range 0 to 80,000 psi, and from the freezing point to 425 F. The lubricants include petroleum fractions of many types, commercial lubricants, polymer blended oils, pure hydrocarbons, and certain synthetic and nonhydrocarbon materials (Table 8).

TABLE 8 LUBRICANT TYPES USED IN CORRELATION

Oil designation[a]	Type
8-C-12C	Pure hydrocarbons
1A, 19D, 56H	Synthetic-diester
53H, 55H	Synthetic-silicone
54H	Synthetic-fluorolube
46G-48G	Synthetic-polybutylene
26E, 27E, 44G, 45G, 50G, 51G	Polymer-blended petroleum fractions
13D, 15D, 17D, 21D, 23D, 28F-30F	Commercial petroleum lubricants[b]
24E, 31G-35G, 41G, 49G	Paraffinic petroleum fractions
25E, 36G-40G, 42G, 52G	Naphthenic petroleum fractions

[a] As given in reference (1).
[b] Probably all contain various additives.

The correlations do not predict solidification points of these materials, so that errors can be made in using these results if under the desired temperature and pressure the lubricant is solid.

While no checks have been made, it is believed that these correlations could be applied to lighter liquid hydrocarbons such as gasoline, diesel fuel, and so on.

BIBLIOGRAPHY

1 "Pressure-Viscosity Report," ASME, New York, N. Y., 1953.
2 Supplement to NBS Circular C-410, U. S. Government Printing Office, Washington, D. C., 1937.
3 ASTM-IP Petroleum Measurement Tables, American edition, ASTM, Philadelphia, Pa., 1952.

4 "Pressure-Volume-Temperature Relations for Fraction of an Oil," by R. B. Dow and M. R. Fenske, *Industrial and Engineering Chemistry*, vol. 27, 1935, pp. 165–168.

5 "Computation of Some Physical Properties of Lubricating Oils at High Temperatures—I Density," by R. B. Dow and C. E. Fink, *Journal of Applied Physics*, vol. 11, 1940, pp. 353–357.

Discussion

A. A. Bondi.[3] The usefulness of the data obtained by the ASME high-pressure project will be greatly enhanced by the development of correlations which permit the calculation of properties at high pressures from those at atmospheric pressure or from chemical-composition data. This paper constitutes, therefore, a most welcome beginning to what will probably become a long trail of investigations.

That it was possible to represent the density-pressure-temperature relations of all the petroleum fractions and synthetic hydrocarbons with an equation containing as property parameters only the atmospheric density and viscosity at their standard temperature is astounding. It would be interesting to know the average and the maximum deviations in $\Delta\rho$ for the extremes of the range, viz., 100,000 psi at 77 and at 425 F. For engineering calculations (e.g., plunger-pump efficiency, liquid-spring performance, etc.), one needs usually the change in density ($\Delta\rho$) rather than the absolute value of the density. A 1 per cent deviation in ρ may represent a 10 per cent deviation in $\Delta\rho$, if—as will often be the case—$\Delta\rho/\rho$ is of the order 0.1.

While an empirical correlation is usually considered satisfactory if it represents the data at hand, it is advantageous if one can understand its inherent limitations. Except for the relation $\alpha = k/\rho^n$ (Equation [4]), which can be derived from molecular theory, the writer fails to find anything resembling a known physical relationship in the correlations of the author. Particularly curious is the relation of compressibility to viscosity given in Equation [2]. If this were a general relation it would have to appear, regardless of the manner in which compressibility is expressed. Some time ago the writer tried to correlate the numerical constants obtained by Bradbury[4] for a somewhat different equation of state from that of the author, but on the same oils. Fig. 5 of this discussion gives the correlation between the bulk modulus (inverse of compressibility) at zero pressure with oil density. Two lines are obtained—completely independent of viscosity—one for the petroleum oils and one for the pure hydrocarbons. Specially narrow petroleum (or polybutene) fractions tend toward the line for pure hydrocarbons. This relation can be understood in terms of the geometrical additivity law for intermolecular forces.

The pressure coefficient n of the bulk modulus could not be correlated satisfactorily with any property. A trend of the point cloud with (log) viscosity (tried because of the author's work) can be observed, but the scatter of points did not justify the setting up of a correlation. Since three fourths of all points are within 5 per cent of the average value of n, the search for a correlation is probably not warranted by the experimental accuracy.[5] The temperature coefficient of m, in Fig. 6, herewith, shows a rather interesting trend with oil composition, being a function of the density and of the average ring content and type of the oils. The temperature coefficient of n could not be correlated with anything, as one might have expected from the scattering of n itself. Assuming an average value for it causes a maximum error of 5 to 6 per cent in $\Delta\rho$ for the maximum range of the experimental data, 400 F. Since the temperature coefficient c of density of petroleum oils (at atmospheric pressure) is a unique function of molecular weight, it appears that we can obtain all constants in Bradbury's equation of state

$$\frac{\rho_0^{25}}{\rho} = \frac{1}{1 - c\,\Delta T} - \frac{1}{n}\log\left(\frac{P}{m/n} + 1\right)$$

from a knowledge of the density, the molecular weight, and the refractive index of the oil (these three constants together permit calculation of the average hydrocarbon composition). The same should be possible for the constants of the Tait-type equation currently being used by Prof. Wayne Webb in the evaluation of the ASME and his own data.

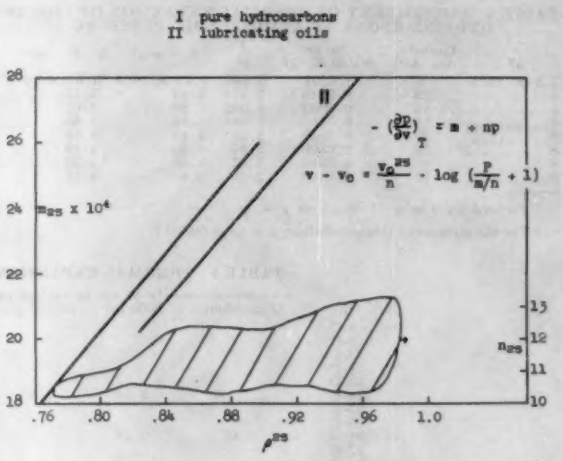

Fig. 5 Correlation of Bulk Modulus With Density ρ (at 25 Deg C)

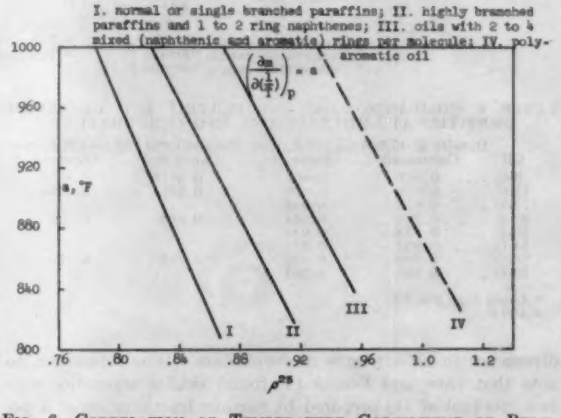

Fig. 6 Correlation of Temperature Coefficient of Bulk Modulus With Density and Composition of Lubricating Oils

Wayne Webb.[6] The author is to be congratulated on this correlation which extends greatly the usefulness of the extensive data of the ASME study as well as permitting predictions for materials not yet studied.

The relation between the thermal coefficient of expansion, the compressibility, and the viscosity is very interesting. That some

[3] Shell Development Company, Emeryville, Calif.

[4] DSc thesis, Harvard University (1950).

[5] The trend with viscosity is perhaps indicative of experimental difficulties.

[6] Professor, Pennsylvania State University, University Park, Pa.

such relationship existed should have been suspected because of the strong dependence of viscosity variation on the specific-volume variation. This dependence is so strong that it has misled some workers into thinking that keeping the specific volume constant would keep the viscosity constant. The fundamental reason for this should certainly be sought.

Since, as shown in the ASME report,[7] a Tait-type equation

$$\frac{V_0 - V}{V_0} = C \log (1 + P/B)$$

can be found that describes the specific volume rather accurately, is it possible to turn the correlation around and predict viscosities as a function of pressure instead of using atmospheric pressure viscosity and thermal coefficients to predict density? Such a correlation would be very useful.

Author's Closure

It certainly should be expected that the compressibility and coefficient of thermal expansion for hydrocarbons are governed by parameters describing molecular size and configuration. To a good approximation, viscosity and density together are such parameters. Undoubtedly, a more complex combination of properties might characterize a lubricant more precisely, leading to better correlation at the expense of more calculating effort.

Dr. Bondi's unsuccessful attempt to find a relation between compressibility and viscosity may be due to the kind of data he used. According to Bradbury, et al.,[8] the constants M and N were obtained as follows: The negative reciprocals of the slopes of the volume-pressure curves were plotted against pressure, the points falling on (apparently) straight lines. The general equation for these lines is that quoted by Dr. Bondi

$$-\left(\frac{\partial P}{\partial V}\right)_T = M + NP$$

The values for M and N are thus empirically derived from slope measurements. In this treatment of the basic data, the small dependence of compressibility on viscosity may be lost. It should be further pointed out that the pure hydrocarbons of reference (1) of the paper were not used in establishing this correlation. They fit it very well, however, Table 6. This is counter to Dr. Bondi's finding in Fig. 5 that pure hydrocarbons follow a different line than lubricating oils. Again, the relations may be confused by the method of handling the original data.

It is true that compressibility might better be represented as a function of viscosity and density together, but for the improved accuracy the increased complexity was thought to be not worth while.

As Dr. Bondi points out, change in density is more sensitive to error than density itself. For the petroleum hydrocarbons, oil 36-G showed by far the poorest fit:

	40000 psi, 210 F	80000 psi, 425 F
ρ	0.8 per cent error	1.7 per cent
$\Delta\rho/\rho_0$	13 per cent	18 per cent

For all other materials, except synthetics, maximum errors are about 40 per cent of the values given here.

Professor Webb raises an interesting question concerning the prediction of viscosity. The present correlation cannot do this, as the viscosity used here is the atmospheric pressure value. However, the idea merits further study, as density measurements at high pressure are much easier to make than viscosity measurements.

The author wishes to thank the discussers for contributing their efforts toward a better understanding of this problem.

[7] Reference (1) of the Bibliography of the paper.

[8] "Viscosity and Density of Lubricating Oils From 0 to 150,000 Psig and 32 to 425 F," by D. Bradbury, M. Mark, and R. V. Kleinschmidt, Trans. ASME, vol. 73, 1951, pp. 667–676.

Finite Journal Bearings With Arbitrary Position of Source

By J. V. FEDOR,[1] SILVER SPRING, MD.

By using different mathematical methods, Muskat and Morgan's theory of force-feed lubrication (2, 3)[2] is put in a compact, convenient form. The first derivative is neglected in the solution of Reynolds homogeneous equation to gain mathematical simplicity for the pressure distribution. Sommerfeld boundary conditions are used and no restriction on length of bearing is made. Explicit equations are derived for the characteristics of finite journal-bearing systems. Values calculated compare with published results when the source is at the crown of the bearing. It is estimated that the solution will give satisfactory results for eccentricity ratios up to 0.4. For relatively short bearings the eccentricity ratio can be extended to higher values.

Introduction

FOR many years engineers have been plagued by the failure to obtain a satisfactory analytical solution of Reynolds differential equation as applied to full journal bearings. The familiar Reynolds equation is

$$\frac{\partial}{\partial\theta}\left(\frac{h^3}{\mu}\frac{\partial P}{\partial\theta}\right)+r^2\frac{\partial}{\partial z}\left(\frac{h^3}{\mu}\frac{\partial P}{\partial z}\right)=6Ur\frac{\partial h}{\partial\theta}$$

where

- P = pressure at any point in oil film above atmospheric pressure
- U = linear velocity of journal
- r = radius of journal
- c = difference between journal and bearing radii
- e = eccentricity of journal and bearing axis
- μ = viscosity of oil: constant
- h = oil-film thickness; $c(1+b\cos\theta)$
- b = eccentricity ratio; e/c
- θ = angular co-ordinate
- z = co-ordinate in axial direction

Solutions for the infinitely long bearing and the very short bearing have been developed. Results obtained, however, were inadequate to describe fully the characteristics of the finite journal bearing. Many attempts have been made to solve the finite journal-bearing problem with some measure of success. Most analytical solutions developed, though, were too complicated for the designer to apply. The crux of the problem centers around solving the homogeneous differential equation

$$\frac{\partial}{\partial\theta}\left(\frac{h^3}{\mu}\frac{\partial P}{\partial\theta}\right)+r^2\frac{\partial}{\partial z}\left(\frac{h^3}{\mu}\frac{\partial P}{\partial z}\right)=0$$

The method of separation of variable leads to the following form for the solution

$$P=X(\theta)Y(z)$$

where $X(\theta)$ and $Y(z)$ must satisfy the following ordinary differential equations, respectively

$$\frac{d^2X}{d\theta^2}-\frac{3b\sin\theta}{1+b\cos\theta}\frac{dX}{d\theta}+m^2X=0$$

$$\frac{d^2Y}{dz^2}-\left(\frac{m}{r}\right)^2Y=0$$

and m^2 is the separation of variable parameter. The equation for $Y(z)$ can easily be solved; the equation for $X(\theta)$ is the stumbling block. Since the coefficient of the first derivative is periodic, the differential equation is a form of the Hill equation. By making the substitution

$$1/b=\frac{1}{2}(a+a^{-1})$$

and using the expansion

$$\frac{-a^{-1}\sin\theta}{1+2a^{-1}\cos\theta+a^{-2}}=\sum_{1}^{\infty}(-a)^{-n}\sin n\theta=\sum_{\pm1}^{\infty\pm}A_ne^{in}$$

where

$$-A_{-n}=A_n=(-a)^{-n}/2i,\quad i=\sqrt{-1}$$

the equation for $X(\theta)$ becomes

$$\frac{d^2X}{d\theta^2}+6\sum_{\pm1}^{\pm\infty}A_ne^{in\theta}\frac{dX}{d\theta}+m^2X=0$$

The equation for $X(\theta)$ can be solved by taking the solution in the following form

$$X(\theta)=e^{k\theta}\sum_{-\infty}^{\infty}B_je^{ij\theta}$$

where the constants k and B_j are determined from the condition that the coefficients of the powers of the exponentials must vanish. In theory this is straightforward but actually to do this is quite tedious since the process leads to infinite determinants. By making the assumption that the first-derivative term can be neglected compared to the other terms in the solution of the homogeneous equation, great mathematical simplicity is obtained. Neglecting the first-derivative term in the homogeneous equation, in effect, is to consider the variation of film thickness small compared to the variation of the first derivative in the θ-direction. This assumption is certainly valid for small values of eccentricity ratio.[3] In design work exact analysis is frequently not necessary. Simple equations with a certain amount of validity are often more useful than complicated equations that result from exact analysis. It is the purpose of this paper to take into account the position of the

---

[1] Naval Ordnance Laboratory. Assoc. Mem. ASME.

[2] Numbers in parentheses refer to the Bibliography at the end of the paper.

Contributed by the Research Committee on Lubrication under the auspices of the Lubrication Activity of The American Society of Mechanical Engineers and presented at the Second Annual ASME–ASLE Lubrication Conference, Indianapolis, Ind., October 10–12, 1955.

Note: Statements and opinions advanced in papers are to be understood as individual expressions of their authors and not those of the Society. Manuscript received at ASME Headquarters, November 19, 1954. Paper No. 55—LUB-14.

[3] It is convenient to call the eccentricity ratio simply eccentricity.

source and develop simple equations and conditions useful as guides in the design of finite journal bearings.

Pressure Distribution

The pressure function will be determined first. Once the pressure distribution in the journal bearing is known, the other journal-bearing characteristics can be determined. The co-ordinate system shown in Fig. 1 will be used in this analysis. Symbols are

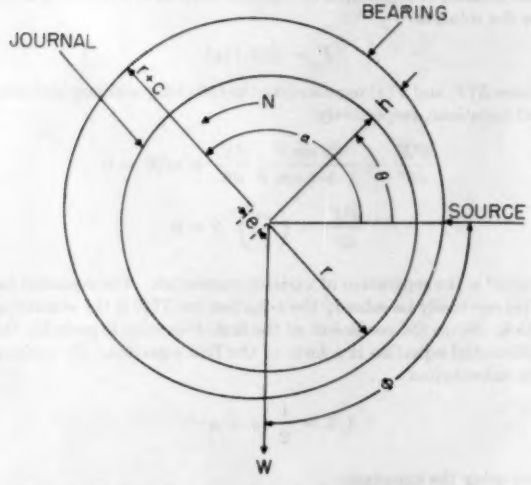

Fig. 1 Cross Section of a Journal-Bearing System

as previously defined. For the present co-ordinate system Reynolds equation is

$$\frac{\partial}{\partial\theta}\left\{\frac{[1+b\cos(\theta-\alpha)]^3}{\mu}\frac{\partial P}{\partial\theta}\right\} + r^2\frac{\partial}{\partial z}\left\{\frac{[1+b\cos(\theta-\alpha)]^3}{\mu}\frac{\partial P}{\partial z}\right\} = -\frac{6Urb}{c^2}\sin(\theta-\alpha) \quad [1]$$

where α is the arbitrary angular displacement of the line of centers from the source. The origin is located midway between the ends of the bearing.

The following boundary conditions will be imposed on the solution:

1 The pressure function and all of its derivatives must duplicate themselves in going completely around the bearing.

2 The pressure function must be axially symmetric with the origin and vanish at the ends of the bearing.

3 The pressure must have a discontinuity at $\theta = 0$, $z = 0$ (source).

4 As the length of the bearing becomes large, and as the source becomes small, the pressure should go over to the Sommerfeld pressure distribution.

The solution for the infinite bearing with the Sommerfeld boundary condition and constant viscosity is

$$P_\infty = \frac{6\mu Urb}{c^2(2+b^2)}\frac{[2+b\cos(\theta-\alpha)]}{[1+b\cos(\theta-\alpha)]^2}\sin(\theta-\alpha) \quad [2]$$

The Fourier series expansion for this function is

$$P_\infty = \frac{12\mu Ur}{c^2(2+b^2)}\sum_1^\infty (-)^{n-1}a^{-n}\left[1+\frac{n}{(1-b^2)^{1/2}}\right]\sin n(\theta-\alpha) \quad [3]$$

where

$$a^{-n} = \left(\frac{b}{1+(1-b^2)^{1/2}}\right)^n$$

Using the previously mentioned assumption, Reynolds homogeneous equation becomes

$$\frac{\partial^2 P}{\partial\theta^2} + r^2\frac{\partial^2 P}{\partial z^2} = 0 \quad [4]$$

The separation of variable solution of Equation [4] is

$$P_1 = \sum_1^\infty A_n' \sin n(\theta-\alpha)\cosh nz/r \quad [5]$$

To satisfy the condition that the pressure vanishes at the ends of the bearing we must have

$$A_n' = -B_n/\cosh n\beta \quad [6]$$

where

$$B_n = \frac{12\mu Ur(-)^{n-1}a^{-n}}{c^2(2+b^2)}\left[1+\frac{n}{(1-b^2)^{1/2}}\right]$$

and

$$\beta = l/2r$$

The pressure equation thus far is

$$P = P_\infty + P_1 \quad [7]$$

A fundamental element of a journal-bearing system is the source. If the source is not present the lubricant will be depleted between the journal and bearing by end leakage and the journal bearing will cease to operate effectively. The following equation will be taken as the source function

$$P_s = \sum_0^\infty C_n \cos n\theta\cosh nz/r - q\ln(\cosh z/r - \cos\theta) \quad [8]$$

This function has a discontinuity at $\theta = 0$, $z = 0$, and is symmetric in θ and z. Using the expansion

$$\ln(\cosh l/2r - \cos\theta) = \beta - \ln 2 - 2\sum_1^\infty \frac{e^{-n\beta}\cos}{n} n\theta$$

the C_n are determined from the condition that the pressure must vanish at the ends of the bearing. Hence

$$C_0 = q(\beta - \ln 2)$$

$$C_n = -2qe^{-n\beta}/n\cosh n\beta = -4q/n(1+e^{2n\beta}) \quad [9]$$

The total pressure equation is

$$P = P_\infty + P_1 + P_s \quad [10]$$

where P_∞, P_1, and P_s are as previously defined.

Journal-Bearing Properties

Proceeding to the journal-bearing characteristics, the load components are given by

$$P_y = 2\int_0^{l/2}\int_0^{2\pi} P\cos\theta r d\theta dz$$

$$P_x = 2\int_0^{l/2}\int_0^{2\pi} P\sin\theta r d\theta dz$$

where

P_p = load parallel to co-ordinate axis passing through source

P_n = load normal to the afore-mentioned axis

Since this is a simple integration, the end results will be given

$$P_p = -W_\infty \left(1 - \frac{\tanh}{\beta}\beta\right) \sin\alpha + 4\pi\bar{q}r^2[1 - e^{-\beta}(1 + \tanh\beta)] \quad [11a]$$

$$P_n = W_\infty \left(1 - \frac{\tanh}{\beta}\beta\right) \cos\alpha \quad [11b]$$

where

$$W_\infty = \frac{12\mu U r^2 b l\pi}{c^2(2 + b^2)(1 - b^2)^{1/2}}$$

At this point it is convenient to define the dimensionless source parameter $\bar{q}$ in the following manner

$$\bar{q} = qr^2/W$$

where W is the load-carrying capacity of the journal bearing. The total load of the journal bearing is given by

$$W = (P_n^2 + P_p^2)^{1/2} = W_\infty K \quad [12]$$

where W_∞ is the load-carrying capacity for the infinitely long bearing and K is given by

$$K = \left(1 - \frac{\tanh}{\beta}\beta\right)\left\{\frac{M\sin\alpha \pm [1 - M^2\cos^2\alpha]^{1/2}}{M^2 - 1}\right\}$$

$$M = 4\pi\bar{q}[1 - e^{-\beta}(1 + \tanh\beta)]$$

The minus sign is used when the source is at the upper portion of the bearing, while the plus sign is used when the source is at the base.

Let ϕ be the arbitrary but specified counterclockwise angle measured from the load vector to the source (c.f. Fig. 1). The equations of equilibrium give

$$-W\cos\phi + P_p = 0$$

$$W\sin\phi + P_n = 0$$

After making the required substitution it will be found that the position of the line of centers is given by

$$\tan\alpha = \frac{\cos\phi - M}{\sin\phi} \quad [13]$$

By an appropriate analysis it will be found that q and $\bar{q}$ are related to the flow Q of the source by

$$q = \frac{3\mu Q}{\pi c^3(1 + b\cos\alpha)^3} = \bar{q}W/r^2 \quad [14]$$

Since the flow entering is equal to the lubricant leaving the bearing, end leakage can be obtained from Equation [14].

Following Muskat and Morgan (2), the friction force acting on the journal-bearing system is given by

$$F = \frac{2\mu U r l\pi}{c(1 - b^2)^{1/2}} \pm \frac{cb}{2r}\{P_n\cos\alpha - P_p\sin\alpha\}$$

where the + sign applies to the journal while the — sign applies to the bearing. By some simple manipulation it will be found that

$$\frac{r}{c}f = \frac{2\pi^2 S}{(1 - b^2)^{1/2}} \pm \frac{b}{2}\left\{\frac{P_n}{W}\cos\alpha - \frac{P_P}{W}\sin\alpha\right\} \quad [15]$$

where

f = coefficient of friction; friction force divided by total load

S = Sommerfeld variable, $\mu N\left(\frac{r}{c}\right)^2 \Big/ W'$

N = rps

W' = load per unit projected bearing area

From Equation [12] it will be verified that the Sommerfeld variable is given by

$$S = S_\infty/K; \quad S_\infty = \frac{(2 + b^2)(1 - b^2)^{1/2}}{12\pi^2 b} \quad [16]$$

where S_∞ is the Sommerfeld variable for the infinitely long journal bearing and K is as previously defined.

The supply pressure is given essentially by

$$P_0 = P_\infty\Big|_{\theta=0} - \sum_1^\infty A_n' \sin n\alpha + \bar{q}\frac{W}{r^2}\left[\beta - 2\ln\rho - 4\sum_1^\infty \frac{1}{n(1 + e^{2n\beta})}\right] \quad [17]$$

where ρ is the radius of the source divided by the radius of the journal. The series converges rapidly and only a few terms are needed to determine the inlet pressure.

To insure that the journal bearing has a continuous oil film around the journal the condition must be imposed that the axial pressure gradient evaluated at the ends of the bearing be negative. This condition will prevent air from being sucked in and rupturing the oil film. The following inequality, which imposes a restriction on $\bar{q}$, must be satisfied to insure a continuous oil film.[4]

$$\frac{\partial P}{\partial z} = \frac{n}{r}\sum_1^\infty [-B_n\tanh n\beta\sin n(\theta - \alpha) + C_n\sinh n\beta\cos n\theta] - q/r\frac{\sinh\beta}{\cosh\beta - \cos\theta} < 0 \quad [18]$$

For small eccentricities and relatively long bearings, the restriction on $\bar{q}$ becomes

$$\bar{q} > \frac{1}{2\pi\beta K\left[2e^{-\beta}\sin\alpha + \frac{\cosh\beta}{\cosh\beta - \sin\alpha}\right]} \quad [19]$$

When ϕ, β, and $\bar{q}$ are specified, K and α are determined. If the foregoing inequality is satisfied, the pressure will be everywhere positive. The restriction on $\bar{q}$ implies that the pressure distribution due to the lubricant source has overcome the negative pressure due to the journal rotation. For small length-to-diameter ratios, Equation [19] will demand too large a value for $\bar{q}$. This is due to neglecting some of the pressure-gradient terms.

Discussion

The numerically simple case of the load along the axis passing through the source was chosen for computation and discussion. With the source at the crown or unloaded portion of the bearing, ϕ is equal to π (c.f. Fig. 1). From Equation [13] the position of the line of centers is found to be $\pi/2$ (the $3\pi/2$ value is superfluous). The load capacity is obtained from Equation [12]

$$W = \frac{W_\infty(1 - \tanh\beta/\beta)}{1 + 4\pi\bar{q}[1 - e^{-\beta}(1 + \tanh\beta)]} \quad [20]$$

[4] The equation, $\cos(\theta - \alpha) = -3b/2 + b^2$ can be used as a guide to determine the point where the greatest tendency for positive gradients occurs ($\pi < (\theta - \alpha) < 3\pi/2$).

The coefficient of friction is obtained from Equation [15]

$$\frac{r}{c}f = \frac{2\pi^2 S}{(1-b^2)^{1/2}} \pm \frac{b}{2} \quad \ldots\ldots\ldots\ldots [21]$$

For a specific journal-bearing application, values must be assigned to the various parameters to fix a design. Since it is intended to show some of the general features of force-feed lubrication and the limitation of the derivated equations, this will not be done.

A plot of $(r/c)f$ versus S for several values of the parameter K is shown in Fig. 2 when the source is at the crown of the bearing. It will be noticed that journal-friction curves plot above the Sommerfeld curve and approach it asymptotically for large values of the Sommerfeld variable. Curve IV is for the friction on the bearing.

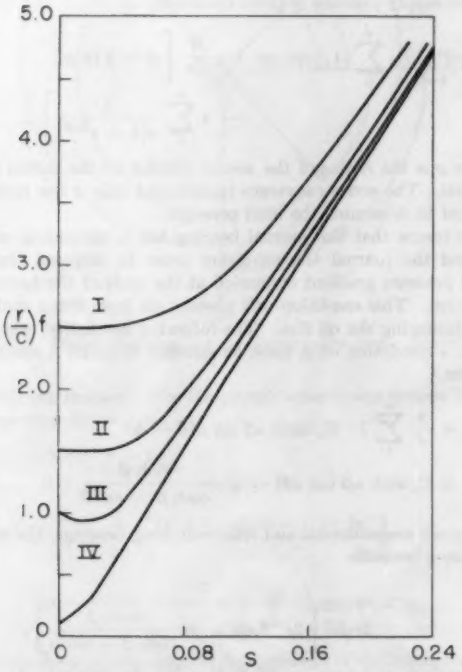

FIG. 2 COEFFICIENTS OF FRICTION f VERSUS S FOR JOURNAL BEARINGS OF FINITE LENGTH

($S = \mu N \left(\frac{r}{c}\right)^2 / W'$; $K = \frac{W}{W_\infty}$, where W is load-carrying capacity of the finite bearing and W_∞ is load-carrying capacity of infinitely long bearing. I: $K = 0.25$; II: $K = 0.50$; III: $K = 1.0$; IV: $K = 0.75$. Curves I and II are friction curves for journal. Curve III is for infinitely long journal. Curve IV is for bearing. All curves are for journal bearings fed with lubricant sources at crown of bearing.)

Fig. 3 depicts the general variation of the Sommerfeld variable for various values of the parameter K. The Sommerfeld variable for the finite bearing plots above the curve for the infinite bearing not only because of the loss of load due to the pressure falling to zero at the ends of the bearing, but also to the fact that the resultant force due to the pressure of the lubricant source is opposing the resultant force produced by the journal rotation.

Equation [13] shows that the value of the source parameter and the position of the source greatly affect the position of the line of centers and hence the behavior of the journal-bearing system. When the lubricant source is at the crown of the bearing, Equation [13] gives a fixed value of $\pi/2$ for α. This is certainly true for

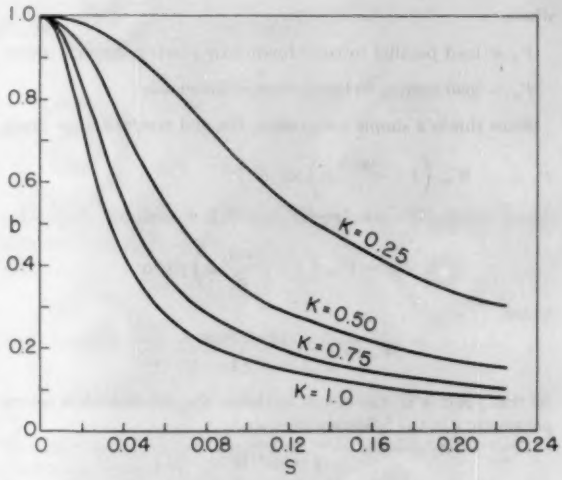

FIG. 3 THE VARIATION OF JOURNAL ECCENTRICITY b WITH THE SOMMERFELD VARIABLE S FOR FINITE JOURNAL BEARINGS WITH LUBRICANT SOURCE AT CROWN OF THE BEARING

($S = \mu N \left(\frac{r}{c}\right)^2 / W'$, where r = journal radius, c = radial clearance, μ = lubricant viscosity, N = journal speed, rps., and W' = bearing load per unit projected bearing area.)

small values of eccentricity. For large eccentricities the angle α will vary somewhat and be less than $\pi/2$. When the source is at the base of the bearing ($\phi = 0$), and $\bar{q}$ is less than the critical value of

$$1/4\pi[1 - e^{-\beta}(1 + \tanh \beta)]$$

Equation [13] gives a fixed value of $3\pi/2$. This narrow restriction can be removed by a slight artifice. Let $\phi = c/r = \lambda$ instead of zero. Replacing $\sin \lambda$ by λ, the position of the line of centers is then determined from

$$\tan \alpha = \frac{1 - M}{\lambda} \quad \ldots\ldots\ldots\ldots [22]$$

The angle α can now vary between $3\pi/2$ and π. The load capacity is obtained from Equation [12] with proper regard for sign. The coefficient of friction is given essentially by

$$\frac{r}{c}f = \frac{2\pi^2 S}{(1-b^2)^{1/2}} \mp \frac{b}{2}\sin \alpha \quad \ldots\ldots\ldots [23]$$

The same artifice can be used when $\bar{q}$ exceeds the critical value. Let $\phi = -\lambda$, Equation [13] becomes

$$\tan \alpha = \frac{M - 1}{\lambda} \quad \ldots\ldots\ldots\ldots [24]$$

The angle α is free to vary from zero to $\pi/2$. The load and coefficient of friction can be obtained from Equations [12] and [23]. What has been done, in effect, is to consider that the journal-bearing characteristics are essentially the same when the lubricant source is displaced slightly. This allows the range of the derived equations to be extended slightly. When $\bar{q}$ is equal to the critical value, the journal will be concentric with the bearing and the load is supported entirely by the source. The load capacity can be obtained from Equation [17] if the eccentricity is set equal to zero and the supply pressure is specified. The coefficient of friction is obtained from the Petroff line

$$\frac{r}{c}f = 2\pi^2 S \quad \ldots\ldots\ldots\ldots [25]$$

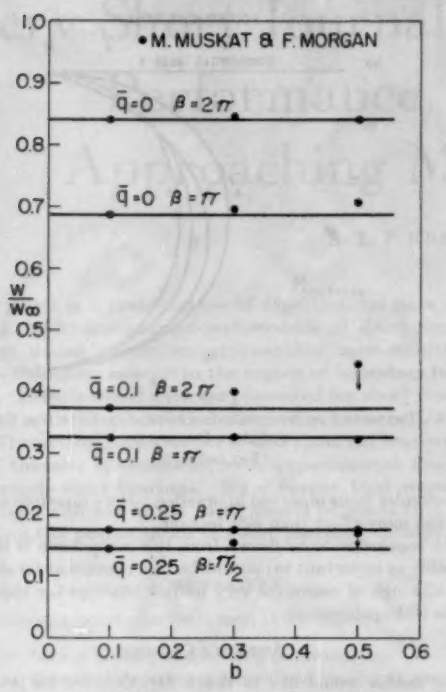

FIG. 4 CALCULATED VALUES OF RELATIVE LOAD-CARRYING CAPACITY, W/W_∞, VERSUS ECCENTRICITY b, ARE COMPARED WITH RESULTS OF M. MUSKAT AND F. MORGAN

(The solid line is the author's calculations. Lubricant source is at the crown of the bearing.)

It is believed that for most design work this analysis will be satisfactory for eccentricities equal to or less than 0.4 for all journal length-to-diameter ratios. Fig. 4 compares the results obtained from this solution with results published by F. Morgan and M. Muskat (3, 4) for relatively long bearings and eccentricities up to $^1/_2$.[8] It will be observed that there is good agreement in general for eccentricities up to 0.4. For short bearings the value of b can be extended since the end flow, that the present analysis fully includes, becomes more important than the flow in the θ-direction. Even if the equations were used for higher eccentricities for any length of bearing, the calculated properties would be on the safe side in design. It will be noticed from Fig. 4 that the load capacity predicted by the equations would be less than theoretically correct. Thus an inherent margin of safety is included in the analysis.

It is felt that the derived equations contain the essential features of the force-feed theory developed by M. Muskat and F. Morgan but obviates most of the tedious calculations necessary to apply the theory. The equations are simple and easily applied in the design of journal bearings using some form of force-feed system and operating in the thick-film region of lubrication.

ACKNOWLEDGMENT

The author is indebted to Millicent Fedor and Mr. S. Globe of the Naval Ordnance Laboratory for the preparation of the manuscript.

BIBLIOGRAPHY

1 "Fourier Series and Boundary Value Problems," by R. V. Churchill, McGraw-Hill Book Company, Inc., New York, N. Y., 1941.

2 "The Theory of the Thick-Film Lubrication of a Complete Journal Bearing of Finite Length," by F. Morgan and M. Muskat, *Journal of Applied Physics*, vol. 9, 1938, p. 393.

3 "The Theory of the Thick-Film Lubrication of a Complete Journal Bearing of Finite Length With Arbitrary Position of the Lubricant Source," by F. Morgan and M. Muskat, *Journal of Applied Physics*, vol. 10, 1939, p. 46.

4 "The Theory of the Thick-Film Lubrication of Flooded Journal Bearings and Bearings With Circumferential Grooves," by F. Morgan and M. Muskat, *Journal of Applied Physics*, vol. 10, 1939, p. 398.

5 "Lubrication," by A. E. Norton, McGraw-Hill Book Company, Inc., New York, N. Y., 1942.

6 "Analysis and Lubrication of Bearings," by M. C. Shaw and E. F. Macks, McGraw-Hill Book Company, Inc., New York, N. Y., 1949.

7 "Modern Analysis," by E. T. Whittaker and G. N. Watson, The Macmillan Company, New York, N. Y., 1945.

8 "The Hydrodynamic Lubrication of Cyclically Loaded Bearings," by E. M. Simons, Trans. ASME, vol. 72, 1950, pp. 805–816.

Discussion

J. A. COLE.[6] In the analysis, the author has found it necessary to assume a complete film. This is said to be valid for eccentricity ratios up to 0.4, the author stating at one point that the pressure distribution attributable to the lubricant source overcomes the negative pressure resulting from journal rotation. While this is theoretically possible, observations with transparent bearings (preliminarily reported upon by Cole and Hughes[7]) indicate that except with very light loads, film rupture is not prevented with feed pressures as high as 40 psi for bearings of standard clearance ratio (0.001) and oil admission via a single hole opposite the load, an axial groove, or a complete circumferential groove.

It is interesting to consider the relative importance of the corrections to the classical Sommerfeld solution (for an infinitely wide bearing with a complete 2π film) necessary to account for side leakage and for film rupture. This may be estimated roughly, for a bearing of width-diameter ratio unity, from Fig. 5, herewith. Here load capacity as a fraction of the Sommerfeld value

$$W_\infty = \frac{\mu U l r^2}{c^2} \frac{12\pi b}{(2 + b^2)\sqrt{1 - b^2}} \quad [26]$$

is plotted in terms of eccentricity ratio b.

Curve A shows the solution for an infinitely wide bearing with the load-carrying film extending from 0 to π only

$$W = \frac{\mu U l r^2}{c^2} \frac{6b\sqrt{\pi^2(1 - b^2) + 4b^2}}{(2 + b^2)(1 - b^2)} \quad [27]$$

while curve B shows the solution for an infinitely narrow bearing with the load-carrying film assumed to be complete (2π)

$$W = \frac{\mu U l r^2}{c^2} \left(\frac{l}{2r}\right)^2 \frac{2\pi b}{(1 - b^2)^{3/2}} \quad [28]$$

Curves A and B may be said to represent the separate effects of film rupture and side leakage, respectively, and it is reasonable to deduce that they are of the same order for unit width-diameter ratio.

It may be objected that the $0 - \pi$ film extent assumption for taking film rupture into account and the infinitely narrow bearing assumption for taking side leakage into account are very crude.

[8] Muskat and Morgan define $\bar{q}$ as $qr^2(1 + b\cos\alpha)^2/W$. Even if $\bar{q}$ were to be defined in this way the numerical results would not be changed since α is equal to $\pi/2$ for the case calculated.

[6] Department of Scientific and Industrial Research, Lubrication and Wear Division, Mechanical Engineering Research Laboratory, Thorntonhall, Glasgow, Scotland.

[7] "Oil-Film Extent in Complete Journal Bearings," by J. A. Cole and C. J. Hughes, *The Engineer*, vol. 199, 1955, pp. 555–557.

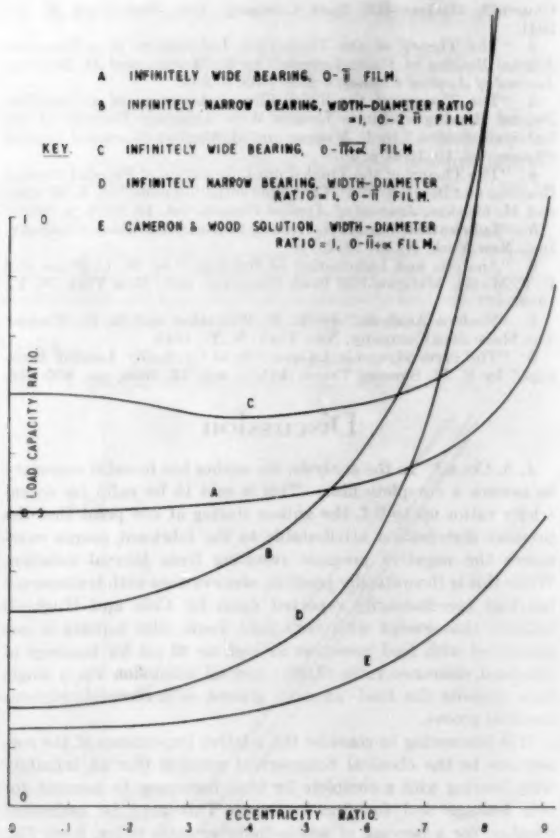

FIG. 5 THEORETICAL LOAD CAPACITY OF COMPLETE JOURNAL BEARINGS
(Expressed as fraction of Sommerfeld value for infinitely wide bearing with complete film.)

However curve C, showing the solution for an infinitely wide bearing with film extent $0 - \overline{\pi + \alpha}$ (where $p_{\pi+\alpha} = (\partial p/\partial\theta)_{\pi+\alpha} = 0$) (Cameron and Wood)[8] is reasonably close to curve A. A comparison of curve D, showing the solution for the infinitely narrow bearing with the load-carrying film extent $0 - \pi$ (Dubois and Ocvirk)[9]

$$W = \frac{\mu U l r^2}{c^2}\left(\frac{l}{2r}\right)^2 b\,\frac{\sqrt{\pi^2(1-b^2)+16b^2}}{(1-b^2)^2} \quad \ldots\ldots [29]$$

and curve E, showing the solution for the bearing of finite width with film extent $0 - \overline{\pi + \alpha}$ (Cameron and Wood, loc. cit.) indicates that the infinitely narrow bearing approximation also is reasonable.

Another important consequence of film rupture is the modification of the bearing attitude-eccentricity locus. Fig. 6 of this discussion shows the loci for the various solutions already noted. Those involving the assumption of a complete film result in a straight-line locus perpendicular to the load line, while those involving film rupture give curves of form similar to the nearly

[8] "The Full Journal Bearing," by A. Cameron and Mrs. W. L Wood, Proceedings of The Institution of Mechanical Engineers, vol. 161, 1949, pp. 59–64.

[9] "Analytical Derivation and Experimental Evaluation of Short-Bearing Approximation and Full Journal Bearings," by G. B. Dubois and F. W. Ocvirk, NACA Technical Report 1157, 1953.

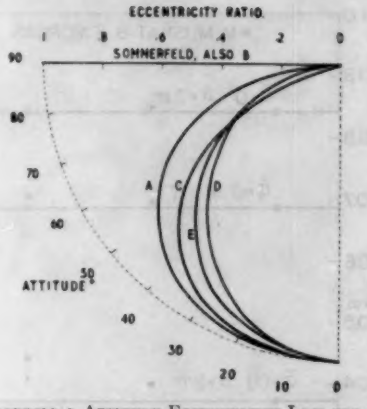

FIG. 6 THEORETICAL ATTITUDE-ECCENTRICITY LOCI FOR COMPLETE JOURNAL BEARINGS
(Key as Fig. 5.)

semi-circular locus observed in practice. Here therefore film rupture has more effect than side leakage.

The conclusion to be drawn from this comparison is that it is probably as important to account for film rupture as for side leakage, although of course for very narrow bearings the importance of side leakage increases.

AUTHOR'S CLOSURE

The author would like to thank Mr. Cole for his interesting discussion on the importance of taking into account oil-film rupture. Simons (8) has shown that feed pressures need not be excessively high for a complete oil film in light to moderately loaded bearings. With a properly located lubricant source the tendency for film rupture can be minimized. Admittedly, with either insufficient lubricant or high loads the oil film will be discontinuous and the derived equations will not apply. If the film is broken over a small arc of the bearing (light to moderate loads), the load-capacity and friction values given by the present equations should not be seriously in error. It is interesting to note that for $\beta = 1$ and $\bar{q} = 0$ (no source present) the author's equation gives a value of 0.238 for the leakage factor (W/W_∞). When the presence of the source is taken into account the leakage factor can be above or below this value depending upon the location and strength of the source. The Cameron and Wood solution (see Fig. 5) gives an essentially constant value of 0.13 in the eccentricity ratio range of 0 to 0.4.

In regard to the attitude-eccentricity locus, Muskat and Morgan's solution (3) has shown that if a complete oil film is postulated this does not require that the line of centers be perpendicular to the load line. Because of the nature of the author's approximation, when the source is parallel to the load vector the line of centers is at right angles to the load line. What has been neglected is the interaction of the eccentricity and source which produces turning of the line of centers. When the source is sufficiently displaced from the afore-mentioned position, the author's equations indicate that the position of the line of centers does indeed vary.

A rigorous solution of the classical journal-bearing problem with steady load would include end leakage, film rupture, and the source. Oil-film rupture can best be handled by numerical methods. When the source is included in the analysis, numerical methods are not convenient to use. Analytical methods can be used to advantage but the ruptured film is difficult to include. Because of these limitations it is doubtful that a rigorous solution will be obtained to the finite journal-bearing problem.

Very Short Journal-Bearing Hydrodynamic Performance Under Conditions Approaching Marginal Lubrication

By L. F. KREISLE,[1] AUSTIN, TEXAS

This paper is a presentation of experimental data concerning the hydrodynamic performance of short journal bearings under conditions approaching zero minimum oil-film thickness near or in the region of boundary lubrication. Experimental data are presented for short journal bearings with length-to-diameter ratios between 1/2 and 1/53. Theoretical performance of short journal bearings by several theories is compared with experimental findings of extremely short bearings. Six different load numbers are defined and are found to be useful in predicting and analyzing the performance of short journal bearings.

Nomenclature

The following nomenclature is used in the paper:

B = bore of bearing at operating conditions, in.
C_d = diametral clearance of journal and bearing at operating conditions, in., equals $B - D$
C_d/D = diametral clearance ratio at operating conditions, dimensionless
D = diameter of journal at operating conditions, in.
D/L = diameter-to-length ratio of the bearing at operating conditions, dimensionless
e = eccentricity of center of the journal relative to center of bearing, in.
h_m = minimum oil-film thickness, in.
h_m/D = minimum oil-film thickness to diameter ratio at operating conditions, dimensionless
L = length of bearing in contact with journal at operating conditions, in.
L/D = length-to-diameter ratio at operating conditions, dimensionless
N_c = clearance-load number at operating conditions, dimensionless, equals $\frac{p}{\mu n'}\left(\frac{C_d}{D}\right)^2\left(\frac{D}{L}\right)^2$
N_c' = experimental clearance-load number at operating conditions, dimensionless, equals $\frac{p}{\mu n'}\left(\frac{C_d}{D}\right)^2\left(\frac{D}{L}\right)^\gamma$
N_h = minimum oil-film thickness-load number at operating conditions, dimensionless, equals $\frac{p}{\mu n'}\left(\frac{h_m}{D}\right)^2\left(\frac{D}{L}\right)^2$
N_h' = experimental minimum oil-film thickness-load number at operating conditions, dimensionless, equals $\frac{p}{\mu n'}\left(\frac{h_m}{D}\right)^2\left(\frac{D}{L}\right)^\gamma$
$N_{D/L}$ = $\frac{D}{L}$ load number at operating conditions, dimensionless, equals $\frac{p}{\mu n'}\left(\frac{D}{L}\right)^2$
N_0 = oil-pressure load number at operating conditions, dimensionless, equals $\frac{p_0}{\mu n'}\left(\frac{C_d}{D}\right)^2\left(\frac{D}{L}\right)^2$
n' = rotational speed of journal relative to stationary bearing, revolutions per sec (rps)
P = radial load on bearing, lb
p = unit loading on projected area of bearing, psi, equals $\frac{P}{LD}$
p_0 = inlet oil pressure to bearing, psig
Q = actual oil flow through bearing, cu in. per sec
Q_s = analytical oil flow through bearing, cu in. per sec, equals $\frac{\pi DLC_d n'\epsilon}{2}$
q = oil-flow factor, dimensionless, equals Q/Q_s
T = friction torque on bearing, in-lb
T_0 = Petroff friction torque on both bearing and journal, in-lb, equals $\frac{\pi^2\mu n' LD^3}{C_d}$
γ = exponent of D/L term of experimental clearance-load number and experimental minimum oil-film thickness-load number, dimensionless
ϵ = eccentricity ratio, dimensionless, equals $2e/C_d$
μ = viscosity of bearing lubricating oil at average operating conditions, lb sec per sq in. = reyns
ϕ = attitude angle between load line on bearing and position of minimum oil-film thickness, deg

Experimental Results

A short journal bearing is a cylindrical bearing in which the proportion of the length L to the diameter D is such that the circumferential pressure gradient is small compared with the axial pressure gradient. For the purpose of this paper, a short journal bearing is defined as a cylindrical bearing in which the length-to-diameter ratio is less than one. Such a bearing supporting a loaded rotating journal is shown in Fig. 1.

Several dimensionless quantities consisting of arrangements of the fundamental variables of bearing lubrication appear in the various theories and approximate solutions applicable to short journal bearings. These quantities are the diameter-to-length

[1] Assistant Professor of Mechanical Engineering, University of Texas. Mem. ASME.

Contributed by the Research Committee on Lubrication under the auspices of the Lubrication Activity of The American Society of Mechanical Engineers, and presented at the Second Annual ASME-ASLE Lubrication Conference, Indianapolis, Ind., October 10–12, 1955.

Note: Statements and opinions advanced in papers are to be understood as individual expressions of their authors and not those of the Society. Manuscript received at ASME Headquarters, November 16, 1955.

ratio D/L, the diametral clearance-to-diameter ratio C_d/D, the minimum oil-film thickness-to-diameter ratio h_m/D, the clearance-load number N_c, the minimum oil-film thickness-load number N_h, the D/L load number $N_{D/L}$, and other possible combinations of the variables. Theoretical values of the foregoing nondimensional quantities by the Ocvirk short-bearing approximation[2] are compared favorably with the corresponding experimentally determined values by use of superposed graphical plots. Similar comparisons are drawn for the bearing-friction torque ratio, oil-flow factor, and attitude angle.

Clearance-Load Number. The clearance-load number N_c is a dimensionless quantity defined as follows

$$N_c = \frac{p}{\mu n'} \left(\frac{C_d}{D}\right)^2 \left(\frac{D}{L}\right)^2$$

Experimentally determined values of the clearance-load number for L/D ratios between 0.0187 and 0.502, faired experimental curves for each bearing tested, and theoretical values versus eccentricity ratio are compared graphically in Fig. 2. Experimentally obtained clearance-load numbers of 190,000 are indicated. The eccentricity ratios predicted by use of the short-bearing approximation appear to agree well with experimentally determined values and are of practical value in predicting the hydrodynamic performance of short journal bearings.

Experimental Clearance-Load Number. The experimental clearance-load number N_c' is a dimensionless quantity defined by

$$N_c' = \frac{p}{\mu n'} \left(\frac{C_d}{D}\right)^2 \left(\frac{D}{L}\right)^\gamma$$

where γ is an experimentally determined exponent which best reduces the deviation of the experimentally determined values of ϵ versus N_c' for each bearing from an average curve for all bearings. Experimental data indicate an approximate value of 1.73 for γ. Considering that $\gamma = 1.7275$, experimental and average curve values of ϵ versus N_c' are given graphically in Fig. 3. The experimental and average curve values of ϵ versus N_c' agree even more closely than did the corresponding values of ϵ versus N_c.

Since the short-bearing theory indicates that the exponent γ of the D/L term of N_c is 2.0 and experimental data indicate a lower value, there is a possibility that accurate theoretical values of N_c determined by including all terms of Reynolds equation may give a value of γ less than 2. This might be accomplished by the lengthy relaxation procedures of Cameron and Wood.[3]

Minimum Oil-Film Thickness-Load Number. By substituting the minimum oil-film thickness h_m for the diametral clearance C_d into the equation for the clearance-load number N_c, the dimensionless quantity minimum oil-film thickness-load number N_h is obtained as

[2] "Short Bearing Approximation for Full Journal Bearings," by F. W. Ocvirk, NACA Technical Note 2808, 1952.

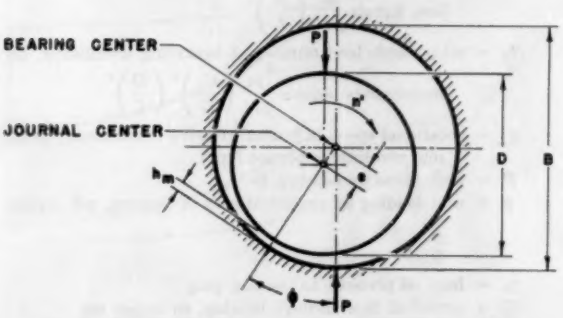

FIG. 1 DIAGRAM OF JOURNAL AND BEARING UNDER LOAD

[3] "The Full Journal Bearing," by A. Cameron and W. L. Wood, Proceedings of The Institution of Mechanical Engineers, vol. 161, 1949, pp. 59–72.

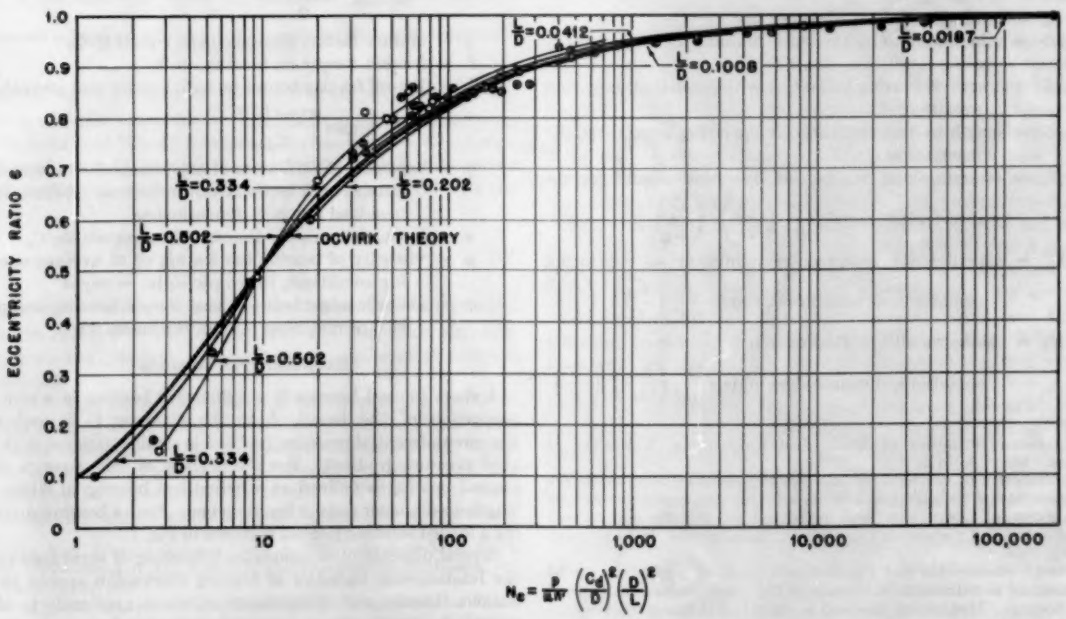

FIG. 2 CLEARANCE-LOAD NUMBER VERSUS ECCENTRICITY RATIO

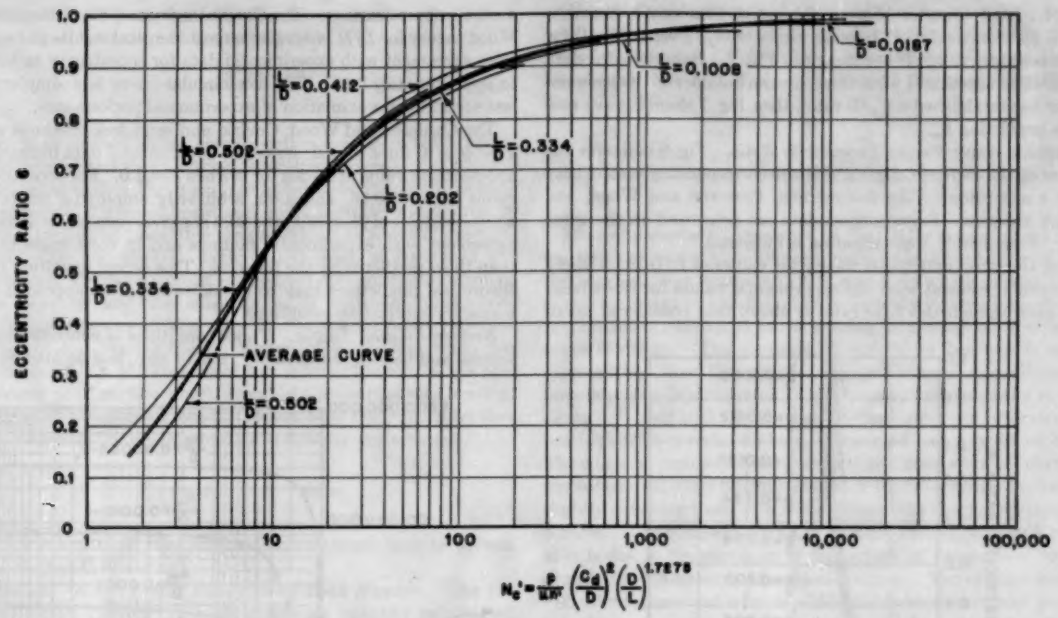

FIG. 3 EXPERIMENTAL CLEARANCE-LOAD NUMBER VERSUS ECCENTRICITY RATIO FOR $\gamma = 1.7275$

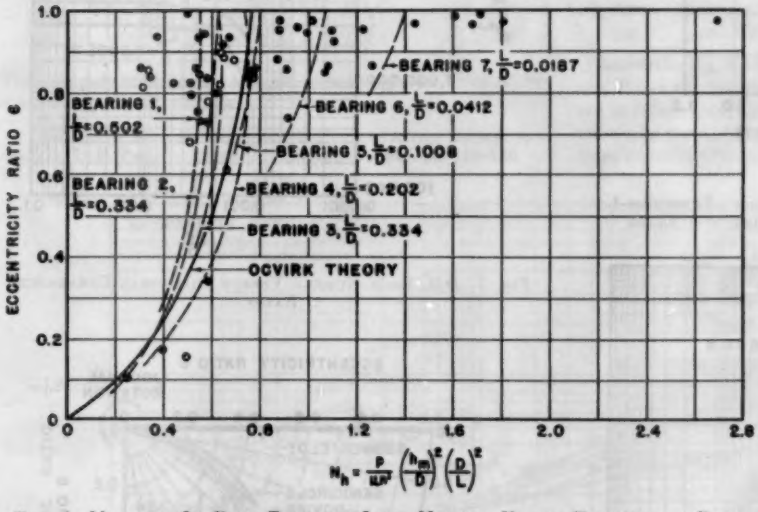

FIG. 4 MINIMUM OIL-FILM THICKNESS-LOAD NUMBER VERSUS ECCENTRICITY RATIO

$$N_h = \frac{p}{\mu n'} \left(\frac{h_m}{D}\right)^2 \left(\frac{D}{L}\right)^2$$

Theoretical values of ϵ versus N_h are compared with experimental values in the curves of Fig. 4. Although the theoretical values appear to give an average curve for all the experimental data, faired curves for the experimental data of several of the individual bearings fall a considerable distance away from the theoretical curve. Part of this difference may be explained by the great difficulty of obtaining accurate measurements of the minimum oil-film thickness. The plot of ϵ versus N_h is very sensitive to comparatively minute changes in the value of h_m.

Experimental Minimum Oil-Film Thickness-Load Number. By changing the exponent of the D/L term of the minimum oil-film thickness-load number from 2.0 to γ, the dimensionless quantity experimental minimum oil-film thickness-load number N_h' is defined as follows

$$N_h' = \frac{p}{\mu n'} \left(\frac{h_m}{D}\right)^2 \left(\frac{D}{L}\right)^\gamma$$

A value of $\gamma = 1.7275$ appears best to bring into agreement the experimental values of N_h' and the average curve values when plotted versus ϵ. Assuming that $\gamma = 1.7275$, Fig. 5 indicates the close agreement between the average curve values of ϵ versus N_h' and the experimentally determined values of the same quantities. It is probable that as the accuracy of measuring h_m increases, the accuracy of determining the exponent γ will improve and the experimental and average curves will come into even closer agreement.

D/L Load Number Versus Minimum Oil-Film Thickness-to-Diameter Ratio. Theoretical values of the D/L load number $N_{D/L}$ versus h_m/D for eccentricity ratios between 0.1 and 1 are shown graphically in Fig. 6. Superposed on this plot are experimental data for eccentricity ratios between 0.8 and 1.

If one desires to determine the value of the minimum oil-film thickness of a given bearing, he would be making a comparatively small error by using the value of h_m determined by the particular value of $N_{D/L}$ he desires and the $\epsilon = 0.8$ line of Fig. 6. Thus the short-bearing theory is useful in giving good approximations for the minimum oil-film thickness of short journal bearings that operate with eccentricity ratios between 0.3 and 1. Only the lightest loaded bearings operate with eccentricity ratios below 0.3.

D/L Load Number Versus Diametral Clearance-to-Diameter Ratio. Theoretical short-bearing values of $N_{D/L}$ versus C_d/D for various values of h_m/D are shown in Fig. 7. Experimental data are in close agreement with these theoretical curves. Once a designer has established a C_d/D ratio, then Fig. 7 should prove useful in predicting h_m.

Attitude Angle Versus Eccentricity Ratio. Fig. 8 indicates the values of the attitude angle ϕ and the corresponding eccentricity ratio ϵ according to the Sommerfeld, Cameron and Wood, and Ocvirk theories. Experimental data are presented on the same plot. A semicircle approximation is indicated.

The Cameron and Wood theory for values of $L/D = \infty$ and 1 approach agreement with the experimental values for short bearings even though the L/D ratio is above that considered maximum for short bearings. The Ocvirk theory and the Cameron and Wood theory for $L/D = 1/4$ give almost identical results and are in close agreement with experimental data for eccentricity ratios up to approximately 0.85. The semicircular curve is a simpler but less accurate approximation of experimental performance.

The Cameron and Wood, Ocvirk, and semicircle methods each give $\phi = 0$ for $\epsilon = 1.0$; however, experimental data indicate an approximate value of 20 deg for ϕ when $\epsilon = 1.0$. For eccentricity ratios of 0.90, 0.95, and 1.00, arbitrarily employing respective attitude angles of 25.0, 22.5, and 20.0 deg gives results in reasonable agreement with experimental findings and in most cases better than those predicted by the theories. This actual deviation from theoretical predictions may be an indication of an approach into boundary-lubrication conditions.

Bearing-Friction Torque. Under conditions of concentricity of journal and bearing, eccentricity ratio of zero, and no load on the

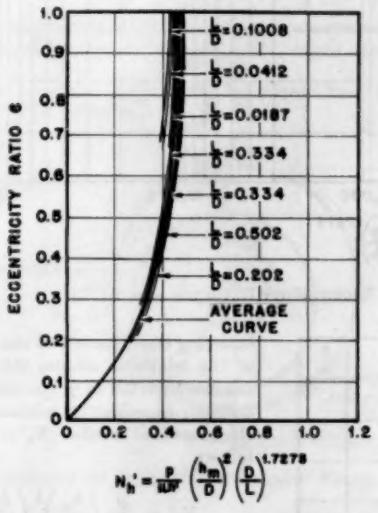

FIG. 5 EXPERIMENTAL MINIMUM OIL-FILM THICKNESS-LOAD NUMBER VERSUS ECCENTRICITY RATIO FOR $\gamma = 1.7275$

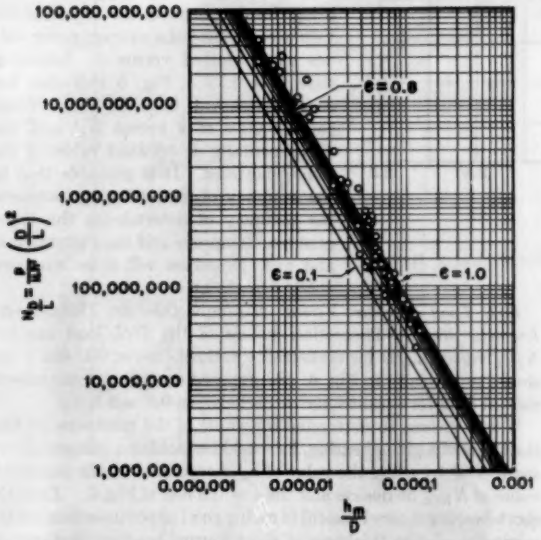

FIG. 6 *D/L* LOAD NUMBER VERSUS MINIMUM OIL-FILM THICKNESS-TO-DIAMETER RATIO

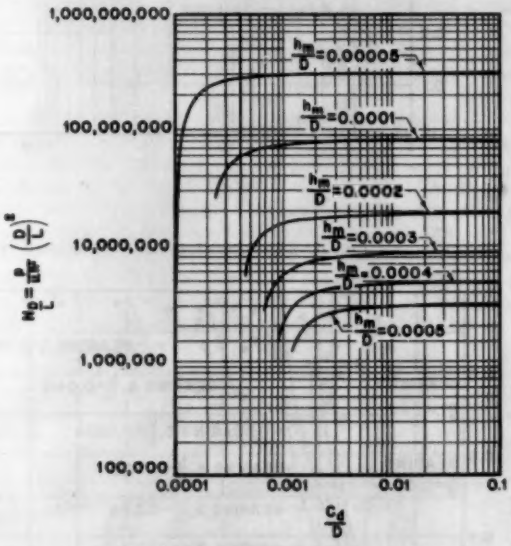

FIG. 7 *D/L* LOAD NUMBER VERSUS DIAMETRAL CLEARANCE RATIO

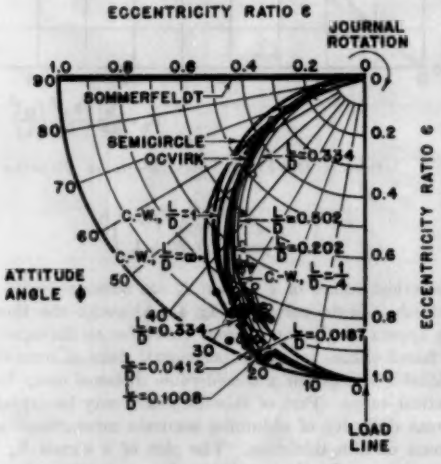

FIG. 8 ATTITUDE ANGLE VERSUS ECCENTRICITY RATIO

bearing, Petroff gives the following expression for the friction torque T_0 on both the bearing and journal

$$T_0 = \frac{\pi^2 \mu n' L D^3}{C_d}$$

Let T be defined as the actual friction torque on the bearing. Experimental and short-bearing theoretical values of T/T_0 versus N_c are compared in Fig. 9 and are found to be in fair agreement. Experimental curves of bearings 6 and 7 indicate a sharp rise in bearing friction at respective clearance-load numbers of approximately 4000 and 80,000. Perhaps this is an indication of the breakdown, at least partially, of the hydrodynamic lubrication of these bearings and the substitution of marginal lubrication. Additional increases of N_c are accomplished with rather rapid increases of the bearing-friction torque. This occurs when the minimum oil-film thickness is of the order of the sum of the predominant peak surface roughnesses[4] of the journal and bearing. From equilibrium conditions it is seen that the journal-friction torque exceeds the bearing-friction torque by the amount

$$P(e \sin \phi) = \frac{P \epsilon C_d}{2} \sin \phi$$

At high values of N_c, the journal-friction torque may be several times that of the bearing.

Oil-Flow Factor Versus Oil-Pressure Load Number. The oil-pressure load number N_0, a dimensionless quantity relating oil flow through a journal bearing to other variables, is defined as follows

$$N_0 = \frac{p_0}{\mu n'} \left(\frac{C_d}{D}\right)^2 \left(\frac{D}{L}\right)^2$$

Thus the oil-pressure load number is nothing more than N_c revised with p_0 substituted for p.

[4] "Relation of Surface-Roughness Readings to Actual Surface Profile," by L. P. Tarasov, Trans. ASME, vol. 67, 1945, pp. 189–196.

The oil-flow factor q is the ratio of the experimentally measured oil-flow rate Q through the bearing to the analytically determined oil-flow rate Q_a determined from the short-bearing theory based upon 180 deg of pressurization of the bearing by the oil film. Thus

$$q = \frac{Q}{Q_a} = \frac{Q}{\left(\frac{\pi D L C_d n' \epsilon}{2}\right)}$$

Plots of q versus N_0 are shown in Fig. 10 for several short journal bearings under two different methods of introducing oil into the bearing. For bearings 1, 2, 3, and 4, in which oil was introduced by means of a radial oil hole centrally located opposite the application of radial load to the bearing, an average oil-flow factor curve is drawn. The q versus N_0 curves for bearings 6 and 7 represent oil flow through bearings with axial circumferential pressurization from one end of the bearing and naturally do not agree very well with the average oil-flow factor curve drawn for bearings with a radial oil hole. Bearing 5 had a radial oil hole. The edges (or corners) of the ends of this bearing were left sharp as machined; all other bearings had their corners slightly broken by slightly touching them with a fine stone as the bearing was spun in a lathe. The comparatively low oil-flow rate of bearing 5 probably is due to the sharpness of its corners in comparison to the slightly broken corners of the other bearings. The oil-flow data of Fig. 10 are presented only as additional information and not as anywhere near a complete study of the oil-flow characteristics of short journal bearings.

Bearing Performance Under Conditions Approaching Marginal Lubrication

As seen in Fig. 8, the attitude angles predicted by the Cameron and Wood solution and the Ocvirk short-bearing approximation are in rather good agreement with the experimentally determined values for eccentricity ratios up to approximately 0.85 but depart from experimental results for higher eccentricity ratios. Under

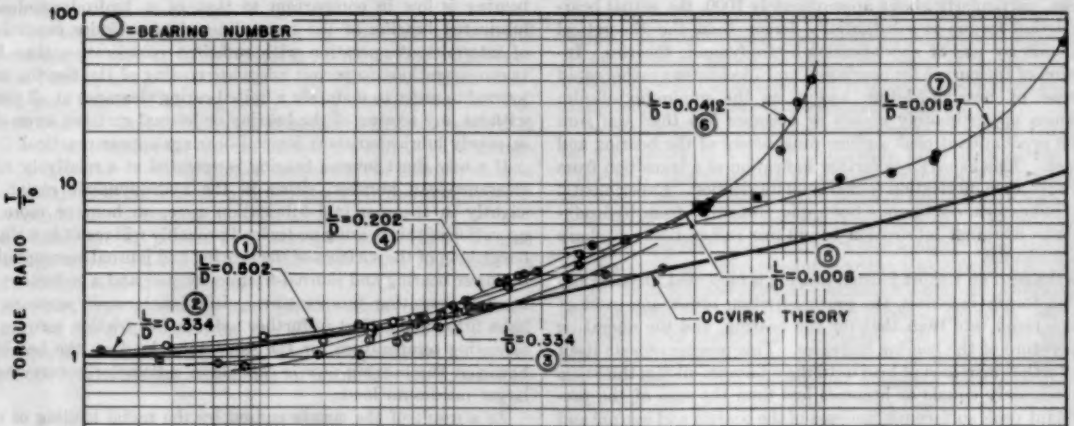

Fig. 9 Clearance-Load Number Versus Bearing-Friction Torque Ratio

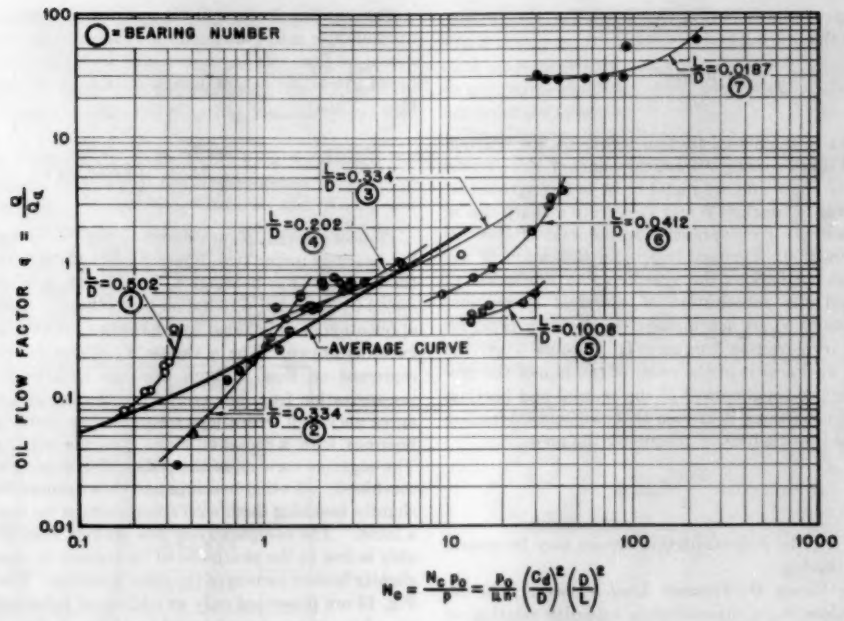

FIG. 10 OIL-PRESSURE LOAD NUMBER VERSUS OIL-FLOW FACTOR

these conditions of very small minimum oil-film thicknesses in which the journal and bearing are approaching contact, the deviation of actual bearing performance from theoretical hydrodynamic predictions is an indication of the departure from pure hydrodynamic film lubrication and the substitution (at least in part) of marginal lubrication conditions.

The bearing-friction torque versus clearance-load number curves of Fig. 9 indicate that as the clearance-load number increases, particularly above approximately 1000, the actual bearing-friction torque is substantially larger than the theoretical prediction by use of short-bearing hydrodynamic theories. Inspection of the curves for bearings 6 and 7 indicates a rather rapid increase of bearing-friction torque as the minimum oil-film thickness approximately equals or becomes less than the sum of the predominant peak surface roughnesses of the bearing and journal. This behavior is further indication of a transition from hydrodynamic lubrication to marginal lubrication. Experimental data indicate a continuous but rapid transition from hydrodynamic to marginal lubrication conditions rather than a sharp abrupt change.

As the load on a short journal bearing is increased, the bearing-friction torque increases, the journal-friction torque increases at a more rapid rate than that for the bearing, and the operating temperature of the bearing increases. This process repeats itself with further increases of load until the minimum oil-film thickness approximately equals or becomes less than the sum of the predominant peak surface roughnesses of the bearing and journal and marginal lubrication conditions are reached. Under these conditions, there is a rapid rise of journal and bearing-friction torques, an increase of temperature, and due to the differential expansion of the journal and bearing often a reduction of diametral clearance to zero with resultant seizure of the bearing and journal and probable damage to bearing and journal. These phenomena are a common cause for the failure of short journal bearings. In view of this and the minimum oil-film-thickness considerations, clearances large enough to avoid temperature seizures are recommended. If a bearing has been operating barely outside the hydrodynamic-film region in the marginal lubrication zone at relatively high-bearing and journal-friction torques and high-bearing operating temperatures, reduction of the radial loading will effect an increase in the minimum oil-film thickness, a reduction of bearing and journal-friction torques, a reduction of bearing operating temperature, and a probable return to full hydrodynamic film-lubrication conditions.

The load capacity of a dry or even only slightly lubricated bearing is low in comparison to that of a hydrodynamically lubricated bearing of the same dimensions. Under conditions of intermittent operation with sufficient recuperation time between operations to permit adequate cooling of the bearing and journal in order to maintain a finite bearing clearance at all times without any scoring of the bearing or journal surfaces, even dry or poorly lubricated short journal bearings appear practical.

If a new short journal bearing is operated at a relatively high clearance-load number, either in the hydrodynamic region or slightly in the marginal lubrication zone, an hour or more of operation of this bearing under load probably will result in a slight burnishing of the surfaces of the bearing and journal accompanied by lower bearing and journal-friction torques and a reduction of bearing operating temperature. Additional run-in appears to have little or no effect in further reduction of friction torques or operating temperature for the same total load on the bearing; however, the bearing now is capable of satisfactorily carrying a larger maximum load.

As a result of the couple caused by the radial loading of the bearing and eccentric journal, the journal-friction torque always exceeds the bearing-friction torque. Under marginal lubrication conditions where the eccentricity of the journal is maximum, the friction torque on the journal may be several times that on the bearing due to the magnitude of this couple.

The inclusion of up to equal parts of air and oil in the lubricant supplied to a lightly loaded journal bearing often has little or no significant effect on the hydrodynamic performance of the bearing. The inclusion of only a small amount of air in the oil of a heavily loaded journal bearing generally is sufficient to cause the hydro-

dynamic film to break temporarily or permanently, causing an increase in the bearing-friction torque, a resulting rise in bearing operating temperature, and often a seizure of bearing and journal. If a journal is started from rest to some finite rotational speed under conditions of high radial loading, the hydrodynamic film may be unable to build up. When this condition appears, often by reducing or removing the load while the journal continues to rotate and then gradually applying the same total load, the hydrodynamic film may be formed.

If oil is supplied to the radial oil hole on the unloaded side of a lightly or heavily loaded journal bearing at atmospheric or slightly below atmospheric pressure, the bearing generally will pump sufficient oil to perform satisfactorily and exhibit hydrodynamic lubrication characteristics.

Conclusions

From the experimental and theoretical data presented in this paper, the following conclusions are drawn:

1 The most useful means of presenting short-bearing theoretical and experimental results appear to be by the use of the $N_{D/L}$ versus h_m/D and the $N_{D/L}$ versus C_d/D curves. Bearing designers will find these particular curves useful for design and analysis.

2 The clearance-load numbers, experimental clearance-load numbers, minimum oil-film thickness-load numbers, experimental minimum oil-film thickness-load numbers, D/L load numbers, and oil-pressure load numbers are basic dimensionless quantities useful for predicting and analyzing the performance of short journal bearings. The T/T_0 versus N_s and the q versus N_0 curves are useful for predicting bearing-friction torques and oil-flow rates. It is probable that the optimum arrangement of the variables of short-journal bearing lubrication has not yet been made in order to obtain the most useful dimensionless quantity.

3 The experimental clearance-load numbers and the experimental minimum oil-film thickness-load numbers appear to be improvements on present short-bearing theories; however, additional analysis is necessary in order to determine the value of the exponent γ more accurately.

4 So long as the minimum oil-film thickness is of the order of or exceeds the sum of the predominant peak surface roughnesses of the bearing and journal measured in the circumferential directions after run-in of bearing and journal, experimental bearing-friction-torque data indicate the presence of hydrodynamic film lubrication. Smaller oil-film thicknesses are indicative of marginal lubrication. Bearing-friction-torque curves indicate a rapid continuous transition from hydrodynamic to marginal lubrication conditions rather than a sharp abrupt change.

5 Although in present engineering practice most journal bearings operate at clearance-load numbers below 100, values of 190,000 and more are attainable.

6 Short journal bearings can operate successfully under conditions of marginal lubrication but with bearing-friction torques and operating temperatures exceeding those predicted by hydrodynamic lubrication considerations for a similarly sized bearing.

Acknowledgments

The author wishes to express his utmost appreciation to the International Business Machines Corporation for its interest in and financial backing of these investigations in addition to providing much of the test equipment. The author further wishes to express his sincere appreciation to the Machine Design Laboratories, Cornell University in providing laboratory and machine-shop facilities for conducting these investigations and the loan of test equipment. Thanks are due Prof. Fred W. Ocvirk, Cornell University, for providing information concerning his short-journal-bearing approximation for correlation with experimental findings.

Discussion

A. Bondi.[5] The writer would expect that the author's experimental results in the thin-film region depend very largely on the running-in procedure employed. The run-in methods were not described in the paper. Should their effect be as noticeable as the writer expects they are, then the initial surface-finish measurements (discussed by the author and by Professor Ocvirk) would hardly be significant for design calculations.

F. W. Ocvirk.[6] The author is to be commended for his experimental exploration into the thinness of hydrodynamic films in journal bearings. The major portion of his experimental data shows measurements of minimum film thickness less than 0.0001 in. and reaching extreme thinnesses of 0.00001 in. or less. Measurement of film thicknesses of these orders of magnitude are difficult, and the question of accuracy of measurement inevitably arises. However, the use of very short double bearings as test specimens appears logical since the effect of shaft deflection, misalignment, and waviness of bore are less apt to be disturbing variables. In view of the author's careful technique and the sensitive performance of the microformers, the order of magnitudes of film thicknesses measured appears reasonable.

The author's statement that surface roughness seems to be the limiting factor in the purely hydrodynamic performance of thin films is logical. Marginal lubrication is apparent first from a rise in friction because of the beginning of metallic contact which is accompanied by a large temperature rise. This does not mean necessarily that a breakdown of load capacity is the primary cause of failure usually signified by temperature rise but that the increase friction is the primary factor because of the rapid reduction in clearance owing to differential thermal expansion caused by the heating. The author's statement that a large clearance would be desirable under marginal conditions is logical in this regard. It would appear that purely hydrodynamic steady-state performance at minimum film thicknesses of much less than 0.00001 in. could be realized with extremely fine finishes and relatively large clearances—and with short bearings.

Perhaps a clearer picture of the influence of surface roughness on the failure of thin hydrodynamic films is apparent from Tarasov's[4] magnifications of surface irregularities of machined surfaces. Tarasov shows that relatively few but very high peaks exist in all machined surfaces (turned, ground, lapped, superfinished) and that these peaks are much higher than the irregularities which are predominant over the major portion of the surface. Thus it is possible that a substantial film exists between the surfaces even though a friction rise becomes apparent because of the contact of the peaks. Moreover, Tarasov shows that the high peaks are of the order of from $4^1/_2$ to 10 times greater than the root-mean-square roughnesses measured with profilometers. Thus, for mating surfaces each having 1-microinch profilometer roughness, the load-carrying film thickness may be as much as $2 \times 1 \times 10 = 20$ microinches when metallic contact first begins. Run-in may reduce the height of the peaks, but this should be accomplished at high loads and low speeds to prevent high heating.

---

[5] Shell Development Company, Emeryville, Calif.

[6] Associate Professor of Mechanical Engineering, Department of Machine Design, Cornell University, Ithaca, N. Y.

D. F. Wilcock.[7] The author is to be commended for his painstaking experimental work which confirms so well the result of the simple theory for zero-length bearings. Efforts to induce a better correlation with the clearance-load number by making the exponent of the D/L term variable tend to reduce the results to those of an empirical relation. As the author points out, accurate results can be obtained by using the relaxation procedures of Cameron and Wood.

Rosenblatt and Wilcock[8] showed the benefits to be obtained by the use of a d-c network analyzer in obtaining more rapid solutions of Reynolds equation for bearings of finite length.

More recently, Pinkus[9] and Wilcock[10] have given more accurate results obtained by the use of digital computers. It would seem preferable, where the results of the simple theory are inadequate, to use solutions of Reynolds equations for finite bearings rather than to attempt correlations between experimental results and theoretical results for extreme conditions.

The substantial agreement obtained by the author between his experimental results for very short bearings and the theory for zero-length bearings lends added evidence to the writer's conviction of several years' standing that with the rapid solution of Reynolds equation for finite bearings available using computers, the amount of experimental work can be reduced sharply. Good bearing analyses can now be made by the right kind of theoretical prediction and only confirmatory experimental runs need to be carried out.

The author does not make clear what temperature is used in arriving at the oil viscosity used in correlating the results. For small bearings such as are discussed in this paper, a large amount of the heat is removed by conduction. Nevertheless, knowledge of oil flow and power loss must be utilized in arriving at the proper operating temperature. Perhaps the author can clarify this point? Similarly, the viscosity data on the oil used in the experiments are not given, and the reader must assume that careful measurements of viscosity at two or more temperatures were made and used. The SAE designation mentioned in the paper covers a rather broad range of possible viscosities.

Author's Closure

The author wishes to express his appreciation for the discussions given by Dr. Bondi, Professor Ocvirk, and Dr. Wilcock and to their interest in and encouragement of the continuation of related investigations.

Inasmuch as the transition from full hydrodynamic-film lubrication to marginal lubrication conditions appears to begin when the minimum oil-film thickness becomes less than the sum of the predominant-peak surface roughnesses of the bearing and journal measured in the circumferential direction after run-in of bearing and journal, Dr. Bondi justifiably requests description of the run-in procedures. The new $1^1/_8$-in-diam test bearings and journals were run in under constant journal rotational speeds of approximately 1000 rpm with continually increasing radial loading until clearance load numbers of approximately 1000 were obtained. This careful increase of loading was accompanied by a continuous monitoring of the bearing-friction torques and bearing operating temperatures in order to prevent high heat generation in the oil film effecting a large reduction of diametral clearance with subsequent scoring of bearing and/or journal. The journals then were permitted to run at clearance-load numbers of approximately 1000 for 1 hr, after which time additional run-in appeared to have little or no effect in burnishing of bearing and journal surfaces with accompanying reduction of bearing-friction torques and operating temperatures. Surface-roughness measurements of both the bearing and journal then were made, the bearing and journal were tested, and surface-roughness determinations were repeated to assure that the testing had effected no further burnishing of the mating surfaces.

The author believes that this run-in procedure results in surface roughnesses corresponding to those of commercial oil-lubricated short journal bearings which have been broken in through conventional usage, provided this break-in period was not accompanied by sufficiently high bearing operating temperatures to cause scoring of bearing and/or journal. Dr. Bondi correctly states that the initial surface-finish measurements of new bearings and journals are not very significant for design calculations unless these initial roughnesses correspond closely to those after run in. Fortunately, a bearing designer has available from experience typical roughnesses of various types of mating bearing and journal materials and surface treatments after conventional break-in conditions and it is these roughnesses that should be used in the design and analysis of short journal bearings.

Surface-roughness measurements in the circumferential direction were made on each journal and bearing axially midway between the ends of the bearing surface and for the bearing at the point estimated at the location corresponding to the position of the minimum oil-film thickness for the heaviest loading of the bearing. Root-mean-square microinch surface-roughness readings were obtained by use of a Brush surface analyzer and a profilometer. These roughnesses were translated into predominant-peak surface roughnesses by use of the methods described by Tarasov.[4] This method was checked experimentally on several of the bearings by use of microtome section of a plastic replica of the bearing surface and a toolmaker's microscope for direct measurement of predominant-peak surface roughness.

Thanks are due Professor Ocvirk for additional information concerning the transition from full hydrodynamic film lubrication to marginal lubrication conditions and the probable effect that the predominant-peak surface roughnesses of the bearing and journal play in this process, and for presenting some of the findings of Tarasov.[4] It is appreciated that Professor Ocvirk amplified the point that the breakdown of load capacity of a short journal bearing operating with marginal lubrication, usually signified by a rise in bearing operating temperature, is not the primary cause of bearing failure but that the increase of function is the primary factor because of the rapid reduction of diametral clearance due to the differential thermal expansion caused by the heating. Increasing diametral clearances of short journal bearings reduces the possibility of seizure of the bearing and journal as a result of this differential expansion and in most cases without any substantial reduction in the maximum load capacity. Reducing the predominant peak surface roughnesses of the journal and bearing surfaces reduces the limiting minimum oil-film thickness at which marginal lubrication begins.

The bearing lubricant employed throughout all investigations was Texaco SAE 20-20W D insulated motor oil. Its viscosity, as determined experimentally by use of a Saybolt universal viscometer and checked by a Brookfield viscometer, was as given in Fig. 11, herewith. These viscosity determinations were made with the test oil at various constant-temperature conditions and at atmospheric pressure. As Dr. Wilcock indicates, it is a difficult task to determine a single effective temperature of the oil in the bearing in order to arrive at a useful value of viscosity. The temperature and pressure in the oil film of a short journal bearing vary

---

[7] Mechanical Engineer, General Engineering Laboratory, General Electric Company, Schenectady, N. Y. Mem. ASME.

[8] "Oil Flow, Key Factor in Sleeve-Bearing Operation," by M. Rosenblatt and D. F. Wilcock, Trans. ASME, vol. 74, 1952, pp. 849–865.

[9] "Analysis of Elliptical Bearings," by O. Pinkus, presented at the Second Annual ASME-ASLE Lubrication Conference, Indianapolis, Ind., October 10–12, 1955.

[10] "Predicting Performance of Starved Bearings," by D. F. Wilcock, ASME Paper No. 55—LUB-9.

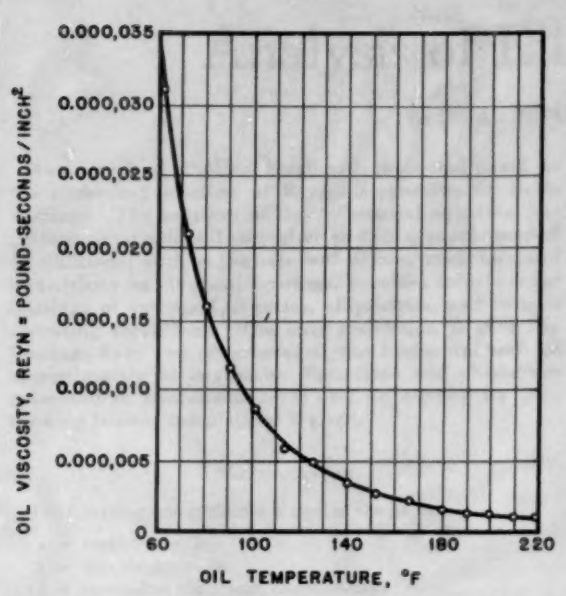

FIG. 11 EXPERIMENTALLY DETERMINED VISCOSITY OF TEST OIL AT ATMOSPHERIC PRESSURE

both circumferentially and axially and the viscosity of the oil varies accordingly. If a complete temperature and pressure traverse of the oil film experimentally were possible without altering the other experimental findings, then it would be a simple matter to determine an average viscosity of the oil in the oil film. Unfortunately, with the smallness of the oil-film thicknesses involved in these experimental investigations, this procedure was not possible. The following method was employed for the determination of oil viscosity in the bearing in correlating the experimental results with theoretical predictions; no attempt was made to take into account the effect of pressure upon viscosity.

A small copper-constantan thermocouple junction was placed within the bearing material at a point $^1/_{64}$ in. from the actual bearing surface at the point at which the load P is shown applied to the bearing in Fig. 1. The temperature indicated by the output of this junction and the viscosity data of Fig. 11 were employed to determine the viscosity of the test oil under test conditions of the bearings and journals.

Dr. Wilcock points out a probable trend in scientific investigations, that of employing computers to obtain solutions of problems rather than resorting to lengthy experimental investigations. Of course, certain conditions must be known about the problem before computers can give useful results. It is possible that in the near future, experimental investigations may be limited to the determination of the minimum information necessary for setting up a computer program and for obtaining a few confirmatory experimental runs of the computer results!

Analysis of Elliptical Bearings

By OSCAR PINKUS,[1] LYNN, MASS.

An analysis of elliptical bearings is presented based on the numerical solution of Reynolds equation for finite bearings. The solution of the differential equation was performed on a digital computer and this, supplemented by additional work on the nature of oil flow, power loss, and eccentricity in elliptical bearings, provides solutions for bearings of various L/D ratios, ellipticities, and various operating conditions. The only restriction is that the bearings have two oil grooves at the horizontal split of approximately 30 deg each. Equations and charts are presented in convenient form and an outline for performing bearing calculations is given.

Nomenclature

The following nomenclature is used in the paper:

e = eccentricity, in.
h = film thickness, in.
j = power-loss coefficient, dimensionless
m = $2\epsilon/C$, ellipticity ratio, dimensionless
n = $2e/C$, eccentricity ratio, dimensionless
p = pressure, psi
q = oil-flow coefficient, dimensionless
x, z = rectangular co-ordinates
C = major diametral clearance, in.
D = diameter, in.
H = power loss, in.-lb/sec
J = mechanical equivalent of heat, 778 in.-lb/Btu
L = length, in.
N = speed, rps
P = unit load, psi
S = Sommerfeld number $\left(\frac{D}{C}\right)^2 \frac{ZN}{P}$, dimensionless
T = temperature, deg F
U = linear speed, in/sec
V = flux-plot coefficient, dimensionless
Z = viscosity, lb-sec/in.
α = attitude angle, deg
ϵ = ellipticity, in.
c_p = specific heat, Btu/cu in., deg F
h_{min} = minimum film thickness, in.
n_B = $2e/C_M$ bearing eccentricity, dimensionless
C_M = minor diametral clearance, in.
F_V = vertical force, lb
F_H = horizontal force, lb
H_P = Petroff's power loss, in-lb/sec
P_i = inlet oil pressure, psi
Q_h = hydrodynamic oil flow, cu in/sec
Q_0 = zero-speed oil flow, cu in/sec

[1] Bearing Development Engineer, Thomson Laboratory, General Electric Company. Assoc. Mem. ASME.

Contributed by the Research Committee on Lubrication under the auspices of the Lubrication Activity of The American Society of Mechanical Engineers and presented at the Second Annual ASME-ASLE Lubrication Conference, Indianapolis, Ind., October 10–12, 1955.

Note: Statements and opinions advanced in papers are to be understood as individual expressions of their authors and not those of the Society. Manuscript received at ASME Headquarters, September 15, 1955. Paper No. 55—LUB-22.

Introduction

The trend to operate present-day bearings at ever-increasing speeds and loads confronts the engineer with many new, often perplexing, problems. Excessive power losses tax the efficiency of engines, high bearing temperatures pose a danger to the babbitt as well as to the lubricant, and instability, mainly in the form of oil whip, may ruin not only the bearings but the machine itself.

New bearing designs are sought to meet the new requirements and these bearings are usually characterized by their noncircular cross section. Almost any noncircular-bearing geometry will enhance shaft stability and under proper conditions this will also reduce power losses and increase oil flow (as compared to an inscribed circular bearing), thus reducing bearing temperatures. Among these noncircular sleeve bearings the elliptical bearing is one of the most commonly used.

The so-called elliptical bearing is actually not elliptic in cross section but is usually made up of two circular arcs whose centers are displaced along a common straight line from the center of the bearing, as shown in Fig. 1. Although these bearings may have any number of axial grooves, they are usually manufactured with

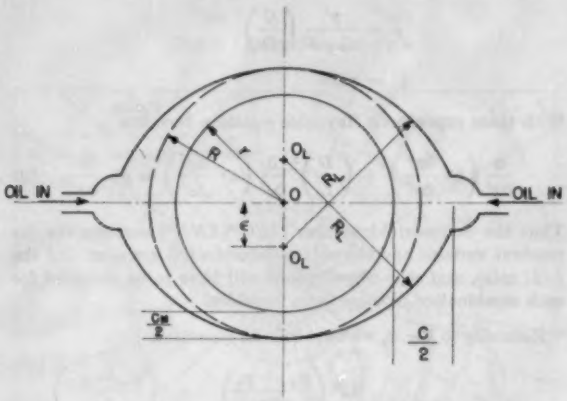

Fig. 1 Geometry of Elliptical Bearings

two grooves at the horizontal split. This paper provides solutions for bearings with 2 axial grooves of 30-deg arc each, for any ellipticity, and L/D ratios ranging from $^1/_4$ to $1^1/_2$. The results embrace the particular case of zero ellipticity which represents a plain circular bearing. All solutions here presented are based on a numerical solution of Reynolds 2-dimensional equation using an IBM digital computer.

Previous numerical solutions of Reynolds equation for journal bearings are confined to circular bearings. Cameron and Wood (1)[2] solved it by Southwell's (2) relaxation methods for a 360-deg bearing. Wilcock and Rosenblatt (3) solved it by electrical analogy for a 150-deg arc. Needs (4) using Kingsbury's (5) electrolytic tank methods solved it for a 120-deg arc. The present solutions are for elliptical as well as circular bearings of 150-deg arcs and these were obtained on an IBM digital computer.

In outline the general approach to the problem is similar to that used by Wilcock and Rosenblatt. However, the introduction of a

[2] Numbers in parentheses refer to the Bibliography at the end of the paper.

new variable ellipticity and the complexity of the bearing geometry call for new approaches. In the following presentation those results that are derived in reference (3) will just be restated but when modifications or additions are introduced the analysis will be given in full.

Solution of Reynolds Equation

The basic differential equation for hydrodynamic lubrication as derived by Reynolds (6) is given by

$$\frac{\partial}{\partial x}\left(\frac{h^3}{\mu}\frac{\partial p}{\partial x}\right)+\frac{\partial}{\partial z}\left(\frac{h^3}{\mu}\frac{\partial p}{\partial z}\right)=6U\frac{\partial h}{\partial x}\quad\ldots\ldots[1]$$

This is a second-order, nonhomogeneous, partial differential equation which is difficult to solve analytically. As it stands it contains μ, e, ϵ, D, N, C, and L as parameters. To solve the equation numerically an attempt must first be made to reduce the number of variables to a few compact dimensionless groups. The following substitutions are used for this purpose

$$x=x'/D$$

$$z=z'/D$$

$$h=h'/C/2=\frac{1+n\cos\theta}{2}$$

$$\mu=\mu'/\mu_{avg}=1$$

$$p=\frac{p'}{\mu_{avg}N}\left(\frac{C}{D}\right)^2$$

$$U=\pi DN$$

With these expressions Reynolds equation becomes

$$\frac{\partial}{\partial x'}\left(h^3\frac{\partial p'}{\partial x'}\right)+\left(\frac{D}{L}\right)^2\frac{\partial}{\partial z'}\left(h^3\frac{\partial p'}{\partial z'}\right)=6\pi\frac{\partial h'}{\partial x'}\quad\ldots[2]$$

Thus the Sommerfeld number $(D/C)^2(ZN/P)$ becomes the dependent variable and the only parameters left are n, α, and the L/D ratio, and separate solutions will have to be obtained for each combination of these three variables.

Referring to Fig. 2, we have infinite quantities

$$\frac{\partial}{\partial x'}\left(h'^3\frac{\partial p'}{\partial x'}\right)=\frac{h_R^3\left(\frac{p_R-p_a}{\Delta x}\right)-h_L^3\left(\frac{p_a-p_L}{\Delta x}\right)}{\Delta x}$$

$$\frac{\partial}{\partial z'}\left(h'^3\frac{\partial p'}{\partial z'}\right)=\frac{h_T^3\left(\frac{p_T-p_a}{\Delta z}\right)-h_B^3\left(\frac{p_a-p_B}{\Delta z}\right)}{\Delta z}$$

$$\frac{\partial h'}{\partial x'}=\frac{h_R-h_L}{\Delta x}$$

and solving for p_a the following expression is obtained

$$p_a=\frac{18.84\frac{h_L-h_R}{\Delta x}+\left(\frac{D}{L}\right)^2\frac{h_T^3}{\Delta z^2}p_T+\frac{h_R^3}{\Delta x^2}p_R+\left(\frac{D}{L}\right)^2\frac{h_B^3}{\Delta z^2}p_B+\frac{h_L^3}{\Delta x^2}p_L}{\left(\frac{D}{L}\right)^2\frac{h_T^3}{\Delta z^2}+\frac{h_R^3}{\Delta x^2}+\left(\frac{D}{L}\right)^2\frac{h_B^3}{\Delta z^2}+\frac{h_L^3}{\Delta x^2}}\quad\ldots[3]$$

This equation is of the form

$$p_a=c_0+c_1p_T+c_2p_R+c_3p_B+c_4p_L$$

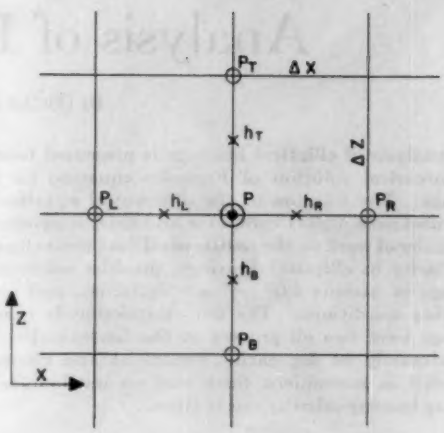

Fig. 2 Element of Bearing Grid

where c_0, c_1, c_2, c_3, c_4 are constants. Thus for n-points in the network a set of n algebraic equations in n-unknowns is obtained which can be solved by any analog or relaxation method.

For this problem a grid of about 50 points was picked and the equations solved on an IBM digital computer. No negative-pressure values were allowed in the expanding oil-film regions which also amounts to a boundary condition of zero pressure gradient at the trailing oil groove. The values of p_a were later integrated numerically on the same computer to provide the horizontal and vertical resultants

$$F_V=\sum_{n=1}^{n}p_a\cos\theta_a(\Delta x)(\Delta z)\quad\ldots\ldots[4]$$

$$F_H=\sum_{n=1}^{n}p_a\sin\theta_a(\Delta x)(\Delta z)\quad\ldots\ldots[5]$$

For any given bearing geometry and n, an equilibrium position of the shaft is given by the requirement that $F_H=0$ which can be obtained by assigning the proper value of α. This, of course, is a trial-and-error method.

As seen from Fig. 1, the elliptical bearing is made up of two circular arcs each with its own center of curvature O_L displaced a distance ϵ, termed the ellipticity, from the geometric center of the bearing O. It is clear that for any given shaft position O' the eccentricities and attitude angles with respect to the bearing and lobe centers will be different. The geometrical relationship between these parameters is shown in Fig. 3 and can be mathematically related as follows:

For the lower lobe

$$\epsilon^2+e^2-2e\epsilon\cos(\pi-\alpha)=e_1^2$$

or dividing out by $(C/2)^2$

$$n_1=\sqrt{n^2+m^2+2nm\cos\alpha}\quad\ldots\ldots[6]$$

where $m=\epsilon/C/2$ is here termed the "ellipticity ratio."

Also

$$\epsilon/\sin\alpha_1=e_1/\sin(\pi-\alpha)$$

or

$$\alpha_1=\text{arc sin}\frac{n\sin\alpha}{n_1}\quad\ldots\ldots[7]$$

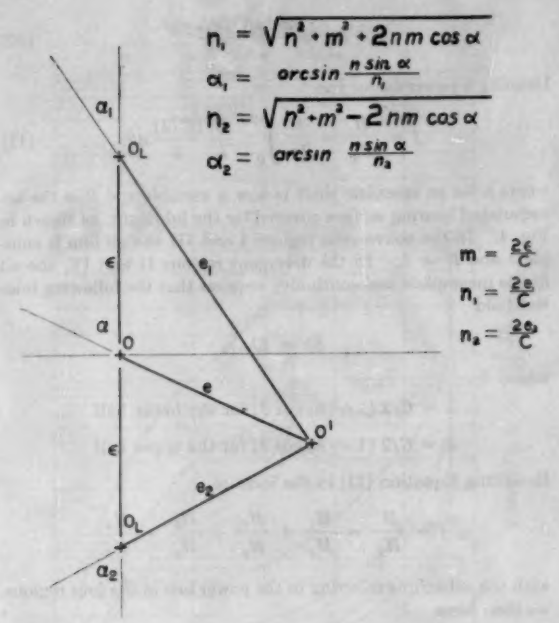

FIG. 3 ATTITUDES IN ELLIPTICAL BEARINGS

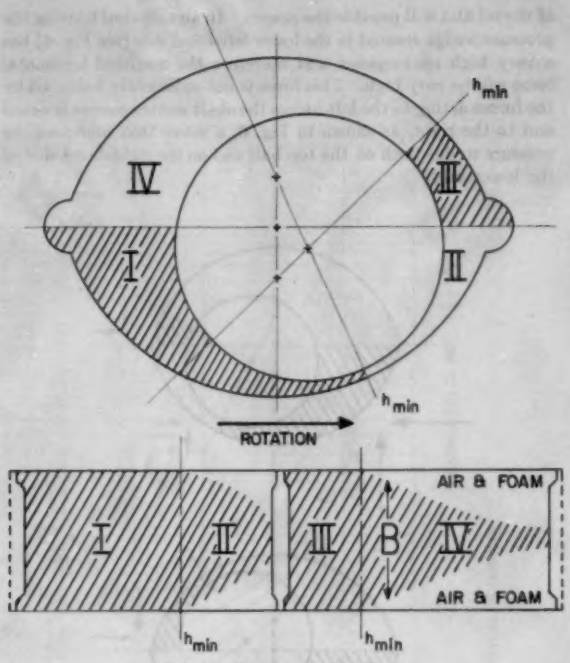

FIG. 4 EXTENT OF OIL FILM

For the upper lobe

$$\epsilon^2 + e^2 - 2e\epsilon\cos\alpha = e_2^2$$

or

$$n_2 = \sqrt{n^2 + m^2 - 2nm\cos\alpha} \quad \ldots\ldots\ldots\ldots [8]$$

$$e/\sin\alpha_2 = e_2/\sin\alpha$$

$$\alpha_2 = \text{arc sin}\,\frac{n\sin\alpha}{n_2} \quad \ldots\ldots\ldots\ldots [9]$$

Thus, given the bearing eccentricity and attitude angle, n and α, all other quantities can be determined from the foregoing relationships.

With a chosen bearing eccentricity and attitude angle picked at random, say, α', there will result a set of lobe eccentricities and attitude angles for which the solution of Reynolds equation will provide the magnitude of forces generated in the pressure wedges I and III of Fig. 4. The sum of the horizontal forces in both wedges must be zero. If this is not the case, a different α is chosen, n_1, n_2, α_1, and α_2 are recalculated and the forces in the horizontal direction summed again. This will eventually locate the shaft at the correct attitude angle where the sum of all forces in the horizontal direction is zero. Then for this equilibrium position the vertical forces are summed to give the load capacity. All other relevant quantities such as oil-flow coefficient, and power-loss factor (derived later) are then computed from the two separate halves and properly summed.

From Equations [6] to [9], it is seen that the lobe eccentricities and attitude angles depend also on the ellipticity ratio m. In this work the four ellipticity ratios picked are $m = 0$, $m = 1/4$, $m = 1/2$, and $m = 3/4$. The $m = 0$ case corresponds to a circular bearing. No need for higher m ratios exists as, in our nomenclature, for $m = 1$ there will be metal-to-metal contact.

ANALYSIS

In going through the following analysis it should be clearly borne in mind that there are two clearances in an elliptical bearing and that the major diametral clearance C is here used as the reference parameter. This is done for mathematical simplicity because the two individual lobes have a clearance C and the analysis is conducted in terms of the two circular lobes. In actual practice, if an elliptical bearing were to replace a circular bearing, it would be circumscribed on it; i.e., its minor clearance would equal the clearance of the circular bearing. It also should be remembered that there are at least three distinct eccentricity ratios, the bearing eccentricity $n_B = 2e/C_M$ and two lobe eccentricities $n_1 = 2e_1/C$ and $n_2 = 2e_2/C$ ($n = 2e/C$ is a fourth one).

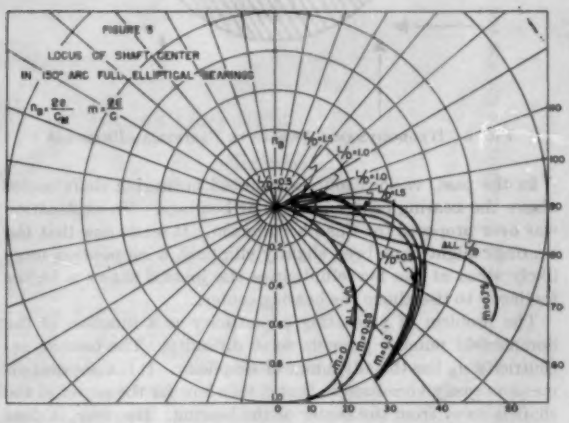

FIG. 5 LOCUS OF SHAFT CENTER

Eccentricity Locus. The most striking result of this analysis is the locus of shaft center, which is given in Fig. 5. As seen, the shaft center often finds itself above the center of the bearing. This may seem surprising but a little thought about the dynamics

of the oil film will provide the reason. In an elliptical bearing the pressure wedge created in the lower left-hand side (see Fig. 6) has a very high convergence and therefore the resultant horizontal force will be very high. This force is not sufficiently balanced by the forces acting to the left unless the shaft center moves upward and to the right, as shown in Fig. 6, a move that increases the pressure wedge both on the top half and on the right-hand side of the lower half.

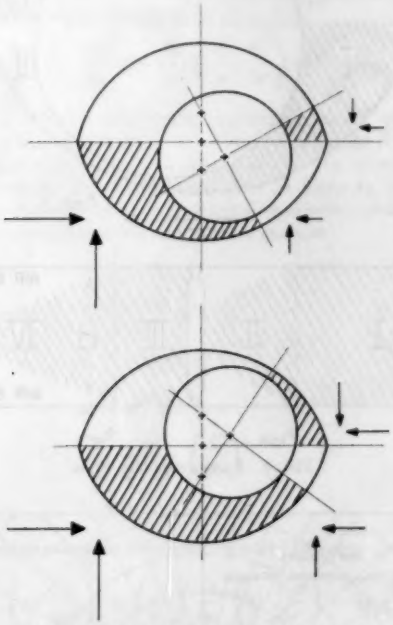

FIG. 6 HYDRODYNAMIC FORCES IN ELLIPTICAL BEARINGS

In the past, various sources reported measuring shaft center above the bearing center in circular bearings. No explanation was ever proposed for this phenomenon. It seems now that the bearings might have been slightly elliptical, a supposition more likely since at the low ellipticities the journal shows a higher tendency to rise above the bearing center.

The problem of presenting eccentricity as a function of the Sommerfeld number presents some difficulty. The bearing eccentricity n_B has the advantage of simplicity. It is a physical dimension easily visualized in that it tells how far the center of the shaft is away from the center of the bearing. However, it does not provide the vital information on minimum film thickness. This minimum film thickness can be obtained only from the knowledge of the lobe eccentricity n_1 or n_2. Since the shaft center may be either above or below the bearing center, the point of minimum film thickness may occur either on the top or bottom half of the bearing. Thus only those lobe eccentricities, either n_1 or n_2, that supply the information on minimum film thickness are used as parameters in Fig. 7. Fig. 8 gives the relation between n_B and n_L, the latter denoting, in general, that lobe eccentricity which provides the value of minimum thickness without reference to either top or bottom half.

Power Losses. The power losses in elliptical bearings for a concentric shaft position were derived in reference (7). Here the effect of eccentricity and the resulting modification for the regions of a complete and incomplete oil film will be taken into account. The approach presented here is similar to that used in reference (3). Petroff's equation (8) for a concentric circular bearing is

$$H_p = \frac{2\pi^3 \mu N^2 D^3 L}{C} \quad \ldots\ldots\ldots\ldots\ldots\ldots [10]$$

Defining a power factor j as

$$j = \frac{H}{H_p} = \frac{1}{2\pi} \int_0^{2\pi} \frac{B}{L} \frac{(C/2)}{h}\, d\theta \quad \ldots\ldots\ldots [11]$$

where h for an eccentric shaft is now a variable and B is the accumulated bearing surface covered by the lubricant, as shown in Fig. 4. In the convergent regions I and III the oil film is complete and $B = L$. In the divergent regions II and IV, the oil film is incomplete and continuity requires that the following relation hold

$$Bh = Lh_{\min}$$

where

$$h = C/2\,(1 - n_1 \cos\theta) \text{ for the lower half}$$

$$h = C/2\,(1 - n_2 \cos\theta) \text{ for the upper half}$$

Rewriting Equation [11] in the form of

$$j = \frac{H}{H_p} = \frac{H_1}{H_p} + \frac{H_2}{H_p} + \frac{H_3}{H_p} + \frac{H_4}{H_p}$$

with the subscripts referring to the power loss in the four regions, we then have

$$\frac{H_1}{H_p} = \frac{1}{2\pi} \int_{\pi/2}^{\pi} \frac{d\theta}{1 + n_1 \cos\theta} = \frac{1}{2\pi\sqrt{1 - n_1^2}} \arccos\left(\frac{\cos\theta + n_1}{1 + n_1 \cos\theta}\right)\Bigg|_{\pi/2 - \alpha_1}^{\pi}$$

$$\frac{H_2}{H_p} = \frac{1 - n_1}{2\pi} \int_{\pi}^{3\pi/2 - \alpha_1} \frac{d\theta}{(1 + n_1 \cos\theta)^2} = \frac{(1 - n_1)}{2\pi(1 - n_1^2)^{3/2}} \left\{\arccos\left(\frac{\cos\theta + n_1}{1 + n_1 \cos\theta}\right) - n_1 \sin \arccos\left(\frac{\cos\theta + n_1}{1 + n_1 \cos\theta}\right)\right\}\Bigg|_{\pi}^{3\pi/2 - \alpha_1}$$

$$\frac{H_3}{H_p} = \frac{1}{2\pi} \int_{\pi/2 + \alpha_1}^{\pi} \frac{d\theta}{1 + n_2 \cos\theta} = \frac{1}{2\pi\sqrt{1 - n_2^2}} \arccos\left(\frac{\cos\theta + n_2}{1 + n_2 \cos\theta}\right)\Bigg|_{\pi/2 + \alpha_1}^{\pi}$$

$$\frac{H_4}{H_p} = \frac{1 - n_2}{2\pi} \int_{\pi}^{3\pi/2 + \alpha_1} \frac{d\theta}{(1 + n_2 \cos\theta)^2} = \frac{1 - n_1}{2\pi(1 - n_2^2)^{3/2}} \left\{\arccos\left(\frac{\cos\theta + n_2}{1 + n_2 \cos\theta}\right) - n_2 \sin \arccos\left(\frac{\cos\theta + n_2}{1 + n_2 \cos\theta}\right)\right\}\Bigg|_{\pi}^{3\pi/2 + \alpha_1}$$

These integrations are accomplished by the use of the Sommerfeld substitution

$$\gamma = \arccos\left(\frac{\cos\theta + n}{1 + n \cos\theta}\right)$$

These four expressions were then evaluated for the various bearing attitudes and Fig. 7 gives the value of j as a function of the Sommerfeld number. The factor j contains here the combined effect of ellipticity, eccentricity, and incompleteness of the oil film. Then to compute the power loss in an elliptical bearing all that is necessary is to compute the power loss in a circular bearing of

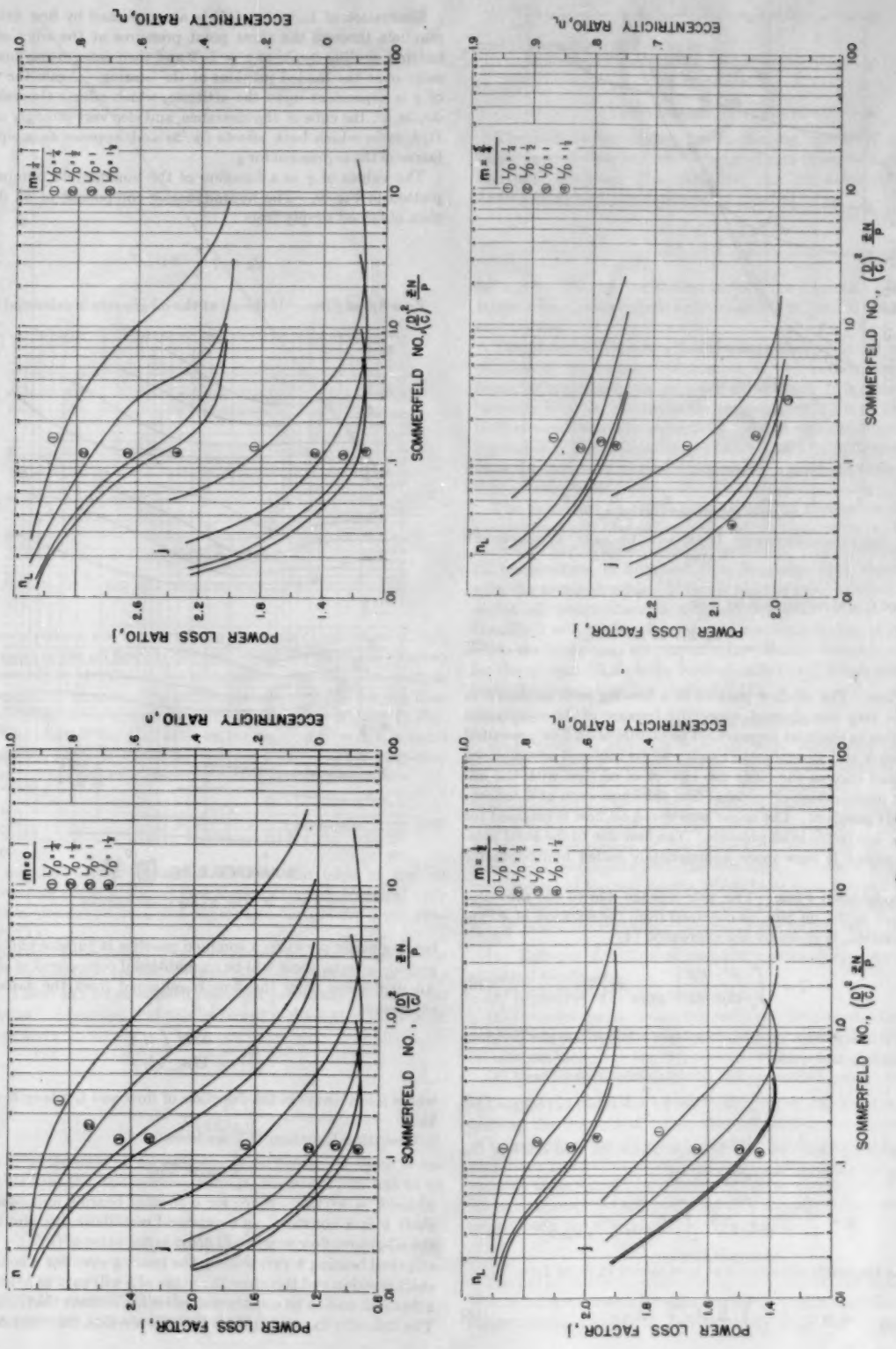

FIG. 7 PERFORMANCE CHARTS FOR ELLIPTICAL BEARINGS

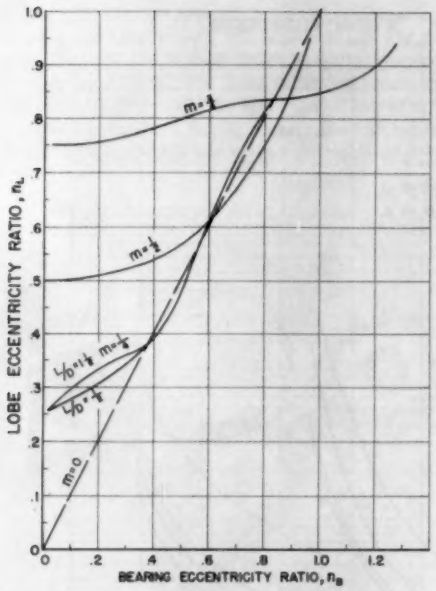

FIG. 8 RELATION BETWEEN LOBE AND BEARING ECCENTRICITY RATIO

clearance C and multiply it by j, or

$$H = j\frac{2\pi^3 ZN^2D^3L}{C} \quad \text{[12]}$$

Oil Flow. The oil-flow pattern in a bearing such as shown in Fig. 1 is very complicated, especially because of the component of flow due to the inlet pressure. The picture of oil flow presented by Wilcock and Rosenblatt (1) with all its inherent assumptions is retained here as the basic mechanism of oil flow with the important modification of variable film thickness even at a concentric shaft position. The name zero-speed oil flow is retained for the flow due to the inlet pressure. The flow due to the axial pressure gradient is here more appropriately called hydrodynamic flow.

Hydrodynamic Flow. The side leakage due to the pressures generated in the oil film, as obtained from the solution of Reynolds equation, is given by the expression (4)

$$Q = \int_c \frac{h^3}{12\mu}\frac{dp}{dz}\bigg|_{\pm L/2} dx \Bigg\} \quad \text{[13]}$$

To get this equation in dimensionless form, we use the previous substitutions and write

$$Q_h = q\frac{U}{2}L\frac{C}{2} = q\frac{\pi}{4}NDLC \quad \text{[14]}$$

Remembering that this side leakage occurs on two sides of the bearing, we have for the coefficient q

$$q = \frac{2\times 4}{12\times\pi}\left(\frac{D}{L}\right)^2\int_C h^3\frac{\partial p}{\partial z}\bigg|_{z=\pm L/2} dx$$

or since Reynolds equation was here solved in finite form

$$q = \frac{2}{3\pi}\left(\frac{D}{L}\right)^2\Sigma h^3\frac{\Delta p}{\Delta z}\bigg|_{z=\pm L/2}\Delta x \Bigg\} \quad \text{[15]}$$

Evaluation of Equation [15] is accomplished by first fitting a parabola through the three point pressures at the edge of the bearing, finding $\partial p/\partial z$ at $z = L/2$ and then integrating numerically over the loaded portions of the bearing. Again the value of q is dependent upon the attitude, which affects the value of $\partial p/\partial z$, h^3, the cube of the clearance, and also very strongly on the D/L ratio which both affects $\partial p/\partial z$ and appears as a squared factor in the expression for q.

The values of q as a function of the Sommerfeld number are plotted in Fig. 9. The hydrodynamic component of oil flow is then obtained simply from

$$Q_h = q\frac{\pi}{4}NDLC \quad \text{[16]}$$

Zero Speed Flow. If the oil at the oil grooves is delivered to the bearing under pressure, a common practice in turbine and marine propulsion sets, there will be an additional component of oil flow. An expression from the flow is obtained from the same basic expression

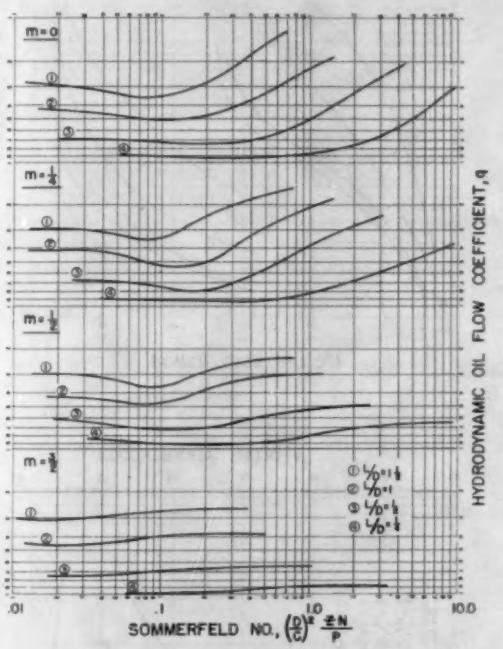

FIG. 9 OIL FLOW COEFFICIENT

$$Q_0 = \frac{\Delta p h^3}{12\mu}\left(\frac{l_1}{l_2}\right) \quad \text{[17]}$$

where l_1 is a length in the direction of flow and l_2 a length normal to l_1.

Rewriting Equation [17] we have

$$l_2\Delta p = kl_1Q$$

where $k = h^3/12\mu$. Since for a circular bearing and concentric shaft k is a constant, an equilateral rectilinear flux plot around the oil-groove flow source will provide the value of (l_1/l_2). For an elliptical bearing h varies along the bearing even for a concentric shaft position and therefore the value of k will vary as h^3 and thus a flux plot had to be constructed in such a manner that $l_2/l_1 \sim h^3$. The difficulty in making such a plot is obvious, but the inaccura-

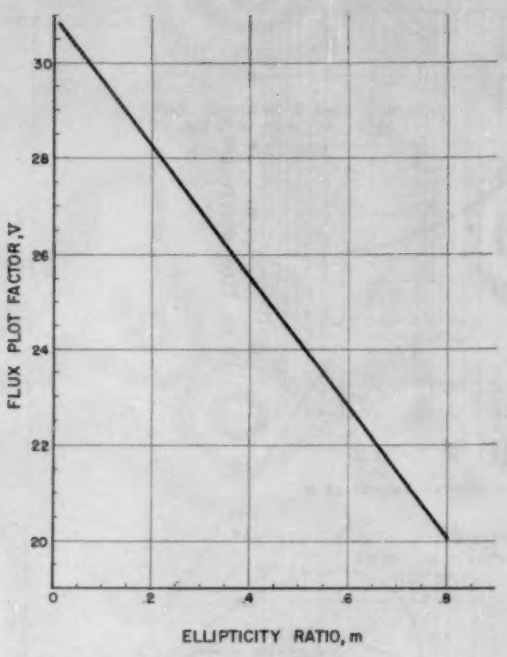

FIG. 10 PLOT OF FACTOR V

cies involved are not too serious as the bulk of the value of l_4/l_1 (i.e., most of the oil flow) is determined by the clearance space in the immediate vicinity of the oil groove. The flux plot there is still relatively simple. These flux plots were made for the four various ellipticities at an $L/D = 1$ and the result is given in Fig. 10. The effect of the L/D ratio on the value of $V = l_2/l_1$ is small (3) and the value of V can be used for all L/D ratios here considered. Thus the expression for zero-speed oil flow is

$$Q_0 = \frac{P_1 C^3}{24\mu} V \quad \ldots\ldots [18]$$

If chamfers—little triangular slots at the edge of the oil grooves—are present, the oil flow through them is identical with that in a circular bearing and expressions for it were given previously (1)

Dependent Quantities. Two remaining important quantities in bearing operation are temperature rise and minimum film thickness. These can be calculated from the previously obtained information. Assuming that all the power is dissipated in form of heat we have

$$c_p Q \Delta T = H/12J$$

or

$$\Delta T = \frac{H}{12Jc_pQ} \quad \ldots\ldots [19]$$

where Q is the sum of all component oil flows. If there is appreciable heat loss to the surroundings, Equation [19] has to be written as

$$\Delta T = \frac{H - J\varphi}{12Jc_pQ} \quad \ldots\ldots [20]$$

where φ is the amount of heat lost.

The minimum film thickness is given by

$$h_{min} = (1 - n_L)\, C/2 \quad \ldots\ldots [21]$$

and the bearing eccentricity by

$$e = n_E\, C_M/2 \quad \ldots\ldots [22]$$

PERFORMANCE CALCULATIONS

The information looked for in bearing operation is usually power loss, oil flow, and eccentricity. From these the temperature rise and minimum film thickness can be calculated. After having evaluated the Sommerfeld number

$$\left(\frac{D}{C}\right)^2 \frac{ZN}{P}$$

for a given bearing, the desired factors like j, q, and n_L can be obtained from the appropriate curves and then used in the foregoing expressions.

The problem that now arises is what viscosity to use in the calculation of the Sommerfeld number as well as in all subsequent formulas containing viscosity as a parameter. It is clear that the viscosity is not a constant as the temperature of the oil film varies both circumferentially and axially. Some representative operating viscosity has to be used and experience and tests have shown that the outlet oil viscosity represents a good approximation to this average value.

The procedure to be followed is thus to assume an outlet oil temperature and proceed with the calculations using the viscosity corresponding to the assumed temperature. The calculated outlet oil temperature, as obtained from Equation [19], should agree with the assumed value. If this is not the case, another value of outlet oil temperature is assumed and the process repeated. Usually 2 or 3 trials will locate the correct solution, particularly when the trial points are plotted on a viscosity-temperature curve for the oil used. This is the method called by Wilcock and Rosenblatt the "operating line method." (1)

EXPERIMENTAL RESULTS

Some tests on elliptical bearings were performed on a test machine described previously (1). Runs were made at various speeds up to 10,000 rpm, loads up to 750 psi, and inlet oil temperatures ranging from 80 to 125 F. Bearings ranging in diameter size from 4 to 8 in. and various ellipticities were tested. Figs. 11 and 12 give a comparison of the theoretical values of oil flow and power-loss coefficients with the test data. There is a markedly wide spread of the test results which have been lumped together from a variety of operating conditions and bearing designs. This spread is not too surprising because of the following:

(*a*) Extreme difficulty of measuring accurately clearances in elliptical bearings.

(*b*) Imperfections in the test machine.

(*c*) Inaccuracies in measuring and recording apparatus.

(*d*) The questionable validity of the assumption that the outlet oil temperature gives the "representative" bearing viscosity.

(*e*) Heat losses to environment not accounted for.

Despite the dispersion of the test points their general trend is to envelop the theoretical curve, thus confirming the proper order of magnitude of the theoretical results. By accounting for all the variations and inaccuracies involved in testing bearings, and if a suitable theory could be developed for a representative viscosity in bearings, the test points would probably follow somewhat more closely the theoretical curves.

ACKNOWLEDGMENT

The author wishes to acknowledge his indebtedness to Dr. D. F. Wilcock of the General Electric Company, for his many invaluable suggestions and to Mr. F. J. Maginniss also of the General Elec-

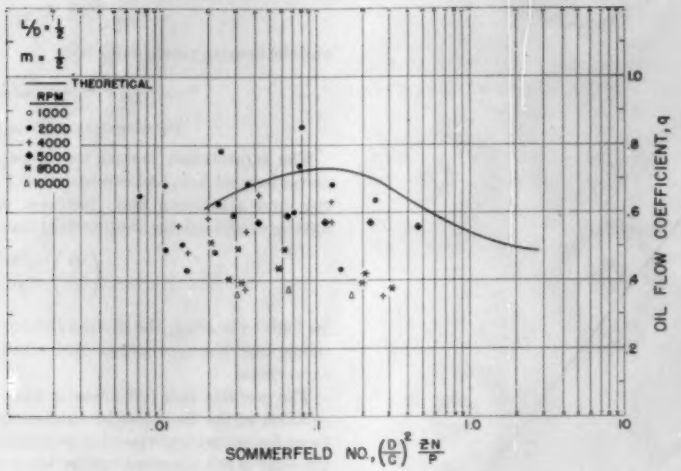

FIG. 11 THEORETICAL AND EXPERIMENTAL VALUES OF q

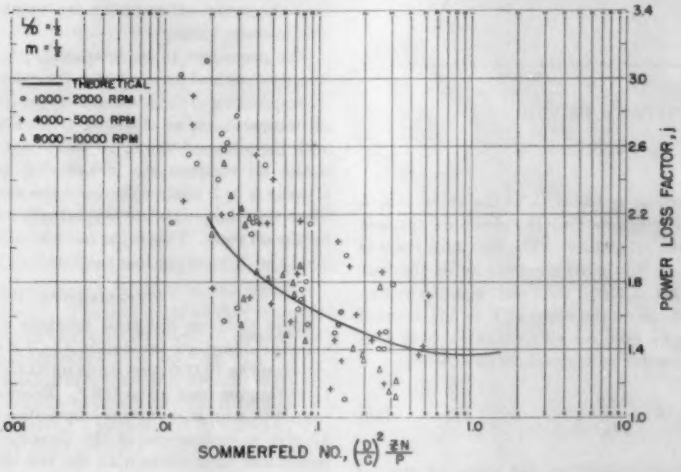

FIG. 12 THEORETICAL AND EXPERIMENTAL VALUES OF j

tric Company, for programming and supervising the numerical calculations on the digital computer.

BIBLIOGRAPHY

1 "The Full Journal Bearing," by A. Cameron and Mrs. W. L. Wood, Proceedings of the Institution of Mechanical Engineers, London, England, vol. 161, 1949, pp. 59–64.

2 "Relaxation Methods in Theoretical Physics," by R. V. Southwell, Oxford University Press, London, England, 1946.

3 "Oil Flow, Key Factor in Sleeve-Bearing Performance," by D. F. Wilcock and M. Rosenblatt, Trans. ASME, vol. 74, 1952, pp. 849–866.

4 "Effects of Side Leakage in 120-Degree Centrally Supported Journal Bearings," by S. J. Needs, Trans. ASME, vol. 56, 1934, pp. 721–732.

5 "On Problems of the Theory of Fluid-Film Lubrication, With an Experimental Method of Solution," by A. Kingsbury, Trans. ASME, vol. 53, Paper APM—53-5, 1931, pp. 59–75.

6 "On the Theory of Lubrication and Its Application to Mr. Beauchamp Tower's Experiments, Including an Experimental Determination of the Viscosity of Olive Oil," by Osborne Reynolds, Philosophical Trans. of the Royal Society, London, England, series A, vol. 177, 1886, pp. 157–234.

7 "Power Loss in Elliptical and 3-Lobe Bearings," by Oscar Pinkus, ASME Paper No. 54—LUB-9, published in this issue, pp. 899.

8 "Friction in Machines and the Effect of the Lubricant," by N. Petroff, *Engineering Journal*, 1883, no. 1, 2, 4.

Discussion

J. A. COLE.[9] The paper is a comprehensive addition to journal-bearing literature. The results for the case $m = 0$, zero ellipticity, are in themselves of great interest, and it is these only the writer wishes to discuss here. The author does not state explicitly the boundary conditions used, but notes that negative pressures were not allowed, and that this amounts to a zero pressure gradient at the trailing oil groove. In view of the presence of the grooves, the film should begin at the groove edge, where $\theta = 105$ deg $- \alpha$, and end at the groove edge $\theta = 255$ deg $- \alpha$ for small eccentricities (in which case $\partial p/\partial\theta$ may not be zero), or earlier at a point determined by $p = \partial p/\partial\theta = 0$ for larger eccentricities. θ is measured, as usual, from the point opposite the

[9] Department of Scientific and Industrial Research, Lubrication and Wear Division, Mechanical Engineering Research Laboratory, Thorntonhall, Glasgow, Scotland.

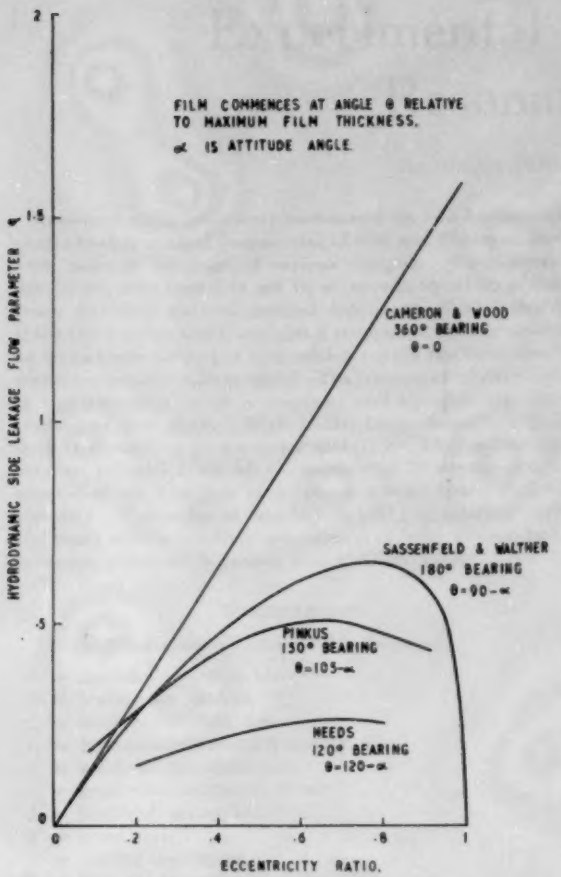

FIG. 13 THEORETICAL SIDE LEAKAGE, $L/D = 1$

minimum film thickness. In Fig. 4 of the paper, however, the full width film is shown to end at the minimum film thickness.

The load capacities evaluated are in good agreement with those of Sassenfeld and Walther[4] for the 180-deg bearing using boundary conditions similar to those just mentioned, and are also very near to those of Cameron and Wood[5] for a 360-deg bearing, indicating that for reasonably narrow bearings the precise form of the boundary conditions is unimportant in this respect.

It is curious, however, that in Fig. 5 the various width-diameter ratios give the same attitude-eccentricity locus. The two analyses mentioned give separate curves.

The hydrodynamic side-leakage values in Fig. 9 are of particular interest. The writer has constructed Fig. 13 of this discussion from Figs. 7(*a*) and 9 of the paper and from other sources to show the effect of the boundary conditions on the oil flow. The differences are seen to be large, especially at high eccentricities. These can be explained qualitatively on the basis that since the side leakage is the difference between the circumferential flows at the beginning and end of the pressure film, the later the film starts after the maximum film thickness the smaller the initial circumferential flow, as the film thickness is smaller and the adverse circumferential pressure gradient is greater. With an axial groove at the parting line to determine the film start, as in the author's analysis, the film commences progressively later relative to the maximum film thickness as the eccentricity increases, accounting for the drooping flow curve.

[4] "Gleitlagerberechnungen," by H. Sassenfeld and A. Walther, *VDI-Forschungsheft* 441, 1954.

[5] Reference (1) of the Bibliography of the paper.

AUTHOR'S CLOSURE

The author appreciates Mr. Cole's stimulating discussion and is glad to have the opportunity to add a few comments. There may have been a misinterpretation of Fig. 4. The sketch makes no reference to the extent of the pressure wave which may end at or after the point of minimum film thickness. In the solution of Reynolds equation the end of the pressure wave was established by the requirement that there be no negative pressures and this point was usually beyond the point of minimum film thickness. Fig. 4 in attempting to illustrate this point picked a case where the pressure wave ends at h_{min} and, as Mr. Cole points out, this may lead to an erroneous generalization. The full oil film may extend to any line between h_{min} and the trailing oil groove. Beyond the extent of the pressure wave a situation develops that there is not enough lubricant to fill out the clearance space. What then actually happens is that the effective width of the oil film is reduced, this reduction increasing with θ. Numerically this contraction of the oil film is given by

$$\text{Reduction} = 1 - \frac{B}{L} = \frac{n(1 + \cos\theta)}{1 + n\cos\theta}$$

and it has to be accounted for in the calculation of the bearing shear losses.

The analysis did yield different values of attitude angle for various L/D ratios. Table 1 shows these values for $m = 0$.

TABLE 1

	α at a given L/D ratio			
n	$^1/_4$	$^1/_2$	1	$1^1/_2$
0.2	70	64	64	62
0.4	57	53	53	51
0.6	43	42	42	42
0.8	29	24	28	29

The differences are of the order of a few degrees and where the loci are plotted on a polar diagram, as was done in Fig. 5, they blend into a single curve. The most pronounced dependence of α on the L/D ratio occurs at $m = {}^1/_2$.

In connection with the eccentricity locus, the author has subsequently run some tests using newly developed mutual-inductance gages. The theoretical and experimental loci for an $8 \times 8 \times 0.024 \times 0.012$ in. elliptical bearing are shown in Fig. 14.

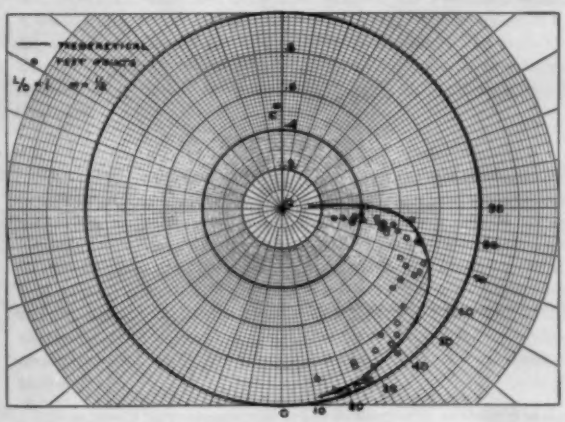

FIG. 14 LOCUS OF SHAFT CENTER

Experimental Investigation of Resonant Whip

By OSCAR PINKUS,[1] LYNN, MASS.

Resonant-whip tests were performed on two horizontal shafts having critical frequencies of 4000 and 6100 rpm and with pairs of bearings of various designs. Whip, when developed, was found to set in at speeds equal to about twice the first natural critical frequency of the shaft. With the heavier shaft, whipping stopped at speeds nearly equal to three times the first critical; with the light shaft whipping could not be stopped. The frequency of vibration in the whipping range is constant and equal to the first critical of the shaft. High loads, high viscosities, and flexible mounting gave greater stability. The load necessary to prevent whip at a viscosity of 70 centipoises is around 40 psi, but this value changes with speed and oil viscosity. The order of bearing stability is, starting with the most stable bearings, as follows: 3-lobe, tilting-pad, pressure, elliptical, 3-groove, and plain circular.

Nomenclature

The following nomenclature is used in the paper:

C = diametral clearance, in.
D = bearing diameter, in.
f_w = frequency of whip, cpm
f_n = first-observed natural frequency, cpm
f_r = rotational frequency, rpm
g = gravitational constant, ft/min^2
L = length of bearing, in.
N = speed, rpm
P = bearing loading, psi
P_i = inlet oil pressure, psi
Q = oil flow, gpm
T = temperature, deg C
W_s = weight of shaft, lb
Z = oil viscosity $\frac{\text{lb-min}}{\text{in.}^2}$
μ = oil viscosity, centipoises

Introduction

Resonant whip (previously called "oil whip") is a vibrational phenomenon encountered in shafts rotating in fluid-film bearings. It is usually associated with high speeds and low loads and is a result of a resonance built up in the oil film. Unlike other resonant vibrations, oil whip once started persists over a wide range of speeds. This shaft vibration is not to be confused with any regular vibration due to the unbalance of the shaft. Resonant whip is independent of balancing, but is excited and supported by the action of the fluid film alone, has a frequency of its own, and is capable of producing extremely high amplitudes of vibration. Resonant whip can be defined as a vibration of shafts in hydrodynamic journal bearings, with the frequency of vibration equal to a resonant frequency of the system regardless of the running speed. Because of the high amplitudes of vibration and the inherent instability of the shaft, resonant whip constitutes a serious threat to the bearings and the machine itself. Bearings have failed and the operation of many machines has been impeded because of the excessive vibrations induced by whip.

The phenomenon of resonant whip was first observed and described by Newkirk in 1924. He first set forth the theory that whipping of the shaft is caused by the action of the oil film in the clearance space, and in his original paper (1)[2] described the basic characteristics of resonant whip. Further investigation treated whip from the analytical standpoint. Robertson (2), by introducing the elasticity of the rotor in the dynamic equations of the shaft, showed that the rotor is inherently unstable at all speeds. Poritsky (3), assuming small shaft displacements and a radial force in the bearing, showed that instability should occur at speeds equal to twice the first critical of the shaft. The work of Newkirk and Grobel (4) was mainly concerned with designing or improving a bearing that would resist whipping. A more general approach to the problem is given in papers by Hagg (5) and by Hagg and Warner (6). Newkirk and Lewis (7) ran tests on horizontal shafts while Booker and Sternlicht (8) investigated unloaded vertical shafts and did some analytical work on stability criteria. A note on resonant whip was also published by the writer (9).

This investigation originally started with the intent of evaluating on a comparative basis the stability of various bearings used in turbines and motors. In the course of realizing the original objective, the program was broadened to include a more basic investigation of resonant whip. Such an understanding became necessary for a rational evaluation of rotor stability in a given set of bearings. Thus the investigation had a threefold purpose: (*a*) To determine the susceptibility of bearings of various designs to whip; (*b*) to obtain a characteristic pattern of resonant whip; and (*c*) to investigate the effect of some of the numerous design and operating variables on whip. Among the variables tested were loading, speed, bearing tightness, viscosity and amount of oil, unbalance, flexibility, and external excitation. The tests included circular (2 and 3 groove), elliptical, 3-lobe (symmetrical and asymmetrical), pressure, tilting-pad, and self-energizing bearings.

Test Equipment

The instability tests were conducted on a test stand described previously (10). This stand has a 200-hp amplidyne-controlled d-c motor with two sets of gears in series giving speeds up to 30,000 rpm. The general arrangement of the test stand is shown in Fig. 1. The dimensions of the test shafts are given in Fig. 2.

A pickup mounted in front of six bolts on the coupling face fed the signal into an Eput meter which recorded the rpm of the shaft directly. The speed could also be measured by an audio-oscillator and cathode-ray oscilloscope set and two Frahm tachometers.

---

[1] Bearing Development Engineer, Thomson Laboratory, General Electric Company. Assoc. Mem. ASME.

Contributed by the Research Committee on Lubrication under the auspices of the Lubrication Activity of The American Society of Mechanical Engineers, and presented at the Second Annual ASME-ASLE Lubrication Conference, Indianapolis, Ind, October 10–12, 1955.

Note: Statements and opinions advanced in papers are to be understood as individual expressions of their authors and not those of the Society. Manuscript received at ASME Headquarters, September 15, 1955. Paper No. 55—LUB-23.

[2] Numbers in parentheses refer to the Bibliography at the end of the paper.

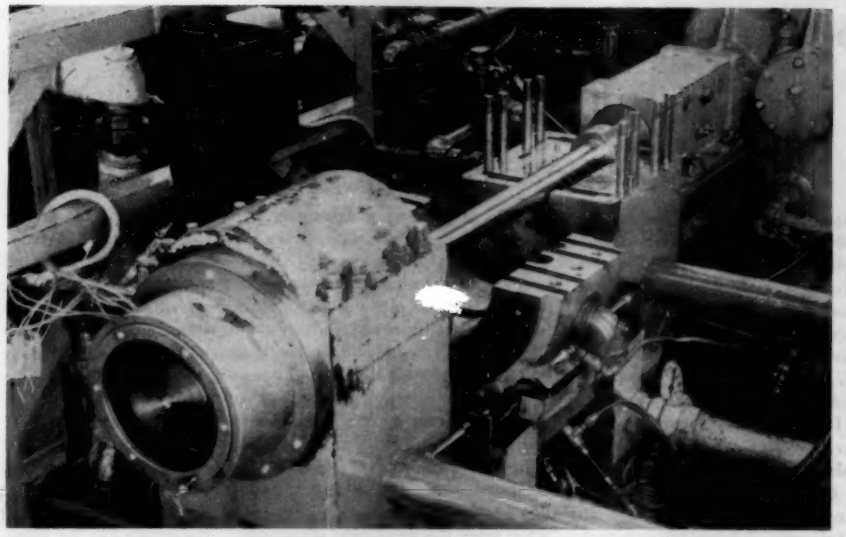

FIG. 1 GENERAL VIEW OF TEST STAND

The locus of the shaft center was traced on an oscilloscope screen. Four magnetic gages were mounted on the bearing liner with a clearance of about 25 mils between the shaft and the gages. The signal whose magnitude depended on the reluctance of the magnetic path was fed into a two-channel ampl fier consisting of bridge balancing circuits, alternators, carrier amplifiers, and detector circuits, then to a voltage booster in a switch box and finally into the x and y-axes of an oscilloscope. The locus of the shaft center could then be observed on the oscilloscope screen and photographed to provide information as to the shape of the locus as well as the amplitudes of vibration. Photographs of the traces were taken with a polaroid photographic camera. The arrangement of the electronic setup is shown in Fig. 3.

For each set of bearings, the gages were calibrated as follows: The shaft was first pulled to its extreme vertical and horizontal positions in the clearance space and coverage of this total displacement range assured on the milliammeter. The shaft was then displaced against a dial indicator in increments of 1 mil and the corresponding change in milliampere readings recorded. A plot of milliamperes versus displacement then gave the appropriate oscilloscope settings for reading of thousandths of an inch as whole divisions on the screen.

EXPERIMENTAL INVESTIGATION

The instability tests described in this report were performed on eight different bearing designs, mostly $2 \times 2 \times 0.005$ in. nominal size. Cylindrical bearings with an L/D ratio of $^1/_2$ and with clearances of 8 mils and 2.5 mils, respectively, were also tested as a preliminary attempt to determine the effect of these variables on whip. The bearings, used in pairs, were tested with two shafts; one weighing 187 lb with a mass in the middle and having a first critical of about 4000 rpm, and one of 64 lb with its first critical occurring at 6100 rpm. Turbine oil with a viscosity of 150 SSU at 100 F and a viscosity index of 102 was used on all tests.

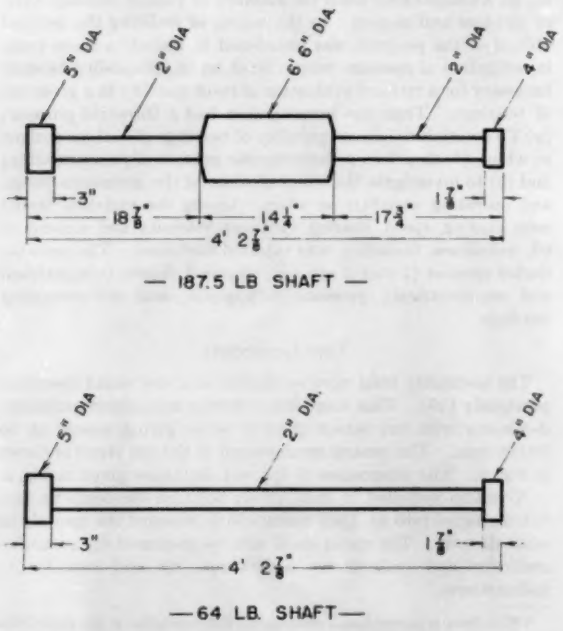

FIG. 2 DIMENSIONS OF TEST SHAFTS

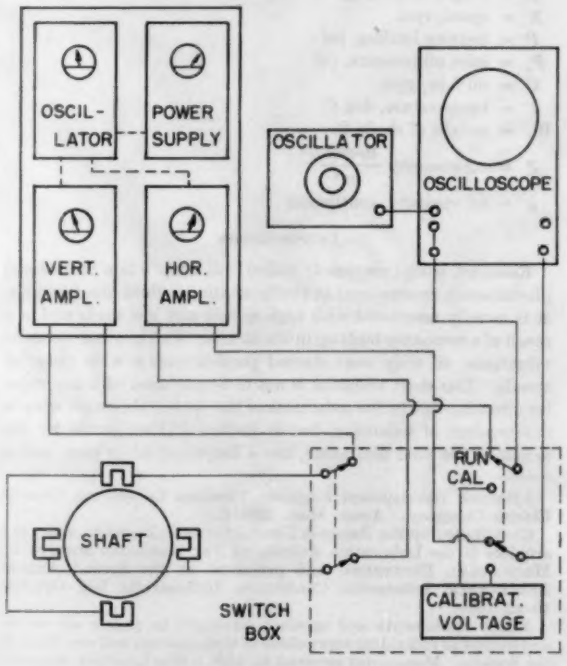

FIG. 3 TRACING THE LOCUS OF SHAFT CENTER

A typical run consisted of increasing the shaft speed and taking the following data: Inlet and outlet oil temperature, frequency of vibration of the shaft, speed, horizontal and vertical amplitudes of vibration, and inlet oil pressure. When required, the load and amount of oil flow were recorded. For certain runs photographs of the locus of the shaft center were taken with a polaroid land camera.

Most of the tests with the 187-lb shaft were stopped in the vicinity of 14,000 rpm. This upper limit of speed was imposed by extremely high amplitudes of vibration encountered. These were due to two reasons. At 14,000 rpm the shaft was reaching another critical speed. Also, it was discovered later that the test stand had a resonant response at this speed and the two stimuli caused excessive vibration. In one case, however, testing continued up to 17,400 rpm. With the 64-lb shaft, tests were run up to 24,000 rpm.

The configuration of the various bearings tested is given in Fig. 4. The self-energizing bearing was designed to increase bearing loading by transferring pressure from the bottom half of the bearing to the top. In the tests with the self-energizing bearing the top of the bearing was utilized to apply an external load on the bearing. This was done by joining the load-transferring tubing with the hydraulic system of the test stand. By closing either valve 2 or valve 1, Fig. 5, the bearing could be either self-energized or externally loaded.

Four kinds of tests were run with the self-energizing bearing. With both valves closed, the bearing was first tested as a plain circular bearing. Then with valve 2 closed and 1 open, the self-loading ability of the bearing was investigated as a function of a particular position of the pressure tap on the bottom of the bearing. The last two types of tests were performed with valve 1 closed and 2 open, the pressure being supplied by a hydraulic pump. In some runs no load was originally applied to the bearing and the speed was increased until whipping stopped. Readings were taken before and after whip stopped. The pressure was then taken off and the speed increased. Enough pressure was again applied to stop the shaft from whipping. This was repeated with higher and higher speeds, and values of the least pressure required to stop whip at a given speed were obtained. Finally, tests were run where pressure was applied at the very beginning and the inception of whip was recorded as a function of loading. The tests were run at oil-inlet temperatures ranging from 10 to 65 C.

In the tests designed to investigate the effect that tightness has on whip, the bearings in the caps were tightened by simply placing 0.0015-in-thick shims on top of the bearing and then bolting the cap. The bearings could be loosened in the caps in two ways. One method was to place 0.003-in-thick shims at the horizontal split of the cap. The other method was to reduce the outside diameter of the bearing by 4 mils. This later method enabled the bearing to move in a horizontal as well as in a vertical direction. All tests were performed with the 187-lb shaft on bearings that were on the border line of whip, i.e., 3-lobe and pressure bearings.

Results and Discussion

As mentioned in the Introduction, resonant whip can be defined as a vibration of shafts in hydrodynamic journal bearings whose frequency of vibration equals the natural frequency of the system regardless of the running speed. This form of vibration differs from ordinary vibration in that it is caused not by the unbalance of the shaft, but by the action of forces generated in the oil film. It also differs from ordinary vibration in that it is not confined to a single speed but persists over a wide range of speeds. No entirely satisfactory explanation of the origin of forces that produce whip exists, nor is there any useful criterion that would delineate the regions or conditions of shaft stability. The interpretation of the experiments, here performed, it is hoped, will furnish useful information about the general characteristics of resonant whip

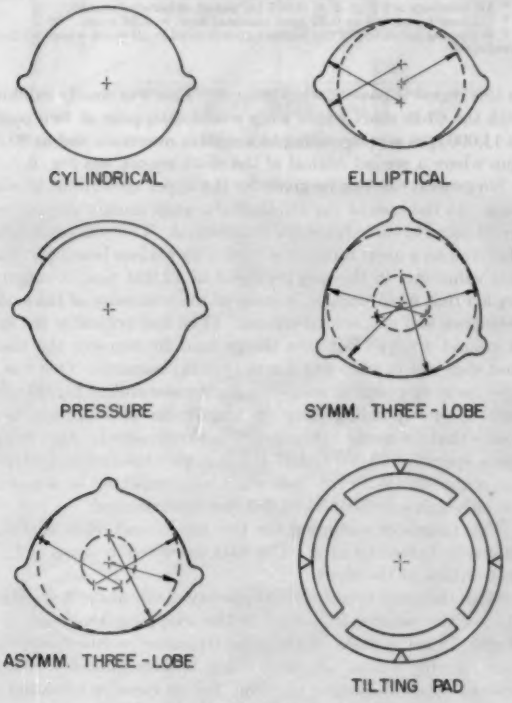

Fig. 4 Geometry of Test Bearings

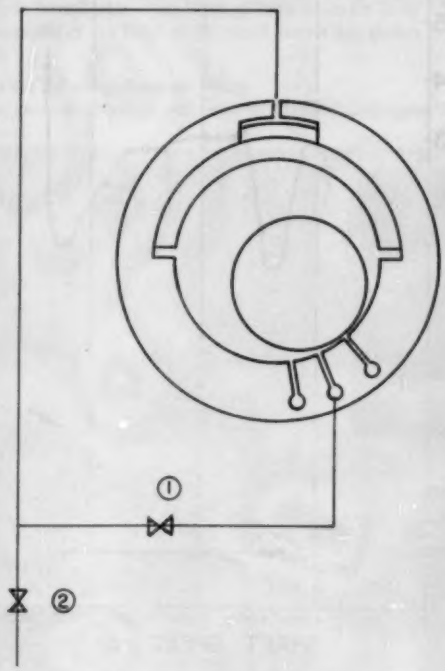

Fig. 5 Self-Energizing Bearing

TABLE 1 SUMMARY OF RESONANT WHIP TESTS WITH 187-LB SHAFT

Bearing[a]	f_n rpm	—Range of whipping at a given inlet oil temperature,[b] f_n— 25 C	45 C	66 C	Maximum speed, f_n
Cylindrical 2 × 1 × 0.005..	4100	1.3–1.6 & 1.9–3.0	.....	1.7–3.2	3.2
Cylindrical 2 × 2 × 0.005..	3800	1.7–3.2	.....	1.5–3.3	3.7
Cylindrical 2 × 2 × 0.0025.	4200	1.5–3.0	1.4–3.0	1.4–3.0	4.2
3-groove cylindrical.....	3800	1.8–3.1	.....	.....	4.0
Elliptical.....	3800	1.9–2.8	.....	1.7–2.8	3.5
Pressure.....	4100	0	2.0–3.0	1.9–3.0	3.6
3-lobe symmetrical.....	4100	0	2.3–2.6	2.0–2.8	3.3
3-lobe asymmetrical.....	4200	0	0	0	3.2
Tilting pad.....	5200	0	0	0	2.5

[a] All bearings are 2 × 2 × 0.005 in. unless otherwise stated.
[b] This includes the portion of half-frequency whirl.

and the effect of some of the operating variables and bearing designs on shaft stability.

Characteristic Pattern of Resonant Whip. Following is a description of the general pattern of resonant whip as exhibited in the series of experiments performed in this investigation. Phenomena of whipping that were qualitatively common to all cases regardless of shafts or bearings used will be classified as inherent characteristics of resonant whip.

In tests run with an increasing shaft speed, the start of whipping is usually characterized by a vibration whose frequency is about half of the running speed (8). This usually covers a relatively narrow range of speeds and is soon overtaken by a vibration where frequency is constant and equal to the first critical of the shaft. This transition occurs at speeds equal to twice the value of the first critical speed.

Resonant whip, unlike other forms of vibration, persists over a wide range of speeds. Whenever a speed is reached corresponding to a higher critical of the shaft or other resonance of the system, whip tends to be damped out and the resonant vibration having a frequency equal to the running speed prevails. As soon as this region is passed, whip returns. This was clearly exhibited with the 64-lb shaft where whip would disappear at two points, at 14,000 rpm corresponding to a system resonance and at 20,000 rpm where a second critical of the shaft occurs, see Fig. 6.

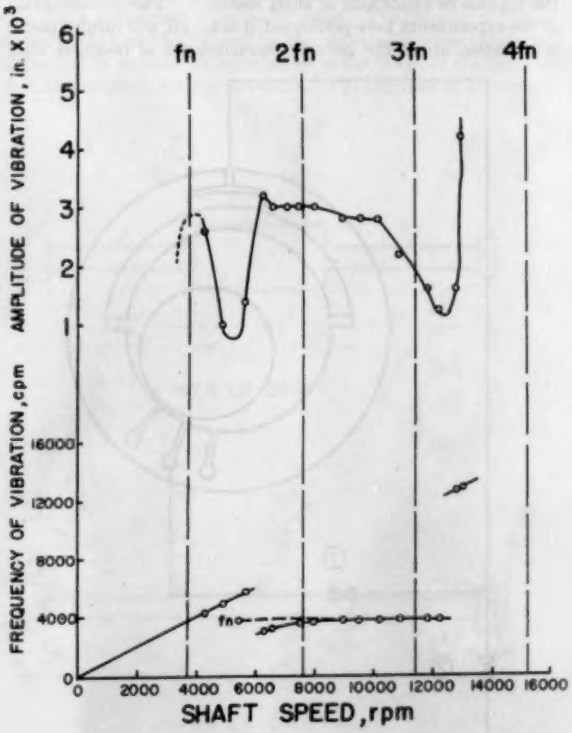

FIG. 6 TYPICAL WHIP CURVES FOR 187-LB SHAFT

TABLE 2 SUMMARY OF RESONANT WHIP TESTS WITH 64-LB SHAFT

Bearing[a]	Inlet oil temp, deg C	Transient whip starts, f_n	Steady whip starts, f_n	Maximum speed,[c] f_n
Cylindrical.....	25	..	1.93	1.93
2 × 2 × 0.005 in.....	45	..	1.93	1.93
f_n = 6100 rpm.....	60	..	1.93	1.93
Cylindrical.....	25	..	2.07	4.0
f_n = 6100 rpm.....	45	..	2.08	3.5
	60	..	1.98	2.8
3-groove cylindrical.....	25	..	..[b]	3.02
f_n = 6200 rpm.....	25	2.00	2.02	3.23
	45	1.95	2.00	2.00
	63	..	1.96	1.96
3-groove cylindrical.....	23	..	2.13	2.13
2 × 2 × 0.008 in.....	46	..	2.13	2.13
f_n = 6200 rpm.....	65	..	2.07	2.07
Tilting pad.....	10	2.33	2.40	..
f_n = 6200 rpm.....	25	2.21	2.30	2.80
	45	..	2.41	2.63
	60	..	1.86	1.86
Elliptical.....	25	2.08	2.48	3.0
f_n = 6100 rpm.....	45	1.97	2.60	3.12
	60	2.03	2.12	2.95
Pressure.....	10	1.96	2.70	3.76
f_n = 6100 rpm.....	20	1.99	2.64	3.51
	40	2.08	2.61	3.69
	60	1.97	2.54	3.73
3-lobe symmetrical.....	25	2.83	..	3.82
f_n = 6100 rpm.....	45	2.25	2.53	3.52
	60	2.08	2.58	3.28
3-lobe asymmetrical.....	25	..	..	3.74
f_n = 6100 rpm.....	45	2.00	2.64	3.48
	60	2.00	2.08	2.62

[a] All bearings are 2 × 2 × 0.005 in. unless otherwise stated.
[b] Oil flow restricted to 0.31 gpm (normal flow = 0.56 gpm).
[c] Whipping persisted to the highest speeds used in all cases where whipping developed.

No general rule can be given for the upper speed limit of whipping. In the case of the 187-lb shaft, whip usually stopped at a speed equal to three times the first critical. This was consistently observed on a great number of tests with various bearings. Since this value was in the neighborhood of 12,000 rpm, it might be argued that whip stopped because of the proximity of the system resonance and of a second critical. (The first critical of the shaft is around 4000.) But two things tend to disprove the theory that stoppage of whip was due to system resonance. One was the very early stoppage of whip—in some cases around 11,000 rpm—with a corresponding drop in amplitudes of vibration which means that the resonant region was not yet reached. Also, in some cases, speeds of 15,000 and 17,500 rpm were reached and whip did not reappear. With the 64-lb shaft whip could not be stopped at all, although speeds up to 24,000 rpm were reached.

The ranges of whipping for the 187-lb and 64-lb shafts are shown in Tables 1 and 2. The data are given in terms of f_n, the first critical of the shaft.

With the onset of whip, the frequency of vibration changes from that of the running frequency to the whipping frequency of the shaft. In many cases, the running frequency would disappear as soon as whip starts. In some cases, both frequencies would be present at the beginning of whip; but as speed is increased, the running frequency is damped out and the whipping frequency is

the only one left. The value of the whipping frequency increases slightly with speed and approaches an asymptotic value.

The second symptom of whipping, in addition to a change in vibration frequency, is an increase in the amplitudes of vibration. In most cases, the change in magnitude is extremely sharp, sometimes equaling the diametral clearance of the bearings. The amplitudes of vibration rise in the vicinity of the speed where whip starts, but tend to level off. Figs. 6 and 7 give a graphical representation of the whip phenomenon. The relation

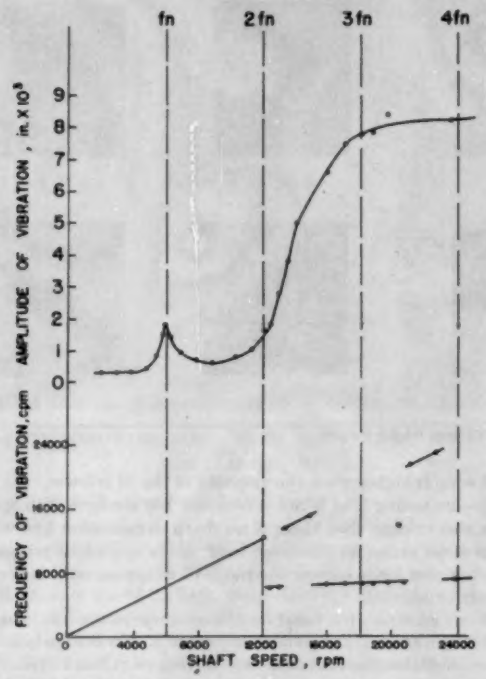

FIG. 7 TYPICAL WHIP CURVES FOR 64-LB SHAFT

between speed, frequency, and amplitudes of vibration is shown for a pair of cylindrical bearings using both the 187-lb and 64-lb shafts.

In a number of experiments, a phenomenon that might be called an inertia effect in resonant whip was observed. In general, it is characterized by a resistance to whip when the shaft is stable and an unwillingness to pull out of whip once it develops. When whipping was observed under conditions of decreasing speeds, it was noted that whip persisted down to speeds lower than those at which whip started when speed was being increased. In many cases, it took some time for whip to develop at a given speed; and in the experiments with variable bearing loading, it took a higher load to stop whip than to prevent it.

In some cases, the stable and unstable states were separated by a region of transient whip. In this transient condition, the shaft would alternately become stable and unstable. All the symptoms of whip, as an increase in amplitudes of vibration, a change of vibrational frequency, and the appearance of the characteristic locus of the shaft center, would correspondingly follow this cyclic change. This state of transient whipping sometimes persisted over an appreciable range of speeds, once over the entire whipping range.

Using the pickup system described under Test Equipment, the trace of the locus of the shaft center assumes a distinctly different appearance when the shaft becomes unstable. For a stable position, the trace is a steady single-contoured loop. In the unstable region the loop, in addition to becoming larger, forms two or more loops and starts to rotate on the oscilloscope screen. As speed is increased, the trace becomes more and more complex, producing the effect of a rotating multiple-boundary network. Some of the loops are apparently due to the unbalance vibration, some to whipping. Having different frequencies, these loops are out of phase and produce the effect of rotation although an actual rotation of the trace is also noticeable. At points where whip disappeared, the trace would first stop rotating and then the multiple boundaries would merge into a single loop. Typical photographs of the locus of the shaft center are shown in Figs. 8 and 9.

Variables Affecting Resonant Whip

The factors affecting whip can be divided into operating and

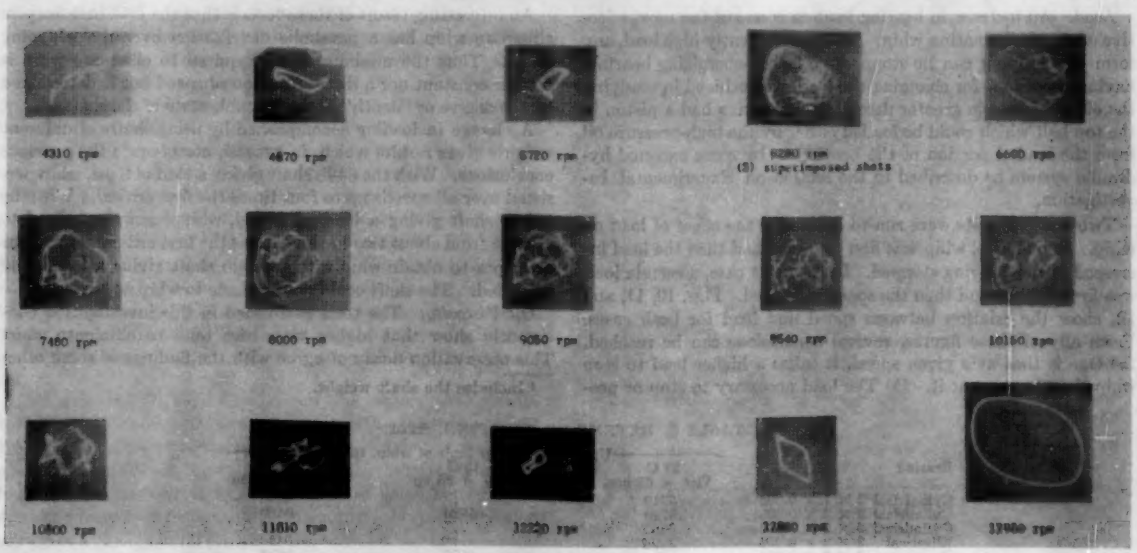

FIG. 8 LOCUS OF SHAFT CENTER FOR 187-LB SHAFT

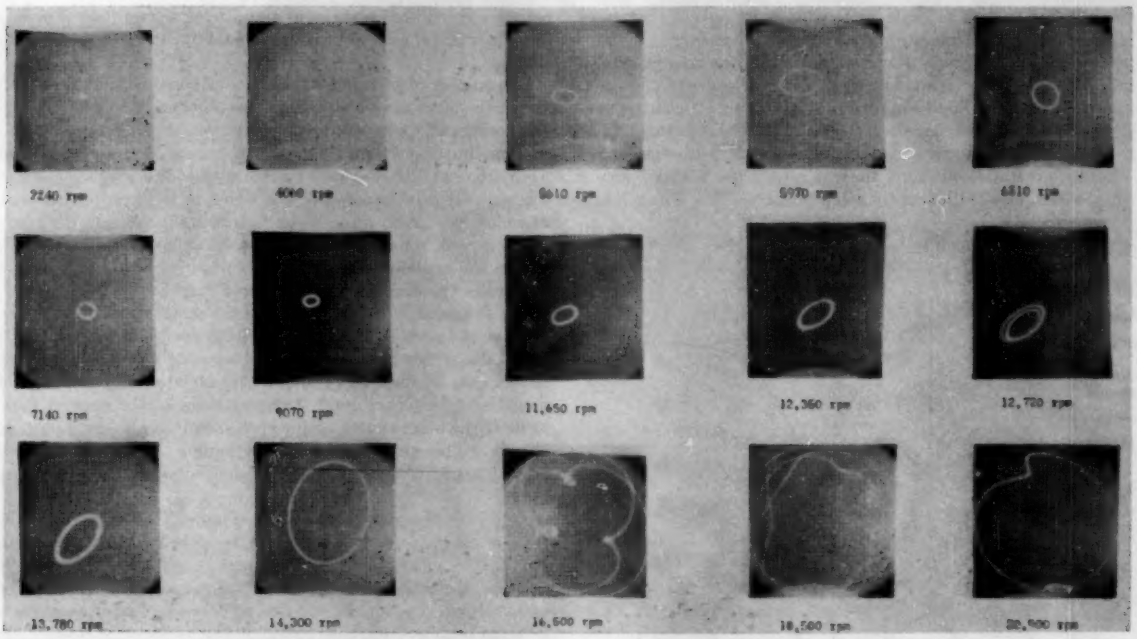

FIG. 9 LOCUS OF SHAFT CENTER FOR 64-LB SHAFT

design variables. The first category refers to conditions or techniques of bearing operation regardless of kinds of bearings used, like viscosity or tightness of bearings. Design variables refer to the proportions or dimensions of a given bearing design, like changes in the L/D ratio or clearance. Each factor affecting oil whip will be taken up individually and discussed.

Speed. Since whip starts at about twice the natural frequency of the shaft, a wider range of stable operating speeds can be obtained by raising the value of the first critical. If the machine is made to operate at speeds below about 1.5 times the first critical, no whip is likely.

Load. An increase in bearing loading is one of the most effective ways of eliminating whip. With a sufficiently high load, any form of whipping can be stopped. The self-energizing bearing, having provisions for changing the load, was utilized in studying the effect of load in greater detail. This bearing had a piston in the top half which could be loaded either by the high-pressure oil from the loaded portion of the bearing or by some external hydraulic system as described in the section on Experimental Investigation.

Two kinds of tests were run to determine the effect of load on whip. In one case, whip was first obtained and then the load increased until whipping stopped. In the other case, a certain load was first applied and then the speed increased. Figs. 10, 11, and 12, show the relation between speed and load for both cases. From any of these figures, several conclusions can be reached. (*a*) One is that at a given speed, it takes a higher load to stop whip than to prevent it. (*b*) The load necessary to stop or prevent whip is higher when the viscosity of the oil is lower. (*c*) The whip-eliminating load is not a constant but changes with speed. It is also evident that there is no sharp demarcation line where whip stops under an increased load. It is a gradual process in which higher loads narrow the range of whipping until it is completely eliminated.

As an example, the total load[3] necessary to prevent whip at 10,000 rpm and an inlet oil temperature of 45 C was 62 psi; for the same conditions the load necessary to stop whip was 75 psi. The load necessary to prevent any whippng at all with a 25-C inlet oil temperature was 40 psi; for 45-C oil, 57 psi.

An interesting result of these tests is that the load necessary to eliminate whip has a parabolic distribution over the whipping range. Thus the minimum load required to eliminate whip is neither constant nor a direct function of speed but is determined by the degree or "depth" of the unstable state of the shaft.

A change in loading accomplished by using shafts of different weights gives results which, in general, corroborate the previous conclusions. With the 64-lb shaft giving a load of 8 psi, whip persisted over all speeds up to four times the first critical. With the 187-lb shaft giving a load of 23 psi, whipping was confined to a range from about two to three times the first critical. Previous attempts to obtain whip with a 400-lb shaft giving a load of 40 psi failed. The shaft could not be made to whip at any speed.

Oil Viscosity. The tests performed in this investigation consistently show that higher viscosities tend to eliminate whip. This observation does not agree with the findings of some other

[3] Includes the shaft weight.

TABLE 3 EXTENT OF WHIPPING, RPM

Bearing	Upper limit–lower limit of whip, rpm 25 C Visc = 65 cp	45 C Visc = 26 cp	60 C Visc = 14 cp
Cylindrical 2 × 1 × 0.005	5710	..	6140
Cylindrical 2 × 2 × 0.008	6720	6880	6590
Cylindrical 2 × 2 × 0.005	5960	..	6840
Elliptical 2 × 2 × 0.005	3990	..	5380
Pressure 2 × 2 × 0.005	0	1150	5290
3-Lobe 2 × 2 × 0.005	0	1330	3510

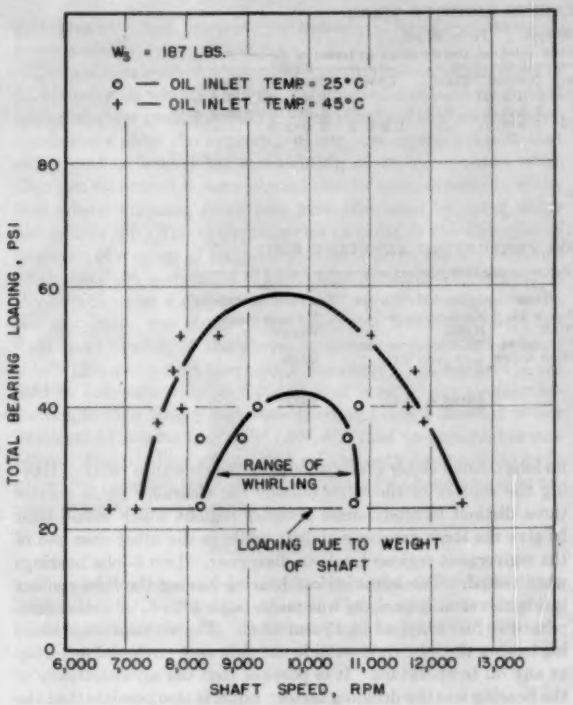

FIG. 10 RANGE OF WHIP VERSUS LOADING

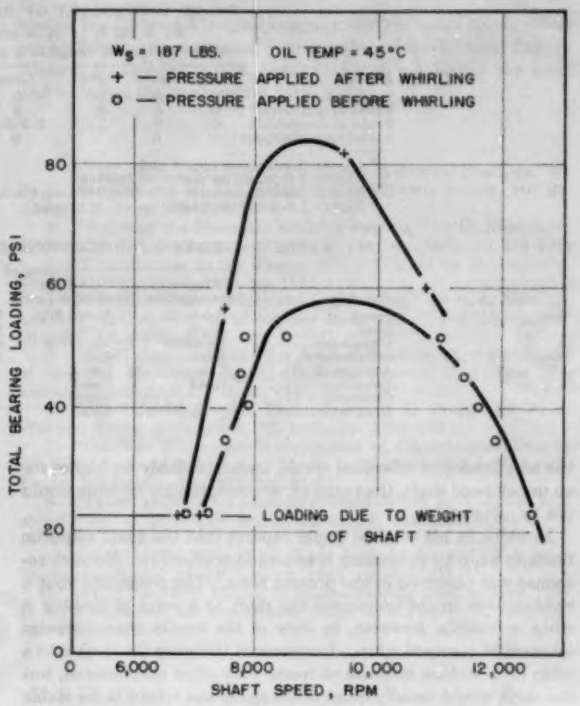

FIG. 11 BEARING LOADING AT BOUNDARY POINTS OF WHIP

investigators, but Table 3 shows how consistently this trend was evidenced in the tests with the 187-lb shaft.

In the case of the 64-lb shaft, the picture is a little less obvious because of the lack of an upper whip limit, but a glance at Table 2 shows that raising the oil temperature tends, in general, to lower the speed at which whip starts. As can be seen from this tabulation, the range of whipping increased with an increase in inlet oil temperature. With several bearings, whipping was entirely eliminated when the oil was cooled down to 25 C.

That higher oil viscosities contribute to greater shaft stability was also evidenced in the tests with the self-energizing bearing. In all cases, the loads required to eliminate whip were lower for cold oil. Even in the cases when whip occurred, the violence of the vibration was higher for the high-temperature oil.

Amount of Oil. Since resonant whip is a vibration produced by the action of the oil film, the amount of oil flowing through the bearing would be expected to have some effect on whip. The only test made here was one in which a reduction in oil flow was accomplished by making a bearing without chamfers. With an oil flow of only 0.31 gpm, no whip developed. When chamfers were made and the oil flow increased to 0.51 gpm, the bearing whipped. It is possible that there is no sharp break between whip and no whip at some particular oil flow, but that there is a gradual reduction in the violence and range of whipping with a reduction in oil flow.

Unbalance and External Excitation. The present tests corroborate the findings of most other experiments that unbalance has little, if any, effect on resonant whip. In a number of tests, unbalance weights were inserted in the shaft, but no significant change in shaft behavior was observed. In some border cases where the transition from a stable to an unstable state depended only upon a change in oil temperature, unbalancing the shaft did not shift the respective boundaries of the two regions. Although

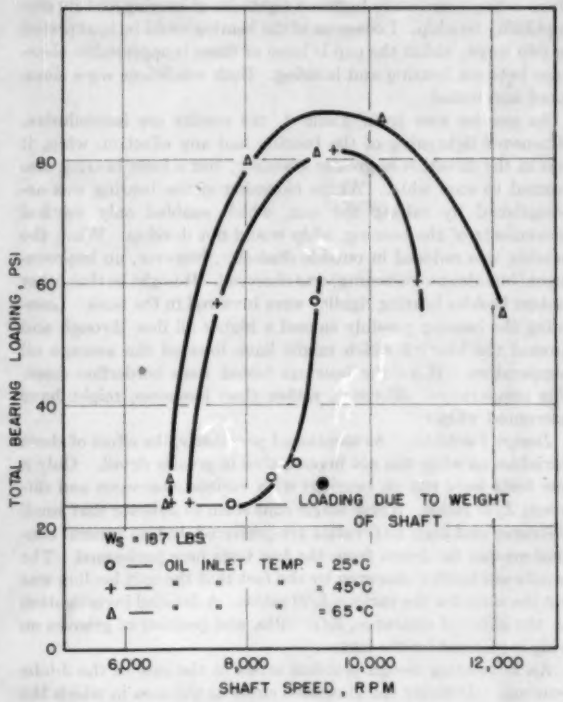

FIG. 12 MINIMUM PRESSURE REQUIRED TO STOP WHIP

TABLE 4 SUMMARY OF BEARING RIGIDITY TESTS

W_s = 187 lb f_n = 4200 rpm P_1 = 20 psi

	Whipping range at a given inlet oil temperature in terms of f_n								
	25 C			45 C			60 C		
Bearing	Loose	Normal	Tight	Loose	Normal	Tight	Loose	Normal	Tight
Pressure[a]	0	0	0	0	2.0–3.0	0	0	1.9–3.0	2.0–3.0
3-lobe symmetrical[a]	0	0	0	0	2.3–2.6	0	0	2.0–2.8	1.7–2.8
3-lobe asymmetrical[b]	0	0	...	2.2–2.6	2.3–2.6	...	1.8–3.2	2.0–2.8	.....
3-lobe asymmetrical[b]	0	0	...	0	0	...	0	0	.....

[a] Loose: 3-mil shims placed under cap.
Tight: 1.5-mil shims placed on bearing.
[b] Loose: Outside diameter of bearing reduced 4 mils.
Tight: 1.5-mil shims placed on top of bearing.

TABLE 5 DESIRABLE CONDITIONS FOR PREVENTING RESONANT WHIP

	Source of recommendation—references				
Variable	Present investigation	(1) & (7) Newkirk & Lewis	(5) Hagg	(6) Hagg & Warner	(8) Boeker & Sternlicht
Speed	Below $2f_n$	Below $2f_n$	Below $2f_n$	No assurance	No assurance
Load	High	High	High	High	High
Unbalance	No effect	No effect	Eliminates	Eliminates air causes	.....
Oil viscosity	High	Low	High & low	Low (and high)	High
Amount of oil	Low	Low	.....	.....	.....
Loose cap	Good	Good	.....	.....	.....
Clearance	....	Large	.....	Large & small	Large
L/D ratio	....	Small	.....	Small	.....

the amplitudes of vibration would understandably be higher for an unbalanced shaft, the range of, or susceptibility to, whip would not be affected.

Newkirk in his original paper reports that the shaft could be made to whip by subjecting it to a sudden blow (1). No such response was observed in the present tests. The possibility that a sudden blow might unbalance the shaft to a point of making it whip is feasible, however, in view of the inertia characteristics inherent in resonant whip. Instances of throwing the shaft into a whip by a sudden increase of speed were often encountered, but the shaft would usually quiet down again and return to its stable operation.

Tightness of Bearing. Bearings being on the border line of whip were chosen for a series of tests designed to establish whether there is any correlation between tightness of bearing and its susceptibility to whip. Looseness of the bearing could be interpreted in two ways; either the cap is loose or there is appreciable clearance between bearing and housing. Both conditions were simulated and tested.

As can be seen from Table 4, the results are inconclusive. Whenever tightening of the bearing had any effect on whip, it was in the direction of greater stability; but a loose bearing also seemed to stop whip. Where loosening of the bearing was accomplished by raising the cap, which enabled only vertical movements of the bearing, whip would not develop. When the bearing was reduced in outside diameter, however, no improvement (but also no worsening) was observed. It might be that other factors besides bearing rigidity were involved in the tests. Loosening the bearing possibly caused a higher oil flow through and around the bearing which might have lowered the average oil temperature. Since the bearings tested were borderline cases, this temperature difference, rather than looseness, might have prevented whip.

Design Variables. As mentioned previously, the effect of these variables on whip was not investigated in greater detail. Only a few tests were run on bearings with various clearances and different L/D ratios. These single runs seem to indicate that small clearance and high L/D ratios are preferred, but no general conclusions can be drawn from the few tests here performed. The results are further obscured by the fact that the unit loading was not the same for the various L/D ratios. A detailed investigation on the effect of clearance, L/D ratio, and position of grooves on whip is planned for the future.

An interesting design problem arises in the case of the 3-lobe bearings. Defining the clearance circle as the area in which the shaft center is free to move a 3-lobe bearing can be designed with its lobe centers either inside or outside the clearance circle. Having the centers of the lobes outside the clearance circle creates three distinct hydrodynamic pressure regions which would tend to give the shaft greater stability, while in the other case one of the convergent regions tends to disappear. Two 3-lobe bearings were tested. The symmetrical bearing having the lobe centers inside the clearance circle was stable with a 25-C oil (inlet temperature) but whipped at 45 and 60 C. The asymmetrical bearing having the lobe radii outside the clearance circle did not whip at any oil temperature. It is possible that the asymmetricity of the bearing was the deciding factor; but it is also possible that the location of the lobe centers outside the clearance circle contributed to the stability of the bearing. This point too will be the subject of future investigation.

Susceptibility of Bearings of Various Designs to Whip

The bearings tested for their susceptibility to whip include circular, elliptical, 3-lobe, pressure, tilting-pad, and self-energizing bearings. When one bearing whips while the other does not, the classification is obvious, but where both varieties of bearings whip an evaluation becomes more difficult. In such cases, the extent of range of whipping was taken as a basis for comparison. Also, such factors as magnitude and violence of vibration were taken into account. Tables 1 and 2 tabulate the bearings in order of increasing stability. Not only does the range of whipping decrease as one moves down the list of bearings but also, the violence and the amplitudes of vibration were smaller for the pressure and 3-lobe bearings.

The 3-lobe and tilting-pad bearings are the most stable ones while plain cylindrical bearings are the most susceptible to whip. The self-energizing bearing is a class in itself. This bearing, sufficiently loaded by some external source, can prevent whipping under the most adverse conditions.

Comparison With Other Investigations

It might be of some interest to compare the findings of this investigation with past literature on whip. Table 5 summarizes test results and conclusions reached here and by some other workers in the field. In this table, the conditions of each variable or design feature that gives greater shaft stability is described.

There is general agreement that keeping the operating speed below $2f_n$ and using a sufficiently high loading is the surest way for preventing resonant whip. The prevalent opinion is also that unbalance has little effect on whip and that a low oil supply is desirable. The question of the effect of clearance and L/D ratio is

problematic. And, surprisingly enough, a loose cap seems to foster stability.

The greatest confusion seems to reign in the case of the effect of oil viscosity on whip. Definite statements have been made that hotter oil gives greater stability. The results of this investigation consistently show the opposite. Some investigators report that either cold or hot oil has a stabilizing effect on resonant whip. This last statement is corroborated also by some experience in the field where whipping conditions were alleviated by using either hot or cold oil. The evidence seems to point in the direction of existence of a range of temperatures for a given set of conditions where the shaft is unstable. In that case, either cooling or heating the oil will cause a change of state. To a certain degree such a stability curve was obtained by Hagg and Warner (6) with the right-hand branch of the curve much flatter than the left-hand side. This also would upset the attempts of some workers in the field to delineate whip as a function of eccentricity alone. According to their theory high eccentricities, being a function of low Sommerfeld numbers, $(D/C)^2\,(ZN/P)$, tend to give higher stability. The peculiar effects that oil viscosity has on whip indicates that resonant whip is too complicated a phenomenon to explain in terms of eccentricity alone.

Acknowledgment

The author wishes to acknowledge his indebtedness to Mr. D. A. Wilhelmson of the General Electric Company for devising the method of measuring the shaft locus, and to Dr. D. F. Wilcock, also of the General Electric Company, for his many constructive suggestions and comments. Acknowledgment is also due to Messrs. E. Beesley and R. Ostrowski who conducted the tests and collected the background data.

BIBLIOGRAPHY

1 "Shaft Whipping Due to Oil Action in Journal Bearings," by B. L. Newkirk and H. D. Taylor, *General Electric Review*, vol. 28, August, 1925, pp. 559–568.

2 "Whirling of a Journal in a Sleeve Bearing," by D. Robertson, *Philosophical Magazine*, series 7, vol. 15, January, 1933, pp. 113–130.

3 "Contribution to the Theory of Oil Whip," by H. Poritsky, Trans. ASME, vol. 75, 1953, pp. 1153–1161.

4 "Oil-Film Whirl—A Nonwhirling Bearing," by B. L. Newkirk and L. P. Grobel, *Journal of Applied Mechanics*, Trans. ASME, vol. 56, 1934, pp. A-607–A-615.

5 "The Influence of Oil-Film Journal Bearings on the Stability of Rotating Machines," by A. C. Hagg, *Journal of Applied Mechanics*, Trans. ASME, vol. 68, 1946, pp. A-211–A-220.

6 "Oil-Whip of Flexible Rotors," by A. C. Hagg and P. C. Warner, Trans. ASME, vol. 75, 1953, pp. 1339–1344.

7 "Oil-Film Whirl—An Investigation of Disturbances Due to Oil Films in Journal Bearings," by B. L. Newkirk and J. F. Lewis, Trans. ASME, vol. 78, 1956, pp. 21–27.

8 "Investigation of Translatory Fluid Whirl in Vertical Machines," by G. F. Boeker and B. Sternlicht, Trans. ASME vol. 78, 1956, pp. 13–19.

9 "Note on Oil Whip," by Oscar Pinkus, *Journal of Applied Mechanics*, Trans. ASME, vol. 75, 1953, pp. 450–451.

10 "Oil Flow, Key Factor in Sleeve-Bearing Performance," by D. F. Wilcock and M. Rosenblatt, Trans. ASME, vol. 74, 1952, pp. 849–866.

Varieties of Shaft Disturbances Due to Fluid Films in Journal Bearings

By B. L. NEWKIRK,[1] SCHENECTADY, N. Y.

Diversities of behavior and some seeming inconsistencies among the disturbances due to the action of fluid films in journal bearings are described. These are shown to be broadly consistent and in accord with findings of analysis. Some items of observed behavior are mentioned and critical speeds due to fluid-film action are listed.

Introduction

THE disturbances heretofore called "shaft whipping," "oil whip," or "oil-film whirl" have been recognized and discussed for some 30 years. Recently, certain apparent inconsistencies of reported behavior have come to light. For example, the disturbance appears with some rotors that run at speeds below their lowest critical speeds and, in other cases, it does not appear unless the rotor runs at more than twice its lowest critical speed. In the field, some rotors exhibiting the disturbance can be quieted by warming up the oil supplied to the bearing and in other cases, cooling the oil supply is effective. There are other diversities of behavior which are discussed in the paper, that indicate a complex situation requiring clarification.

Two Typical Cases

To make a start in reconciling the apparent inconsistencies in shaft disturbances, two typical cases already described in the literature will be reviewed.

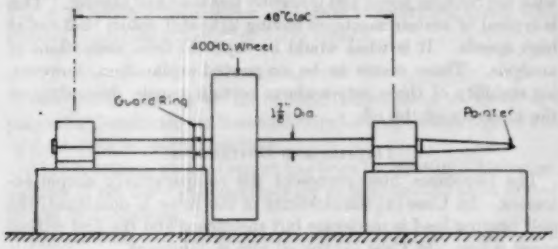

FIG. 1

Case a. In reference (1),[2] fig. 1, a rotor is described consisting of a 1 1/8-in. shaft, having a span of 40 in., carrying at its center a 400-lb disk, and running in bearings 1 7/8 × 2 1/2 in., with a diametral clearance of 0.003 to 0.004 in. The unit bearing pressure was approximately 42.5 psi and the lowest critical speed was stated to be "about 1210 rpm." (With bearings having so large a length-diameter ratio, the critical speed is not sharply defined—depending on alignment of bearings and amplitude of the critical-speed whirl). See Fig. 1.

The model ran smoothly at lower speeds, but at higher speeds, over the range of running speeds from 2300 to 5000 rpm, the rotor whirled about as it did at critical speed, with whirling frequencies of 1205 to 1280 per min. The severity of the whirl increased with increasing speed. The 5000 rpm was the top speed for this model. This is a resonant motion in the sense that its frequency is the natural frequency of the shaft.

Case b. In reference (2), fig. 8 (shorter rotor), and pages 5 and 6, a short very stiff shaft[3] is shown, having a ball bearing or a small journal bearing at one end and, at the other end, a bearing of 2 in. diam, 1 1/8 in. long (see Fig. 2). There was no critical speed within the range of operation, up to 30,000 rpm. The unit bearing load was about 4 psi. This shaft whirled at low speeds, and the whirl frequency in cycles per minute was "somewhat less than one half the running speed" in rpm. It "would not whirl at higher speeds, and the limiting speeds, above which whirling would not occur, varied from 7000 rpm to 18,000 rpm, depending on the temperature (viscosity) of the oil, the higher limit corresponding to the lower viscosity." This is a nonresonant motion.

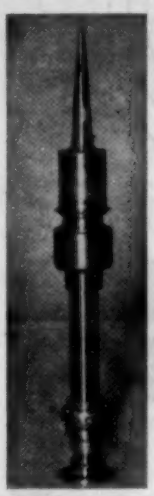

FIG. 2

Hydrodynamics of Journal Whirl

An analytical basis for whirling of a journal due to oil-film action was offered by Harrison (4). Making the usual assumptions, of constant viscosity, a full bearing without end leakage, etc., he found that a running position of the journal is indicated for each load, but that if the speed or load changes, the journal will not move to the new position of equilibrium but it will revolve in a closed orbit. Robertson (5) pointed out that, in view of the mass of the journal, the whirling would become an outward spiral, with the inference that all journal bearings should be unstable (see Fig. 3; this is Harrison's fig. 7). Robertson rejected this inference as contrary to well-established facts. However, there seems to be a sound analytical explanation for the instances of whirling of vertical rotors in guide bearings, and of stiff horizontal rotors with lightly loaded journal bearings. A recent investigation (6) reports cases of similar whirling of a lightly loaded journal. The situation seems, therefore, to call for an explanation for the stability of some rotors as well as for the instability in other cases.

Rotor Flexibility the Key Factor

In Case (*a*) the elasticity of the shaft plays a decisive role in the development of disturbances stimulated by the oil film. Consider a sequence of events as follows, referring to Fig. 1.

A jar results in a transverse vibration of the shaft in its own natural frequency.[4] This vibration of the shaft causes displace-

[1] Consultant. Fellow ASME.

[2] Numbers in parentheses refer to the Bibliography at the end of the paper.

Contributed by the Research Committee on Lubrication under the auspices of the Lubrication Activity of THE AMERICAN SOCIETY OF MECHANICAL ENGINEERS and presented at the Second Annual ASME-ASLE Lubrication Conference, Indianapolis, Ind., October 10–12, 1955.

NOTE: Statements and opinions advanced in papers are to be understood as individual expressions of their authors and not those of the Society. Manuscript received at ASME Headquarters, August 31, 1955. Paper No. 55—LUB-12.

[3] The same rotor is shown in reference (3), fig. 6.

[4] For rotors of moderate flexibility, as in Case (*a*), this frequency is substantially the same for all running speeds. At critical speed the natural frequency in cycles per minute is equal to the running speed in rpm. There is a slight increase in natural frequency with increasing running speed, due perhaps to an elastic property of the oil film.

ments of the journal in the same frequency. The tendency of the oil film to convert a displacement of the journal into a whirl, according to Harrison's analysis, adds components of motion to the journal at right angles to those due to its vibration, but without changing the frequency. This builds the journal motion out into a whirl, the frequency of the whirl being that of the shaft vibration. If this frequency is less than the whirl frequency indicated by analysis for the journal alone (between four and five tenths of the running speed), the oil forces urge the journal forward and build up a whirl of the rotor. This is the case when running speed is more than two to two and a half times the critical speed.

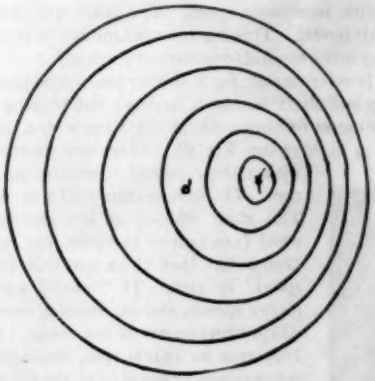

FIG. 3

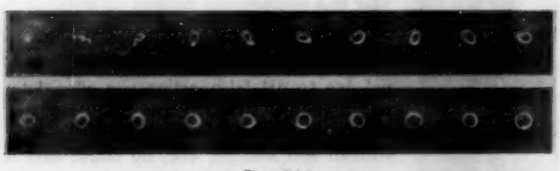

FIG. 3(a)

A build-up of this sort is shown in Fig. 3(*a*) which is taken from reference (12). The figure shows successive photographs of the tip of a pointer, like the one shown in Fig. 1. These photographs were made with a motion-picture camera, making approximately 16 exposures per sec. The exposure time for each frame was about $^1/_{36}$ sec.

The first frame shows the rotor running smoothly. The second frame shows the effect of striking the shaft with a stick. The following frames show the build-up of the whirl by the addition of components at right angles to the longer axis of the motion. The arc of whirl that was recorded on each frame, together with the exposure time, gives an approximate value of the frequency of the whirl, which is a natural frequency of the rotor.[5]

On the other hand, if the whirl frequency is greater than the whirl frequency indicated by analysis for the journal, the oil forces retard the whirl and cause it to die out. This is the case when running speed is less than two to two and a half times critical speed.

It should be emphasized that the action of the oil forces does not increase or decrease the frequency of the whirl. It either adds energy to the whirl or absorbs energy from it without changing the frequency.

It appears, therefore, that the tendency of the oil film in a journal bearing to support a whirl of the journal explains the instability of this rather flexible rotor at speeds above twice critical speed and the stable operation at speeds below twice critical.

Any whirling of the journal in frequencies determined by the oil-film forces would not build up much response of this more flexible rotor, except when the rotor speed is close to twice critical speed, so that the journal whirl frequency coincides with the natural frequency of the rotor. This has been observed (see Fig. 4 which is fig. 7 of reference 1).

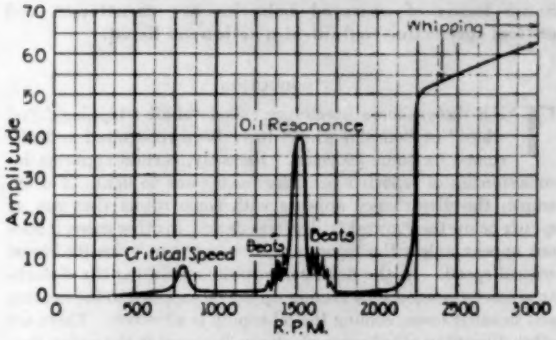

FIG. 4

Case (*b*) is simpler except for one matter. The shaft runs much below its critical speed. A jar causes very little flexing of the shaft, and the oil forces are dominant. The shaft whirls with a frequency determined by the journal whirl, which varies with the running speed and is slightly less than half thereof. This is typical of certain machines having light stiff rotors that run at high speeds. It is what would be expected from indications of analysis. There seems to be no proved explanation, however, for stability of these rotors above certain speeds, depending on the viscosity of the oil.

DETAILS AND DEVIATIONS

The two cases cited represent the comparatively simple extremes. In Case (*a*) the elasticity of the rotor is dominant; the unit bearing load is moderate but significant and the first critical speed is low. In Case (*b*) the oil film is dominant.

In cases of intermediate shaft critical speeds and running speeds, with greater or less unit bearing loads and short bearings, diversities of behavior must be expected.

The resonant whirl, Case (*a*), does not always develop at all speeds above twice critical. Cases have been reported (7) in which the speed reached five or six times critical before instability developed. This is a matter of considerable economic importance. Conditions favoring stability at speeds over twice critical are short bearings, rather large clearance, moderate loading, and low oil viscosity. A severe jar or blow applied to the rotor starts the whirl at speeds for which it would otherwise be stable—but not at any speed below twice critical.

Another feature worthy of note is that a very little external damping overcomes the whirling stimulus; also small changes of bearing alignment affect the occurrence of the whirl. Consequently both of the whirl phenomena are regarded as somewhat erratic and unpredictable.

Less information is available about the nonresonant half-running-frequency whirl. Its occurrence is usually with lightly loaded stiff shafts running at high speed. Pinkus (8) reported a

[5] It should be stated that shaft whirl discussed in reference (12), and shown building up in these photographs, was not due to oil-film action, but to internal friction of the rotor. The actions in the two cases are similar in that vibration in a plane builds out into a whirl (without change of frequency) due to force components at right angles to the displacements.

case of a rotor that developed this nonresonant whirl at speeds below twice critical, and went over into the resonant whirl as it passed through twice critical speed. He added that his rotors become stable at speeds above three times their first critical speeds, and that more viscous oil inhibits a disturbance that develops if the oil is heated up. In both respects the behavior of his (stiffer) rotors differs from that of the more flexible rotors described under Case (*a*).

In some cases either of these disturbances has been quieted by grooves in the bearing or other means to load the journal.

The nonresonant whirl at approximately half-running-speed frequency has been observed, appearing erratically, coming and going, as a flexible rotor running at well over twice critical speed builds up the resonant whirl.

Fluid-Film Critical Speeds

In 1925 Stodola (9) showed that oil films in journal bearings have quasielastic properties and that these might be responsible for critical speeds, i.e., resonant vibration or whirl, occurring over a limited speed range. The shaft is assumed to be rigid and the centrifugal force due to unbalance is the stimulus. His pupil, Hummel (10), made a more detailed analytical study of the matter, assuming a bearing arc of 180 deg and taking account of end leakage. The rotor was assumed stiff. He concluded that there are two such critical speeds—one of them involving severe vibration. He concluded also that instability develops if the eccentricity ratio becomes less than seven tenths. He made a careful experimental investigation and found that the results confirmed his analysis. His clearances were large, and he stated that with a top half bearing the disturbances were much reduced.

Recently Dr. Cameron (11) has questioned Hummel's conclusion of instability with eccentricity ratios less than 0.7 and concluded that there is a third critical speed in that region. He mentions no experimental support for his findings.

This category of fluid-film critical speeds includes also cases, Fig. 4, in which a disturbance appears at twice critical speed, with smooth operation at higher or lower speeds.

Nomenclature

The Design Group of the ASME Lubrication Activity appointed a Committee on Nomenclature for shaft disturbances due to fluid films in journal bearings.

At this writing, no final report has been brought in. However, authors of the three papers presented at this meeting have agreed to use the following:

The phenomenon described under Case (*a*) will be called "resonant fluid-film whirl,"[6] which may be abbreviated to "resonant whirl." It is defined briefly as "a resonant vibration of a shaft in a fluid-film journal bearing which occurs at speeds equal to or above twice the first critical of the rotor, and at a frequency equal approximately to a natural frequency of the rotor at the running speed."

The phenomenon of Class (*b*) is called "half-running-frequency whirl,"[7] which may be abbreviated to "half-frequency whirl." This is defined briefly as "a vibration of a shaft in a fluid-film journal bearing which may occur at any rotative speed, and at a frequency of approximately one half of such speed."

The third classification is called "fluid-film critical speeds," which may be abbreviated to "fluid criticals." These are defined as "rotor instabilities of limited speed range due to fluid-film action in journal bearings." They include a resonant disturbance that develops at twice critical speed, in case the rotor runs quietly at speeds above and below that value; also the two critical speeds found by Hummel, and the one by Cameron.

[6] Some prefer the word "whip."

[7] Theory indicates, and precise observations confirm, that the frequency of the Class (*b*) whirl is always less than half-running-speed frequency. However, the whirl frequency is usually so close to half-running frequency that less exact measurements (for example, with a reed tachometer) fail to indicate the divergence of the whirl frequency from half-running-speed frequency.

BIBLIOGRAPHY

1 "Shaft Whipping Due to Oil Action in Journal Bearings," by B. L. Newkirk and H. D. Taylor, *General Electric Review*, August, 1925, pp. 559–568.

2 "Whirling Balanced Shafts," by B. L. Newkirk, Third International Congress of Applied Mechanics, Stockholm, Sweden, August, 1930.

3 "Oil-Film Whirl—A Non-Whirling Bearing," by B. L. Newkirk and L. P. Grobel, *Journal of Applied Mechanics*, Trans. ASME, vol. 56, 1934, Paper No. APM—56-10.

4 "The Hydrodynamical Theory of Lubrication of a Cylindrical Bearing Under Variable Load and of a Pivot Bearing," by W. J. Harrison, Trans. Cambridge Philosophical Society, vol. 22 (1912–1923), April 24, 1919, pp. 373–388.

5 "Whirling of a Journal in a Sleeve Bearing," by David Robertson, *Philosophical Magazine*, series 7, vol. 15, January, 1933, p. 113.

6 "Whirling of a Journal Bearing. Experiments Under No-Load Conditions," by G. S. A. Shawki, *Engineering*, vol. 179, February 25, 1955, pp. 243–246.

7 "Oil Film Whirl—An Investigation of Disturbances Due to Oil Films in Journal Bearings," by B. L. Newkirk and J. F. Lewis, Paper No. 54—LUB-4, presented at the First Annual ASME-ASLE Lubrication Conference, Baltimore, Md., October 18–20, 1954. See also the 1955 Air Force Publication, WADC TR 54–188.

8 "Note on Oil Whip," by Oscar Pinkus, *Journal of Applied Mechanics*, Trans. ASME, vol. 75, 1953, pp. 450–451.

9 "Kritische Wellenstörungen Infolge der Nachgiebigkeit des Ölpolsters," by A. Stodola, *Schweitzerische Bauzeitung*, vol. 85, p. 265.

10 "Kritische Drehzahlen Als Folge der Nachgiebigkeit des Schmiermittels im Lager," by Charles Hummel, *Forschungsarbeiten-VDI*, heft 287, 1926.

11 "Oil Whirl in Bearings—Theoretical Deduction of a Further Criterion," by A. Cameron, *Engineering*, vol. 179, February 25, 1955, pp. 237–239.

12 "Shaft Whipping," by B. L. Newkirk, *General Electric Review*, March, 1924, fig. 3, p. 171.

Discussion

B. Sternlicht.[8] This paper makes a valuable contribution to the field of journal-bearing instability. The author clarifies the physical phenomena that take place in journal bearings.

Because of the great complexity of the problem, the author has not as yet arrived at a complete solution although he has spent some 30 years working on it. In this paper he attempts to differentiate between the various forms of instability and arrives at some common definitions to be used in the future by those interested in this topic. Various phenomena are defined but it may be found, in the future, that all these phenomena are interrelated and might be encompassed by one definition. At the present these definitions are valuable as tools of communication.

The author implies here that "Case (*b*)" occurs only in machines having vertical shafts or in lightly loaded stiff rotors of horizontal machines. The writer's experience has been that "half-frequency whirl" also will occur in a flexible rotor of horizontal machines which are not necessarily lightly loaded. In vertical machines the writer has never observed stabilizing effects at high speeds. Of course it is quite possible that the speeds in the writer's experiments were not high enough and that the whirl amplitude eventually might have decreased.

The writer questions whether we can attribute "Case (*a*)" solely to rotor flexibility and consider it the key factor. Mr. Hagg, has attributed it to rotor, fluid, and bearing flexibility and to rotor, fluid, and bearing damping properties, which is believed to be more nearly correct.

It is probably due to the complexity of this problem that we

[8] General Engineering Laboratory, General Electric Company, Schenectady, N. Y.

have experienced so many deviations, some of which the author describes.

This paper paves the way for future work as it provides the necessary common working ground.

ALFRED SLIBAR.[9] The author discusses two sets of experiments from his own extended research work in this field. The given results clearly indicate the diversities in the behavior of journal bearings. The two test devices *a* and *b*, to which the author refers, differ greatly in their length-to-diameter ratio, as well as in their unit bearing load, and finally in their damping characteristics.

With respect to the first point we have to keep in mind that all analytical criteria up to now are based on Harrison's relations (4) which are derived for the infinite journal bearing and—as H. Poritsky (12)[10] states it—should be considered outdated. Also, the influence of the difference in the unit bearing load cannot be predicted by analysis, as all theoretical treatments have been carried out for the condition of light loading or no loading at all.

It is believed to conform with the author's demand for clarification of this rather complex situation to mention preliminary results found in a recent analytical study of the subject under particular consideration of unloaded gas-lubricated bearings. Applying the usual bearing assumptions and superimposing parallel whirl to the angular velocity of the shaft, we can draw the following conclusions from the resulting differential equation for the finite bearing:

1 In the expression for the pressure field the term due to rotation must be proportional to the sum of the angular velocities. If the film thickness is a symmetrical function about the connecting line from bearing center to shaft center the resulting force—created by rotation only—acts perpendicular to this line of symmetry and has zero amount if the shaft whirls with half the running frequency in the positive direction.

2 If the system of external feeding also is symmetrical about the same axis the term in the pressure distribution accounting for the feeding of the lubricant results in a force acting in the line bearing center-journal center.

A more extended calculation furthermore predicts that for statically not perfectly balanced shafts certain resonance areas exist even in the stable area given by the Poritsky condition (12),[10] the angular velocity of these vibrations being equal to the critical of the shaft.

[9] Department of Mechanical Engineering, Stanford University, Stanford, Calif.

[10] Reference to author's Bibliography.

AUTHOR'S CLOSURE

Any complete solution of this problem must take account of the bearing parameters, those of the rotor (mass, stiffness, critical speed), those of the structure (rigidity, damping, alignment), also of the shocks which may reach the bearing. All of these factors affect the incidence of the whirling, and any complete solution must take account of all of them.

The one simple underlying cause of these disturbances (except fluid-film critical speeds) seems to be the tendency of the journal to whirl in the bearing. The manifestations of this unstable characteristic are so diverse, however, that it is desirable to make some classification of the phenomena. The critical speed is the key factor in the sense that resonant whirl does not occur unless the rotor runs above twice its lowest critical speed.

The suggested approach to the problem is to assume that journals have a tendency to whirl, with a whirl frequency somewhat less than half the running frequency, and to look for inhibiting effects to account for cases of stable operation. Behavior of the more flexible rotors discussed under Case (*a*) is accounted for on this basis; also the whirling of stiff rotors under Case (*b*). The reported stability of stiff rotors at higher speeds, and with more viscous oil, is not accounted for.

In the author's limited experience with Class (*b*) disturbances they have not been conspicuous except where the journal runs at small eccentricity, as in the case of lightly loaded bearings. With large bearings at high speeds this condition would occur at higher loads. Little has been published on these "half-frequency" whirls and a detailed account of cases would be of interest.

The Harrison analysis was quoted because he seemed to be the first to show, by analysis, the tendency of the journal to whirl. This has been confirmed. He neglected axial flow, and any rupture of the film that might occur in unloaded portions of the bearing; i.e., he assumed a 360-deg bearing. Burwell took account of the axial flow and neglected part of the peripheral flow, assuming a 360-degree bearing. He found orbital motion of the journal similar to that found by Harrison.

For the general case of a loaded short bearing with liquid lubricant, experiments have shown the whirling tendency at eccentricities greater than nine tenths, with a bearing of L/D ratio one half. In this case the active peripheral bearing length must have been short.

The information offered by Mr. Slibar is interesting. It seems to indicate that the unloaded finite gas-lubricated bearing should have the same whirling characteristic. Whirling in such bearings has been observed.

Effect of Combustion-Resistant Hydraulic Fluids on Ball-Bearing Fatigue Life[1]

By H. V. CORDIANO,[2] E. P. COCHRAN, JR.,[3] AND R. J. WOLFE,[4] BROOKLYN, N. Y.

Phosphate ester, phosphate ester-base, and water-glycol-base combustion-resistant fluids and a petroleum oil were investigated to determine the relative effects of the fluids, used as flood lubricants, on the life of angular-contact ball bearings. Bearing life was lower in the combustion-resistant fluids than in oil, ranging from 58 per cent of the life in oil for the phosphate ester, to 6 per cent for the water-base fluid. Fatigue failures of the bearing races were prevalent for all fluids and additional investigations are required to determine the causes of the wide variation in bearing life in the various fluids.

Introduction

PRESENT-DAY industrial and military use of hydraulic fluids demands on many occasions a high performance not readily obtained with petroleum lubricants (1).[5] In this connection, the Material Laboratory, New York Naval Shipyard, and other Naval laboratories, working under the general direction of the Bureau of Ships, have been investigating the properties of combustion-resistant hydraulic fluids and their effects on the various components of shipboard machinery and equipment. During the early stages of the evaluation of these fluids in variable-delivery axial-piston-type pumps, it was found that pump life was relatively short and that failure always occurred in the angular-contact ball bearing which resisted the thrust of the rotating unit. Damage was severe but it was not difficult to identify the typical fatigue failure of the bearing races. Similar bearing failures in piston-type pumps using water-glycol-base fluids have been previously reported (2).

These repeated bearing failures suggested that the combustion-resistant hydraulic fluids have a significant effect on the life of ball bearings, and efforts were directed toward this phase of the over-all problem. Because of the large variability in the life of ball bearings and in order to obtain the quantity of data required for statistical analysis, the fluids were evaluated on four bearing testing machines designed to permit operation of eight bearings at a time. This test equipment was designed to simulate, as closely as practicable, the conditions of lubrication, load, and temperature found in axial-piston-type pumps on Naval vessels.

Fluids Evaluated

Three combustion-resistant fluids and a petroleum oil were evaluated in the test equipment. The properties of these fluids are given in Table 1. In the compression-ignition tests (3) conducted at the U. S. Naval Engineering Experiment Station, Annapolis, Md., the fluids showed different degrees of combustion resistance and only one was considered "satisfactorily noncombustible" for shipboard hydraulic systems. It should be understood that combustion resistance is a relative property and that the suitability of a fluid, from the standpoint of fire and explosion hazard, depends on the service use and safety requirements.

TABLE 1 PROPERTIES OF FLUIDS

Fluid	A	B	C	D
Type of fluid	Petroleum oil	Phosphate ester	Phosphate ester-base	Water-glycol-base
Color (ASTM)	2	1½	1½	1
Viscosity, SSU at 100 F	182.0	214.0	231.4	280.2
150 F	70.6	68.8	72.9	125.5
210 F	44.3	42.3	44.2	69.5
Viscosity index	80	<0	16	156
Specific gravity, 60/60 F	0.8960	1.1470	1.2677	1.0792
Pour point, deg F	−30	−5	−5	<−65
pH	.....	.....	.....	10.0
Neutralization number	0.08	0.04	0.06	.....
Refractive index at 20 C	1.489	1.553	1.583	1.411
Flash point, deg F	410	535	450	260[a]
Fire point, deg F	425	600	555	270[a]
Water content, per cent	.....	.....	.....	35.0

[a] Cleveland open-cup method—after water had evaporated.

Apparatus

The test equipment for evaluating the effect of various hydraulic fluids on the life of angular-contact ball bearings is shown in Fig. 1. The equipment consists of a fluid-transfer system and four bearing testing machines in which eight angular contact bearings are operated to failure.

The fluid-transfer system, shown schematically in Fig. 2, is used to supply a continuous flow of the sample fluid to each of eight bearings mounted in individual housings. The fluid is drawn from the reservoir by a centrifugal pump and passed through a filter, heat exchanger, feed manifold, sight-flow indicator, and flexible metallic hose, in succession, before entering the bottom of each bearing housing. The fluid flows into the housing on one side of the test bearing, passes through the bearing to the opposite side, and is discharged from the top of the housing, through flexible metallic hose and a return line, to the reservoir. The temperature of the fluid is measured by means of a dial-type

[1] The opinions or assertions contained in this paper are the private ones of the authors and are not to be construed as official or reflecting the views of the Navy Department or the Naval Service at large.

[2] Head, Structural Mechanics and Hydrodynamics Section, Material Laboratory, New York Naval Shipyard.

[3] Lieutenant Commander, USN, Mechanics Branch Program Officer, Material Laboratory, New York Naval Shipyard. Assoc. Mem. ASME.

[4] Assistant Head, Structural Mechanics and Hydrodynamics Section, Material Laboratory, New York Naval Shipyard.

[5] Numbers in parentheses refer to the Bibliography at the end of the paper.

Contributed by the Research Committee on Lubrication under the auspices of the Lubrication Activity of THE AMERICAN SOCIETY OF MECHANICAL ENGINEERS, and presented at the Second Annual ASME-ASLE Lubrication Conference, Indianapolis, Ind., October 10–12, 1955.

NOTE: Statements and opinions advanced in papers are to be understood as individual expressions of their authors and not those of the Society. Manuscript received at ASME Headquarters, August 31, 1955. Paper No. 55—LUB-21.

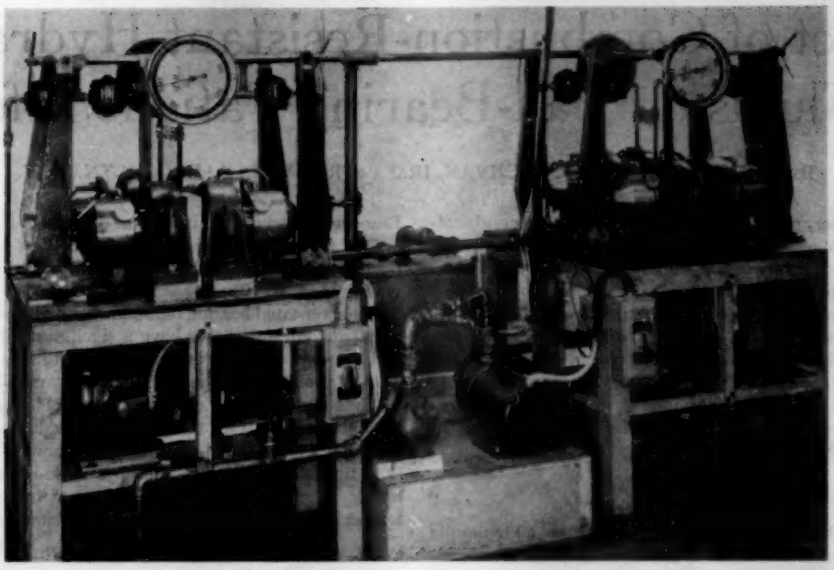

FIG. 1 BEARING TEST APPARATUS

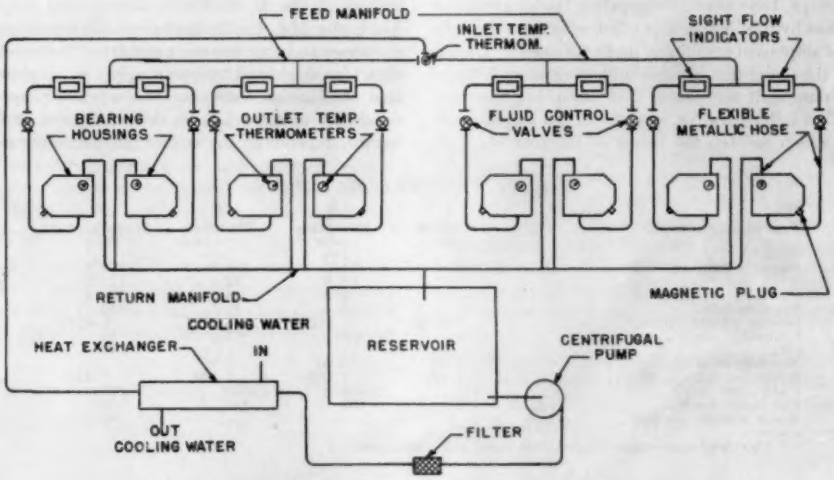

FIG. 2 SCHEMATIC OF FLUID-TRANSFER SYSTEM

stem thermometer inserted into the stream at the discharge from each housing.

A similar thermometer is also inserted in the feed manifold to permit measurement of the supply-fluid temperature. Control of the temperature is obtained by regulation of the flow of cooling water through the heat exchanger and the quantity of the fluid flowing through each bearing. A removable magnetic plug is fitted to the bottom of each housing to attract and hold ferrous particles that may be released to the fluid. The main-line filter consists of a 60-mesh bronze screen wrapped around a perforated steel cylinder. The valves, piping, metallic hose, and interior parts of the pump and heat exchanger are of brass or bronze. The bearing housings are of steel and the fluid reservoir is of stainless steel. Other materials in contact with the fluid are glass in the sight-flow indicators, and silicone rubber in the gaskets and in the shaft-sealing elements of the bearing housing. The capacity of the fluid reservoir is 13 gal and that of the remainder of the system, which includes the heat exchanger, bearing housings, piping, and sight-flow indicators, is 3 gal.

The bearing testing machines consist of four identical units, one of which is shown in Fig. 3. Each unit permits testing two bearings at a time under identical conditions of load and speed. Referring to Fig. 3, the test bearings 1, AFBMA Code No. 85BA02 angular-contact ball bearings, are mounted opposed in pairs, on the drive shaft 2, and enclosed by housings 3 and 4. The housings also are provided with AFBMA Code No. 50RU02 cylindrical roller bearings 5, for aligning purposes. The shaft is mounted in two ball-bearing pillow blocks 6, and is driven at 2150

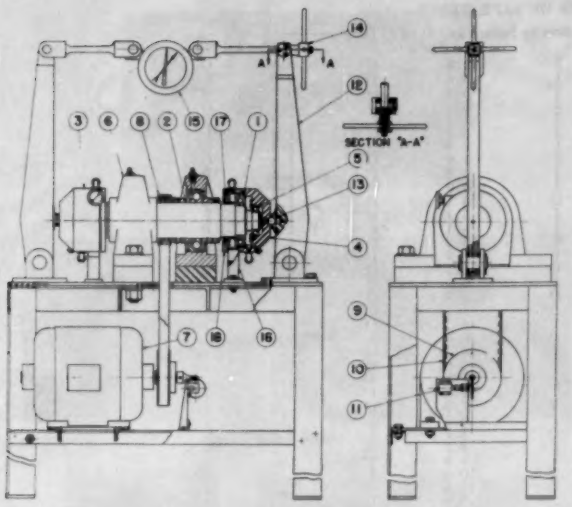

FIG. 3 CROSS-SECTIONAL ASSEMBLY OF BEARING TESTER

rpm by the motor 7, through grooved reduction pulleys 8 and 9 and cog belt 10. The motor is of the polyphase-induction type with a full-load speed of 3450 rpm. A mechanical counter 11, driven through a 100 to 1 speed-reduction gear, is used to indicate the number of revolutions of the drive shaft. Thrust load is transmitted from the levers 12, through hardened steel balls 13, to the housings and thence to the outer race of the test bearings. The load is controlled by rotation of the hand wheel 14, and is measured by means of the dynamometer 15, which indicates one fifth of the load applied to the bearing because of the 5 to 1 lever ratio. The test bearings take all of the thrust load and are not subjected to radial load other than that imposed by the weight of the housings. The test bearings are push-fitted into the housings and onto the drive shaft. The inner race revolves at drive-shaft speed while the outer race is held stationary in the housing, which is restrained from rotating by the stop 16. Shaft seal 17, mounted in cover plate 18, prevents leakage of fluid from the cup.

BEARINGS

Two hundred AFBMA Code No. 85BA02 angular-contact bearings of one brand were procured for this work under specifications requiring that this material be part of a single production run. These bearings were randomly selected and assembled into groups of eight for evaluating the fluids. Prior to receipt of these bearings, however, part of the evaluation of fluids A, C, and D was completed, using for each fluid 16 85BA02 bearings of the same brand as the lot of 200, drawn from Navy supply sources. Thus out of a total of 120 bearings used for evaluating 4 fluids, 72 were randomly selected. In reporting the results of this work data obtained with bearings from both sources have been assembled together because results obtained with each fluid on bearings from both sources were not significantly different.

PROCEDURES

The general procedure for evaluating each fluid was to circulate the fluid through the system and flood-lubricate the angular-contact ball bearing operating under the prescribed conditions, until each bearing in two groups of eight failed. Eight bearings from the first group were started simultaneously at eight stations on the machines, and as failure occurred at each station the bearing was replaced by a sample from the second group of eight, thereby insuring an equal distribution of bearings among the stations. Additional dummy bearings were used when necessary to permit running all bearings in the second group of eight to failure. Prior to the evaluation of each fluid, the bearings, fluid-transfer system, and housings were thoroughly cleaned and then flushed with about 3 gal of the test fluid which was pumped through the system and discarded.

Great care was exercised to insure duplication of test procedures and conditions. The bearings were mounted on the testing machines opposed in pairs under one half the full operating thrust load and the fluid circulating pump was started. As soon as the bearings were flooded, the machines were started and when the full operating speed of 2150 rpm was attained, the thrust load was increased to the value of 12,900 lb established for the work. The flow of fluid to each bearing was regulated to 1.5 units on the sight flowmeter, or approximately 0.5 gpm, and the bulk temperature of the fluid leaving the bearings was maintained at 150 to 160 F by regulating the flow of cold water to the heat exchanger. Under these conditions the inlet temperature for each fluid was maintained essentially constant, but because of the differences in thermal characteristics, this temperature was not the same for each fluid. The inlet temperature for all fluids investigated ranged between 110 and 125 F.

Each bearing was run continuously to failure which was considered to have occurred when either an outer or inner race spalled or when a ball spalled, chipped, or fractured. Failure was detected by a change in operating-noise characteristics of the bearings. This method was found to be sufficiently effective to permit immediate detection of the presence of a very small spalled spot.

RESULTS

Table 2 summarizes the results showing the effect of various hydraulic fluids on the life of AFBMA Code No. 85BA02 angular-contact ball bearings operating under a thrust load of 12,900 lb and a speed of 2150 rpm. The data are arranged in the order of increasing lives with notations indicating the types of failure. First indication of failure was detected from a change in noise characteristics of the bearings to within 10,000 revolutions in most cases. Failures of inner races, outer races, and balls were obtained with all fluids. Evaluation of the water-glycol-base fluid was stopped after 16 bearing failures because the fluid had already given a significantly poor performance and, in addition, caused early failures of the lightly loaded cylindrical roller bearings which maintain alignment of the housings.

The data listed in Table 2 are shown plotted in Fig. 4 on extreme probability paper. The straight lines drawn through the data were determined by the "order-statistics method" proposed by J. Lieblein (4). In using this method it is assumed that bearing life conforms to the extreme value distribution

$$P = e^{-e^{-Y}}$$

where

P = probability of failure
$Y = (L - \mu)/\beta$
L = life
μ = mode or highest point of the frequency distribution (life at $P = 0.368$)
β = a scale parameter of extreme value distribution (slope of line when distribution is plotted as a straight line on extreme probability paper)

The data plotted in Fig. 4 follow the fitted lines fairly closely and are well within the 95 per cent confidence bands (not shown).

The predominant types of bearing failures resulting from opera-

TABLE 2 RESULTS OF LIFE TESTS

Order of increasing life	Millions of revolutions to failure and type of failure							
	Fluid A		Fluid B		Fluid C		Fluid D	
1	2.7	B	3.3	I	2.8	O	0.8	O
2	3.9	I	3.4	I	3.4	I	0.8	I
3	6.0	B[a]	4.8	I[a]	3.4	O	0.9	B[a]
4	6.1	I	5.3	I	3.4	O	1.0	O
5	8.9	I	6.1	I	3.5	I	1.0	O
6	9.5	O	6.2	I	3.7	O	1.2	I
7	12.6	I[a]	8.1	I	3.8	I	1.3	I
8	12.8	O	8.3	I	3.9	O	1.3	O
9	14.6	O	8.5	I	4.3	I	1.4	B
10	17.3	B	9.0	I	5.0	O	1.4	B
11	17.5	B	10.1	O	5.1	B	1.4	O
12	18.3	I	10.1	I	5.1	B	1.7	I
13	20.2	O	10.9	I	5.1	I	1.7	B
14	20.2	O	11.1	I	5.2	I	1.8	O
15	22.1	I	11.4	I	5.2	I	2.4	B
16	23.3	O	11.6	O	5.3	O	2.6	I
17	23.4	O	13.7	I	5.7	B	...	..
18	24.0	O	14.6	O	5.7	O	...	..
19	28.1	I	14.7	O	6.1	I	...	..
20	29.2	I	14.8	I	6.1	O	...	..
21	29.6	O	15.0	O	6.2	I	...	..
22	30.6	O	15.6	I	6.2	O	...	..
23	41.0	O	15.6	I	6.6	O	...	..
24	45.1	I	17.3	I	7.6	I	...	..
25	45.6	I	18.9	I	7.8	I	...	..
26	49.8	O	21.9	B	7.8	O	...	..
27	52.3	I	24.9	I	8.5	I	...	..
28	53.3	B	27.6	O	8.7	I	...	..
29	55.5	O	28.4	I	8.7	B	...	..
30	63.3	B[a]	32.1	I	9.0	I[a]	...	..
31	66.8	O	34.4	B	10.0	I	...	..
32	69.3	B	44.3	O	10.5	O	...	..
33	..	..	..	..	10.8	I	...	..
34	..	..	..	..	10.9	I	...	..
35	..	..	..	..	11.7	I	...	..
36	..	..	..	..	12.3	O	...	..
37	..	..	..	..	13.7	I	...	..
38	..	..	..	..	15.9	O	...	..
39	..	..	..	..	16.9	I	...	..
40	..	..	..	..	17.6	I	...	..

NOTES:
[a] More than one type of failure was observed. Type indicated was predominant.
O—Spalling of outer race.
I—Spalling of inner race.
B—Breakage, chipping, or spalling of ball.

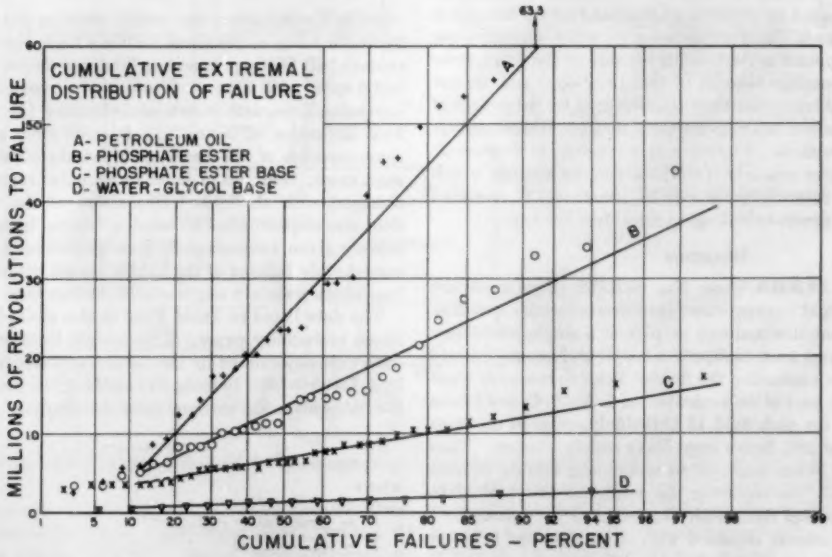

FIG. 4 EFFECT OF PETROLEUM OIL AND COMBUSTION-RESISTANT HYDRAULIC FLUIDS ON THE LIFE OF ANGULAR CONTACT BALL BEARINGS

tion in the various fluids were spalling of the inner or outer races as shown in Figs. 5(*a*, *b*). Less frequent failures occurred by spalling, chipping, or fracture of one or more balls as shown in Figs. 5(*c*, *d*). The failures obtained with the four fluids were similar and failures of any other type were not observed.

Except for viscosity there was little change in the properties of the fluids as a result of use in the bearing test apparatus. The viscosity of the water-glycol-base fluid increased 8.2 per cent, whereas the viscosity of the petroleum oil and the phosphate ester-base fluid decreased 9.3 and 27.8 per cent, respectively.

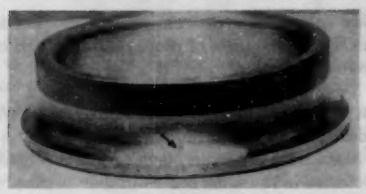

(*a*) Spalled inner race

(*b*) Spalled outer race

(*c*) Spalled ball

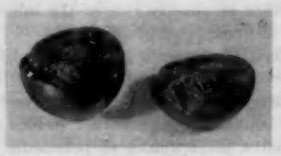

(*d*) Fractured ball

FIG. 5 TYPICAL BEARING FAILURES

DISCUSSION

The plotted data shown in Fig. 4 and the numerical values given in Table 3 indicate that the combustion-resistant fluids tested have an appreciable effect on the modal and median lives of angular-contact ball bearings. The phosphate ester is the most effective of the combustion-resistant fluids as a ball-bearing lubricant with a relative modal life of 0.58, while the water-glycol-base fluid is the least effective with a relative modal life of 0.06. The phosphate ester-base fluid is intermediate between these two. Morrison (7) has found that these fluids significantly affect the life of radially loaded bearings.

TABLE 3 MODAL AND MEDIAN LIVES OF ANGULAR-CONTACT BALL BEARINGS OPERATED IN PETROLEUM OIL AND THREE COMBUSTION-RESISTANT FLUIDS

Fluid	Type	Life in millions of revolutions		Relative life	
		Modal	Median	Modal	Median
A	Petroleum oil	18.6	24.9	1.00	1.00
B	Phosphate ester	10.7	13.5	0.58	0.54
C	Phosphate ester-base	5.8	6.8	0.31	0.27
D	Water-glycol-base	1.2	1.3	0.06	0.05

Caution must be exercised in drawing general conclusions for conditions of load, temperature, and type of lubrication other than those used in this investigation without a sufficient background of information on the cause for such wide differences in the results obtained.

The types of failure obtained with the various combustion-resistant fluids were similar to those obtained with petroleum oil and were characterized by flaking or spalling of the races or balls. These failures are typical of what are generally recognized as fatigue failures and some evidence has been given (5, 6) to show that failure usually starts below the surface of the race. Since ball-bearing fatigue life varies inversely as the ninth power of the stress (5), a small change in subsurface stress will have an appreciable effect on bearing life.

If it is assumed that failure actually started below the surface during these tests, then the question arises as to what property of the fluid could affect the stress distribution in the vicinity of the contact area in such a manner as to have an appreciable effect on ball-bearing fatigue life. One possible answer to this question may be found in the viscosity of the fluid under the conditions of pressure and temperature existing in the fluid between the balls and the races. It is quite possible that the viscosity of the fluid may have an effect on the stress distribution between the ball and the race and therefore the pressure-viscosity characteristics of the fluid may be an important factor in ball-bearing fatigue life. An investigation of the pressure-viscosity relations at different temperatures of the fluids herein reported is now under way for correlation with the results of the bearing tests.

Corrosive effects combined with high stress and chemical action of the fluids should not be ignored as possible causes for the differences obtained with the various fluids. However, preliminary studies of the surface condition of the balls and races after failure indicate that a corrosive attack from any of the fluids tested is very minor or nonexistent.

CONCLUSIONS

The results of this investigation were obtained under conditions simulating the use of a hydraulic fluid as a ball-bearing lubricant in an axial-piston-type pump and therefore any conclusions drawn have particular significance for this or similar applications.

The three combustion-resistant fluids evaluated have a significant effect on the life of angular-contact ball bearings. When compared with petroleum oil the per cent reduction in ball-bearing modal life caused by the combustion-resistant fluids is as follows:

Fluid	Per cent reduction in modal life
Phosphate ester	42
Phosphate ester-base	69
Water-glycol-base	94

The large differences in results obtained with the fluids evaluated have not been explained. The increasing use of these fluids in industrial and military applications indicates the need for additional research to determine the cause of these differences and to furnish information for possible improvement of the fluids as ball-bearing lubricants.

ACKNOWLEDGMENT

The assistance of Mr. T. W. Morrison of SKF Industries, Inc., in connection with the design of the bearing test apparatus, and of Mr. L. Diamond of the Material Laboratory, New York Naval Shipyard, in connection with the statistical analysis of the results, is gratefully acknowledged.

BIBLIOGRAPHY

1 "Review of Synthetic Lubricants," by D. H. Moreton, *Lubrication Engineering*, vol. 10, April, 1954, pp. 65–73.

2 "Aqueous Nonflammable Hydraulic Fluids," by J. E. Brophy, V. G. Fitzsimmons, J. G. O'Rear, T. R. Price, and W. A. Zisman, *Industrial and Engineering Chemistry*, vol. 43, April, 1951, p. 884.

3 "Compression-Ignition Tests of Hydraulic Fluids," by A. R. Schrader, Naval Engineering Experiment Station Report 070243K of February 15, 1955.

4 "A New Method of Analyzing Extreme-Value Data," by J. Lieblein, NACA TN 3053, January, 1954.

5 "Fatigue Strength of Ball Bearing Races and Heat-Treated 52100 Steel Specimens," by H. Styri, Proceedings of the ASTM, vol. 51, 1951, pp. 682–700.

6 "Metallographic Observations of Ball Bearing Fatigue Phenomena," by H. B. Jones, Proceedings of the ASTM, vol. 46, 1946, p. 853.

7 "Some Unusual Conditions Encountered in the Lubrication of Rolling Contact Bearings," by T. W. Morrison, presented at the April, 1955, Annual ASLE Meeting.

Discussion

F. T. Barwell[5] and D. Scott.[5] The paper is an interesting and valuable contribution to the literature on an important subject, namely, pitting failure of bearings. Some of the nonflammable fluids have been causing considerable concern by the premature failure of bearings by pitting action in some hydraulic systems where the pumps embody rolling bearings which are required to be lubricated by the hydraulic fluid being pumped.

It has always been recognized that a limiting factor in the life of rolling-contact bearings has been the disintegration of the surface, pits being formed by a process having fatigue characteristics. It has been considered generally that this phenomenon was attributable to the stresses at and immediately within the surface and was characterized by the properties of the materials. Some preliminary experiments carried out at the Mechanical Engineering Research Laboratory using a simple apparatus in which conventional ball bearings were used as test specimens also have established that the nature of the lubricant may have considerable bearing on the incidence of failure, some nonflammable hydraulic fluids leading to lives of only $^1/_8$ of that to be expected from a conventional lubricant.

The test rig consisted of a conventional Boerlage four-ball machine modified so that the three lower balls, instead of being rigidly held, were allowed to rotate in a ball race. The ball race was so proportioned that failure occurred on the surface of the balls. About 30 different fluids have been tested including mineral-based lubricants, water-based hydraulic fluids, and synthetic hydraulic fluids. The conditions used in the tests were more severe than in practice, the loads used being selected to obtain rapid failure and the results are therefore subject to confirmation at normal working stress. The general conformity of the results to the inverse cube law, however, provides some support for extrapolation while actual running of pumps confirms the assessment of fluids by the modified four-ball rig.

The results disclose that the adapted four-ball machine is clearly capable of differentiating between lubricants by showing detectable differences in the time to pitting failure and this simple apparatus offers many experimental conveniences. The results are reasonably reproducible and use of four commercial steel balls for each test is an economical method of obtaining a fairly uniform test specimen, eliminating the cumulative inaccuracies of machining and assembly which possibly increase the scatter of results when using more elaborate test apparatus and specimens. Details of test procedure and complete results are to be published shortly.

From the test results obtained, viscosity of the lubricant does not seem to be a dominant factor in the time taken to pitting failure as some very low-viscosity fluids give as long a life as others with much higher viscosity. However, increased stress cycles to failure with increased viscosity with the same type of lubricant was found with some lubricants (e.g., mineral oil) but not with others. It is possible that compressibility and variation in viscosity with pressure may be more important than the viscosity at atmospheric pressure and it is pleasing to learn from the authors that an investigation along these lines is under way. As suggested by the authors, corrosive effects combined with high stress, and chemical action of the fluids should not be ignored as possible causes of the differences in bearing life obtained with different fluids as rapid deterioration of the bearing surfaces to a state of continuous fine pitting was found when using the poorer nonflammable fluids. Sections through such pitted races revealed numerous subsurface cracks, spreading from existing pits to ultimately enlarge pits or form new ones. These numerous small cracks in various states of propagation may be indicative of stress corrosion.

A. Bondi.[7] A decision between the mechanical and the (surface) chemical mechanism of fatigue failure might be made by a few rotary flexural-fatigue experiments in the test fluids. Failure of such specimens in the same order of fluids as that found by the author would strongly support the surface chemical mechanism. The probability of such an outcome is suggested by previous observations of the much longer flexural-fatigue life of steel specimens in oil than in aqueous environments.

D. H. Moreton.[8] The authors are to be congratulated for this good work in a field of knowledge where a technical vacuum seems to exist. The literature is replete with information on the fatigue characteristics of rolling-contact bearings generally in the presence of the petroleum-type lubricant. Even in these cases, however, the methods by which the lubricants have been applied have left doubt in the minds of many lubrication engineers as to whether or not the role of the lubricant in ball-bearing fatigue had been explored properly.

Certainly an even greater lack of information exists in the case of synthetic-type lubricants now finding increased usage in industry. This work clearly reveals that at least under these test conditions some rather serious differences exist in the comparative performance of petroleum oils and some of the synthetics. We agree with the authors that much further work is necessary to answer the question as to what property or properties of fluids could cause these differences. We disagree with the authors, however, in their first conclusion that these results necessarily have particular significance for ball-bearing life in an axial-piston-type pump. This conclusion is believed to be unduly broad and questionable even when related to these specific types of pumps employing the types of fluids investigated.

Aircraft manufactured by our company have accumulated several million hours of service on a phosphate ester type of synthetic lubricant in use in Vickers' axial piston-type pumps with no indications of foreshortened ball-bearing life as a result. There are as many as six pumps of this type on a single aircraft operating at pressures of 3000 psi, at varying flow rates, and at speeds up to 4000 rpm. The design weight of these units is necessarily low; conditions are considered by the manufacturers to be relatively more severe than most industrial usage; and the majority of all of these pumps are returned to our factory for overhaul of the units on which they were employed. Careful records are therefore available for assessing performance of the various elements in the pump. No differences have appeared as compared to previous and concurrent experience on petroleum-type oils. Other phosphate ester fluids have been used successfully in similar pumps in the die-casting industry for many years with apparently little or no distress being observed in the ball bearings.

That the authors found a serious difference, however, is not to be questioned; therefore it suggests itself that their conditions of test have either amplified or induced a variable not present in at least many other types of service employing these pumps and these types of lubricants. Even further, their results indicate a median life performance on petroleum oil of approximately twenty-five million revolutions. At their test speed and conditions chosen to represent the actual service installation, this reduces to a median bearing life of approximately 193 hours. This seems an unusually low life span for a machine of this type and certainly could not be tolerated in an aircraft hydraulic

[5] Department of Scientific and Industrial Research, Lubrication and Wear Division, Mechanical Engineering Research Laboratory, Thorntonhall, Glasgow, Scotland.

[7] Shell Development Company, Emeryville, Calif.

[8] Project Co-Ordinator, Douglas Aircraft Company, Inc., Santa Monica, Calif.

pump. Since the purpose of their investigation was to simulate conditions found in these pumps now in service, it would be interesting to know if a pump life factor for the presently used petroleum oil on which they must have considerable experience in actual use had been determined and, further, if this actual service life had been rationalized against the laboratory life of the same bearings with this same oil under their test conditions. If pump-bearing failures are being experienced in service from as low a life as 2.7 million revolutions or 21 hr to a maximum life of approximately 70 million revolutions or 540 hr, then we would agree that the chosen laboratory test conditions are simulating service performance. If this is not the case, then it is suggested that a severity factor has been introduced by the laboratory tests. This would call for a thorough investigation of these differences to make sure that this severity factor has not introduced a reason for failure which might never be encountered in the service counterpart of this laboratory test.

Over the past 8 years we have tested over 50 axial-piston-type pumps to incipient or actual failure on many synthetic lubricants. Reference runs have been made periodically on petroleum fluids. With regard to ball-bearing failures in these pumps, we can confirm the experience of the authors on water-base fluids. Numerous early ball-bearing fatigue failures resulted from pump tests on many different water-glycol-type fluids. On the ester-base fluids including dibasic acid esters, phosphates, and silicates, generally good ball-bearing experience has been obtained, contrary to the authors' findings. On the critical parts of these pumps which operate under boundary-layer-type lubrication conditions, the phosphate ester-type lubricants show, in fact, a considerable improvement over service with petroleum oils. In general, our full-scale pump-testing program agrees favorably with the rather broad background of industry experience that has accumulated on these types of fluids in hydraulic pumps.

T. W. Morrison.[9] We wish to commend the authors on the sound approach they have taken to evaluate the effect of combustion-resistant hydraulic fluids on rolling-bearing fatigue life and the alacrity with which they have gotten their program under way. We already have published data for similar materials which substantiate their findings completely.

The effect of lubricants on the fatigue life of bearings is a very important consideration, not only where hydraulic fluids are used but in all bearing applications. A vast amount of investigation will be necessary to evaluate the effects of the various lubricants on bearing endurance and to determine the basic reasons for the endurance being affected by the lubricants.

In addition to the field of hydraulic fluids, another critical group of products is the lubricants that are to be developed for high-temperature aircraft power plants. It is extremely important in evaluating these that consideration be given to their effect on bearing fatigue.

To establish definitely that the results of their testing correlated with service results, and to obtain directly from the tests, if possible, data that could be used to evaluate bearing lives in certain pumps handling the hydraulic fluids, the authors justifiably chose the bearing size used in their investigations. We would like to emphasize, however, that in any program to evaluate relative effects of lubricants on bearing fatigue life, or to study the basic reasons for the materials affecting bearing endurance, smaller and less expensive bearings can be used.

C. R. Schmitt.[10] The writer wishes to compliment the authors for the extensive test work completed on fire-resistant fluids. This work should certainly form the basis for continued investigations along the same lines.

As in all laboratory tests, however, the results require evaluation solely in terms of speeds, loads, temperatures, etc., embodied in the test in question. It is well to follow the suggestions of the authors that caution be exercised in drawing general conclusions from these tests for application to other conditions where different loads, temperatures, and type of lubrication are encountered.

These tests confirm the fact, known for some time, that at extremes of loadings and temperatures, water-base fluids are not adaptable to angular-contact antifriction bearings. It must be recognized, however, that water-base fluids are performing satisfactorily in hundreds of applications involving antifriction bearings operating at normal loadings, speeds, and temperatures. Water-base fluids are performing very satisfactorily in hydraulic die casters, welders, presses, oven-door mechanisms, and many other kinds of equipment where ball and roller bearings are involved.

The important thought behind these comments is that water-base fluids have been researched and are being marketed for use in the vast majority of hazardous industrial applications where operating conditions are such that they are entirely satisfactory. Systems employing pumps and equipment operating at temperatures, or antifriction-bearing pressures, lying outside their operating limits, cannot be considered as possible applications for such fluids.

Authors' Closure

The comments made by Messrs. Barwell and Scott are most welcome. In particular, the indication that a modified Boerlage four-ball machine is capable of differentiating between lubricants by showing detectable differences in the time to pitting failure is of considerable interest since the Shell four-ball machine and other types of E. P. testers have not been used successfully to detect significant differences in the qualities of the various fluids under investigation as ball-bearing lubricants. It has been the authors' intention to obtain additional information on the fluids, including work at lower loads for at least two bearing sizes, and to establish clearly the differences in the fluids as ball-bearing lubricants and then follow up this work with the development of a less expensive bench tester which would produce results that correlate satisfactorily with those established under bearing operating conditions. The results indicated for the modified Boerlage machine are encouraging in this connection.

A crude attempt at the rotating-beam fatigue experiments with specimens of drill rod exposed to the fluid, as suggested by Mr. Bondi, has been made with negative results. However, the speed of the machine was rather high, 13,000 rpm, and as a result time for chemical action was limited. In addition, the specimen was subjected to a stream of the fluid rather than immersed completely. Definite steps have been taken to conduct these experiments at a lower speed with specimens of hardened 52100 steel completely immersed in the fluid. It is expected that these results will be published in the near future.

The comments made by Mr. Moreton are noteworthy. However, in disagreeing with the authors' conclusion that the results have a particular significance for ball-bearing life in axial-piston-type pumps or similar applications, he apparently fails to recognize that this conclusion is identified with the conditions of load, temperature, and type of lubrication which have been simulated by the tests. Although the results reported in the paper apply to angular-contact bearings, the substantiation of these results by Morrison in tests of similar fluids in radially loaded bearings of a much smaller size indicates that the conclusion could have been more general. No conclusion has been made

[9] Manager, Research Laboratory, SKF Industries, Inc., Philadelphia, Pa.

[10] Manager, National Lubrication Sales Department, E. F. Houghton & Company, Philadelphia, Pa.

to suggest that the results apply to lighter loads; however, it is expected that the same order of merit will be retained at moderately lighter loads by the various fluids in view of the wide differences shown at a relatively heavy load.

The service records accumulated by the Douglas Aircraft Company, Inc., on a phosphate ester type of synthetic lubricant used in Vickers' axial-piston-type pumps are certainly of considerable value for assessing the suitability of this fluid for these specific applications. Although it is indicated that the service conditions for these pumps is more severe than most industrial usage, a proper evaluation of the fluid as a bearing lubricant in terms of bearing life can be made only if due consideration is given to the actual loads on the bearings and the wide scatter of results. In stating that no differences have appeared in the service performance of a phosphate ester-type fluid and petroleum oil, Mr. Moreton does not indicate a specific basis for making the comparison. It is conceivable that if a maintenance schedule requires periodic replacement of bearings prior to reaching the expected minimum life, little difference can be detected in the performance of two fluids which show significant differences in systematic evaluations.

Mr. Moreton suggests that the wide differences in results reported may be due to test conditions which have either amplified or induced a variable not present in many other types of service employing these pumps and these types of lubricants. The authors doubt that this is the case since the conditions of test were established only after a survey was made of the conditions found in various pumps encountered and after reasonable assurance was obtained from three reputable bearing manufacturers that the conditions established would give reliable results. In this connection there are tabulated in Table 4 thrust-bearing data for five sizes of axial-piston-type pumps found in Naval Service.

TABLE 4

Pump	P Max equivalent thrust load, lb	C Basic dynamic bearing load, rating, lb	C/P	Expected minimum life, revolutions
A	4,460[a]	15,700	3.52	45,000,000
B	6,080	11,900	1.96	7,500,000
C	6,080[a]	32,000	5.26	146,000,000
D	7,950[a]	25,000	3.15	31,000,000
E	29,590[a]	53,500	1.81	6,000,000

[a] Tandem bearing mounting.

In setting up the conditions of test reported in the paper, consideration was given to the values of C/P for the pumps operating continuously under the maximum load. As seen from the tabulation, the design load for the bearings in the five pumps varies considerably giving values of C/P from 1.81 to 5.26. Since bearing manufacturers select a load corresponding to a C/P of 2 for evaluation of bearings, it was considered that this value would be satisfactory for our evaluations since it represented actual conditions in the two pumps with the most heavily loaded bearings. Thus the loads used in the tests, although high, are not out of line with those found in actual service.

Mr. Moreton points to the median bearing life of 193 hours obtained for operation in petroleum oil and indicates that this is an unusually low life span for a pump. It must be remembered that this is the median-bearing life for continuous operation at maximum load, and that under actual service conditions the pump operates at maximum load for only a small portion of its life. Since the life of the bearing varies inversely as the cube of the load, the number of hours of operation under variable-load conditions will be many times the 193 hr determined in the tests. In addition, the service use of these pumps is intermittent and life under these conditions may be much greater than one year. Of course, for lighter loading, or higher values of C/P, pump life should be still greater.

Regarding the correlation of results obtained in the Laboratory with those obtained in actual pump operation, the amount of available information is very limited. A single pump test was conducted in the Laboratory with petroleum oil under variable load conditions equivalent to a C/P of approximately 3.5. Based on a median bearing life of 25,000,000 revolutions established in our tests, the median life of the pump is calculated to be 1280 hr. The actual life found for the bearing in the pump was 515 hr, which is within the range of lives that could be expected, if due consideration is given to the wide scatter obtainable with ball bearings.

The comments made by Mr. Morrison are much appreciated. It is gratifying to note the agreement of his results on radially loaded bearings with those of the authors on angular-contact thrust bearings. His remarks regarding the use of smaller and less expensive bearings are well taken. The authors have already taken steps to design machines for continuing the investigation with smaller bearings. The first evaluation will involve the size effect and then the investigation will proceed in the direction of determining the effect of load, temperature, viscosity, and speed.

The authors acknowledge the remarks made by Mr. Schmitt with due respect and appreciation and agree with his comment that within certain limits of bearing loading satisfactory life can be obtained with water-base fluids in hazardous industrial applications.

Operating Characteristics of High-Speed Ball Bearings at High Oil-Flow Rates

By C. C. MOORE[1] and F. C. JONES,[1] WEST LYNN, MASS.

Using 1005 petroleum oil as a lubricant, 202, 203, and 204-size ball bearings were operated in a speed range of between 0.6 to 1.7 × 10^6 *DN* value. Under lightly loaded conditions, oil-flow rates were varied between 1 and 500 range while friction power, oil-inlet, and outer-race temperatures were measured at speeds between 30,000 and 100,000 rpm.

Nomenclature

The following nomenclature is used in the paper:

a, b, c = constants in power-loss equations
D = bearing bore diameter, mm
$\% H_R$ = per cent friction power rejected to oil
H_R = friction power (dimensionless)
N = inner-race speed, rpm
Q = oil flow (dimensionless)
T = oil-inlet temperature, deg F
T_0 = oil-outlet temperature minus oil-inlet temperature, deg F
T_R = outer-race temperature minus oil-inlet temperature, deg F

Introduction

The series of tests reported here was sponsored by the Aircraft Accessory Turbine Department of the General Electric Company at West Lynn, Mass. The purpose of the tests was to investigate lubrication of ball bearings at speeds up to 100,000 rpm and *DN* values up to 1.7 × 10^6. The information here is concerned with friction power measurements with high oil-flow rates delivered by positive cross-feed.

In past years a machine designer's main concern with rolling-element bearings was generally with fatigue life. Usually the bearing friction was so small as to be an insignificant part of the power loss in the over-all machine system in which the bearing was used. Although this is still generally the case, a new design problem of cooling rolling-element bearings has accompanied the recent development of aircraft gas turbines and accessory units which operate at high temperatures and high speeds. This paper reports friction power losses in small bearings as a function of speed and oil flow and shows that increasing oil flow through bearings will result in cooler operation in a 30,000 to 100,000-rpm speed range.

Historically speaking, friction power-loss measurements have not been made in rolling-element-bearing tests. With the exception of analyses by H. Styri (1)[2] and M. Muzzoli (2), no efforts have been expended by any of the workers in this field to correlate friction power loss in a bearing as a function of the operating parameters such as speed, load, oil flow, and bearing size. Fogg (3) used friction factor as a parameter in reporting operation data on high-speed bearings, but did not express these data mathematically. Fogg concluded that high oil-flow rates can be used for cooling with no appreciable increase in friction power generation. This paper expresses the same conclusions. Macks and Nemeth (4) have developed a jet-cooling correlation analysis for one size of bearing relating the outer-rate temperature of the bearing to speed, load and oil flow, and viscosity; but friction power loss was not measured.

An analytical approach to friction power loss in rolling-element bearings has likewise been incomplete. The primary reason for this situation has been the failure of any worker to establish a successful theory on the mechanism of lubrication which takes place in rolling-element bearings. Muzzoli first suggested, but did not accomplish, integration of the parabolic stress distribution in the elliptical contact area between the balls and the races with a suitable coefficient of friction to obtain a value of friction torque. Muzzoli suggests that the coefficient of friction would be a function of load and speed. Recently, Poritsky et al. (5) performed this integration for a low-speed angular-contact bearing with a constant coefficient of friction. The results indicated that friction torque was independent of speed which the data in this paper indicate clearly is not the case for higher speed bearings. Michell (6) attempted to relate friction power loss to energy deformation of the balls and races. Again, this result indicated friction torque to be independent of speed which, as he himself pointed out, did not agree with experimental data.

The purpose of this paper is not to examine friction in rolling-element bearings from an analytical or mechanistic viewpoint, but to show the relative change in the friction in the bearing as a function of bearing speed, size, and oil-flow rates. The oil flows are greatly in excess of the minimum necessary for lubrication in the bearing and represent quantities of oil needed to cool the bearing. Correlation of data shows that, contrary to prevailing ideas, high oil flows by positive feed will cool bearings.

Test Equipment and Bearings

The drive motor of the first of two units employed is a two-pole induction motor and the drive motor of the other unit is a four-pole machine. Both of these units are driven by power from a variable-frequency alternator whose frequency range is from 1000 to 1700 cycles per sec (cps). Fig. 1 shows the test stand with the disassembled 100,000-rpm unit. To the left of the housing are two cantilever beams with strain gages used for torque measurement. The housing contains 24 capillary tubes which act as restrictors for the hydrostatic air bearing. The hydrostatic air-bearing assembly is seen at the left of the housing in Fig. 1. This assembly consists of two dynamometer air bearings which house the two test bearings. These test bearings, which cannot be seen in Fig. 1, support the shaft and motor rotor which drives the shaft. The oil pump under the stand is used for supply pressure when the test bearings are being lubricated with liquid oil. At the upper left of the panel is an air-mist unit which also can be used for lubrication.

---

[1] Thomson Laboratory, General Electric Company.

[2] Numbers in parentheses refer to the Bibliography at the end of the paper.

Contributed by the Research Committee on Lubrication under the auspices of the Lubrication Activity of The American Society of Mechanical Engineers, and presented at the Second Annual ASME-ASLE Lubrication Conference, Indianapolis, Ind., October 10–12, 1955.

Note: Statements and opinions advanced in papers are to be understood as individual expressions of their authors and not those of the Society. Manuscript received at ASME Headquarters, August 11, 1955. Paper No. 55—LUB-10.

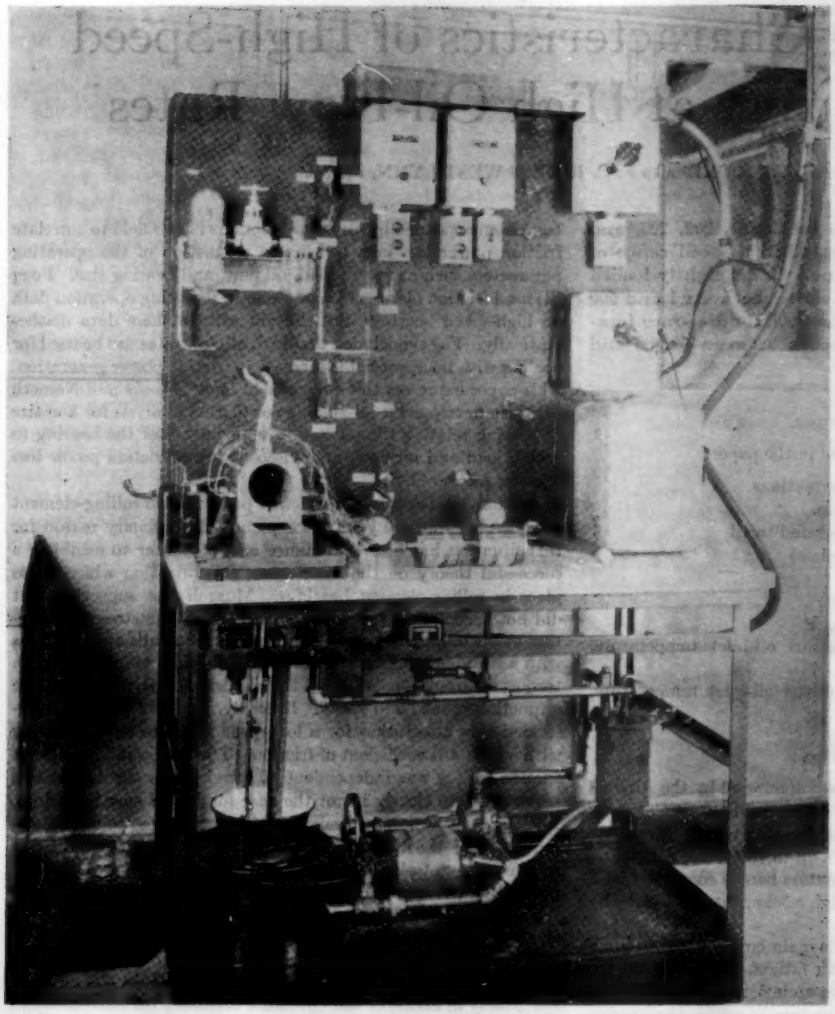

FIG. 1 VIEW OF 100,000-RPM UNIT AND TEST STAND

The bearings used in these tests were all of the deep-groove, Conrad type. The radial clearance was 0.0003 in. in the 202, 203, and 204 sizes. Calculations considering centrifugal force on a 202-size bearing rotating at 100,000 rpm were made by A. B. Jones (7) to determine the maximum radial clearance allowable. It was found that with a thrust load of 20 lb the pressure ellipse on the inner race would just begin to extend over the shoulder of the race at a radial clearance of 0.0013 in.

All the bearings had laminated phenolic retainers which are recommended by the bearing manufacturers for high speed because of (*a*) a high strength/weight ratio, and (*b*) low friction characteristics. These retainers were of the inner-race riding type. All bearings were of the precision type, i.e., ABEC 5 tolerances or better.

TEST CONDITIONS

Positive lubrication by cross-feed was accomplished by putting the oil in on one side of the bearing and leaving no convenient exit for the oil except through the bearing. This method proved to be quite adequate and is illustrated in Fig. 2 using various supply pressures and orifice diameters so that a flow range of 500 to 1 was achieved. The oil used in all of the tests was the light grade 1005

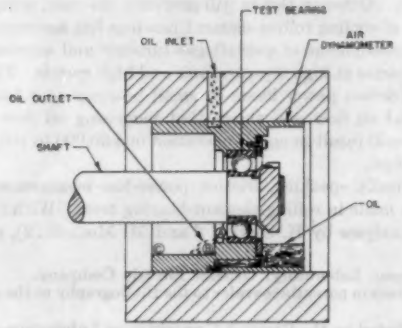

THERMOCOUPLE POSITON	TEMPERATURE, °F 60,000 RPM	80,000 RPM
A	169	220
B	158	195
C	129	164

FIG. 2 DYNAMOMETER MOUNTING OF TEST BEARING SHOWING CROSS-FEED OILING

petroleum oil, MIL-O-6081A (Amend. L), which has a viscosity of 5 centistokes at 100 F.

Oil-mist and jet-lubrication methods were used unsuccessfully and did not deliver enough oil to the bearing for lubrication and cooling. A typical failure was evidenced by thermal expansion of the balls, removal of all of the radial clearance in the bearing and finally seizure.

Most of the tests were run with a light 20-lb thrust load on the bearings to prevent ball skidding. The only radial load present was an unbalance load of between 10 and 100 lb depending, of course, on the speed of rotation. This represented the best balance that could readily be obtained on the shafts. The 204-size bearing was operated at a speed range of between 30,000 and 50,000 rpm, while the 202 and 203 size bearings were operated at a speed range between 30,000 and 100,000 rpm. No external heat was applied.

As oil flows were varied in a 500 to 1 range, friction power loss, oil-temperature rise, and outer-ring temperatures of the bearing were measured. Friction torque was measured through an air-dynamometer bearing which housed the outer ring of the bearing and which was restrained from rotation by a previously calibrated strain gage mounted on a cantilever beam.

TABLE 1 PERFORMANCE DATA FOR NO. 202 BALL BEARINGS
Radial clearance 0.0003 in.; 7 balls 1/4 in. diam; ABEC 5; synthetic retainer

Speed RPM	Oil Flow (Dimensionless)	T_i, °F	T_R, °F	T_o, °F	% HP_R
30,000	500	110	2	4	57.8
	200	84	24	22	153.5
	100	97	18	19	66.1
	50	90	34	24	44.5
	25	85	35	26	27.2
	20	74	46	34	29.8
	15	74	48	34	21.3
	10	75	46	35	16.7
	5	75	49	37	9.7
	3	74	48	29	5.2
	1	74	52	31	2.6
40,000	500	98	11	12	118
	200	90	20	25	103
	100	86	33	36	81.3
	50	77	43	43	59.5
	25	76	53	48	32.4
	20	75	57	57	32.8
	15	71	59	56	24.7
	10	66	63	60	17.6
	5	66	65	65	10.5
	3	67	65	65	6.5
	1	68	66	64	1.6
50,000	500	108	12	14	63.2
	200	87	29	38	86.2
	100	87	45	48	56.4
	50	76	61	49	36.0
	25	76	71	62	22.8
	20	77	77	66	19.8
	15	69	77	73	16.2
	10	68	78	73	11.4
	5	67	80	75	7.1
	3	67	80	75	4.7
	1	67	82	77	1.6
60,000	500	82	49	70	245
	200	87	43	63	80.5
	100	79	71	86	66.0
	50	82	84	90	37.6
	25	73	87	87	19.8
	15	74	105	103	16.1
	5	78	99	96	5.7
	1	70	94	91	1.2
80,000	500	92	72	96	210
	200	97	69	95	87.6
	100	82	99	108	40.5
	50	80	117	112	33.9
	25	74	118	114	17.7
	15	76	126	118	13.0
	5	78	124	116	4.6
	3	73	119	109	2.7
	1	Bearing failed			
100,000	500	100	119	142	187
	200	80	126	140	78.5
	100	82	153	158	49.7
	50	82	166	156	29.4
	25	78	156	142	14.9
	15	79	168	146	10.5
	10	78	170	149	7.1
	3	Bearing failed			

Test Data

The data for the 202, 203, and 204-bearing tests are presented in Tables 1, 2, and 3, respectively. The percentage of the friction power rejected to the oil has been included in the tables. It will be noted that the oil-outlet temperature is greater than the bearing temperature in a number of the tests. This is due to the difficulty encountered in obtaining the average outlet-oil temperature. Fig. 2 shows the outlet-oil temperature at three thermocouple positions in the bearing housing for a 202 bearing running

TABLE 2 PERFORMANCE DATA FOR NO. 203 BALL BEARINGS
Radial clearance 0.0003 in.; 8 balls 7/32 in. diam; ABEC 5; synthetic retainer

x = Power consumption too great for steady-state operation

Speed RPM	Oil Flow (Dimensionless)	T_i, °F	T_R, °F	T_o, °F	% HP_R
30,000	500	116	1	4	42.6
	200	94	12	18	85.9
	100	83	29	35	95.8
	50	78	39	44	64.5
	25	77	32	35	27.6
	20	83	39	38	23.2
	15	79	41	39	19.4
	10	69	46	41	12.3
	5	77	45	40	7.0
	3	77	45	40	4.2
	1	77	46	41	1.5
40,000	500	113	5	10	62.0
	200	95	20	27	82.0
	100	79	40	48	83.5
	50	79	49	53	50.5
	25	81	50	53	26.6
	20	79	54	53	22.7
	15	80	53	51	18.8
	10	67	62	56	12.8
	5	74	58	52	6.1
	3	74	58	52	3.7
	1	74	60	54	1.4
50,000	500	94	18	33	134
	200	108	24	39	75.9
	100	82	52	68	73.0
	50	79	65	76	48.3
	25	77	75	81	27.0
	20	78	75	81	21.6
	15	81	73	81	24.6
	10	81	73	81	11.6
	5	83	78	83	6.4
	3	83	78	83	3.8
	1	85	76	86	1.4
60,000	500	106	25	37	92.6
	200	93	61	68	97.3
	100	80	92	87	64.4
	50	83	107	96	38.1
	25	76	111	98	22.2
	20	95	97	101	18.7
	15	82	98	98	14.7
	10	75	120	97	10.0
	5	82	107	107	5.45
	3	80	108	108	3.37
	1	84	111	111	1.14
80,000	500	x	x	x	x
	200	108	75	101	69.4
	100	100	96	94	52.0
	50	84	158	136	37.5
	25	88	161	139	21.2
	20	87	168	146	16.1
	15	87	168	146	12.2
	10	78	176	167	9.2
	5	Bearing failed			
100,000	780	x	x	x	x
	500	x	x	x	x
	400	x	x	x	x
	300	x	x	x	x
	200	x	x	x	x
	100	Bearing failed			

TABLE 3 PERFORMANCE DATA FOR NO. 204 BALL BEARINGS
Radial clearance 0.0003 in.; 8 balls 9/32 in. diam; ABEC 5; synthetic retainer

Speed RPM	Oil Flow (Dimensionless)	T_i, °F	T_R, °F	T_o, °F	% HP_R
30,000	500	117	6	12	77.0
	200	65	26	35	95.0
	100	90	40	49	82.0
	50	80	56	62	52.4
	25	82	55	58	38.0
	15	91	58	59	18.0
	3	91	54	59	4.1
40,000	500	118	11	19	79.0
	200	90	32	44	88.0
	100	87	51	62	75.8
	50	77	73	80	51.0
	25	83	67	75	25.0
	15	91	75	81	15.6
	3	90	67	72	4.4
50,000	500	112	21	32	92.5
	200	94	46	60	63.0
	100	77	92	97	76.4
	50	78	91	103	42.0
	25	88	94	104	25.2
	15	90	94	102	16.0
	3	89	90	97	3.2

at 60,000 and 80,000 rpm and at an intermediate oil-flow rate. The temperatures tabulated in Tables 1, 2, and 3 were obtained from a thermocouple at position A, and may be greater than the average. The temperature at A is higher than the temperature at C for two reasons: (*a*) The temperature at A reads the oil temperature just coming out of the bearing before mixing occurs, and (*b*) heat transfer from the oil to the dynamometer bearing cools the oil by the time C is reached. It is difficult then to read average temperature because heat has been lost from the oil by the time sufficient mixing has occurred. This discrepancy is reflected as high values in the percentage of friction power rejected to the oil, but it does not change the general sense of the data.

Several effects of the rate of flow may be noted directly from the data shown in Tables 1, 2, and 3. An increase in oil flow at any given speed resulted in the following action:

1 Increased friction power loss.

2 Increased percentage of the friction power loss rejected to the oil.

3 Decreased temperature difference between the outer race and the inlet oil.

4 Decreased temperature difference between the inlet oil and outlet oil.

The lowest oil flow that could be delivered by the supply system was sufficient at all bearing operating conditions less severe than those listed in Table 4. At high speeds, however, it was discovered that the rates in Table 4 were required to prevent failure.

TABLE 4 OIL-FLOW RATES FOR HIGH-SPEED OPERATION

Size	Speed, rpm	$DN \times 10^{-6}$	Relative minimum oil-flow rate
202	80000	1.2	1
202	100000	1.5	3
203	80000	1.36	5
203	100000	1.7	100

The effects of speed are easily seen in Tables 1, 2, and 3. An increase in speed at any given flow resulted in the following:

1 Increased friction horsepower.

2 Increased temperature difference between the inlet oil and the outer race.

3 Increased temperature difference between the inlet oil and the outlet oil.

4 Generally a decreased percentage of friction power rejected to the oil.

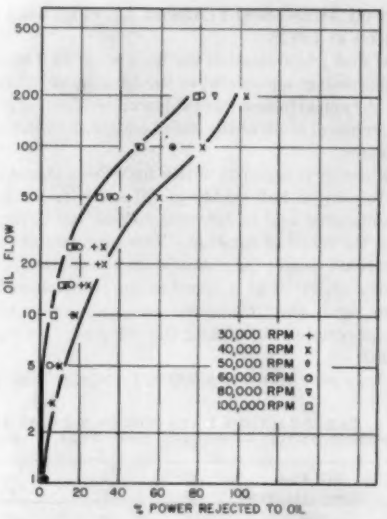

FIG. 3 OIL FLOW VERSUS POWER REJECTION TO OIL NO. 202 ABEC-5 BALL BEARING, 1005 OIL

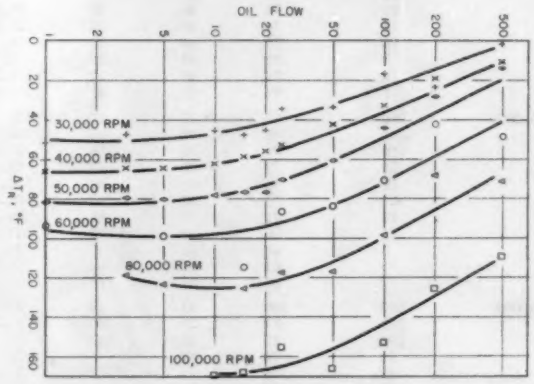

FIG. 4 OIL FLOW VERSUS ΔT_R FOR NO. 202 ABEC-5 BALL BEARING, 1005 OIL

Fig. 3 is a plot of oil flow versus the percentage of the friction power rejected to the oil for the 202 bearing. It will be noted that the power rejected to the oil approaches 100 per cent at high oil-flow rates. The cooling effect of high oil flows is demonstrated again in Fig. 4, a plot of the oil flow versus the difference in temperature between the inlet oil and the outer race for the 202 bearing. At high flow rates the temperature difference decreases rapidly, since more of the friction power is being absorbed by the oil. These two figures show the marked effect of oil flow in cooling the bearing.

An analysis of the data to determine the relative importance of bore diameter, speed, and oil flow upon friction power has been made in Fig. 5 and the ranked importance of these variables is shown in Table 5. The tests reported here did not include load as a variable, but tests of 140-mm-bore bearings indicated that the effect of load and oil flow are of comparable magnitude. For example, changing the axial load from 1000 to 5000 lb had approximately the same effect on the friction power as a change in flow rate from 0.5 to 2.5. From Table 5 it can be seen that the bore and speed are the most important factors in the friction

TABLE 5 RELATIVE IMPORTANCE OF BEARING SIZE, SPEED, AND OIL FLOW ON FRICTION POWER

(Refer to Fig. 6)

	Variable	From	Increase in HP_f (X), per cent	Produced by (Y)	Relative importance (X/Y)
1	Bearing size...	E to A	47	13% in bore size	350
2	Speed.....	B to D	232	100% in speed	220
3	Oil flow.....	B to A	52	4900% in oil flow	1

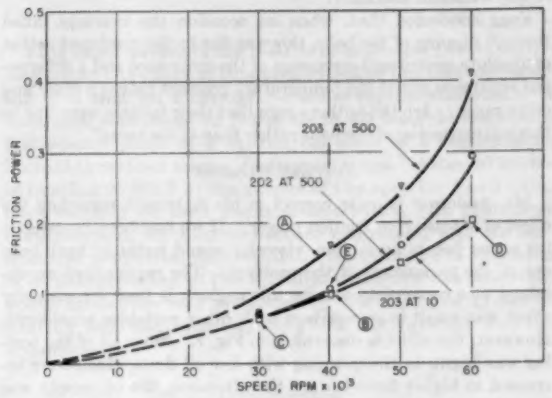

FIG. 5 FRICTION POWER LOSS VERSUS SPEED FOR NO. 202 BALL BEARING—ABEC-5 BEARING, 1005 OIL

power loss in the bearing, and that oil flow has only a minor effect.

Figs. 6, 7, and 8 are plots of the friction power loss versus the oil flow at various speeds for 202, 203, and 204 bearings, respectively. The similarity of these figures is rather striking. At each bearing size the data at different speeds form a family of straight lines. Equations for the groups are of the form

$$H = aN^bQ^{cN^d}$$

It is felt that similar equations will hold for other bearing sizes and types of lubricants.

CONCLUSIONS

The conclusions of this study are as follows:

1 Within the scope of this study small high-speed bearings can best be lubricated by cross-feed or puddling techniques. Jet and mist lubrication were unsuccessful.

2 Friction power is more a function of speed and bearing size than of oil flow.

3 Increasing the oil-flow rate lowers the outer-race temperature but increases the total friction power being created by the bearing.

4 High oil flows will cool a bearing with only a relatively small increase in friction power.

BIBLIOGRAPHY

1 "Friction Torque in Ball and Roller Bearings," by Haakon Styri, *Mechanical Engineering*, vol. 62, 1940, pp. 886–890.

2 "Friction in Rolling Bearings," by Manlio Mussoli, Ricerche de Ingegneria, September-October, 1934.

3 "The Lubrication of Ball and Roller Bearings at High Speed," by A. Fogg and J. S. Webber, *Journal of the Institute of Petroleum*, vol. 39, November, 1953, pp. 743–764.

4 "Investigation of 75 Millimeter-Bore Cylindrical Roller Bearings at High Speeds III," by E. F. Macks and Z. N. Nemeth, NACA TN 2420, July, 1951.

5 "Sliding Friction of Ball Bearings of the Pivot Type," by H. Poritsky, C. W. Hewlett, and R. E. Coleman, Jr., *Journal of Applied Mechanics*, Trans. ASME, vol. 69, 1947, p. A-261.

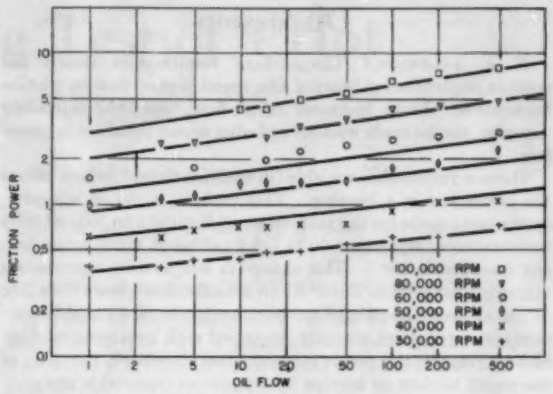

FIG. 6 FRICTION POWER LOSS VERSUS OIL FLOW FOR NO. 202 BALL BEARING—ABEC-5 BEARING, 1005 OIL

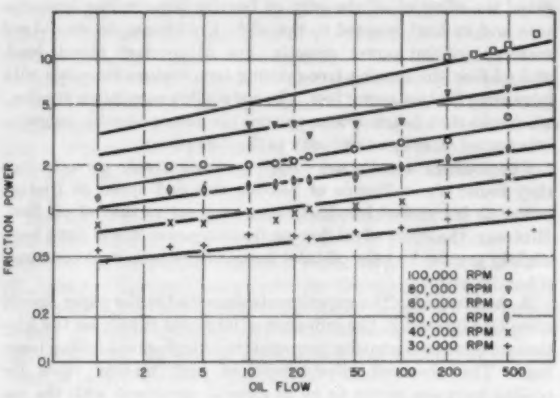

FIG. 7 FRICTION POWER LOSS VERSUS OIL FLOW FOR NO. 203 BALL BEARING—ABEC-5 BEARING, 1005 OIL

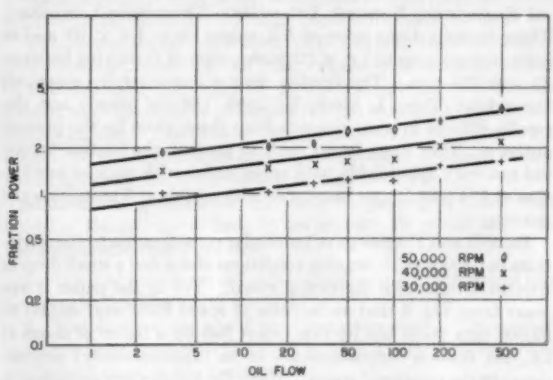

FIG. 8 FRICTION POWER LOSS VERSUS OIL FLOW FOR NO. 204 BALL BEARING—ABEC-5 BEARING, 1005 OIL

6 "Lubrication, Its Principle and Practice," by A. G. M. Michell, Blackie and Sons, Ltd., 1950.

7 Private communication by A. B. Jones, Fafnir Bearing Company, 1953.

8 "Design Technique Forecasts Supercharger Performance," by R. J. S. Pigott, *SAE Journal*, January, 1947, pp. 59–64.

Discussion

W. J. Anderson.[3] The authors' results show clearly the relative importance of bearing size, speed, and oil flow on friction horsepower. Large increases in oil flow, and thus in cooling capacity, can be made without suffering severe penalties in power loss.

There is yet another variable (in addition to load) which affects the power loss in a bearing. This variable is the oil viscosity. In the tests made by the authors at oil flows of 1 to 500, oil-inlet temperatures varied from 66 to 118 F (although not that much in any one specific test). This change in temperature represents a viscosity change from about 8.5 to 4 centistokes—more than 2 to 1. In all tests, the oil-inlet temperature increased with oil flow or, in other words, inlet viscosity decreased with increasing oil flow. Since it requires less power to shear a less viscous oil, the effect of increasing oil flow on friction horsepower as reported is probably somewhat less than the true effect that would have been obtained had oil-inlet temperature been held constant.

In some of our tests of 75-mm-bore roller bearings, we investigated the effect of oil viscosity on bearing free-running temperature and on heat rejected to the oil.[4] Unfortunately, we did not measure friction power directly, but at constant speed, load, and oil flow the bearing free-running temperature increases with increasing friction power loss. In our cooling correlation studies,[4] we found that bearing temperature rise above oil-inlet temperature varied directly as viscosity to the 0.25 power.

The authors' results are certainly qualitatively correct since they found the influence of bearing size and speed on friction power to be several hundred times as great as that of oil flow. However, the effect of oil flow on friction power would have been slightly greater had the oil-inlet temperature been kept constant.

A. A. Milne.[5] The experiments described in the paper should stimulate interest in the influence of lubricant supply on the friction torque and operating temperature of high-speed rolling bearings. The observed effectiveness of high oil-flow rates for cooling purposes seems to be in general agreement with the experience of Fogg at the National Physical Laboratory, Teddington, England (in which the writer had the privilege of assisting) and, later, of Barwell and Hughes at the N.P.L. and at the Mechanical Engineering Research Laboratory, Thorntonhall, Scotland. These investigations covered DN values up to 1.4×10^6 and in some instances up to 1.8×10^6 with values of D varying between 35 and 125 mm. The friction torque was carefully measured throughout (Proc. I. Mech. E., 1955, 169 [in press]) and the results differed in some respects from those given by the present authors. Thus Fogg found that, in general, the friction torque did not vary appreciably with speed either with oil-mist lubrication at 1/4 pint/hr per bearing or with oil jets at 3 pints/min per bearing.

Barwell and Hughes gave particular consideration to the variations in friction with running conditions and noted a small drop in friction torque with increasing speed. Yet in the paper it appears from Fig. 6 that an increase of speed from, say, 40,000 to 80,000 rpm raises the friction power loss by a factor of about 4; i.e., the friction torque appears to be (approximately) proportional to the rotational speed. Have the authors any explanation of their observed much larger effect of speed than in the earlier work? Could it be due to the large increase in effective bearing load with increasing speed due to rotor unbalance; the proportionate effect of this might be particularly marked at the low nominal thrust loads employed by the authors?

The reported lack of success with oil-mist and oil-jet lubrication is puzzling in view of the previously reported successful experience with these methods, up to DN-values of at least 1.4×10^6. Can the authors offer any explanation of the failure of their systems to supply sufficient lubricant?

Fogg concluded that, when on occasion the bearings failed through nipping of the balls, this was due to the combined action of absolute centrifugal expansion of the inner race and a differential expansion due to the temperature gradient between inner and outer races. Are the authors sure that their failures were due to thermal expansion of the balls rather than of the races?

Authors' Closure

Mr. Anderson is quite correct in his statement regarding the effect of viscosity on friction power. If we had been investigating power loss in an oil line, viscosity would certainly have been one of the parameters of the problem. The reason that we obtained nice correlation despite this neglect, is that the viscosity effect was small in comparison with other variables considered. However, the effect is discernible in Fig. 7. Since all of the testing was begun in the morning with low oil flows which were increased to higher flows toward the afternoon, the oil supply was heated gradually throughout the day. As a consequence, viscosities were higher for lower oil flows. In Fig. 7 the experimental data show higher power losses than the curve predicts owing to these higher viscosity values at low oil-flow rates.

In answer to Mr. Milne's questions regarding variation in friction torque with oil flow, speed, and load, the authors would like to mention that we are reporting friction power, not friction torque. Friction power, of course, is the product of friction torque and speed, and therefore definitely varies with speed. We are not familiar with the work of Barwell and Hughes which indicated no variation of friction torque with speed. This report is contrary to our work and the work of Styri and Mussoli. We noticed a much smaller effect from oil flow compared with speed and bearing size on friction torque and in other tests not reported here have observed about the same effect with loads. Summing up, friction torque seems to be mostly a function of speed and bearing size with oil flow and load playing a smaller part.

The effect of oil flow seems to have been negligible in Fogg's work because of the smaller range of oil flow through the bearing used in the testing. Since jets were used, only about 20–40 per cent of the 3 pints per min actually got through the bearing and contributed to friction. In our test all of the oil was required to go through the bearing and at higher flow rates we had near-submersion operation. One of the features of this type of lubrication is that, although friction power is higher, the bearing is cooler and the greatest cooling effect is obtained in submerged operation. It is believed this is a new concept in high-speed rolling-bearing lubrication and cooling.

Our lack of success with oil mist in lubricating these bearings resulted from the fact that, since we had small internal clearances, insufficient cooling was provided compared with solid oil. Insufficient cooling results in differential internal expansion of the balls and races to remove the radial clearances in the bearing. We did not measure ball and inner-race temperatures and are not sure which element contributed the most toward removal of this clearance. Because of the thermally insulated condition of the ball, it is suspected that its temperatures are considerably above those of the inner and outer rings. We estimate that a 150-deg F temperature differential between the balls and other elements was sufficient to remove a radial clearance of 0.0003 in.

[3] National Advisory Committee for Aeronautics, Washington, D. C.

[4] "Influence of Lubricant Viscosity on Operating Temperatures of 75-Millimeter-Bore Cylindrical-Roller-Bearing at High Speeds," by E. F. Macks, W. J. Anderson, and Z. N. Nemeth, NACA TN 2636, February, 1952.

[5] Lubrication Division, Mechanical Engineering Research Laboratory, Thorntonhall, Glasgow, Scotland.

Thermal-Cycling Test of a Hot Spot on a Vessel

By P. N. RANDALL[1] and H. A. LANG[2]

This paper presents the results of laboratory tests which simulated the effect of repeated cycles of heating and cooling of a spot on a catalytic-cracker regenerator shell. A specimen was made to resemble in all feasible respects a 6-ft-square piece of a cylindrical shell of a regenerator, including welded seams and vapor stops. After 50 cycles of heating to 900 F at the center of the spot for 1 or 2 days, then cooling to near room temperature, the plate was radiographed, its microstructure examined, and its mechanical properties determined. No evidence of cracking or of deterioration of the metallic structure was observed. Some distortion was produced by the first few cycles of heating but continued cycling did not produce further distortion.

Introduction

THE regenerator shells of fluidized catalytic-cracking units can develop surface hot spots when erosive catalyst destroys portions of the internal insulation. Since bursting of the regenerator shell could easily result in heavy loss of life and property, it is natural that operators are inclined to shut down a unit and make repairs as promptly as possible, although such a shutdown may seriously reduce the output of the refinery. It is desirable to evaluate the hazards of continued operation where thermal cycling exists, since fluctuating stress states produced by hot spots can be expected to recur in other refinery units.

On the basis of these considerations, it was decided to run a simulated service test upon a portion of a regenerator shell. Temperature cycles created by electric heaters were imposed and measurements of strain and deformation were made.

The test was designed to answer the following questions:

1 Can cracks be produced and made to propagate?

2 Will increased plastic flow take place as temperature cycles are continued?

3 Will the mechanical properties of the material be seriously affected by the thermal cycles?

The number of repetitions of a "hot spot" that a refinery vessel, such as a regenerator, undergoes throughout its life is too small to indicate that the design should be based on the avoidance of fatigue failure. It is sufficient to determine whether the cycling produces further plastic deformation or whether the vessel supports the thermally induced stress state in an elastic manner after plastic flow has occurred in the first few cycles. This latter occurrence is called "shakedown." It is important for field engineers to recognize this state and to realize that shakedown states are not hazardous if the number of cycles is small.

Review of Previous Investigations

A review of the literature prior to the date of these tests revealed no studies from which one could estimate the danger of cracking at a hot spot. Some studies of specific cases had been reported, the one most applicable to this problem being cyclic heating tests upon ferritic and austenitic-steel test pieces welded together, conducted by Weisberg.[3] The test program simulated full-size welds occurring in the main-steam-piping joint of the Sewaren generating station. Since austenitic steel has a coefficient of thermal expansion about 50 per cent greater than that of ferritic steel, high stresses were expected. One hundred cycles of heating and cooling revealed no new cracks and no propagation of cracks initially present in the unsound welds. The heating temperature of 1100 F was reached in 4 hr for the first 25 cycles and in 2 hr for the next 75 cycles. The holding periods were $1\frac{1}{2}$ and 0 hr, respectively. Test pieces were always cooled to 200 F in 2 hr.

Surveys of available information on thermal fatigue and thermal shock have recently been published by Thielsch[4] and Manson.[5] From the work of various investigators, it appears that the likelihood of damage from a particular thermal cycle is related to the total range of mechanical strain which it imposes on the material. Whether cracking will occur depends on this range of imposed strain, and also on the strength and ductility of the material at both extremes of the thermal cycle.

Choice of Specimen

Three types of test specimen were considered; a tension-compression member, a scale model of the entire regenerator shell, and a full-scale duplicate of part of the regenerator shell.

To simulate the service conditions of thermal fatigue would require that the histories of both the stresses and the temperatures of the hot spot be duplicated in the test specimen. Unfortunately, only the thermal history of the hot spot was even approximately known. Therefore it seemed impossible to estimate the degree to which a simple tension-compression specimen would have duplicated the stress history in the vessel.

Maintaining geometrical similarity by testing a small scale model of the cylindrical body of the regenerator would have had the serious disadvantages that:

1 It would have been difficult to duplicate the mechanical and metallurgical properties of the steel.

2 The vapor stops would have been too small. They could not have been welded to the shell in such a way that the welds duplicated those in the regenerator.

3 Stress raisers resulting from other steps in the fabrication process would have differed between model and prototype.

---

[1] Project Engineer, Engineering Research Department, Standard Oil Company (Indiana), Chicago, Ill.

[2] Missiles Division, Rand Corporation, Santa Monica, Calif. Mem. ASME.

Contributed by the Materials Committee of the Petroleum Division and presented at the Petroleum-Mechanical Engineering Conference, New Orleans, La., September 25–28, 1955, of The American Society of Mechanical Engineers.

Note: Statements and opinions advanced in papers are to be understood as individual expressions of their authors and not those of the Society. Manuscript received at ASME Headquarters, May 10, 1955. Paper No. 55—PET-2.

[3] "Cyclic Heating Test of Main Steam Piping Joints Between Ferritic and Austenitic Steels—Sewaren Generating Station," by H. Weisberg, Trans. ASME, vol. 71, 1949, p. 643.

[4] "Thermal Fatigue and Thermal Shock," by H. Thielsch, Welding Research Council, Bulletin Series No. 10, April, 1952.

[5] "Behavior of Materials Under Conditions of Thermal Stress," by S. S. Manson, NACA Technical Note 2933, July, 1953.

4 Surface oxidation would have been of much greater consequence in the model than in the prototype.

5 The temperature gradient through the shell wall may have been significant in the prototype. In the model this gradient could not have been easily produced.

The disadvantages cited for the first two types of test pieces were largely avoided by using a specimen made identical in all respects to a 6-ft-square portion of the regenerator shell. A difficulty then arose, namely, how much less restraint to the deformation of the shell in the region of the hot spot was there in the test specimen than in the vessel? To minimize this difference, the test specimen was made as large as could be handled and the temperature gradient around the spot was made as sharp as possible. Data presented in a later section indicate that a larger specimen would have been desirable; however, the authors believe that the conclusions would not have been changed. The fact that the specimen was not a complete cylinder was not considered significant.

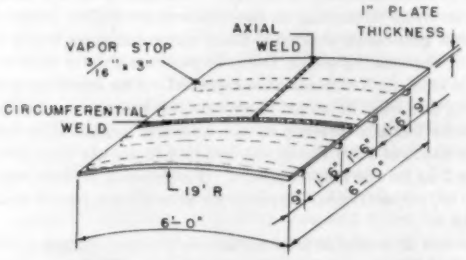

FIG. 1 SKETCH OF SPECIMEN

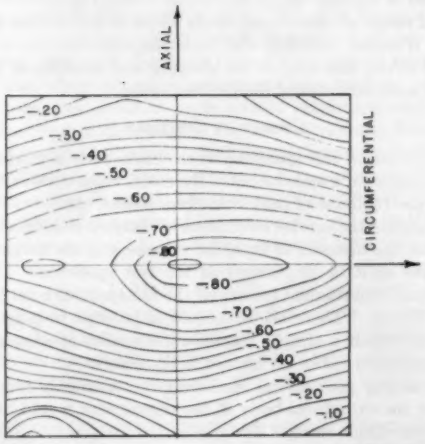

FIG. 2 CONTOURS SHOW RADIAL DISTANCE FROM SURFACE OF SPECIMEN TO CYLINDRICAL REFERENCE SURFACE OF 19-FT RADIUS

The specimen, Fig. 1, was made as follows. First, a piece of 1-in. plate, 6 ft wide × 8 ft long, of ASTM A-201 Grade A firebox-quality steel, was rolled cold to a radius of 19 ft, the curvature being in the direction of rolling at the mill. Then a 1-ft strip was burned off each end and the plate was cut into three pieces which were then rejoined by welding so the center of the specimen resembled the junction of a circumferential weld and an axial weld in the regenerator shell. The plate edges were prepared by burning for double-Vee butt welds, which were made with $^{3}/_{16}$-in-diam, E6010, cellulose-sodium welding rod with the specimen standing on edge as in the field. The welding procedure duplicated that used on one of the regenerator vessels in question. The weld reinforcement was ground off. Radiographs revealed a defect at the weld junction. The defect was removed by chipping and rewelding, followed by a recheck set of radiographs. The vapor stops were made of $^{3}/_{16}$-in-thick ASTM A285 steel plate. They were burned to shape and attached as shown in Fig. 1, using $^{1}/_{4}$-in. continuous fillet welds made with $^{3}/_{32}$-in-diam welding rod. Vapor stops on the regenerator shell acted as barriers to the flow of gases between the shell and the internal insulation. The specimen was then stress-relieved by holding at 1030 F for 15 hr. Heating and cooling rates were 50 F and 160 F per hr, respectively.

The specimen as received was not perfectly cylindrical in form, but had a saddle shape caused by unequal shrinkage of the circumferential weld. This shape is shown in Fig. 2 which is a contour map showing the departure of the top surface of the plate from that of a cylindrical reference surface of 19 ft radius. The effect of the saddle shape on bulging or on the maximum values of tensile and compressive strain is not known. Measurements of the deformation during heating showed no evidence of "snap action" or buckling as the bulge developed.

APPARATUS

The specimen was tested in a horizontal position, with the vapor stops down as shown in Fig. 3. It was supported on four pipe legs spaced 4 ft apart, and was electrically heated from below by a flat spiral of 0.289-in-diam nichrome resistance wire, which rested on a steel and transite platform carried by the pipe stand. Power, provided by a welding transformer, was typically about 175 amp at 37 volts. The top surface of the plate and the bottom surface, except above the heater, and also the edges, were covered with 4 in. of a block-type insulation made of diatomaceous silica and asbestos fiber.

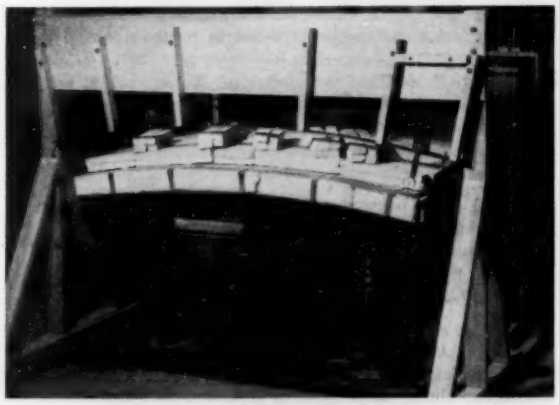

FIG. 3 SPECIMEN AND TEST EQUIPMENT
(Contour gage in position for reading on heated plate.)

Temperatures were measured by means of iron-constantan thermocouples attached to the top surface of the plate, at locations shown by small circles in Fig. 4, by peening the wires into a pair of small drilled holes. Also, thermocouples were attached to one vapor stop to measure the circumferential and radial temperature gradients in it. These were all connected to a 12-point, strip-chart, temperature recorder. The maximum temperature, at the center of the specimen, was controlled by manual adjustment of the welding transformer to balance heat input against losses to the room.

Radial movements of points on the top surface of the specimen

were measured by means of an Ames dial mounted on a block which slid along a curved track spanning the plate as shown in Fig. 3. The curved track could be moved the length of the specimen on wooden rails. A square grid of punch marks 5 in. apart, Fig. 4, covering the surface of the specimen provided fixed points of reference. The effect of temperature changes on the Ames dial and on the curved track when readings were taken on the hot specimen was checked by taking readings on a standard bar before and after taking readings on the plate. Fortunately, the net effect was small and has been neglected.

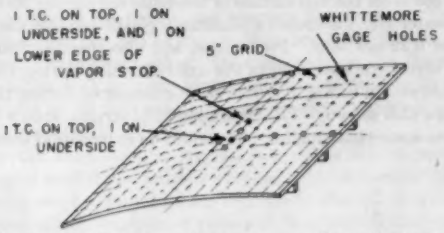

FIG. 4 SKETCH SHOWING LOCATION OF THERMOCOUPLES AND REFERENCE POINTS FOR MEASUREMENT OF STRAIN AND RADIAL MOVEMENT

The four supporting columns for the plate were each located 1 ft inside the edge of the plate. Because of this, the motion of the center of the plate during heating was upward relative to the contour track, and the motion of the corners of the plate was downward. To present a clearer picture, the data were converted to show radial movements of the top surface of the plate relative to three corner reference points.

Strains on the top surface of the plate in both the hot and cold states were measured with a 10-in. Whittemore gage. Gage holes were made in one quadrant of the specimen, Fig. 4, with a No. 54 drill, following the pattern of the 5-in. grid of punch marks. When the plate was hot, readings were taken by removing insulation (which had been cut into blocks of special size for this purpose) only from the region near the gage points in question in order to minimize the temperature drop. The record of strains included also the record of temperatures taken simultaneously in order that thermal strain could be subtracted from the total strain.

PROCEDURE

A temperature cycle consisted of a period of heating from near room temperature to 900 F at the plate center, which required about 12 hr; a period of holding at that temperature for about 1 day to permit as much creep as possible; and a period of cooling to near room temperature with the heater turned off and the insulation removed from the top surface of the plate, which required about 6 hr. Practical considerations affected the length of time spent in the hot and cold states and dictated a frequency of about 3 cycles per week. Complete sets of readings of strains and radial movements were taken in the hot and cold states for the first two cycles and again for the 26th cycle. Then the size of the heater was reduced and another 25 cycles were run, a complete set of readings being taken on the last cycle. Skeleton readings were taken for intermediate cycles to check on the progress of bulging at the center and to check the maximum strain readings. The vapor stops and the plate surface were visually examined at intervals for evidence of cracking.

The temperatures measured along the center line of the specimen in a circumferential direction are plotted in Fig. 5 for both heaters. The values shown were duplicated in the axial direction and also in succeeding cycles with a variation of plus or minus 30 deg F. The center temperature of 900 F was chosen to simulate the worst condition in the regenerator. For heater No. 1 the edge temperature of 550+ F was considered satisfactory, since thermal cycling in the "blue-brittle" range was a matter of some concern. The change was made to heater No. 2 when it appeared the specimen was not being damaged by cycling with heater No. 1 and a steeper temperature gradient was desired to produce higher restraint stresses. Heater No. 2 was made from No. 1 by forming two flat spirals instead of one, and placing one above the other to concentrate the heat input.

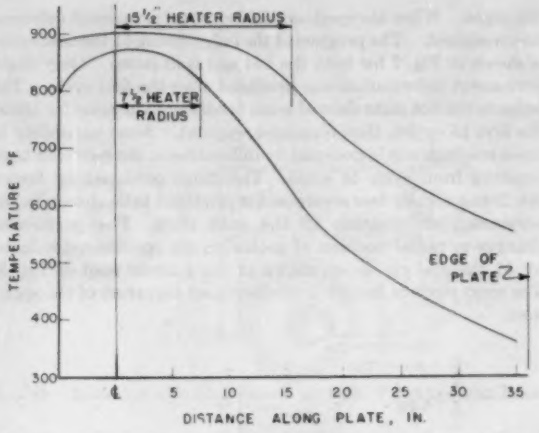

FIG. 5 TEMPERATURES ALONG CIRCUMFERENTIAL CENTER LINE

RESULTS

The primary objective of the experimental program was to determine if the test conditions were severe enough to cause cracking at any point on the specimen. Visual inspection of the surfaces of the plate and of the vapor stops revealed no evidence of cracking or damage. Radiographs of the shell seams also revealed no evidence of damage.

The shape of the bulge produced when the specimen was heated for the first time is shown in Fig. 6. The specimen behaved as though it were hinged at the circumferential center line and bulged by flexing about this line. The radial movement of points along this line was about 50 per cent greater at the center than at

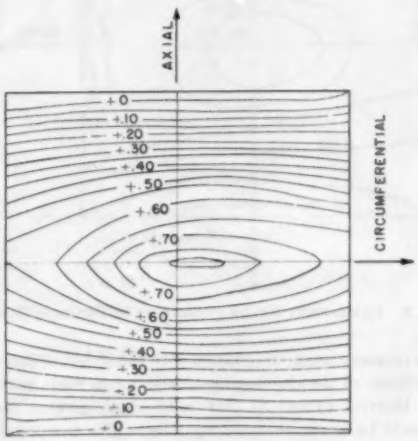

FIG. 6 BULGE PRODUCED ON FIRST HEATING
(Contours show radial movements in inches. All points moved radially outward.)

the edges. When the specimen cooled, some permanent deformation remained. The progress of the bulge during 51 thermal cycles is shown in Fig. 7 for both the hot and cold states. Only slight permanent deformation was produced after the first cycle. The bulge in the hot state showed some tendency to increase for about the first 15 cycles, then remained constant. Some variability in these readings was introduced by differences in the specimen temperature from cycle to cycle. The bulge produced by heater No. 2 was slightly less severe and it produced little change in the permanent deformation in the cold state. The permanent changes in radial position of points on the specimen, produced by 51 thermal cycles are shown in the contour map of Fig. 8. The most obvious feature is the increased curvature of the specimen.

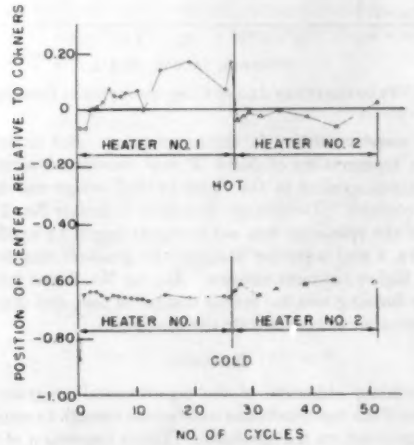

FIG. 7 CURVES SHOWING PROGRESS OF BULGE DURING THERMAL CYCLING

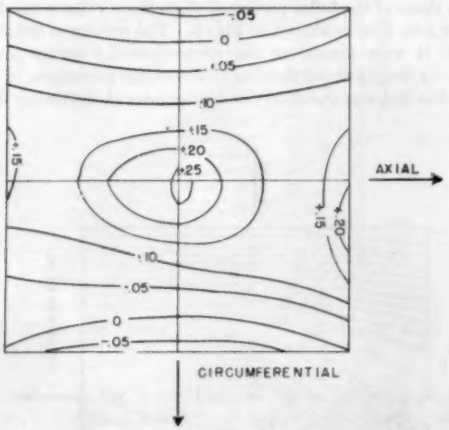

FIG. 8 PERMANENT BULGE FORMED BY 51 THERMAL CYCLES

Strain measurements were taken with the object of determining the amplitude of the elastic-plus-plastic strain cycle accompanying the thermal cycle. If this were much greater than that which could be accommodated by tensile plus compressive elastic strains alone, it was felt that the repeated plastic working would eventually produce a crack. It was assumed that plastic flow would take place during the first few cycles in such a way that the specimen would shake down to purely elastic behavior if possible, limited only by the elastic limit of the specimen material at that instant. Hence the maximum strain amplitude which could be supported elastically was assumed to be the sum of the strains at the yield point in tension and in compression, measured at the temperatures existing when the maximum tension and compression occurred. This value was felt to be approximately 0.2 per cent. It was known to be dependent upon the temperatures reached at the point in question and upon the amount of plastic deformation produced by previous thermal cycles. Measurements made on the top surface of the plate during the 26th cycle with heater No. 1 revealed a maximum elastic-plus-plastic strain cycle of 0.22 per cent. Its location and also the distribution of strain across the specimen in the axial direction during the 26th cycle are shown in Fig. 9. The strains measured during the 51st cycle are also shown. The circumferential strains, shown in Fig. 10, were somewhat smaller. It should be emphasized that these

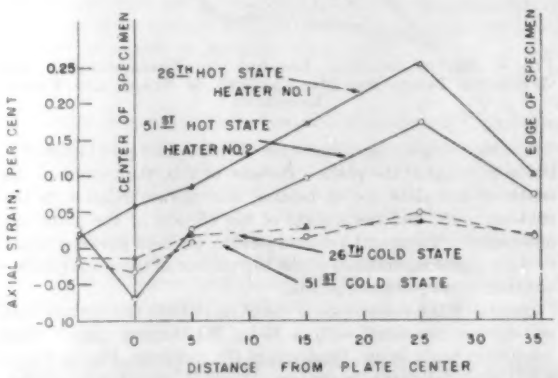

FIG. 9 DISTRIBUTION OF AXIAL STRAIN (ELASTIC-PLUS-PLASTIC) ALONG SPECIMEN CIRCUMFERENCE

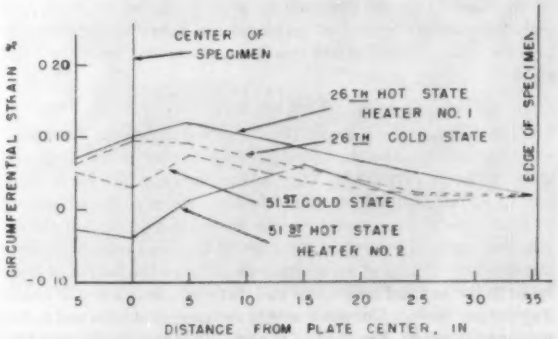

FIG. 10 DISTRIBUTION OF CIRCUMFERENTIAL STRAIN ALONG SPECIMEN AXIS

values are surface strains, the algebraic sum of direct strains and bending strains. It is possible that strain cycles of greater amplitude occurred on the underside of the specimen at the center, but it was not possible to make measurements there.

ANALYSIS OF MECHANICAL PROPERTIES

Tensile tests were made using twenty standard test specimens of 2 in. gage length. The locations of the test specimens, shown in Fig. 11, were chosen according to a factorial plan. Sixteen

specimens were machined from the plate and four specimens were machined from an additional piece of steel which had been subjected to the same mechanical treatment and heat-treatment as the test plate. The sixteen specimens constitute eight pairs of duplicates. The locations of the specimens were such that there were eight test bars which had welds and eight which had no welds. Also, eight test bars were parallel to the direction of roll while the remaining eight were perpendicular to the direction of roll. Again, eight test bars were located in the center of the plate in contrast to the eight located at the edge of the plate where the temperature during heating reached the blue-brittle range.

The results of the tensile test program are shown in Table 1. Examination of the ASTM specifications for A-201 Grade A firebox-quality steel showed that all test results lay within the specification limits with but one exception. Specimen No. 10 had a yield point of 27,000 psi compared to the minimum allowable yield point of 27,500 psi.

Since the mechanical properties fell within ASTM specifications, more careful comparisons were needed to determine whether thermal cycles had produced any significant effects. A statistical procedure called "analysis of variance" was used to compare the test results of Table 1. Some of the conclusions of this analysis are shown in Table 2. The numbers denote percentages (1, 5, and 10 per cent), while NS denotes "not significant." To explain the table, consider item 3. Here the sixteen specimens formed two equal groups and the analysis indicates whether the mechanical properties between specimens heated to 900 F differed significantly from the specimens heated to temperatures in the blue-brittle range. The 1 per cent denotes that there was less than one chance in 100 that the differences in mechanical properties were the result of accidental and experimental errors. This was a highly significant result and we can conclude that the location of a specimen had a definite effect upon the four mechanical properties shown. The table of means, Table 3, indicates which group had a property of greater magnitude.

The four "as-received" test bars showed no significant differences. They are combined as a control group having the means shown in Table 3. Furthermore, no duplicate bars were significantly different.

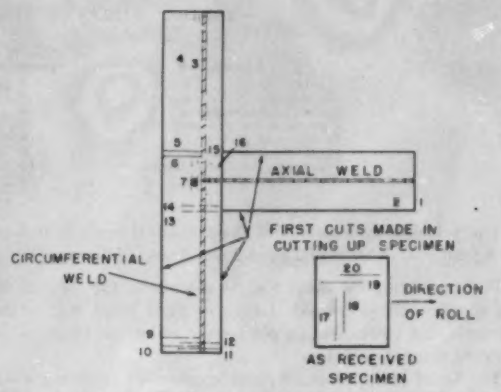

FIG. 11 LOCATION AND NUMBERING OF 8-IN. TENSILE-TEST BARS

TABLE 1 SUMMARY OF TENSILE TESTS MADE ON REGENERATOR-SHELL SPECIMENS

Spec. no.	Upper yield point, psi	Ultimate strength, psi	Elongation, per cent	Reduction in area, per cent	Designation
1	31840	56610	32.0	68.1	Pa B W
2	31200	56350	34.0	67.4	Pa B W
3	29400	60750	40.0	67.0	Pa B
4	31200	61000	40.0	64.7	Pa B
5	32600	59550	38.0	55.2	Pe C
6	34000	59500	36.0	56.0	Pe C
7	32000	60000	41.0	66.2	Pa C
8	35000	60000	41.0	64.0	Pa C
9	29000	58300	35.5	59.0	Pe B
10	27000	58100	35.5	60.0	Pe B
11	27660	56910	28.0	63.9	Pe B W
12	30500	57250	27.5	62.4	Pe B W
13	31000	59750	34.5	59.8	Pe C W
14	31200	59800	33.0	60.8	Pe C W
15	31350	58000	35.5	66.0	Pa C W
16	31750	57350	32.0	59.8	Pa C W
17	31600	59950	32.5	55.2	Pe
18	31940	59700	31.0	51.6	Pe
19	33230	58900	42.0	65.1	Pa
20	35500	59100	39.5	64.2	Pa

NOTE:
W = specimen contained weld.
B = specimen near edge of plate.
C = specimen near plate center.
Pa = specimen parallel to direction of roll.
Pe = specimen perpendicular to direction of roll.

TABLE 2 RESULTS OF VARIANCE ANALYSIS

		Upper yield point	Ultimate strength	Per cent elongation	Per cent reduction in area
1	Between welds and no welds	1	NS	5 to 10	1
2	Parallel and perpendicular to direction of roll	1	NS	1	NS
3	Center specimens and specimens in blue-brittle range	1	1	1	1
4	Interaction of (1) and (2)	NS	NS	5 to 10	1
5	Interaction of (1) and (3)	NS	1 to 5	NS	1 to 5
6	Interaction of (2) and (3)	1 to 5	1 to 5	NS	1
7	Interaction of (1), (2), and (3)	1 to 5	NS	1	NS
8	Between as-received specimens and specimens from test plate	1 to 5	1	NS	1

NOTE:
NS denotes "not significant."
Each figure represents per cent probability that difference in item in left column was due to inherent variability in test.

TABLE 3 TABLES OF MEANS FOR MECHANICAL PROPERTIES

Designation	No. of specimens	Upper yield point, psi	Ultimate strength, psi	Per cent elongation	Per cent reduction in area
Welds	8	30790	57500	32.4	63.5
No welds	8	31280	59650	38.4	61.5
Parallel to direction of roll	8	31720	59280	37.9	65.4
Perpendicular to direction of roll	8	30350	57870	32.9	59.6
In center of plate	8	32360	59060	36.4	60.9
In blue-brittle range	8	29700	58160	34.4	64.1
Specimens from test plate	16	31040	58570	35.4	62.5
As received specimens	4	33070	59410	36.9	59.0

The principal conclusions of the statistical analysis indicated by a joint examination of Tables 2 and 3 are as follows:

1 Considering the sixteen plate specimens, the thermal cycling significantly decreased the upper yield point and ultimate strength and increased the percentage reduction in area. The per cent elongation did not change.

2 Considering the eight plate specimens containing a weld, the thermal cycling led to a reduction in upper yield point and per cent elongation and an increase in per cent reduction of area.

3 The upper yield point and per cent elongation were greater for specimens in the direction of roll than for specimens perpendicular to the direction of roll.

4 Thermally cycling specimens to 900 F in contrast to heating to the blue-brittle range affected all four properties significantly. The higher temperature resulted in higher values of yield point, ultimate strength, and per cent elongation, and a lower value for per cent reduction in area.

5 The double and triple interactions are occasionally significant. They measure the significance of one comparison between two factors at several different levels of comparison of the remaining factors. For example, Table 2 indicates that the effect of direction of roll did not significantly influence the comparison between welded and not-welded specimens.

It is to be emphasized that while variance analysis indicates some statistically significant differences, the tensile test data do not exhibit any large changes in properties. There is no indication that the plate was likely to develop or propagate cracks.

The two principal welds in the plate, Fig. 1, were radiographed before and after the completion of thermal cycling. The radiographs after thermal cycling showed no cracks or inclusions. No other evidence of unsound welds was found.

The microstructures of three of the tensile specimens, Fig. 11, Nos. 3, 7 and 18, were examined. One specimen was taken from the blue-brittle zone at the edge of the plate. A second was taken from the plate center; the third was not subjected to any thermal cycling. The metallographic study did not reveal any significant differences.

Model of Shakedown

Since the concept of shakedown states has appeared rather recently as an element of plastic-limit design, it seems desirable to explain the term by means of a mechanical model. The arrangement to be described is about the simplest possible but the idea of shakedown is readily extended to much more complicated structures. In fact, general theorems concerning the occurrence of shakedown in trusses and space frames have been developed within the past few years. The shakedown state refers to the state of residual stress possessed by a statically indeterminate structure after being loaded until the weakest sections have deformed plastically. The existence of the residual stresses may permit a repetition of the same load without again exceeding the yield-point stress of the weakest member, hence without further plastic deformation of any part.

The elastic structure of Fig. 12 consists of a cylindrical bar, 2, surrounded by a cylindrical tube, 1. Both bodies are attached to a support and a tensile load P is applied to the system. If the force carried by the tube is P_1 and the force carried by the bar is P_2, equilibrium requires that $P_1 + P_2 = P$. If the bar and tube have the same area and modulus of elasticity, but the bar has a lower yield-point stress in both tension and compression than the tube, increasing the load P sufficiently will produce some plastic flow in the bar while the stress in the tube remains elastic. If

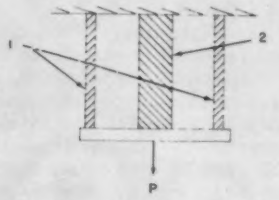

Fig. 12 Statically Indeterminate Structure to Illustrate Shakedown State

the external load P is now gradually removed, the structure will possess some residual strain energy because of the restraint between the elastic tube, in which some tensile stress still exists, and the permanently stretched bar, which now carries a compressive stress. A reapplication of the tensile load P will now be supported elastically by the structure. This is a shakedown state characterized by alternating or fluctuating loads which cause no plastic flow except during the first loading.

Conclusions

1 The test procedure applied to a specimen of the regenerator shell indicated that the production of hot spots with a maximum temperature of about 900 F and thermal cycling of the order of 50 cycles resulted in a shakedown state. There was no evidence of progressive growth of the bulge. Further cycles beyond the first few hot states did not store additional energy in the structure.

2 If shakedown exists, several thousand thermal cycles should be carried by the plate without failure occurring. The same conclusion could be applied to a regenerator (and other vessels with hot spots) provided the temperatures do not vary markedly from the test conditions.

The present work confirmed the results of other investigators who generally heated to higher temperatures and used more rapid heating and cooling rates. Even under these more severe conditions, several investigators found no evidence of crack initiation or propagation for about 100 test cycles. It is unwise to extrapolate the conclusions of these investigators to a number of cycles far in excess of 100. They did not measure deformations and consequently were not able to determine the existence or absence of shakedown.

3 Tests of the mechanical properties of the plate after thermal cycling showed results which fell within the ASTM specification limits with but one minor exception. A statistical analysis of variance showed significant differences in yield strength, ultimate strength, per cent elongation, and reduction of area before and after the temperature cycles. However, these differences were small. It should be kept in mind that mechanical properties

of steel (and other metals) have not been analyzed statistically to the point where engineers can correlate the significance of small differences with the design and service behavior of vessels.

4 Where hot spots and plastic flow occur on refinery vessels, and we can be reasonably certain that failure can occur only with increasing plastic flow, it is recommended that a test program be arranged and instruments constructed which will map the flow at critical points. Failure to find increased deformations would give reasonable assurance that the structure is in a shakedown state. Operators should recognize that such a state is not hazardous since the thermal expansion and contraction is then accommodated by purely elastic deformation, which should not cause cracking unless repeated thousands of times.

The instrumentation for such a program is not necessarily elaborate and expensive. It is more important to provide a test program promptly when the hot spots have been discovered.

Acknowledgments

The authors wish to acknowledge the guidance of Mr. G. W. Watts, Director of Engineering and Engineering Research, and that of Dr. W. M. Dudley, Associate Director, Engineering Research, in the conduct of this project, and to express their gratitude to the Standard Oil Company of Indiana for permission to publish the results.

Discussion

Helmut Thielsch.[6] The authors are to be complimented on the preparation of this very interesting and informative paper. Although it is fortunate that thermal-fatigue failures occur with relative infrequency, they do occur and, at times, are very costly in life and property. Studies similar to this paper are essential to the better understanding and evaluation of conditions which may, or may not, lead to service failures by thermal fatigue or shock.

Unfortunately, it is extremely difficult to correlate laboratory test results to actual service conditions. Often such correlations are impossible since at elevated temperatures gradual changes tend to occur in the metallurgy of the materials involved in the service application which are not apparent from the simulated laboratory studies usually conducted over relatively short periods of time.

The conclusions of this paper, therefore, should be interpreted with considerable caution. As pointed out by the authors themselves, it is even more unwise to extrapolate such data.

It must be recognized also that service conditions may be more critical than those employed in the tests by the authors. Examples are the thermal fatigue or shock incurred by the sudden heating produced by flowing hot oil or superheated steam through piping.

Most actual or "near" service failures associated with thermal fatigue occur in materials in which metallurgical changes have reduced significantly the ductility and toughness; i.e., have resulted in a gradual embrittlement of the affected area.

Typical conditions well known to power-plant engineers have occurred in carbon and carbon-molybdenum steel piping in service at temperatures exceeding 800 F where graphitization has occurred in the heat-affected zones. The resulting embrittlement has set up a weakened zone particularly susceptible to cracking and gradual crack propagation by thermal fatigue. An example of a crack which has been propagated gradually through a graphitized zone is shown in Fig. 13.

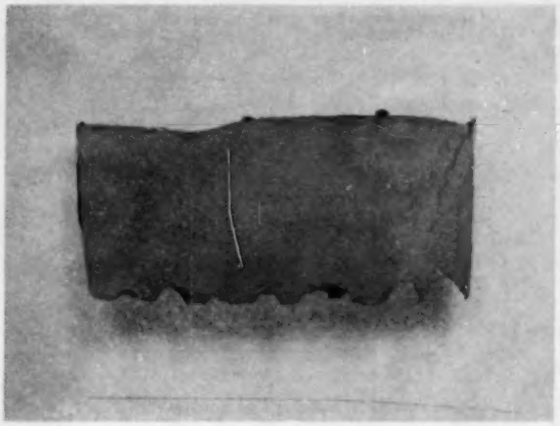

Fig. 13 Crack Propagation Through Graphitized Zone

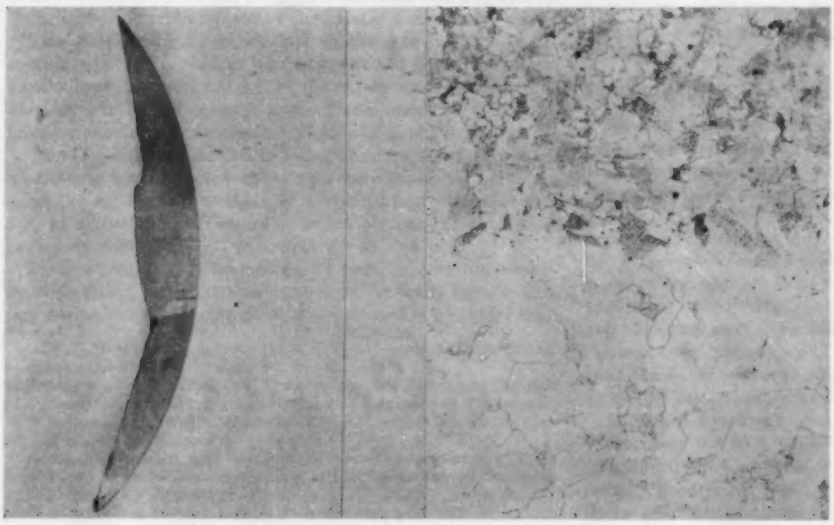

Fig. 14 Crack Through Carbon-Steel Weld Area Adjacent to Carbon-Molybdenum-Steel Base Metal and Microstructure Showing Decarburization

[6] Metallurgical Engineer, Grinnell Company, Providence, R. I. Assoc. Mem. ASME.

Another fairly common condition where metallurgical changes at elevated temperatures reduce significantly the ductility and toughness occurs in dissimilar-metal joints. Even joints between carbon and carbon-molybdenum steel may suffer seriously, though the differences in chemical compositions may seem negligible. An example of this is shown in Fig. 14 where a crack traversed a carbon-steel weld area adjacent to carbon-molybdenum-steel base metal. The microstructure indicates the carbon-steel weld metal to be decarburized along the bond (fusion zone).

Authors' Closure

The authors wish to thank Mr. Thielsch for his discussion, which is a valuable addition to the paper. We concur heartily in his observations on the need for caution in the application of these results to service problems. Our findings should be regarded as a piece of evidence which the reader must combine with other data from his own or other people's experience to form a basis for a decision on his current problem.

We do believe that thermal fatigue is a mode of failure which the engineer must consider in many refinery situations. The essential condition, mechanically speaking, is an elastic-plus-plastic strain cycle of sufficient magnitude to produce failure within the service life of the part. Stress raisers or, if you like, strain-concentrating features, are, of course, very important factors; and certainly, metallurgical changes which reduce ductility or toughness are also present in many problems of this kind.

The authors feel that a valuable contribution to the problem of thermal fatigue, one which reduces it to quantitative terms, is that of L. F. Coffin, Jr.,[7] whose published experimental results have thus far dealt with small test pieces of stainless-steel type 347. In contrast with his work, experiments such as ours are needed when either: (*a*) it is not possible to compute the amplitude of the strain cycle, or (*b*) a large uncertainty exists about the severity of the stress raisers present.

[7] "Apparatus for Study of Effects of Cyclic Thermal Stresses on Ductile Metals," by L. F. Coffin, Jr., and R. P. Wesley, Trans. ASME, vol. 76, 1954, pp. 923–930.

Also, "A Study of the Effects of Cyclic Thermal Stresses on a Ductile Metal," by L. F. Coffin, Jr., Trans. ASME, vol. 76, 1954, pp. 931–950.

Some Cases of Stress Due to Temperature Gradient

By D. J. BERGMAN,[1] DES PLAINES, ILL.

In dealing with this problem, the cause of stress must be considered, and whether the stress remains constant, decreases, or increases as yield or creep occurs as a result of high stress. A qualitative analysis of the stress due to a maintained temperature differential in a flat bar is given for both free and restrained bar, and a comparison with the cases of a flat plate and a thick pipe. Practical cases are reviewed, including a pipe heated from the inside, heater tubes with internal pressure and high heat inputs, stresses set up by localized heating when welding a corrosion liner in a vessel, differential expansion due to noncompatible welds, vapor barriers through an insulation wall, and the temperature-transition skirt for hot vessels.

Introduction

THE subject of stresses in piping, vessels, or structures, caused by temperature gradient has been less thoroughly covered in the interpretive or application field than in the mathematical and applied mechanics fields, and it is hoped that this paper may assist in filling a gap and also in pointing out areas where more accurate analyses are needed. Answers both by recent graduates and experienced engineers run better than four out of five wrong on the question, "Where would a mechanic apply heat in order to straighten a bent shaft?" Perhaps after following through the cases to be cited, the reader can reverse that ratio.

Three different loading systems may be set up, with regard to the effects of yield in the case of high stress and short time, or creep in the case of long exposure to lower stress at high temperature. In Fig. 1 these are illustrated by simple mechanical cases.

In case *a* yield of the simple beam caused by a load which produces stress above the elastic limit results in no change in moment. In case *b* too much cold spring of a bent pipe between fixed supports causes stress above the elastic limit and consequent yield. Hence the natural length of the pipe is increased and the moment is decreased from that figured on the basis of a completely elastic system because the force required to elongate the pipe is decreased. In case *c* yield in the beam stressed above the elastic limit allows the load to deflect outwardly and increases the moment arm of the constant load. Hence moment and stress increase, resulting in accelerated yield, and probable failure.

These loading systems should be kept in mind constantly when considering cases of differential-temperature stress, since in many cases the satisfactory working of a structure at economic cost may be dependent upon case *b*. Fortunately many cases of stress caused by differential temperature are of this nature.

Furthermore, it is important not to consider only the steady-state condition, because transient stresses caused by temperature lags during start-up or shutdown of a system may be higher than those of the steady state, and cause failure. Surely in the petroleum industry most people are aware that piping failures generally occur during the adjustments due to starting or shutting down a plant.

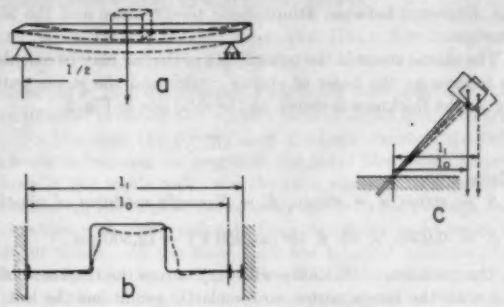

Fig. 1 Effect of Yield on Stress Systems

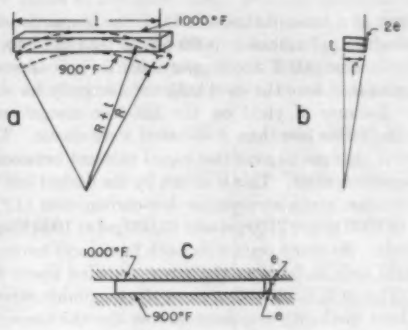

Fig. 2 Expansion of Free and Restrained Bar

Flat Bar, Plate, and Pipe, With Differential Temperature

An elementary analysis of an application of differential temperatures is presented in Fig. 2. If a straight flat bar of low-carbon steel be maintained without restraint with one surface at 900 and the other at 1000 F, we would expect to have it bow as shown in Fig. 2(*a*). We also would expect to have a uniform gradient of temperature from face to face, so that the mid-point would be at 950 F and other points would have temperatures directly proportional to the distance from each of the surfaces. For simplification let us consider that the temperatures are brought up slowly and uniformly so that permanent deformation does not occur because of temperature shock. Further, let us disregard variations from the linear temperature distribution assumed, which may be caused by loss of heat from sides or ends.

At this temperature level the coefficient of expansion is approximately 0.000010 in/in/deg F so the difference in natural length of the two surfaces of the bar is 0.000010 × 100 = 0.0010 in/in. The free bar bows as a result until this differential length is the difference between the arc length of the inner and outer

[1] Chief Engineer, Engineering and Development Department, Universal Oil Products Company. Mem. ASME.

Contributed by the Materials Committee of the Petroleum Division and presented at the Petroleum-Mechanical Engineering Conference, New Orleans, La., September 25–28, 1955, of The American Society of Mechanical Engineers.

Note: Statements and opinions advanced in papers are to be understood as individual expressions of their authors and not those of the Society. Manuscript received at ASME Headquarters, July 7, 1955. Paper No. 55—PET-12.

faces, from a center with radii of R and $R + t$ (see Appendix and Fig. 2*b*). With a free bar there is little or no stress due to this bowing, as each differential layer maintains its natural length at the temperature imposed.

However, consider the case if restraint is placed on the bar to maintain the two faces flat. Fig. 2(*c*) shows the bar held straight with the hot face now compressed by one half of the differential expansion or 0.0005 in/in. and the cooler face extended by the same amount. Of course the whole bar has expanded, owing to the difference between atmospheric temperature and the 950 F average.

The elastic stress in the outer fibers of the bar may be calculated as follows on the basis of elastic strain, and the stress pattern across the thickness is shown as the solid line in Fig. 3

$$S = eE \quad \ldots\ldots [1]$$

where

S = stress, e = strain, E = Young's modulus of elasticity

$$S = 0.0005 \times 25 \times 10^6 \text{ (at 950 F)} = 12{,}500 \text{ psi}$$

The modulus of elasticity will vary across the thickness of the bar with the temperature, so for elastic conditions the hot face might be expected to be compressed slightly more than the cooler face was elongated, changing the stress pattern across the thickness.

However, at a temperature of 1000 F the proportional limit of carbon steel is approximately 9000 psi, so that yield occurs. On the cooler face at 900 F the proportional limit is approximately 12,500 psi so that here the steel behaves elastically for short-time loading. Because of yield on the hot-face elongation will be greater, and stress less than if the steel were elastic. The stress distribution changes to maintain equal moment between tension and compression sides. This is shown by the dashed line in Fig. 3.

Furthermore, creep stresses for low-carbon steel (1)[2] for 0.10 per cent in 1000 hr are 2700 psi and 13,000 psi at 1000 F and 900 F, respectively. So creep occurs on both faces, and inward toward the neutral axis as long as the stress remains above the creep values. This still further decreases the maximum stresses, and makes them distinctly nonlinear across the thickness. This is illustrated in the short-dashed line in Fig. 3.

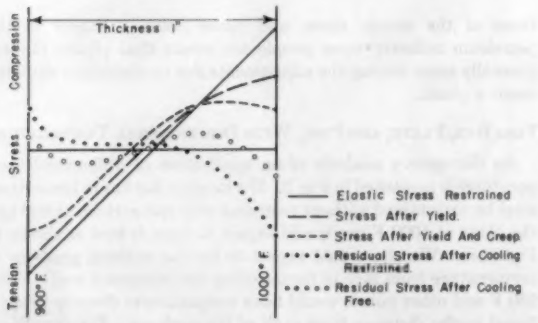

FIG. 3 STRESS DUE TO DIFFERENTIAL TEMPERATURE

The deformation which has occurred is indicated by the departure of the stress curve across the thickness of the bar from the prolongation of the straight portion of the curve for the elastically stressed portion of the thickness.

Now consider what happens when the bar is cooled back down to atmospheric temperature after, say, 4000 hr under these temperature conditions. The top fiber has shortened due to both yield and creep, and the bottom fiber has lengthened due to creep, and in this process the stresses near the two surfaces have diminished.

When brought back to atmospheric temperature the top fiber wants to be shorter than the shape of the bar will permit by the amount of yield and creep which has occurred, and likewise the bottom section wants to be longer; so a reversal of stress occurs, the top being under tension and the bottom under compression. The dotted line in Fig. 3 shows the residual-stress pattern when the bar is maintained under restraint during and after cooling.

If the restraint holding the bar flat be removed after cooling there will be a bow in the opposite direction, owing to the fact that the hot face has been upset and the cooler face permanently stretched. The stress pattern then is shown by the circled curve in Fig. 3. Part of the permanent deformation which has occurred is taken up by bow and the rest by residual stress which is much smaller than under the restrained conditions.

This is an illustration of the complications which are involved in trying to arrive at actual values of stress under simple conditions of differential temperature. Confirming in a general way this qualitative analysis, Clark (2) gives data on creep tests of killed carbon steel by the Barr and Bardgett method in which a specimen stressed to an initial value of 11,000 psi at 1000 F dropped in 24 hr to a value of 4000 psi, while a similar specimen stressed to 11,000 psi at 900 F dropped to 8000 psi in the same time.

In most cases, because of the greater strength of the cold metal, the residual stress will be well below the cold yield point; so although there is a residual stress, no ill effects occur. When the material is reheated the residual stress starts decreasing, passes through zero, and then reversing, increases up to the working conditions again.

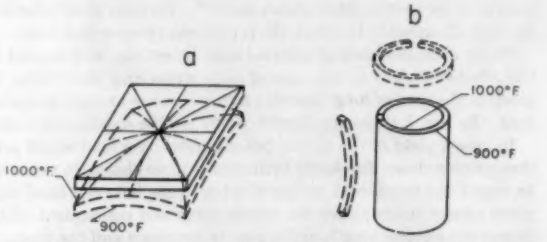

FIG. 4 EXPANSION OF FLAT PLATE AND THICK PIPE DUE TO TEMPERATURE GRADIENT

Taking a slightly more complicated case of a flat plate, Fig. 4(*a*) shows the effect of temperature differential, in that the plate attempts to assume a spherical shape. As long as the differential is small it can do this with little or no stress, but for large temperature differentials the necessity of bending in two directions introduces stresses even though the plate be free. If the plate be restrained at the edges, or over all, stresses are set up which may reach values high enough to cause yield or creep.

Formulas for calculation of the stress in a round or square plate held at the edges are given by Goodier (3), but in application of them, if the stresses calculated are above yield or creep values at the temperatures given the elastic conditions on which they are derived no longer apply.

HEAT TRANSFER FROM INSIDE A PIPE

Taking one step further, consider the thick-walled pipe in Fig. 4(*b*) subjected to temperature differential due to flow of heat from inside to outside. Because of the inherently stiff shape of a cylinder it is impossible for the metal to move and relieve the stresses set up by the temperature gradient as happens with the free bar.

[2] Numbers in parentheses refer to the Bibliography at the end of the paper.

A longitudinal strip cut out of the pipe would bow like the bar discussed earlier. Hoop stresses prevent this. A circular element slit at one point would open up because of the increase in natural length of the inner fiber compared to the outer one, but this cannot occur in the pipe either. All the pipe can do is take the stresses set up, with no opportunity for relief except through yield and creep.

The stresses in such a case can be material, as illustrated by a carbon-molybdenum spool piece installed on one of the wartime catalytic-cracking units in place of a second slide valve in the regenerated catalyst standpipe. This spool, made of $1^1/_4$-in-thick carbon-molybdenum steel and flanged on each end, was cut through the middle, installed in the line, and welded to make a neat fit in the piping. Since it was so short that bolt heads interfered, no insulation was provided around it.

After some months of operation it had bowed outwardly above and below the weld line. In seeking for reasons, the obvious ones of high temperatures, internal pressure, and end load due to an expansion joint seemed to be possible causes. It was expected that more uniform operation with no runaway temperatures would prevent any further deformation. But deformation went on.

The possible reasons just outlined were then investigated and the stress due to internal pressure and end load were each evaluated to be less than 200 psi. Such a stress is too low to cause the deformation found. However, Timoshenko (4) gave a formula for differential temperature stress at inner and outer fiber as follows

$$S = \frac{Ea(t_1 - t_2)}{2(1 - u)} \qquad [2]$$

where S = stress, E = Young's modulus, a = coefficient of expansion (0.00001 at 950 F), $t_1 - t_2$ = radial temperature gradient across shell (assumed 100 deg F), and u = Poisson's ratio = 0.3. Substituting in this formula for the values assumed, the stress appears to be

$$S = \frac{25 \times 10^6 \times 0.000010 \times 100}{2(1 - 0.3)} = 17{,}800 \text{ psi}$$

Perhaps it might be questioned whether 100 deg F is a reasonable temperature drop across the $1^1/_4$-in. thickness of the pipe. Curves for loss of heat from bare pipe at 900 F in still air indicate values of the order of 7000 Btu/hr/sq ft. Flux values of 30,000 Btu/hr/sq ft are given in Kern (5) for water. So a figure of 20,000–25,000 Btu/hr/sq ft for a rain-washed pipe appears to be reasonable. At a temperature of 950 deg F the conductivity of steel is approximately 275 Btu/hr/sq ft/in/deg F. For $1^1/_4$ in. thickness the conductivity is 275/1.25 = 220 Btu/hr/sq ft/deg F. Then dividing the heat flux by the conductivity to get the temperature drop gives a value of the order of 100 deg F.

The stress found in the foregoing is based upon elastic conditions which naturally do not hold at this temperature. Variations in temperature plus complete cooling at shutdowns resulted in so much permanent deformation that this detail acquired the nickname—"The Pregnant Spool Piece"—and had to be replaced.

Another similarly located spool piece in a different catalytic-cracking unit also started to bulge, causing concern over possible failure. It was recommended that the piece be insulated, and also that the outside temperature of the pipe wall be measured. This spool piece was located immediately over the slide valve controlling flow of fluid catalyst at a temperature of 1100 F. Tempilstik measurements showed variations at a given point of as much as 150 deg F in $^1/_2$ hr and also variations of as much as 400 deg F at a given time between quadrant points.

At this time the spool piece had a diameter of $18^1/_{16}$ in. at the flanges, and $18^7/_{16}$ and $18^{11}/_{16}$ in. in the middle. The data indicated temperature gradients of at least 28 deg per in. circumferentially, as well as high radial gradients. However, it does not seem that there would be much more than 100 deg F actual radial gradient through the pipe wall. It is probable that the large differences around the circumference were due to catalyst settling and packing along the inside of the pipe wall above the slide-valve deck. Occasional variations in the slumping of this catalyst would result in the changes with time. Lining the inside of the spool piece with 1 in. of high-temperature concrete reduced the heat transfer enough to stop further growth.

Tubes With Internal Pressure and Heat Applied From Outside

Luster (6) in 1930 developed the optimum thickness for a tube under internal pressure and subject to heat input from the outside. In this case the temperature gradient through the tube wall tends to increase the length of the outer fibers with respect to those of the inside wall. So the tube expands to something approximating the circumference comparable to the average wall temperature with compression in the outer fibers and tension in the inner fibers. At the same time the internal pressure puts tension completely across the thickness of the tube although in the case of thick tubes this tension stress is higher at the inside than the outside fiber. Combining these two stresses as shown in Fig. 5 shows a high tension at the inner face and a comparatively low stress at the outer face. For the optimum thickness of tube the stress at the outer face would be zero. In the example given in the paper an 18-8 tube of 5-in-OD by $^3/_8$-in-thick wall is shown as having an inside hoop stress of approximately 12,200 psi with a heat input of 10,000 Btu/sq ft/hr based on outside

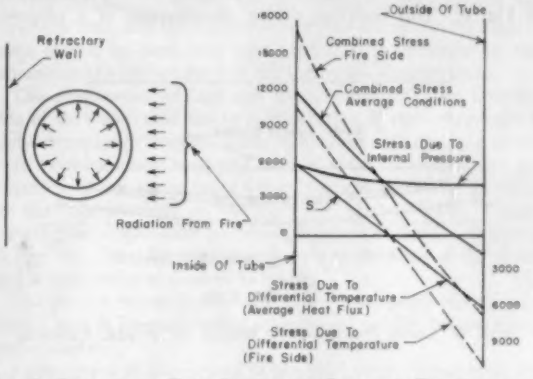

Fig. 5 Stresses in Tube Subject to Internal Pressure and High Heat Transfer

tube surface. It should be recognized, particularly in the case of radiant wall tubes, that the localized heat-transfer rate on the fire side of the tube will be considerably above the average heat input so that the calculation of the differential-temperature stresses on the fire side would result in values about 80 per cent above those given. Furthermore, average hourly heat-input rates of up to 15,000 Btu/sq ft of outside surface may be found in the petroleum industry and even much above that in the power field.

Application of the formulas in Luster's paper to a number of existing thermal-cracking units with carbon-steel tubes resulted in calculated stress so much above the yield point that failure might well have been expected. Still, these heaters had in many cases operated satisfactorily for years. Apparently the calculated high stresses were something that did not occur in practice since mother nature took care of this situation by allowing the

metal to yield and creep on the inside while the tube was hot, resulting in a reversed stress of compression on the inside and tension on the outside wall of the tube when it was cold.

In order to check the validity of this theory a 3¼-in-OD × 5/16-in. tube was slit on the roof side. The saw kerf was 0.053 in. and after cutting the slit opened to 0.081 in. Although the heat rates are not available there seems to be little question but that the inside of the tube was in compression and the outside in tension due to relief of the high tension stress at the inner wall of the tube because of yield and creep under operating conditions.

In the Appendix is derived the amount of spring which might be expected on slitting a tube in this way on the assumption that the heat input had occurred uniformly from all directions and that the residual-stress pattern across the tube wall when cold was a straight-line function. Neither of these assumptions is accurate, but using the formula as an approximation, the extreme fiber stress in the tube wall was found to be 8350 psi.

The adjustment which occurs in a tube wall subject to high heat-input densities at high temperature follows along the idea expressed in Fig. 1(*b*); namely, that stress relief or relaxation of the tube due to yield or creep reduces the stress in the steel from that calculated for elastic conditions to a value approximating that due only to internal pressure. Accordingly, it appears entirely safe, based upon years of experience, to design tube-wall thickness for an allowable creep stress caused by internal pressure only. Perhaps this should be limited to relatively thin-wall tubes.

Bowing of Bar Due to Localized Heating

A good example of the effects of localized heating is illustrated in Fig. 6. This occurred during consideration of a proposed

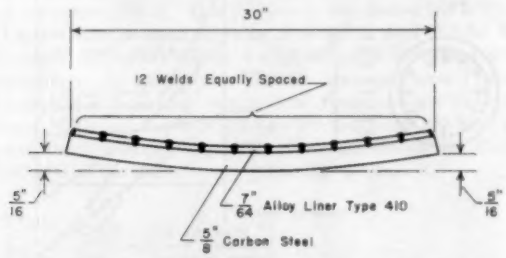

Fig. 6 Lined Plate With Welds on 2½-In. Centers

method of lining a pressure vessel with a 7/64-in. layer of 12-chrome steel. The proposed method consisted of welding vessel rounds for an 8-ft-diam vessel 10 ft long, fitting sheets of liner as closely to the inside wall as possible, and then with the vessel course mounted on dollies, rotating it slowly while a continuous-feed automatic welding head burned through the 12-chrome liner into the steel vessel wall. Several different types of rods, including 25-20, 25-12, and 18-8, several different rod diameters, and variations in welding voltage and current were tried to determine the best procedure to obtain a satisfactory weld bond between liner and vessel steel. This was done on a flat slab of 5/8-in. steel at the shop.

After completion of these tests a section 6 in. wide × 30 in. long and containing about 12 welds spaced evenly along the 30-in. length was sent into the office for examination. It was observed that this strip of steel was bowed to the extent that the two ends rose 5/16 in. and the question of residual stresses resulting from the welding operation came up. It was calculated that, were the steel bar to be forced into a flattened position, stresses of approximately 30,000 psi would be the result, and since this was assumed to be similar to the case where the vessel course already welded up was unable to move to relieve itself these stresses would be locked in the steel unless the vessel was stress-relieved.

Since many vessels have been protected successfully against internal corrosion in the field by hand-welding strips of 12-chrome steel at 2½ to 4-in. intervals without stress-relieving, perhaps we may give secondary consideration to the earlier problem.

If the liner were applied to a flat sheet of steel constrained to remain flat the yield and creep which would occur, stretching each of the welds as it cooled, would result in a greater natural length on the lined side so that although the sheet would indeed try to bow toward the welds when cold the amount of permanent deformation during plastic condition would be greater. So the bow would be reduced and the calculated average residual stresses due to welding would have been correspondingly reduced. The fact that the welding had been applied to the sheet in a free position allowed it to adjust itself on cooling with a minimum of yield giving a greater bow and indicating higher stresses than actually would be the case in the constrained vessel wall.

The Appendix shows a method of calculating the apparent stresses due to flattening a free circular arc of steel.

Junction of Noncompatible Metals

An allied problem dealing not with stresses caused by differential temperatures but with differential expansion between dissimilar metals is the case of a 5-chrome pipe welded with 25-20 chrome-nickel rod and subject to an operating temperature of 1000 F. The expansion of the 5-chrome between 70 and 1000 F is approximately 0.0067 in. per in. The expansion of the 25-20 weld deposit over the same temperature range is approximately 0.0083 in. per in. The 25-20 weld deposit has a lower expansion rate than either 18-8 or 25-12 which perhaps is one reason why it has become popular as a field welding material for low-chrome alloys. The modulus of elasticity of 25-20 at 1000 F is about 22.5×10^6 while that of 5-chrome is approximately 25×10^6. Disregarding this difference which would tend to throw a somewhat greater amount of the deformation in the 25-20 alloy deposit, we may take an average value of 23.7×10^6. Assuming what is highly improbable, that the two dissimilar metals were stress-relieved to have essentially zero stress at 535 F and that the elongation of the 5-chrome and shortening of the 25-20 weld material were equal, the elongation and compression of each metal would amount to one fourth the difference between the two expansion rates given previously, or 0.00040 in. per in. The stress on an elastic basis would be approximately $0.00040 \times 23.7 \times 10^6 = 9480$ psi.

Five-chrome steel at 1000 F has approximately 7000 psi creep strength for 1 per cent in 100,000 hr. Accordingly, some creep may be expected. Although this joining of dissimilar metals has not been looked on with favor by metallurgists, its use, particularly in the petroleum industry, has grown over past years as a field-welding procedure for piping using preheat and then letting the weld cool slowly instead of using compatible rod with the requirement of careful stress relieving. Some have encountered microscopic cracking in or adjacent to the weld but the practice has been expanded and the power industry is also using it, as indicated by papers presented by Lien, Eberle, and Wylie, and by Weisberg and Soldan at the Annual Meeting of the ASME in 1953 (7, 8). Cycling tests resulted in surface notches and subsurface cracks in the fusion zone. Removal of the cracks which showed up and continued operation under test conditions indicated that the welds would be safe for operation in spite of the apparent high stress level caused by the differential expan-

sion. It is probable that the thickness of the materials thus welded together plays a very important part in the stress pattern. While the procedure works very satisfactorily for thin pipe, it should be considered questionable for thicknesses of over 1 in., and probably also for temperatures over 1100 F.

A quantitative study of the residual stresses in a composite bar of carbon steel clad with a heavy corrosion-resistant lining of type 347 alloy is given in the report of the American Petroleum Institute task force assigned to study the requirements for welded pressure vessels constructed of internally clad plate. This report is dated May 10, 1955. The data were obtained by cutting a slot successively deeper in the bar and noting the change in bow. This study shows a complicated stress pattern because of the use of two dissimilar materials fastened rigidly together.

Supports for Hot Vessels

As an important example, consider the case of a coke chamber and its supports. These vessels have been built in sizes up to 17 ft diam and up to 80 ft tangent lengths. They are subjected to unusually severe temperature shocks by their operating conditions. They may go through a cycle of operation and cleanout every 24 hr. During this time the vessel is brought up to a temperature of approximately 850 F by vapor and liquid from the coking heater. When the coke level gets up to about 75 or 80 per cent of the vessel volume after perhaps 12 or 14 hr of operation, the flow from the heater is switched to an empty vessel, and the connecting lines are blanked off for cleanout. Pressure is reduced to a sump, and steam is introduced at the bottom of the vessel in order to start cooling. After steaming for a period of perhaps 1 hr, water is pumped into the bottom of the chamber. The hot coke turns this into steam often resulting in high local pressures because of the volume of steam generated, and resulting in a quick drop in temperature of the vessel walls. This temperature drop proceeds up the chamber as the coke becomes cooled down to water temperature. Hence it is possible for the bottom of the vessel to be at a temperature of 100 F while the top is in the order of 700 F. As the vessel wall cools it also tries to contract. The coke, formed when the vessel is hot, does not have nearly as high a temperature coefficient of expansion, and so the cooling operations may set up apparent high internal pressures approximating the ultimate compression or crushing strength of the coke. Following the cooling the vessel is unheaded and the coke is removed, either by mechanical drilling or hydraulic jets.

It is common experience for these vessels to swell in service and cases are known where a 10-ft-diam $1^1/_2$-in-thick vessel swelled to 10 ft 6-in diam in the course of about 8 years of operation. This swelling was mainly between the circumferential welds. It appears that the weld metal, having a cast structure, was not subject to creep or yield as much as the rolled plate. Application of a 2-in. gunnited concrete lining to the inside of the shell, even though it had a low insulating value compared to the external insulation, greatly suppressed this swelling action, presumably by cushioning the temperature shocks on water cooling. Thin-wall vessels will show less tendency to bulge than thick ones, because of lower temperature difference across the wall.

While the vessel wall is thus being mistreated by the frequent and relatively fast temperature changes, another point of high stress concentration may be set up at the vessel support. Many hot vessels have been supported on lugs welded to the vessel wall, which in turn rest on a concrete or steel beam, as shown in Fig. 7(*a*). Because the weight of the vessel acts offset from the point of support, a moment is produced which must be resisted by tension at the lower, and compression at the upper, attachment of the lug to the vessel wall. Frequently it is recognized that these support stresses are in addition to the design basis of internal pressure, and compression and tension rings are added at the top and bottom of the lug. When these rings are welded flat to the shell and insulated there is not a great temperature difference, but sometimes a designer will endeavor to gain an advantage in section modulus and strength by installing the reinforcing rings edgewise extending 4 or 5 in. out from the vessel and perhaps even outside of the insulation. Then differential-temperature problems are liable to appear.

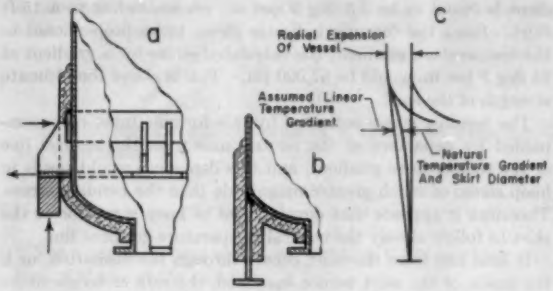

Fig. 7 Hot-Vessel Supports

(*a*) Lug supports; (*b*) temperature transition skirt support; (*c*) linear and actual temperature gradient for skirt support.

An additional load thrown into the vessel wall that is frequently overlooked is the fact that the lugs, even though placed on sliding bearing supports, still require a considerable force to start moving. And move they must, because a 10-ft-diam vessel heated from 100 to 900 F will expand approximately $^3/_4$ in. In expanding, a push results at the bottom and a pull at the top of the lug attachment to the vessel. When cooling occurs, the reverse is true, and the compression at the top of the lug attachment caused by dead load plus wind load is increased by the moment of the friction force of the lug on the support plate.

The combination of high and variable loads thrown into the side of the vessel shell led to consideration of skirt supports for high-temperature vessels. Early difficulties with cracking at the weld between vessel head and skirt of some coke chambers appeared to be due to the use of a short thick skirt, further stiffened by the lugs provided on the skirt for anchor bolts. Consequently the temperature transition skirt was evolved. As shown in Fig. 7(*b*), the skirt support is welded to the head of the vessel and is insulated over most of its length.

The skirt is normally made of $^3/_8$ or $^1/_2$-in. plate and may be from 3 to 5 ft long depending upon vessel weight, temperature, and diameter.

At the point of attachment of the skirt to the vessel both are at the same temperature, hence have the same natural diameter. At the support, the support plate and lower part of the skirt are losing heat to the atmosphere, and since this heat must travel the long narrow path through the skirt there is a considerable temperature drop and the bottom of the skirt is close to the temperature of the support; hence no expansion need be provided for. At intermediate points the skirt diameter varies with the skirt temperature with practically no stress with the exception of the zone near the vessel head weld. Here internal pressure in the vessel causes expansion and hoop stress which is transmitted also to the skirt.

It may be theorized that the top of the skirt, being fixed at the head, must remain parallel to the vessel wall, and then change in direction as indicated by the temperature gradient. Wolosewick (9) analyzed this condition and set up a formula for the stress due to bending. He gives an example for a skirt 130 in. diam, and $^1/_2$-in wall thickness with a vessel temperature of 700 F. The calculated bending stress is given as 9350 psi. Skirt length is not given but solving back his equations the temperature gra-

dient is found to be 3.5 deg F per in., corresponding to a 15-ft skirt. Since the formula indicates stress to be proportional to the temperature gradient, the calculated stress for a gradient of 25 deg F per in. would be 67,000 psi. This is above the ultimate strength of the steel.

The bending stress indicated by this formula must be accompanied by departure of the neutral axis from the natural line of the temperature gradient, and this departure would result in hoop stress of much greater magnitude than the bending stress. Therefore it appears that development of hoop stress forces the skirt to follow closely the natural temperature-gradient line.

If heat loss from the skirt occurs through the insulation, or if the inside of the skirt be not insulated, the rate of temperature drop per inch of skirt length will be greatest near the head and least near the support, resulting in a curve for the natural diameter of the skirt along its axial length. This will still further increase calculated stresses based on an end condition parallel to the vessel wall.

Against this, pressure and loss of heat from the end of the vessel wall to the skirt tend to incline the end of the wall inward in the direction of the temperature-gradient line, decreasing stress.

Several hundred vessels, ranging up to reactors of catalytic-cracking units 27 ft diam, have been supported by this means with no trouble where consideration was given to provision of a temperature transition skirt with gradients of the order of 15 to 25 deg F per in. Therefore it appears that practice should outweigh calculations indicating stresses far above the yield point, since these calculations are based on elastic properties and lose track of the natural adjustments caused by temperature, yield, and creep. So as long as the conditions are such that the stress is reduced as yield occurs, failure should not be expected, even though the stress-relieving which occurs during operation may result in residual stress during shutdown.

Having covered this group of case experiences in differential temperatures the time has come to revert to the question propounded at the start of this paper: "On which side does a mechanic heat a bent shaft in order to straighten it?" Reference to the bowing of the free plate caused by welding as indicated in Fig. 6 will make it quite obvious that the heat would be applied to the outside of the bend in the shaft. The localized heating causes this side to expand against the resistance of the cold side setting up stresses above the elastic limit with a small permanent upset or shortening of the longest fiber. If the proper amount of heating has been applied the natural length of the two sides is the same when the shaft is cooled, and the shaft becomes straight. Heating on the inside of the bow will similarly result in upsetting the metal. Only in this case when the shaft cools there will be more bow.

BIBLIOGRAPHY

1 "Compilation of Available High-Temperature Creep Characteristics of Metals and Alloys," Joint Research Committee ASTM and ASME, 1938.

2 "High-Temperature Alloys," by C. L. Clark, Pitman Publishing Corporation, New York, N. Y., 1953.

3 "Thermal Stress," by J. N. Goodier, *Design Data and Methods*, ASME, July, 1953, pp. 74–77.

4 "Theory of Plates and Shells," by S. Timoshenko, McGraw-Hill Book Company, Inc., New York, N. Y., 1940.

5 "Process Heat Transfer," by D. Q. Kern, McGraw-Hill Book Company, Inc., New York, N. Y., 1950.

6 "Design of Thick-Walled Tubes Subjected to Pressure and Heat Input," by E. W. Luster, Trans. ASME, vol. 53, 1931, Paper No. FSP—53-8, pp. 161–172.

7 "Results of Service Test Program on Transition Welds Between Austenitic and Ferritic Steels at the Philip Sporn and Twin Branch Plants," by G. F. Lien, F. Eberle, and R. D. Wylie, Trans. ASME, vol. 76, 1954, pp. 1075–1083.

8 "Cyclic Heating Test of Main Steam Piping Materials and Welds at the Sewaren Generating Station," by H. Weisberg and H. M. Soldan, Trans. ASME, vol. 76, 1954, pp. 1085–1089.

9 "Supports for Vertical Pressure Vessels," by F. E. Wolosewick, *Petroleum Refiner*, vol. 30, December, 1951, pp. 151–153.

Appendix

Curvature of Bar Due to Differential Expansion

Referring to Fig. 2(*b*)

$$\frac{2e}{t} = \frac{1}{R} \quad \ldots\ldots [3]$$

e = ½ differential expansion between inner and outer faces of free bar, in/in., t = thickness of bar, in., R = radius, in.

For a steel bar 1 in. thick with temperatures of 1000 F and 900 F on the two faces the radius of curvature would be obtained as follows

$$e = \frac{0.000010 \times 100}{2} = 0.0005 \text{ in/in.}$$

$$R = \frac{t}{2e} = \frac{1}{2 \times 0.0005} = 1000 \text{ in.}$$

As a rule these bows are of relatively large radius and the subtended arc is small, so by an approximation the height between the chord and the inside of the bow may be found as follows

$$\frac{2h}{\frac{1}{2}c} = \frac{\frac{1}{2}c}{R} \quad \ldots\ldots [4]$$

or

$$h = \frac{c^2}{8R} \quad \ldots\ldots [5]$$

h = height from chord to bow, c = chord length = approximately arc length.

Residual Stress in Heater Tube

In order to make an approximate evaluation of the residual stresses in a heater tube after service refer to Fig. 8. Assuming

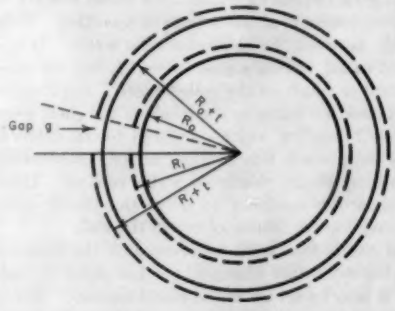

Fig. 8 Expansion of Slit Tube Section Due to Residual Stresses

that the heat input has a constant value around the circumference of the tube and the stress distribution across the thickness is linear, the residual stress may be found as follows:

Measure inside diameter and thickness of a short section of the tube, then slit and measure the gap formed when the tube opens up (allowing for saw kerf).

Before cutting the tube the ratio of outside circumference to inside circumference is

$$\frac{2\pi(R_0 + t)}{2\pi R_0} = 1 + \frac{t}{R_0} \quad [6]$$

After slitting the tube and allowing it to move to eliminate the residual compression at the inside face and tension at the outside face, the outside fiber length will decrease and the inside will increase by S/E in/in. each, where S = extreme fiber stress and E = Young's modulus of elasticity.

Therefore, after cutting, the ratio of outside to inside circumference is

$$1 + \frac{t}{R_0} - \frac{2S}{E} \quad [7]$$

The tube will expand to a new diameter

$$R_1 = R_0 + \frac{\text{gap}}{2\pi} \quad [8]$$

After cutting, the ratio of outside to inside circumference is

$$\frac{2\pi(R_1 + t)}{2\pi R_1} = 1 + \frac{t}{R_0} - \frac{2S}{E} \quad [9]$$

Simplifying and rearranging

$$1 + \frac{t}{R_1} = 1 + \frac{t}{R_0} - \frac{2S}{E} \quad [10]$$

$$\frac{t}{R_1} = \frac{t}{R_0} - \frac{2S}{E} \quad [11]$$

$$R_0 tE = R_1 tE - 2SR_1R_0 \quad [12]$$

$$2SR_1R_0 = R_1 tE - R_0 tE \quad [13]$$

$$S = \frac{tE(R_1 - R_0)}{2\,R_1R_0} \quad [14]$$

Substituting the value of $R_1 - R_0$ obtained from Equation [8] in Equation [14]

$$R_1 - R_0 = \frac{\text{gap}}{2\pi} \quad [15]$$

$$S = \frac{tE\,g}{4\pi R_1R_0} \quad [16]$$

This was used to determine the cold residual stress in a tube from a thermal-cracking heater. The tube was carbon steel, $3^3/_4$ in. OD × $^5/_{16}$ in. wall and heat rates are not available.

This was a roof tube, fired from one side, so the residual stresses would not be expected to be uniform. However, slits made at different points on the circumference show the following:

	Gap, in.
Fire side	0.029
Roof side	0.028
Side next to adjacent tube	0.025
Average	0.027

Taking the average of these gaps the calculated stress is as follows

$$S = \frac{0.312 \times 30 \times 10^6 \times 0.027}{4\pi 1.562 \times 1.566} = 8350 \text{ psi}$$

Straightening a Bowed Bar

The stress due to straightening a bar bowed with radius R may be found as follows:

In straightening the bar the outside is compressed and the inside is stretched $^1/_2$ the total difference in length per inch of inside diameter

$$\frac{2e}{t} = \frac{1}{R} \quad [3]$$

Substituting the defined value of $e = S/E$ in Equation [3] and rearranging

$$S = \frac{tE}{2R} \quad [17]$$

For a bar 30 in. long and $^5/_8$ in. + $^7/_{64}$ = 0.734 in. thick with a bow of $^5/_{16}$ in. at the middle

$$R = \frac{c^2}{8\lambda} = \frac{30^2}{8 \times 5/16} = 360 \text{ in.}$$

$$S = \frac{tE}{2R} = \frac{0.734 \times 30 \times 10^6}{2 \times 360} = 30{,}600 \text{ psi}$$

Discussion

F. E. Wolosewick.[8] This interesting paper discusses in a novel manner stresses due to temperature differences occurring in a large number of industrial applications. Without formal mathematics, which is somewhat regrettable, the author portrays the physical behavior pattern caused by temperature differences in types of construction used in the chemical field, and indicates the importance of plasticity in metals.

The utilization of plastic flow, or the yield properties of steel within certain narrow limits, is recognized by structural engineers, judging by the number of papers appearing in the Transactions of ASCE. A very important Seminar on the Plastic Behavior of Structural Steel was recently conducted at Lehigh University, where full-scale model tests demonstrated plastic behavior, and in the resulting discussions, new concepts of analysis were demonstrated. Although this Seminar was concerned with structural steel, the underlying philosophy and the unorthodox approach should be welcomed by engineers employed in the chemical fields.

In the field which the author is describing, yielding may, or may not, be beneficial, depending on the degree of yielding, and on the geometrical distortions which the structure sustains during such yielding actions. It may be that such yielding may accumulate creep in sections least desired, resulting in permanent distortions requiring corrective treatments. This condition has been known to exist in piping systems, and in cylindrical containers.

Specific references are made by the author in the opening part of his paper to the apparent lack of information on temperature-gradient stresses. This is understandable, since the problem is essentially complicated theoretically, and by introducing geometrical discontinuities, cannot be handled conveniently. It would require a high degree of mathematical skill, an aptitude for this type of work on the part of the analyst, and wealth of experimental data, before he could reach reasonable conclusions. The normal procedure is to ignore these problems completely, or use some expedient which will minimize thermal stresses. It appears to be more convenient to say that plastic yielding should cause a more favorable stress distribution, than to hypotheticate a premise, develop a conclusion, without the means of experimental verification.

Apparently the author's intent in using Fig. 1 is to demonstrate the three possible types of structures: determinate, indeterminate, and instability conditions. In so far as Fig.1 (*b*) is con-

[8] Sargent and Lundy, Chicago, Ill.

cerned, forces in this system due to cold springing can have two additional limiting values; those due to plastic flow up to the strain-hardening range, and higher values of stress and force beyond the strain-hardening zone approaching the ultimate values in tension. It should be recognized that in Fig. 1(*c*) elastic instability can develop at very low stress values, considerably below the elastic limits of materials, since the behavior pattern is a function of geometrical dimensions of the structures. In short, it is possible to have fully elastic systems, undergoing large displacements, and still possess structural stability upon the removal of the load.

In determining the values shown in Fig. 3, the writer wonders whether frictional resistance at the contacting faces was considered, since the curves have unequal stress areas above and below the zero stress line. This would presuppose that tangential forces are present.

The writer is not familiar with the experimental tests by Clark, but believes in the importance of accumulated strains which can, and do, become critical. In the more complex structures like pipe bends, rings, castings, or cylinders, creep can accumulate in the highly stressed fibers, while the less stressed fibers may add additional elastic deformations, which may further increase creep in the critical zones. This perhaps may be one of the possible explanations of the "pregnant spool pieces," and the bulging pressure vessels mentioned by the author.

The illustrated example cited by the author in calculating the stresses in the spool piece, the temperature ranges, and the resulting deformations, lead the writer to suspect that the value of the Poisson's ratio should be somewhat higher than that used by the author. The limiting case of Poisson's ratio is 0.5, in which instance the magnitude of the stress would be about 25,000 psi, instead of 17,800.

The increased value of Poisson's ratio can be evaluated from the plasticity equation, on the assumption that volume change is zero. Hence

$$e_v = \frac{1 - 2\nu}{E}(S_x + S_y + S_z)$$

where e_v is the volume change, and the values in the parentheses are triaxial stresses. Since they cannot be zero, then $\nu = {}^1/_2$.

After publication of Luster's article on stresses due to heat input, two additional studies, one in ASME publications, the other in Russian,[4] but translated into English, discuss this problem in detail. It appears that more conservative results can be predicted by the use of equations from the later publication; however the strains are quite high from theoretical considerations, and the adjustments which the author mentions undoubtedly occur.

When thin-wall pressure vessels are supported by lugs, reinforcing rings are necessary to prevent large distortions, and to keep stresses within reasonable limits. The introduction of reinforcing rings develops longitudinal bending stress in the wall of the pressure vessel, depending on the degree of stiffness in the rings, and stresses due to thermal differences in the rings themselves. The longitudinal flexural stresses have short amplitudes and are additive to the axial stresses from internal pressure.

When properly designed, and resting on lubricated bronze plates, whose surfaces have "vulcanized" layers of graphite several mils in thicknesses permitting expansions, with properly proportioned and well-insulated ring reinforcements suitably attached to the pressure vessel, lugs have given excellent service, and are more economical than skirt supports. There is no recorded case of failure in such construction although, in a few instances, large distortions have been observed, requiring corrective measures to prevent further structural damage. Another advantage in the lug construction, when compared with the skirt support, is the elimination of thermal stresses, because of the ability of the lugs to move with diametral increase of the pressure vessel.

The writer recalls clearly a problem of supporting a 25-ton stripper directly from the wall of a high-temperature reactor operating at 900 F, thereby eliminating a tall structural support, with considerable simplification in piping, and elimination of an expansion joint.

A satisfactory design was evolved, using an external reinforcing ring, consisting of a structural tee, approximately 8 in. in depth, with the web of the tee perpendicular to the vertical axis of the reactor, and encircling the reactor approximately 240 deg. Such section was required, since the flat-plate reinforcement of the type, indicated by the author in Fig. 7 (*a*), did not have the desired structural stiffness. Stresses resulting from thermal differences between the outside of the flange of the tee and the pressure vessel were anticipated, and were provided for by ample insulation. Since the ring was discontinuous, bending stresses along the circumference of the reactor could not be critical, while stresses due to thermal differences between the flange of the tee, and wall of the vessel were evaluated on a basis of small differentials. This type of construction has been used successfully on a large number of similar installations, without any visible distortions in the supports, or in the walls of the reactor.

The author refers to the writer's article on temperature stresses in skirts,[5] and uses the equation (which the writer developed) in his subsequent discussion. As originally printed, the equation in question was typographically in error, and should read as follows

$$f = \frac{[3(1 - \nu^2)]^{1/4}}{(1 - \nu^2)} \sqrt{Rt}\, Ea \frac{dT}{dx}$$

where

f = bending stress
R = radius of skirt
t = thickness of skirt
E = Young's modulus, 25,500,000 at 700 F
a = unit elongation per unit of length per degree F, and is 7.6×10^{-6} at temperature of 700 F
dT/dx = temperature drop per inch of height, or instantaneous value, if some explicit function expressing temperature drop through insulated skirt could be obtained
ν = Poisson's ratio, used as 0.27 in this illustration

In the third part of the same article, and published in the *Petroleum Refiner*, in October of the same year, the writer developed an empirical equation for temperature gradient through an insulated skirt, based on some experimental test data. This equation is as follows

$$T_x = (T_v - 50) - 6.037x - 0.289x^2 + 0.009x^3$$

where

T_x = metal temperature at any distance below the tangent line
T_v = vapor temperature, or liquid
x = distance below tangent line, in inches

If dT/dx is known experimentally, or by differentiation of explicit function like the one listed in the foregoing, then an approximate stress value can be determined. In the case under

[4] "Distribution of Temperature Heat Stresses and Thermal Strains in the Radiant Tubes of Tubular Furnaces," by I. A. Charnyi, Process Management Corporation, Foreign Literature Service, Special Translation S16, July 29, 1938.

[5] Author's Bibliography (9).

discussion, dT/dx was obtained by differentiation of the foregoing equation, as 6.588 deg per in. of height, resulting in an approximate stress value of 9350 psi.

In this particular illustration the skirt was approximately 40 in. in height, with thermocouple recordings of 700 F at the tangent line, and approximately 250 F at the base angles. On the basis of linear temperature difference, the variation per inch of height is approximately 11 deg F, while the estimated temperature variation near the tangent line was about 25 deg F over a height of 3 in., or approximately 8 deg F per in. Apparently any reasonable stress value can be obtained, depending on the accuracy of dT/dx.

The writer is in agreement with the author that thermal differences in insulated skirts are not large, and that resulting stresses in them are not critical, assuming of course that skirts are reasonably high, and are of nominal thicknesses. With short stubby skirts, with thicknesses equal to the vessel wall itself, high temperature stresses are anticipated, and if they do occur, there is yielding in the steel, which reduces the stress to those of yield value, for the given temperature. In other words, the steel knows which way to bend when heated.

Author's Closure

Mr. Wolosewick deplores the lack of formal mathematics in this paper. It seemed more practical to try to develop a basic understanding of the problem than to submit the cases to mathematical treatment (if the author were able). The resulting equations surely would be used indiscriminately and would give answers as erroneous as those obtained from elastic theory applied to semiplastic conditions. Even the primitive mathematics in the paper will no doubt be used outside the limitations set around it.

The temperature gradient along a skirt support is a case in point on the use of mathematics. For a rough approximation, use of an empirical equation gives a number. When the equation is based on test data, considerable confidence may be placed in the number so obtained. But it seems preferable to understand that this number actually depends upon the temperature of the vessel contents, the temperature and weather conditions at the base, the length, thickness, and conductivity of the skirt, the thickness and conductivity of the skirt insulation, and the ratio of insulated area to the area of the bare base. Having these factors, a stepwise trial-and-error method can be set up to calculate dT/dx which is equal to the heat flow at any point along the skirt divided by the conductivity of the path. With all the possibilities for error in assumptions, there are many cases where the laborious calculation is not justified as against a simple linear approximation.

High-Temperature Stability of Insulating and Refractory Castables in Reducing and Oxidizing Atmospheres

By C. M. VOGRIN[1] and H. HEEP,[2] NEW YORK, N. Y.

Beginning with the installation of a castable lining in a regenerator of a fluid catalytic-cracking unit in 1946, the authors' company became particularly interested in the use of castables as a means for temperature reduction and erosion protection. Encouraged by successful service coupled with the growing acceptance by industry of castables, it was decided to investigate the possible application of castable linings for services involving temperatures up to 2400 F in a reducing atmosphere of CO, H_2, CO_2, CH_4, and H_2O. In the course of the test program, the investigation was broadened to include applications which require protection not only against heat, but also corrosion and erosion. The paper reviews the test program and the results achieved.

SOON after installation of a castable refractory lining in a regenerator for a catalytic-cracking unit in 1946, the authors' company undertook a study of castable linings for services involving temperatures up to 2400 F.

During the initial stages of investigation it became apparent that a test program be evolved to clear up the following points:

1 The usual source of information concerning maximum service temperature and other physical data of castable refractories is the manufacturers' catalogs advertising these products. Generally, the basis of such figures is not indicated. Especially difficult to define is the maximum service temperature. To a large extent, this figure is a matter of opinion depending on the assumed margin of safety. For a design which has to include provisions to handle runaway temperatures the knowledge of such margins becomes important.

2 With regard to hydraulic binders of castable materials divergence of opinion was found about the comparative merits of aluminous-type cements (calcium-aluminate) versus special Portland cements (calcium-silicate) developed for castables. While there seems to exist general acceptance of the merits of aluminous cements as a refractory material, the opinions on Portland cement are divided.

In this course of the test program, the investigation was broadened to include castables for applications which require protection not only against heat, but also corrosion and erosion.

Test Materials

The castables chosen for the investigation were considered representative of commercially available products. In common, these materials can be handled like ordinary concrete. They develop a hydraulic bond and when exposed to elevated temperatures, a ceramic bond. Differences existed with regard to type of hydraulic binder and with regard to suitability for specific service conditions. Considering the hydraulic binder, three variations exist as follows:

1 Portland cement of the high-early-strength type.

2 Aluminous cement of the ordinary type as characterized by the following analysis:

	Per cent
Al_2O_3	36–39
CaO	37–39
SiO_2	5–5½
Fe_2O_3	11–13
FeO	4–5
TiO_2	1½–2

3 High-purity aluminous cement, a special calcium-aluminate binder essentially featuring a reduced iron content of 1 per cent or less combined with a corresponding higher percentage of alumina.

On the basis of their service the tested castables belong to the following groups:

1 Refractory castables, standard weight (100–130 pcf) with refractory qualities comparable to firebrick.

2 Insulating refractory castables:

(*a*) Medium weight (70–100 pcf), a compromise between insulating qualities, structural strength, and erosion resistance for single liner application.

(*b*) Lightweight (30–50 pcf), where strength is sacrificed in favor of low conductivity.

3 Erosion-resistant refractory castables.

Test Program

The test program was planned to obtain a qualitative classification of various refractory castables regarding stability at elevated temperatures in oxidizing as well as reducing atmosphere; further to gain better knowledge of what can be expected from specific hydraulic binders; and finally to study the type of breakdown as well as its preceding circumstances for individual castables, when failure occurs due to temperature.

The test program included a graduated heat-soaking test and a cyclic heating test, both in oxidizing atmosphere of air and a reducing atmosphere of illuminating gas. Each test specimen was subjected to one heat-treatment only. The behavior of the specimens during the test as visually observed, their change in weight and linear dimensions, was recorded.

During the progressive heat-soaking test each charge was heated from ambient to test temperature as quickly as the furnace allowed and soaked at this temperature for the remainder of 8 hr. The specimens were then allowed to cool overnight and removed from the furnace prior to placing the next charge.

HEAT-SOAKING SCHEDULE

Charge no.	1	2	3	4	5	6
Soaking temp, deg F	1150	1500	1750	2000	2250	2500

[1] Section Engineer, The M. W. Kellogg Company.

[2] Senior Engineer, The M. W. Kellogg Company.

Contributed by the Materials Committee of the Petroleum Division and presented at the Petroleum-Mechanical Engineering Conference, New Orleans, La., September 25–28, 1955, of The American Society of Mechanical Engineers.

Note: Statements and opinions advanced in papers are to be understood as individual expressions of their authors and not those of the Society. Manuscript received at ASME Headquarters, September 27, 1955. Paper No. 55—PET-31.

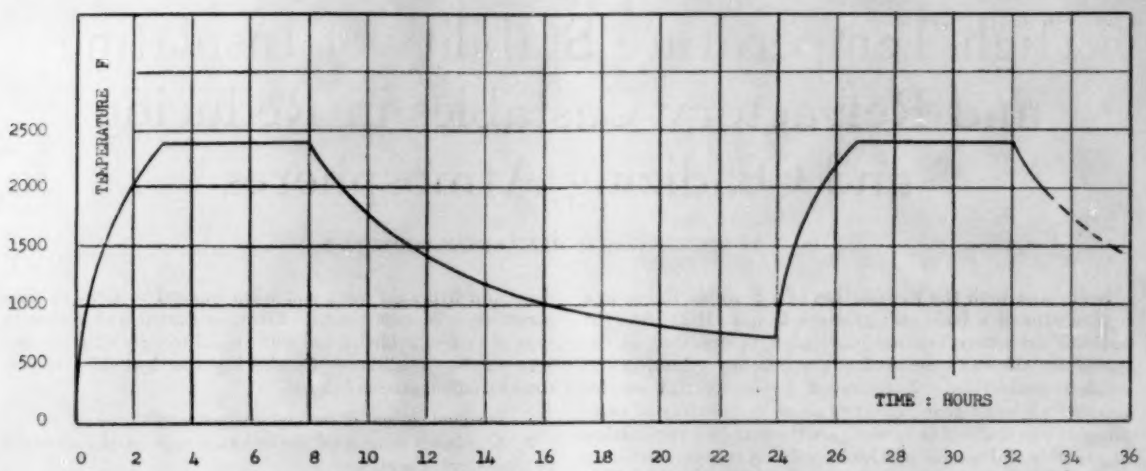

FIG. 1 TYPICAL TIME-TEMPERATURE RECORDING OF CYCLIC REHEATING TEST

The cyclic heating test was a repetitive soaking following the same pattern with one cycle per day. The number of cycles in the beginning was 10 and later was reduced to 5. Fig. 1 depicts a typical time-temperature recording of such a test. The cycling took place for oxidizing atmosphere between ambient and 1800 or 2300 F. For reducing atmosphere, the range was between ambient and 1200, 1800, or 2400 F.

Chemical analyses of unfired and fired specimens were made to determine relations between carbon depositions and iron content of the castable.

After each cycle the furnace muffles were opened for inspection. A specimen was considered to have failed if either one of the following conditions existed:

1 Specimen fused.

2 Specimen revealed signs of plastic deformation as a result of firing.

3 Specimen cracked or crumbled seriously.

After the test, the fired specimens were stored at room temperature and periodically checked for 6 months.

TEST EQUIPMENT

Since the test called for temperatures possibly up to 3000 F at various atmospheres, it was considered necessary to design a special electric furnace with Glo-Bar heating elements (Fig. 2). Four silicon-carbide muffles of rectangular shape were arranged across the furnace. Each muffle could hold 4 test specimens measuring 2 in. × 2 in. × 6 in. Temperature control was automatic by on-and-off temperature relay actuated from a control thermocouple in muffle No. 3. Temperature of each muffle was continuously recorded by a multipoint potentiometer. Up to 2000 F the control thermocouple was chromel alumel and the recording couples iron constantan. Beyond 2000 F, all thermocouples were platinum rhodium in protective porcelain wells.

TEST SPECIMENS

In casting the test specimens, efforts were made to obtain the same consistency of wet mix for each material. The flow table procedure ASTM C91-40 was used to determine the necessary wet-mix ratio. A flow of 75 per cent provided sufficient workability to cast uniform specimens without drawing water to the surface. Specimens were cast vertically. Determination of initial and final set followed the Gillmore needle method in accordance with ASTM A191.

TEST RESULTS

The test data, our observations, and the review of pertinent literature led us to the following:

Temperature Stability

Refractory castables (standard weight) recommended by manufacturers for maximum service temperature of 3000 F:

Castables belonging to this group basically combine a high-purity alumina binder with an aggregate of either crushed alumina firebrick or calcined clay. The iron content of these mixes is low, about 1 per cent or less and the percentage of aluminum high, up to 70 per cent. As a result of the low iron content, the color is white or near white. During heat soaking, plastic deformation set in at 2400-2500 F.

Softening gradually increased until fusion occurred slightly beyond the maximum recommended service temperature. Consequently, temperatures above 2400 F must be strictly limited to hot-face temperatures if there is any appreciable load to be supported.

In general, materials of this group displayed stability during all tests under both oxidizing and reducing conditions for all soaking temperatures up to 2400–2500 F. Out of four materials tested, one castable was selected for liners of combustion chambers operating from 1700 to 2300 F and has given satisfactory service over an operating period of about 2 years.

Insulating refractory castables (medium-weight) recommended by manufacturers for maximum service temperatures up to 2250 F:

Castables of this type are a mix of regular aluminous cement such as Lumnite and an aggregate of Haydite and Dicalite or just Haydite. The iron content of these mixes varies between 5–10 per cent.

During soaking at the maximum recommended service temperature of 2250 F indications of some softening were observed. However, when cycled at 1800 F in illuminating gas all materials of this group disintegrated or cracked considerably, but were stable during the same test in oxidizing atmosphere. Cracked specimens pressed between fingers crumbled into fine powder of black and rusty-red color and generally unharmed pieces of aggregate. No other test produced failures of this type which evidently were caused by carbon depositions inside of castables containing more than $1^1/_4$ per cent of iron. The temperature of 1800 F for this type of failure was surprising because the familiar

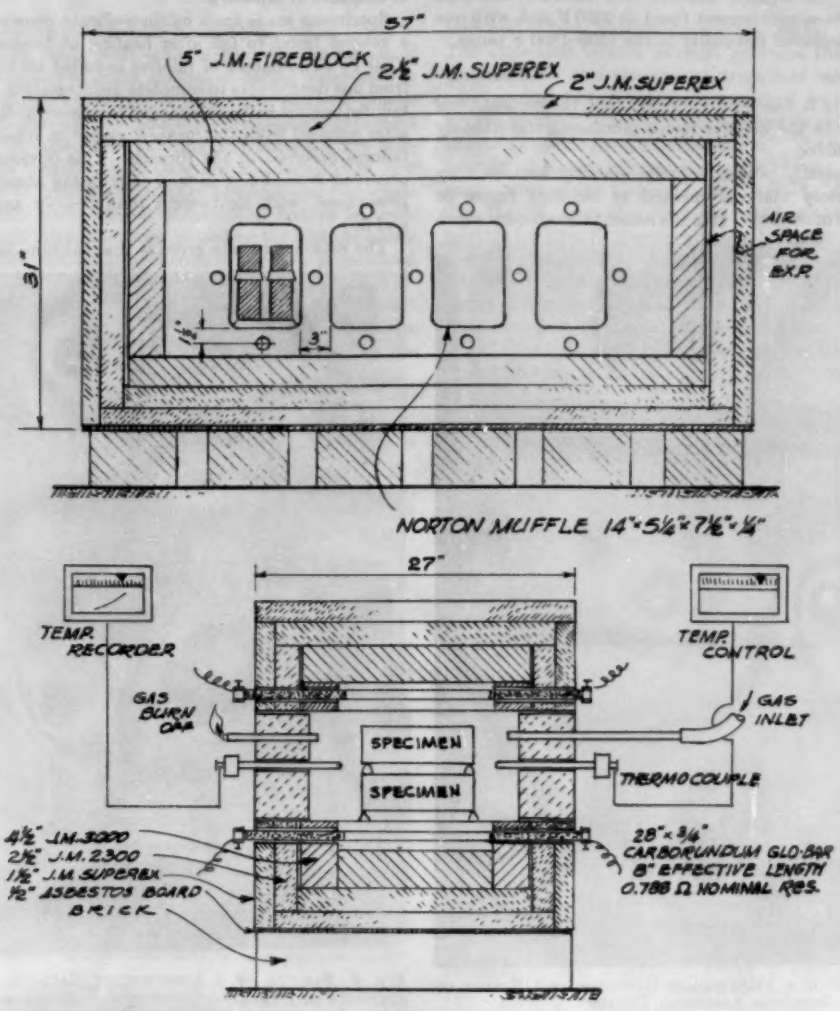

FIG. 2 TEST FURNACE

case of carbon disintegration is more likely to occur at lower temperatures. The tentative ASTM Carbon Disintegration Test calls for temperatures of only 900–950 F. This phenomenon prompted a study which is added in Appendix 1.

Insulating refractory castables (lightweight):

The lightweight castables which were tested, contained a high-early-strength calcium-silicate binder, for example, Incore, and aggregates such as crushed insulating brick, expanded vermiculite, pearlite, and diatomaceous earth.

Maximum recommended service temperatures ranged from 1800–2000 F. No castable of this group was found unconditionally stable above 1300 F. In the range between 1500–1800 F, specimens cracked or crumbled, particularly during cycling. Those recommended for up to 2000 F were stable at that temperature. At 2250 F all of them fused completely into a black or green glossy mass which covered the bottom of the muffle. Moreover permanent shrinkage after exposure to temperatures above 1300 F was high. In some cases a shrinkage of 5 per cent was measured for 1500–1700 F, compared with 0.2–0.3 per cent for refractory concrete of standard weight under the same circumstances.

Some specimens cracked several months later after exposure to temperatures between 1500–1800 F.

Special care was necessary during artificial drying of lightweight castables. On account of their porous nature, more moisture is retained which developed a destructive steam pressure if temperatures were raised too fast, Fig. 3.

Erosion-resistant refractory castables:

These castables are recommended for erosion resistance up to 1200 F. Correlations are known to exist between erosion rate and compressive strength or fracture strength. For that reason the cement-aggregate ratio is on the cement-rich side to provide maximum strength. A cement-rich ratio in turn is detrimental at elevated temperatures when, due to dehydration, the hydraulic bond is diminished.

The materials tested contained a calcium-aluminate or a high-early-strength calcium-silicate binder. The comparatively coarse aggregate was either crushed firebrick, silicon carbide, or corhart.

Regarding temperature stability, the castables behaved as could be expected from their binders. For instance, the ones containing calcium-silicate cement fused at 2250 F and, with one exception, also displayed instability in the 1500–1800 F range.

Cementitious Binder

In the foregoing it has been indicated that the cementitious binder proved to be the decisive factor influencing the stability of refractory castables.

Aggregates generally possess superior stability because they are either refractory material prefired to incipient fusion or stabilized in some other way. It is the cementitious binder which undergoes drastic changes of its properties with temperature and atmosphere or exposure.

Specimens made from calcium-silicate cement mixes revealed a general trend to fail after heating at temperatures of 1500–1750 F. The nature of failures included all intermediate steps from fine deep cracks to complete disintegration. The time when failures became noticeable ranged from several days to five months after removal from the furnace, except in reheating tests where failures occurred in the furnace. This obvious instability was observed in oxidizing as well as reducing atmosphere and more pronounced with lightweight than heavier aggregates, Figs. 4 and 5.

The reason generally given is that calcium-silicate cements re-

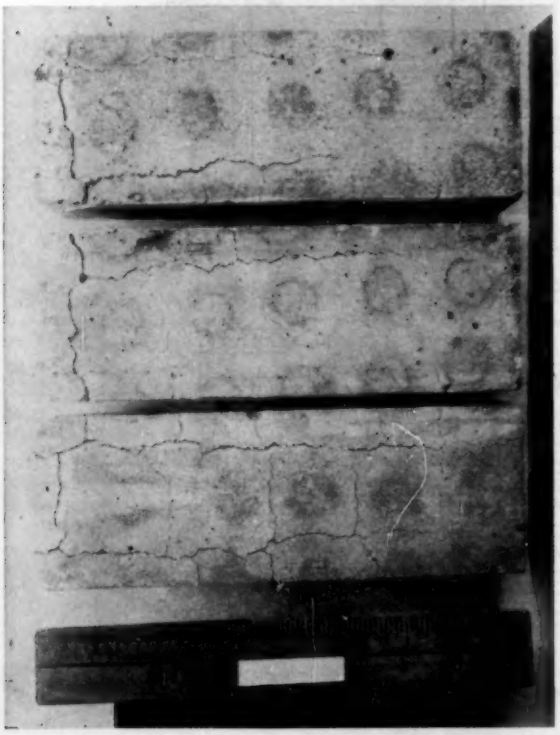

FIG. 3 CRACKING OF A LIGHTWEIGHT CASTABLE AS A RESULT OF IMPROPER ARTIFICIAL DRYING

(Maximum temperature of 500 F was attained faster than specified. Internal build-up of steam pressure caused the damage. Cracks outline spots which correspond to holes in the electric oven tray.)

FIG. 4 FAILURE OF A LIGHTWEIGHT CASTABLE INDUCED BY INSTABILITY OF HYDRATED COMPOUNDS OF CALCIUM-SILICATE CEMENT AFTER FIRING ONCE AT 1750 F IN ILLUMINATING GAS ATMOSPHERE

(Specimen was removed from furnace without defects. Photograph depicts condition 6 months later.)

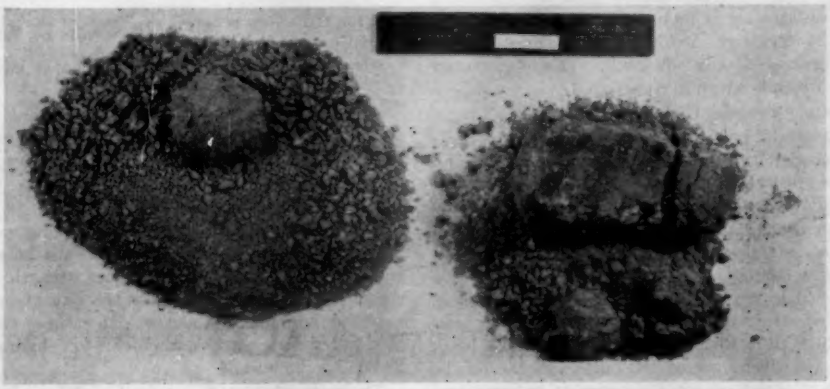

FIG. 5 FAILURE OF AN EROSION-RESISTANT CASTABLE INDUCED TO INSTABILITY OF HYDRATED COMPOUNDS OF CALCIUM-SILICATE CEMENT

(Specimen on the left was fired at 1750 F and the other at 2000 F, both in oxidizing atmosphere. Specimens left furnace without defects. Several days later deep cracks developed. Photo was taken three weeks later.)

lease free lime during dehydration which upon cooling tends to rehydrate or easily reacts with other elements. The release of calcium oxide increases with the amount of gaging water used in the mix. Overgaging easily occurs with lightweight or porous aggregates which absorb excess moisture. The tested lightweight castables were developed for gunniting and naturally are difficult to pour into forms because they are not designed to flow easily. In order to facilitate pouring of homogeneous test specimens greater than recommended water ratios had to be used. This, together with internal stresses caused by the high shrinkage rate, may have been contributing factors to the more pronounced failures of calcium-silicate cements in lightweight castables.

Besides reactions of the free lime, Portland-type cements at temperatures above 1300 F can be subject to mineral inversions which result in volume changes developing disruptive forces (Appendix 2).

Finally, all castables containing calcium-silicate cements with one exception failed completely by fusion when vitrification set in between 2000–2250 F. The high percentage of silicates is responsible for this.

Specimens bonded with regular calcium-aluminate cement consistently failed when cycled at 1800 F in illuminating gas atmosphere. Gas of the following analysis was used:

CO_2	CO	O_2	H_2	CH_4	C_2H_4	N
2%	9.2%	3.7%	9%	26%	12%	Rest

Disintegration of samples obviously was caused by destructive internal carbon depositions around nuclei of iron particles. The attendant volume increase produces the disruptive force. Unfortunately also, the rupture strength of castables is at a minimum around 1800 F because the original hydraulic bond is lost by dehydration while the temperature is still too low for an effective ceramic bond by vitrification. The relatively high iron content of regular calcium-aluminate cement catalyzed the decomposition of the hydrocarbons CH_4 and C_2H_4 into C and H_2. The H_2:CH_4 ratio of subject gas was less than the equilibrium mixture for 1800 F; therefore carbon had to be deposited to reach a stable equilibrium. Actually from 1750 F upward hot gas leaving the furnace muffles contained a lot of soot, which kept on plugging the burn-off pipe. However, at 2000 F and above, destructive carbon deposits were not observed, probably because vitrification set in and coated the iron particles with glassy silicates thus eliminating the catalytic surfaces, Figs. 6 to 9.

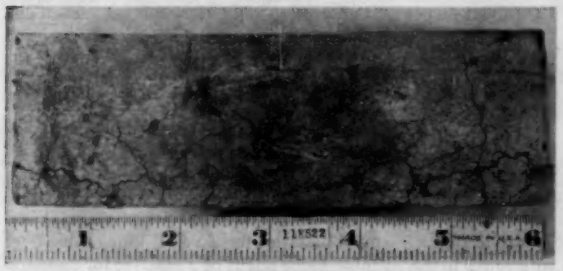

FIG. 6 EXAMPLE OF CARBON-DISINTEGRATION FAILURE OF A MEDIUM-WEIGHT CASTABLE AFTER 3 CYCLES AT 1800 F IN ILLUMINATING GAS ATMOSPHERE

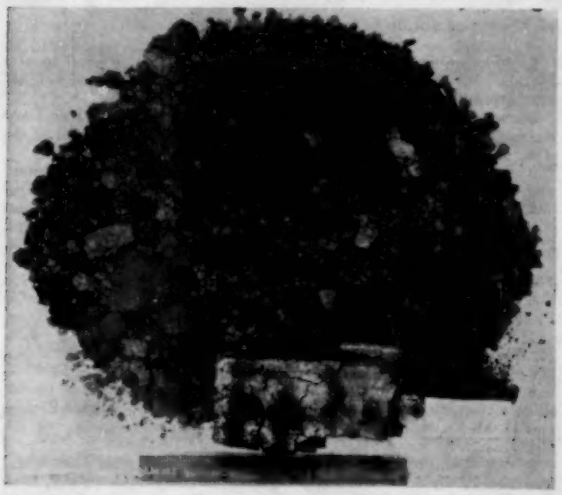

FIG. 8 EXAMPLE OF CARBON-DISINTEGRATION FAILURE AFTER 4 CYCLES AT 1800 F IN ILLUMINATING GAS ATMOSPHERE
(Material is identical to that of Fig. 7.)

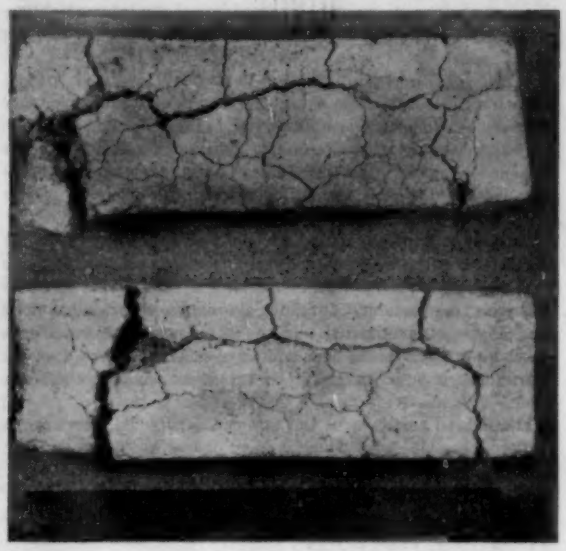

FIG. 7 EXAMPLE OF CARBON-DISINTEGRATION FAILURE OF A STANDARD-WEIGHT CASTABLE AFTER 2 CYCLES AT 1800 F IN ILLUMINATING GAS

FIG. 9 EXAMPLE OF CARBON-DISINTEGRATION FAILURE OF AN EROSION-RESISTANT CASTABLE AFTER 5 CYCLES AT 1800 F IN ILLUMINATING-GAS ATMOSPHERE

The better-known carbon disintegration resulting from the reaction

$$2\,CO \rightleftharpoons CO_2 + C$$

which is most likely to occur around 1000 F was not observed. The latter requires a much higher percentage of CO than 9 per cent as found in illuminating gas. Possibly more than 50 per cent is necessary as reported by one observer.

Disruptive carbon depositions were not observed when calcium-silicate cement was used. In this binder the iron content is lower and also sulphur compounds are added to facilitate quick setting. Sulphur is an effective catalyst poison, which may explain the different behavior.

Only castables with a special iron-free aluminous binder proved to be stable over the whole temperature range in oxidizing as well as reducing atmosphere. They were not subject to any disruptive carbon depositions and also were free of the inherent shortcomings of calcium-silicate cements.

Types of Failures

With regard to the type of failures as a result of excessive temperature the following is noteworthy:

The atmosphere of environment oxidizing or reducing did not influence essentially the softening or fusion temperature; however, it seemed slightly higher in oxidizing atmosphere.

Castables with calcium-silicate binder generally failed by fusing completely into a liquid when fired within a 100-deg F margin above the maximum recommended service temperature. This sudden and complete breakdown is significant. On the other hand, all castables containing aluminous cement failed more gradually when overheated. In the latter case there was a progressive softening spread over a range of several hundred degrees, providing a greater margin of safety against runaway temperatures.

The unfired castables of the test can be divided colorwise in two groups: One type which is more or less white and another which comprises various shades of typical gray concrete colors.

The white mixes derive their color from their pure iron-free alumina binder or pure iron-free Portland-type cement. When fired up to the point of incipient fusion these castables did not change their color. Above this, light brown spots appeared giving them resemblance to alumina firebrick.

The gray mixes underwent more pronounced color changes. Up to 1500 F or as long as some hydraulic bond existed, the basic gray or greenish-gray was retained, assuming only lighter shades above 200 F. From 1500 F up specimens changed to biscuit-like colors, growing more and more brown or reddish brown until failure occurred. These permanent color changes seem rather characteristic. An effort was therefore made to record the individual colors by matching color snips. This color chart has possibilities for determining in the field the maximum temperature to which a certain castable liner has been exposed, especially when all other means of temperature recording have failed.

Conclusions

When selecting commercial refractory castables, careful consideration must be given to all possible service conditions. It is not enough to note the maximum service temperature. Cycle temperature variations during operation, type of atmosphere, and expected frequency of shutdown with attendant cooling influence decisively the choice of a castable.

The information handed out by reputable manufacturers of commercial castables was found fairly correct, but incomplete. Therefore appropriate tests are advisable whenever castables have to be specified for new service conditions. The unexpected disruptive carbon deposits on catalytic-iron particles from the decomposition of CH_4 at 1750–1800 F proved this point.

The ASTM specifies an atmosphere of 100 per cent CO for the standard disintegration test. An atmosphere of CO alone should be a rare occasion in any process. Indications are that a certain minimum percentage, possibly more than 50 per cent of CO, is required to produce such damage. More work is desirable to determine exactly the critical range of CO concentrations.

The maximum service temperature as recommended by reputable manufacturers of commercial castables is reliable. Materials with ratings up to 2000 F will not fail even if soaked at the maximum temperature. However, ratings from 2250 to 3000 F must be considered more or less as hot-face temperatures.

Castables containing high-early-strength Portland cement as hydraulic binder can be used without limitations up to 1300 F. Regarding service at higher temperatures it must be kept in mind that during subsequent cooling and shutdown periods some instability exists due to reaction of dehydrated lime with the surrounding atmosphere or to mineral inversions. Excessive hydration during application increases this instability. Portland-cement mixes, however, offer good resistance against carbon disintegration.

Castables containing regular calcium-aluminate cement combined with suitable aggregates possess temperature stability up to 2250 F. Service environment containing high percentage of CO (about 50 per cent and more) and CH_4 will cause carbon disintegration in a temperature range of 900–1700 F. The reaction is catalyzed by the high iron content of the cement.

Castables for hot-face temperatures of 2500–3200 F require special iron-free (less than 1 per cent) calcium-aluminate cement for reasons of temperature stability. These castables, if mixed with an equivalent inert aggregate, possess also the greatest stability against various service environments.

If one would condense the results derived from this test program into one sentence, it might be stated:

In selecting a castable material for a vessel lining, check for substances in the castable which might be a catalyst for undesirable reactions or which react chemically with the service environment in a way to cause damage to the liner itself or to substances inside the contained equipment, for instance, sensitive catalysts.

References

1 "Decomposition of Carbon Monoxide by Ferromagnetic Metals," by Francois Olmer, *Journal of Physical Chemistry*, vol. 46, 1942, pp. 405–414.

2 "Some Effects of Zinc and Carbon Monoxide on Fire Clay Refractories," by R. F. Patrick and R. B. Sosman, *Journal of the American Ceramic Society*, vol. 32, 1949, pp. 133–140.

3 "Equilibrium in the System Alumina-Silica," by R. B. Sosman, *Journal of the American Ceramic Society*, vol. 16, 1933, pp. 60–68.

4 "Linear Force of Growing Crystals," by G. F. Becker and A. L. Day, Proceedings of the Washington Academy of Sciences, vol. 7, 1905, pp. 283–288; *Journal of Geology*, vol. 24, 1916, pp. 313–333.

5 "Some Problems of the Oxides of Iron," by R. B. Sosman, *Journal of the Washington Academy of Sciences*, vol. 7, 1917, pp. 55–72.

6 "Diffusion in Solids, Liquids, Gases," by W. Jost, Academic Press, New York, N. Y., 1952.

7 "Manufacture and Use of Fireclay Grog Refractories," by R. R. West and W. J. Sutton, American Ceramic Society Bulletin No. 30, 1951.

8 "Observations on Solid-Phase Inversions of Calcium Orthosilicate, Constituent of Dolomite Silica Brick," by Samuel Zerfoss and H. M. Davis, *Journal of the American Ceramic Society*, vol. 26, 1943.

9 "A Comprehensive Treatise on Inorganic and Theoretical Chemistry," by J. W. Mellor, Longmans, Green and Company, London, England, vol. 4, 1923.

TABLE 1 CARBON-DISINTEGRATION DATA

Material	Hydraulic binder	Fe content of specimen, per cent	C content before firing, per cent	C content after firing, per cent	No. of cycles and temp, deg F	Remarks
Castable A	Calcium aluminate	8.82	2.49	4.02	6–1800	One specimen disintegrated after 2 cycles, one after 3, two after 4, and one after 6 cycles.
		...	...	9.12	2–1800	
		...	...	1.48	10–1200	No defects after cycling at 1200 F.
Castable B	Calcium aluminate	6.38	2.94	8.17	5–1800	Two specimens cracked after 2 cycles, disintegrated after 5.
		...	...	...	5–1200	No defects after cycling at 1200 F.
Castable C	Calcium aluminate	7.52	0.53	4.23	6–1800	One specimen disintegrated after 2 cycles one after 3, two after 4, and one after 6 cycles.
		...	...	0.10	10–1200	No defects after cycling at 1200 F.
Castable D	Calcium aluminate	4.79	1.85	3.00	5–1800	Two specimens had fine cracks after 5 cycles.
Castable E	High-purity calcium aluminate	0.64	0.31	0.20	10–1800	No defects.

Appendix 1

Tentative Explanation for Consistent Failures of Certain Castables During Testing in Reducing Atmosphere

During the cycling test at 1800 F in the reducing atmosphere of illuminating gas it was observed that only a few cycles were sufficient to cause disintegration of specimens made from regular calcium-aluminate cement, while castables containing high-early-strength calcium-silicate cement or a special pure calcium-aluminate cement did not fail. To find the cause of this consistent behavior, some of the specimens were checked for iron content and carbon depositions. Based on a study of related literature, an explanation of this kind of failure is attempted.

Test Results. The test results are condensed in Table 1. More than one soaking at 1800 F was necessary to produce failure. During the 1200 F reheat test none of the castables disintegrated. The analysis did not indicate any carbon deposits at 1200 F. There was rather a decrease of the original carbon content. This carbon in the unfired specimens stems either from organic impurities or organic additives, intended to improve the workability of the wet mix.

Explanation. The disintegration of refractories by deposition of carbon from dissociation of CO in the presence of iron is a well-known and often published fact. The favorable temperature range for this reaction is between 800 and 1400 F. At higher temperatures the percentage of CO_2 in equilibrium with CO is very small, while at lower temperatures the reaction rate is too slow.

However, difficulties were not experienced during subject tests within this temperature range because the CO percentage was not enough to favor carbon depositions. The observed failures occurred at 1750–1800 F, probably as a result of methane cracking. Contrary to CO, methane becomes increasingly unstable at higher temperatures. As the original $H_2 : CH_4$ ratio of the reducing atmosphere was less than the equilibrium composition for elevated temperatures, CH_4 had to dissociate into C and H_2 to reach a new stable state. The destructive results of this carbon deposition resemble those from CO dissociation. There is literature on the latter but none on the first. The following explanations on the mechanics of carbon disintegration are assembled from literature on carbon-monoxide dissociation with the conviction that they are applicable to methane as well.

The first destructive effects of carbon depositions were noticed in blast furnaces, where accumulated carbon caused the refractory liner to expand and build up enough pressure to burst steel shells of 1 in. thickness. Thus most of the published papers were initiated by problems of the steel industry.

According to these references, the disintegration of refractories is caused by deposition of carbon from CO on nuclei formed from particles of free iron oxides in the refractory material. Besides iron oxides other effective catalysts such as nickel, cobalt, and zinc oxide do exist, but are not found in our refractory liners.

While the fact of carbon depositions in the presence of a catalyst is easy to understand, there remains to explain how the disruptive force is developed, because refractory linings have enough voids where carbon could deposit freely without developing any pressure. Preferentially, carbon seems to deposit on iron surfaces which are in tight contact with fire clay thus exerting a linear force. An analogy of this is reported by Becker and Day,[3] in that some crystals when depositing out of water solutions grow on a face that is under pressure from a superimposed weight rather than on a free surface. Darker suggested to Sosman that the effect may be an instance of Ostwald's rule of successive reactions:

"According to this principle, a substance which is unstable under the prevailing temperature and pressure, because its free energy is greater than that of the thermodynamically stable form, does not always change directly to that form but goes first to a form having intermediate free energy....Now a crystal under unidirectional stress has a greater energy content than the same crystal when free and unstressed. Hence, when carbon forms out of gaseous carbon monoxide under the stimulus of a catalytic surface, it preferentially deposits in a position where it is under stress."

Appendix 2

Discussion of Consistent Failures of Castables With Portland Cement After Heating to 1500–1750 F

The test revealed a definite instability of castables with Portland-type-cement binders when tested between 1500–1750 F. It is significant that failures generally did not occur during firing but rather in cooling and generally after the specimens were removed from the furnace. Only during the reheating tests did the specimens crack in the furnace. All Portland-cement mixes tested, with the exception of one, gave indications of the same type of instability, which was not observed in alumina-cement mixes. In the following, explanations are offered which are the result of a literature survey.

Test Results. All castables of the subject test containing Portland-type cements, with the exception of one, indicated instability after heating to 1500–1750 F. The severity of the failure and the percentage of occurrence varied widely between the different makes. The types of failures included everything between fine deep cracks and complete disintegration into a mixture of powdered cement and granular aggregate. The elapsed time after which cracks and disintegration became apparent ranged from several days to several months.

However, heating to temperatures higher than 1750 F reduced the occurrence of failures for most castables of this group. For instance, except for one insulating castable, failures were not observed during and after reheating cycles at 1750-1800 F or after single soaking at 2000 F and higher. Cyclic heating up to 1500

[3] See reference (4) at the end of the paper.

F proved to be most disastrous for these castables as it consistently caused specimens to fail in the furnace.

Concerning the influence of atmosphere, the evidence is not conclusive. All material, except for one which appeared sensitive only to oxidizing atmosphere, failed when exposed to either atmosphere.

Discussion. In no case was the Portland cement of the castables comparable to the regular type which is used in concrete construction. It was either high-early-strength cement or a special type of white color unknown in composition.

For high-early-strength cement the ASTM Specification for Portland Cement (C 150-49) requires 15 per cent of tricalcium aluminate ($3CAO\ AL_2O_3$), while none is specified for general construction cement. This substantial fraction of aluminates appears to be the essential difference which makes Portland cement, which is basically a calcium-silicate cement, a more acceptable ingredient of refractory castables. The special white Portland cements of unknown composition can also be assumed to have a sizable fraction of calcium aluminates which must be particularly high because the castable displayed considerable refractoriness up to 2400 F.

Concerning the failures, consideration must be given to the reactions of tricalcium silicate, the major hydrable constituent of Portland cement. During hydration the basic tricalcium silicate is decomposed according to the formula

$$3CaO \cdot SiO_2 + 4^1/_2\ H_2O = 2Ca(OH)_2 + CaO \cdot SiO_2 \cdot 2^1/_2\ H_2O$$

Upon heating dehydration sets in and free lime is liberated. The tendency of the free lime to rehydrate or combine with other elements is detrimental to strength and stability. R. R. West and W. J. Sutton determined by a simple test the correlation between free lime and stability of castables. They found that specimens which show presence of calcium oxide over the entire surface crumble and crack after storing from 1 to 7 days. On account of the higher fraction of calcium silicates, Portland-cement bond released more CaO after heating to 1000–1500 F than calcium-aluminate-cement bond. The amount of calcium oxide liberated also increased with the amount of gaging water used in the mix. Based on similar evidence, the generally accepted opinion appears to be that on account of the greater fraction of free lime liberated upon heating and its tendency for rehydration after cooling, regular Portland cement is inferior to calcium-aluminate cement as bonding agent in refractory castables.

As it has been pointed out before, the Portland cements in successful refractory castables must be of a special type to prevent an excess of free lime. This is done by increasing the fraction of calcium aluminate which at the same time is mandatory for an early set. There may be other chemical additives unknown to the author which bind free lime upon dehydration.

However, the foregoing explanation is not entirely satisfactory because there remains to explain the consistent failures of portland mixes during the reheating at 1500 F where between cycles temperatures in the furnace did not drop below 300 F, which is too high for rehydration. Therefore another mechanism of failure is suggested, which is based on the mineral inversion of calcium orthosilicate Ca_2SiO_4, another hydraulic bonding agent of portland cement. It crystallizes in three distinct forms, the α, β, and γ forms. The changes are reversible according to the following formula

$$\alpha - Ca_2SiO_4 \overset{1250\ F}{\rightleftharpoons} \beta - Ca_2SiO_4 \overset{2600\ F}{\rightleftharpoons} \gamma - Ca_2SiO_4$$

The transformation of the β to the α form in cooling is attended by an expansion of about 10 per cent. This volume change develops the disruptive force shattering the specimen.

S. Zerfoss and H. M. Davis report that the inversion takes place spontaneously and is autocatalytic. The low-temperature α form does not possess the property of rehydration. This is contrary to free lime. The inversion initiates at some flaw in the lattice; it then proceeds autocatalytically from grain to grain until the whole mass is inverted. To invert, the grain must expand the surrounding material. No material could withstand the enormous total pressure of the inverting grains. This pressure, however, is not developed instantaneously but rather progressively. Any original restraint which is capable of withstanding the initial pressure will physically prevent the inversion from initiating. For instance, if the specimen is heated to the point of vitrification, which apparently starts around 1750 F, the surrounding vitreous material can provide the necessary isolation and restraint to inhibit inversion. Otherwise at 1500 F with dehydration rather complete and no ceramic bond initiated, resistance against inversion is practically nonexistent.

Besides physical inhibition there are chemical inhibitors as P_2O_5, B_2O_3, etc. Only a few per cent of these inhibitors are necessary to be effective. This was accidentally discovered when it was observed that slag of steel furnaces, which generally "dusted," did not disintegrate when it contained P_2O_5.[4]

Conclusions. The failures of Portland-type mixes can thus be ascribed to two possible causes, excess of free lime and mineral inversion of calcium orthosilicate. Both failures can be prevented (1) by increasing the fraction of calcium aluminates and low water-mixing ratio, and (2) by adding chemical inhibitors, as P_2O_5, B_2O_3. The dangerous temperature range is between 1300-1500 F. Failures are unlikely in hot conditions but, if at all, will rather occur during cooling. The worst condition appears to be reheating between a lower temperature and 1500 F.

The test revealed that there were two materials which appeared to be free of the usual shortcomings attributed to Portland-type cements.

It seems to be safe to state, that the regular calcium-silicate cement is not a satisfactory refractory cement unless a big fraction of calcium aluminates is added. Thus the difference disappears and the question arises when to call a cement a Portland type (calcium silicate) or an aluminous type (calcium aluminate).

Discussion

J. F. Wygant.[5] The authors have done a service to the petroleum industry in calling attention to the distinctions which exist among castable refractories, and to some of their characteristics which require experienced engineering judgment for their proper use. This work confirms earlier investigations of carbon disintegration of fireclay brick in the presence of hydrocarbons.[6] Considerable evidence exists that iron carbides, usually formed from reducible iron oxides, are the catalysts for the reaction. The role of sulphur and sulphates in suppressing the reaction has been investigated quite recently.[7] Appendix 1 therefore might be considered more than a tentative explanation.

It should not be inferred that all other hydrocarbons behave as

[4] See reference (8) at the end of the paper.

[5] Section Head, Standard Oil Company (Indiana), Whiting, Ind.

[6] "A Study of the Effect of Natural Gas and of Hydrogen Upon Various Refractories," by B. C. Ruprecht, R. H. Pierce, and F. A. Harvey, *Journal of the American Ceramic Society*, vol. 17, 1934, pp. 185–193.

"Studies on Effect of Methane," by E. Rowden and A. T. Green, Trans. British Ceramic Society, vol. 38, no. 7, 1939, pp. 418–424.

"A Study of Effect of Ethylene on Refractory Materials—Part 4," by E. Rowden, Trans. British Ceramic Society, vol. 39, no. 9, 1940, pp. 266–278; vol. 43, no. 7, 1944, pp. 105–130.

[7] "Effect of Impurities in Carbon Monoxide and in Iron Oxide on Deposit of Carbon and Formation of Hagg Carbide," by T. F. Berry, R. N. Ames, and R. B. Snow, Paper No. 6, Refractories Division, Annual Meeting of the American Ceramic Society, 1954.

methane does in causing carbon disintegration. Ethylene, for example, apparently does not.[4] Instances of this type of failure in refinery equipment are rare, although one such occurrence recently has been identified without much doubt. It took place at about 1300 to 1350 F, and was distinct from the normal deposition of coke in refractory-vessel linings.

The writer does not agree that there is little distinction between Portland and aluminous cements. ASTM Designation C-150 limits the calculated tricalcium-aluminate (C_3A) content of Type III (high early strength) Portland to a maximum of 15 per cent, rather than a minimum as construed by the authors. This is because C_3A has a very high heat of hydration and tends to cause flash setting. Actually, the average calculated C_3A contents of normal (Type I) and high early strength Portland cements are almost identical, at about 11 per cent.[5] Both have about the same setting time, controlled by additions of calcium sulphate, and the initial set is due primarily to calcium silicates. Tricalcium aluminate does not exist in any appreciable quantities in aluminous cements (although $C_3A \times H_2O$ is a hydration product), and C_3A is not considered to be a good cementing compound. On these points, the authors' analogy breaks down. An examination of the phase relationships in the $CaO - SiO_2 - Al_2O_3 - H_2O$ and related (e.g., hydrogarnet) systems indicates quite clearly that the similarity between siliceous and aluminous hydraulic cements is primarily one of hydration kinetics and physical states of the hydration products. There is little duplication of chemical compounds. Other research on the behavior of these cements at elevated temperatures confirms the authors' conclusion that the dehydration, fusion, shrinkage, and other properties are quite dissimilar.

Since indiscriminate substitution of Type III Portland cement for aluminous cements could be disastrous in many cases, it seems imperative to distinguish clearly between them.

[5] "The Chemistry of Portland Cement," by R. H. Bogue, Reinhold Publishing Corporation, New York, N. Y., 1947.

Authors' Closure

In general, the authors agree with Mr. J. F. Wygant's comments. They are grateful to learn about literature references reporting similar experiences with carbon disintegration resulting from the cracking of methane. It is correct that in the subject tests when the gas composition resulted in methane cracking, the iron oxides were converted into metallic FeC. However, at lower temperatures and with a gas composition favoring CO cracking, the same iron oxides would be reduced to a metallic-iron catalyst. Other effective catalysts, but unlikely to be found in castable refractories, are copper, nickel, cobalt, and zinc.

Finally, the reviewer comments at length on two sentences in Appendix 2, which contained an error regarding the percentage of tricalcium aluminate as well as its significance in Portland cement. The authors regret that this caused a misleading interpretation of their views on calcium-silicate cement as a constituent of refractory castables. Reference is therefore made to the text of the paper where the inherent merits and shortcomings of calcium-silicate versus calcium-aluminate binders are compared and the best service applications pointed out.

Yield and Bursting Characteristics of Heavy-Wall Cylinders

By J. H. FAUPEL,[1] WILMINGTON, DEL.

Data obtained from nearly 100 static cylinder tests under internal pressure have been examined statistically and design formulas proposed for elastic-breakdown pressure and bursting pressure. The formulas are reliable within ±15 per cent of the observed value on a 90 per cent certainty basis.

Nomenclature

The following nomenclature is used in the paper:

K = efficiency of longitudinal seam in vessel, per cent
P = maximum design pressure (ASME Code), psi
R = cylinder-wall ratio, b/a
S = allowable working stress (ASME Code), psi
a = bore radius of hollow cylinder, in.
b = radius to outside of cylinder, in.
d = inside diameter of cylinder, in
ln = symbol for natural logarithms
p = internal pressure in cylinder, psi
p_b = bursting pressure of cylinder, psi
p_y = elastic-breakdown pressure in cylinder, psi
r = variable radius in cylinder, in.
t = cylinder-wall thickness, in.
σ_h = hoop stress in cylinder, psi
σ_h' = residual hoop stress in cylinder, psi
σ_r = radial stress in cylinder, psi
σ_u = ultimate tensile strength, psi
σ_y = yield strength in tension (0.01 per cent offset or lower yield strength for p_y calculation and 0.20 per cent offset or lower yield strength for p_b calculation), psi
σ_z = longitudinal stress in cylinder, psi
σ_z' = residual longitudinal stress in cylinder, psi
μ = Poisson's ratio (also symbol for "micro" as in microinches per in. strain)

Introduction

During the past 7 years, nearly a hundred heavy-wall cylinders have been tested to bursting at the Engineering Research Laboratory of the author's company. The heavy-wall cylinders were constructed of plain-carbon steel, various low-alloy steels, various stainless steels, and aluminum bronze, Table 1. The materials covered a range of mechanical properties as follows: Ultimate strength, 66,000 to 188,000 psi; transverse ductility (elongation in 1 in.), 4–66 per cent; and longitudinal ductility (elongation in 2 in.), 12–83 per cent. As a result of the work, formulas have been developed which predict elastic-breakdown pressure and bursting pressure for static loading. These predictions are based on a mathematical theory which uses the results of tensile tests made on small specimens of the cylinder material. For the most part, the new design formulas developed are corrected or modified versions of previously existing equations. Thus the basic theories have only been modified to meet the requirements of commercial materials.

The work reported in this paper deals primarily with the yield and bursting characteristics of monobloc, initially stress-free, heavy-wall cylinders in the temperature range 75–660 F. Work has already been reported on cylinders containing residual stresses imparted (*a*) by heat-treatment,[2] (*b*) by shrink-fitting,[3] and (*c*) by autofrettage.[2,4]

Design Considerations

For cylinders operating below a temperature of about 650 F but above room temperature, reliance is commonly placed on data obtained from short-time tensile tests of the material. Above a temperature of about 650 F, use of the mechanical strength of the material, as determined by short-time tensile tests, may give rise to inadequate design, since creep may occur; consequently, at temperatures over about 650 F time as well as load becomes important and design must be based on creep and stress-rupture data.

Elastic-Breakdown Pressure. For heavy-wall cylinders with uniform wall temperature below the creep range the elastic-breakdown and bursting pressure can be predicted to at least ±15 per cent of the true value on a 90 per cent certainty basis. In the formulas the values of yield and ultimate tensile strength used are those obtained on specimens of the cylinder material at the temperature in question.

Consider Fig. 1 which indicates the cylinder geometry. The dimensions have been chosen to facilitate analyses for both thick and thin-wall vessels. Based on this geometry wall stresses developed in the elastic range for the internal-pressure condition are

$$\sigma_h = \frac{p}{R^2 - 1}\left[1 + \frac{b^2}{r^2}\right] \quad [1]$$

$$\sigma_r = \frac{p}{R^2 - 1}\left[1 - \frac{b^2}{r^2}\right] \quad [2]$$

$$\sigma_z \text{ (open ends)} = 0 \quad [3]$$

$$\sigma_z \text{ (closed ends)} = \frac{p}{R^2 - 1} \quad [4]$$

$$\sigma_z \text{ (restrained ends)} = \frac{2\mu p}{R^2 - 1} \quad [5]$$

When the internal pressure reaches a certain value, plastic flow of the cylinder wall begins at $r = a$, in accordance with the distortion-energy theory of failure

---

[1] Research Associate, Engineering Research Laboratory, Engineering Department, E. I. du Pont de Nemours & Co., Inc. Mem. ASME.

Contributed by the Materials Committee of the Petroleum Division and presented at the Petroleum Conference, New Orleans, La., September 25–28, 1955, of The American Society of Mechanical Engineers.

Note: Statements and opinions advanced in papers are to be understood as individual expressions of their authors and not those of the Society. Manuscript received at ASME Headquarters, January 25, 1955. Paper No 55—PET-1.

[2] "Influence of Residual Stress on Behavior of Thick-Wall, Closed-End Cylinders," by J. H. Faupel and A. R. Furbeck, Trans. ASME, vol. 75, 1953, pp 345–354.

[3] "Designing for Shrink-Fits," by J. H. Faupel, *Machine Design*, vol. 26, January, 1954, pp. 114–124.

[4] "Residual Stresses in Heavy-Wall Cylinders," by J. H. Faupel, *Journal of The Franklin Institute*, vol. 259, no. 5, May, 1955, pp. 405–419

TABLE 1 MECHANICAL PROPERTIES OF MATERIALS

A—Room-Temperature Tests

Material	Cylinder test no.	See Fig.	Longitudinal Properties: Yield strength, psi 0.01% offset	Yield strength, psi 0.20% offset	Lower yield	Ultimate strength, psi	Elong. in 2 in., per cent	Elong. at ultimate, per cent	Reduction of area, per cent	Transverse Properties: Yield strength, psi 0.01% offset	Yield strength, psi 0.20% offset	Lower yield	Ultimate strength, psi	Elong. in 1 in., per cent	Reduction of area, per cent	Charpy impact, ft-lb 70 F	Charpy impact, ft-lb 40 F
AISI 4337, heat-treatment not known, but probably quenched and tempered	1		68250	104000		118800	21		65								
AISI 3130, normalized	2				54000	94750	28		55								
AISI 4130, heat-treatment not known, but probably normalized	3				60200	91250	31		67								
Jalloy No. 3 (C-Mn-Fe alloy), normalized	4		56000	73950		98400	22		64							15.1	5.1
Jalloy No. 3, normalized	5		56000	73950		98400	22		64								
Jalloy No. 3, normalized	6		56500	73750		98750	22		60								
AISI 8630, normalized	7				62000	90480	34		64								
AISI Type 347 stainless steel, annealed	8		24600	36350		91200	58 (1 in.)		71								
AISI Type 347 stainless steel, annealed	9		24600	36350		91200	58 (1 in.)		71								
AISI Type 347 stainless steel, annealed	10		24600	36350		91200	58 (1 in.)		71								
AISI 8630, normalized	11				62000	90480	34		64								
AISI 6130, heat-treatment not known	12				64400	99100	28		60								
AISI 1030, annealed	13		22100	35400		69300	33		60	29800	36900		67400	27	45	34.4	4.75
AISI 1030, quenched, drawn at 750 F	14				64400	89100	32		69			64800	94000	14	28	51.8	18.42
AISI Type 304 stainless steel, annealed	15		26900	39000		103500	67		61								
AISI Type 304 stainless steel, annealed	16		26900	39000		103500	67		61								
AISI Type 304 stainless steel, annealed	17		29900	39000		103500	67		61								
AISI 1035 (had been proof-tested)	18		27800	38800		66600	35		57								
AISI 1035 (had been proof-tested)	19		30700	41900		70400	32		48								
AISI 1035 (had been proof-tested)	20		30700	41900		70400	32		48								
AISI 1035 (had been proof-tested)	21		30700	41900		70400	32		48								
AISI 4140, quenched, drawn at 1100 F	37	22	92500	119000		119000	31		53								
AISI Type 304 stainless steel, annealed	39		27800	35900		90100	80	50	75	27400	34300		89300	66	53	103.5	71.7
Ampco No. 15, aluminum bronze, annealed at 1650 F, heated to 1000 F, air cooled	40		31600	34200		81400	39	33	38	30800	33900		79800	28	27	13.3	11.3
AISI 1035, annealed at 1450 F	41				42400	76700	31	21	50			38600	73100	25	32	14.4	2.8
AISI 1035, quenched, drawn at 900 F	42				69600	106800	25	16	29			65600	102500	13	27	15.5	6.2
AISI 1151, quenched, drawn at 450 F	43		72300	80400		121400	16		28	71000	81000		105000	4	3	4.92	2.75
AISI 3320, quenched, tempered and quenched from 1200 F	44		58800	76000		107700	27	12	68	68800	78700		103600	18	45	48.7	37.3
AISI 3320, quenched, tempered at 950 F	45	6	120000	124500		136900	20	10	57	115800	125500		138800	16	37	2	1.6
AISI 3320, quenched, tempered and quenched from 1200 F	46		71500	81300		104700	27	13	72	75800	82500		106300	25	56	57.0	39.2
AISI 3320, quenched, tempered and quenched from 1200 F	47				84900	106100	27	12	70			85800	107300	25	55	48.2	21.8
AISI 3320, annealed at 1450 F	48				68100	107700	23	15	49			68500	112600	20	41	19.8	11.0
Mn-Mo-V, welded ends	55		77000	86000		103000	18		45								
AISI 4140, cold-worked	56				113500	116000	17		69								
Bethlehem gun steel (Cr-Ni-Mo-V) slack-quenched	72		120800	135800		149600	19		65	109800	125500		142100	12	29	14.5	8.0
Bethlehem gun steel, annealed	73				44900	87300	27		50			45300	83300	25	37	16.0	4.8
AISI 3320, quenched, tempered and quenched from 1200 F	74		66500	79000		105800	28	13	71	74300	79500		105400	24	50		
Mn-Mo-V, tube salvaged from fire at plant	76		103500	111300		120300	22		50								
Mn-Mo-V, tube salvaged from fire at plant	77		103500	106000		114500	22		52								
AISI 4140, quenched and tempered, shrink-fit construction	79		138000	156000		162300	17		55								
AISI 4140, quenched and tempered	80		138000	156000		162300	17		55								
AISI 1025, drawn tubing	82		80000	80000		90000	15		45								
AISI 3320 centrifugal casting, quenched and tempered	83	9	109700	112700		129600	16		39	110300	114800		124800	16	48	3.5	
Bethlehem gun steel, quenched and tempered	84	10								125000	149000		163000	12	36	9.3	4.5
Bethlehem gun steel, quenched and tempered, autofrettaged	85	11								133000	149000		164000	11	33	9.3	4.5
Bethlehem gun steel, quenched and tempered, shrink-fit	86	12							(shell)	125000	140000		153000	12	35		
									(liner)	103000	111000		128000	15	43		
Bethlehem gun steel, quenched and tempered	87	13								113000	122000		131000	14	43		
Bethlehem gun steel, quenched and tempered, autofrettaged	88	14								113000	122000		131000	14	43		
Bethlehem gun steel, quenched and tempered, shrink-fit	89	15							(shell)	125000	130000		143000	16	55		
									(liner)	103000	111000		128000	15	43		
AISI 4340 + V, quenched and tempered	90											90000	111700	15	28	32.5	
AISI 4340 + V, quenched and tempered	91											94600	114400	15	36	34.9	
AISI 4340 + V, quenched and tempered	92				94000	112800	21		66			89900	111900	16	45	32.5	
AISI 4340 + V, quenched and tempered	93				100000	115900	22		67			94400	113300	15	40	34.0	
Bethlehem gun steel, annealed	94		43000	48000		96400	23		48	47000	47800		93100	16	23		
Bethlehem gun steel, quenched, tempered, and quenched from 1000 F	95		155500	174000		187700	18 (1 in.)		61	141200	159800		177500	9	20		
AISI 4340, quenched and tempered	96											121400	124600	22	50		
AISI 4340, quenched and tempered	98											121400	124600	22	50		

TABLE 1 (*Continued*) MECHANICAL PROPERTIES OF MATERIALS

A—Room-Temperature Tests

Material	Cylinder test no.	See Fig.	Longitudinal Properties: Yield strength, psi 0.01% offset	0.20% offset	Lower yield	Ultimate strength, psi	Elong. in 2 in., per cent	Elong. at ultimate, per cent	Reduction of area, per cent	Transverse Properties: Yield strength, psi 0.01% offset	0.20% offset	Lower yield	Ultimate strength, psi	Elong. in 1 in., per cent	Reduction of area, per cent	Charpy impact, ft-lb 70 F	40 F
AISI Type 304 stainless steel, annealed	100		24300	30500		83500	83		80	22100	28200		85000	82	72		
AISI Type 316 stainless steel, annealed	104		82800	127500		152000	12		52								
AISI 4340, quenched, drawn at 1200 F	105	16	97500	103600		124500	24		63	99400	103900		124100	16	31		
AISI 4340, quenched, tempered, and quenched from 1200 F	106	17	97000	103000		124000	24		65	94500	101900		123900	19	42		
AISI 4340, normalized, drawn at 1200 F	107	18	82500	86300		114900	24		59	83400	86500		115300	17	33		
AISI 1045, quenched, drawn at 800 F	108	19	63000	63800		103400	25		52	61400	62900		103100	18	27		
AISI 1045, quenched, drawn at 800 F, plugged end hollow cylinder	109	20	60800	62000		102900	24		51	57500	60900		101800	18	28		
AISI 1045, quenched, drawn at 800 F, surface-bore quenched	110	21	78600	82000		124200	20		47	76800	81600		122200	13	28		
AISI Type 316 stainless steel, annealed	111		72500	121500		146000	16		50								
AISI Type 410 stainless steel, drawn 1000 F	135			118400		135300	12		49								
AISI Type 410 stainless steel, drawn 1000 F	136			119200		139300	13		49								
AISI Type 410 stainless steel, drawn 1100 F	137			100400		120600	15		54								
AISI Type 410 stainless steel, drawn 1100 F	138			100000		121400	15		53								
AISI Type 410 stainless steel, drawn 1200 F	139			85600		105400	19		60								
AISI Type 410 stainless steel, drawn 1200 F	140			84500		106600	17		54								
Mn-Mo-V + Lan-Cer-Amp, thermit welded tube	128*		62000	81500		108500	7 (1 in.)		12								
Nickel-lined Mn-Mo-V tubing	28		83500	93000		93000	33		53								
Nickel-lined Mn-Mo-V tubing	29		67000	88300		89000	34		54								
Nickel-lined Mn-Mo-V tubing	31		76500	121000		128000	23		51								
Nickel-lined Mn-Mo-V tubing	32		39000	56500		72000	44		68								
Nickel-lined Mn-Mo-V tubing	26		77700	95200		103500	26		51								
B—Elevated-Temperature Tests																	
AISI 4140, quenched, drawn 1100 F, tested 570 F	56	27	71500	91500		112000	17		57								
AISI 4140, quenched, drawn 1100 F, tested 570 F	57	26	71500	91500		112000	17		57								
AISI 4140, quenched, drawn 1100 F, tested 660 F	58	28	61200	86500		106000	17		65								
AISI 4140, quenched, drawn 1200 F, tested 300 F	70	25	59500	73500		115000	17		60								
Mn-Mo-Cr steel, quenched, drawn 1100 F, tested 400 F	119	23	83000	99000		115000											
Mn-Mo-Cr steel, quenched, drawn 1100 F, tested 400 F	120	24	83000	99000		115000											

* After burst test.

9% (1 in. ultimate) 12% (at ultimate)

9% (1 in. ultimate) 12% (at ultimate)

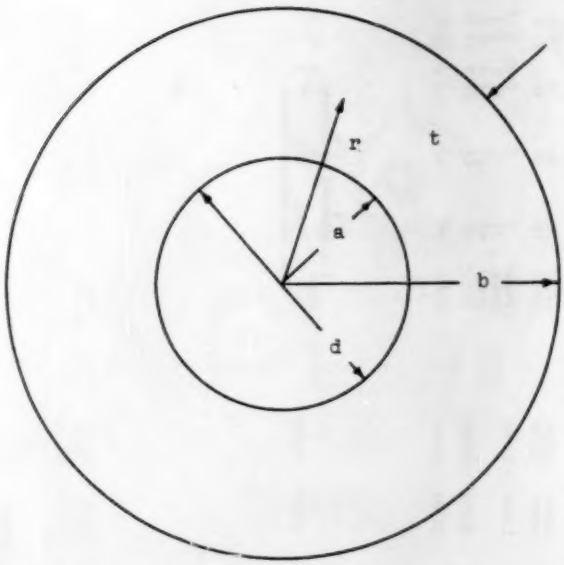

FIG. 1 GEOMETRY OF CYLINDER

$$\sigma_y^2 = \sigma_h^2 + \sigma_r^2 + \sigma_a^2 - \sigma_h\sigma_r - \sigma_r\sigma_a - \sigma_a\sigma_h \quad [6]$$

Substituting the maximum values ($r = a$) of Equations [1] to [5] into Equation [6] gives three formulas for the yield or elastic-breakdown pressure, p_y

$$p_y \text{ (open ends)} = \frac{\sigma_y(R^2 - 1)}{\sqrt{3R^4 + 1}} \quad [7]$$

$$p_y \text{ (closed ends)} = \frac{\sigma_y}{\sqrt{3}}\left[\frac{R^2 - 1}{R^2}\right] \quad [8]$$

$$p_y \text{ (restrained ends)} = \frac{\sigma_y(R^2 - 1)}{\sqrt{(3R^4 + 1) + 4\mu(\mu - 1)}} \quad [9]$$

The hoop and radial stresses are independent of the end conditions of the cylinder and the longitudinal stress is always intermediate to these stresses. For initial yielding the open-end cylinder yields first; however, the differences between the pressures predicted using Equations [7], [8], or [9] are small, particularly for wall ratios greater than about 2.00; and for engineering work the differences are inconsequential. All tests described in this paper were conducted on closed-end cylinders so that the formula substantiated and recommended is given by Equation [8].

If residual stresses are present in the cylinder they will contribute to the elastic-breakdown pressure[3] and must be included in the analysis. Such stresses are added to those given by Equations [1] to [5] and the elastic-breakdown pressure is then calculated from the quadratic

$$p_y^2\left[\frac{R^2}{R^2 - 1}\right]^2 + p_y\left[\frac{R^2}{R^2 - 1}\right]\sigma_h' + \frac{1}{3}\left[(\sigma_z')^2 + (\sigma_h')^2 - \sigma_z'\sigma_h' - \sigma_y^2\right] = 0 \quad [10]$$

Bursting Pressure. The theoretical prediction of bursting pressure received considerable attention in this investigation and a formula was developed for predicting this pressure. It is postulated that, if the cylinder wall yields at constant stress, as stated by classical plasticity theory, it will burst at the pressure required to overstrain the wall; that is, the lower limit would be

$$p_b = \frac{2\sigma_y}{\sqrt{3}} \ln R \quad [11]$$

If the ratio of the tensile yield strength σ_y, to the tensile ultimate strength, σ_u, were unity, bursting would occur at an upper limit defined as

$$p_b = \frac{2\sigma_u}{\sqrt{3}} \ln R \quad [12]$$

However, for yield/ultimate ratios less than unity the bursting pressure will be somewhere between the pressures defined by Equations [11] and [12]. Consequently, it is postulated that the bursting pressure will be a function of both the overstrain pressure, Equation [11], and the pressure defined by Equation [12]. Assuming direct proportionality

$$p_b = \frac{\sigma_y}{\sigma_u}\left(\frac{2\sigma_u}{\sqrt{3}} \ln R\right) + \left(1 - \frac{\sigma_y}{\sigma_u}\right)\left(\frac{2\sigma_y}{\sqrt{3}} \ln R\right)$$

which reduces to

$$p_b = \frac{2\sigma_y}{\sqrt{3}} \ln R \left[2 - \frac{\sigma_y}{\sigma_u}\right] \quad [13]$$

Effect of Wall Ratio. Some authors have reported success in predicting yielding and bursting of cylinders by using the maximum-stress theory and Equation [1], letting $r = a$. This success has usually been with thin-wall tubes of low wall ratio. However, the influence of wall ratio on calculated yield or bursting pressures is considerable. To illustrate this point, formulas have been tabulated in Table 2 and corresponding curves plotted in Figs. 2 and 3 which show how both mechanical properties and geometry influence cylinder characteristics. From the plots in Figs. 2 and 3 it is seen that as the wall ratio decreases the theories tend toward predicting the same result.

Provision is made as follows in the ASME Code for calculating the wall thickness of cylindrical vessels operating under an internal pressure of 3000 psi or less, when the shell thickness exceeds $a/2$ or when P exceeds $0.385\,SK$

$$t = a\left[\sqrt{\frac{SK + P}{SK - P}} - 1\right] \quad [14]$$

Assuming 100 per cent joint efficiency in Equation [14] (i.e., a monobloc vessel with no flanges, welds, etc.), the formula can be rewritten

$$t = a\sqrt{\frac{S + P}{S - P}} - 1 \quad [15]$$

If the allowable working stress is taken as the yield strength of the material and the maximum design pressure as the elastic-breakdown pressure, then

$$p_y = \sigma_y\left[\frac{R^2 - 1}{R^2 + 1}\right] \quad [16]$$

which is a statement of the maximum-stress theory, see Table 2, the most conservative design for a cylindrical vessel under internal pressure. Equation [16] differs from Equation [8] by a factor

$$\frac{R^2 + 1}{\sqrt{3}}\left(\frac{1}{R^2}\right)$$

which approaches $1/\sqrt{3}$ as the wall ratio increases.

TABLE 2 YIELD AND BURSTING-PRESSURE FORMULAS FOR CLOSED-END TUBES

Theory	Yield Pressure	Reference	Bursting Pressure	Reference
Thin wall				
$S = \frac{pd}{2t}$	$p_y = \frac{2\sigma_y t}{d} = \sigma_y(R-1)$	Fig. 2, Plot A	$p_b = \frac{2\sigma_u t}{d} = \sigma_u(R-1)$	Fig. 3 Plot A
Thin wall				
$\sigma_h = \frac{pd}{2t}$ $\sigma_z = \frac{pd}{4t}$ $\sigma_r \approx -\frac{p}{2}$ + Eq. [6]	$p_y = \frac{4\sigma_y\left(\frac{t}{d}\right)}{\sqrt{3 + 6\frac{t}{d} + 4\frac{t^2}{d^2}}}$	Fig. 2, Plot B	$p_b = \frac{4\sigma_u\left(\frac{t}{d}\right)}{\sqrt{3 + 6\frac{t}{d} + 4\frac{t^2}{d^2}}}$	Fig. 3, Plot D
	or $p_y = \frac{2\sigma_y(R-1)}{\sqrt{R^2+R+1}}$	Fig. 2, Plot B	or $p_b = \frac{2\sigma_u(R-1)}{\sqrt{R^2+R+1}}$	Fig. 3, Plot D
Thick wall				
Max. value of Equation [1]	$p_y = \sigma_y\left(\frac{R^2-1}{R^2+1}\right)$	Fig. 2, Plot C	$p_b = \sigma_u\left(\frac{R^2-1}{R^2+1}\right)$	Fig. 3, Plot F
Thick Wall				
Equation [8] or [13]	$p_y = \frac{\sigma_y}{\sqrt{3}}\left(\frac{R^2-1}{R^2}\right)$	Fig. 2, Plot D	$p_b = \frac{2\sigma_y}{\sqrt{3}} \ln R\left(2 - \frac{\sigma_y}{\sigma_u}\right)$	Fig. 3, Plots B, C, E, G

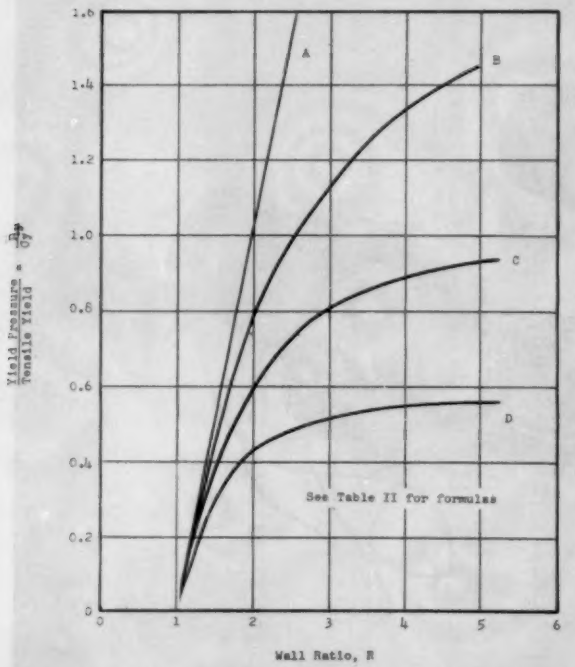

FIG. 2 COMPARISON OF METHODS USED TO PREDICT INITIAL YIELDING IN CYLINDERS

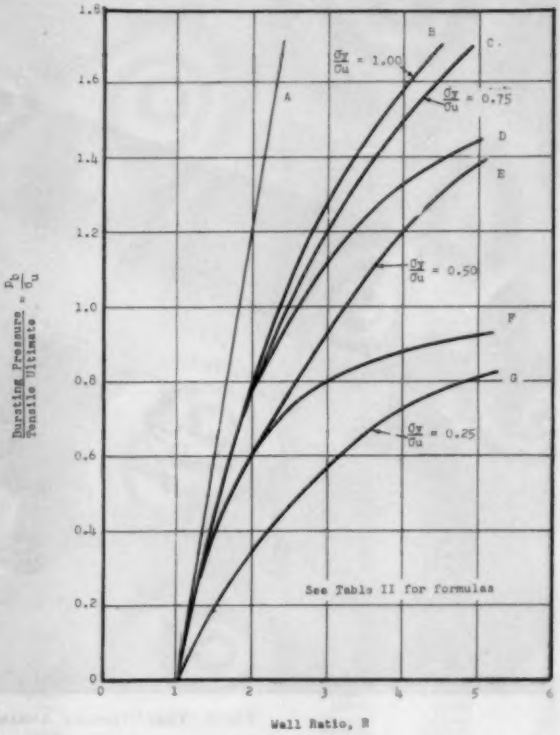

FIG. 3 COMPARISON OF METHODS USED TO PREDICT BURSTING OF CYLINDERS

EXPERIMENTAL PROGRAM

Internal-Pressure Testing. The general test-cylinder arrangement is shown in Fig. 4. Cylinders varied in size, and the geometry shown in Fig. 4 varied correspondingly. Hydrostatic internal pressure was applied to the cylinders after attaching several SR-4 electrical resistance strain gages on the outside surface of the cylinders in both the hoop and longitudinal directions. Cylinders tested above room temperature were equipped with several Baldwin EBD-1S bakelite, 350-ohm self-compensated electrical strain gages and heating of the cylinder was uniformly (±5 deg F) controlled by induction coils mounted on transit pipe, Fig. 5.

Strains were recorded for small increments of pressure. Pressures were determined at initial yielding of the cylinder at the bore and at bursting. Initial yielding of the bore of the cylinder

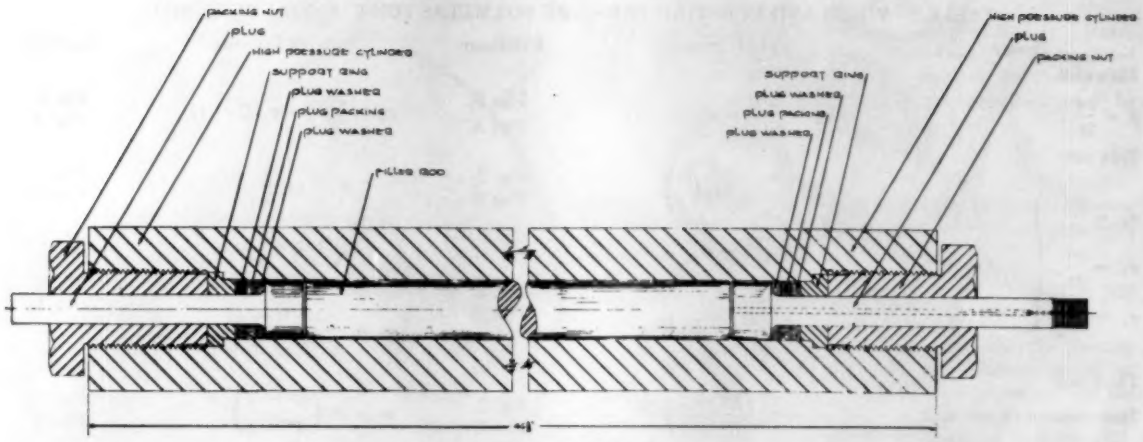

FIG. 4 HIGH-PRESSURE TEST ASSEMBLY

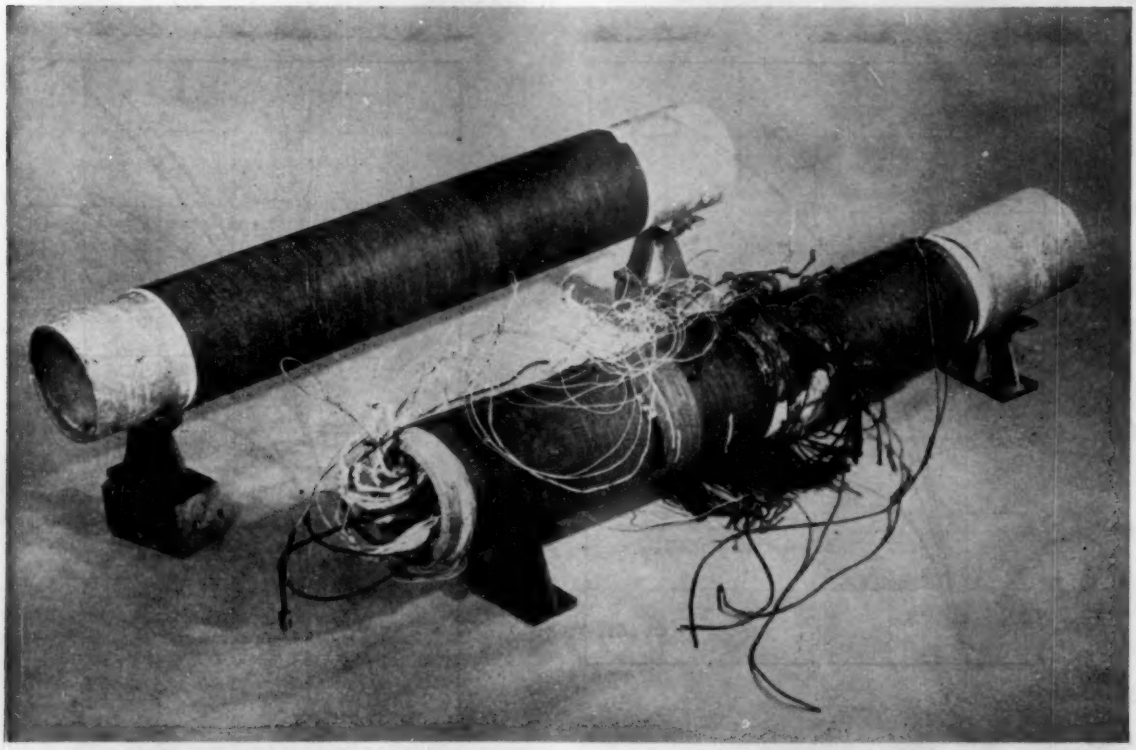

FIG. 5 TEST-CYLINDER ARRANGEMENT—HIGH TEMPERATURE
(Before and after test.)

was taken as the end of the straight-line portion of the pressure-hoop strain curve. Because of this, the correlation value from the tensile test, σ_y, was taken as the 0.01 per cent offset yield strength, or the lower yield-strength (point), if such existed. Actually the elastic limit in tension should be used, but this is usually too difficult to obtain from the stress-strain curve. The bursting pressure recorded was the maximum pressure reached within the cylinder before failure. As explained later, the correlation value from the tensile test, σ_y, was taken as the 0.20 per cent offset yield strength, or the lower yield point, if one existed.

Testing of the cylinders was done by raising the pressure to a predetermined level and holding it constant while recording the data from the strain gages. Strain data were recorded at 2000-psi intervals in the elastic range and at 1000-psi intervals in the plastic range.

When testing cylinders in the plastic range, it was necessary to

increase the time between readings to allow the material to work-harden and reach equilibrium at each pressure for which strain data were recorded. At increments of 1000 psi 1/2 to 3/4 hr was required between readings. This rate of strain is much lower than that used in the tensile tests, where a rate of 20,000 microinches/min was used. For a ductile cylinder, approximately 6 to 8 hr were required to complete a test after initial yielding of the bore.

Internal pressure-external strain curves were plotted from the data recorded. Several of these curves plus some photographs of the burst cylinders are reproduced in this paper in Figs. 6 to 28.

Analysis of Data. All cylinders tested were of the closed-end type; consequently the elastic-breakdown pressure for cylinders initially stress-free is given by Equation [8]. For the case of pre-stressed cylinders, as mentioned earlier, initial yielding is influenced by the presence of residual stresses at the bore of the cylinder, and yielding is calculated in accordance with Equation [10].

Values of calculated and observed elastic-breakdown pressures are given in Table 3 for room-temperature tests and in Table 4 for elevated temperature tests. Calculated values were obtained from either Equation [8] or [10], depending on the circumstances; the observed values, for comparison, were obtained by noting the end of the straight-line portion of the cylinder pressure-strain curve, for example, Curve B in Fig. 6. In several cases in Table 3

TABLE 3 RESULTS OF CYLINDER TESTS (ROOM TEMPERATURE)

Test no.	Fig. no.	OD, in.	ID, in.	Wall ratio	Length, in.	Cylinder Test Data[a] Elastic-breakdown pressure at bore, psi			Bursting pressure, psi		
						Observed	Calculated	Deviation, per cent	Observed	Calculated	Deviation, per cent
1		4.34	1.76	2.47	24	40000			85000		
2		3.75	1.50	2.50	12	25000	26200	+5	76500	81800	+7
3		3.75	1.50	2.50	12	30000	29200	−3	82000	85500	+4
4	8	3.75	1.50	2.50	47	25000	27200	+9	91000	97400	+7
5		3.75	1.50	2.50	47	30000	27200	−7	86000	97400	+13
6		3.75	1.50	2.50	47	25000	27400	+10	87000	97600	+12
7		3.74	1.50	2.49	47	28000	30000	+7	79000	85700	+9
8		1.75	0.77	2.27	12	19000			59000	54800	−7
9		1.77	0.77	2.31	36	15000			53000	56400	+6
10		1.77	0.81	2.19	30	12000			56000	52600	−6
11		3.74	1.49	2.51	47	28000	30200	+8	No Burst		
12		3.79	1.50	2.53	12	32000			89000	93400	+5
13		4.28	1.76	2.43	36	12000	10600	−12	57000	54000	−5
14		4.28	1.75	2.44	36	25000			83000	84700	+2
15		0.7535	0.3845	1.96	30	9000			45000	49300	+10
16		0.7538	0.3845	1.96	30	8000			44000	49400	+12
17		0.7533	0.3834	1.97	30	7500			47000	49400	+5
18		0.8804	0.3743	2.32	30	15000			50000	53500	+7
19		0.8756	0.3800	2.30	30	18000			51000	56600	+11
20		0.7499	0.3765	1.99	30	16000			43000	46800	+9
21		0.7505	0.3801	1.97	30	18000			43000	46250	+8
26		1.254	0.511	2.45	30	30000			88000		
28		1.251	0.514	2.43	30	25000			85000	95500	+12
29		1.252	0.515	2.43	30	15000			87000	91500	+5
31		1.252	0.514	2.44	20	17500			127500	131000	+3
32		1.251	0.514	2.43	20	5000			65000	70500	+8
37	22	1.50	0.50	3.00	24	45000	47500	+6	138000	143500	+4
39		4.127	1.50	2.75	46	9000			63000	67400	+7
40		4.130	1.498	2.76	34	18000			55000	63000	+15
41		4.120	1.50	2.75	46	21000			67500	66500	−2
42		4.095	1.509	2.74	46	25000			98500	111300	+13
43		7.130	1.539	4.63	46	25000			No Burst		
44		2.620	1.501	1.75	46	20000			59000	63000	+7
45	6	4.130	1.502	2.75	46	57000			143000	158500	+11
46		5.625	1.525	3.69	46	26000			168000	152000	−10
47		7.112	1.509	4.71	46	27500			192500	184000	−4
48		4.125	1.502	2.75	46	28000			98000		
55		7.50	3.00	2.50	40	35000			99000	106000	+7
56		1.50	0.50	3.00	15				128000	142700	+12
72		4.129	1.503	2.75	46	60000			162000	164000	+1
73	7	4.126	1.503	2.75	46	20000			81000	83700	+3
74		4.125	1.504	2.74	46	21000			106000	115700	+9
76		2.641	1.013	2.61	18	40000			115000	132700	+15
77		2.639	1.005	2.62	18	40000			110000	126500	+15
79		1.498	0.495	3.026	12	50000			177000	207500	+17
80		1.500	0.492	3.047	8				200000	209000	+5
82		0.734	0.125	5.86	12	45000			161000	182000	+13
83	9	4.500	1.566	2.874	46	65000			146000	151000	+3
84	10	4.128	1.501	2.75	46	65000	63000	−4	188000	189000	+1
85	11	4.128	1.501	2.75	46	65000	66700	+3	190000	188500	+1
86	12	4.128	1.498	2.756	46	76000	82000	+8	164000	159000	−3
87	13	5.502	1.377	4.00	46	65000	71000	+9	>200000	209000	
88	14	5.502	1.377	4.00	46	69000	71000	+3	>200000	209000	
89	15	5.502	1.374	4.01	46	85000	96000	+13	>200000	212000	
90		0.750	0.251	2.99	7				130000	136000	+5
91		0.750	0.251	2.99	7				126000	140500	+12
92		2.248	0.750	3.00	18				126000	136000	+8
93		6.002	2.002	3.00	45	40000			136000	140000	+3
94		2.751	1.003	2.74	15	20000			96000	83000	−14
95		2.751	1.003	2.74	15	70000			>200000	204000	
96		1.250	0.500	2.50	7	45000			117000	131500	+12
98		1.248	0.500	2.50	7	40000			118000	131500	+11
100		4.125	1.500	2.75	36	6600			59500	55000	−8
104		0.624	0.250	2.50	18				161000	155500	−3
105	16	4.128	1.502	2.75	36	45000			133000	141500	+6
106	17	4.125	1.503	2.74	36	37000			134000	152000	+13
107	18	4.123	1.497	2.75	36	43700			120000	127000	+6
108	19	4.127	1.505	2.74	36	35000			109000	102000	−6
109	20	4.126	1.50	2.75	36	21000			107000	100000	−7
110	21	4.126	1.498	2.75	36	57500			119000	127500	+7
111		0.436	0.146	2.99	11	40000			200000	179500	−10
128		2.625	1.00	2.63	18	40000	40000	0	95000	95000	0
135		0.375	0.125	3.00	10	60000			163000	169500	+4
136		0.375	0.125	3.00	10	70000			170000	173500	+2
137		0.375	0.125	3.00	10	65000			142000	143500	+1
138		0.375	0.125	3.00	10	65000			142000	149500	+5
139		0.375	0.125	3.00	10	55000			120000	129000	+8
140		0.375	0.125	3.00	10	55000			125000	129000	+3

[a] Omissions of calculated values due to inadequate mechanical-property data.

TABLE 4 RESULTS OF CYLINDER TESTS
(Elevated temperature)

Cylinder no. (also Table 1)	See Fig.	Test temp, deg F	Material	Wall ratio	Elastic-breakdown pressure, psi — Observed	Predicted	Deviation, per cent	Bursting pressure, psi — Observed	Predicted	Deviation, per cent
56	27	570	AISI-4140	3	35000[a]	36000	+3	128000	124000	−3
57	26	570	AISI-4140	3	45000[b]	47500	+6	123000	124000	+1
58	28	660	AISI-4140	3	35000	31600	−10	118000	111000	−6
70	25	570	AISI-4140	3	35000	30600	−12	118000	127000	+8
119	23	400	Chrome-moly	2.75	45000	41500	−8	126000	131000	+4
120	24	400	Chrome-moly	2.75	46000	41500	−10	132000	131000	−1

[a] At 480 F. (Cycle of pressure before final cycle at 570 F.) Observed elastic-breakdown pressure was 59,000 psi on final cycle (see note below).
[b] At 75 F. (Cycle of pressure before final cycle at 570 F.) Observed elastic-breakdown pressure was 50,000 psi on final cycle (see note below).
NOTE: Cylinders 56 and 57 were pressurized at intermediate temperatures to check dilation characteristics. Prediction of elastic-breakdown pressure on final cycle is not possible because residual stresses, and possible changes in tensile properties of the materials, were not measured following the initial pressure cycles.

TABLE 5 BURSTING DATA FOR PRESTRESSED CYLINDERS

Cylinder no.	Material	Wall ratio	Method of stressing	Observed	Calculated	Deviation from observed, per cent
18	AISI-1035	2.32	15–35% autofrettage[a]	50000	54000	+8
19	AISI-1035	2.30	15–35% autofrettage[a]	51000	57000	+11
20	AISI-1035	1.99	15–35% autofrettage[a]	43000	47000	+9
21	AISI-1035	1.97	15–35% autofrettage[a]	43000	46000	+8
74	AISI-3320	2.74	σ_h' = 35000; σ_z' = 45000[b]	106000	112000	+5
85	Beth. gun stee	2.75	57% autofrettage	190000	185000	−3
96	AISI-4340	2.50	σ_h' = 26000; σ_z' = 32000	117000	129000	+11
110	AISI-1045	2.75	σ_h' = 34000; σ_z' = 37000	119000	123000	+3

[a] Cylinder autofrettaged at 15,000 psi, which amounted to 15–35 per cent autofrettage (see footnote 4 of text).
[b] Cylinder quenched in order to induce residual hoop stress, σ_h' of 35,000 psi and residual longitudinal stress of σ_z' = 45,000 psi.

no calculation of elastic-breakdown pressure is shown; in fewer instances no observed value is given. The reason for the former is that information on the cylinder was not complete enough to justify a prediction; in the latter case, the cylinders had been proof-tested so that the fundamental elastic-breakdown pressure was not known.

A statistical analysis of the elastic-breakdown data shown in Table 3 indicated that out of 100 calculations using Equations [8] or [10], at least 10 calculations would deviate from the experimental value by more than —6.2 to +13.6 per cent. In other words, the results of theory will check the results of experiment 90 per cent of the time within —6 to +14 per cent; or, as stated in earlier papers, the formulas are good to at least ±15 per cent.

The bursting pressure has been defined as the maximum pressure sustained during a test. Observed and calculated values of bursting pressure are given in Table 3 for room-temperature tests and in Table 4 for elevated-temperature tests; calculations have been based on Equation [13]. In the initial development of the bursting-pressure formula use was made of the 0.01 per cent offset-yield-strength value from a tensile test. It was found, however, that in all cases the behavior of cylinders of austenitic stainless steels (which can undergo a phase transformation during plastic straining) could be better expressed by use of the standard 0.20 per cent offset value. Because of this situation and also because most handbooks give only the 0.20 per cent offset-yield-strength value, calculations were made on various types of steel and nonferrous cylinders using Equations [13] with σ_y as the 0.20 per cent offset yield strength, or the lower yield-strength (point), if one existed. It was found, and proved statistically, that the 0.20 per cent offset yield strength (or the lower yield point) was satisfactory for the other materials as well as for austenitic stainless steel. Consequently, for bursting-pressure calculations the 0.20 per cent offset-yield strength value, or the lower yield strength, is used in Equation [13].

A statistical analysis showed that out of 100 cylinder bursting tests 10 would be expected to fall outside the range of —4 to +15 per cent of the value predicted by the use of Equation [13]; or, as stated earlier, the bursting-pressure formula is also good to at least ±15 per cent.

The influence of residual stresses on the elastic-breakdown pressure has been discussed in previous papers and will not be repeated here. However, no mention has yet been made of the possible influence of residual stresses on bursting pressure. The data obtained suggest that bursting pressure is not influenced in any major way by the presence of residual stresses; this is illustrated in Table 5.

Photographs of several burst cylinders are included in Figs. 6 to 28. The fractures give little, if any, quantitative information. Primarily, the fractures indicate brittle or ductile failure of the cylinder. Correlation between theory and experiment did not appear to be influenced by the tendency for a cylinder to fail in either a brittle or a ductile fashion. For example, the fractures shown in Figs. 6 and 9 are brittle; the ductility reported for the cylinder materials in Table 1 indicates good tensile-test ductility but poor impact strength. Good prediction was made of bursting pressure, however. Fig. 8 also shows brittle behavior but the ductility and impact strength of the material are both fairly high. Finally, there did not appear to be any unusual differences in fractures of cylinders tested at elevated temperatures (cylinders 56, 57, 58, 70, 119, and 120). There is some indication that the ductility of the steel tested is less at elevated temperature than at room temperature, although all fractures noted were ductile and very similar to fractures of cylinders tested at room temperature.

SUMMARY

A large quantity of data has been assembled on the performance of thick-wall cylinders that were tested under internal pressure and with uniform wall temperatures that varied from ambient temperature to 660 F. Design formulas have been developed (Equations [8], [10], and [13]), for predicting the elastic-breakdown and bursting pressure of the cylinders that are reliable 90 per cent of the time to better than ±15 per cent of the observed value.

FIGURE 6

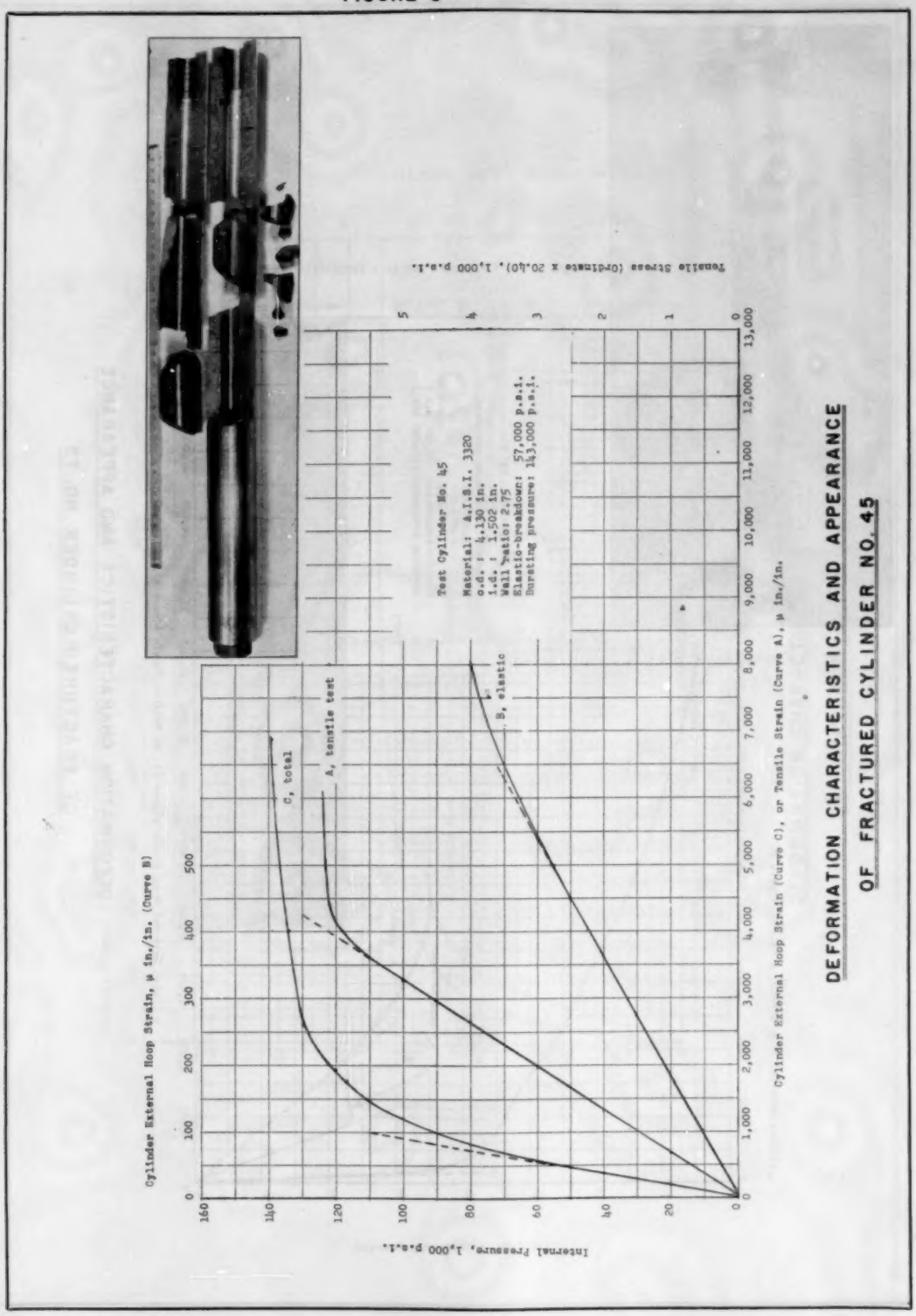
DEFORMATION CHARACTERISTICS AND APPEARANCE
OF FRACTURED CYLINDER NO. 45
Test Cylinder No. 45
Material: A.I.S.I. 3320
o.d. : 4.130 in.
i.d. : 1.502 in.
Wall ratio: 2.75
Elastic-breakdown: 57,000 p.s.i.
Bursting pressure: 143,000 p.s.i.
A, tensile test
B, elastic
C, total
Internal Pressure, 1,000 p.s.i.
Cylinder External Hoop Strain, μ in./in. (Curve B)
Cylinder External Hoop Strain (Curve C), or Tensile Strain (Curve A), μ in./in.
Tensile Stress (Ordinate x 20.40), 1,000 p.s.i.

FIGURE 7

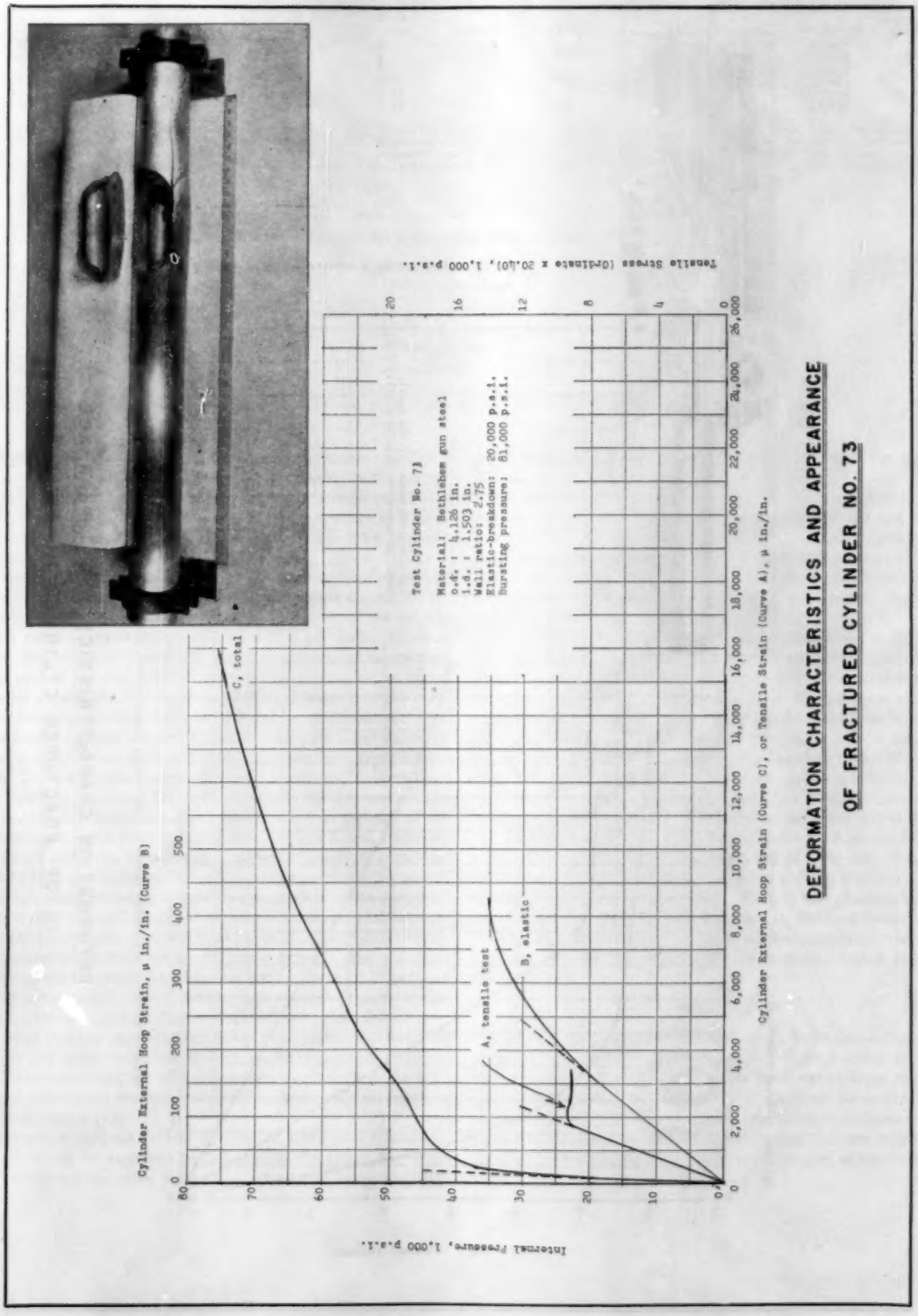

DEFORMATION CHARACTERISTICS AND APPEARANCE OF FRACTURED CYLINDER NO. 73

FIGURE 8

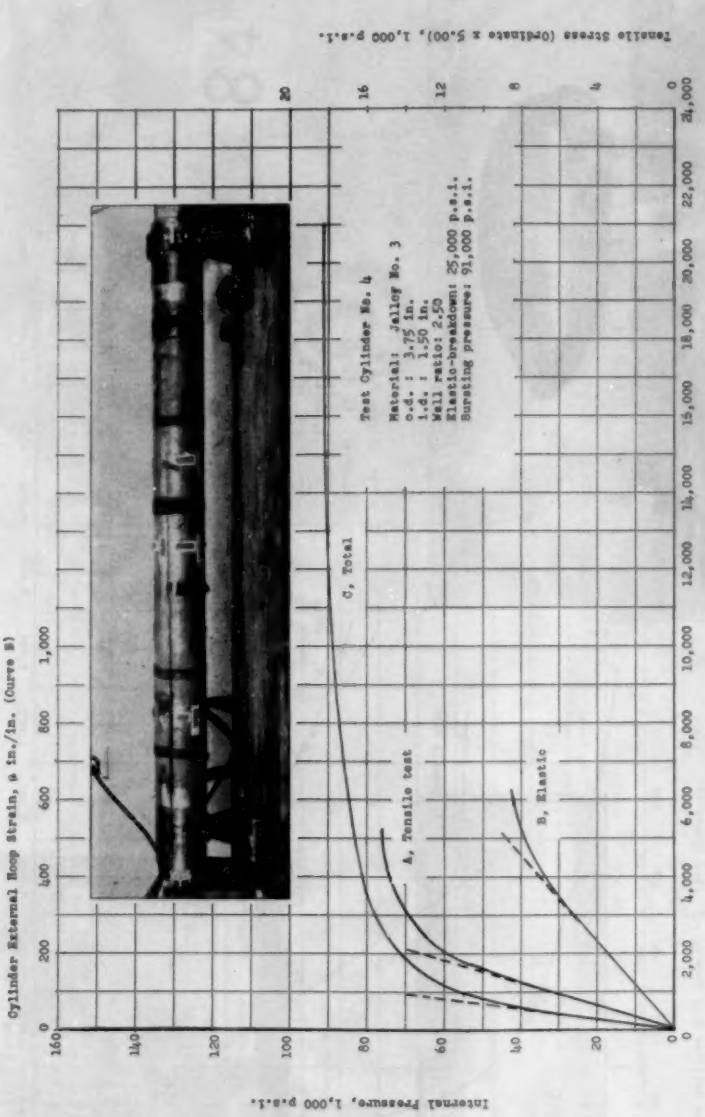

DEFORMATION CHARACTISTICS AND APPEARANCE OF FRACTURED CYLINDER NO. 4

FIGURE 9

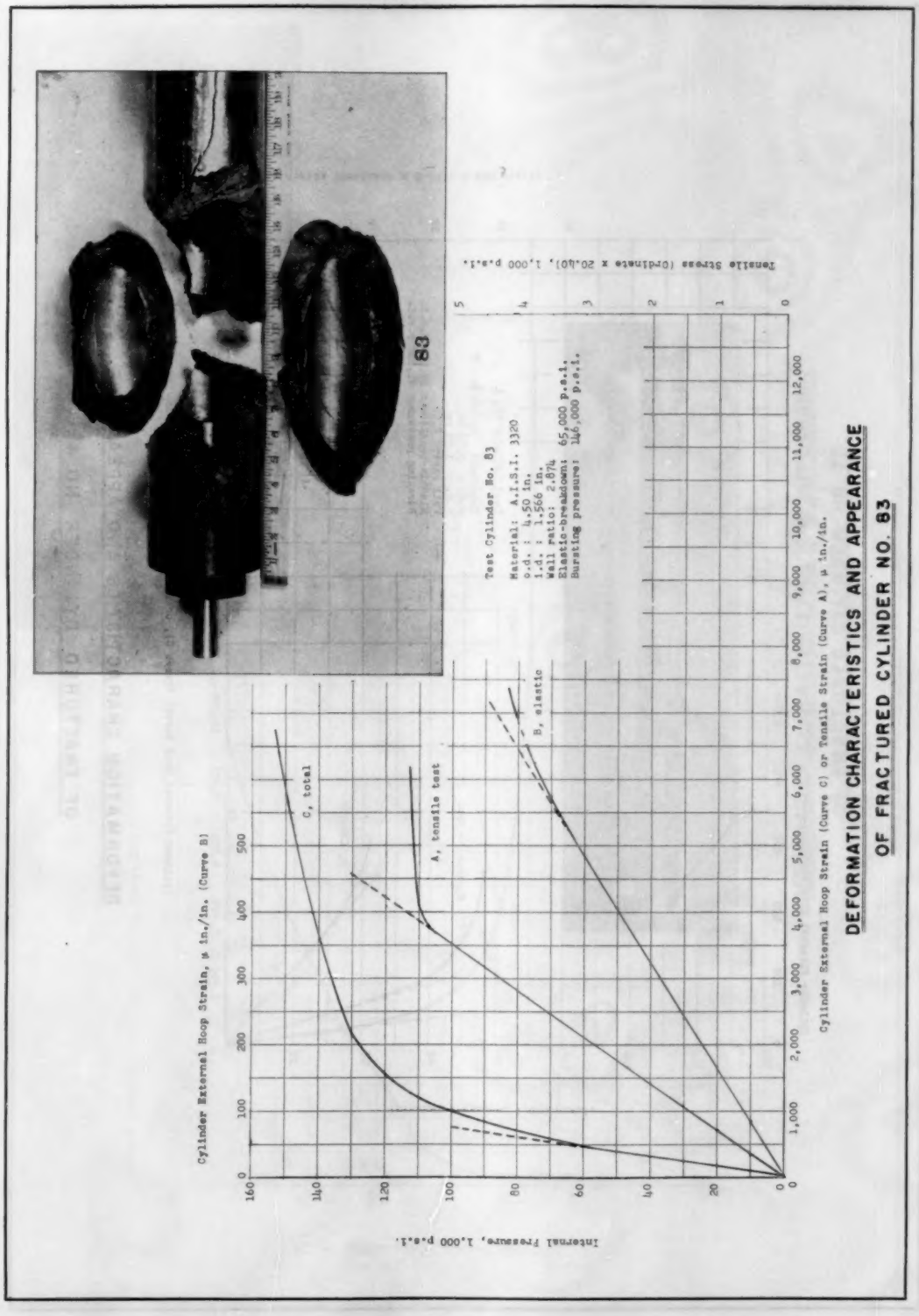
83
Test Cylinder No. 83
Material: A.I.S.I. 3320
o.d. : 4.50 in.
i.d. : 1.566 in.
Wall ratio: 2.874
Elastic-breakdown: 65,000 p.s.i.
Bursting pressure: 146,000 p.s.i.
Tensile Stress (Ordinate x 20,000), 1,000 p.s.i.
Internal Pressure, 1,000 p.s.i.
Cylinder External Hoop Strain, μ in./in. (Curve B)
Cylinder External Hoop Strain (Curve C) or Tensile Strain (Curve A), μ in./in.
C, total
A, tensile test
B, elastic
DEFORMATION CHARACTERISTICS AND APPEARANCE
OF FRACTURED CYLINDER NO. 83

FIGURE 10

DEFORMATION CHARACTERISTICS AND APPEARANCE OF FRACTURED CYLINDER NO. 84

FIGURE 11

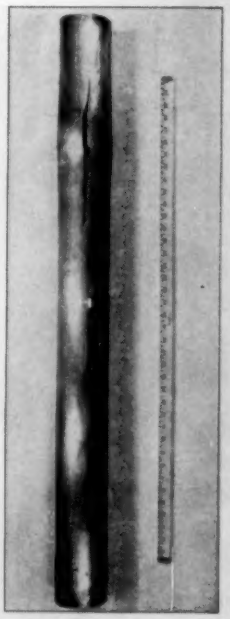

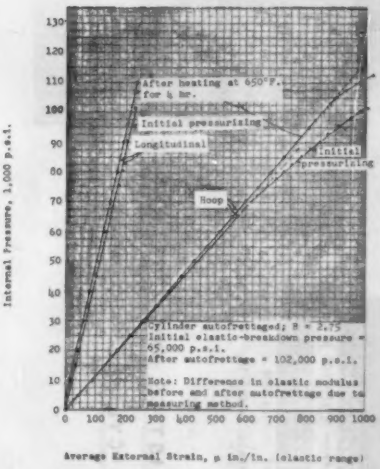

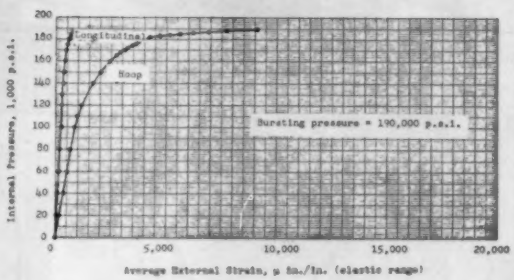

DEFORMATION CHARACTERISTICS AND APPEARANCE OF FRACTURED CYLINDER NO. 85

FIGURE 12

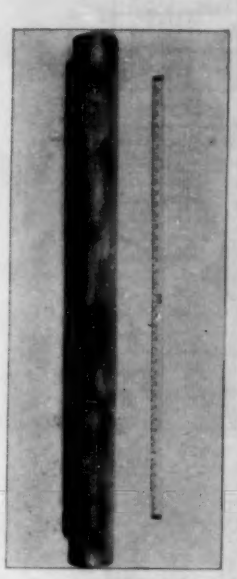

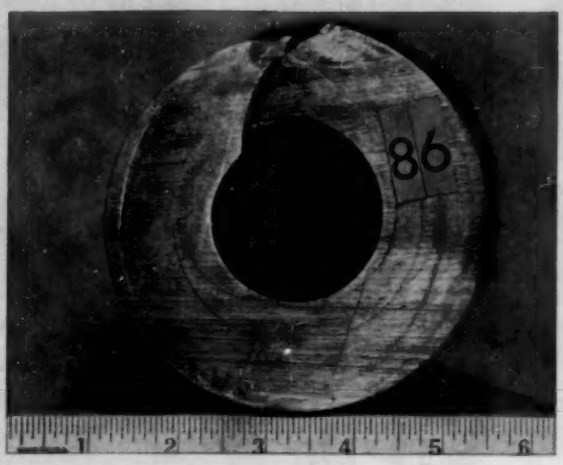

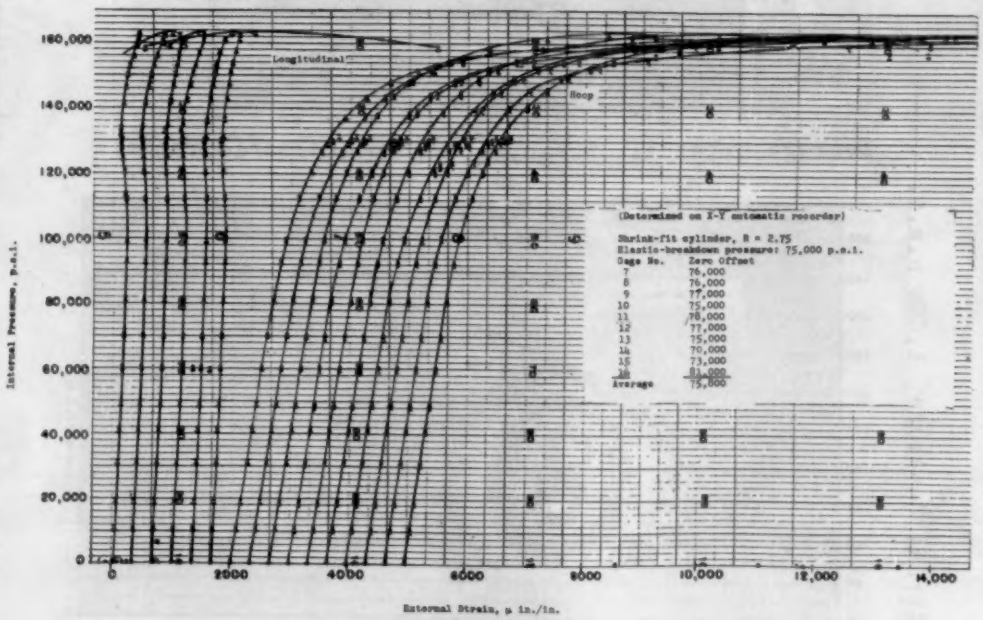

DEFORMATION CHARACTERISTICS AND APPEARANCE OF FRACTURED CYLINDER NO. 86

FIGURE 13

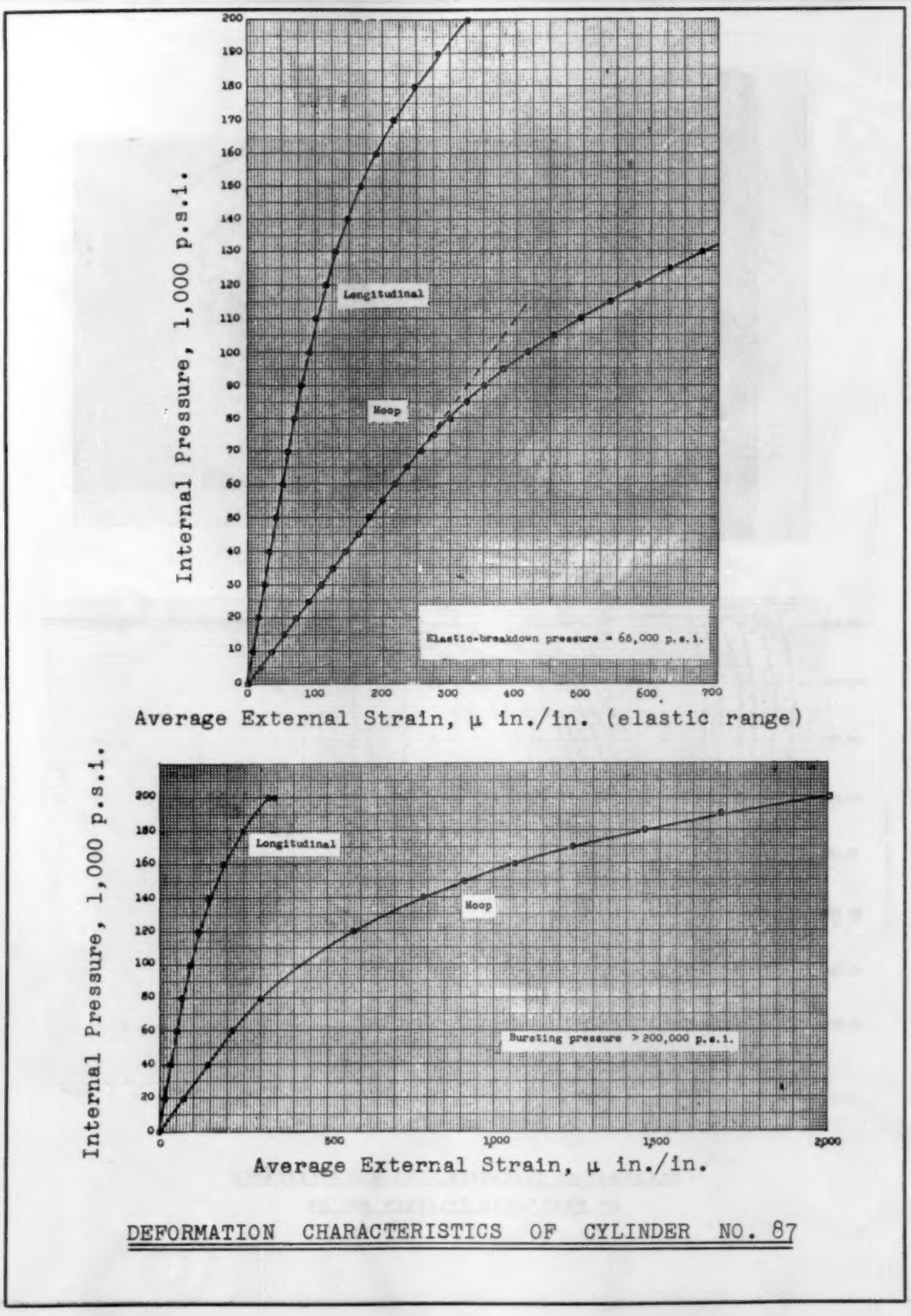

DEFORMATION CHARACTERISTICS OF CYLINDER NO. 87

FIGURE 14

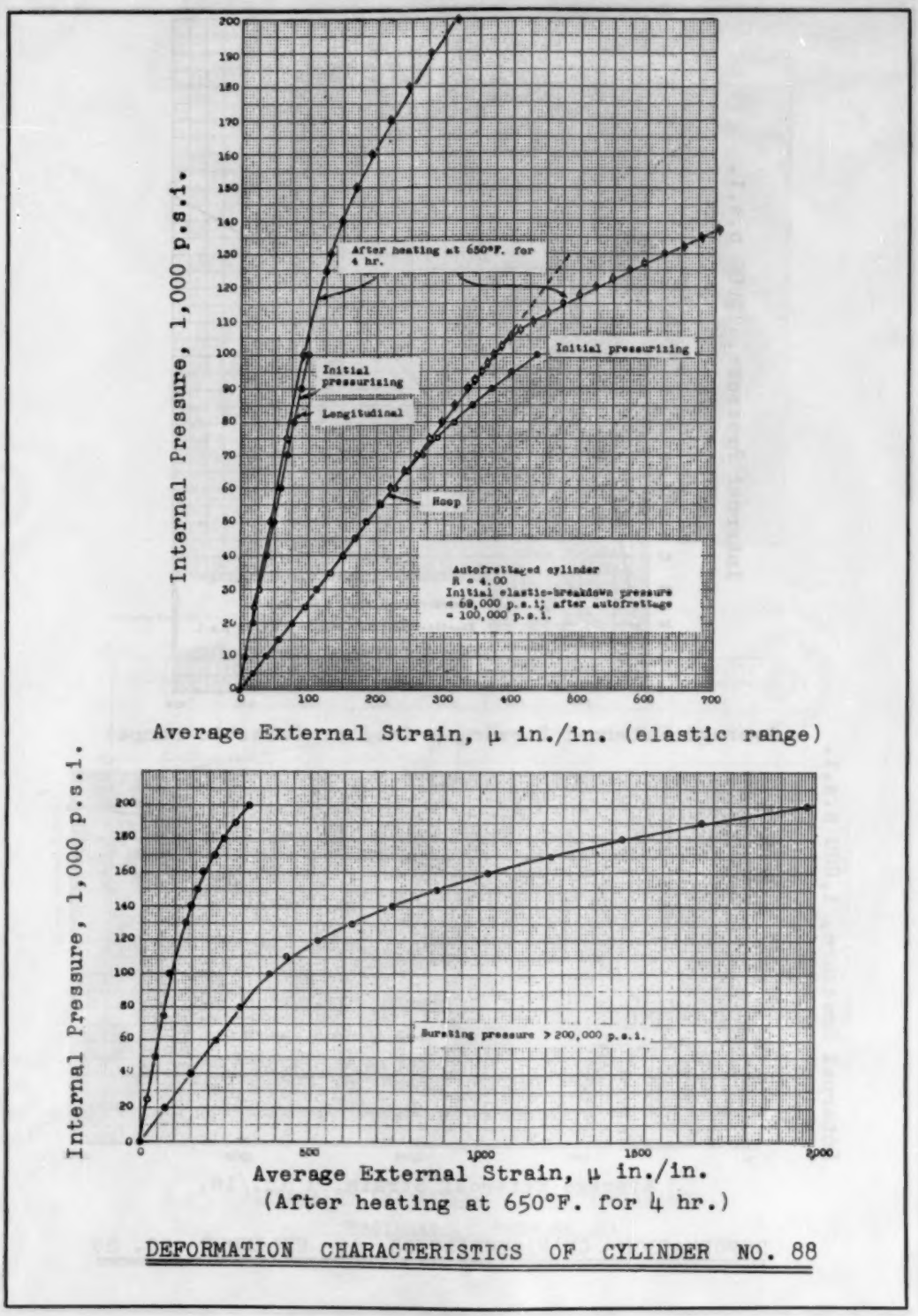

DEFORMATION CHARACTERISTICS OF CYLINDER NO. 88

FIGURE 15

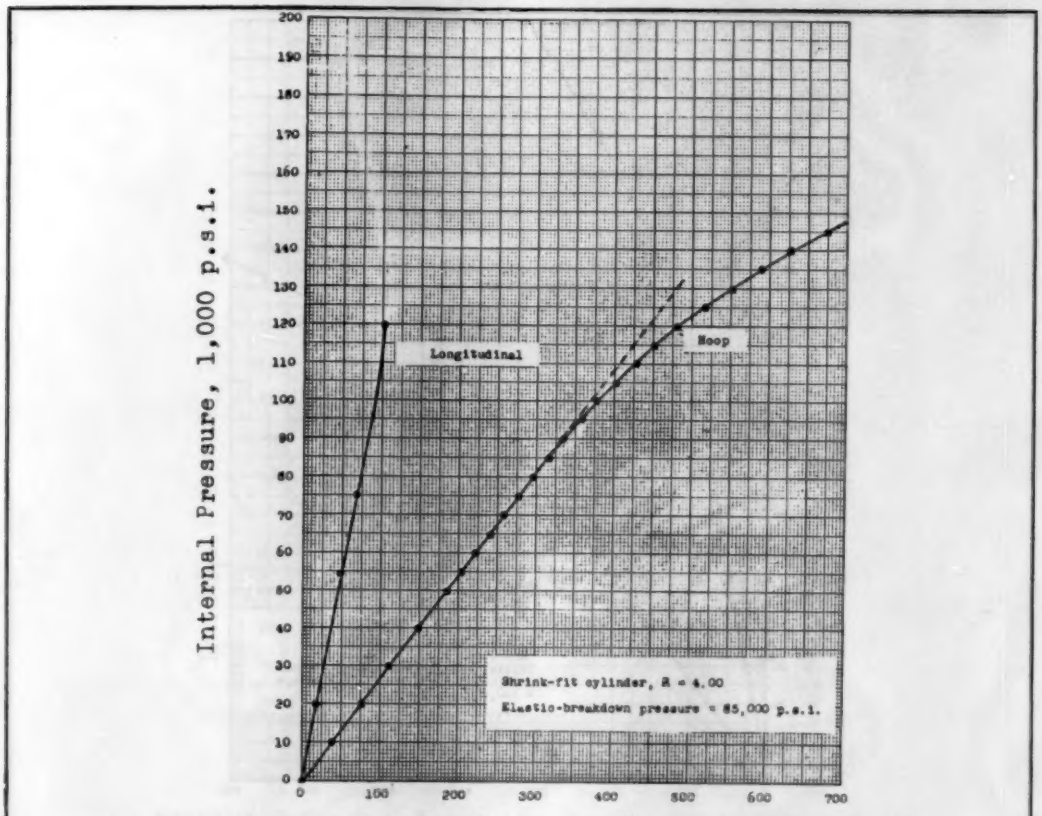

DEFORMATION CHARACTERISTICS OF CYLINDER NO. 89

FIGURE 16

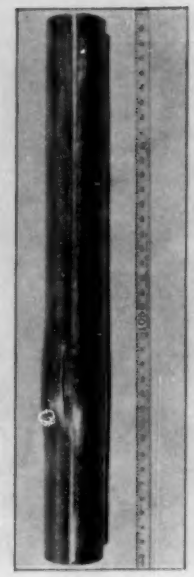

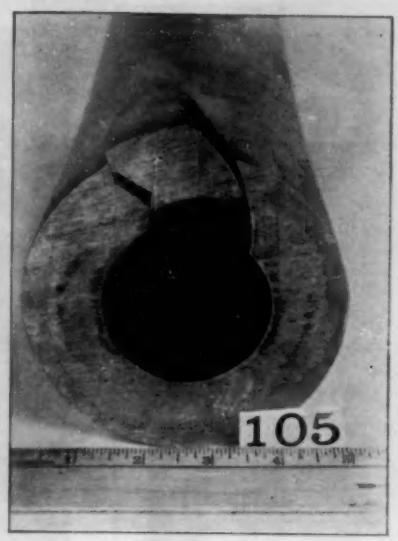

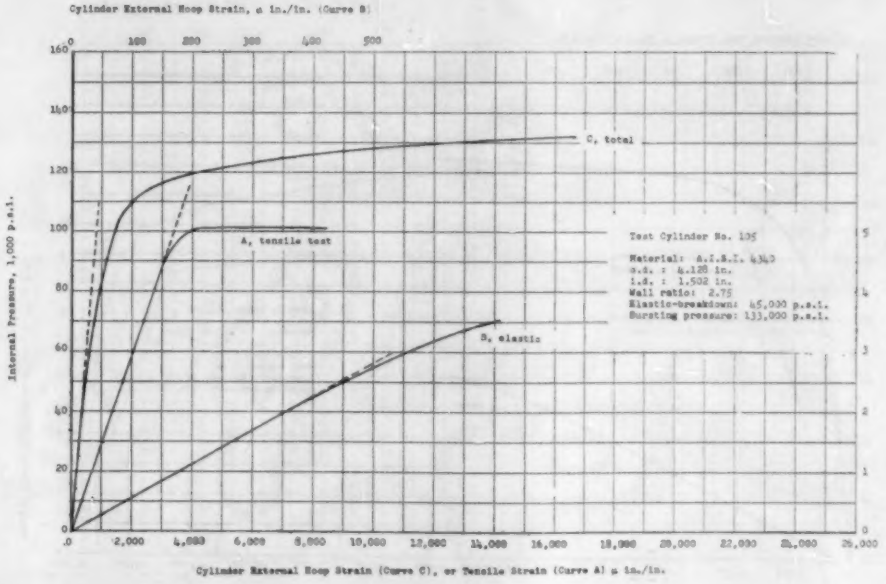

DEFORMATION CHARACTERISTICS AND APPEARANCE OF FRACTURED CYLINDER NO. 105

FIGURE 17

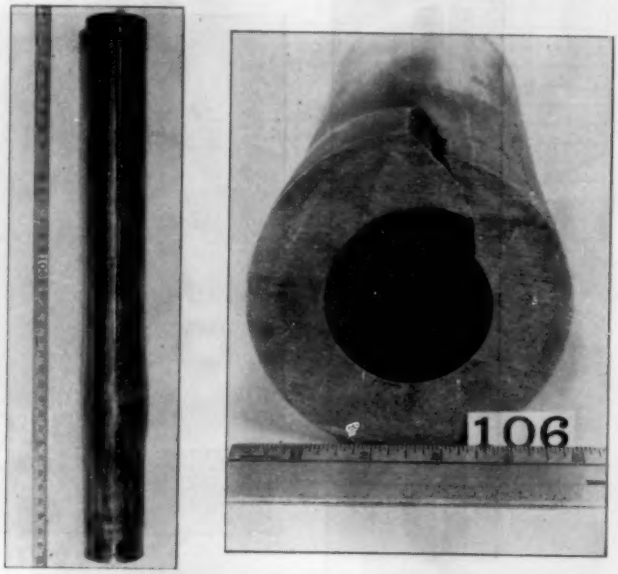

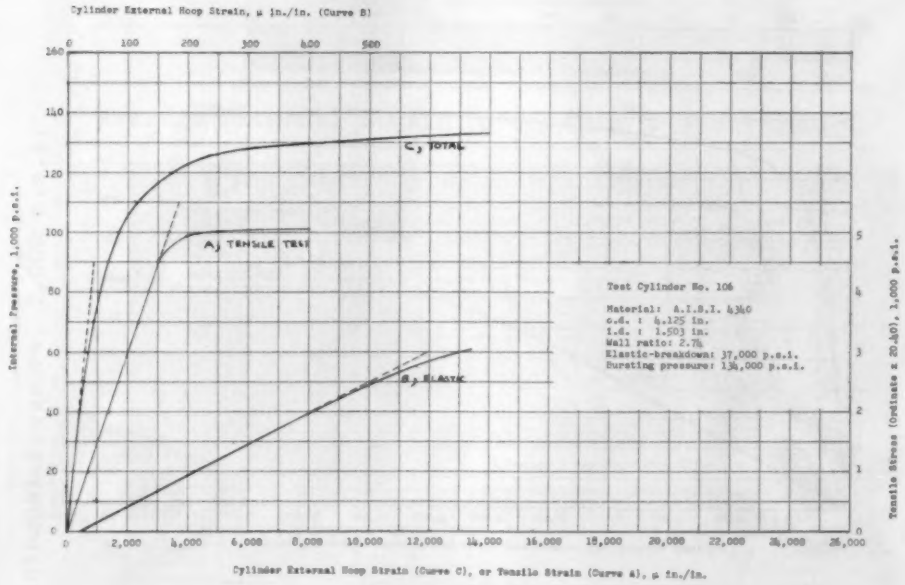

DEFORMATION CHARACTERISTICS AND APPEARANCE OF FRACTURED CYLINDER NO. 106

FIGURE 18

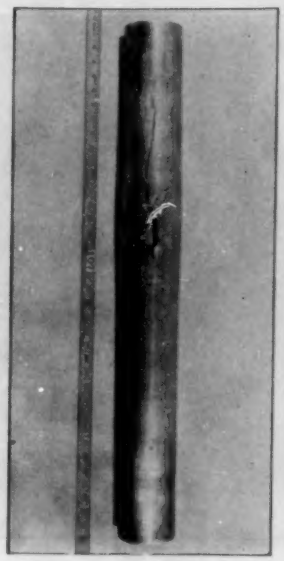

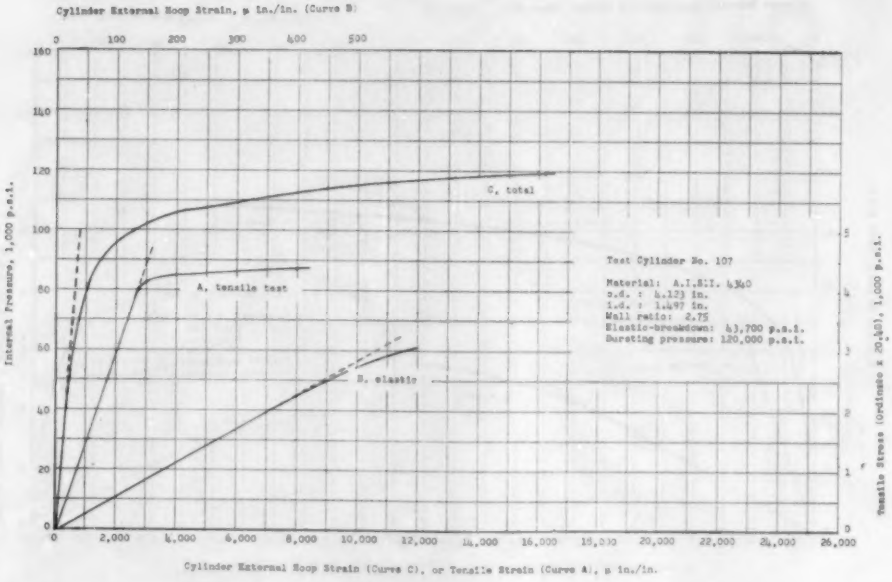

DEFORMATION CHARACTERISTICS AND APPEARANCE OF FRACTURED CYLINDER NO. 107

FIGURE 19

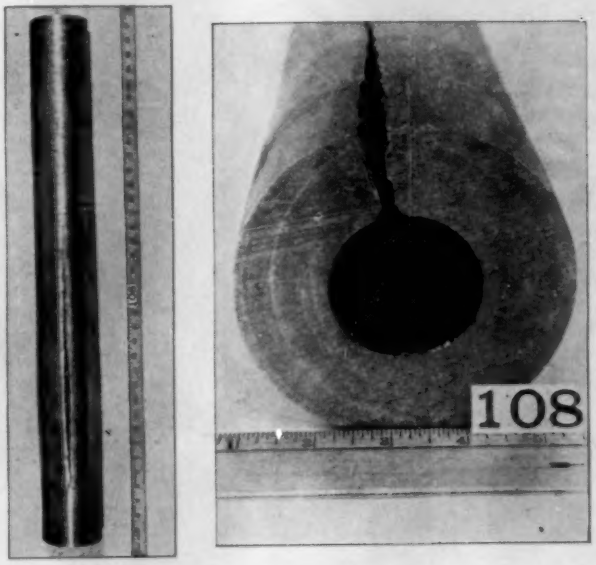

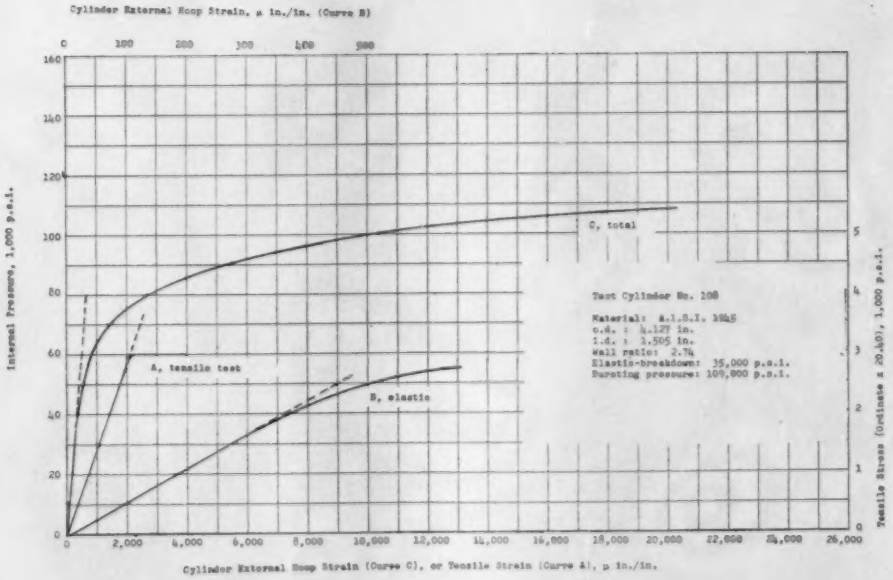

DEFORMATION CHARACTERISTICS AND APPEARANCE OF FRACTURED CYLINDER NO. 108

FIGURE 20

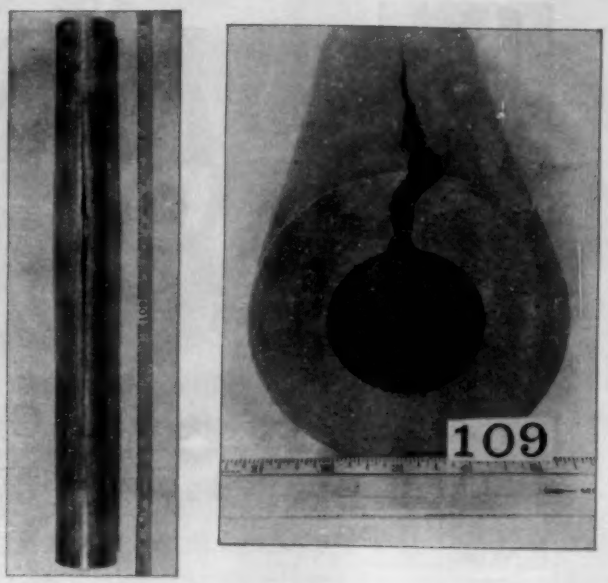

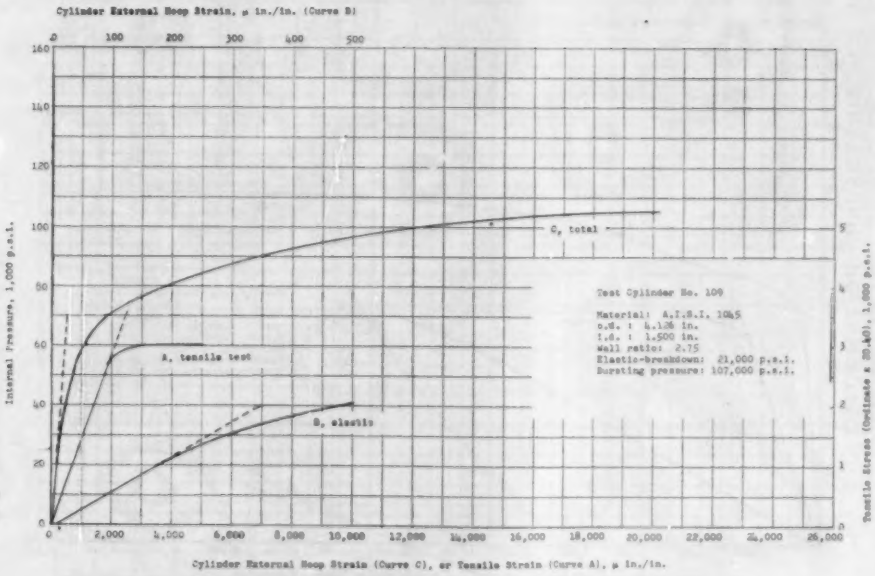

DEFORMATION CHARACTERISTICS AND APPEARANCE OF FRACTURED CYLINDER NO. 109

FIGURE 21

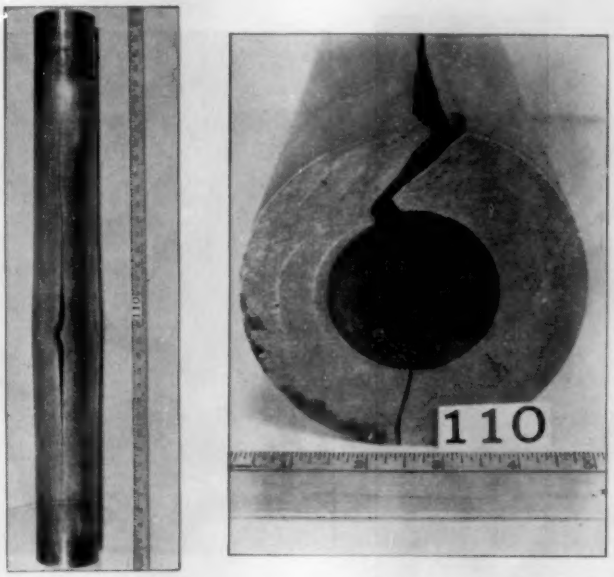

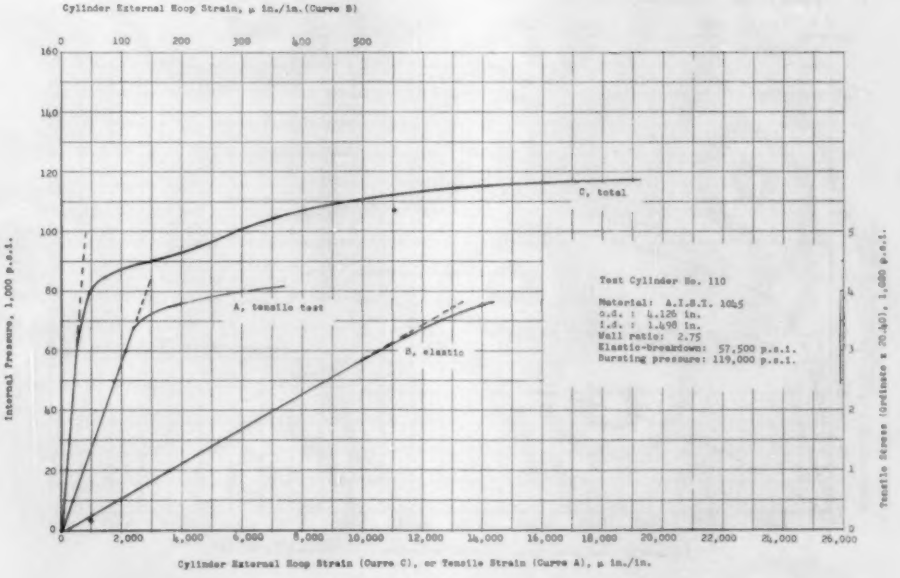

DEFORMATION CHARACTERISTICS AND APPEARANCE OF FRACTURED CYLINDER NO. 110

FIGURE 22

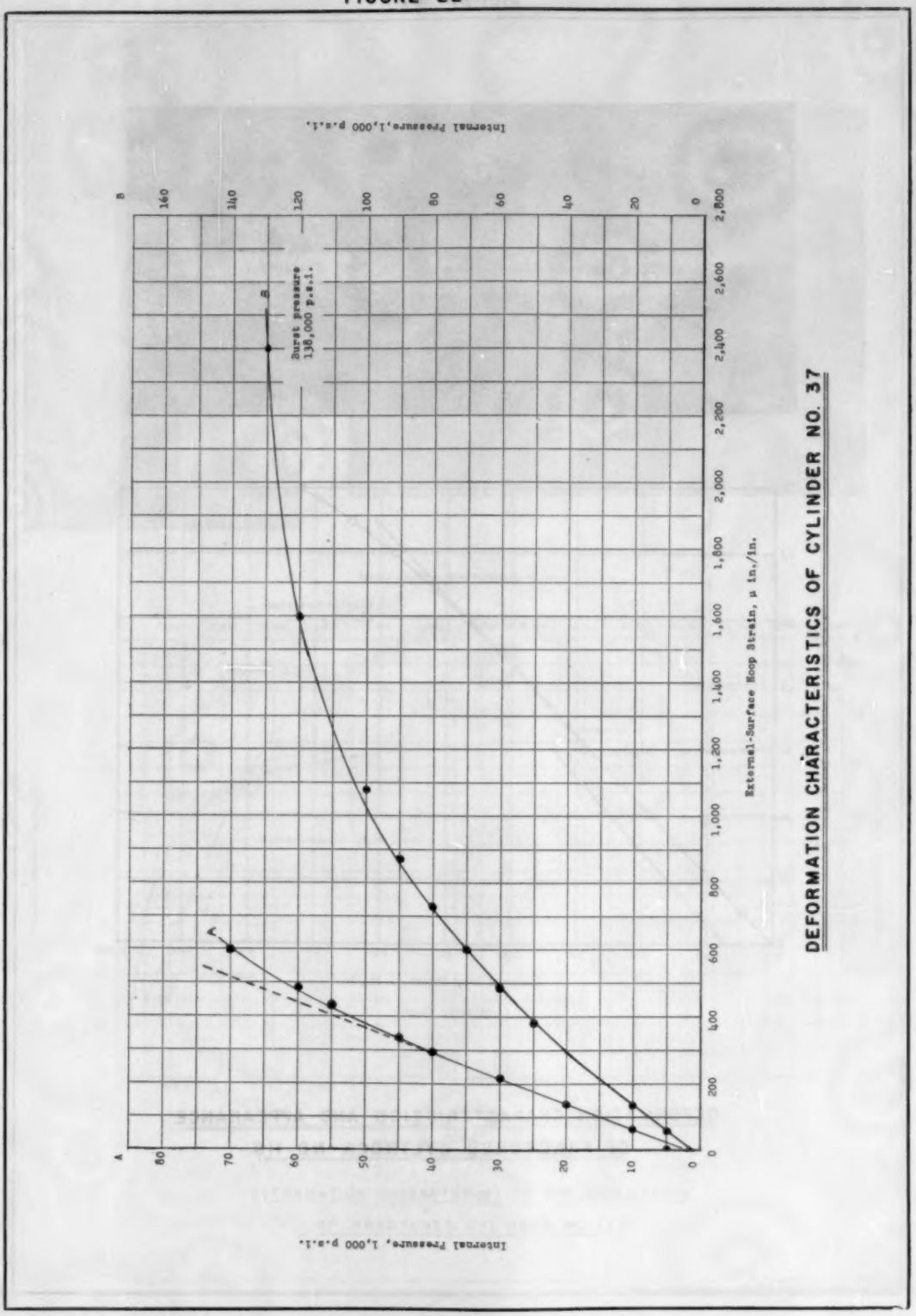
DEFORMATION CHARACTERISTICS OF CYLINDER NO. 37
Burst pressure 138,000 p.s.i.
A
B
External-Surface Hoop Strain, μ in./in.
Internal Pressure, 1,000 p.s.i.
Internal Pressure, 1,000 p.s.i.

FIGURE 23

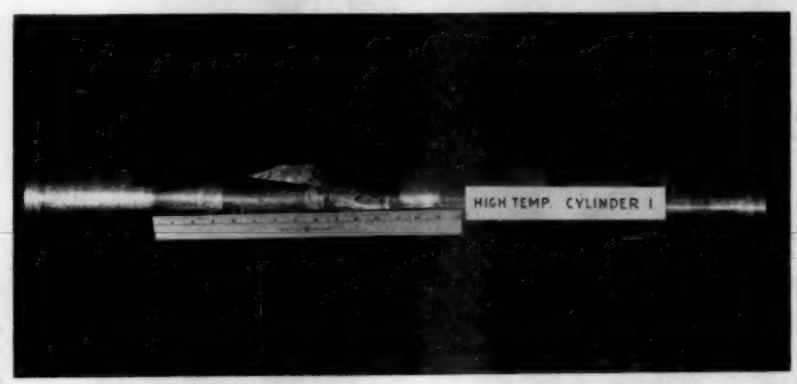

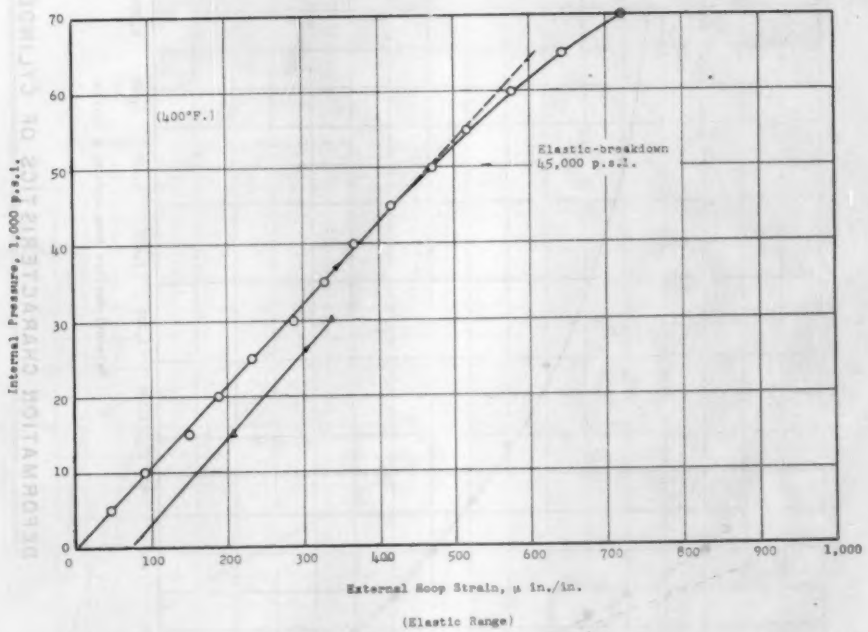

DEFORMATION CHARACTERISTICS AND APPEARANCE OF FRACTURED CYLINDER NO. 119

FIGURE 24

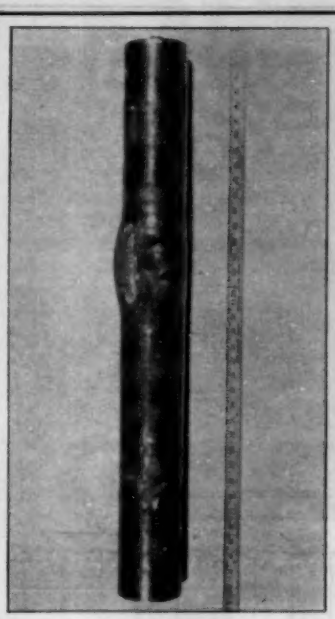

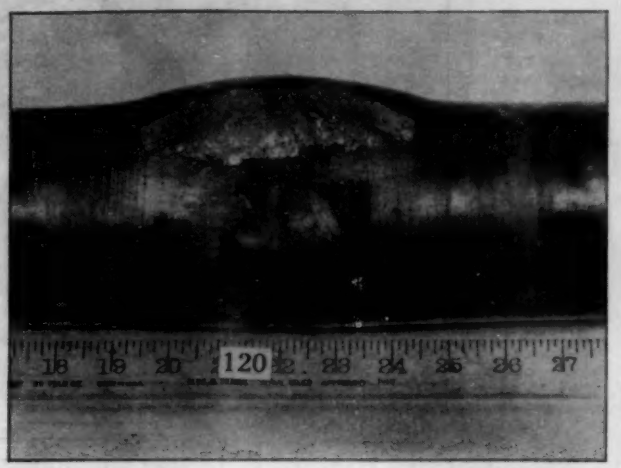

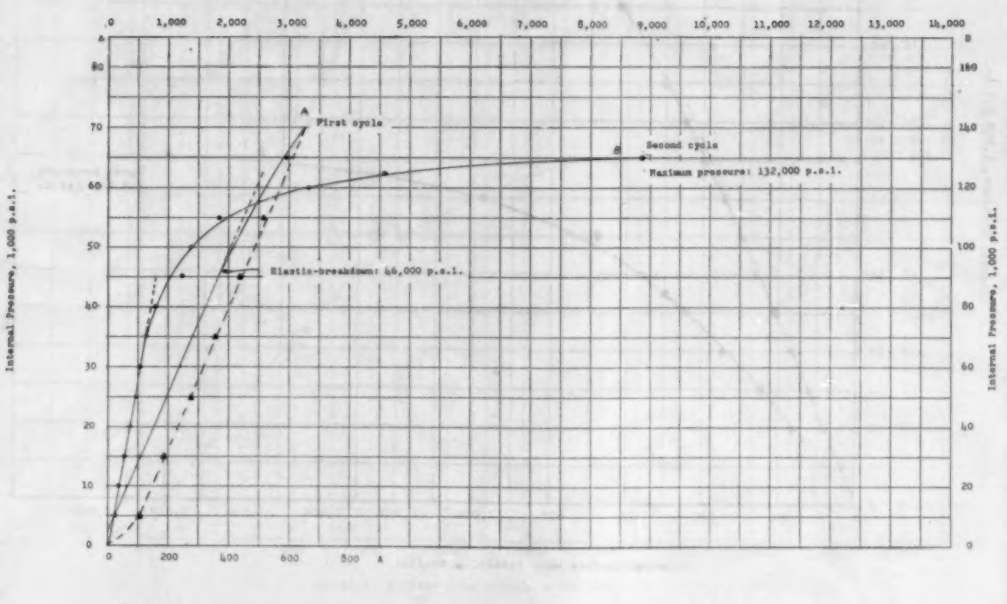

DEFORMATION CHARACTERISTICS AND APPEARANCE OF FRACTURED CYLINDER NO. 120

FIGURE 25

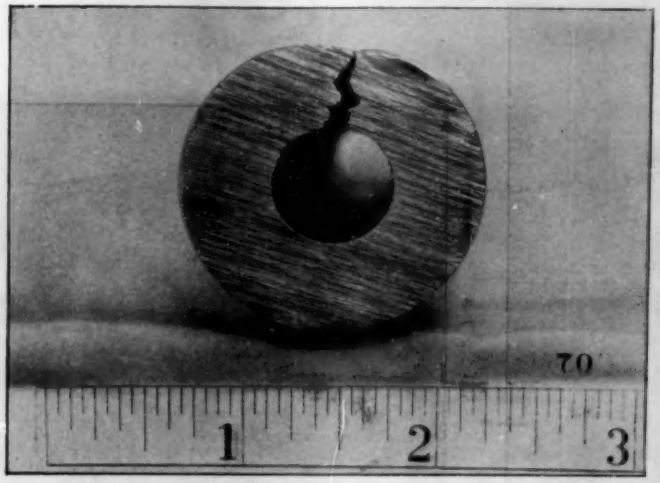

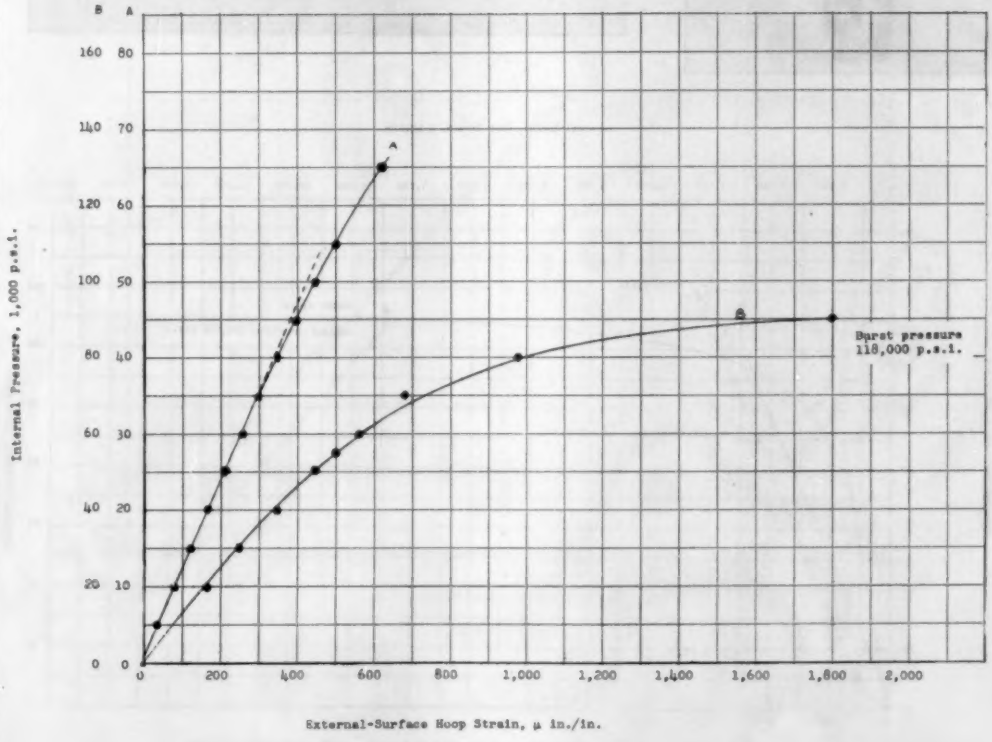

DEFORMATION CHARACTERISTICS AND APPEARANCE OF FRACTURED CYLINDER NO. 70

FIGURE 26

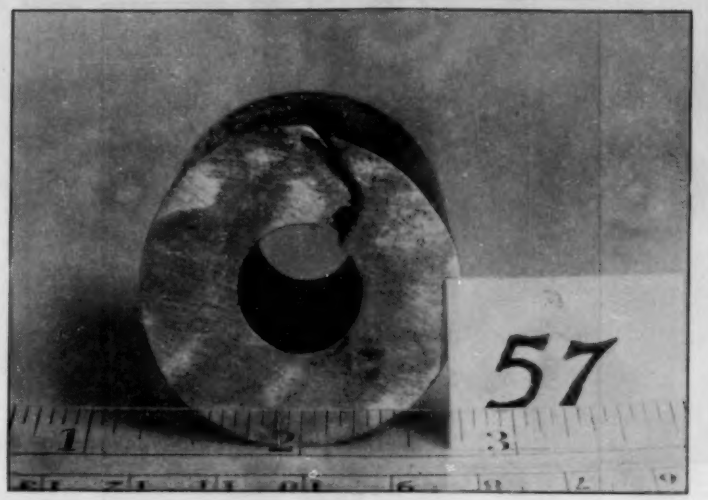

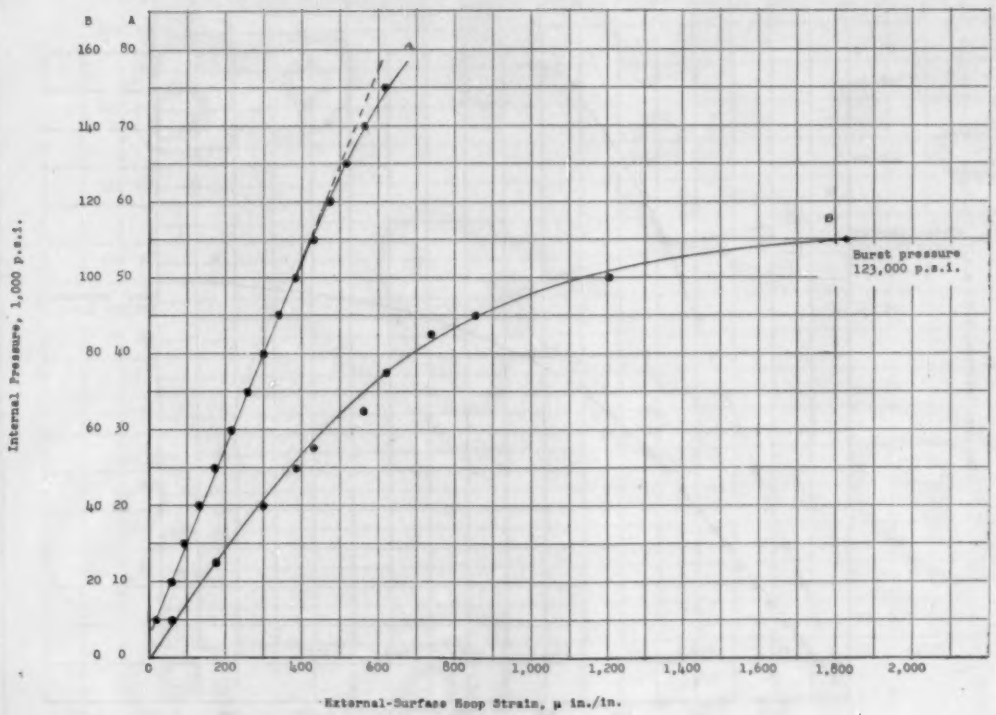

DEFORMATION CHARACTERISTICS AND APPEARANCE OF FRACTURED CYLINDER NO. 57

FIGURE 27

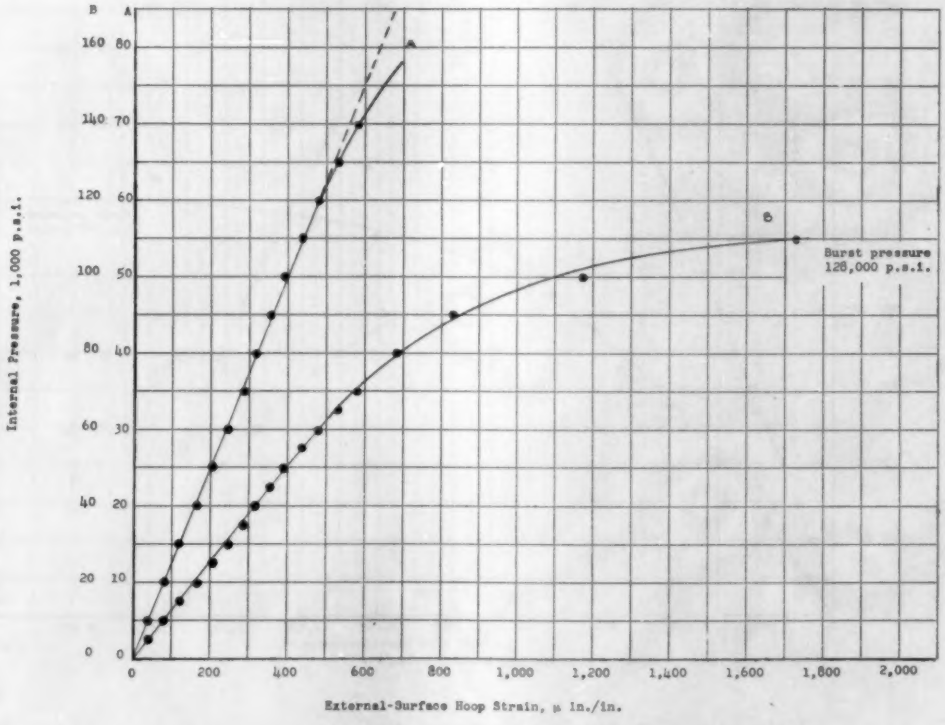

DEFORMATION CHARACTERISTICS AND APPEARANCE OF FRACTURED CYLINDER NO. 56

FIGURE 28

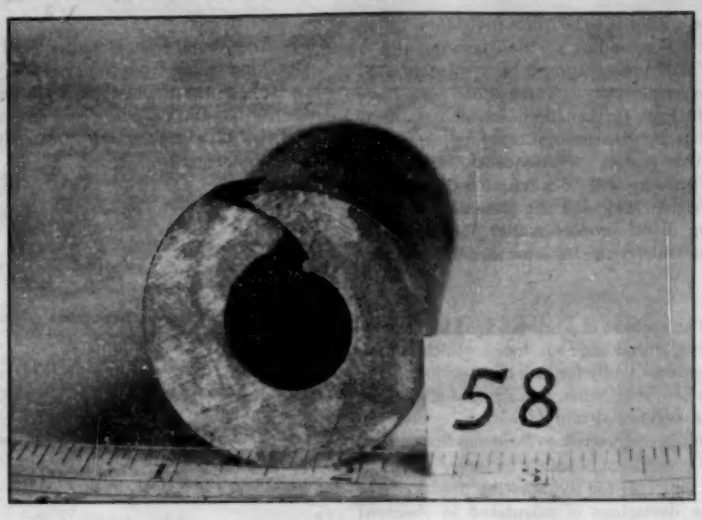

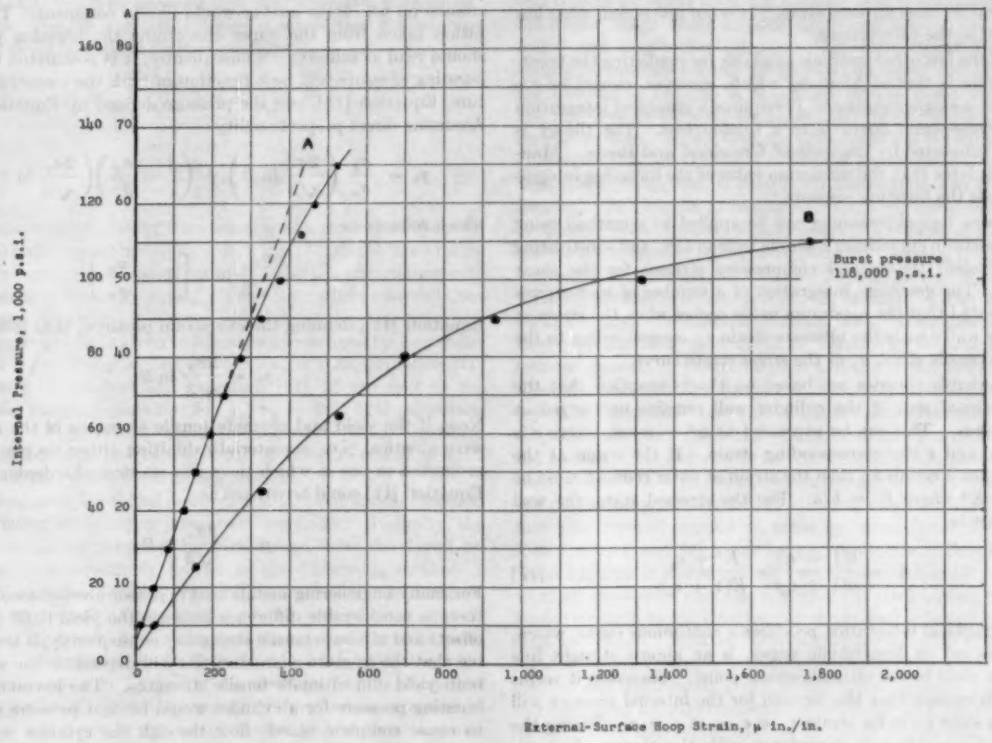

DEFORMATION CHARACTERISTICS AND APPEARANCE OF FRACTURED CYLINDER NO. 58

Discussion

E. W. Comings.[5] The author is to be commended for a valuable contribution to our understanding of the characteristics of heavy-walled cylinders. His presentation is well substantiated both theoretically and experimentally. There is one part, however, which would benefit from further discussion and clarification. This has to do with the discussion of bursting pressure in the paper where the author states: "Consequently it is postulated that the bursting pressure will be a function of both the overstrain pressure, Equation [11], and the pressure defined by Equation [12], assuming direct proportionality." This statement is not clear, and particularly the basis for assuming a direct proportionality.

S. M. Jorgensen.[6] The amount of work involved in developing this paper is impressive, containing as it does a wealth of data on a subject which has suffered badly for lack of attention. The importance of such work is evident when it is realized that there are thousands of vessels engineered and operating beyond the scope of any code, and often engineered to formulas that do not apply, and with no clear conception of safety factors.

For this reason, Equation [13] for the bursting pressure is of particular interest. The deviations of calculated to observed pressures in Table 3 are mainly on the plus side. This may be because the wall ratio used in the formula is the ratio in the unstressed rather than stressed state. It is not quite clear what has been used in the calculations.

One of the few other methods available for predicting the bursting pressure is that of Manning which, however, cannot be expressed in a single equation. It requires a graphical integration of the stress-strain curve from a torsion test. The theory is strongly supported by the tests of Crossland and Bones. Manning postulates that the maximum value of the foregoing integration equals the bursting pressure.

The same logical reasoning can be applied to a method using the stress-strain curve from a simple tension test, and substituting the equivalent tensile and compressive stresses for the shear stresses. The graphical integration of a number of such curves has indicated that the maximum value occurs when the strain at the inner wall equals the ultimate strain ϵ_u, corresponding to the ultimate tensile stress σ_u of the stress-strain curve.

All workable theories are based on the assumption that the cross-sectional area of the cylinder wall remains unchanged at all pressures. This can be expressed as $\epsilon r^2 = \text{const}$, where r is a radius, and ϵ the corresponding strain. If the strain at the inner radius a equals ϵ_u, then the strain at outer radius b must be $\epsilon_b = \epsilon_u/K^2$ where $K = b/a$. For the stressed state, the wall ratio must be

$$K' = \frac{b(1 + \epsilon_b)}{a(1 + \epsilon_u)} = \frac{K^2 + \epsilon_u}{K(1 + \epsilon_u)} \quad \ldots\ldots [17]$$

The graphical integration produces a continuous curve, which, when plotted on logarithmic paper, is an almost straight line from the yield to the ultimate-stress point. Therefore it seems logical to assume that the formula for the internal pressure will take the same form for strain ϵ_u or ϵ_{yield} at $r = a$. Taking the formula for yielding in accordance with the theory of plastic deformation, the internal pressure at the time of bursting should then be

$$p_b = \frac{2\sigma_u}{\sqrt{3}} \log_e K' \quad \ldots\ldots [18]$$

where K' is found from Equation [17] of this discussion.

Checking values from the graphical integration against Equation [18], it was found that Equation [18] gave higher values than the integration curve at high values of K'. It was also found that almost complete agreement occurred when the equation was changed to

$$p_b = \frac{\sigma_u + \sigma_b}{\sqrt{3}} \log_e K' \quad \ldots\ldots [19]$$

σ_b = stress at OD strain ϵ_b

$$\epsilon_b = \frac{\epsilon_u}{(K')^2}$$

with K' according to Equation [17].

It will be noted that Equation [19] is of the same form and closer to the author's equation for p. The conclusion must be, however, that more work must be done before a final bursting formula can be written. It is therefore gratifying to see a research program of the type and magnitude described in this paper.

Author's Closure

Several interesting points have been brought out in the discussion on which the author would like to comment. The quotation taken from the paper concerning the bursting pressure should read as follows: "Consequently, it is postulated that the bursting pressure will be a function of both the overstrain pressure, Equation [11], and the pressure defined by Equation [12]. Assuming direct proportionality

$$p_b = \frac{\sigma_y}{\sigma_u}\left(\frac{2\sigma_u}{\sqrt{3}} \ln R\right) + \left(1 - \frac{\sigma_y}{\sigma_u}\right)\left(\frac{2\sigma_y}{\sqrt{3}} \ln R\right)$$

which reduces to

$$p_b = \frac{2\sigma_y}{\sqrt{3}} \ln R \left[2 - \frac{\sigma_y}{\sigma_u}\right] \quad \ldots\ldots [13]"$$

Equation [11], defining the overstrain pressure, is as follows

$$p_b = \frac{2\sigma_y}{\sqrt{3}} \ln R$$

Now, if the yield and ultimate tensile strengths of the material were identical (i.e., a material exhibiting either no plastic flow properties or one in which there was no strain-hardening effect), Equation [11] could be written as

$$p_b = \frac{2\sigma_u}{\sqrt{3}} \ln R \quad \ldots\ldots [12]$$

For many engineering metals used in pressure-vessel construction there is considerable difference between the yield (0.02 per cent offset) and ultimate tensile strengths; consequently, it is reasonable that the fracture characteristics will depend on the values of both yield and ultimate tensile strengths. The lowest expected bursting pressure for a cylinder would be that pressure required to cause complete plastic flow through the cylinder wall; this pressure is called the "overstrain" pressure, Equation [11]. Also, the highest expected bursting pressure for a cylinder would be that pressure required to cause complete plastic flow through the cylinder wall if the material strength were σ_u, Equation [12]. It is evident that lower and upper bounds have been placed on the bursting pressure and that, in all probability, the bursting pressure will be somewhere between the lower and upper limits.

---

[5] Head, School of Chemical and Metallurgical Engineering, Purdue University, Lafayette, Ind.

[6] Process Plants Division, Foster Wheeler Corporation, New York, N. Y.

TABLE 6 BURSTING PRESSURE OF CYLINDERS

Test no. (Table 3)	R	σ_u (psi)	p_b Observed (psi)	Calculated p_b (psi) A — Lamé[a] method	Dev. (%)	B — Mean-diameter[b] method	Dev. (%)	C — Classical[c] method	Dev. (%)	D — Faupel[d] method	Dev. (%)	E — Manning Method	Dev. (%)
7	2.49	90,480	79,000	65,300	−17	77,500	− 2	95,000	+20	85,700	+ 9	85,000	+ 8
13	2.43	68,350	57,000	48,500	−15	57,000	0	70,500	+24	54,000	− 5	59,500	+ 4
14	2.44	91,550	83,000	65,000	−22	77,000	− 7	94,500	+14	84,700	+ 2	89,000	+ 7
39	2.75	89,700	63,000	68,700	+ 9	81,000	+29	115,000	+83	67,400	+ 7	70,000	+11
40	2.76	80,100	55,000	61,500	+12	75,000	+36	106,500	+94	63,000	+15	69,000	+25
41	2.75	74,900	67,500	57,300	−15	74,200	+10	96,000	+42	66,500	− 2	70,000	+ 4
42	2.74	104,650	98,500	79,750	−19	97,500	−10	131,000	+43	111,300	+13	105,000	+ 7
44	1.75	105,650	59,000	53,600	− 9	57,500	− 3	68,300	+16	63,000	+ 7	64,500	+ 9
45	2.75	137,850	143,000	105,500	−26	128,500	−10	178,000	+24	158,500	+11	150,000	+ 5
46	3.69	105,500	168,000	91,200	−45	121,000	−28	160,000	− 5	152,000	−10	191,000	+14
47	4.71	106,700	192,500	97,600	−49	138,500	−28	191,000	− 1	184,000	− 4	157,000	−18
No. (Crossland and Bones, *Eng.* 1/21, 1/28 (1955)				F		G		H		J		K	
1	1.57	66,000	31,000	27,800	−10	29,300	− 6	34,400	+11	25,800	−17	29,000	− 6
2	1.33	66,000	18,640	18,200	− 2	18,700	0	21,700	+16	16,300	−13	18,000	0
3	1.99	66,000	44,600	39,400	−12	43,700	− 2	52,500	+18	39,400	−12	43,500	− 2
4	2.29	66,000	54,000	45,000	−17	52,000	− 4	63,200	+17	47,400	−12	53,000	− 2
5	2.66	66,000	60,100	49,500	−18	60,000	0	74,600	+24	56,000	− 7	62,000	+ 3
6	1.78	66,000	38,400	34,200	−11	37,000	− 4	44,000	+15	32,700	−15	38,000	− 1
7	2.90	66,000	65,300	52,000	−20	64,500	− 1	81,000	+24	60,600	− 7	67,000	+ 3
8	1.88	66,000	40,200	36,800	− 8	40,400	0	48,200	+20	36,000	−10	41,000	+ 2
9	2.48	66,000	57,400	47,500	−17	56,100	− 2	69,500	+21	52,000	− 9	57,000	− 1
10	3.18	66,000	70,000	54,000	−23	68,700	− 2	88,500	+26	66,100	− 6	72,000	+ 3
11	2.13	66,000	47,800	42,000	−12	47,700	0	57,800	+17	43,200	−10	47,000	− 2
12	3.60	66,000	76,000	56,500	−26	74,500	− 2	93,200	+23	73,000	− 4	78,000	+ 3
13	3.72	66,000	79,000	57,000	−28	76,000	− 4	100,400	+27	74,800	− 5	81,000	+ 3

[a] $\sigma_u\left(\frac{R^2-1}{R^2+1}\right)$ [b] $2\sigma_u\left(\frac{R-1}{R+1}\right)$ [c] $\frac{2\sigma_u}{\sqrt{3}}\ln R$ [d] $\frac{2\sigma_y}{\sqrt{3}}\ln R\left(2-\frac{\sigma_y}{\sigma_u}\right)$

As a guess, it could be assumed that the "critical failure stress" would be $\frac{1}{2}(\sigma_y + \sigma_u)$. If this were assumed then the bursting pressure could be defined by the equation

$$p_b = \frac{1}{2}\left[\frac{2\sigma_y}{\sqrt{3}}\ln R + \frac{2\sigma_u}{\sqrt{3}}\ln R\right]$$

or

$$p_b = \frac{\ln R}{\sqrt{3}}(\sigma_y + \sigma_u) \quad \ldots\ldots\ldots\ldots\ldots [20]$$

In Equation [13], rather than arbitrarily assume that the critical stress value would be $\frac{1}{2}(\sigma_y + \sigma_u)$, it was thought more realistic to "weight" the effects of both σ_y and σ_u in accordance with the yield/ultimate ratio, σ_y/σ_u. Thus, for various materials, the strain-hardening effect is allowed for; but, at the same time, proportional weighting is given to the pressures defined by Equations [11] and [12]. For example, when $\sigma_y/\sigma_u = 0.25$, Equation [11] contributes 75 per cent and Equation [12], 25 per cent to the calculated bursting pressure; for $\sigma_y/\sigma_u = 0.5$, both equations contribute 50 per cent, while for $\sigma_y/\sigma_u = 0.75$, Equation [11] contributes 25 per cent and Equation [12] contributes 75 per cent to the calculated bursting pressure.

Mr. Jorgensen has raised some questions about another method for predicting the bursting pressure of a cylinder. Basically, the method originally proposed by Nadai, and later developed by Manning (now commonly known as the "Manning method"), utilizes the results of torsion tests. This method is indeed ingenious and represents an application of the principles of applied mechanics for which the orginators of the method are to be commended. There is no doubt that the Manning method is reliable; this is shown in Table 6 which gives the results of various calculations on the bursting pressure of cylinders reported in Table 3 of this paper as well as cylinders tested by Crossland and Bones.[7] Under Column A of Table 6 the results of calculations on several cylinders listed in Table 3 using the so-called "Lamé method" are given. It is seen that most of the predictions are considerably at variance with the observed bursting pressure; this is to be expected since the formula used is applicable only in the elastic range of strain and completely ignores the effect of radial and longitudinal stresses. Likewise, under Column B results are tabulated using the "Mean-Diameter" formula. Like the formula in Column A this expression is based on Hooke's law and thus should not be expected to predict results dependent on plastic flow. Under Column C the classical bursting formula (Equation [12], text) is used to furnish predictions; it is evident that this formula, too, is completely inadequate and should not be used. In Column D results are tabulated using the formula proposed by the author (Equation [13], text) and in Column E results are presented which were deduced by using the Manning method.[8] Comparison of Column D and E shows that both methods provide adequate predictions of bursting pressure. For further comparison consider the data obtained by Crossland and Bones (Columns F through K of Table 6). Several points of interest show up in this tabulation which warrant brief mention. First, the results under Column K (Manning method) are almost unbelievably precise; the same is true of the results under Column G (Mean-diameter formula). Crossland and Bones state that the results under Column G for their material are probably fortuitous since the Mean-diameter formula has no justification in the plastic range of strain. It is interesting, however, to note that this method applied to some cylinders listed in Table 3 (No. 7, 13, 14, and 44) yielded very precise predictions as shown under Column B of Table 6; in fact, Cylinder No. 13, for which an exact prediction was made, is made of steel having the same tensile strength as the steel used in the cylinders tested by Crossland and Bones. What all of this appears to say is that, of the various formulas and methods presented, only the Manning method and the formula given in this paper (Equation [13]) can be expected to provide consistent predictions for a variety of materials. It is interesting to note in Table 6 that the Manning method applied to cylinders made of a variety of steels of different composition and strength level provides about the same degree of prediction accuracy as Equation [13]. It may be that the

[7] "The Ultimate Strength of Thick-Walled Cylinders Subjected to Internal Pressure," by B. Crossland and J. A. Bones, *Engineering*, January, 1955, pp. 80–83; 114–117.

[8] The Manning calculations were made by F. R. Klauck, Design Division, Engineering Department, E. I. du Pont de Nemours and Co., Inc., Wilmington, Delaware (formerly a member of the staff of the Engineering Research Laboratory).

Manning method is best suited for cylinders made of soft low-carbon annealed steel. The principal drawback of the Manning method is the fact that torsion test data are required; few agencies conduct torsion tests and virtually no design handbooks supply such data. Consequently, the engineer faced with the problem of predicting a bursting pressure for a cylinder should have other means at his disposal. A bursting pressure for a cylinder can be quickly and accurately (±15 per cent on a 95 per cent certainty basis) determined by use of Equation [13]; in the Manning method, even if torsion data were available, it would require many hours of computation and analysis to arrive at the desired answer. Furthermore, if dilation analyses are required, the Manning method also requires hours of computation, as compared with a few minutes by the method given in footnote 2.

Mr. Jorgensen has raised some additional questions which require brief comment. First, in Equation [13], the initial value of the wall ratio R is used in all calculations; all of our tests have shown that this is satisfactory. To try and correct for the continuously changing wall ratio (Equation [17]) introduces some additional difficulties which can be handled analytically, but which complicate the situation considerably. For example, if the wall ratio defined by Equation [17] is used, then the value of σ_s in Equation [18] should be the true stress. Use of Equation [18] with true values of R and σ_s gives predicted bursting pressures which are even further out of line than obtained by Equation [12]; this would be expected because the effect of σ_r is completely ignored. Mr. Jorgensen's Equation [19] contains both nominal and true values, which is inconsistent, and in addition he proposes a prediction, based on maximum stress or maximum strain values, which has been proved inadequate for ductile metals. On the other hand, the alternate proposal of Mr. Jorgensen to use tensile data rather than torsion data appears to have considerable merit, and it is hoped that more details will be published at some future time.

Ebullition Cooling of Gas Engines

By G. O. BATES,[1] J. E. ENGLISH,[2] and G. M. FRANKLIN,[3] TULSA, OKLA.

The ebullition system is defined as a method for cooling internal-combustion engines by boiling water in the engine jackets. No pump is required because thermal circulation is maintained. Relationships of power requirements, equipment prices, and installed costs for ebullition systems and conventional forced-circulation water systems are shown graphically. Satisfactory performance over an initial operating period of ten months is reported for the cooling equipment and engines on five units equipped with ebullition systems. Observations on those units during the same period indicate that engine maintenance will be less than for similar engines with conventional cooling. In view of its economy, simplicity, and satisfactory functional performance, ebullition cooling is expected eventually to supersede conventional water cooling.

Introduction

EVER since man invented the internal-combustion engine, he has been faced with the economical and mechanical problems of the unused heat in such engines. Now, a method by which heat is removed by boiling water in the engine jackets is being used successfully on many installations. That system, known as latent cooling or ebullition cooling, costs less to install, uses less power, and gives better engine performance than conventional jacket-water cooling. In addition, it effects substantial savings in fuel, water, and equipment if the steam can be utilized. For these reasons everyone who designs or uses internal-combustion engines should be interested in further use and development of ebullition cooling. Therefore it is the purpose of this paper to present the results of design and operating experience with several ebullition installations for such help as they may be in such development.

Development of Ebullition Cooling

Ebullition-cooling systems were first used on single-cylinder engines fitted with open tanks filled with water in which the power cylinders were immersed. Cooling occurred as water boiled from the hot surfaces within the jacketing vessels. The forerunner of today's ebullition system appeared on such engines as early as 1920 when they were fitted with closed hoppers and steam-condensing, air-cooled radiators to prevent loss of cooling water. Modern horizontal engines using such cooling systems were developed for oil-field pumping service during the 1940's.

As far as is known, there was no directed attempt to elevate the temperature of the cooling water to the range of 212 to 250 F in jacket systems for vertical multicylinder industrial engines until the late 1930's. About that time, a high-temperature cooling system was introduced which claimed to reduce cylinder wear, to permit use of sulphur-bearing fuel gas and to increase thermal efficiency through recovery of waste heat. That system differed from an ebullition system in that a pump was provided to force circulation through the jackets in order to suppress free boiling within the engine. From 1939 to 1952 this system won a gradually increasing acceptance, usually being favorably considered only when the ability to burn sulphur-bearing fuel or the recovery of waste heat was significantly advantageous. The effort to attain recognition for the system as a cooling method for engines was resisted by most engine users and builders who were uncertain as to what troubles might arise from high-temperature cooling and were satisfied with cooling from conventional closed water systems operating in the medium-temperature range.

In 1952 O. B. Freeman of the Tidewater Associated Oil Company, Ventura, Calif., experimented on vertical multicylinder gas engines with high-temperature cooling without the jacket-water pumps. In his experiments, boiling was permitted within the jackets to promote natural circulation through the engine. A paper reporting the favorable results of his work was presented by Mr. Freeman before the California Natural Gasoline Association in 1953. Apparently, the additional economy permitted by the omission of the water-circulating pump created general interest in ebullition-type high-temperature cooling among operators of oil-field gas engines. As a result, over 40,000 engine horsepower in compressor service alone has been equipped with ebullition cooling since 1953.

Comparison of Ebullition and Conventional Cooling Systems

Fig. 1 shows a conventional forced-circulation water system with the engine, the surge tank, the pump, and the cooler.

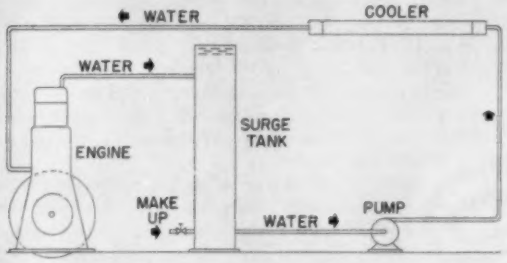

Fig. 1 Conventional Cooling System

Fig. 2 shows a simplified ebullition-cooling system with the engine, the separator, and the steam condenser. A mixture of water and steam from the engine enters the separator. The steam flows to an elevated condenser from which condensate is returned by gravity to the fluid stream entering the separator. This mixing ahead of the separator provides uniform temperature in case the condensate has been subcooled. There is no pump because all circulation is maintained by the difference in densities between the water in the separator and the mixture of water and steam in the jackets.

The ebullition system requires less heat-transfer surface and a smaller cooling-air fan than a comparable forced-circulation water system because of the greater temperature differences and

---

[1] Mechanical Engineering Supervisor, Stanolind Oil & Gas Company. Mem. ASME.

[2] Senior Mechanical Engineer, Stanolind Oil & Gas Company.

[3] Senior Mechanical Engineer, Stanolind Oil & Gas Company. Assoc. Mem. ASME.

Contributed by the Petroleum Division and presented at the Petroleum-Mechanical Engineering Conference, New Orleans, La., September 25–28, 1955, of The American Society of Mechanical Engineers.

Note: Statements and opinions advanced in papers are to be understood as individual expressions of their authors and not those of the Society. Manuscript received at ASME Headquarters, September, 25, 1955. Paper No. 55—PET-18.

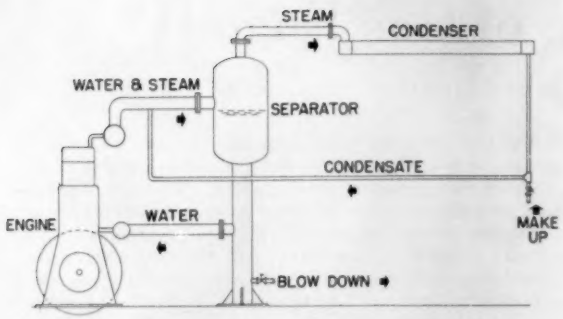

FIG. 2 EBULLITION-COOLING SYSTEM

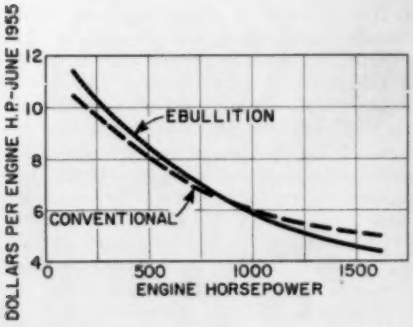

FIG. 3 PRICE OF COOLING EQUIPMENT FOR SLOW-SPEED ENGINES

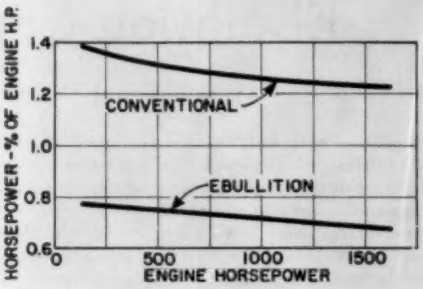

FIG. 4 POWER FOR COOLING SLOW-SPEED ENGINES

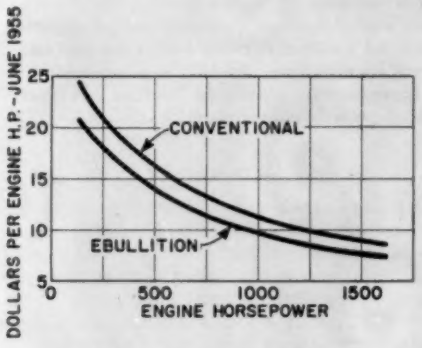

FIG. 5 INSTALLED COSTS OF COOLING EQUIPMENT FOR SLOW-SPEED ENGINES

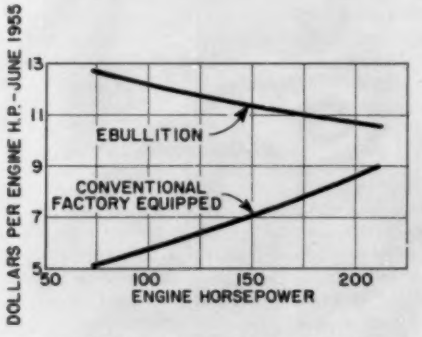

FIG. 6 PRICE OF COOLING EQUIPMENT FOR HIGH-SPEED ENGINES

higher heat-transfer rates that result when condensing steam.

Power requirements are less because of the smaller fan and driver and the elimination of the engine-jacket water pump. Obviously, operating and maintenance costs are lower for the same reasons.

In addition, engine maintenance costs are reported by several operators to be less. Uniform heat transfer at a high rate is achieved by the turbulent boiling action and there is little or no gradient in the temperature of the coolant. Therefore the cylinder walls have more uniform temperatures and less distortion or taper than with conventional cooling. Those conditions result in less wear of the cylinders and pistons, thereby reducing piston blowby and oil sludging.

Fig. 3 compares the initial costs of cooling equipment for both the ebullition system and the conventional system for slow-speed engines. Cost in dollars per engine horsepower based on June, 1955, prices is plotted against engine horsepower. The costs for ebullition systems include the purchase prices for a separator, an air-cooled steam condenser, and the necessary instruments and controls to maintain a steam pressure less than 5 psi. The costs for conventional systems include the purchase prices for a jacket-water surge tank, a jacket-water pump, an air-cooled exchanger, and the necessary instruments and controls to maintain a maximum water temperature of 170 F.

Fig. 4 compares the auxiliary power required by cooling equipment covered by Fig. 3 for both the ebullition system and the conventional system for slow-speed engines. Auxiliary horsepower, expressed in per cent of engine horsepower, is plotted against engine horsepower. The power for the ebullition system is that required by the fan. The power for the conventional system includes that required by the fan and the jacket-water pump.

Fig. 5 compares the installed costs of slow-speed engine-cooling equipment for both the ebullition system and the conventional system. The units and the basis for the indicated values are similar to those of Fig. 3. The costs include all labor and material which are required to make the installation ready for operation.

Fig. 6 compares the initial costs for cooling equipment for both the ebullition system and the conventional system for high-speed engines. The units and the basis for the indicated values are similar to those of Fig. 3.

Fig. 7 compares the auxiliary power required by cooling equipment for both the ebullition system and the conventional system for high-speed engines. The units and the basis for the indicated values are similar to those of Fig. 4.

The costs and auxiliary-power requirements for the factory-equipped conventional systems (radiators) furnished with high-speed engines are based on data obtained from a limited number

of engine manufacturers. Power requirements and costs for engines furnished by other manufacturers may vary slightly from the data indicated. However, these values are considered sufficiently accurate to be satisfactory for this comparison.

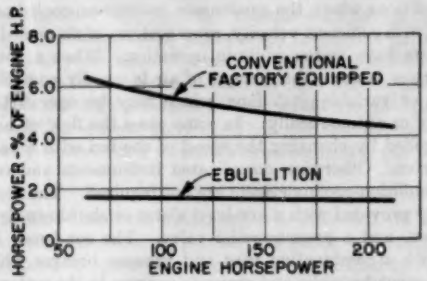

FIG. 7 POWER FOR COOLING HIGH-SPEED ENGINES

In all cases, the data apply to complete systems for cooling only jacket water on single engines. For cases where a single system is used for cooling several engines or jacket cooling is integrated with other services, somewhat different data will apply.

Installed costs for cooling equipment on high-speed engines are not given because such data were not available.

No data are given for high-temperature water-cooling systems because there are no economic or operational advantages for such systems in comparison with ebullition systems.

At least 15 per cent, and in many cases as much as 30 per cent, of the heating value of the engine fuel goes into steam which is generated in an ebullition system. Therefore very appreciable fuel savings can be made if the steam can be utilized, although it is normally condensed in an air-cooled unit. If the steam is used, a condensate-return system is usually required, but that cost is offset to some extent by a reduction in size of the steam condenser. In addition, boiler feedwater and steam generating facilities can be reduced. Usually, a small excess steam condenser is required to handle variations between the rates of steam generation and demand. At present, steam pressures above 25 psig are not feasible in standard engine jackets. Such low-pressure steam can be used for space heating, process heating, and absorption refrigeration. If higher pressures could be generated, more general use of the steam could be made, with attendant savings in boiler facilities. High temperatures associated with the higher steam pressures would probably have some effect upon cooling efficiency. However, potential savings are so great that considerable experimental and development work on high-pressure jackets is justifiable.

DESCRIPTION OF STANOLIND'S INSTALLATIONS

Each of four engine-driven compressors (two Clark RA-8's and two Clark RA-6's) at the Midland Farms Plant is equipped with an ebullition-cooling system similar to that shown in Fig. 2. The steam is condensed in the upper section of an elevated air-cooled unit, while water used for cooling the compressor cylinders and the lubricating oil is cooled in the lower section of the unit. Each unit is equipped with two small forced-draft fans which blow air vertically across the two coils in series. Those fans and a pump for circulating cooling water through the compressor-cylinder jackets are equipped with hydraulic-motor drivers. Each compressor engine drives a hydraulic pump which supplies hydraulic power to the motors. Originally, a manual by-pass around each hydraulic motor provided speed control for varying the flow of air and water. The fans are now equipped with automatically controlled by-passes which are actuated by steam pressure. Controlling the fan speed in this manner prevents fluctuation of the steam pressure with changes in atmospheric temperature.

One engine-driven compressor (Clark HRA-8H) at the South Fullerton gasoline plant is equipped with an ebullition-cooling

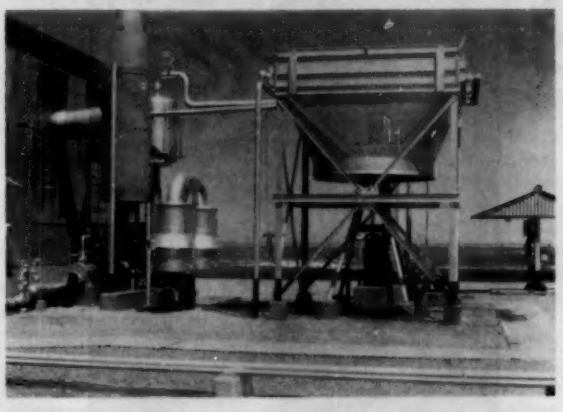

FIG. 8

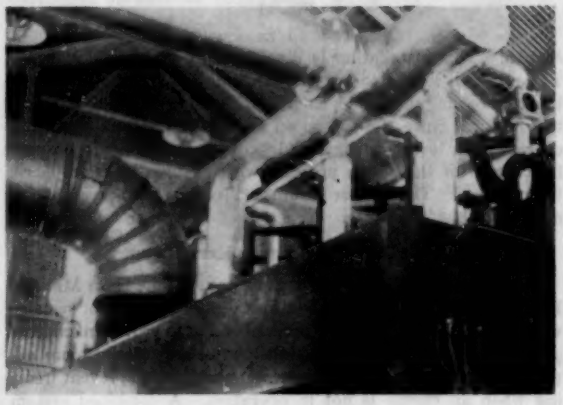

FIG. 9

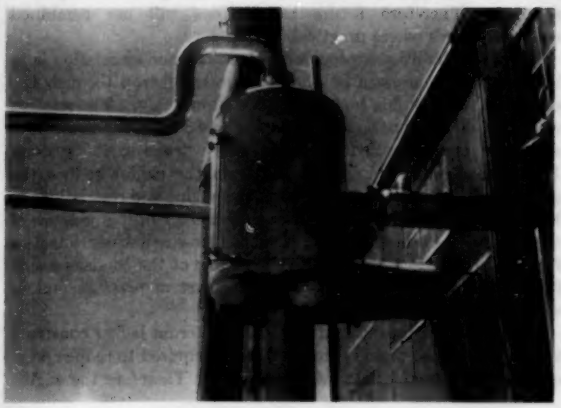

FIG. 10

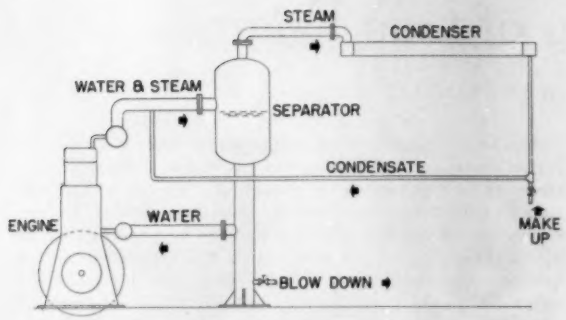

FIG. 2 EBULLITION-COOLING SYSTEM

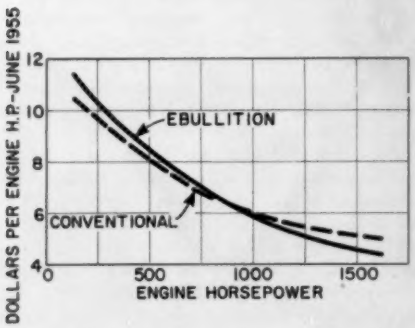

FIG. 3 PRICE OF COOLING EQUIPMENT FOR SLOW-SPEED ENGINES

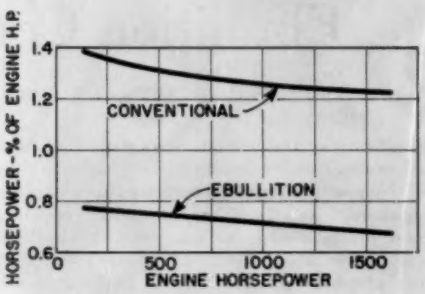

FIG. 4 POWER FOR COOLING SLOW-SPEED ENGINES

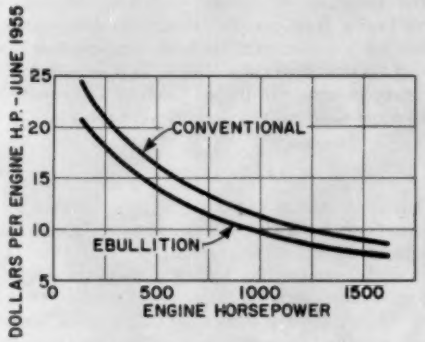

FIG. 5 INSTALLED COSTS OF COOLING EQUIPMENT FOR SLOW-SPEED ENGINES

higher heat-transfer rates that result when condensing steam.

Power requirements are less because of the smaller fan and driver and the elimination of the engine-jacket water pump. Obviously, operating and maintenance costs are lower for the same reasons.

In addition, engine maintenance costs are reported by several operators to be less. Uniform heat transfer at a high rate is achieved by the turbulent boiling action and there is little or no gradient in the temperature of the coolant. Therefore the cylinder walls have more uniform temperatures and less distortion or taper than with conventional cooling. Those conditions result in less wear of the cylinders and pistons, thereby reducing piston blowby and oil sludging.

Fig. 3 compares the initial costs of cooling equipment for both the ebullition system and the conventional system for slow-speed engines. Cost in dollars per engine horsepower based on June, 1955, prices is plotted against engine horsepower. The costs for ebullition systems include the purchase prices for a separator, an air-cooled steam condenser, and the necessary instruments and controls to maintain a steam pressure less than 5 psi. The costs for conventional systems include the purchase prices for a jacket-water surge tank, a jacket-water pump, an air-cooled exchanger, and the necessary instruments and controls to maintain a maximum water temperature of 170 F.

Fig. 4 compares the auxiliary power required by cooling equipment covered by Fig. 3 for both the ebullition system and the conventional system for slow-speed engines. Auxiliary horsepower, expressed in per cent of engine horsepower, is plotted against engine horsepower. The power for the ebullition system is that required by the fan. The power for the conventional system includes that required by the fan and the jacket-water pump.

Fig. 5 compares the installed costs of slow-speed engine-cooling

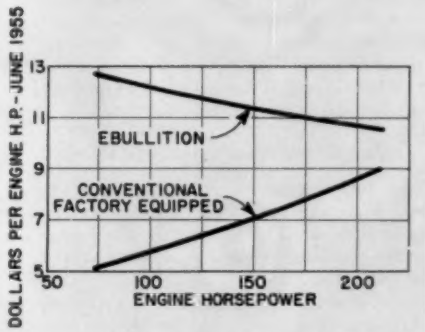

FIG. 6 PRICE OF COOLING EQUIPMENT FOR HIGH-SPEED ENGINES

equipment for both the ebullition system and the conventional system. The units and the basis for the indicated values are similar to those of Fig. 3. The costs include all labor and material which are required to make the installation ready for operation.

Fig. 6 compares the initial costs for cooling equipment for both the ebullition system and the conventional system for high-speed engines. The units and the basis for the indicated values are similar to those of Fig. 3.

Fig. 7 compares the auxiliary power required by cooling equipment for both the ebullition system and the conventional system for high-speed engines. The units and the basis for the indicated values are similar to those of Fig. 4.

The costs and auxiliary-power requirements for the factory-equipped conventional systems (radiators) furnished with high-speed engines are based on data obtained from a limited number

of engine manufacturers. Power requirements and costs for engines furnished by other manufacturers may vary slightly from the data indicated. However, these values are considered sufficiently accurate to be satisfactory for this comparison.

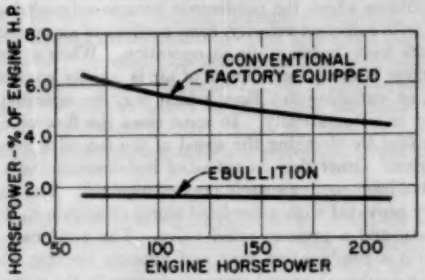

FIG. 7 POWER FOR COOLING HIGH-SPEED ENGINES

In all cases, the data apply to complete systems for cooling only jacket water on single engines. For cases where a single system is used for cooling several engines or jacket cooling is integrated with other services, somewhat different data will apply.

Installed costs for cooling equipment on high-speed engines are not given because such data were not available.

No data are given for high-temperature water-cooling systems because there are no economic or operational advantages for such systems in comparison with ebullition systems.

At least 15 per cent, and in many cases as much as 30 per cent, of the heating value of the engine fuel goes into steam which is generated in an ebullition system. Therefore very appreciable fuel savings can be made if the steam can be utilized, although it is normally condensed in an air-cooled unit. If the steam is used, a condensate-return system is usually required, but that cost is offset to some extent by a reduction in size of the steam condenser. In addition, boiler feedwater and steam generating facilities can be reduced. Usually, a small excess steam condenser is required to handle variations between the rates of steam generation and demand. At present, steam pressures above 25 psig are not feasible in standard engine jackets. Such low-pressure steam can be used for space heating, process heating, and absorption refrigeration. If higher pressures could be generated, more general use of the steam could be made, with attendant savings in boiler facilities. High temperatures associated with the higher steam pressures would probably have some effect upon cooling efficiency. However, potential savings are so great that considerable experimental and development work on high-pressure jackets is justifiable.

DESCRIPTION OF STANOLIND'S INSTALLATIONS

Each of four engine-driven compressors (two Clark RA-8's and two Clark RA-6's) at the Midland Farms Plant is equipped with an ebullition-cooling system similar to that shown in Fig. 2. The steam is condensed in the upper section of an elevated air-cooled unit, while water used for cooling the compressor cylinders and the lubricating oil is cooled in the lower section of the unit. Each unit is equipped with two small forced-draft fans which blow air vertically across the two coils in series. Those fans and a pump for circulating cooling water through the compressor-cylinder jackets are equipped with hydraulic-motor drivers. Each compressor engine drives a hydraulic pump which supplies hydraulic power to the motors. Originally, a manual by-pass around each hydraulic motor provided speed control for varying the flow of air and water. The fans are now equipped with automatically controlled by-passes which are actuated by steam pressure. Controlling the fan speed in this manner prevents fluctuation of the steam pressure with changes in atmospheric temperature.

One engine-driven compressor (Clark HRA-8H) at the South Fullerton gasoline plant is equipped with an ebullition-cooling

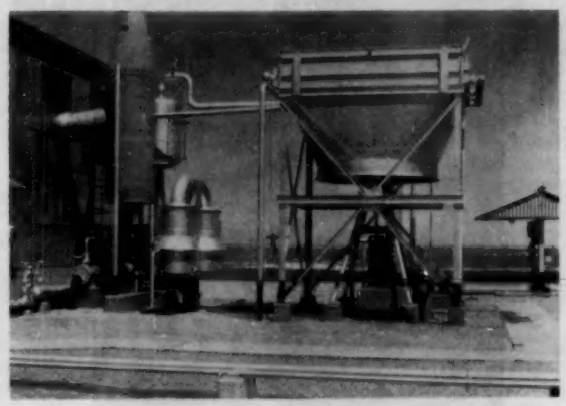

FIG. 8

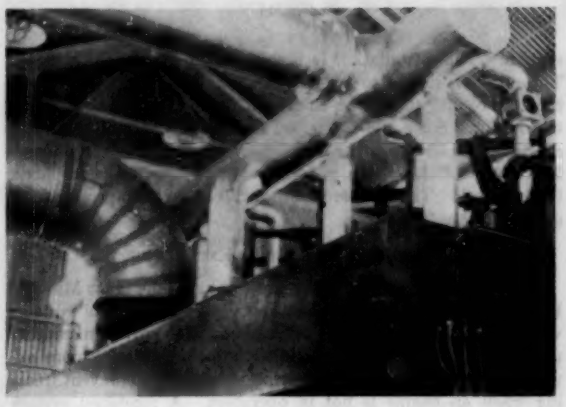

FIG. 9

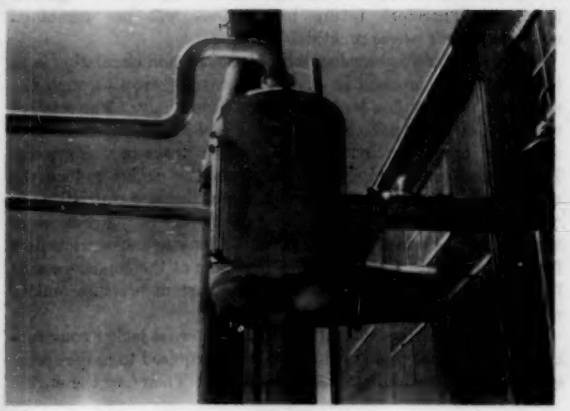

FIG. 10

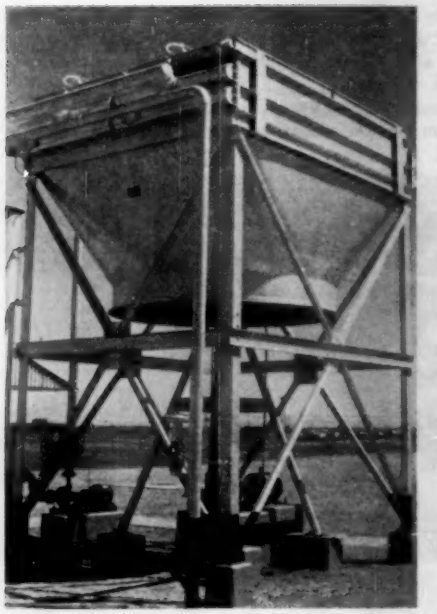

FIG. 11

system. This installation is illustrated in Figs. 8 through 11. The system is similar to those at the Midland Farms Plant except that the cooling unit has a single fan which is driven by an electric motor. Since the fan speed is constant, an automatically operated shutter is provided on top of the steam coil to prevent fluctuation of the steam pressure with changes in atmospheric temperature. The shutter is actuated by the steam pressure and maintains it at 2 to 3 psig.

RESULTS OF OPERATING EXPERIENCE

A single system to serve all engines was considered for Midland Farms but since that was a trial installation, individual systems were used in order to simplify operations and to provide maximum performance data. The individual units are usually more expensive and they necessitate special precautions to prevent freezing when an engine is not in operation. A combined system minimizes the freezing hazard because some thermal circulation is maintained throughout the system as long as one engine is running. Therefore future installations will use combined cooling systems where practical.

When an ebullition system with thermosiphon circulation is to be installed, it is essential that the pressure drop through the equipment and piping be investigated thoroughly. The relative elevation of the separator and engine and of the condenser and separator are controlled by the pressure drops in the system. Restrictions in the piping to and from the engine reduce the amount of water circulated through the engine and restrictions in the steam piping to the condenser raise the operating pressure of the system. An inadequately sized condensate line restricts flow from the condenser, thereby flooding some of the condenser surface. This condition results in higher system pressure and in subcooled condensate.

With some engines alterations of the internal jacket construction or additional piping connections are required to reduce pressure drop or to eliminate vapor pockets. Therefore the engine manufacturer should always be consulted regarding the use of ebullition cooling.

Experience has indicated that it is advisable both to control the flow of air and to slope the tubes for drainage in any air-cooled equipment in which the fluid is subject to freezing. Under certain conditions where the condensate became subcooled and did not flow with sufficient velocity, some sections of air-cooled steam condensers have frozen while in operation. When a constant-speed driver is used, the amount of air is usually controlled by shutters or variable-pitch fans, which may be operated either manually or automatically. In some cases the flow of air may be controlled by changing the speed of the fan with a variable-speed drive. Otherwise, complicated instruments and controls for an ebullition-cooling system are not required. The separator is usually provided with a low-level alarm or shutdown device, a gage glass, and a pressure-relief valve. The condenser is provided with a combination vent and vacuum breaker which removes noncondensables and prevents vacuum in the system when it cools after shutdown.

Some difficulties were experienced in operating the hydraulic-drive systems on the Midland Farms units owing to faulty hydraulic equipment and foreign material in the hydraulic lines. However, replacement of the faulty equipment and modification of the system have improved operation appreciably. Operators report no particular difference in operation from conventionally cooled engines, except for the freezing problem which was discussed earlier. No detonation difficulty has been reported although the fuel has a rather high Btu content. The oil has not been affected adversely to any detectable degree by ebullition cooling. No extraordinary sludging is indicated in the full-flow oil filters.

Engine-performance tests demonstrated that the South Fullerton engine could handle 120–125 per cent of its altitude horsepower rating after six months of operation. Such performance is obtainable only if the engine is in good mechanical condition and therefore it indicates that no unusual wear has occurred. No inspection has been made of the condition of crankcase, bearings, or power cylinders, but there is no indication of piston blowby or sludging of the oil. There has been no detonation except for a slight pinging when the engine was overloaded. Operators report that the engine cooled by ebullition requires less attention and runs more smoothly than any other compressor engine at the location (eight BA-8's). There are no particular start-up, shutdown, or operating problems.

Proper water treatment is essential for low maintenance and continuous operation in any system which uses water. Normally, treatment for steam systems is more expensive and requires closer attention than treatment for liquid systems. However, treatment of ebullition systems for engine cooling is not difficult because of low make-up requirements with the closed cycle. If possible, steam condensate or rain water should be used in any type of jacket-water cooling system. With such water, satisfactory protection against corrosion can be obtained in ebullition systems with the same high chromate treatment that is suitable for conventional systems. If raw water must be used in an ebullition system, a phosphate treatment suitable for low-pressure boilers will protect against formation of scale. With such treatment, a sulphite residual must be maintained in the system at all times to prevent oxygen attack.

CONCLUSION

On the basis that ebullition cooling is economical, efficient, and simple, as indicated by the cost and operating information presented herein, the authors' company expects to make general use

of such cooling on future installations of slow-speed gas engines, except for unattended units in areas with serious freezing problems.

Several companies already have similar plans and others may be expected to follow the trend to make ebullition the generally accepted method for cooling internal-combustion engines. Therefore manufacturers should be ready to provide engines that are satisfactory for ebullition cooling without alteration of the jackets or installation of complicated piping. Jackets also should be designed for high pressures so that steam generated in them can be used for general service. Then the internal-combustion engine will be more efficient than was ever hoped in the past.

Acknowledgment

The authors thank the management of Stanolind Oil and Gas Company for permission to publish this paper. Appreciation is also expressed to operating personnel who provided information from the plants and to Mr. G. C. Hickman who assisted in preparation of the cost data.

References

1 "Engine Cooling by Ebullition," by O. B. Freeman, *Oil and Gas Journal*, vol. 51, February 23, 1953, pp. 172–174, 178.

2 "Boiling Heat Transfer," by O. B. Freeman, *The Petroleum Engineer*, October, 1953, pp. B108, B112, and B115–B116.

3 "Boiling Point Cooling Systems," by G. M. Jackson, paper presented before the 28th Annual Fall Meeting of the CNGA, October, 1953, *Petroleum Engineer*, vol. 26, July 15, 1954, pp. D32, D34, and D36.

4 "Engine Cooling by Ebullition," by R. P. Bland, *Oil and Gas Journal*, vol. 52, March 22, 1954, pp. 324–325, 327, and 329.

5 "Vapor Phase Engine Cooling," by L. C. Harbert, *The Petroleum Refiner*, vol. 33, April, 1954, pp. 127–131.

6 "Latent Cooling of Compressors," by H. Menard and E. D. Blossom, *Oil and Gas Journal*, vol. 52, April 26, 1954, pp. 231–236.

7 "How Large Gas Compressors Utilize Vapor Phase Engine Cooling," by L. C. Harbert, *Gas*, vol. 30, August, 1954, pp. 91–92, 94–96, 98, and 101–102.

8 "Advantages of Latent Cooling of Compressors," by H. Menard and E. D. Blossom, *The Petroleum Engineer*, vol. 27, August, 1955, pp. C-12, C-14–C-15, and C-18.

Discussion

Harvey Menard.[4] We have found that the condensate should be returned to the steam-water system in such a fashion that the condensate temperature is raised to the boiling point. Merely returning the condensate stream to the flowing steam-water mixture is not always sufficient to allow the subcooled condensate to absorb sufficient heat to bring it to boiling temperature. One scheme of accomplishing this is to bring the condensate into the separator in a pipe coil or distributing channel that would allow heat transfer between the steam and the condensate. This also might reduce the condenser load by a very nominal degree. Recent experience in Signal's installations at Oklahoma and North Dakota have indicated that a length of ordinary pipe laid horizontally makes a perfectly adequate separator. A horizontal separator gives more separating surface.

We do not have any particular need for low-level heat and are not using the same. For those that can use it, the heat would be valuable. We are pleased to see an expression in this paper reiterating that high-pressure steam produced in engine jackets might relieve the load on boiler facilities.

Conceivably, high-pressure steam might replace boilers in some plants with high compressor horsepower and low steam requirements. We are convinced this can be done without serious engine-maintenance problems. Now that there is so much interest in latent cooling it is time that the engine manufacturers contributed to the available information on this type of operation.

Authors' Closure

Mr. Menard's remarks are appreciated. They support the authors' conclusion that further study and improvement can make ebullition cooling even more attractive than it is at present. The authors also agree with Mr. Menard that the engine manufacturers should contribute to such study and experimentation.

[4] General Superintendent, Signal Oil and Gas Company, Long Beach Field Office, Long Beach, Calif.

Resistance Coefficients for Accelerated and Decelerated Flows Through Smooth Tubes and Orifices

By J. W. DAILY,[1] W. L. HANKEY, JR.,[2] R. W. OLIVE,[3] and J. M. JORDAAN, JR.[4]

This paper is a summary of the results of investigations of the drop in potential and boundary resistance in unsteady motion for cases of surface resistance caused by boundary shear stresses and cases of form-type resistance associated with the high shear and generation and diffusion of turbulence accompanying jet formation. These cases were obtained using uniform diameter conduits and orifices in conduits. From tests in the MIT unsteady flow water tunnel, the effects of accelerated and decelerated flows were studied. In the case of flow through a uniform tube, it was found that the boundary resistance at any instant during accelerated motion was slightly greater than the equivalent steady-state case while, for decelerated motion, it was slightly less. In the case of flow through orifices, it was found that the combined resistance of the orifice and the conduit was less during accelerated motion and more during decelerated motion than for the equivalent steady-state cases.

Introduction

IN the prediction of transients involving hydrodynamic or aerodynamic phenomena, it has been customary to calculate pressure variation and fluid resistance, neglecting possible effects of unsteadiness on the mechanics of the fluid motion. There are several areas for which knowledge of the effects of unsteadiness on resistance would be useful. Included, for example, are transient resistance and stability of accelerating missiles and other immersed objects, flowmeter coefficients with pulsating flows, and transient hydrodynamic performance of pumps, compressors, and turbines. The latter is a category where under many circumstances steady-state performance has been used with good results in predicting transient pressures and machine accelerations and decelerations. Yet, recently, in connection with pumps of special design, discrepancies between measured and calculated transients have indicated what is probably an effect of unsteadiness on the basic fluid motion. In all cases, a basic question is the effect of unsteadiness on fluid shear and turbulence generation, and the resulting effects on the inertial and frictional components contributing to the instantaneous total potential drop.

This paper summarizes the results of investigations in the MIT unsteady flow water tunnel (1–4)[5] of accelerated and decelerated flow through uniform conduits and orifices in conduits. In the uniform conduit shear and turbulence are generated through boundary-layer friction and are essentially uniform along the duct. The orifices cause separation and jet formation with accompanying high shear and turbulence which vary along the duct as the jet diffuses and the turbulence is dissipated.

Unsteady Flow Equations

As a basis for analyzing experimental results, the following momentum analysis was made in which the effects of all the variables including turbulence are considered. Thus while the equations are reduced ultimately to essentially a one-dimensional form, more insight is given to the significance of each term than is readily apparent from an ordinary one-dimensional analysis.

Consider a constant-diameter conduit which may be unobstructed or may contain constrictions such as orifices or venturi sections. Let the dotted boundary shown in Fig. 1 define a control volume for a general case.

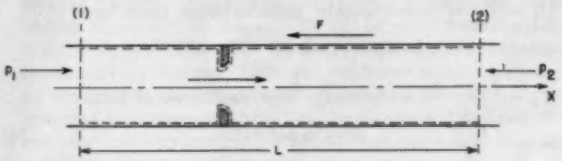

Fig. 1 Constant-Diameter Conduit

Applying the momentum principle to unsteady turbulent liquid flow through such a system, we can write the instantaneous balance

(External forces) = Σ (net flux of momentum from control volume + rate of change of momentum within the volume)

or, for the x-direction

$$\int^{A_1} P_1 dA - \int^{A_2} P_2 dA - F = \int^{A_2} \rho U_2^2 dA - \int^{A_1} \rho U_1^2 dA + \int^{V} \rho \frac{\partial U}{\partial t} dV \quad \ldots\ldots [1]$$

where

P = x-component of local pressure intensity
F = lumped boundary resistance due to wall shear and any constrictions
U = local velocity
V = liquid volume within control surface

[1] Associate Professor of Hydraulics, Massachusetts Institute of Technology, Cambridge, Mass. Mem. ASME.

[2] First Lieutenant, USAF, and Project Engineer, Transonic Wind Tunnel, Wright Patterson Air Force Base, Ohio.

[3] Manufacturing Supervision Trainee, Manufacturing Training Program, General Electric Company, River Works, Lynn, Mass. Mem. ASME.

[4] Research Assistant, Hydrodynamics Laboratory, Massachusetts Institute of Technology, Cambridge, Mass.

Contributed by the Hydraulic Division and presented at the Diamond Jubilee Semi-Annual Meeting, Boston, Mass., June 19–23, 1955, of The American Society of Mechanical Engineers.

Note: Statements and opinions advanced in papers are to be understood as individual expressions of their authors and not those of the Society. Manuscript received at ASME Headquarters, June 29, 1955. Paper No. 55—SA-78.

[5] Numbers in parentheses refer to the Bibliography at the end of the paper.

Analogous to "steady" turbulent flow we will assume that at each instant during a transient the velocity field can be described as a "mean flow" plus a "fluctuating flow" and introduce the usual notation

$$U = u + u' \quad \ldots\ldots [2]$$

Here then u is a kind of mean value like the temporal mean value of statistically steady turbulent motion. Using Equation [2] gives

$$\int^{A_1} P_1 dA - \int^{A_2} P_2 dA - F = \int^{A_2} \rho u_2^2 dA - \int^{A_1} \rho u_1^2 dA + \int^{A_2} \rho u_2'^2 dA - \int^{A_1} \rho u_1'^2 dA + 2\int^{A_2} \rho u_2 u_2' dA - 2\int^{A_1} \rho u_1 u_1' dA + \int^{V} \rho \frac{\partial u}{\partial t} dV + \int^{V} \rho \frac{\partial u'}{\partial t} dV \quad \ldots\ldots [3]$$

At this stage it is customary in analyzing turbulent flows to take temporal mean values of all terms in the equations in order to obtain a relation governing the main flow. This ignores the contribution of the terms that are linear in the turbulent components, because they drop out in the averaging process. For very rapid changes of the main flow this may not be justified. We will leave the equation in terms of the instantaneous velocity fluctuations so that the relative importance of the instantaneous turbulence can be examined. Let us introduce the definitions

$p = \dfrac{\int P dA}{A}$ = average pressure intensity over cross section

$U_0 = \dfrac{Q}{A}$ = instantaneous cross-sectional mean velocity in conduit

$K_u = \dfrac{p_1 - p_2}{\rho \dfrac{U_0^2}{2}}$ = unsteady flow coefficient of total drop in potential $\quad \ldots\ldots [4]$

$K = \dfrac{F}{\dfrac{\rho U_0^2 A}{2}}$ = unsteady flow coefficient of boundary resistance $\quad \ldots\ldots [5]$

$\beta = \dfrac{\int^A u^2 dA}{U_0^2 A}$ = distribution factor for mean velocity $\quad \ldots\ldots [6]$

$I = \dfrac{\int^A u'^2 dA}{U_0^2 A} + \dfrac{2\int^A u\, u' dA}{U_0^2 A}$ = distribution factor for turbulent fluctuations $\quad \ldots\ldots [7]$

$c_1 = \dfrac{\int^V \dfrac{u}{U_0} dV + \int^V \dfrac{u'}{U_0} dV}{V}$ = inertial coefficient $\quad \ldots\ldots [8]$

Using these definitions, Equation [3] is expressed dimensionlessly as

$$K_u = K + 2[(\beta_2 - \beta_1) + (I_2 - I_1)] + \frac{2V}{U_0^2 A} \frac{\partial}{\partial t}(c_1 U_0) \quad \ldots\ldots [9]$$

If in Equation [8] we introduce the approximations that the space average values of u/U_0 and u'/U_0 are independent of time, we can write Equation [9] as

$$K_u = K + 2[(\beta_2 - \beta_1) + (I_2 - I_1)] + c_1 \frac{2aV}{U_0^2 A} \quad \ldots\ldots [9a]$$

where $a = \partial U_0/\partial t$ = acceleration of mean flow in conduit.

The last term in Equation [9] is the dimensionless force due to the inertia of the turbulent fluid to local accelerations. The second right-hand term gives the effect of nonuniformity of the mean flow and turbulence intensity between sections 1 and 2. It is the dimensionless x-component of the flux of momentum of the absolute motion. While the effect of turbulence appears explicitly only in the last two right-hand terms, it also appears indirectly in the resistance coefficient K. The velocity and turbulence distributions within the liquid volume are interdependent with the boundary shears and pressures and hence the boundary resistance.

Also, to the extent that the establishment of each instantaneous velocity and turbulence distribution requires some absolute time interval for the adjustment from a previous condition, the relative magnitudes of the several terms in this force-momentum balance may depend on the rate of change of acceleration as well as the magnitude of the acceleration.

By the preceding formulation the boundary resistance for a constricted tube includes the extra pressure drag of the constriction due to the accelerated flow past the boundary. This extra drag corresponds to the additional apparent mass effect of immersed bodies in unsteady motion. If the coefficient c_1 were allowed to absorb the apparent mass contribution, the coefficient K would include only the resistance associated with the presence of viscosity and turbulence. For the experiments to be described, c_1 is calculated by the approximation

$$c_1 \approx \frac{1}{L}\int_0^L \frac{V}{U_0} dx \quad \ldots\ldots [10]$$

where V = average velocity over the cross section of the main stream (jet) at any x. By this equation, c_1 is increased over values given by Equation [8] by an order of magnitude approximating the added inertia effect.

While Equation [9] is useful for qualitative indication of how turbulence, flow uniformity, and acceleration affect the total potential drop and boundary resistance, it cannot be used for quantitative comparisons because the required instantaneous velocity and turbulence distributions cannot be calculated or measured. Because of this, and because it is desirable to make comparisons with steady-state conditions corresponding to given instantaneous rates of discharge, we introduce the following simplifications. Let

$$\left.\begin{aligned} K_u &= K + 2[(\beta_2 - \beta_1) + (I_2 - I_1)] \\ &= K_s + K_t \end{aligned}\right\} \quad \ldots\ldots [11]$$

where

K_u = unsteady flow coefficient of boundary resistance and momentum flux of absolute local velocity
K_s = one-dimensional steady-state "resistance" coefficient
K_t = correcting coefficient to measure the additional transient effects on boundary resistance and momentum flux of absolute local velocity

Equation [9] becomes

$$K_u = K_s + K_t + c_1 \frac{2aV}{U_0^2 A} \quad \ldots\ldots [12]$$

For steady flow this reduces to the relation given by the conventional one-dimensional energy equation where the resistance coefficient is taken as a measure of the energy dissipation.

Equation [12] can be simplified further with the aid of an analogy to Schonfeld's analysis for smooth round tubes (5). Schonfeld presents the solution for the special case of slowly varied motion in which the resistance dominates (as opposed to quickly varied motion where the inertia dominates). He obtains for uniform diameter tubes

$$p_1 - p_2 = \frac{\rho g L}{R_h C'^2}\frac{Q^2}{A^2} + N\frac{dQ}{dt} \quad [13]$$

where

Q = rate of discharge
R_h = hydraulic radius
C' = steady flow Chezy coefficient

$$N = \frac{\rho L}{A}\left[1.0 + \frac{234}{(C' + 14.0)^2}\right] \quad [14]$$

By substituting $Q = AU_0$, $R_h = D/4$, and $C' = \sqrt{(8g/f_s)}$, Equation [13] can be written for the tunnel test section thus

$$\frac{p_1 - p_2}{\rho\frac{U_0^2}{2}} = f_s\frac{L}{D} + \frac{0.91}{\left(\frac{1}{\sqrt{f_s}} + 0.87\right)^2}\frac{2aL}{U_0^2} + \frac{2aL}{U_0^2} \quad [15]$$

where

f_s = steady flow friction factor

We note that this can be put in the form of Equation [12] if we make the substitutions

$$\frac{2a\mathrm{V}}{U_0^2 A} = \frac{2aL}{U_0^2}$$

$$c_1 = 1.00$$

$$K_s = \frac{f_s L}{D} \quad [16]$$

$$K_i = \frac{0.91}{\left(\frac{1}{\sqrt{f_s}} + 0.87\right)^2}\frac{2aL}{U_0^2} \quad [17]$$

As these substitutions indicate, Schonfeld's analysis considers the turbulence to be fully developed at every instant and uniform conditions to exist along the length of the conduit. Thus, referring to Equation [8], we see that the value $c_1 = 1.00$ implies that the mean value of the turbulent fluctuations over the liquid volume of the uniform tube is zero at all times so that the inertial coefficient is merely

$$c_1 \approx \frac{\int^{\mathrm{V}}\frac{u}{U_0}d\mathrm{V}}{\int^{\mathrm{V}}d\mathrm{V}} = 1$$

Furthermore, if similar flow conditions exist at all sections along the conduit, the term $(\beta_2 - \beta_1)$ will be zero and the term $(I_2 - I_1)$ will approach zero for sufficiently random values of u' at each instant over each annular increment of flow area at the two sections. Thus K_i as given by Equation [17] implies no influence of nonuniformity in velocity or turbulence.

Returning now to the more general case which may include tubes with constrictions, let us write in analogy to Equation [17]

$$K_i = c_2\frac{2a\mathrm{V}}{U_0^2 A} \quad [18]$$

In Equation [18] c_2 is a measure of the deviations, due to unsteadiness, of the boundary resistance and flux of momentum. Using Equation [18], Equation [12] reduces to

$$K_u = K_s + c\frac{2a\mathrm{V}}{U_0^2 A} \quad [19]$$

with

$$c = c_1 + c_2 \quad [20]$$

We can also write this as

$$\frac{K_u}{K_s} = 1 + c\frac{2a\mathrm{V}}{K_s U_0^2 A} \quad [21]$$

or, noting from Equations [11] and [12] that

$$K_u = K_s + K_i = K_u - c_1\frac{2a\mathrm{V}}{U_0^2 A}$$

$$\frac{K_u}{K_s} = 1 + c_2\frac{2a\mathrm{V}}{K_s U_0^2 A} \quad [22]$$

Equations [19], [21], and [22] are alternate statements of the balance of forces specified by the momentum principle. Moreover, to the extent that the quantity $2[(\beta_2 - \beta_1) + (I_2 - I_1)]$ in Equation [11] approaches zero, K_u becomes equal to K and the equations will be useful for comparing the steady and unsteady boundary resistance at given instantaneous discharge rates. Here we note, that as for a clear conduit, flow through a constricted conduit having a test length L much longer than the disturbed flow zone caused by the constriction should exhibit approximately the same velocity and turbulence distributions at sections 1 and 2. Hence only a small error is introduced by assuming $K_u = K$.[8] In this case, it will be noted from Equation [22] that, for accelerated flow where a is positive, positive values of c_2 will indicate that *more* boundary resistance is developed than for steady flow and negative values will indicate less. For decelerated flow where a is negative, positive c_2 will indicate that *less* boundary resistance is developed than for steady flow and negative values will indicate more.

Using experimental results in Equation [19] will give the coefficient c. The coefficient c_1 can be evaluated from a flow net of the jet profile through the constriction using the definition of Equation [10]. The resulting value of c_2, obtained as $(c - c_1)$, will absorb the difference between the true total inertial effects and the value calculated by Equation [10], as well as the deviations, due to unsteadiness, of the boundary resistance and flux of momentum.

Experimentally, it is convenient to evaluate the comparison between steady and unsteady behavior from a simple series of measurements of total potential drop along the conduit versus instantaneous flow rate. From each such basic experiment, the comparison can be obtained for each of a range of values of the ratio

[8] Subsequent to the initial preparation of this paper, a series of steady-state mean velocity traverses were made upstream and downstream of the 0.5 orifice in the 1-in. conduit. Profiles were obtained at distances 7.5 diameters upstream and 3, 4.5, 6, 7.5, 10.5 diameters downstream. According to these measurements, some difference exists between profiles at the measuring stations used of 4.5 diameters upstream and 7.5 diameters downstream. This results in a correction $2[(\beta_2 - \beta_1) + (I_2 - I_1)]$ which is the order of magnitude 1 per cent of K_s, based on the calculated difference $(\beta_2 - \beta_1)$, plus an allowance for some difference $(I_2 - I_1)$. It appears to be important only for near-zero values of a/U_0^2.

$$\frac{aV}{U_0^2A} = \frac{aL}{U_0^2}$$

Finally, note that the term

$$\frac{aV}{U_0^2A} = \frac{aL}{U_0^2}$$

is a parameter proportional to the ratio of local to convective acceleration. If all the effects of unsteadiness are fundamentally dependent on the acceleration of the mean flow, the coefficients in Equations [21] and [22] will be constants, otherwise not.

Experimental Apparatus

The apparatus used for these experiments is a nonreturn unsteady-flow water tunnel (6). As shown by the schematic section in Fig. 2, the tunnel consists of two cylindrical tanks mounted one above the other and connected by a 1-in-diam smooth brass conduit 99 diameters in length. This conduit constitutes the test section in which constrictions such as orifices or venturi sections can be placed. Water is caused to flow from one tank to the other under pneumatic control. Compressed air is admitted to the spaces above the water surfaces in the two tanks to provide a driving force for a desired flow rate and acceleration or deceleration. To obtain the desired ranges of acceleration and pressure in the working section, compressed air must be admitted to, or released from, either tank according to some time schedule. To prevent cavitation and the introduction of air into the piezometric system, the test section is maintained at positive pressure by throttling the exhaust from the bottom tank. The square-edged orifices employed were dimensioned according to ASME standards and constructed from 0.102-in-thick sheet brass. The conduit and orifice combinations used and the principal dimensional data and location of piezometer taps are given in Table 1 and Fig. 3.

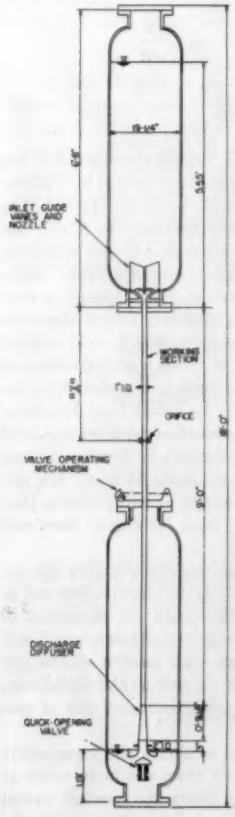

Fig. 2 Schematic Section of Tunnel Showing Location of Orifice

In all experiments the beginning of the test length over which potential drops were measured was located well beyond the calculated transition distance necessary to establish a fully developed turbulent velocity profile in the 1-in. tube. In most tests the test length began at approximately 33 diameters from the entrance nozzle, the orifice being located at $x = 37.5$ diameters, Fig. 2. In some cases a 28-diameter approach was used ($x = 32.5$ diameters). The actual test length L was 27 diameters for the unobstructed tube and 12 diameters for the cases of orifice-constricted tube. For the latter, the piezometer taps were located 4.5 diameters upstream and 7.5 diameters downstream of the orifice plate. The 7.5-diameter downstream distance was chosen to include the expected zone of influence of the orifice on the local flow conditions (7).[6] Some measurements also were made with the downstream piezometer taps 22.5 diameters from the orifice as checks in case the orifice disturbance persisted for greater distances for unsteady flow than for steady. The results of these checks did not alter the conclusions drawn from the measurements over the shorter distance.

TABLE 1 TEST COMBINATIONS AND PRINCIPAL DIMENSIONS

	Area ratio	$\frac{d}{D}$	Assumed jet dimensions $\frac{d_j}{D}$	Diffusion angle for 4-diam expansion
Smooth tube.....	1.0	1.0		
Orifice in tube.....	0.7	0.837	0.72	4°22′
Orifice in tube.....	0.5	0.707	0.59	6°38′
Orifice in tube.....	0.3	0.548	0.44	9°06′

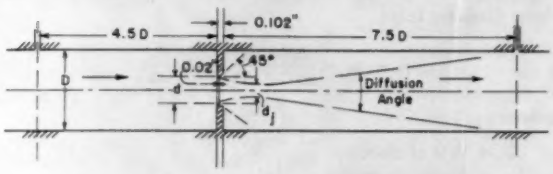

Fig. 3 Conduit and Orifice Combinations, Dimensional Data and Piezometer-Tap Locations

The nozzle at the inlet to the working section is used for flow measurements. The instantaneous pressure drops recorded during unsteady flows are corrected to account for the inertia force due to the local acceleration of the fluid through the nozzle. The correction calculated assuming potential flow is equal to

$$\frac{0.2}{g}\frac{dU_0}{dt}$$

The several differential pressures were measured with diaphragm-type pressure cells in which the diaphragm deflection actuates a differential transformer. Each pressure-gage signal is sent through a separate amplifying and detecting unit and is then recorded versus time. Two amplifying-recording systems were used during the experiments; in one, a photographic record was obtained using a Hathaway Type S8-C oscillograph; in the other, the record was traced with a temperature stylus on Sanborn "Permapaper" using a four-channel Sanborn recorder, Model 150. Measured natural frequencies of the pressure cells and oscillograph-recording system connected as for testing including water-filled lead lines, exceeded 165 cycles per second (eps). With the Sanborn recorder the limit of accurate response is about 100 cps. Instantaneous differential pressures were evaluated using static calibrations of each gage before and after test runs.

Experimental Program

The range of variables for the experiments reported here are given in Table 2. As the table indicates, a range of velocities and accelerations or decelerations was included. In addition, the several tests included different rates of change of acceleration.

Acceleration tests were made from zero velocity or were preceded by an initial period of steady flow. All deceleration tests were preceded by an initial period of steady flow. At the start of each unsteady period was an initial impulse phase during which the acceleration (or deceleration) changed rapidly ($|da/dt| \gg 0$). Following this was an "established" phase, distinguished by either constant or more slowly changing acceleration. In general, the acceleration or deceleration varied continuously although, in the case of the uniform diameter conduit, several runs,

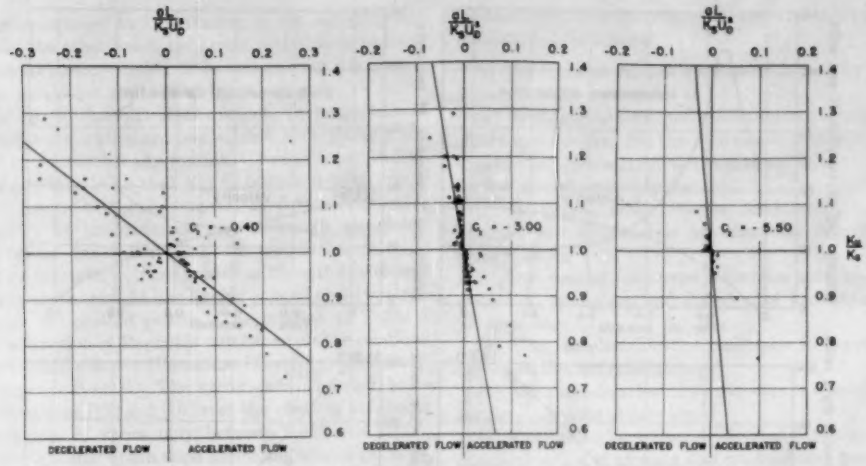

FIG. 4 ORIFICE-AREA RATIO 0.7 FIG. 5 ORIFICE-AREA RATIO 0.5 FIG. 6 ORIFICE-AREA RATIO 0.3

(Parametric presentation of unsteady flow frictional resistance coefficients for orifices and smooth conduits.)

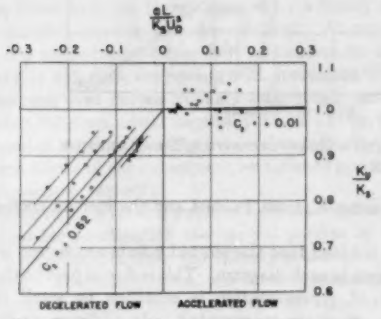

FIG. 7 SMOOTH CONDUIT—AREA RATIO 1.0

(Parametric presentation of unsteady flow frictional resistance coefficients for orifices and smooth conduits.)

each with essentially constant deceleration, were obtained. The period of the initial impulse phase varied and it was not always possible to obtain reliable recordings of the instantaneous pressures. Typical test results appear in Figs. 8(*a*) and 8(*b*). These diagrams show instantaneous conduit velocity U_0, acceleration dU_0/dt, and total potential head drop H_s as calculated from oscillograph recordings.

From such data values of

$$K_s = \frac{H_s}{U_0^2/2g} \text{ versus } \frac{aL}{U_0^2}$$

were obtained for successive time intervals throughout the test. Any one run gives a wide range of values of aL/U_0^2. From steady flow data, values of K_s versus Reynolds number were computed. These were used to relate the successive instantaneous conditions of unsteady flow to steady-state conditions for the same Reynolds number. With computed values of the inertial coefficient c_1 the combined boundary resistance and momentum flux during unsteady flow was evaluated using Equation [22].

As previously mentioned, the inertial coefficients c_1 were calculated for the orifices by numerical integration of Equation [10] from a flow net of the jet profile. This profile is known only approximately and in addition is assumed to be essentially the same over the range of velocity and acceleration of the tests. Therefore values of K_s can be determined only within some range. Table 3 gives the computed magnitudes of c_1 together with extreme limits of possible deviations.

RESULTS AND CONCLUSIONS

Steady Flow. The experimentally determined steady-flow re-

TABLE 3 INERTIA COEFFICIENTS FOR UNSTEADY FLOW THROUGH ORIFICES

Orifice area ratio	c_1 based on 4-diam jet-diffusion length	c_1 possible range of variation	c_1 assumed for calculation purposes
0.7	1.14	1.00 to 1.50	1.15
0.5	1.27	1.00 to 1.80	1.30
0.3	1.51	1.00 to 2.00	1.50

TABLE 2 RANGE OF EXPERIMENTAL INVESTIGATION

Equivalent area ratio	Maximum conduit velocity at steady-state discharge, fps	Maximum conduit Reynolds number	Maximum throat Reynolds number	Conduit acceleration range, fps² Max	Avg	Conduit deceleration range, fps² Max	Avg
			ORIFICES				
0.7	38.7	320000	620000	80	40	50	25
0.5	29.75	248000	720000	60	30	50	25
0.3	18.00	150000	770000	30	15	30	15
			SMOOTH CONDUIT				
1.0	9 to 60[a]	500000	...	80	40		
	36 to 18[b]	300000	...			7.11, 16.20	

[a] Runs 39, 40, by Deemer for accelerated flow.
[b] Runs UJ, by Jordaan for decelerated flow.

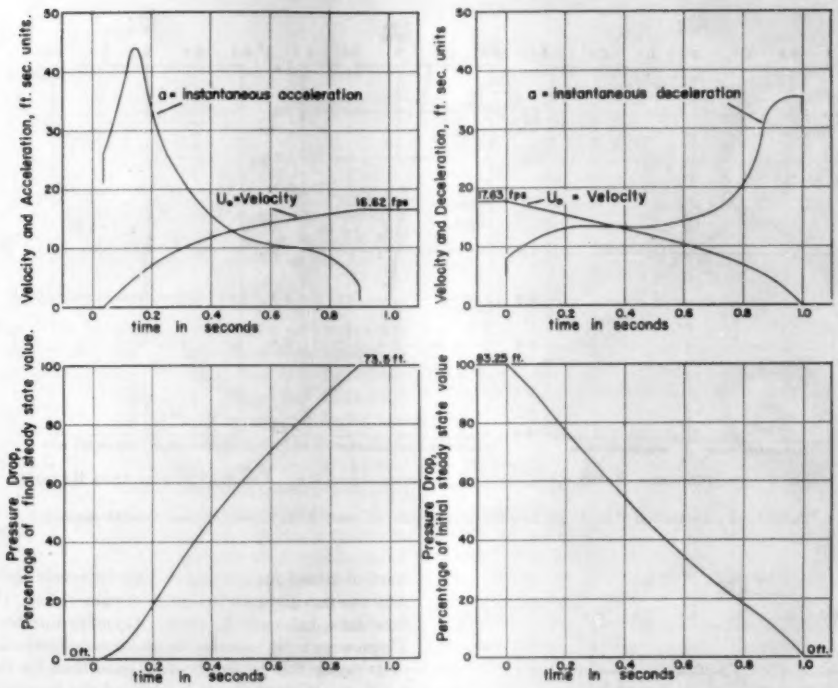

FIG. 8(a) FLOW CHARACTERISTICS, ACCELERATION FIG. 8(b) FLOW CHARACTERISTICS, DECELERATION
(Orifice area ratio, $m^2 = 0.3$.)

sistance coefficients K_s are presented in Table 4. The coefficients for orifices are in fair agreement with values calculated from the sudden expansion formula. Some dependence on Reynolds number is indicated for the 0.7-area-ratio unit. Otherwise the coefficients are essentially constant over the velocity range covered by the experiments. The pipe-friction coefficients are given by the relation

$$\frac{1}{\sqrt{f_s}} = 2.0 \log_{10} (\mathsf{R} \sqrt{f_s}) - 0.8$$

where

$$\mathsf{R} = \text{conduit Reynolds number} = \frac{U_o D}{\nu}$$

f_s = steady-state pipe-friction factor

Substituting

$$K_s = f_s \frac{L}{D} \quad \text{with} \quad \frac{L}{D} = 12$$

gives the equation in Table 4 for a foot length of test conduit.

TABLE 4 STEADY-STATE DISCHARGE COEFFICIENTS

	Area ratio	Loss coef, K_s	Remarks
Orifices	0.7	0.93	Low velocities
		0.98	High velocities
	0.5	3.81	
	0.3	17.00	
Smooth conduit	1.0	$1/\sqrt{K_s} = 0.59 \log_{10} (\mathsf{R} \sqrt{K_s}) - 0.54$	

Unsteady Flow. The comparison of the unsteady and steady behaviors are given in Figs. 4–7 in the form of diagrams of K_u/K_s versus $aL/(K_s U_o^2)$. Each point plotted on these diagrams was evaluated using K_s from Table 4 and the inertial coefficient from Table 3.

First, it is noted that the plotted points are spread over a considerable area in each diagram. This is due in part to the fact that this form of representation is sensitive to small differences. Therefore, errors are exaggerated. In addition, as the data included a range of velocities, accelerations, and rates of change of acceleration (or decelerations) the plotted spread is an indication that the actual unsteady velocity and turbulence distribution and resulting boundary shear and boundary pressures are in some way dependent on these factors.

Nevertheless, it is seen that in each diagram the data fall essentially in two opposite quadrants, indicating definite, even though qualitative, trends in the relative magnitudes of K_u and K_s. Merely to emphasize these trends the data are represented by single straight lines with positive or negative slopes. These slopes are measures of c_2 in Equation [22] and values of c_2 are indicated. However, it is emphasized that only the sign of the slope, and of c_2, is significant, not the magnitude. In drawing these lines, emphasis was given to the "established phase" portion of the test run, where the rate of change of acceleration is not large.

For accelerated flow through the three orifices, the unsteady coefficient K_u is less than the steady K_s at the same instantaneous velocity. Assuming, as previously mentioned, that the net flux of momentum is zero for the volume between the measuring stations, the indication is that the boundary resistance during acceleration is less than for the equivalent steady motion. For decelerated flows through these orifices $K_u > K_s$ and the boundary resistance exceeds that for steady flow.

It is recognized that the results are qualitative, and, because of the uncertainty in the value of the calculated inertial coefficient, this would be the case even in the absence of the factors

which were just mentioned as contributing to the spread of observed data. On the other hand, the errors probable or possible in the experimental measurements, or in determining the inertial head drop term, would not alter the stated conclusions.

In the case of the uniform diameter conduit, the magnitude of the boundary resistance during accelerated flow is very nearly the same as for the equivalent steady motion. Nevertheless, in Fig. 7 there is a definite indication that K_u/K_s is greater than unity. Thus the case of resistance due to boundary-layer shear stresses is affected differently by unsteadiness than resistance associated with the turbulence generation and diffusion accompanying separation and jet formation. For these data, Schonfeld's theory is used as a guide, and a straight line having a small positive slope is drawn through the plotted points. The relation in Table 4 shows K_s to be a function of Reynolds number while the relations derived from Schonfeld's theory (Equations [15–17]) predict c_2 and K_u also to be dependent on R. The variation in c_2 is small, however. Using Equations [17] and [18] over the range of Reynolds number investigated, c_2 varies only between 0.010 and 0.015. Hence a single straight line with a slope indicating a constant $c_2 = 0.010$ was arbitrarily chosen to represent test data qualitatively.

For decelerated flow the boundary resistance of the uniform tube is less than for steady flow. In this case, however, there is a clear indication of effects not predicted by Schonfeld's results. As shown, these data can be represented by a family of lines, essentially parallel, one for each deceleration. At any particular velocity, the proportion of boundary resistance to over-all potential drop is different, decreasing with increasing deceleration. All of these runs were started from the same steady-state velocity, but included different initial impulse periods. From the parallel displacement of the lines for different decelerations, it appears that the flow conditions of the subsequent established phase depend on the previous flow history.

These observations for the uniform tube are consistent with the view that under acceleration the central portion of the stream moves somewhat bodily while the velocity profile steepens, giving higher shear. For deceleration, the reverse seems to hold. In either event, it appears that unsteadiness does not result in marked changes from equivalent steady-state flows.

In the case of the orifices, however, it appears that the imposition of a transient results in flows having quite different velocity and turbulence characteristics. This was indicated not only by the relative magnitude of K_u and K_s, but also by what was first thought to be an anomalous experimental result. For decelerated flow through the smaller orifices, it was observed that as the unsteady run proceeded the magnitude of the potential drop changed from less than the equivalent steady-state drop (as required to establish the deceleration) to more; i.e., K_u/K_s became greater than 1.0 as the test run proceeded. This observation was repeated on many runs and cannot be attributed to measurement errors. For acceleration through the 0.3 orifice, there was some indication that a corresponding change to $K_u/K_s < 1.0$ occurred late in the run. However, experimental errors conceivably could account for the shift in this case. Such results could only mean that as the unsteady flow proceeded the internal structure of the velocity and the turbulence distribution changed to the point that it was no longer comparable to any steady-state flow condition.

Such effects as mentioned in the preceding paragraph clearly indicate that the particular state from which an unsteady run was initiated would affect the subsequent flow history. In fact, more generally it means that any particular unsteady state is dependent on the previous flow history, as seemed to be indicated by the deceleration tests with the uniform tube.

Summary

In summary, it is concluded that the imposition of an unsteady transient produces different effects for the two basic types of flow investigated, as follows:

1 For cases of surface resistance caused by boundary shear stresses.

(*a*) With acceleration the resistance is slightly but not appreciably greater than for the equivalent steady state.

(*b*) With deceleration the resistance is appreciably less than for the equivalent steady state.

(*c*) With either acceleration or deceleration, it appears that the internal flow structure is not markedly different from that for steady states.

2 For cases of form-type resistance associated with the high shear and generation and diffusion of turbulence accompanying jet formation.

(*a*) With acceleration the resistance is appreciably less than for the equivalent steady state.

(*b*) With deceleration the resistance is appreciably more than for the equivalent steady state.

(*c*) For intense jet action as obtained with small orifice-to-tube-diameter ratios, it appears that unsteadiness produces an internal flow structure that is no longer comparable to any steady-state condition.

Acknowledgment

The investigations described in this paper have been conducted under the sponsorship of the Office of Naval Research at the Hydrodynamics Laboratory of the Massachusetts Institute of Technology.

BIBLIOGRAPHY

1 "Measurements of Fluid Friction With Steady and Unsteady Motion," by J. W. Daily and K. C. Deemer, M.I.T. Hydrodynamics Laboratory Report No. 9, July, 1952.

2 "Resistance Coefficients for Accelerated Flow Through Orifices," by J. W. Daily and W. L. Hankey, Jr., M.I.T. Hydrodynamics Laboratory Report No. 10, October, 1953.

3 "Resistance Coefficients for Decelerated Flow Through Orifices," by R. W. Olive, SM thesis, Course I, Massachusetts Institute of Technology, Cambridge, Mass., 1954.

4 "Resistance Coefficients for Unsteady Flow Through Fluid Meters," by J. M. Jordaan, Jr., CE thesis, Course I, Massachusetts Institute of Technology, Cambridge, Mass., 1955.

5 "Resistance and Inertia of the Flow of Liquids in a Tube or Open Canal," by J. C. Schonfeld, *Applied Scientific Research*, vol. A1, 1949, pp. 169–197.

6 "The Unsteady-Flow Water Tunnel at the Massachusetts Institute of Technology," by J. W. Daily and K. C. Deemer, Trans. ASME, vol. 76, 1954, pp. 87–95.

7 "Further Investigation of Fluid Flow Through Orifices in Series," by C. H. Fink and S. D. Pollis, BS thesis, Course XIII, Massachusetts Institute of Technology, Cambridge, Mass., 1950.

Discussion

F. S. Weinig.[7] The writer would appreciate having stated the nondimensional quantities which control the unsteady flow in addition to the equations derived in the paper, especially since the nonlinear effects play a role in the range of the tests.

Authors' Closure

In reply to Dr. Weinig's suggestion, the authors appreciate that there are other approaches to the analysis of unsteady flow effects. The procedure chosen in this instant seemed especially appropriate to the evaluation of effects on resistance and was used for these experiments in preference to the formulation of nondimensional parameters by dimensional analysis methods.

---

[7] Manager, Aerodynamics, Aircraft Gas Turbine Division, General Electric Company, Cincinnati, Ohio. Mem. ASME.

Streamlined Pitot-Tube Bar for Measuring Water Flow in Large Pipe

By F. NUMACHI,[1] H. MURAI,[2] and S. ABE[3]

With the aim of measuring flow through pipes of large diameter, a "streamlined pitot-tube bar" was devised. Basic studies, both theoretical and experimental, were carried out in a preliminary way on the cross-sectional form of the bar in order to obtain the best results. Based on the sectional form finally selected, a full-size model was prepared and tested, from which the pitot coefficient and other pertinent data were obtained. Two actual pitot-tube bars of 60 mm chord and 2 m length were constructed and used in measuring the flow in the main pipe of the pump installed at the Numazawanuma storage system hydroelectric station.

Difficulties in Measurement of Large Flow Through Ducts

ACCURATE measurement of the statical head and the rate of flow is required in order to clarify the characteristics of hydraulic machinery. In practice, however, difficulties are encountered frequently in the determination of the rate of flow. This is particularly so in the case where it is required to measure the flow through tubular ducts in conjunction with test runs of large hydraulic machinery. This has led to the development of various methods for measuring large flow, resulting in further comparative studies of the different methods thus devised (1),[4] but so far there has not been established a really convenient and at the same time sufficiently reliable method.

Granted that the velocity at each point of the cross section of the duct be accurately measured, for instance, by the use of a Prandtl-type pitot tube, we could logically expect the information on the rate of flow based on these data to be duly and sufficiently accurate. However, three difficulties confront us in our endeavor to realize this aim: (*a*) The practical problem of boring a hole of sufficient size in the wall of the duct to be measured to permit the insertion of the pitot tube with its projections and supporting arm. (*b*) The flow directions at the measuring points on the pipe radius are not always axial owing to the secondary rotational flow induced by pipe bends, elbow, etc., which are often unavoidable. Hence there exists the difficulty in adopting the adequate values of pitot-coefficient corresponding to the deviation in the flow direction at every measuring point. (*c*) The difficulty of measuring simultaneously the velocities at several points of the cross section—necessary from the fact that the velocities often vary with time.

B. W. Proebstel (2), as well as W. M. White and W. J. Rheingans (3) have overcome the third difficulty through the use of the so-called photoflow method. A really perfect solution to the difficulties (*a*) and (*b*), however, were not provided. The method described in the foregoing references still leaves some question in that, similarly to the case of the so-called total head-tube method (4), the static pressure at points on the pipe wall only are measured, which pressure is presumed to represent the value of the whole cross section. The foregoing are purely hydrodynamical considerations, which, in actual practice, must be further complemented by such structural questions as strength, or rather, strain.

Development of a Streamlined Pitot-Tube Bar

The foregoing considerations led us to consider the possibility of devising an instrument that would at once solve all three difficulties mentioned and be convenient to use without any sacrifice of accuracy. The final outcome of our study, which was conceived by one of the authors (Numachi), shaped up to what we named the streamlined pitot-tube bar, which will be described in the following.

The streamlined pitot-tube bar possesses the following advantages: (*a*) Having a streamlined cross section, less strain is caused in the bar than with other forms (e.g., cylindrical). (*b*) The magnitude and direction of the velocity of the flow may be measured accurately even when the direction of the flow deviates to some extent from that of the axis of the duct (the error in the measured speed being within 1 per cent for a deviation of 10 deg in the incidence angle). (*c*) There is little change in the pitot-tube constant (static-pressure constant) caused by variation in the Reynolds number ($\mathrm{Re} = vl/\nu$, where v = velocity of flow, l = chord length of the section). The statement between parentheses in item (*b*) applies in a range of $\mathrm{Re} = (0.24 \sim 2.5) \times 10^6$. (*d*) The form is not inconvenient for insertion in the duct, and lends itself to simultaneous measurement of all points on the cross section.

Study of Streamlined Profile

Theory of the Streamlined Pitot-Tube Bar. In order to analyze the performance of the streamlined pitot-tube bar, let us first consider the two-dimensional flow around any given streamlined form. According to Imai's theory (5), any streamlined form symmetrical to the x-axis may be expressed as follows with the use of the parameter φ (Fig. 1)

$$\left.\begin{aligned} x &= \frac{1}{2}(1+\cos\varphi) + A_0 + (A_{-1}+A_1)\cos\varphi + \sum_{n=2}^{\infty} A_n \cos n\varphi \\ y &= (A_{-1}-A_1)\sin\varphi - \sum_{n=2}^{\infty} A_n \sin n\varphi \end{aligned}\right\} \quad \ldots [1]$$

where $A_{-1}, A_0, A_1, A_2, \ldots\ldots A_n \ldots$ are constants determined by the form of the streamlined body. Therefore, if we let p_∞, v_∞ be the static pressure and velocity, respectively, at infinity, and p_o and p_u the surface pressure on both sides at points R_o and R_u, the relationship of p_o and p_u to p_∞ may be expressed thus

---

[1] Professor, Faculty of Engineering, and Director of Institute of High Speed Mechanics, Tōhoku University, Sendai, Japan.

[2] Assistant Professor of Institute of High Speed Mechanics, Tōhoku University.

[3] Deceased; formerly Assistant Professor of Institute of High Speed Mechanics, Tōhoku University.

[4] Numbers in parentheses refer to the Bibliography at the end of the paper.

Contributed by the Hydraulic Division and presented at the Diamond Jubilee Semi-Annual Meeting, Boston, Mass., June 19–23, 1955, of The American Society of Mechanical Engineers.

Note: Statements and opinions advanced in papers are to be understood as individual expressions of their authors and not those of the Society. Manuscript received at ASME Headquarters, March 11, 1955. Paper No. 55—SA-25.

$$p_m = (p_o + p_s)/2 = p_\infty - \epsilon_m \rho v_\infty^2/2$$

$$\epsilon_m = \left(\frac{1}{2} + 2A_{-1}\right)^2 \frac{\sin^2\varphi_1 + \sin^2\alpha\{(1-\cos\varphi_1)^2 - \sin^2\varphi_1\}}{\left(\frac{dx}{d\varphi}\right)^2_{\varphi=\varphi_1} + \left(\frac{dy}{d\varphi}\right)^2_{\varphi=\varphi_1}} \quad \ldots\ldots [2]$$

where ρ = density of water.

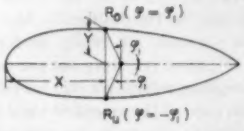

FIG. 1 REPRESENTATION OF STREAMLINED FORM BY φ

If we measure the total pressure p_t against the head of the body and the surface pressures p_o and p_s registered at appropriate points on the surface of the body, the velocity of flow v_∞ may then be obtained as follows

$$v_\infty = \sqrt{\frac{2g}{k}\frac{\left[p_t - \frac{1}{2}(p_o + p_s)\right]}{\gamma}} = \sqrt{\frac{2g\Delta H}{k}} \quad \ldots\ldots [3]$$

$$k = (1 + \epsilon_m), \quad \Delta H = \left[p_t - \frac{1}{2}(p_o + p_s)\right]\Big/\gamma \quad \ldots [4]$$

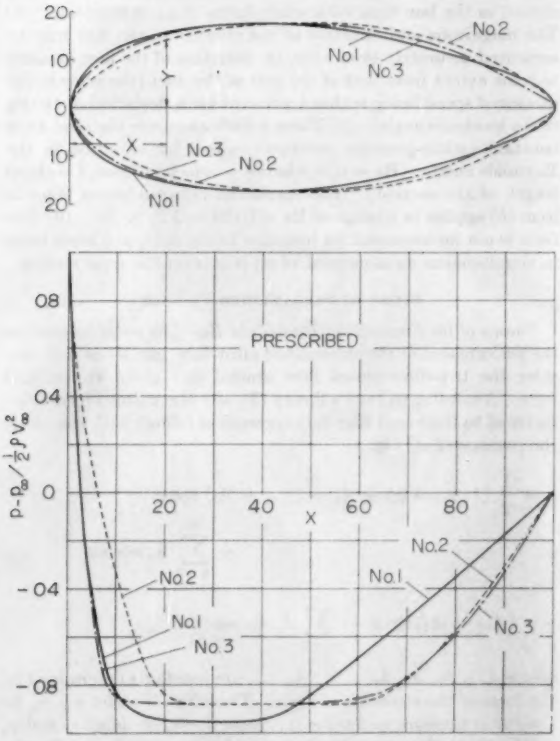

FIG. 2 PRESCRIBED PRESSURE DISTRIBUTIONS AND STREAMLINED FORMS OBTAINED

where k is what is usually called the pitot-tube coefficient, while we will call ΔH the "mean pressure difference." The value of ϵ_m may be obtained from Equation [2] in the case of a potential flow, but should deviate more or less from the theoretical in actual flow, and therefore this should be determined previously and precisely in a known velocity field.

The streamlined form to be utilized for the cross section of a pitot-tube bar should be such as would produce a stable flow around it in the range of Reynolds number to be measured. In order to obtain such a form, the proper approach is first to give a suitable surface pressure distribution, and then to calculate theoretically the streamlined form that should produce the same pressure distribution around it. What is inferred by a "suitable" pressure distribution is such a one as would on the one hand be free of cavitation and of mobile separation of the boundary layer, and on the other hand cause little error in the measured static

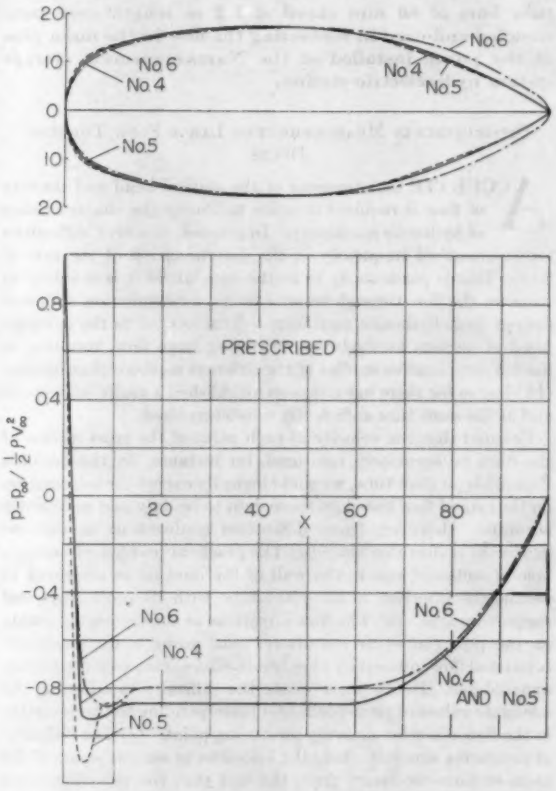

FIG. 3 PRESCRIBED PRESSURE DISTRIBUTIONS AND STREAMLINED FORMS OBTAINED

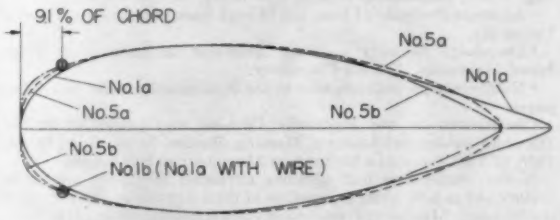

FIG. 4 ADDITIONAL PROFILES FOR PITOT-TUBE BAR

TABLE 1 PRESSURE DISTRIBUTIONS PRESCRIBED IN CALCULATING PROFILES FOR PITOT-TUBE BAR

No. 1		No. 2		No. 3		No. 4		No. 5		No. 6	
X %	$\frac{P-P_\infty}{\frac{1}{2}\rho V_\infty^2}$	X %	$\frac{P-P_\infty}{\frac{1}{2}\rho V_\infty^2}$	X %	$\frac{P-P_\infty}{\frac{1}{2}\rho V_\infty^2}$	X %	$\frac{P-P_\infty}{\frac{1}{2}\rho V_\infty^2}$	X %	$\frac{P-P_\infty}{\frac{1}{2}\rho V_\infty^2}$	X %	$\frac{P-P_\infty}{\frac{1}{2}\rho V_\infty^2}$
0.00	1.0000	0.00	1.0000	0.00	1.0000	0.00	1.0000	0.00	1.0000	0.00	1.0000
0.69	0.7052	0.97	0.6186	0.84	0.7190	0.50	0.8080	0.39	0.8141	0.46	0.7314
2.56	0.0639	3.77	0.2350	3.10	-0.0620	1.89	-0.0796	1.63	-0.1371	1.97	-0.0978
5.73	-0.5145	7.66	-0.1296	6.46	-0.6470	4.36	-0.9237	3.93	-1.1109	4.58	-0.8092
10.17	-0.8315	12.59	-0.5168	10.93	-0.8600	8.54	-0.9145	8.12	-0.8691	9.07	-0.8840
15.70	-0.9326	18.38	-0.8029	16.59	-0.8720	14.17	-0.8670	13.83	-0.8621	15.10	-0.7996
22.40	-0.9510	25.06	-0.8803	23.25	-0.8760	20.88	-0.8670	20.52	-0.8670	22.44	-0.7996
29.84	-0.9510	32.56	-0.8803	30.65	-0.8800	28.43	-0.8670	28.08	-0.8670	30.10	-0.7996
37.91	-0.9510	40.55	-0.8803	38.62	-0.8800	36.41	-0.8670	36.06	-0.8670	38.52	-0.7996
46.22	-0.8980	49.00	-0.8803	46.93	-0.8800	44.85	-0.8670	44.50	-0.8670	47.19	-0.7996
54.67	-0.7430	57.34	-0.8803	55.32	-0.8688	53.19	-0.8670	52.84	-0.8670	55.88	-0.7996
63.16	-0.6390	65.41	-0.8430	63.50	-0.8420	61.24	-0.8624	60.91	-0.8649	64.30	-0.7830
71.40	-0.5030	72.96	-0.7320	71.15	-0.7590	68.69	-0.8030	68.33	-0.8070	72.44	-0.7300
79.30	-0.3650	79.82	-0.5870	78.03	-0.6330	75.45	-0.7120	75.08	-0.7180	79.38	-0.6270
86.27	-0.2420	85.95	-0.4380	84.79	-0.4750	81.82	-0.6020	81.45	-0.6080	85.68	-0.4910
92.11	-0.1410	91.35	-0.2700	90.16	-0.3270	88.08	-0.4420	87.77	-0.4580	91.18	-0.3240
96.44	-0.0630	95.73	-0.1410	95.26	-0.1630	93.76	-0.2570	93.45	-0.2630	95.94	-0.1770
99.05	-0.0180	98.89	-0.0370	98.76	-0.0450	98.23	-0.0890	98.11	-0.0930	98.94	-0.0580
100.00	0.0000	100.00	0.0000	100.00	0.0000	100.00	0.0000	100.00	0.0000	100.00	0.0000

TABLE 2(a) DIMENSIONAL PROPORTIONS OF PROFILES FOR STREAMLINED PITOT-TUBE BAR
(x, y: cf. Fig. 2)

No. 1		No. 2		No. 3		No. 4		No. 5		No. 6	
X %	Y %	X %	Y %	X %	Y %	X %	Y %	X %	Y %	X %	Y %
0.00	0.00	0.00	0.00	0.00	0.00	0.00	0.00	0.00	0.00	0.00	0.00
0.69	3.54	0.97	2.52	0.84	3.10	0.50	4.18	0.39	4.37	0.46	4.00
2.56	6.98	3.77	5.30	3.10	6.36	1.89	7.86	1.63	8.10	1.97	7.54
5.73	9.97	7.66	8.30	6.46	9.48	4.36	10.69	3.93	10.86	4.58	10.37
10.17	12.56	12.59	11.19	10.93	12.11	8.54	12.82	8.12	12.84	9.07	12.56
15.70	14.57	18.38	13.61	16.59	14.23	14.17	14.59	13.83	14.61	15.10	14.29
22.40	16.09	25.06	15.41	23.25	15.89	20.88	15.99	20.52	16.01	22.40	15.70
29.84	17.10	32.56	16.62	30.65	17.02	28.43	16.97	28.08	16.99	30.10	16.77
37.91	17.50	40.55	17.33	38.62	17.56	36.41	17.51	36.06	17.52	38.52	17.39
46.22	17.35	49.00	17.54	46.93	17.54	44.85	17.54	44.50	17.54	47.19	17.50
54.67	16.40	57.34	17.21	55.32	17.02	53.19	17.03	52.84	17.03	55.88	17.07
63.16	14.94	65.41	16.31	63.50	15.92	61.24	15.98	60.91	15.97	64.30	16.12
71.40	12.97	72.96	14.83	71.15	14.36	68.69	14.29	68.33	14.29	72.44	14.62
79.30	10.79	79.82	12.74	78.03	12.13	75.45	12.00	75.08	11.70	79.38	12.52
86.27	8.62	85.95	10.09	84.29	9.17	82.50	9.20	80.00	10.10	85.68	9.94
92.11	6.41	91.35	7.14	90.16	5.96	87.50	6.95	87.50	6.90	91.18	7.13
96.44	4.30	95.73	4.32	95.26	3.26	92.50	4.45	92.50	4.45	95.94	4.43
99.05	2.12	98.89	1.96	98.76	1.37	97.50	1.80	97.50	1.85	98.94	2.08
100.00	0.00	100.00	0.00	100.00	0.00	100.00	0.00	100.00	0.00	100.00	0.00

TABLE 2(b) DIMENSIONAL PROPORTIONS OF PROFILES FOR STREAMLINED PITOT-TUBE BAR

No. 1a		No. 5a		No. 5b	
X %	Y %	X %	Y %	X %	Y %
0.00	0.00	0.00	0.00	0.00	0.00
0.69	3.54	0.39	4.37	0.00	4.78
2.56	6.98	1.63	8.10	0.90	8.18
5.73	9.97	3.93	10.86	3.43	10.70
10.17	12.56	8.12	12.84	7.77	12.78
15.70	14.57	13.83	14.61	13.49	14.58
22.40	16.09	20.52	16.01	20.52	16.01
29.84	17.10	28.08	16.99	28.08	16.99
37.91	17.50	36.06	17.52	36.06	17.52
46.22	17.35	44.50	17.54	44.50	17.54
54.67	16.40	52.84	17.03	52.84	17.03
63.16	14.94	60.91	15.97	60.91	15.97
71.40	12.97	68.00	14.54	68.33	14.29
79.30	10.80	75.00	12.78	75.08	11.70
86.27	8.55	80.00	11.27	80.00	10.10
92.11	6.60	85.00	9.56	87.50	6.90
97.50	4.95	90.00	7.57	92.50	4.45
100.00	4.20	95.00	4.81	97.50	1.85
102.50	3.50	98.00	2.63	100.00	0.00
105.00	2.60	100.00	0.00		
107.50	1.60				
110.00	0.45				

pressure with error or displacement within reasonable limits in the position of the measuring openings. For this reason it should be necessary to have a surface pressure distribution that features little or no pressure gradient for a fairly long stretch around the measuring points R_s and R_w. A further point to be borne in mind is to select a distribution that gives a profile with a sufficiently large thickness ratio in order to obtain a form amply rigid under a condition of flow hitting it at an angle within reasonable limits.

Specimen Streamlined Forms and Method of Experimentation. In determining the cross section of our pitot-tube bar on the basis of the foregoing considerations, we finally adopted for calculating the profiles, the configurations of prescribed pressure distribution by turns shown in Figs. 2 and 3 and specified in Table 1. (In these figures and table, p = surface pressure, p_∞ = static pressure in front of the body.) A common thickness ratio of 35 per cent was used, based on common practice for pitot tubes and on requirements for rigidity. The resulting streamlined forms are shown in Figs. 2, 3, and 4 and specified in Tables 2(a) and 2(b).

$$p_m = (p_o + p_u)/2 = p_\infty - \epsilon_m \rho v_\infty^2/2$$

$$\epsilon_m = \left(\frac{1}{2} + 2A_{-1}\right)^2 \frac{\sin^2\varphi_1 + \sin^2\alpha\{(1-\cos\varphi_1)^2 - \sin^2\varphi_1\}}{\left(\frac{dx}{d\varphi}\right)^2_{\varphi=\varphi_1} + \left(\frac{dy}{d\varphi}\right)^2_{\varphi=\varphi_1}} \quad \ldots\ldots [2]$$

where ρ = density of water.

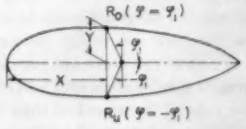

FIG. 1 REPRESENTATION OF STREAMLINED FORM BY φ

If we measure the total pressure p_t against the head of the body and the surface pressures p_o and p_u registered at appropriate points on the surface of the body, the velocity of flow v_∞ may then be obtained as follows

$$v_\infty = \sqrt{\frac{2g}{k}\frac{\left[p_t - \frac{1}{2}(p_o + p_u)\right]}{\gamma}} = \sqrt{\frac{2g\Delta H}{k}} \quad \ldots\ldots [3]$$

$$k = (1 + \epsilon_m), \quad \Delta H = \left[p_t - \frac{1}{2}(p_o + p_u)\right]\Big/\gamma \ldots [4]$$

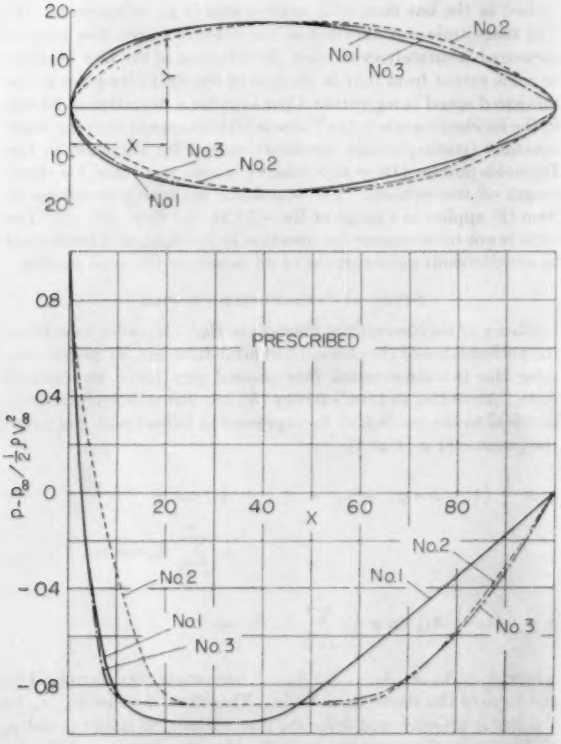

FIG. 2 PRESCRIBED PRESSURE DISTRIBUTIONS AND STREAMLINED FORMS OBTAINED

where k is what is usually called the pitot-tube coefficient, while we will call ΔH the "mean pressure difference." The value of ϵ_m may be obtained from Equation [2] in the case of a potential flow, but should deviate more or less from the theoretical in actual flow, and therefore this should be determined previously and precisely in a known velocity field.

The streamlined form to be utilized for the cross section of a pitot-tube bar should be such as would produce a stable flow around it in the range of Reynolds number to be measured. In order to obtain such a form, the proper approach is first to give a suitable surface pressure distribution, and then to calculate theoretically the streamlined form that should produce the same pressure distribution around it. What is inferred by a "suitable" pressure distribution is such a one as would on the one hand be free of cavitation and of mobile separation of the boundary layer, and on the other hand cause little error in the measured static

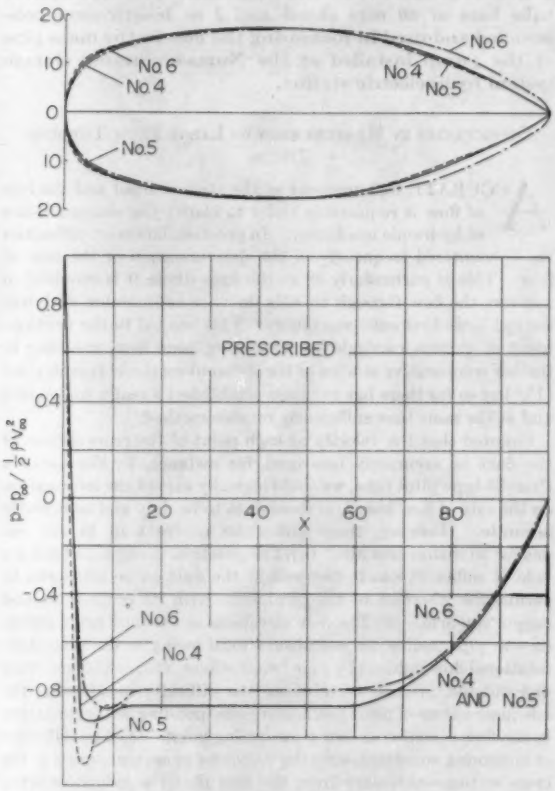

FIG. 3 PRESCRIBED PRESSURE DISTRIBUTIONS AND STREAMLINED FORMS OBTAINED

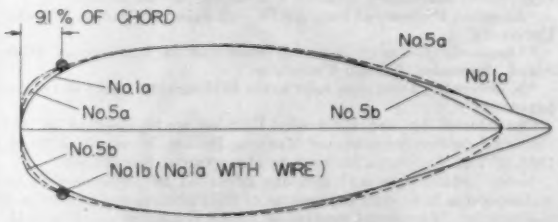

FIG. 4 ADDITIONAL PROFILES FOR PITOT-TUBE BAR

TABLE 1 PRESSURE DISTRIBUTIONS PRESCRIBED IN CALCULATING PROFILES FOR PITOT-TUBE BAR

No. 1		No. 2		No. 3		No. 4		No. 5		No. 6	
X %	$\frac{P-P_\infty}{\frac{1}{2}\rho V_\infty^2}$	X %	$\frac{P-P_\infty}{\frac{1}{2}\rho V_\infty^2}$	X %	$\frac{P-P_\infty}{\frac{1}{2}\rho V_\infty^2}$	X %	$\frac{P-P_\infty}{\frac{1}{2}\rho V_\infty^2}$	X %	$\frac{P-P_\infty}{\frac{1}{2}\rho V_\infty^2}$	X %	$\frac{P-P_\infty}{\frac{1}{2}\rho V_\infty^2}$
0.00	1.0000	0.00	1.0000	0.00	1.0000	0.00	1.0000	0.00	1.0000	0.00	1.0000
0.69	0.7052	0.97	0.6186	0.84	0.7190	0.50	0.8080	0.39	0.8141	0.46	0.7314
2.56	0.0639	3.77	0.2350	3.10	-0.0620	1.89	-0.0796	1.63	-0.1371	1.97	-0.0978
5.73	-0.5145	7.66	-0.1296	6.46	-0.6470	4.36	-0.9237	3.93	-1.1109	4.58	-0.8092
10.17	-0.8315	12.59	-0.5168	10.93	-0.8600	8.54	-0.9145	8.12	-0.8691	9.07	-0.8840
15.70	-0.9326	18.38	-0.8029	16.59	-0.8720	14.17	-0.8670	13.83	-0.8621	15.10	-0.7996
22.40	-0.9510	25.06	-0.8803	23.25	-0.8760	20.88	-0.8670	20.52	-0.8670	22.44	-0.7996
29.84	-0.9510	32.56	-0.8803	30.65	-0.8800	28.43	-0.8670	28.08	-0.8670	30.10	-0.7996
37.91	-0.9510	40.55	-0.8803	38.62	-0.8800	36.41	-0.8670	36.06	-0.8670	38.52	-0.7996
46.22	-0.8980	49.00	-0.8803	46.93	-0.8800	44.85	-0.8670	44.50	-0.8670	47.19	-0.7996
54.67	-0.7430	57.34	-0.8803	55.32	-0.8688	53.19	-0.8670	52.84	-0.8670	55.88	-0.7996
63.16	-0.6390	65.41	-0.8430	63.50	-0.8420	61.24	-0.8624	60.91	-0.8649	64.30	-0.7830
71.40	-0.5030	72.96	-0.7320	71.15	-0.7590	68.69	-0.8030	68.33	-0.8070	72.44	-0.7300
79.30	-0.3650	79.82	-0.5870	78.03	-0.6330	75.45	-0.7120	75.08	-0.7180	79.38	-0.6270
86.27	-0.2420	85.95	-0.4380	84.79	-0.4750	81.82	-0.6020	81.45	-0.6080	85.68	-0.4910
92.11	-0.1410	91.35	-0.2700	90.16	-0.3270	88.08	-0.4420	87.77	-0.4580	91.18	-0.3240
96.44	-0.0630	95.73	-0.1410	95.26	-0.1630	93.76	-0.2570	93.45	-0.2630	95.94	-0.1770
99.05	-0.0180	98.89	-0.0370	98.76	-0.0450	98.23	-0.0890	98.11	-0.0930	98.94	-0.0580
100.00	0.0000	100.00	0.0000	100.00	0.0000	100.00	0.0000	100.00	0.0000	100.00	0.0000

TABLE 2(a) DIMENSIONAL PROPORTIONS OF PROFILES FOR STREAMLINED PITOT-TUBE BAR
(x, y: cf. Fig. 2)

No. 1		No. 2		No. 3		No. 4		No. 5		No. 6	
X %	Y %	X %	Y %	X %	Y %	X %	Y %	X %	Y %	X %	Y %
0.00	0.00	0.00	0.00	0.00	0.00	0.00	0.00	0.00	0.00	0.00	0.00
0.69	3.54	0.97	2.52	0.84	3.10	0.50	4.18	0.39	4.37	0.46	4.00
2.56	6.98	3.77	5.30	3.10	6.36	1.89	7.86	1.63	8.10	1.97	7.54
5.73	9.97	7.66	8.30	6.46	9.48	4.36	10.69	3.93	10.86	4.58	10.37
10.17	12.56	12.59	11.19	10.93	12.11	8.54	12.82	8.12	12.84	9.07	12.56
15.70	14.57	18.38	13.61	16.59	14.23	14.17	14.59	13.83	14.61	15.10	14.29
22.40	16.09	25.06	15.41	23.25	15.89	20.88	15.99	20.52	16.01	22.40	15.70
29.84	17.10	32.56	16.62	30.65	17.02	28.43	16.97	28.08	16.99	30.10	16.77
37.91	17.50	40.55	17.33	38.62	17.56	36.41	17.51	36.06	17.52	38.52	17.39
46.22	17.35	49.00	17.54	46.93	17.54	44.85	17.54	44.50	17.54	47.19	17.50
54.67	16.40	57.34	17.21	55.32	17.02	53.19	17.03	52.84	17.03	55.88	17.07
63.16	14.94	65.41	16.31	63.50	15.92	61.24	15.98	60.91	15.97	64.30	16.12
71.40	12.97	72.96	14.83	71.15	14.36	68.69	14.29	68.33	14.29	72.44	14.62
79.30	10.79	79.82	12.74	78.03	12.13	75.45	12.00	75.08	11.70	79.38	12.52
86.27	8.62	85.95	10.09	84.29	9.17	82.50	9.20	80.00	10.10	85.68	9.94
92.11	6.41	91.35	7.14	90.16	5.96	87.50	6.95	87.50	6.90	91.18	7.13
96.44	4.30	95.73	4.32	95.26	3.26	92.50	4.45	92.50	4.45	95.94	4.43
99.05	2.12	98.89	1.96	98.76	1.37	97.50	1.80	97.50	1.85	98.94	2.08
100.00	0.00	100.00	0.00	100.00	0.00	100.00	0.00	100.00	0.00	100.00	0.00

TABLE 2(b) DIMENSIONAL PROPORTIONS OF PROFILES FOR STREAMLINED PITOT-TUBE BAR

No. 1a		No. 5a		No. 5b	
X %	Y %	X %	Y %	X %	Y %
0.00	0.00	0.00	0.00	0.00	0.00
0.69	3.54	0.39	4.37	0.00	4.78
2.56	6.98	1.63	8.10	0.90	8.18
5.73	9.97	3.93	10.86	3.43	10.70
10.17	12.56	8.12	12.84	7.77	12.78
15.70	14.57	13.83	14.61	13.49	14.58
22.40	16.09	20.52	16.01	20.52	16.01
29.84	17.10	28.08	16.99	28.08	16.99
37.91	17.50	36.06	17.52	36.06	17.52
46.22	17.35	44.50	17.54	44.50	17.54
54.67	16.40	52.84	17.03	52.84	17.03
63.16	14.94	60.91	15.97	60.91	15.97
71.40	12.97	68.00	14.54	68.33	14.29
79.30	10.80	75.00	12.78	75.08	11.70
86.27	8.55	80.00	11.27	80.00	10.10
92.11	6.60	85.00	9.56	87.50	6.90
97.50	4.95	90.00	7.57	92.50	4.45
100.00	4.20	95.00	4.81	97.50	1.85
102.50	3.50	98.00	2.63	100.00	0.00
105.00	2.60	100.00	0.00		
107.50	1.60				
110.00	0.45				

pressure with error or displacement within reasonable limits in the position of the measuring openings. For this reason it should be necessary to have a surface pressure distribution that features little or no pressure gradient for a fairly long stretch around the measuring points R_e and R_w. A further point to be borne in mind is to select a distribution that gives a profile with a sufficiently large thickness ratio in order to obtain a form amply rigid under a condition of flow hitting it at an angle within reasonable limits.

Specimen Streamlined Forms and Method of Experimentation. In determining the cross section of our pitot-tube bar on the basis of the foregoing considerations, we finally adopted for calculating the profiles, the configurations of prescribed pressure distribution by turns shown in Figs. 2 and 3 and specified in Table 1. (In these figures and table, p = surface pressure, p_∞ = static pressure in front of the body.) A common thickness ratio of 35 per cent was used, based on common practice for pitot tubes and on requirements for rigidity. The resulting streamlined forms are shown in Figs. 2, 3, and 4 and specified in Tables 2(a) and 2(b).

We first obtained the forms Nos. 1 to 3 from pressure configurations featuring a falling surface pressure along the chord from the leading edge to a certain point, followed by a level stretch and ending in a gentle rise toward the tail. Of the three forms thus obtained, No. 1 was calculated to have the level stretch between the points 20 per cent and 40 per cent from the leading edge, but upon actual experimentation with the model of 20-mm chord length, it was found that its performance became unstable in the range Re = $(0.6 \sim 1.0) \times 10^5$. In order to discover the cause of this instability, we prepared a modification of this form featuring a 2-mm (10 per cent of the chord) extension of the profile toward the rear. This profile, which we named No. 1a (Fig. 4) did not give a performance very much better than its predecessor, and so next, a wire of 0.5 mm diameter was attached on the body at a position 2 mm from the head, as measured along the chord. This model designated No. 1b gave good results, being free of the instability seen in the No. 1 model, owing, we believe, to the fact that the wire caused the prompt transference of the boundary layer.

The drawback of the No. 1b model was the undesirability from the structural standpoint of the wire along the body. This led us to devise models Nos. 4 and 5, with pressure configurations as shown in Fig. 3, with a view to producing with the form of the body itself an effect similar to that caused by the wire. However, the very pointed tail of the No. 5 model does not recommend itself because of its frailness and from the necessity of passing numerous measuring tubes along the bar through this part of the body. A modification to No. 5 is No. 5a, with the tail rounded up to the extent of that of No. 3, while No. 6 has it rounded even further. In No. 5b the dip in the pressure curve was advanced well forward, to constitute a series for the position of this dip in conjunction with the Nos. 4 and 5, in an attempt to find the optimum position for the dip.

The models of 20-mm chord were tested in the cavitation tunnel for single profiles (6), while the tunnel for cascade profiles (7) was utilized for experiments with the 60-mm models. The experiments were conducted with the movable duct walls (7) behind the cascade set parallel to the water channel.

A protruding tube with outer and inner diameters, respectively, d_o and d_i and with a length of λ was attached to the leading edge facing the stream for the purpose of measuring the total pressure, while holes of inner diameter d_i were bored on the two sides of the body at points 20, 30, and 40 per cent of the chord measured from the front end, for measuring the static pressure. Each of these holes connected with a channel bored in the specimen parallel to the axis of the bar, which channel in turn led to manometers placed outside the tunnel. The specimen length L, the dimensions of the measuring tubes and holes d_o, d_i, d_s, and λ vary according to the chord l of the specimen, as follows:

Dimension (mm)	l	L	d_o	d_i	λ	d_s
Smaller specimen	20	70−0.05	1	0.6	2	0.55
Full-sized specimen	60	100−0.05	3.8	1.8	5	1.2

Characteristics of Different Streamlined Forms Developed. Specimens of 1/3 actual size (20-mm chord) were tested in the velocity range of Reynolds number $(0.6 \sim 1.9) \times 10^5$, taking the chord length l as the linear dimension. Omitting the details of the data obtained, the summarized results are given in Table 3. The following remarks relate to the suitability of the forms when applied to pitot tubes.

1 *Stability of the performance:* With respect to the static pressure, the major number of the specimens, excepting Nos. 1b, 3, 4, and 6, proved to present unstable phenomena and to give scattering of the data at certain speeds when the incidence angle was between 0 and 3 deg.

2 *Discontinuity of characteristic curve:* Except for those of Nos. 1 and 1a, none of the characteristic curves revealed marked discontinuity in the curves representing the relationship between the static-pressure coefficient and the velocity.

3 *Vibrations caused in streamlined body:* Nos. 1, 1a, 1b, 2, 3, and 5b, being free from such vibrations, may be said to be more suitable from this standpoint.

4 *Stability of pitot coefficient:* From this standpoint, the profiles with the most stable characteristics would be Nos. 1, 1a, 1b, 5, and 5a.

5 *Over-all performance:* We are therefore left with No. 3, which, with its pitot coefficient rather too sensitive to changes in the Reynolds number, may still be regarded as the best of the ten designs developed.

Performance of Full-Size Streamlined Cross Section. As a preliminary step to the adoption in actual practice of the model cross section No. 3, which gave the best performance, we prepared a full-scale model of 60-mm chord and performed exhaustive tests on it. Fig. 5 represents a part of the results. It has been observed that with incidence angles between 0 and 15 deg the performance is stable in the whole range tested of Re = $(0.6 \sim 2.1) \times 10^5$, while the scattering of the data is less than 1 per cent in terms

TABLE 3 TABLE OF CHARACTERISTICS OF THE DIFFERENT STREAMLINED FORMS DEVELOPED (AT REYNOLDS NUMBER Re = $(0.6 \sim 1.8) \times 10^5$)
(α: INCIDENCE ANGLE, — MEANS "NO OCCURRENCE," < MEANS "SMALLER THAN.")

Characteristics	α	Profile Form									
		No.1	No.1a	No.1b	No.2	No.3	No.4	No.5	No.5a	No.5b	No.6
Reynolds' Number R/10^5 where flow becomes unstable	0°	<1.0	< 0.9	—	around 1.6	—	—	—	around 1.1	around 1.1	—
	±3°	<1.1	< 1.0	—	—	—	—	around 1.8	—	—	—
R.N./10^5 where Pitot Coefficient is discontinuous	0°	1.0	—	—	—	—	—	—	—	—	—
	±3°	1.1	—	—	—	—	—	—	—	—	—
R.N./10^5 where Vibration are set up	0°		—	—	—	—	—	—	—	—	—
	±3°		—	—	—	—	1.4 ~1.6	1.4 ~ 1.6	around 1.4	—	1.3 ~1.6
Max. Variation of Pitot Coeff. in Terms of Velocity	0°	1 %	1 %	2 %	6 %	8 %	4 %	1 %	1 %	5 %	6 %

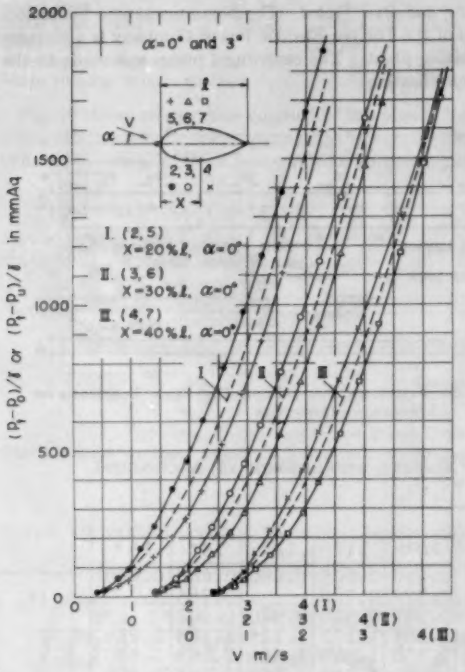

FIG. 5 DIFFERENCE BETWEEN TOTAL AND SURFACE PRESSURES $(p_t - p_o)/\gamma$ OR $(p_t - p_o)/\gamma$ OF PROFILE FORM NO. 3 ACCORDING TO VELOCITY v, INCIDENCE ANGLE $\alpha = 0°$ AND 3°

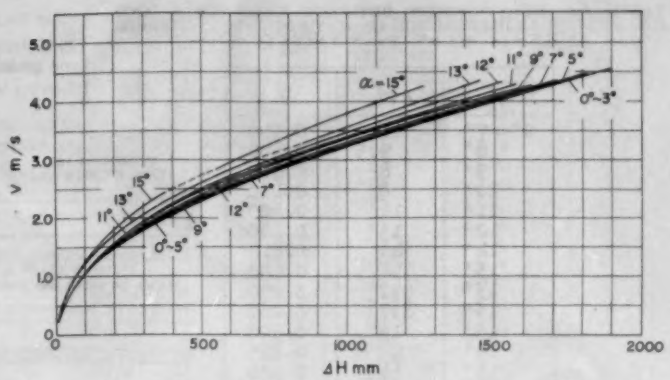

FIG. 6 RELATIONSHIP BETWEEN VELOCITY OF FLOW v, M PER SEC, AND MEAN PRESSURE DIFFERENCE ΔH, MM WATER COLUMN, ACCORDING TO INCIDENCE ANGLE α

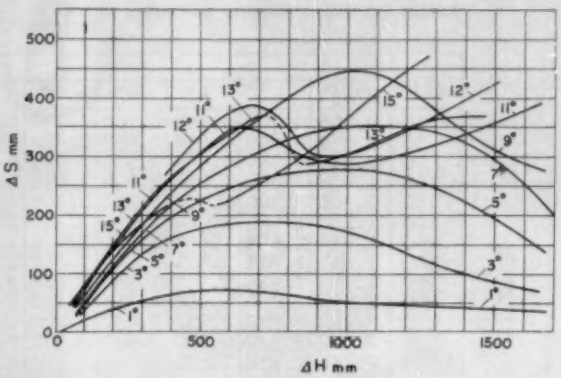

FIG. 7 RELATIONSHIP BETWEEN MEAN PRESSURE DIFFERENCE ΔH AND SURFACE PRESSURE DIFFERENCE ΔS (BOTH IN MM WATER COLUMN), ACCORDING TO INCIDENCE ANGLE α

of velocity. Neither is any discontinuity nor irregularity seen in the present curve. However, with the incidence angle at 11 to 15 deg, discontinuity is seen in a certain range of Reynolds number, which differs according to the incidence angle. It is further a desirable quality for a pitot tube to have the value of the mean pressure difference ΔH vary as little as possible with incidence angle. Therefore, in the present instance, the mean pressure difference was based on measurements of surface pressure registered at the holes bored at the distance of 40 per cent of the chord from the head.

Fig. 6 represents the relation between this ΔH and the velocity v (designated v_m in Equation [3]). Detailed values are given in Tables 4(a) and 4(b). With α between 3 and 15 deg a gradual shifting of the $v - \Delta H$ curve may be observed. Therefore, in measuring velocity, it should be desirable to know also the value of the incidence angle α and to read the velocity from the $v - \Delta H$ curve corresponding to α. This α may be obtained from ΔH and ΔS, the difference in surface pressure between the two measuring points on opposite sides, and in Fig. 7 the relationship between ΔH and ΔS is given with α as parameter [detailed values in Tables 5(a) and 5(b)].

It may be mentioned here that in Fig. 7 the $\Delta H - \Delta S$ relation changes irregularly in the range $\alpha > 10$ deg, and, moreover, becomes triple-valued against the values of ΔH and ΔS. In such cases, reference to adjoining plotted points will help in determining which of the three values to take. Alternatively, the pitot-tube bar could be revolved so as to have the head point toward the stream within 10 deg.

MEASUREMENT OF THE FLOW AT NUMAZAWANUMA PUMP

The Streamlined Pitot-Tube Bar Employed. With the object of measuring the flow through a duct of 2 m diam, we constructed a brass pitot-tube bar possessing the streamlined cross section of the profile given by our model No. 3, with a chord of 60 mm and a total effective length of 2 m. The dimensions of the bar were decided upon considering that the strength and the strain in the bar under service conditions should be well within the prescribed limits (21 mm or about 1 per cent of the duct diameter for a flow of 3.5 m/s). The bar is provided with 10 measuring points as shown in Figs. 8 and 9. Fig. 8 shows how the 10 openings for the total pressure are situated along the leading ridge, and those for the surface pressure along the sides, 10 on each, at a position 40 per cent of the chord behind the leading edge. The positions along the bar of the sets of three measuring openings have been determined in such manner as to enable the most appropriate information to be obtained for an accurate measurement of the flow. The pressures registered at the total of 30 openings along the bar are transmitted by means of copper tubes running along the tail portion of the streamlined bar to one or the other end, Fig. 9.

Method of Measurement. For reading of pressure registered at the total openings, the photoflow method was adopted, but a manometer set was devised and constructed with special provisions to bring the menisci into the camera field with sufficient accuracy of measurement. Consequently, two pitot-tube bars were constructed and inserted in the water tube at right angles to each other and one of them was set parallel to the horizontal plane, as illustrated in Fig. 10.

TABLE 4(a) RELATIONSHIP BETWEEN VELOCITY v AND MEAN PRESSURE DIFFERENCE ΔH, ACCORDING TO INCIDENCE ANGLE α (v: M/S, ΔH: MM IN WATER COLUMN)

α	ΔH	V
0°~7°	11	0.400
8°	9.5	0.400
9°	8	0.400
10°	8	0.400
11°	14	0.400
12°	13	0.400
12°	46	0.815
13°	14	0.400
13°	692	3.050
13°	837	3.260
15°	13	0.400
15°	46	0.815
15°	64	0.920
15°	380	2.450
15°	553	2.850

The Pump and Duct Tested. The Numazawanuma hydroelectric station of the Tōhoku Electric Power Company is a storage-type generating plant. The centrifugal pump was made to the following specification:

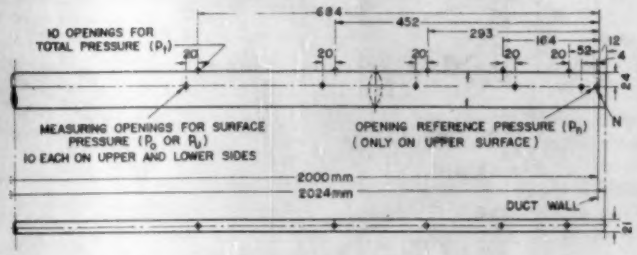

FIG. 8 DIMENSIONS OF STREAMLINED PITOT-TUBE BAR AND POSITIONS OF MEASURING OPENINGS

TABLE 4(b) RELATIONSHIP BETWEEN VELOCITY v AND MEAN PRESSURE DIFFERENCE ΔH, ACCORDING TO INCIDENCE ANGLE α

ΔH	α											
	0°~3°	4°	5°	6°	7°	8°	9°	10°	11°	12°	13°	15°
30	0.708	0.708	0.708	0.708	0.708	0.708	0.708	0.708	0.605	0.680	0.648	0.680
50	0.850	0.850	0.850	0.850	0.850	0.853	0.853	0.870	0.780		0.783	
70	0.959	0.959	0.959	0.959	0.959	0.962	0.970	0.997	0.918	0.920	0.942	
100	1.098	1.098	1.098	1.098	1.098	1.110	1.118	1.163	1.101	1.115	1.163	1.255
150	1.300	1.300	1.300	1.302	1.303	1.313	1.332	1.390	1.349	1.369	1.463	1.590
200	1.484	1.484	1.484	1.490	1.500	1.509	1.527	1.580	1.565	1.590	1.703	1.855
250	1.653	1.653	1.653	1.670	1.682	1.697	1.711	1.745	1.760	1.782	1.906	2.052
300	1.811	1.811	1.811	1.830	1.851	1.868	1.880	1.898	1.934	1.960	2.078	2.220
350	1.955	1.955	1.955	1.980	2.003	2.022	2.032	2.043	2.086	2.124	2.223	2.368
400	2.090	2.090	2.090	2.113	2.140	2.158	2.170	2.183	2.224	2.276	2.361	
450	2.212	2.212	2.212	2.230	2.260	2.278	2.294	2.317	2.357	2.413	2.490	
500	2.327	2.327	2.327	2.340	2.374	2.393	2.412	2.435	2.473	2.530	2.610	
550	2.434	2.434	2.434	2.450	2.482	2.503	2.523	2.548	2.582	2.637	2.725	
600	2.540	2.540	2.540	2.560	2.586	2.608	2.633	2.657	2.685	2.740	2.840	2.960
650	2.638	2.638	2.639	2.658	2.688	2.713	2.737	2.760	2.780	2.840	2.952	3.078
700	2.730	2.730	2.736	2.755	2.784	2.810	2.833	2.860	2.870	2.938		3.193
750	2.820	2.825	2.830	2.850	2.875	2.900	2.930	2.955	2.961	3.029		3.310
800	2.905	2.912	2.922	2.941	2.968	2.994	3.028	3.048	3.050	3.120		3.420
850	2.993	3.000	3.013	3.030	3.058	3.083	3.120	3.140	3.140	3.210	3.283	3.526
900	3.080	3.085	3.100	3.119	3.145	3.174	3.210	3.230	3.230	3.302	3.385	3.630
950	3.169	3.173	3.190	3.210	3.233	3.261	3.300	3.320	3.320	3.393	3.483	3.731
1000	3.253	3.265	3.277	3.297	3.320	3.352	3.384	3.405	3.410	3.483	3.582	3.832
1050	3.338	3.350	3.361	3.383	3.402	3.433	3.470	3.490	3.497	3.575	3.680	3.929
1100	3.420	3.431	3.447	3.464	3.485	3.516	3.546	3.570	3.583	3.668	3.776	4.027
1150	3.502	3.515	3.530	3.553	3.565	3.597	3.623	3.645	3.670	3.757	3.870	4.123
1200	3.583	3.597	3.610	3.636	3.657	3.672	3.697	3.722	3.753	3.843	3.960	4.222
1250	3.663	3.675	3.687	3.713	3.726	3.750	3.770	3.795	3.840	3.930	4.047	
1300	3.740	3.750	3.762	3.780	3.800	3.821	3.843	3.870	3.918	4.012	4.129	
1350	3.818	3.825	3.835	3.860	3.876	3.893	3.915	3.942	3.996	4.090	4.210	
1400	3.892	3.900	3.908	3.930	3.950	3.964	3.985	4.018	4.075	4.170	4.290	
1450	3.963	3.970	3.978	3.997	4.022	4.033	4.051	4.090	4.145	4.240		
1500	4.033	4.040	4.047	4.068	4.090	4.106	4.120	4.162	4.220	4.312		
1550	4.100	4.108	4.118	4.135	4.159	4.170	4.184	4.234	4.293			
1600	4.168	4.178	4.190	4.210	4.225	4.233	4.250	4.308	4.367			
1650	4.245	4.240	4.257	4.270	4.287	4.300	4.318	4.380				
1700	4.298	4.310	4.327	4.337	4.350	4.365	4.383					
1750	4.364	4.375	4.393	4.403	4.411							
1800	4.427											

Speed (rpm)	500		
Input power (kw)	1810	1910	2000
Head (m)	226	211	194
Discharge in m³ per sec	6.95	7.90	8.84
Mean velocity in tube (m/sec)	2.21	2.52	2.81

Fig. 10 shows an elevation diagram of the pipe layout. In deciding the location for the pitot-tube bar, it was thought desirable to have the measuring point removed from the point A where there

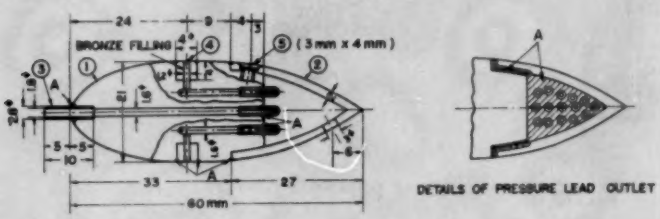

FIG. 9 CROSS SECTION OF PITOT-TUBE BAR
(Part A soldered together. 1 brass bar, 2 brass plate, 3 total pressure tube, 4 static pressure hole, 5 set screw.)

TABLE 5(a) RELATIONSHIP BETWEEN MEAN PRESSURE DIFFERENCE ΔH AND SURFACE PRESSURE DIFFERENCE ΔS, ACCORDING TO INCIDENCE ANGLE α (ΔS: MM IN WATER COLUMN)

α	ΔH	ΔS
0°	11	0
1°	11	0
3°	11	0
5°	11	2
7°	11	2
9°	7.5	1
10°	8.5	5
11°	15	0
12°	13	0
12°	26	4
12°	32	26
13°	15	6
13°	27	10
13°	55	48
15°	13	6
15°	24	8
15°	46	7
15°	64	62

TABLE 5(b) RELATIONSHIP BETWEEN MEAN PRESSURE DIFFERENCE ΔH AND SURFACE PRESSURE DIFFERENCE ΔS, ACCORDING TO INCIDENCE ANGLE α

ΔH	α														
	0°	1°	2°	3°	4°	5°	6°	7°	8°	9°	10°	11°	12°	13°	15°
30	0	4	7	9	13	15.5	16	18	20.5	25	24	16			
50	0	7.8	13.5	18.5	24	28.3	30	32	34	40.5	39.8	33.5	38		
70	0	11.6	20.5	28	35	40.3	43	45	48	53.8	54.3	49.3	52	56	
100	0	17.5	31	42	50.5	57	59.5	62.7	66	72	74.5	72	73	77	86
150	0	22	48.5	65.5	76	83	86	90	94	101.3	106.7	108.3	110	113	114
200	0	37.5	66	89	101	108	112	116.6	122	130	137	144.5	147	149	138.5
250	0	47	84	112	124	132	135	143	150	157.6	168	177.3	183.5	183	162.5
300	0	54	100	134	145.5	155.5	163	169.5	177	185	199.3	206	219	212	185
350	0	60	113.5	151	165	177	186	194.5	203	213	229.5	233	251.5	237.5	205
400	0	64	122	163	182	197	207	216.5	226.5	238	258.4	259	281.2	263	217
450	0	67	126.5	170.5	196.5	213	224	235.5	248	260.5	286	264	309	286	
500	0	69.5	129	176	208	226	239.5	252	269	282	310.5	307	335.5	304.5	
550	0	70.5	130	180.5	217	237	252.5	266	289	304	333.5	327.5	360	322	212
600	0	70.5	129.5	183.5	224	245.5	264	280	307.5	324	355	344	378	339	223.5
650	0	70	127.5	185.5	230	252.5	274	293	326	344	374	352.5	384.5	354.5	237
700	0	68	124	187	234	259	282	306	343	364.5	389.5	350	384	369	251
750	0	65.5	119	187	236.5	264	289.5	319	359	384	400.5	331.5	373		267.5
800	0	62	112.5	186.5	238	268	296.5	331	375	403	410	309.5	346		284
850	0	58.5	106	184.5	239	271.5	303	341	389	419	416.5	296	310	284	303
900	0	54.5	99.5	180.5	239	274	308	347	401	432	419	287.5	298	285.5	323
950	0	51	94	175	237	276	311.5	350	411	441	415	284	297.5	292	345.5
1000	0	48.5	89.5	168.5	233	277	313.5	351.5	417	445	406	284	301.5	301	368.5
1050	0	46.5	86	160.5	228	277	314	351.5	419	444	391	286	308.5	312	391
1100	0	45.5	82.5	152	221.5	275	313	350	412.5	439	372	290	318.5	322	411
1150	0	44	79.5	143	213.5	271	311	348	403	431	349.5	295	330	333.5	429
1200	0	44	77	134	205	264	307	345.5	391	418	330.5	302	342	345.5	446
1250	0	43	74.5	124.5	195	255	301	342	378	402.5	320	309	355.5	355.5	459
1300	0	42	72	116	185	244	293	337	363	383	316	317.5	369	363	
1350	0	41.5	69	108	174	232.5	284	330.5	346	360	316.5	326	382	368	
1400	0	40	66.5	100	161	220	273	322	330.5	339	319	336	394.5	369	
1450	0	39.5	64	93	148	208	260	310	315.5	321.5	324	345.5	406.5		
1500	0	38	61.5	86	133.5	192	245.5	294	301	307	330.5	355.5	418		
1550	0	37.5	59	79.5	120	178	229	274	287	295.5	338.5	366			
1600	0	36.5	56	73	106.5	162.5	211	251	273	288	348	376.5			
1650	0	35.5	53.5	66.5	94	147.5	191	224		283.5	360.5				
1700	0	34	51	60.5	82	132	170	194			376				
1750	0	33.5		54		116									
1800	0														

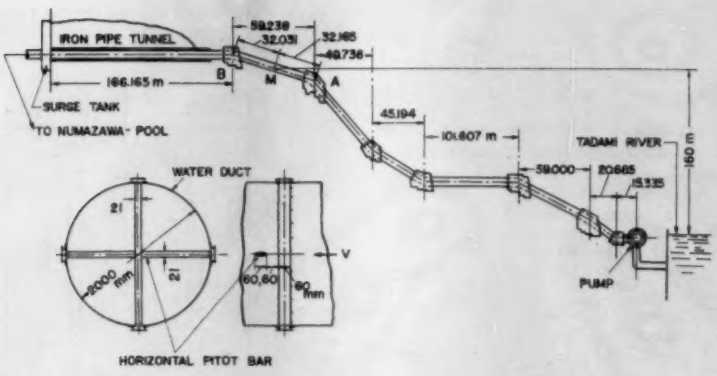

FIG. 10 ELEVATION OF PUMP-DELIVERY DUCT AND POSITION OF TWO PITOT-TUBE BARS IN DUCT

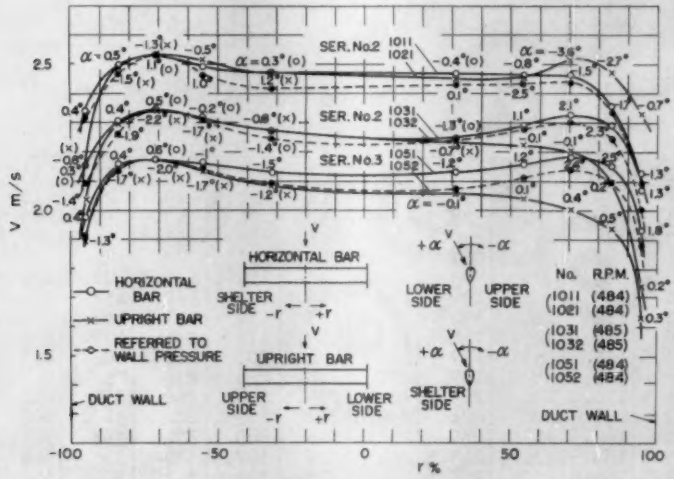

FIG. 11 VELOCITY DISTRIBUTION MEASURED BY PITOT-TUBE BAR

is a bend in the duct, and a point M midway between A and B was finally selected.

Flow Measurement at Pumping Test. At the time of the pumping tests, the actual head between the two levels of the Tadami River and the Numazawa Pool was 196 m. Before commencing the actual measurements, preliminary tests were conducted to ascertain that the direction of the flow in the duct did not deviate from its axis by more than 10 deg. Based on this, the streamlined bars were set with their chords parallel to the duct axis. Fig. 11 gives examples of the velocity distribution in the duct as obtained from the tests. The following points may be noted concerning the results obtained: (*a*) In spite of the fact that the measuring point was removed by a distance of 16 times the diameter of the duct from the bend in the duct, there existed a rotational motion accompanying the flow, evidenced by deviation in the flow direction that was larger toward the periphery, the maximum being 3.6 deg. (*b*) The velocity distribution is not symmetrical around the axis. The distribution curve is seen to have a sag in the middle. However, the shape is not symmetrical, especially in the upright direction, being faster in the upper portion of the duct as compared to the lower half.

Method of Measuring Static Pressure at Wall. In the usual methods (2, 3, 4), the static pressure is assumed to be constant throughout the whole cross section and equal to that registered at the duct wall or at a point near it. If we take the foregoing single value of static pressure as a common basis for all the points across the whole cross section and calculate the velocities on this basis, we obtain values, as marked in Fig. 10, by the solid circles. The resulting error is thus seen to amount to a range of $-2 \sim +3$ per cent.

BIBLIOGRAPHY

1 "Die Genauhigkeit einer Wassermessverfahren," by O. Kirschmer, *VDI-Zeitschrift*, vol. 74, 1930, p. 1499.

2 "Measuring Water Flow in Conduit," by B. W. Proebstel, *Electrical World*, vol. 85, 1925, p. 711.

3 "Photoflow Method of Water Measurement," by W. M. White and W. J. Rheingans, Trans. ASME, vol. 57, 1935, p. 273.

4 "Measurement of Air Flow," by E. Ower, Chapman and Hall Ltd., London, England, third edition, 1949, p. 186.

5 "On the Theory of Arbitrary Wing Section," by I. Imai, *Journal of the Japan Society of Aeronautical Engineering*, vol. 9, 1942, p. 535.

6 "Kraftmessungen an vier Flügelprofilen bei Hohlsog," by F. Numachi, *VDI-Forschung*, vol. 11, 1940, p. 303.

7 "Cavitation Tests on Hydrofoils in Cascade," by F. Numachi, Trans. ASME, vol. 75, 1953, p. 1257.

Discussion

L. J. Hooper.[5] This paper describing the streamlined pitot-tube bar represents an excellent piece of research work which quite possibly may lead to advances in the application of pitot tubes in the measurement of flow in large pipes. However, there are several points brought up by this paper which would seem to require further study. It is regrettable that there is no reference in the bibliography on pitot tubes to the excellent work that has already been done, particularly by Mr. Edward S. Cole,[6] Mr. Clyde Hubbard,[7] and Mr. E. Shaw Cole.[8] The references mentioned emphasize in detail the points which are only briefly enumerated in this discussion.

In American practice it is customary to plot the coefficient of a pitot tube, this coefficient being defined as the ratio of the actual velocity divided by the theoretical velocity. Plotting the coefficient allows a ready expansion of the "error" scale so that 1 per cent deviations are easily evaluated. This suggestion applies particularly to the presentation of the pressure distribution in Figs. 5 and 6 of the paper. With velocity plotted against differential head a square-law curve is plotted on rectangular coordinates and small differences are readily obscured in the plotting. If differential head had been plotted against mean velocity head, for instance, the resulting curves probably would have been straight lines where differences in performance would have been more easily detected.

In determining the efficiencies of pumps and water wheels it is customary to require a flow measurement which is accurate within 1 per cent and this is usually established for inferential methods by calibrations with weighing tanks or volumetric tanks. In this case, no over-all coefficient or over-all calibration has been so determined. It would seem that such a calibration would add a great deal of weight in the conclusions as to the accuracy and desirability of the rod.

The point is made in the paper that the angularity of flow can be determined and corrected with this type of pitot bar where there are two piezometers on opposite sides of the bar reading the pressure. This statement is true in so far as angles measured in a plane normal to the principal axis of the pitot bar are concerned. However, this bar is completely insensitive to angularity in a plane normal to the axis through the piezometers. It is not easy to imagine how such angularity corrections can be incorporated in this design.

Both Mr. E. S. Cole and Mr. C. W. Hubbard pointed out that the presence of a pitot rod in a pipe disturbs the flow and pressure distribution in the measuring section itself. This is the basis of the area correction which Mr. Cole developed at some length in his experimental program. Mr. Hubbard reported on pressure changes around a pitot tube in a pipe in considerable detail. Inasmuch as the pressure measured on a bar is subject to changes induced by local accelerations of velocity it is not possible to compute pressure change directly. Experimental work must be done to develop the correction factor for change in area brought about by the presence of the rod.

Mr. C. W. Hubbard demonstrated that turbulence has an effect upon the calibration of any pitot tube. With some designs the effect is very slight but in other designs the change in coefficient can be several per cent. Mr. E. Shaw Cole in his discussion of Hubbard's paper adds to the evidence of turbulence effects upon the pitot coefficient. In the discussion of Hubbard's paper, Mr. Kalinski[9] discusses this feature and gives further references, namely, Goldstein[10] and Fage.[11] It is obvious from all of this work that has gone before that the effects of turbulence on a particular design cannot be easily worked out analytically. It certainly requires experimental work to determine the various effects of turbulence upon the registration of the impact and reference tubes of such a pitot bar.

The authors are to be congratulated on the excellent work that already has gone into this design and it is hoped that they will continue this good work to answer some of the doubts that have been raised.

S. L. Kerr.[12] This paper gives somewhat of a detailed discussion of the problem in measuring large quantities of water in closed conduits and develops a multiple pitot-tube arrangement whereby such flows can be measured.

Similar work was done in the United States and elsewhere in an attempt to develop a simple and accurate method by using stationary pitot tubes with multiple impact orifices instead of the conventional traversing tube.

Unfortunately, the authors have used the so-called "photoflow method" as a basis for their studies. This method was tried out on several installations in the United States and was described in a publication by White and Rheingans.[13] This method was proposed to the ASME Power Test Code Committee No. 18 on Hydraulic Prime Movers and was thoroughly studied by them. The comparative tests called for in any method of water measurement to qualify for consideration by PTC-18 indicated that the photoflow method was not sufficiently accurate to be included as an improved method in the Test Code.

The errors in measuring the static pressures affected the accuracy of flow measurement to such an extent that it could not qualify within the 1 per cent accuracy range. The proponents of the method withdrew their proposal that it be included in the Test Code and hence the method is not recommended as being an accurate one in so far as American and Canadian practice is concerned.

One of the most thorough investigations of pitot tubes and their accuracy was conducted by Mr. Edward S. Cole[6] and his son, Mr. E. Shaw Cole[8] of The Pitometer Company. This work included much information of great value and it is to be regretted that the authors did not include this in their study as this most valuable work would have undoubtedly changed their conclusions.

W. J. Rheingans.[14] The authors have presented a very comprehensive analysis of pitot-tube design and also have presented valuable data based on experiments with various shapes of pitot-tube bars.

The paper emphasizes the importance of the measurement of the static pressure throughout the cross section of the pipe. During experiments with the photoflow method of water measurement,[15] and subsequent to the publication of that paper, the writer realized the importance of such static pressure measure-

---

[5] Professor of Hydraulic Engineering and Director of Alden Hydraulic Laboratory, Worcester Polytechnic Institute, Worcester, Mass. Mem. ASME.

[6] "Pitot-Tube Practice," by E. S. Cole, Trans. ASME, vol. 57, 1935, pp. 281–294.

[7] "Investigation of Errors of Pitot Tubes," by C. W. Hubbard, Trans. ASME, vol. 61, 1939, pp. 477–492.

[8] Ibid., discussion by E. Shaw Cole, pp. 495–497.

[9] Footnote 7, discussion by A. A. Kalinski, pp. 498–499.

[10] "Measurement of Total Head and Static Head in Turbulent Streams," by S. G. Goldstein, Proceedings of the Royal Society of London, England, vol. 155, series A, 1936, p. 570.

[11] "On the Static Pressure," by A. Fage, Proceedings of the Royal Society of London, England, vol. 155, series A, 1936, p. 576.

[12] Consulting Engineer, Flourtown, Pa. Fellow ASME.

[13] Reference (3) of Bibliography of paper.

[14] Manager, Hydraulic Department, Allis-Chalmers Manufacturing Company, Milwaukee, Wis. Mem. ASME.

[15] Bibliography of the paper (3).

ments. An attempt was made to obtain static measurements by means of four streamlined cylindrical rods equally spaced inside the pipe on a radius corresponding to the center of the area. Four piezometer openings were located on the side of each rod, all leading to single pressure tube. These static-pressure readings throughout the pipe were compared with the readings registered at the pipe wall and it was found that there was considerable variation in the results as well as evidence of relative erratic behavior.

The results of these experimental tests, where the photoflow method was being checked against a standard calibrated method of water measurement, indicated that while it was possible to obtain accurate and reliable measurements of the total (pitot) pressure, the measurement of the static pressure was in considerable doubt. This eventually resulted in the abandonment of the photoflow method as an accurate means of flow measurement.

The authors were aware of this problem and all of their analyses and experimentations were directed toward obtaining accurate static-pressure readings. By designing a streamlined pitot-tube bar, making it possible to obtain static pressure readings near all the points where the pitot readings are taken, they apparently have developed a method which gives consistent results.

Fig. 11 shows a sag in the velocity curves near the center of the pipe. This sort of sag seems to be common to all types of point-velocity measurements when obstructions are placed in the pipe. It is quite possible that no matter how well streamlined the obstruction is (in this case, the pitot-tube bars), such obstruction will affect the flow of the water in such a manner that it reduces the velocity near the obstruction, particularly where the supporting bars or rods cross. Prof. H. Gerber of the Institute of Technology, Zurich, Switzerland, encountered this in connection with current meter measurements in penstocks and found that the only way to eliminate this dip in the velocity curve was to make a special calibration of the current meter which was to be located in the center of the penstock. During calibration this meter was fastened to a cross similar to the supporting bars used in the actual test. All of the other current meters were calibrated fastened to lengths of the supporting bar.

With reference to the accuracy of the use of the authors' pitot-tube method to measure the flow in pipes, this is subject to the usual possible errors of point-by-point velocity measurement in a pipe, due to the inability to obtain measurements close to the wall. For example, in Fig. 11 the closest measurement to the wall of the pipe was at 95 per cent of the pipe radius. This means that for 10 per cent of the area of the pipe the velocity curve has to be extrapolated beyond the test data and since the velocity varies rapidly near the wall, such extrapolation can produce a considerable error in the results.

It is also unfortunate that the authors did not make an actual calibration of the method of measuring flow with the pitot bars and compare it to some standard method, such as weighing, or a calibrated venturi meter. It is suggested that if at all possible, such comparison be made because new methods of water measurement are generally not accepted until they have been proved to be reliable by comparison with some accepted standard.

It also would be interesting if the authors were able to furnish some additional information as to the results obtained in the field test of the pump, such as efficiency and discharge and whether they were in accordance with the pump manufacturer's expectations. Such information usually gives some indication of the reliability of the method of water measurement.

F. S. Weinig.[16] The writer has known the work of Professor Numachi since the late 1920's and always has recognized him as an excellent and meticulous experimenter in the field of fluid flow. If the pitot tube should be applied the way it has been done by Numachi, certainly there can be no better way. However, the writer believes it is intended more for a continuous check with a minimum of pressure loss of an existing pipe if something is going wrong like silt deposit or some other obstruction.

If the pressure principle should be applied for better accuracy, one probably has to suffer higher pressure losses in order to achieve a better-defined and more uniform flow by use of a venturi nozzle or an orifice.

[16] Manager, Aerodynamics, Aircraft Gas Turbine Division, General Electric Company, Cincinnati, Ohio. Mem. ASME.

Authors' Closure

(Written by F. Numachi)

The authors wish to thank the discussers for their interest and pertinent discussions.

Mr. L. J. Hooper suggests the plotting with mean velocity head in place of velocity in Figs. 5 and 6 of the paper. However, the resulting curves thus obtained do not come out as straight lines excepting on $\alpha = 0$ deg in Fig. 5, and on $\alpha = 9$ deg in Fig. 6. Since velocity is what we want to know, we believe our presentation to be more practical than that by velocity head. Depending on velocity, the errors are clarified in Tables 4(*a*) and 4(*b*). Actually, they are very small.

In reply to suggestions concerning the determination of over-all coefficient or calibration with weighing tanks or volumetric tanks, isn't it generally difficult to be equipped with tanks capable of calibrating a flow of 4.9–7.6 ton per sec with sufficient accuracy? Perhaps this is one of the reasons why the inferential method for measuring water flow in a large pipe has not hitherto been established. If experimental results obtained by the use of a miniature pipe and a miniature rod capable of the said calibration be applied to the prototype of large scale, the problem of scale effect will still remain to be solved.

As to insensitiveness of the bar to angularity in a plane normal to the axis through the piezometer, we would think it advisable to have the bar not too sensitive to the angularity (namely, radial velocity) in measuring a flow quantity. As to the total head by a protruding tube, it has been confirmed that there is no change where the angle in question is smaller than ±5 deg. Concerning pressure change at the piezometer, we have confirmed the fact that it shows no change where the angle in question is smaller than ±5 deg in the circular cylindrical section,[17] though we have not yet made experiments on the streamlined section. It is believed that more nearly equal or more stable readings may be expected in the case of the streamlined bar having no surface pressure gradient for a fairly long stretch around the piezometer hole. It would seem undesirable to choose a point on the pipe where the component of a considerable amount of radial velocity is expected to exist as the location for pitot-tube bars for measuring water flow in a large pipe.

Mr. Hooper suggests considering the possibility of the presence of a pitot rod disturbing the flow and pressure distribution, quoting Mr. E. S. Cole's and Mr. C. W. Hubbard's papers. As to this problem, we think it necessary to have a separate study on the treatment of scale effect when we try to apply the experimental results relating to small pipes (e.g., 4–12 in. diam by E. S. Cole) with a small pitot bar to large pipes with a large pitot bar. Mr. Hubbard's method is of measurement of static pressure at the opening bored on the wall, and he treated quite properly those details subject to changes in reading at the opening on account of presence of the total head tube rod. But his is entirely different from ours in principle of measurement. In our method a piezome-

[17] "Über zylindrische Staurohre zur Messung von Geschwindigkeit, Richtung und statischen Druck von Wasserströmung," by F. Numachi, Technological Reports, Tōhoku University, Japan, vol. 11, 1934, p. 353.

ter hole is bored on the streamlined rod and the reading at the hole is treated as one of the measurements of velocity head. Incidentally, the size of our pitot bar is as small as possible proportionately for the pipe within the scope of allowable deformation.

We agree with Mr. Hubbard's opinion that with some designs the turbulence effects upon the pitot coefficient are slight, as well as with Mr. Hooper on his proposal emphasizing the research along that line. It may be stated that the turbulence effects consist largely of the changes of state of boundary layer as influencing readings at the side hole. With reference to this question, the calculation of the transition point of the boundary layer is possible as it relates to the plate,[18] but seems impossible to us at present as to our pitot-bar section, especially as to the section of Cole's pitot tube. Since an accurate and convenient method for measuring the degree of turbulence in water at a given velocity has not as yet been developed, theoretical as well as experimental research on the effects of the degree of turbulence seems to involve considerable difficulty at the present time. In our model experiment, turbulence degree is represented by critical Reynolds number Re_k. In case of an arbitrary velocity, however, it would involve considerable trouble to represent the turbulence degree by the same Re_k either in model experiment or actual measurement.

With reference to this question, we tried to obtain theoretically the effect of Reynolds number Re, a factor of the changes of boundary layer. Then the transition points in boundary layer were calculated[19] from thickness of boundary layer around the streamlined section at each of the two Reynolds numbers, and from those values the separation point of the boundary layer was calculated.[20] The separation point of the boundary layer in either case shows only a slight difference with relation to each other as follows:

Velocity (m/s)	Re × 10^5	Transition point, per cent	Separation point
2.35	1.4	39.2	90.1% of chord length
1.18	0.7	45.4	91.6%

[18] "Laminar Boundary Layer Oscillations and Stability of Laminar Flow," by G. B. Schubauer and H. K. Skramstad, *Journal of the Aeronautical Sciences*, vol. 14, 1947, p. 69.

[19] "Grenzschicht-Theorie," by H. Schlichting, Verlag C. Braun, Karlsruhe, Germany, 1951, p. 304.

[20] "The Theoretical Determination of the Lift Coefficient for a Thin Elliptic Cylinder," by L. Howarth, Proceedings of the Royal Society of London, England, series A, vol. 149, 1935, p. 574.

Mr. S. L. Kerr is correct when he says the photoflow method is not sufficiently accurate in so far as the method hitherto followed is concerned.

Taking that point into account, a photoflow method was devised with special provision to bring the menisci into the field of the camera with sufficient accuracy of measurement, the details of which, however, had to be omitted.[21]

Mr. E. S. Cole's paper[2] will be referred to in our description of the process in which the calculation of flow quantity is carried out from velocity distribution.[21] One of the authors was not satisfied with the Schuster type of pitot tube,[22] similar in some respects to Cole's type,[23] but essentially different since the piezometer opening is not in the direction of unstable dead-water space. He devised a cylindrical pitot tube[17] at the time of Mr. Cole's work. We could give a better answer if Mr. Kerr would state specifically in what point our conclusion should change depending on Mr. E. S. Cole's paper.

As to the sag in the velocity curve which Mr. W. J. Rheingans points out, we cannot as yet give a satisfactory explanation. A sag is similarly shown in the results of measurements by other test groups conducted at the same time as ours, in which only one pitot bar of another type was inserted. If the flow pattern in the latter case is also affected by the obstruction, it would be found to be more noticeable close to the wall than near the center of the pipe.

Mr. Rheingans points out the possible errors due to inability to obtain measurements close to the wall, with which we are entirely in agreement. However, the error of velocity at the part closer to the wall than 95 per cent of the pipe radius does not incur any considerable error in our calculation of flow quantity.[21]

Some information as to the results obtained in the field test of the pump was omitted.[21] The discharge and efficiency of the pump were in accordance with the manufacturer's expectation.

---

[21] The details were given in our original manuscript, but the limitation to the length of the text obliged us to omit them. They will be published in the Rep. I.H.S.M., Tōhoku University, Japan, before long.

A copy of the report will be sent to a reader on request.

The manometer gradation taken on the 35-mm film could be read up to $^1/_3$ mm and it corresponded to 0.33~0.05 per cent of the water-column height.

[22] "Experimentelle Untersuchung der Strömungsvorgänge in einer Schnellläufer-Francis-Turbine, unter Anwendung eines neuen Verfahrens zur Bestimmung von Stromrichtungen mit Pitot-Röhren," by P. Schuster, *VDI-Forschungsarbeiten*, Heft 82, 1910, p. 1.

[23] Bibliography (6), p. 283.

A Comparison of Regenerative-Pump Theories Supported by New Performance Data

By YASUTOSHI SENOO,[1] FUKUOKA, JAPAN

Several theories of the fluid-dynamic mechanism of a regenerative pump have been presented in the literature. The author has compared these theories and believes that in principle they are compatible. The differences occur in the assumptions made. Experimental data show that, although each assumption is useful for a limited operating condition and geometry, none covers a wide enough range for a complete analysis of the phenomenon. In addition, he presents a series of experimental data concerning the geometry of the pumping channel. Although the influence of the geometry of the pumping channel on performance is complicated, consistent tendencies are found. These tendencies and experimental data are available not only as an aid to design but also may serve as a guide for the improvement of any simple semiempirical theory of the regenerative pump as well as for testing any complete theories.

Nomenclature

The following nomenclature is used in the paper:

- A = pumping channel area shown in Figs. 2, 3
- a = effective exit area of momentum-exchange flow
- b = width of impeller vane, Figs. 2, 3
- $C_1 C_2 \ldots$ = proportionality constant
- D = impeller diam
- g = gravity
- H = head
- h = height of impeller vane, Figs. 2, 3
- p = pressure
- Q = rate of flow through area A
- r_G = radius of centroid of pumping channel cross section
- s = depth of side channel, Figs. 2, 3
- T = torque
- t = depth of tip channel, Figs. 2, 3
- U = peripheral velocity of impeller
- v = mean velocity component of moment exchange flow normal to exit area ($v\,a$ = momentum-exchange flow)
- η = efficiency
- θ = angle around axis of impeller
- ρ = density of fluid
- ω = angular speed
- ϕ = dimensionless flow coefficient Q/AU
- ψ = dimensionless pressure rise $2p/\rho U^2 = 2gH/U^2$

Comparison of Some Theories of the Regenerative Pump

The term "regenerative pump" is used in this paper to denote a hydrodynamic unit often referred to in the literature as periphery pump, turbulent pump, friction pump, turbine pump, traction pump, etc.

Several hypotheses concerning the principle of the operation of the regenerative pump have been presented and discussed. Some authors (1, 2)[2] consider that a kind of turbulent theory is applicable; others (3, 4) disagree and insist that the mechanism is based on the circulatory flow between the impeller and the fluid in the casing. But most of these theories are compatible.

Relationship Between Torque and Pressure Rise

If it is assumed that the flow is steady and uniform along the periphery of the impeller, the torque of the impeller is equal to the sum of the torque due to the pressure rise along the periphery and the torque due to the friction force on the fixed wall. This relationship exists whether the force exerted on the impeller is a friction force or any other kind of force. Since it is difficult to estimate the friction force on the fixed wall and there is no theory which treats this force reasonably, the force is left out of the consideration in this comparative study.

If a unit angle of the channel is taken as a control volume, the torque due to the pressure force T/θ is the product of the cross-sectional area A, the radius of the center of gravity of the cross section r_G, and a mean pressure difference across a unit angle p/θ, i.e., $T/\theta = A\,r_G(p/\theta)$. This relationship between the torque and the pressure rise in the pump exists independently of the mechanism of the pumping action.

Relationship Between Through-Flow and Pressure Rise

Momentum-Exchange Theories. Some investigators (3, 4) say that the fluid in the impeller vanes is thrown out and flows across the channel supporting the pressure gradient p/θ at the cost of losing its angular momentum and then it re-enters the impeller with a smaller angular momentum. The rate of change of the angular momentum is the torque exerted by the impeller. Other investigators (2, 6) insist that some amount of fluid is projected from the impeller vanes with a large angular momentum into the fluid in the channel which has less angular momentum. A violent mixing will occur in the channel and the angular momentum will spread over the channel. At the root of the impeller vanes, the same amount of fluid as projected enters the impeller from the channel, with less angular momentum. The rate of change of the angular momentum is the torque exerted by the impeller.

In the second hypothesis, the mechanism includes a mixing process which is not isoentropic unless the fluid in the channel has the same angular momentum as has the fluid in the impeller. On the other hand, in the first hypothesis the process does not include mixing; therefore the process can be isoentropic in an idealized case. This is an object of argument. However, in both cases, the torque exerted by the impeller is the difference of angular momentum between the fluid projected from the impeller and the fluid

[1] Assistant Professor, Research Institute for Applied Mechanics, Kyushu University; Visiting Fellow, Mechanical Engineering Department, Massachusetts Institute of Technology, Cambridge, Mass.

Contributed by the Hydraulic Division and presented at the Diamond Jubilee Semi-Annual Meeting, Boston, Mass., June 19–23, 1955, of The American Society of Mechanical Engineers.

Note: Statements and opinions advanced in papers are to be understood as individual expressions of their authors and not those of the Society. Manuscript received at ASME Headquarters, April 1, 1955. Paper No. 55—SA-44.

[2] Numbers in parentheses refer to the Bibliography at the end of the paper.

entering the impeller. In simplified analysis only this relationship is adopted. Therefore, as far as simple theories are concerned, these two hypotheses are compatible.

The rate of change of angular momentum per unit time is the product of the mass of exchange flow per unit time and the difference of angular momentum per unit mass between the projected fluid and the entering fluid. Some investigators (3) try to estimate theoretically the difference of angular momentum per unit mass by adopting certain assumptions, but in simple theories most researchers simply assume that it is proportional to the difference between the peripheral velocity of the impeller U and the mean velocity of the through-flow in the channel ϕU, where ϕ is the dimensionless rate of through-flow Q/UA. If the difference of the radii at which the fluid is projected and enters is neglected for simplicity, this assumption is reasonable. The mass of momentum exchange flow per unit time is shown by $\rho v a$, where ρ is the fluid density, v is the mean velocity component normal to the exit area, and a is the effective exit area. (a may be proportional to the radius of the impeller $D/2$ times the tip length or the total length of the free edge of the impeller vane $b + h$. In this paper it is assumed to be $a \sim (b+h)D/2$.) The following equation expresses the relation between the angular momentum exchange and the torque on the impeller

$$\frac{T}{\theta} = \frac{p}{\theta} A r_G = C_1 U(1-\phi)\frac{D}{2}\rho v a$$

$$= C_2 U^2(1-\phi)D^2\rho\frac{v}{U}(b+h) \quad \ldots\ldots [1]$$

where C_1 and C_2 are proportionality constants.

The problem is how to estimate the value of v. A researcher (4) assumes that the rate of momentum-exchange flow is proportional to the peripheral velocity of the impeller and it is independent of the rate of through-flow. Another simple assumption is that the rate of momentum-exchange flow is proportional to the difference of the peripheral velocity of the impeller U and the mean velocity of through-flow in the channel ϕU. Since r_G is proportional to D, Equation [1] leads to the following equations if these assumptions for the rate of exchange flow are adopted

$$\left(\frac{p}{\theta}\Big/\rho U^2\right)\frac{A}{D(b+h)} = C_3(1-\phi) \qquad \text{if } v \sim U \quad \ldots\ldots [2]$$

$$\left(\frac{p}{\theta}\Big/\rho U^2\right)\frac{A}{D(b+h)} = C_4(1-\phi)^2 \qquad \text{if } v \sim U(1-\phi) \quad \ldots [3]$$

These are the basic equations deduced from simple momentum exchange theory.

Turbulent-Flow Theories

Other kinds of simple theories are reported by a number of researchers (1, 2, 5, 6, 10) on the fluid-dynamic mechanism of a regenerative pump. According to their hypotheses, a kind of turbulence is the mechanism with which the impeller exerts the torque on the fluid in the channel. One researcher (1) assumes that the turbulence in the channel is the same kind as the turbulence in a pipe but the intensity cannot bear comparison; that is, the shear stress exerted by the impeller is proportional to the square of the difference between the impeller peripheral velocity and the mean velocity of the through-flow $U^2(1-\phi)^2$.

Others (5, 6) assume that the shear stress is proportional to the peripheral velocity of the impeller as well as to the difference between the impeller peripheral velocity and the mean velocity of the through-flow. The reason for this assumption is that the turbulence in a regenerative pump is chiefly influenced by the peripheral velocity of the impeller itself; that is, the turbulence in a regenerative pump is different from the turbulence in a pipe.

Since the effective area of the impeller on which the shear stress works is proportional to $(b+h)D/2$ in both cases, the relationship between the torque exerted by the impeller and the torque due to the pressure gradient is reduced to Equations [3] and [2], respectively. This is not an accidental coincidence. Since turbulence is a kind of momentum-exchange phenomenon, turbulence theory intrinsically includes a treatment like that in the momentum-exchange explained before. In other words, the momentum-exchange phenomenon can be compared qualitatively to a kind of turbulence. Thus either Equation [2] or [3] represents most of the simple theories.

Circulatory Flow Theory

An MIT group (3) has reported a complicated theory. The principle of the theory is explained under the subheading, Momentum-Exchange Theories. The basic equation is similar to Equation [1] except that $(C_3 - \phi)$ is used instead of $(1-\phi)$. Although C_3 is a function of slip coefficient at the impeller tip and of the shapes of the impeller and the channel, the numerical value is close to unity.

The momentum-exchange flow v is not assumed directly as in simple theories, but it is shown as a function of the through-flow and the pump geometry. Roughly speaking, $(v/U)^2$ is a quadratic function of ϕ, so the relationship may be more realistic than those of simple theories.

In all of these theories, at least one coefficient is included which is to be decided experimentally. The coefficient is not constant if the geometries of the channel and the impeller vary. At the present stage of the theories on regenerative pumps, some reports of experimental analysis are required which will not only be directly available for design purposes but also indicate directions for the improvement of theories of operation.

Relationship Between Momentum-Exchange Flow and Through-Flow

In theoretical investigations of regenerative pumps, some researchers (1) have assumed that the momentum-exchange flow is proportional to the difference between the peripheral velocity of the impeller U and the mean velocity of the fluid in the channel ϕU. Other researchers (4, 5, 6) insist that the momentum-exchange flow is approximately proportional to the peripheral velocity of the impeller U. Since most people agree that the angular momentum change per unit mass of the momentum-exchange flow is proportional to the difference $U - \phi U$, the relationship between the momentum-exchange flow v/U and the through-flow ϕ is calculable from experimental performance by Equation [1].

In Fig. 1, some examples of the relationship are exhibited. As will be explained later, the performance is influenced by t/s, t/b, s/b, and $A/(b+h)D$, so the relationship between v/U and ϕ cannot be expressed by a simple relationship such as v/U is proportional to $1-\phi$ or v/U is independent of ϕ.

No simplified method is applicable for a thorough theoretical analysis of the performance of a regenerative pump. The only method is to consider the mechanism of pumping action directly introducing some reasonable hypotheses as Prof. W. A. Wilson and his colleagues have done.

An Analysis of Experimental Data

Some researchers (1) explain that a head-discharge performance curve is upward concave and others (3) insist that it is upward convex. Recently, Prof. W. A. Wilson's group reported a series of experimental data concerning a regenerative pump of variable geometry. The present author performed a complementary experiment which, together with the former data, implies a strong and complex influence of pumping channel geometry on performance. Some papers (8, 9) have indicated that this influence is

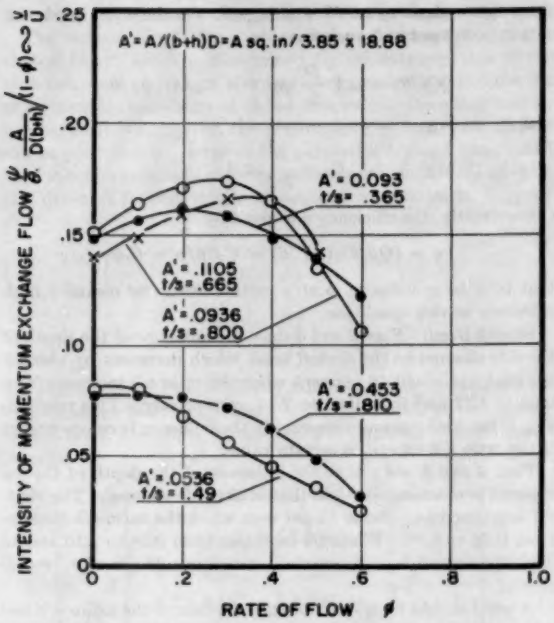

FIG. 1 RELATIONSHIP BETWEEN MOMENTUM-EXCHANGE FLOW AND THROUGH-FLOW

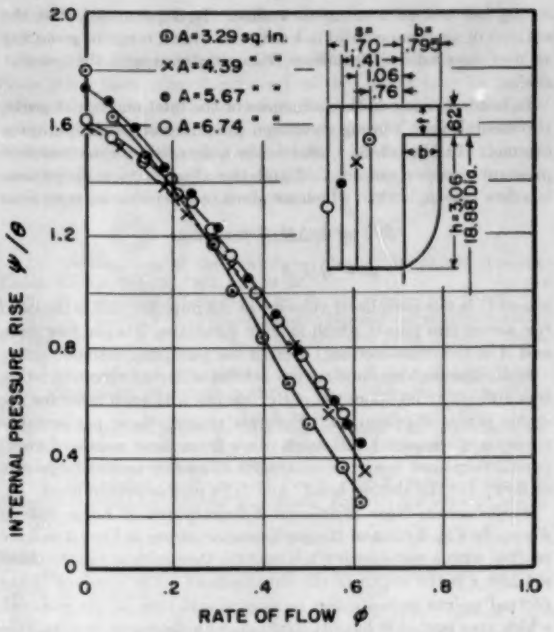

FIG. 2 INFLUENCE OF SIDE-CHANNEL DEPTH ON INTERNAL PERFORMANCE (1)

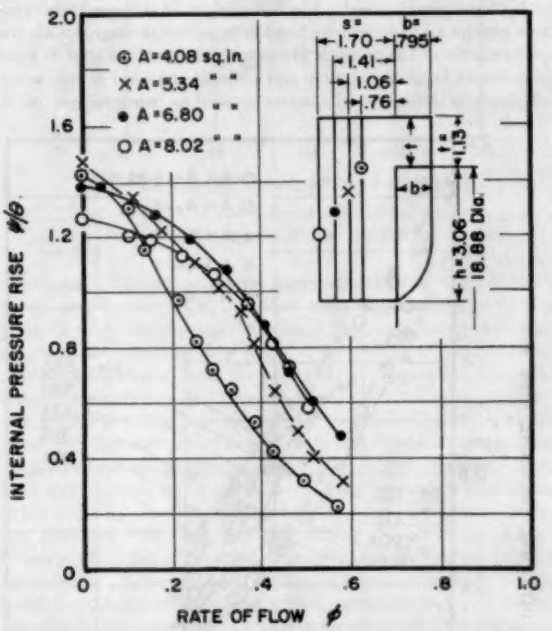

FIG. 3 INFLUENCE OF SIDE-CHANNEL DEPTH ON INTERNAL PERFORMANCE (2)

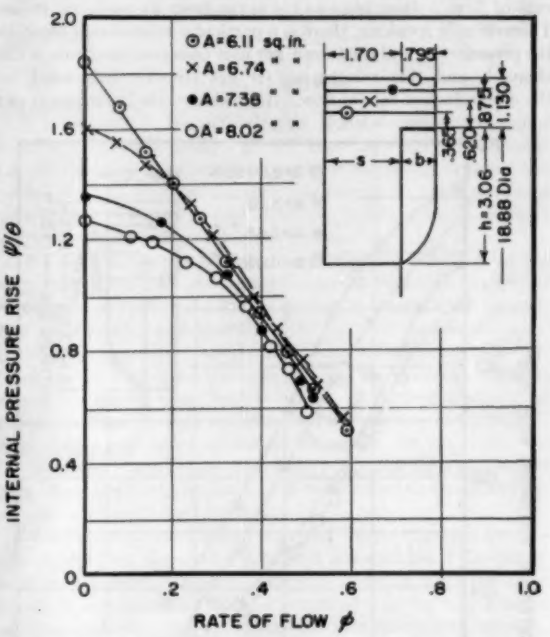

FIG. 4 INFLUENCE OF TIP-CHANNEL DEPTH ON INTERNAL PERFORMANCE (1)

strong but not of a complex nature. It is presumed that the authors of such papers did not cover so wide a range of geometry as was covered by Professor Wilson's group and the present author.

In order to exclude the influences of the inlet and outlet ports, Professor Wilson's group measured pressure rise in the pumping channel. In Figs. 2, 3, 4, and 5, the ordinate is a dimensionless pressure rise per radian ψ/θ and the abscissa is a dimensionless flow rate ϕ, both of which are given by the following equations

$$\psi/\theta = 2g\Delta H/U^2\theta \text{ radians}^{-1}$$

$$\phi = Q/UA$$

where U is the peripheral velocity of the impeller, ΔH is the head rise across two points which include θ radians, Q is the flow rate, and A is the cross-sectional area of the pumping channel.

Since the performance curves exhibit different characteristics, it is difficult to compare the performances with each other for the whole range of operation. For this reason, these performance curves are compared with each other from three points of view: (*a*) Performance near the maximum efficiency and at large rate of flow; (*b*) the shutoff head; and (*c*) a characteristic head.

Performances Near Maximum Efficiency and at Large Rate of Flow. In Fig. 6 most of the performance curves in Figs. 2 to 5 are plotted with a parameter t/s, where t is the depth of the tip channel and s is the depth of the side channel. The symbols of the plotted points indicate the cross-sectional area of the channel, which area probably has little influence on the pump performance within this experimental range. Although the influence of the parameter t/s is not uniform, these data show that a ratio of about 0.4 gives optimum performance; thus, for any constant ψ/θ, the rate of flow ϕ diminishes as t/s varies from its optimum value. Theoretically speaking, there is a particular relationship between the pressure rise and the torque per unit cross-sectional area of the channel, and this relationship is not directly influenced by the dimensionless rate of flow. Accordingly, the input power per unit angle is given by $\omega T/\theta = \omega A r_G p/\theta$. On the other hand, the output power per unit angle is

$$Q(p/\theta) = \omega A \frac{D}{2} \phi p/\theta = C_s \omega A r_G \phi p/\theta$$

where

$$C_s = \frac{D}{2r_G} \cong 1$$

Consequently, the efficiency η is given by

$$\eta = (Qp/\theta)/(\omega T/\theta) = C_s \phi p/p = C_s \phi$$

that is, a large value of ϕ at a certain head rise means a high efficiency at that condition.

Shutoff Head. Figs. 2 and 3 show the influence of the depth of the side channel on the shutoff head, which decreases by about 3 per cent and about 10 per cent when the ratio s/b increases from 0.95 to 1.77 and from 0.95 to 2.14, respectively. This relationship is not uniform and presumably the influence becomes serious if the ratio s/b exceeds a certain value.

Figs. 4 and 5 show that the influence of the depth of the tip channel is more serious than that of the side channel. The shutoff head increases about 15 per cent when the ratio t/b changes from 0.78 to 0.46. When t/b increases from 0.78 to 1.10 and to 1.42, the shutoff head decreases about 15 and 22 per cent, respectively.

A word should be said about the adoption of the ratios s/b and t/b as measures of the depths of the channel. This adoption is due to the intuitive preference of the author who believes the width of the impeller to be more important than the other dimensions such as the diameter D or the height of the blade h.

A Characteristic Head. For comparison of different regenerative pumps a characteristic head is required through which the performance of the pump is predictable. Since the shutoff head is seriously influenced by t/b and s/b, and the head at maximum efficiency is difficult to determine as well as being subject to in-

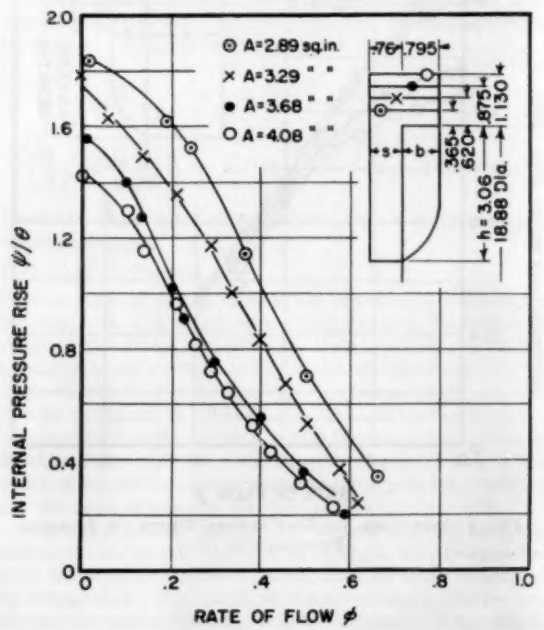

FIG. 5 INFLUENCE OF TIP-CHANNEL DEPTH ON INTERNAL PERFORMANCE (2)

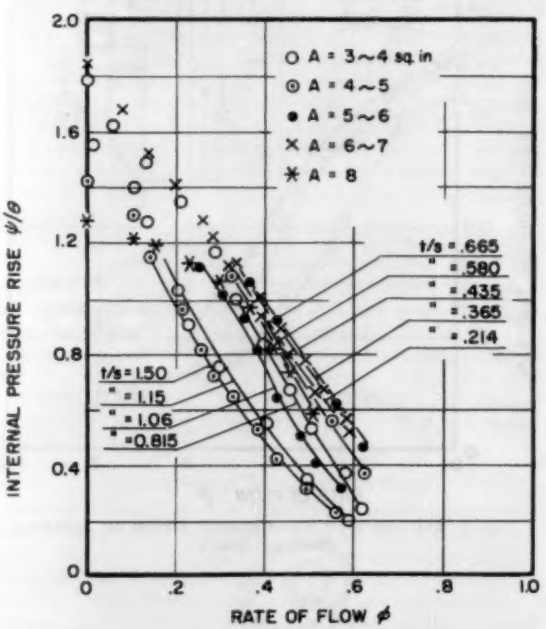

FIG. 6 INFLUENCE OF TIP-SIDE CHANNEL DEPTH RATIO ON INTERNAL PERFORMANCE

fluence by t/s, neither of these is desirable as a characteristic head.

The author adopts for a characteristic head an "imaginary shutoff head" which is determined by an extrapolation of the high-flow-rate portion of the flow-performance curve (ignoring experimental data obtained at low flow rate). Once this characteristic head is indicated, the performance at large rate of flow can be predicted by virtue of the parameter t/s and the shutoff head can be predicted by the parameters t/b and s/b. Equation [1], deduced from a simple theoretical consideration, suggests that

$$\left(\frac{H}{\pi}\Big/\frac{U^2}{2g}\right)\left(\frac{A}{D(b+h)}\right)\Big/(1-\phi) \sim \left(\frac{p}{\theta}\Big/\frac{\rho U^2}{2}\right)\left(\frac{A}{D(b+h)}\right)\Big/(1-\phi) \sim \frac{v}{U}$$

is a parameter which is explicitly influenced only by the momentum-exchange flow. The values of the parameter at the characteristic head, where $\phi = 0$, are shown in Fig. 7 by the double-circle symbol.

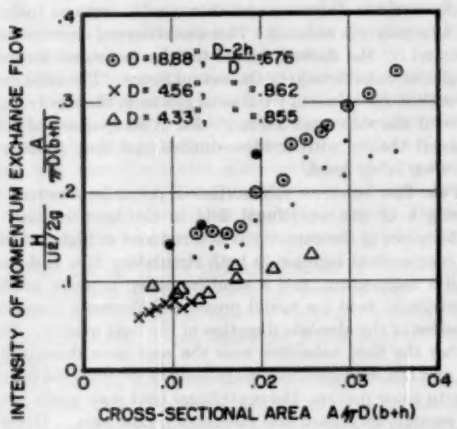

A: One half of channel area, for a usual pump

FIG. 7 MOMENTUM-EXCHANGE FLOW AND CHANNEL AREA

Although the values of the parameter at the shutoff head shown by the symbol of point are scattered, the values of the parameter at the characteristic head increase linearly with increase of the dimensionless area. Two groups of experimental data (8, 9) of shutoff head are plotted in the figure for comparison. Each of the groups was performed with the same impeller but with different geometries of the channel. The three black points are not a series of experiments but represent extraneous data for three different pumps having good performances. The head used for calculating the value of the co-ordinate is a function of the angle between the inlet and the outlet ports, internal leakage, geometry of the impeller, geometry of the inlet (7), and outlet ports, etc.; therefore different groups of experimental data do not coincide. However, in all of them, a tendency is clearly recognized for the intensity of momentum exchange flow v/U to be magnified by an increase of the dimensionless cross-sectional area.

ACKNOWLEDGMENT

The present study was undertaken under the auspices of Prof. William A. Wilson of the Department of Mechanical Engineering, Massachusetts Institute of Technology. The author wishes to thank the professor for encouragement, useful suggestions, funds, and laboratory facilities. The author also expresses his deep appreciation to Prof. Miguel A. Santalo for his contribution to this study.

It is acknowledged that some significant theories and correlations other than those mentioned in this paper may be in the current literature, and indeed that the author possibly has failed to do complete justice in his interpretations of those which are discussed here. Although a sincere effort has been made to avoid such injustices, the author apologizes to any persons who may have been misinterpreted or overlooked.

BIBLIOGRAPHY

1 "Performance of the Periphery Pump," by H. W. Iversen, Trans. ASME, vol. 77, 1955, pp. 19–22.

2 Discussion of reference (1) by W. E. Wilson, pp. 24–25.

3 "A Theory of the Fluid-Dynamic Mechanism of Regenerative Pumps," by W. A. Wilson, M. A. Santalo, and J. A. Oelrich, Trans. ASME, vol. 77, 1955, pp. 1303–1311.

4 Discussion of reference (1) by A. M. Wright, pp. 25–27.

5 Discussion of reference (3) by G. F. Wislicenus, pp. 1314–1315.

6 "Theoretical Research on Friction Pump," by Y. Senoo, *Reports of Research Institute for Fluid Engineering*, Kyushu University, Fukuoka, Japan, vol. 5, no. 1, 1948.

"Researches on Peripheral Pump," by Y. Senoo, *Reports of Research Institute for Applied Mechanics*, Kyushu University, vol. 3, no. 10, 1954.

7 "Influences of the Suction Nozzle on the Characteristics of a Peripheral Pump and an Effective Method of Their Removal," by Y. Senoo, *Reports of Research Institute for Applied Mechanics*, Kyushu University, Fukuoka, Japan, vol. 3, no. 11, 1954.

8 "Performance of a Shallow-Well Pump" (in Japanese), by M. Fujiwara, *Hitachi Hyoron*, vol. 30, no. 3, 1948, p. 104.

9 "On the Performance of the Periphery Pump" (in Japanese), by S. Terada and B. Nanya, *Hitachi Hyoron*, vol. 25, no. 5, 1942, p. 268. Data are adopted in reference (6).

10 "Theory of Westco Rotary Pump," by A. Miyazu, Transactions of the Society of Mechanical Engineers of Japan, vol. 15, no. 18, 1939.

Discussion

J. A. OELRICH.[3] In comparing the various regenerative-pump theories, the author accepts a very important but very difficult task of resolving what appeared to be diametrically opposed hypotheses. This is seldom an easy role to assume, since one must point out the weak as well as the strong points of the position of all parties involved, including one's own.

One of his important observations is that the definition of the term turbulence as sometimes applied to the regenerative pump is erroneous. He points out that it cannot be compared to the turbulence associated with pipe flow; the intensity cannot bear comparison. In general, classical fluid mechanics considers as turbulence the small-scale macroscopic momentum exchange which is superposed on the mean fluid velocities. A further definition or extension of this concept would appear unnecessary in the field of regenerative pumps for, as the author agrees, the mechanism of the pumping action is best deduced by introducing a reasonable hypothesis and applying the laws of motion and thermodynamics as used in classical fluid mechanics.

As to the complicated theory involved, this, of course, is a necessity dictated by the device itself and unavoidable if the theory is to be complete. It should be noted, however, that the complexity is only relative. While a simplified solution may contain an equal number or fewer configuration parameters than the complicated one, the simplified-solution parameters are generally such complicated functions of geometry as to defy analysis—analysis well initiated for the "complicated" theory. Further, the simplified theories are incapable of satisfying the observed details of the fluid motion. It is the writer's viewpoint that any theory which

[3] Research Engineer, Research and Development Department, Worthington Corporation, Harrison, N. J. Assoc. Mem. ASME.

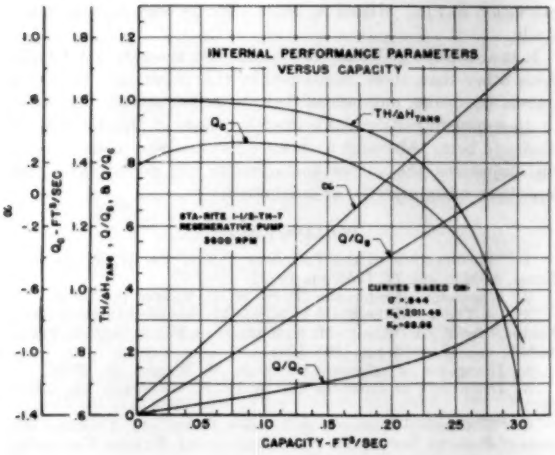

FIG. 8

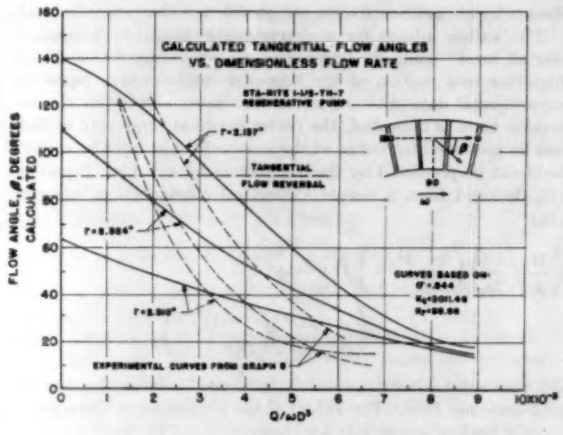

FIG. 9

does not eventually predict the observed and measurable details is not as apt to lead eventually to an optimization of the efficiency for a particular specific speed.

The author's point that configuration plays a decided role in whether the curve is convex or concave upward is well put. The writer has been mildly surprised that this known difference in observations has been made a point of issue in the way it has. The important consideration is not the shape of the curve, but the understanding of why the performance curve takes the shape it does. Reiterating the authors' viewpoint of (3),[4] the centrifugal field creating the radial pressure gradient inside the rotor is constant, or essentially so, at a given speed. However, the centrifugal field in the open channel weakens as capacity is reduced, that is, as the tangential velocities in the open channel decrease. Therefore qualitatively the circulatory flow may be expected to increase as we approach zero through-flow. Actually, for the configuration tested by the authors of reference (3) as well as by the present author, it has been calculated that the circulatory flow does not, in general, continually increase as shutoff conditions are approached, but reaches a maximum and then decreases. This variation in Q_c is shown in a previously unpublished curve,[5] Fig. 8 of this discussion, from the writer's graduate thesis,[6] and is comparable to the curves deduced in the author's Fig. 1. While the curve is calculated from theory (3), the explanation for its shape and the resultant shape of the head-capacity curve is based on a comparison with theory of the observed through-flow behavior, as shown in a second previously unpublished curve[6] (Fig. 9, herewith). To explain this figure we again review the theory (3).

To maintain a tangential pressure gradient in the open channel the angular momentum of the circulatory flow continually decreases after it leaves the rotor. This indicates that an increase in pressure rise requires either a greater reduction of the tangential velocity along the meridional flow path from the exit of the rotor to the blade root, an increase in the rate of circulatory flow, or both. Reductions in the tangential velocity outside the rotor result in reductions in the capacity. In Fig. 8 the parameter α is the ratio of the fluid tangential velocity at the blade entrance to the rotor velocity at this point. As shown here the theory predicts that the tangential velocity of the fluid outside the rotor near the blade entrance decreases and then finally reverses (negative values) as capacity is reduced. This was observed experimentally as indicated by the dashed curves for the measured tangential flow angles at various radii in the second figure. The solid curves are the calculated values of the flow angles from the theory. (The diameter of the rotor was 5.4 in.) For a comparison of a two-dimensional theory with a three-dimensional flow pattern the agreement is fairly good.

With the flow behavior substantiated, it can be reasoned that the strength of the centrifugal field in the open channel certainly decreases as the capacity is first reduced at high flow rates, with a concomitant increase in both circulatory flow and change in angular momentum, and a resulting steep pressure gradient. The centrifugal field (or radial pressure difference), however, is independent of the absolute direction of the fluid motion. Therefore, after the fluid velocities near the root have decreased, reversed, and attained sufficient magnitude in the reversed direction counter to rotor motion, the centrifugal field may again become strong enough to reduce the circulatory flow rate. While observed for certain configurations, this full range of conditions cannot be ascribed to all. In addition, it should be noted that the change in angular momentum continually increases with decreasing capacity, so the head-capacity curve will not reflect the full significance of the circulatory flow variation. The interrelation between these two effects, plus slight variations of the coefficient of slip and meridional streamline with capacity, go far to explain why particular regenerative-pump performance curves are convex or concave upward. The slight variations of the meridional streamline have been indicated by experimental observations.

Unfortunately, the curves deduced by the author in Fig. 1 do not include a configuration similar to the unit for which the variation of circulatory flow is presented by the writer, and so a direct comparison cannot be attempted. An almost exact geometrical comparison, including the rotor, is the unit in Fig. 2 for A equal to 4.39 sq in., t equal to 0.620 in., and s equal to 1.06 in., based on a $3\frac{1}{2}:1$ scale ratio. As indicated, it is believed that the trend of the curves reported in Fig. 1 is correct although the proportionality as given is greatly oversimplified. Values of v/U as given, of course, are comparable only for each curve. Calculations show that the ratio of the average radial velocity at the rotor discharge to the peripheral velocity will run approximately twice the values reported by the author. The divergence depends on the value of the ignored proportionality factor for each particular unit, which itself is a function of configuration.

Optimum configuration is defined by the author on the basis of

[4] Numbers in parentheses refer to the author's Bibliography.

[5] Commercial double-sided unit: Sta-Rite $1\frac{1}{2}$ TH-7.

[6] "Development of an Analysis of a Regenerative Pump," Thesis for the Degree of Mechanical Engineer, Massachusetts Institute of Technology, August, 1955.

the unit with the maximum flow coefficient for a particular ψ/θ. It is agreed that the usual definition does not apply to the *internal performance* of a regenerative pump; that is, considering cavitation performance separately, it is generally accepted that the optimum configuration is that which gives the highest efficiency at a particular specific speed, where the efficiency is the best efficiency point for the complete unit. The theoretical deduction of the internal efficiency certainly does indicate that the configuration with the maximum internal efficiency can be determined. This derivation was previously reported (3) and corresponds to the curve for Q/Q_s in the first figure below, where Q_s equals $r_G A\omega$. It is felt, however, that the addition assumption that $2r_G \cong D$ is far too loose for the range of configurations, and where the actual centroidal radii are used another configuration might be indicated. With this correction to the method, it is believed that for a particular performance point, or specific speed, no unit could have a greater internal efficiency than indicated by such an analysis. With rotor variations included, however, dimensional correlation would undoubtedly be more complicated than the simple t/s parameter indicated.

J. R. PARKER.[7] The continued interest in analysis of the regenerative-pump performance as related to the physical dimensions of the unit is appreciated by the writer.

Progressively the explanation of the pumping theory has been reduced to practical understanding and is felt that with a few additions the subject paper might supply some interesting answers to a regenerative-pump analysis. The writer thinks that if the author had started out with a conventional performance curve showing head, capacity, power, and efficiency and carried an analysis through, it might simplify the study of his paper. The difficulty in analysis might be overcome by answers to the following:

1 What are the proper term dimensions to the formula of ψ over θ, a representation of the internal-pressure rise?

2 What are the dimensions of capacity, gravity, density, flow, and so forth, which figure so prominently in the other formulas?

3 The analysis shows the area of one half of the channel and it is assumed that the entire capacity is used for calculations.

4 It is noted that the pump plotted in Figs. 2, 3, and 4 had an impeller diameter of 18.88 in. while in Fig. 7 the characteristic head data were obtained from the diameter mentioned as well as from two others of 4.56 and 4.33 in. How do these smaller-diameter impellers plot on Figs. 2, 3, and 4?

We calculated the characteristic head as shown in Fig. 7 for impellers $3^3/_4$ to $6^1/_2$ in. diam and obtained the results given in Table 1.

TABLE 1 CHARACTERISTIC HEAD CALCULATIONS

Diameter, in.	$\frac{A}{\pi D(b+h)}$	$\frac{H}{U^2/2g}\frac{A}{\pi D(b+h)}$
$3^3/_4$	0.012	0.18
$4^1/_2$	0.013	0.29
$4^3/_4$	0.014	0.27
$5^1/_2$	0.022	0.29
$6^1/_2$	0.019	0.19

These data fall in an agreeable range only in two cases.

It has been our experience that when the size of the channel becomes large with respect to the impeller dimensions the head-capacity characteristic shows an abrupt change from those shown. It is possible to reduce the shutoff head to one half the conventional value and at the same time obtain twice the capacity at peak efficiency.

We would welcome an explanation of how, once the "imaginary shutoff head" is obtained, the performance at large rates of flow can be predicted.

The author is to be commended on his presentation of a very difficult subject and it is hoped that clarification that may result from the discussion will make it more easily applied and encourage further tests and analysis.

M. A. SANTALO.[8] It is fitting that the author should write this discussion of present theories on regenerative-pump operation because of his extensive investigations on the subject. His comparison of the theories in terms of the "mixing velocity" v is excellent and allows a quick recognition of the assumptions involved in each of them. This paper wisely points out the advantages and disadvantages of the simple theories. It also encouraged the writer to review the previous analysis he presented with Professor Wilson and Mr. Oelrich (3).[9] An attempt to simplify the final relations has been made in order to make them more workable and to be able to compare them with the author's presentation.

The previous analysis considered that the fluid follows a regular helical pattern leaving the impeller at the tip with a tangential velocity component $V_{t_2} = \sigma r_2\omega$ and re-entering the impeller at the side of the blades with a velocity $V_{t_1} = \alpha r_1\omega$. (For simplicity, $r_2 = D/2$ and $r_1 = r_2 - h/2$.) σ represents a slip coefficient and is a measure of the lack of perfect guidance to the flow provided by the blades. The application of the angular momentum relation to a suitable control volume, led to

$$\frac{\psi}{\theta} = 2\frac{r_2}{r_G}\frac{Q_e}{Q_s}\left(\sigma - \alpha\frac{r_1^2}{r_2^2}\right) \quad \ldots\ldots\ldots\ldots [4]$$

An energy balance, adopting some hypothesis regarding flow losses, led to

$$\frac{Q_e}{Q_s} = \frac{r_2 d}{A}\frac{\sqrt{2}}{\sqrt{k_e}} \sqrt{\left(\sigma - \alpha\frac{r_1^2}{r_2^2}\right)(1-\phi) - \frac{1}{2}(1-\alpha)^2\frac{r_1^2}{r_2^2}} \quad \ldots\ldots\ldots [5]$$

where k_e is a loss coefficient and d is a "typical dimension" of the open channel, to be determined experimentally or by further analysis of the flow losses.

The third equation necessary to establish ψ/θ versus ϕ was the flow equation. This expression was previously (3) very long. A simpler relation may be obtained if the average tangential velocity of the flow in the pump open channel is assumed to be the arithmetic mean of V_{t_1} and V_{t_2}

$$\left.\begin{aligned} Q &= A\,\frac{\sigma r_2\omega + \alpha r_1\omega}{2} \\ \text{or} \qquad \phi &= \frac{1}{2}\left(\sigma + \frac{r_1}{r_2}\alpha\right) \end{aligned}\right\} \quad \ldots\ldots\ldots\ldots [6]$$

The numerical values of the coefficients of σ and α in this equation have been found to differ little from the more complex ones derived before.

Equations [4] to [6] can be combined eliminating α and Q_e/Q_s

$$\frac{\psi}{\theta} = \frac{4\sqrt{2}\,r_1 d}{A\sqrt{k_e}}\frac{r_2}{r_G}\sqrt{1-\frac{r_1}{r_2}}\,(C_1 - \phi)\sqrt{C_2 + \sigma\phi - 2\phi^2} \quad \ldots\ldots\ldots [7]$$

[7] Senior Design Engineer, Rocketdyne, Division of North American Aviation Inc., Canoga Park, Calif.

[8] Assistant Professor in Mechanical Engineering, Massachusetts Institute of Technology, Cambridge, Mass.

[9] Numbers in parentheses refer to the author's Bibliography. Symbols used are taken from his nomenclature or are defined in the text.

where

$$C_1 = \frac{\sigma}{2}\left(1 + \frac{r_2}{r_1}\right)$$

$$C_2 = \frac{\sigma\left(1 - \frac{\sigma}{2}\right) - \frac{1}{2}\frac{r_1^2}{r_2^2}}{1 - \frac{r_1}{r_2}}$$

The form of this equation can best be seen in Fig. 10 where it is plotted for one value of r_1/r_2 and several values of σ. This expression, as all the other theories, can be matched reasonably well with most experimental data by choosing proper values of σ and $\sqrt{k_e}/d$.

As indicated by the author this expression has a term of the form $(C_1 - \phi)$ instead of $(1 - \phi)$. Here $C_1 \approx \sigma$ and is less than unity. It is believed that this form is more realistic since when $\psi/\theta = 0$, ϕ is always less than unity. The simple expressions mentioned in the paper always terminate the head-flow curve at $\phi = 1$. This results from the fact that momentum transferred to the flow in the open channel is assumed to come from fluid at the impeller velocity U neglecting an inevitable slip factor σ.

In addition, Expression [7] results in what the author calls a "rate of momentum transfer" v/U proportional to

$$\sqrt{C_2 + \sigma\phi - 2\phi^2}$$

instead of the simple forms $(1 - \phi)$ or a constant. This radical is plotted in Fig. 11 of this discussion for one particular case and shows a shape much closer to the experimental curve of Fig. 1 of the paper than the other two simpler assumptions.

Recent tests carried out at MIT by Theis and McArthur showed the effect of r_1/r_2 by cutting the blades successively, i.e., changing the height of the blade h while keeping the dimensions t, s, and b constant. The area A of the open channel inevitably changed. The experimental points are plotted in Fig. 12, herewith. The values of σ and $\sqrt{k_e}/d$ were obtained to match one curve. When using the new value of r_1/r_2 and A, with all other parameters kept constant, the new theoretical curve is shown to follow the experiment not only qualitatively but also quantitatively.

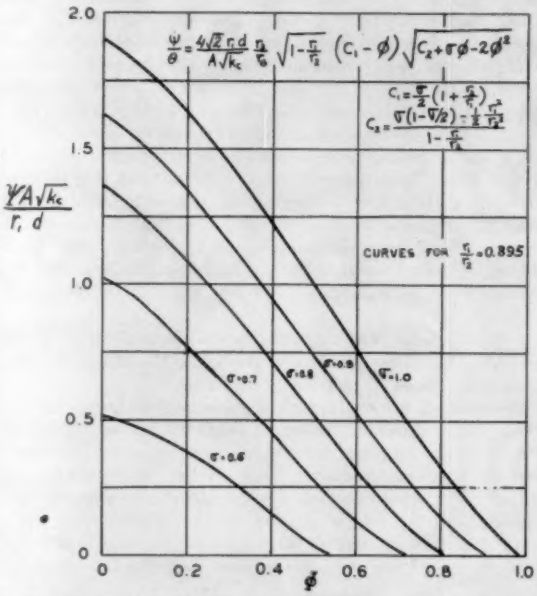

FIG. 10 THEORETICAL PLOT OF INTERNAL HEAD RISE VERSUS FLOW FOR VARIOUS VALUES OF THE PARAMETER σ

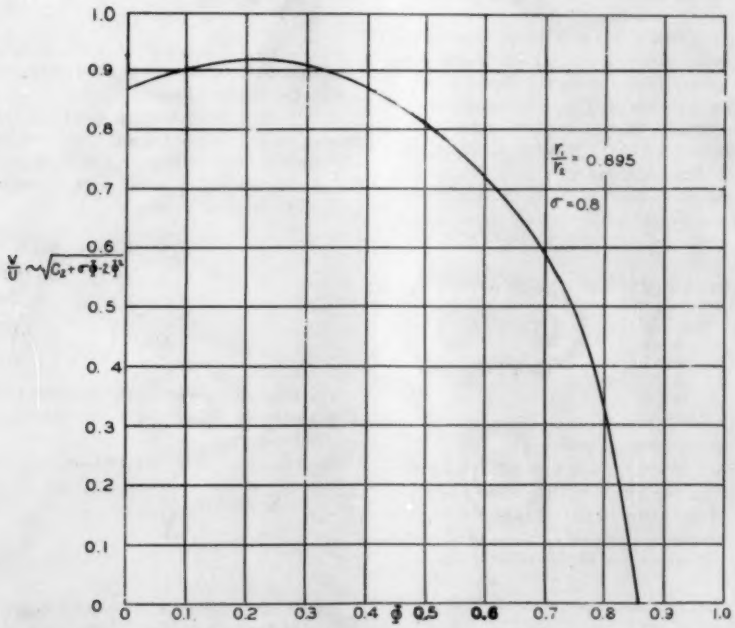

FIG. 11 THEORETICAL PLOT OF THE RATE OF MOMENTUM TRANSFER VERSUS FLOW
(Compare with Fig. 1 of Dr. Senoo's paper.)

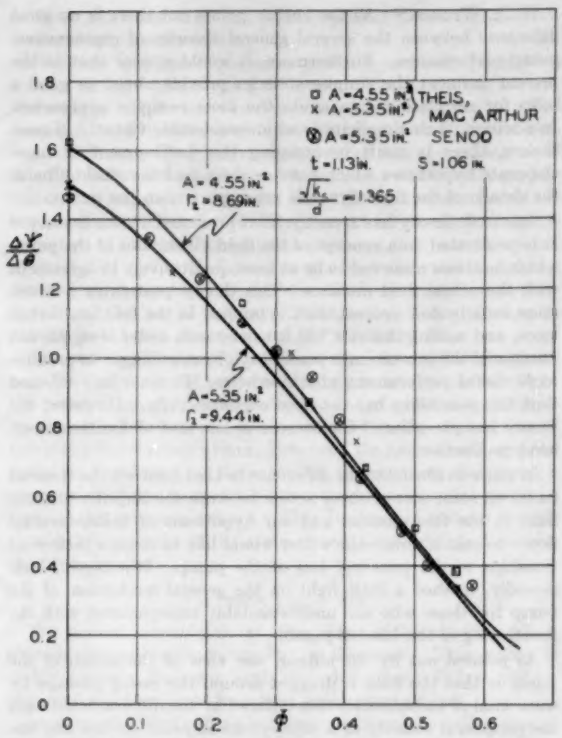

FIG. 12 COMPARISON BETWEEN THEORY AND EXPERIMENT WHEN BLADE HEIGHT IS CHANGED, ALL OTHER DIMENSIONS REMAINING CONSTANT

In conclusion, it is felt that this analysis reflects three more phenomena than the simpler expressions; namely, the presence of slip, the variation of the rate of momentum transfer v with flow, and the effect of a new geometrical parameter r_1/r_2. The latter has often been neglected and is shown to be significant. More systematic testing like that done by the author together with specific analyses of the flow through the pump should show the effect of geometry on the parameters that the author has so cleverly defined.

F. S. WEINIG.[10] The writer is thankful that in the discussion of his paper[11] no one took advantage of the fact that the work was done five years ago and that reference could not be made to test results. The approach is similar to that of H. W. Iversen, which was not known to the writer at that time. An attempt was made to consider all the side effects in the analysis and less consideration was given to quantity than to quality of the results. Therefore the writer may have chosen for the numerical examples somewhat too high disk and casing friction and may have underestimated the exchange losses of inlet and exit, although it is thought these losses could be reduced considerably from the quantities of present-day designs.

The analysis is based on similarity, hence, the conclusion is reached that the ratio α of average radial exchange velocity v, and the difference of $u - v_m$ of blading speed and peripheral-flow velocity in the ring space, in first-order approximation, should be independent of the volume coefficient or the ratio of this peripheral-flow velocity v_m to the tip speed u of the blades. This leads to a quadratic dependency of the blade forces on the difference velocity $u - v_m$ of blade-tip speed and peripheral-flow speed. The value α has been estimated to be of the order of 0.1 and it has been said that it might depend to a certain degree on a series of geometric as well as kinetic conditions. The writer had not suspected so great an influence of the ratio of the radial and axial dimensions as the test results of the present paper would indicate. Evaluation of Fig. 1 of the paper, where the ordinate, if the writer's nomenclature is used, is equivalent to $\alpha(1 - \varphi)$, leads to the conclusion that α covers a range of at least 0.07 to 0.30. The reasons for this variation of α for a given wheel and changing ring-space configuration may establish an intriguing fluid-mechanics problem.

The writer has based his analysis quite conservatively on acknowledged principles of fluid mechanics. In no way is the in-the-main-helical movement of the flow, as observed by W. A. Wilson and co-workers, excluded. It is supposed, however, that the entire free rim of the blades is a flow-separation line and the stream surface originating there at least for a short distance has the properties of Helmholtz's and Kirchhoff's free surface. Except for the following turbulent mixing process, the writer cannot see any reason for the angular momentum change in the free-ring space, except that the nonstationary condition of the flow would take care of it. It might well be that if such effects are sufficiently analyzed one may arrive not only at a more basic understanding of the pump under discussion, but also to a better understanding of the mixing process itself and of the large-scale turbulence going along with it. This might also lead to obtaining a better key to the problem of hydrodynamic drag in separated flow.

Once in a while the writer finds it difficult to accept the use of names for certain things. The names "turbine pumps," "re-entry pumps," "regenerative pumps," for the paddle-wheel types of pumps are examples. To the writer these names are associated with a different pump type entirely.

In explanation—for the purpose of pumping fluids, different working principles may be applied. One may differentiate between the principles of displacement, cross force, friction, and traction. The principle of displacement is realized by means of pistons which alternately induce pressure or suction on the working parts of their surfaces. The remaining parts of the surface serve for sealing and driving. The working process occurs in cycles, also called strokes. The pumping thus effected is a periodic process. There are two principal kinds of piston movement—reciprocating and rotating.

The principle of cross force is realized by means of blades on which the flow of the fluid medium induces forces comparable to the forces on an airfoil. Basically these forces are normal to the main flow direction and are connected with a so-called circulation around the blades. By the flow pressure and suction, forces are imposed on the working surfaces, i.e., on the pressure and suction sides of the blades. These blades have a leading and a trailing edge. The other parts of the blade serve partially for sealing, partially for driving. The pumping thus effected is practically continuous. Such pumps usually are distinguished by the terms axial and radial pumps, according to the principal direction of the meridian components of the velocities.

The principle of friction can be realized by means of rotating rotational surfaces of small mutual distance which induce rotational velocity components into the flow. This principle has the disadvantage of limited delivery head and small efficiencies. However, it could be considered when extreme danger of cavitation exists since only very small excess velocities would occur.

[10] Manager, Aerodynamics, General Electric Company, Cincinnati, Ohio.

[11] "Analysis of Traction Pumps," by F. S. Weinig, ASME Paper No. 55—SA-35.

The pumping effected by the friction principle also would be continuous.

The principle of traction is accomplished by means of blades on which the flow effects a drag comparable to the forces on the blades of the wheel of a side-wheeler steamboat. Contrary to the blades used in applying the cross-force principle—where the resulting forces are essentially normal to the main flow direction—the forces on the blades used in application of the traction principle have a resultant parallel and opposite to the main flow direction.

It may be mentioned that there also are other means for pumping, such as the principles of the hydraulic ram and of the ejector. With the hydraulic ram a part of the flowing mass is brought to a higher-pressure level at the cost of the energy of the other part. With the ejector, an additional mass is pumped at the cost of some of the energy of the working or driving mass. The realization of these principles may be considered to be gadgets rather than machines.

The principle of traction is somewhat similar to the principle of friction and would be equivalent to it if a more or less rough surface were substituted for the blading. A certain difference, however, is that on the blades essentially normal forces, i.e., pressure or suction, are induced instead of the tangential forces of friction. The more important difference is that in the friction principle the flow would be essentially meridional with gradually increasing circumferential components while according to the traction principle flow is essentially peripheral and very high-pressure increase may be achieved.

By use of smooth surfaces instead of the blading and by use of flow velocities which conform to laminar flow the theory of the traction pump would be based on the same principles as the theory of bearings. The traction pump, however, should use rather turbulent flow. Basically, this would render the exact theory of the traction pump more difficult than the theory of bearings. Practically, the so-called quadratic law of drag may be used which simplifies the theory.

With this in mind, the product of association of turbine pump, re-entry pump, and regenerative pump would be a pump which has some similarity with a hydrodynamic brake, the difference being the shaping of the blading for pumping instead of braking, and interrupting the geometrically axisymmetric flow pattern for exit and inlet with sealing in between.

The pump would be essentially radial or centrifugal. It would be distinguished from the ordinary centrifugal pump by operation of the blades pumping in series instead of parallel to each other.

The pump is dissimilar to a paddle-wheel type or traction pump, because stator blades would be used for changing the peripheral momentum instead of a free-ring space, where mixing between the medium in the free-ring space and in the space between the rotor blades would have to be accomplished.

The working of the blades in series would necessitate application of relatively low reaction blading. Decreasing the reaction is one means of increasing mass flow and decreasing pressure ratio. Another means of adapting the principle is choice of the radius ratio.

The flow enters the "inlet," which serves as an inlet guide vane for the passing "rotor channel," passes through this rotor channel and the "stator channel," then enters the next passing rotor channel, and so on, until the last "stator passage" directs the flow into the last open rotor passage which leads to the exit. This serves as a stator for the last step, while the remaining rotor passages are sealed off.

The writer does not know whether this type of pump exists. He would expect that pressure coefficients up to 10 or 20 might be achieved and volume coefficients as low as 0.05 to 0.15 with efficiencies between 50 and 65 per cent. This would mean, of course, a pump of very low specific speed.

W. A. WILSON.[12] As the author points out there is no great difference between the several general theories of regenerative-pump performance. Furthermore, it would appear that at the present moment the simpler theories provide about as good a basis for correlating data as do the more complex approaches. In addition, their simplicity is no inconsiderable virtue. Nevertheless, there is merit in pursuing the development of more elaborate hypotheses which have as their goal the elucidation of the details of the fluid dynamic processes within the pump.

One such theory has recently been presented to the Society.[13] It is predicated on a concept of the fluid kinematics of the pump which has been observed to be at least qualitatively in agreement with the actual fluid motions. This theory postulates a much more orderly flow process than is implied in the friction, turbulence, and mixing theories. If it exists, such order is significant because of the concomitant possibility of controlling it to produce more useful performance characteristics. It must be confessed that this possibility has not been exploited fully. However, the theory has pin-pointed the sources of loss and of limitations on head production.

In order to illustrate the difference in kind between the theories based on some sort of shear action between the impeller and the fluid in the free channel and our hypothesis of helico-toroidal flow—to coin a term—the writer would like to discuss their relationships to the principal loss of the pump. It is hoped, incidentally, to shed a little light on the general mechanism of the pump for those who are understandably unacquainted with the functioning of this kind of pump.

As pointed out by the author, one view of the action of the pump is that the fluid is dragged around the casing passage by some kind of turbulent friction induced by the difference between the peripheral velocity of a super-rough impeller surface and the mean velocity of the fluid in the open channel. The existence of a velocity difference or slip is viewed not only as necessary to the functioning of the pump but as an obvious source of irreversibility. Presumably, the slip work is dissipated in turbulent motion and is inherently irrecoverable as pumping work.

On the other hand, the hypothesis of an ordered flow pictures the progress of a typical fluid element from inlet to discharge as following a regular path—roughly a helix wound on a circular axis. That portion of the helix lying within the impeller cross section progresses circumferentially at the local velocity of the impeller. In the open channel the pitch of the helix is progressively reduced by the adverse pressure gradient and actually may reverse before it re-enters the impeller passages. The momentum-exchange process implied in this picture is the result of large-scale effects on the entire flow and does not necessarily involve the inherent irreversibilities of small-scale turbulence. The author states that the possibility of approaching reversibility in an ideal case is an object of argument. The case for this possibility rests on what seems to the writer to be the reasonable premise that the entire flow participates in the helicoidal motion and that irreversible discontinuities in velocity are not inherent nor are irreversible mixing processes.

Here we seem to be face to face with a paradox. All analysts of this pump agree that the slip loss is the most characteristic feature of its performance, yet here is a theory based on directly observed kinematic behavior which does not appear to involve inherent irreversibility. This naturally raises the question of what happens to that part of the work input which does not appear as useful head rise. We think we have identified the slip loss with a more or less conventional resistance to the meridional component

[12] Associate Professor of Mechanical Engineering, Massachusetts Institute of Technology, Cambridge, Mass. Mem. ASME.

[13] Reference (3) of the Bibliography of the paper.

of flow. Such resistance is probably subject to reduction by attention to hydraulic details.

Since the total loss is the same in either case, this might seem to be a distinction without a difference. This is not our view of the matter. There are two reasons for this opinion: (1) The head produced by the pump is directly proportional to the meridional flow rate. Thus anything which reduces the resistance to this flow will result in a more effective pump albeit with no *percentage* improvement in the slip loss. (2) In the absence of resistance to meridional flow there would be a continuing acceleration of this flow from inlet to discharge, i.e., a continuation of the initial build-up of pressure gradient observed in existing pumps. Conceivably, the kinetic head associated with this meridional flow could be convertible to static head. Such conversion would be a direct recovery of the "slip" loss.

The author's review of the various theories suggests that, except for the process of accumulating more data on the effects of the rather large number of geometric design parameters, we have reached the point of diminishing returns in the exploration of this pump in its present form. However, the understanding of the pump as developed by these several investigators has posed a very real challenge to produce one or more fundamental modifications of this pumping system. This discusser is grateful for this thoughtful appraisal of the state of our knowledge and for the challenge implied.

Author's Closure

The author appreciates the discussions and comments which provide an opportunity to supplement the paper. The comments of Mr. Oelrich, Professor Santalo, and Professor Wilson will be answered together, since they refer to the same subject.

In answer to Mr. Parker's first two questions, the author should say that all influential factors have been combined so as to form dimensionless groups. Therefore any consistent system of units may be used. That is, once the units of length, time, and force are arbitrarily selected, the units of all other terms are fixed as combinations of these units.

Concerning the third question, the author has to apologize for his insufficient explanation, which may have misled readers. Since the test pump is one half of a conventional pump, as shown in Fig. 2, some confusion occurs. In order to plot characteristics of a conventional pump in Fig. 7, one half of the conventional pump should be used. That is, one half of the pumping-channel area is taken as A and one half of the through-flow is taken as Q. Another way of thinking of a conventional pump is to double the effective exit area of momentum-exchange flow, i.e., $2(b + h)$ is taken instead of $b + h$. All data in Fig. 7 are calculated in this way. Mr. Parker's data, calculated in this way, agree with Fig. 7.

The answer to the fourth question is included in the first answer. Since ψ/θ and ϕ are dimensionless, the performance of any regenerative pumps can be plotted on this co-ordinate system.

It is most important, but difficult, to predict the performance of a pump accurately. A simple method is as follows: a characteristic head is connected to the maximum rate of flow (about $\phi = 0.8$) with a suitable curve in Fig. 6 depending upon the value of t/s. For small values of flow rate ϕ, the curve is modified to take care of the influences of tip and side channel depth as suggested by Figs. 2 to 5.

The author is pleased to see Professor Santalo's modification of the theory (3). The performance Equation [7] is simple enough to see the general trend of the pump characteristics. This equation convinces the author of his correct understanding of the theory. In this simplification, Professor Santalo has changed the definition of d from the length of the impeller tip to a typical dimension of the open channel. Since d is defined so that $(k_e/2)(Q_e/r_2 d)^2$ represents the circulatory-flow head loss excluding the inlet shock loss, both impeller tip length and a typical dimension of the open channel have respective significance. However, the maximum velocity in a circuit is usually a dominant factor for the loss of head in the circuit. According to the hypothesis (3), the maximum circulatory velocity occurs at the impeller tip. Therefore the impeller tip length b appears to be the representative dimension. However, if the impeller tip length b is assumed as d, the experimental data in Fig. 7 show that the circulatory flow velocity at the shutoff condition increases as the cross-sectional area of the open channel increases, or the resistance coefficient k_e decreases as the cross-sectional area increases.

This difficulty may be overcome by an assumption that the effective area for the circulatory flow increases with an increase of the open-channel area. In reference (3) it is assumed that the entire circulatory flow is discharged from the tip of the impeller and that the side of the impeller vane is partly blocked. However, it is conceivable that the blocked zone decreases as the open-channel area increases; that is, d increases with the cross-sectional area of the open channel. If this is true, it is reasonable that d is a representative dimension of the "open channel."

In simple theories, an increase in the effective area of the circulatory flow (momentum exchange flow) is expressed as an increase of a instead of a constant value $a \sim b + h$. In such a way the theory of reference (3) and the simple theories can be improved together, and there is no serious contradiction. If this hypothesis shows a realistic picture of the pumping action, the success is due both to the simple theories, which arrange the experimental data meaningfully and indicate the direction of revision of an assumed hypothesis; and the advanced theory, which shows the detail of the mechanism.

It is excellent that Professor Santalo has shown the influence of r_2/r_1 theoretically and verified it experimentally. The maximum value of ϕ, or σ, does not depend significantly upon the configuration of pump. However, a difficulty exists in the estimation of the resistance coefficient k_e. Since the head of a pump is inversely proportional to $\sqrt{k_e}$ an error in the estimation of k_e may mask all other effects. According to Fig. 6, the value of k_e apparently varies not only with the configuration of the open channel but with the rate of flow as well. Unfortunately, these two influences are not independent of each other. Since the flow inside the open channel is a complicated three-dimensional flow with pressure gradient, there is no reliable way for an estimation of the loss of head, even if the flow pattern outside the boundary layer is accurately known. However, it is hoped that specific analysis of the flow through the pump, together with systematic experiment, will clarify the effect of geometry on the pump performance.

Professor Wilson has presented a clear and interesting exposition of their theory. This stimulates the author to compare the helicotoroidal flow with a turbulent flow again. If there were no energy dissipation in turbulent flow, the energy, equivalent to the slip loss, would be conserved as the kinetic energy of the fluctuation. It is impossible to recover this kinetic energy, because the fluctuation is too small and random. The scale of the circulatory flow in a regenerative pump is apparently large enough to control. Additionally, because the scale is large, it may take a long time before the kinetic energy dissipates completely. Certainly there is no reason to give up controlling the circulatory flow before the kinetic energy dissipates. The author recommends an attempt to reduce the entry shock-loss of the circulatory flow using an impeller with radial vanes which intersect meridional planes at a certain angle.

It is to be regretted that Mr. Oelrich has not understood the author's intention. Mr. Oelrich insists that the various theories

are diametrically opposed, but the author has a different opinion. He believes that the reference (3) belongs to the same category as other theories, and this has been clarified by Professor Santalo, one of the authors of reference (3), in the discussion. The difference is that reference (3) bases the theory on the observed details of the fluid motion.

In this paper the author has purposely simplified the theories which have been compared. Proportionality factors are combined together. For example, effective exit area of momentum exchange flow a is taken to be proportional to $(b + h)$. Evidently, if one half of the free edge of the impeller vane is the effective exit area and the other half is the entrance area, this should be one half. However, this is not essential, because the proportionality coefficient takes care of this. A similar thing can be said for the value of r_G. When r_G is substituted by $D/2$, the ratio is included in a proportionality coefficient. Certainly the ratio of r_G to $D/2$ depends upon the configuration. Numerical calculation shows, however, that $2r_G/D = 0.87$ for $t/s = 0.214$ and $2r_G/D = 0.94$ for $t/s = 1.50$. Even in such extreme cases the error due to the assumption that r_G is constant is ± 4 per cent. In most cases the error is less than 1 per cent. Fig. 6 shows that the pump configuration radically influences the performance and obscures such a secondary effect as the change of $2r_G/D$. Therefore the assumption that r_G is proportional to D is acceptable for the present purpose.

Dr. Weinig's classification of pumping action is interesting. According to his definition, what is usually called turbulent friction on a rough surface is "traction" instead of friction, because the resistance is mainly due to the form drag of protrusions from the surface, while laminar friction and turbulent friction on smooth surfaces are real friction. In this sense, a regenerative pump should not be called a friction pump.

The author is not qualified to name the pump. However, he does not object to the name "Regenerative Pump," which is used in reference (3). In order to get a pressure coefficient larger than unity, which is a feature of the pump, there is no doubt that an "average" particle of fluid enters the impeller and gains momentum more than once. Therefore the name Regenerative Pump reflects an important feature of the pump better than the other names proposed.

Process Design of Tubular Heaters

By L. A. MEKLER,[1] NEW YORK, N. Y.

Factors defining the principal process requirement of tubular heaters—the "time-temperature effect," and means of obtaining different rates of heat input in portions of the coil of a heater to produce the desired time-temperature relationship are discussed. The most popular types of process tubular heaters used, at present, are briefly described and evaluated as to their general adaptability to operate with single and multiple streams and varying heat-input rates. Numerical examples of the effects of change in spacing of tubes and the use of single and double-row banks are given.

PROCESS tubular heaters are designed to supply to the fluid being processed, usually called "the charge," a definite quantity of heat of a specific quality as determined by requirements of the process. Generally, the charge to the heaters consists of hydrocarbons or other thermally unstable organic fluids which decompose when heated above a certain temperature specific for each fluid. The extent of decomposition depends on the temperature profile or the "heating curve" through the heater and on the time the fluid is at temperatures above that of initial decomposition. The combined influence of time and temperature on the extent of decomposition in the heater is often referred to as the time-temperature effect of the heater. For thermophysical processes, the heater is designed to avoid decomposition because it will destroy part of the charge and will contaminate the product. Heaters for these processes are therefore designed for a minimum time-temperature effect at the desired outlet temperature. In thermochemical processes the aim is to decompose all or a portion of the charge into specific products and the heater is designed to supply the time-temperature effect required to obtain optimum yields of the desired constituents.

The quantity of heat supplied in a process heater is determined by the difference in enthalpy of the charge at the inlet and the outlet of the heater and generally represents no serious design problem. The quality of heat supplied is determined mainly by how well the time-temperature effect obtained in the heater meets the process requirements and is usually the determining factor whether a certain type of heater is best-suited for the process.

Time-Temperature Effect

The time-temperature effect is a linear function of the time; i.e., at any given temperature the effect and the extent of decomposition are directly proportional to the time at the temperature. The influence of temperature is logarithmic and varies in accordance with the Arrhenius relationship

$$\ln \frac{Kt_2}{Kt_1} = \frac{A}{R}\left(\frac{1}{T_1} - \frac{1}{T_2}\right)$$

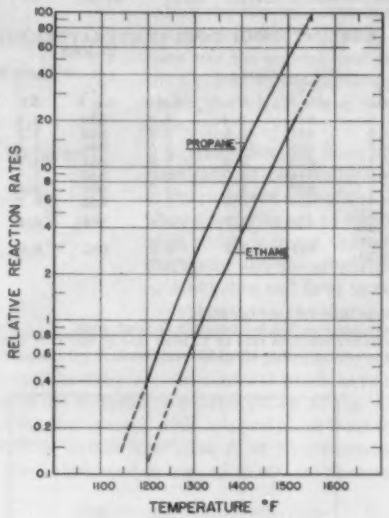

Fig. 1 Reaction Rates, Decomposition of Ethane and Propane

where

Kt_2, Kt_1 = reaction velocities at T_1 and T_2
T_1, T_2 = reaction temperatures, absolute
A = energy of activation
R = gas-law constant

Fig. 1 shows a typical relationship between reaction rates and temperature as they apply to the cracking of ethane and propane to produce ethylene. In this reaction the rates double approximately every 40 deg F, so that if the desired decomposition can be obtained in 4 sec at 1400 F, it also can be obtained in 2 sec at 1440 F or in $^1/_2$ sec at 1520 F. The interchangeability of time and temperature indicated by the relationship applies only to the disappearance of the charge. In most thermochemical processes the desired constituents, obtained by the dominant reaction are mixed with by-products of side reactions, and the net product yield depends both on the extent of decomposition of the charge and on the "conversion efficiency" of the reaction or the fraction of decomposed charge converted into desired product. Usually the efficiency decreases with temperature so that the highest yields are obtained at some optimum temperature where both decomposition and efficiency are relatively high.

In the series of runs in Table 1 the optimum temperature is 1428 F.[2]

Commercial processes are seldom carried out at uniform temperatures. Normally, the charge is heated through a range of temperatures for a period of time during which the sum of the time-temperature effects through the range is equal to the desired effect at the optimum temperature. Table 2 and Fig. 2 illustrate the general method used by some designers in de-

[1] Consulting Engineer, Petro-Chem Process Company and Petro-Chem Development Company. Mem. ASME.

Contributed by the Process Industries Division and presented at the Diamond Jubilee Semi-Annual Meeting, Boston, Mass., June 19–23, 1955, of The American Society of Mechanical Engineers.

Note: Statements and opinions advanced in papers are to be understood as individual expressions of their authors and not those of the Society. Manuscript received at ASME Headquarters, March 11, 1955. Paper No. 55—SA-27.

[2] "Ethylene Production by Thermal Cracking of Propane-Ethane Mixtures," by C. K. Buel and L. J. Weber, *Petroleum Processing*, vol. 5, 1950, pp. 266–272.

TABLE 1 EFFECT OF REACTION TEMPERATURE ON YIELD OF ETHYLENE AND PROPYLENE

Run number	1	2	3	4
Average effective react temp, deg F	1407	1428	1468	1471
Weight per cent of C_2H_4 and C_3H_6 decomposed	65.1	72.4	83.7	86.6
Conversion efficiency, per cent	60.4	58.8	49.9	40.1
Yields, weight per cent	39.3	42.5	41.7	34.3

TABLE 2 EVALUATION OF TIME-TEMPERATURE EFFECT OF A RANGE OF TEMPERATURES

		Curve A			Curve B			Curve C		
Zone	t, min	T_a, deg F	K_T	$K_T t$	T_a, deg F	K_T	$K_T t$	T_a, deg F	K_T	$K_T t$
1	1.0	824	2.1	2.1	830	2.6	2.6	824	2.1	2.1
2	0.5	831	2.6	1.3	840	3.5	1.8	831	2.6	1.3
3	0.5	835	3.0	1.5	846	4.1	2.0	836	3.1	1.6
4	0.5	840	3.5	1.8	851	4.7	2.4	842	3.7	1.8
5	0.5	844	4.0	2.0	856	5.4	2.7	847	4.2	2.1
6	0.5	849	4.5	2.2	859	5.8	2.9	852	4.9	2.4
7	0.5	853	5.0	2.5	862	6.3	3.1	858	5.7	2.9
8a	0.25	858	5.7	2.8	864	6.7	3.4	862	6.3	1.6
8b	0.25							866	7.0	1.8
9a	0.25	862	6.3	3.2	865	6.9	3.4	869	7.6	1.9
9b	0.25							877	9.2	2.3
				19.4			24.3			21.8

NOTE:
t = time interval through zone.
T_a = average reaction temperature through zone.
K_T = relative reaction rate at T_a with rate at 800 F = 1.0.
$K_T t$ = time-temperature effect through zone.

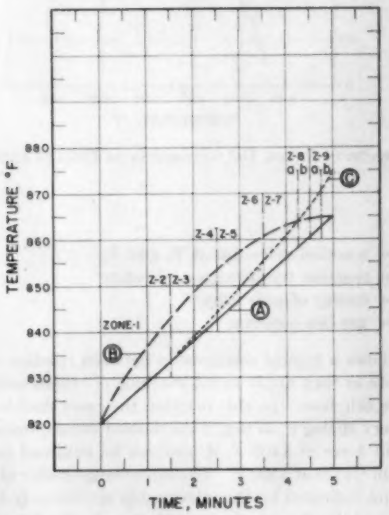

FIG. 2 EVALUATION OF TIME-TEMPERATURE CURVES, VISC-BREAKING

termining the effect through a range of temperatures. The curves are divided into zones, usually of different time intervals. Zone 1 is for an interval of 1 min because through this zone the reaction rates are relatively low. Zones 2 through 7, where the reaction rates increase relatively fast, are for $^1/_2$-min intervals. At the end of curve C the temperature rise is greater than in curves A and B; therefore zones 8 and 9 of C are split into $^1/_4$-min intervals. In heaters, a zone may correspond to several tubes near the inlet and fractions of a tube near the outlet of the coil.

As shown in Table 2 the shape of the curve through the temperature range is the determining factor of the time-temperature effect of the range. Curve B with the same initial and final temperature has a 20 per cent higher effect than curve A. Curve B also has a 10 per cent higher effect than C, even though B has a lower outlet temperature.

FILM CRACKING

The time-temperature effect determines the extent of mass decomposition with each particle assumed to be decomposed to the same degree. There is another type of decomposition produced in heaters, "film cracking," which is independent of mass decomposition and which occurs when the film is overheated because of higher heat inputs to the tubes than the charge can absorb. Film cracking can occur below temperatures of mass decomposition and may become serious where evaporation in the heater forms a viscous emulsion of vapors and liquid with liquid as the outer phase. Film cracking, occurring when the charge is above the temperature of initial decomposition, may cause heavy coke deposits in the tubes and a premature shutdown of the heater. A well-designed heater not only must produce the desired time-temperature effect but do this with linear and mass velocities through the tubes which will produce a sufficiently turbulent flow to tear up the film so that even if it is overheated temporarily, it is quickly quenched in the main flow.

The main problem in design of process tubular heaters is to obtain the proper relationship between the total quantity of heat required by the charge and the physical dimensions of the coil which will meet the time-temperature requirements without film cracking. The quantity of heat and the heat-input rates into the coil are determined by the surface of the coil which is a function of the length and of the first power of the OD of the tubes. The mass velocities required to supply the heat without film cracking vary as the square of the ID of the tubes. The actual residence time and the time-temperature effect are determined by the mass velocities and the specific volume of the fluid inside the coil. With a given outlet pressure, determined by the process, the specific volume of the fluid depends on the pressure drop through the coil which is a function of the fifth power of the ID and of the first power of the length of coil. With these interrelationships the coil of one heater cannot be prorated from a smaller or larger heater on the same service. A backlog of successfully operated heaters on different processes may assist in selecting a first approximation of the size of the coil but the final design is usually obtained by trial-and-error calculations until the length and tube diameter of the coil meet the requirements.

Table 3 and Fig. 3 show the results of such calculations for a relatively simple heater where reduced crude is heated with a short residence time above the temperature of initial decomposition to keep cracking to a minimum. Examples of detailed design procedures for heater of more complicated processes are available in literature.[3,4]

TYPICAL PROCESS HEATERS

Fig. 4 shows schematic cross sections of the most popular types of process heaters. In spite of diversity of shapes, they all have the following characteristics:

1 The fluid is forced through continuous coils of tubes in series by a pump, compressor, or pressure accumulator to assure positive measurement and definite velocity through the tubes.

2 The major portion of the heat is supplied primarily by ra-

[3] "Vacuum Distillation of Petroleum Residues," by W. W. Kraft, *Industrial and Engineering Chemistry*, vol. 40, 1948, p. 807.

[4] "Vaporization in Furnace Tubes," by G. Baars, *Journal of the Institute of Petroleum*, vol. 34, 1948, pp. 417–442.

TABLE 3 SUMMARY OF TRIAL-AND-ERROR CALCULATIONS FOR VISC-BREAKING FOR CURVES IN FIG. 3

Station	Tube no.	Heat content, Btu/lb	Vaporization volume, per cent	Temp, deg F	Pressure, psig	Velocity, fps	Pressure drop, psi	Residence time, sec (cumul.)	
1	56 (outlet)	520	42	852	6.5	65.9	1.8	275.6	
2	55	514	38	850	8.1	52.1	1.6	275.2	10.1 sec
3	53	503	32	846	10.3	31.2	2.2	274.7	
4	52	498	20	843	11.1	20.6	0.7	273.1	
5	51	493	14	840	11.6	16.1	0.5	271.8	
6	49	482	10	835	12.2	4.8/8.2[a]	0.6	265.5	7.5 sec
7	48	...	2	...	...	...	...	...	
8	47	474	0	825	12.7	3.36/4.64[a]	0.6	258	
9	inlet	306	0	600	27.4	4.10	14.7	0	

Operating Conditions

Charge = 5000 B/SD = 71000 lb/hr
Inlet temperature, 600 F
Outlet pressure, 6.5 psig

Gravity of charge, 13.1°API
Outlet temperature, 850 F
Evaporation in heater, vol. %, 42

No. of tubes from outlet	Size of tubes	Btu/hr/sq ft of circ. surface
8	8-in. × 0.75-in. wall	10000
2	6-in. × 0.50-in. wall	10000
46	5-in. × 0.375-in. wall	10000

All tubes 22-ft, 6-in. exposed, 24-ft, 0-in. total length.

[a] Change in tube size

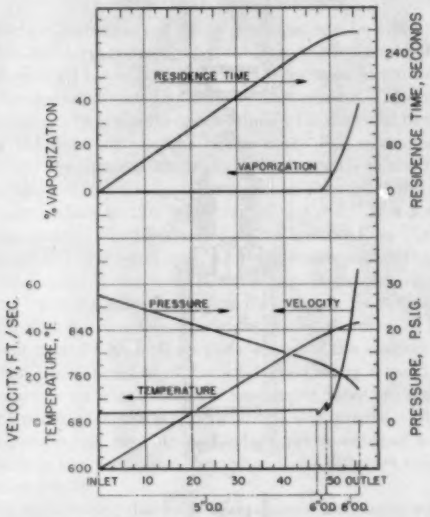

FIG. 3 SUMMARY, TRIAL-AND-ERROR CALCULATIONS FOR ATMOSPHERIC DISTILLATION HEATER

diation to "radiant" tubes located in the combustion chamber or the "radiant section" of the heater. The tubes are placed out of the path of the main stream of gases to prevent superimposing upon the tubes a forced-convection component from high-temperature gases. Theoretically, and to a great extent in actual practice, the radiant-heat absorption by the individual tubes in a radiant bank is close to the average for the bank so that the time-temperature effect of any portion of the bank can be calculated with a fair degree of accuracy. Forced convection, particularly if applied only to the full length or a portion of a few tubes, will add an unknown increment of heat input to these tubes and will impair the accuracy. Some heat is applied to the tubes by free convection from the thermal eddies in the heater but the amount is significant only in floor-fired heaters with high vertical tube banks, where it may be as high as 10 per cent of the total rates. Therefore, in calculating the time-temperature effect of the coil, free convection can be assumed to be uniform for all tubes without appreciable error in the results.

3 The residual heat of the gases leaving the radiant section is utilized in a separate convection bank, marked C, located either completely out of sight of the radiant heat in the combustion chamber, as in heaters A, B, C, H, J, and K, or placed behind a "shock bank," marked SB, with tubes usually spaced on wider centers than the convection bank, to reduce the convection component upon the shock tubes. Usually the shock bank has the highest heat rates and is often placed in the portion of the flow where the charge can absorb these rates.

4 Most heaters have a relatively large ratio of bare refractory surfaces to the projected area of the tube banks. The refractories act as reradiating surfaces which increase the emissivity of the heater and the effectiveness of the radiant tubes and tend to equalize the radiant rates in the heater. The bare refractory surfaces are particularly effective reradiators when they are washed by the main stream of gases as the center wall in heater E, and the outer walls of heater G which have the highest emissivity of the rectangular heaters shown in Fig. 4.[5]

5 The heaters operate with relatively low heat-input rates, usually 8000 to 15,000 Btu/hr/sq ft of circumferential surface. Rates as low as 5000 and as high as 25,000 are used occasionally.

STRUCTURAL CLASSIFICATION

Structurally process heaters can be divided into three groups: Chamber or "box" heaters with the width of the main structure approximately equal to its height as heaters A, B, C, and D; cell heaters, with the height 2 to 3 times the width, as heaters E, F, G, L, and M; and cylindrical or circular heaters as heaters H, J, and K. In all heaters, except G, L, and M, the tubes are placed along the furnace envelope so that they are exposed to primary radiation from the gases and from the bare refractories on one half of the circumference (the "exposed" face), and to reradiation from the refractories behind the tubes on the other half (the "shielded" face).

With tubes in a single row, spaced on two diameters, the exposed face of the tubes is approximately three times as effective as the shielded face and the flux distribution around the circumference of the tubes is substantially as shown in Fig. 5(*a*). The main tube banks in heaters G and L and the center bank in heater M are located along the center line of the combustion chamber and are subjected to direct radiation from both sides of the tubes. With tubes a single-row bank, as the center bank in heater M, both halves of the tube circumference have the same effectiveness, as shown in Fig. 6(*b*), and with a given maximum flux density at point A, the whole tube will have approximately 50 per cent higher average rates than a tube irradiated from one side. However, with the double-row banks exposed to radiation from both sides, as in heaters G and L, the flux distribution along the circumference of the tube and the average heat-input rates are the same as for tubes irradiated from one side. This difference in heat-absorption characteristics of single and double-row banks irradiated from both sides is not always recognized and is sometimes the cause of erroneous interpretation of performance of this type of heater.

Because of interrelationship between the physical dimensions

[5] "Evaluation of Radiant Heat Absorption Rates in Tubular Heaters," by L. A. Mekler and R. S. Fairall, *Petroleum Refiner*, vol. 31, 1952, June, pp. 101–107; November, pp. 128–132; and December, pp. 151–155.

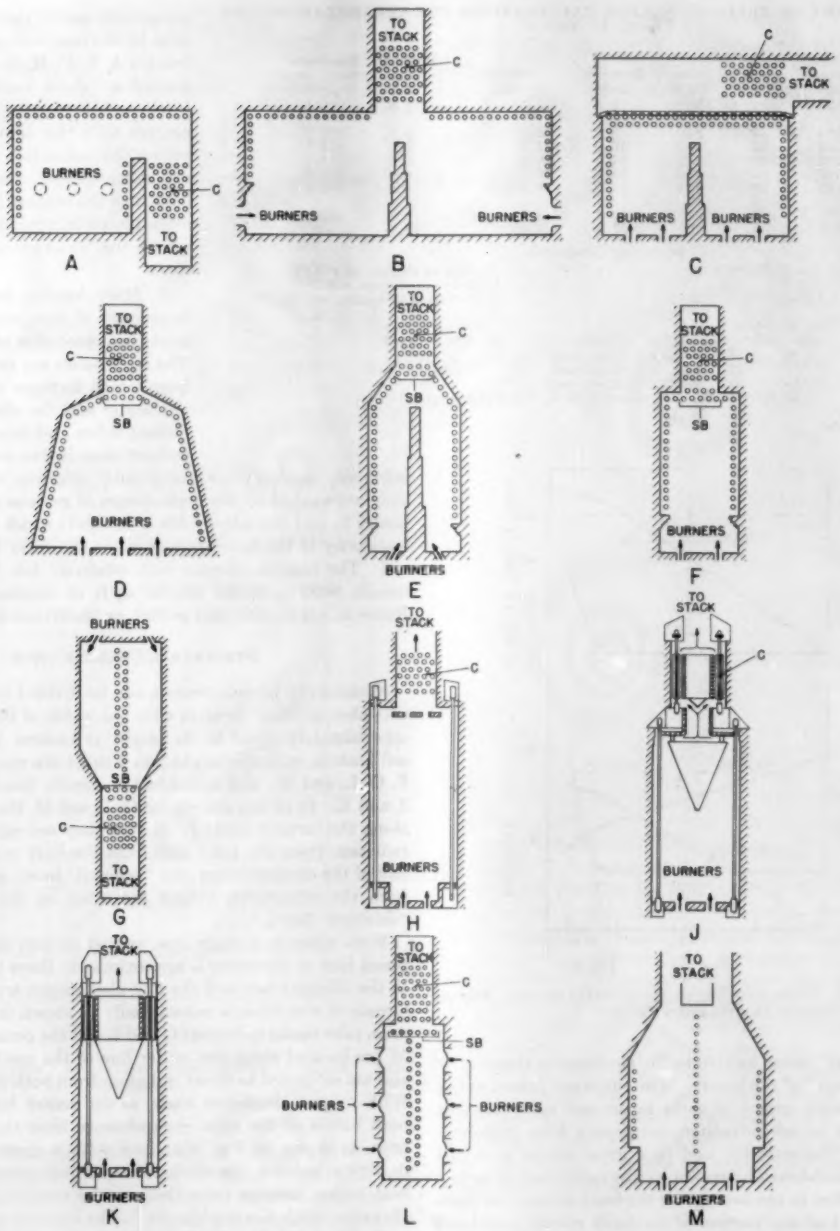

(C, Convection section; SB, Shock bank)

FIG. 4 SCHEMATIC SECTIONS OF PROCESS HEATERS

of the coil and the time-temperature relationship obtained in a coil, it is often necessary not only to use different size tubes, as shown for the heater in Table 3, but also to split the charge into a number of parallel streams. When only two streams are required, any of the heaters except A and M can be used to give identical thermal treatment to the streams by splitting the total tube bank along the vertical center line of the heater. The separating walls in heaters B, C, and E, which permit independent firing of the two halves, make these heaters particularly suitable for the service. With the other heaters it may be necessary to manipulate the burners and the flows to obtain substantially the same thermal treatment for both streams.

If more than two streams are required to process the charge, it can be done in one structure in a multicompartment heater C and particularly in the circular heaters. In circular heaters the tubes are arranged symmetrically with respect to the main stream

of gases and the bare refractories so that with equal firing of the burners equal portions of the coil will give identical thermal treatment to equal portion of the stream. Heater K is the oldest of the circular heaters and together with its companion, heater J, is the most widely used on a large variety of processes. The principal feature of these heaters is the alloy cone at the top of the heater which is washed by the gases as they leave the combustion chamber. The reradiation from the cone is almost equal to the radiation from the gases and gives these heaters the same order of emissivity as of heaters E and G.[4] The cone also acts as a directional dam which gradually deflects the stream of gases into the restricting annulus between the base of the cone and the wall which tends to equalize the flow of gases through the heater and approach in practice the theoretically uniform heat-input rates in circular heaters. In heater J the top portion of the tubes is provided with extended surface and acts as a convection section. Heater K has a separate convection section usually with extended surface, is somewhat more efficient than J, and is used where the value of fuel saved justifies its extra cost.

Process Heat Requirements

The heat requirements of many processes can be met with uniform heat-input rates throughout the coil, particularly if the rates are high enough to meet the maximum increase in enthalpy per degree temperature rise required by the process. However, in some processes, best results are obtained with different heat-input rates in the different sections of the coil. For example, where most of the evaporation or decomposition occurs in the last few tubes of the coil, the heat requirements at the end of the coil are much higher than at the beginning of the coil. If a minimum time-temperature effect is desired, as with curve C in Fig. 2, the rates at the end of the coil must be considerably higher than those at the beginning of the coil. Conversely, if process requires a "soaking" section where reaction rates must be slowed down as equilibrium is approached near the outlet, the rates at the end of the coil must be lower than those ahead of the soaking section to prevent decomposition of the products already formed.

The manner in which different heat-input rates are applied to different portions of the coil depends on the process. Often the desired results can be obtained with uniform rates of a certain magnitude in one portion of the coil and of a different magnitude in another portion.

If the relationship between the rates is unknown, as in the case with experimental units intended to process a variety of stocks with different time-temperature effects or with a first commercial unit of a new process with operating conditions not fully established, separately fired structures for each section of the coil may be required to obtain the best results. Heaters B, C, and E can be used if the desired range of variations in the time-temperature effect can be obtained with the two separately fired zones by using all tubes for a single stream in series. The separating wall permits firing the two halves of the heater independently of each other. Heater C can be built with more than two compartments and can be used for more than two firing rates.

In heater L, the burners are arranged in horizontal rows in the sidewalls. By varying the firing of each row of burners, different heat-input rates can be obtained in the sections of the tube bank affected most by each row. The change in heat-absorption rates in adjacent sections of the coil is not as distinct as in the separately fired compartments, because of overlapping influence of the burners in the adjacent rows, but the heat-input rates are sufficiently responsive to changes in firing to produce the desired over-all results.

If the exact relationship between the rates in the different sections of the coil is constant and is known, as in established processes, any number of different rates can be obtained in one heater structure, particularly in the circular heaters, by using a

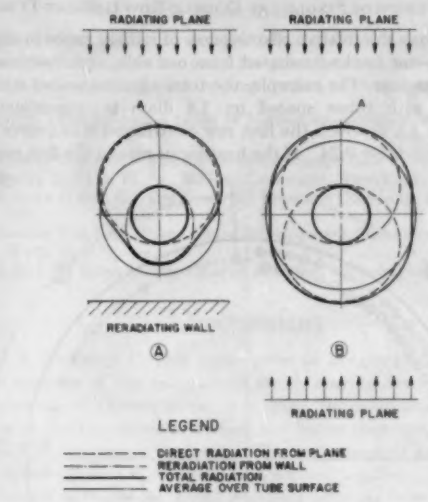

Fig. 5 Flux-Distribution Diagrams

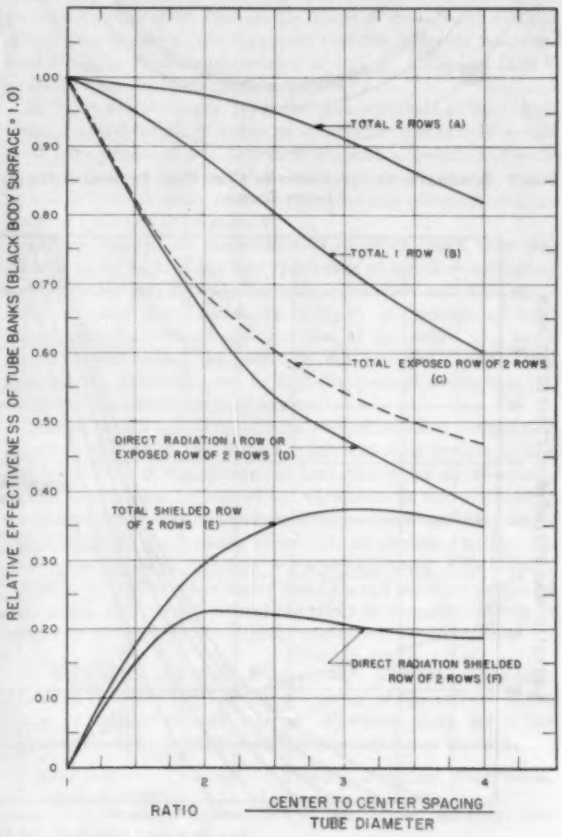

Fig. 6 Relative Effectiveness of Tube Banks

combination of single and double-row tube banks and by varying the spacing between the tubes.

Effectiveness of Single and Double-Row Radiant Tubes

Fig. 6 shows the relative effectiveness of radiant tubes in single and double-row banks irradiated from one side, as a function of the tube spacing. For example, the total effectiveness of a two-row bank with tubes spaced on 1.8 diam is approximately 0.98 (curve A), of which the first row contributes 0.74 (curve D) and the second row 0.24. If the heat-input rate to the first row is 10,000 Btu/hr/sq ft, the rate to the second row will be approximately 3200, or less than one third of the rate to the first row. With a spacing of 3.6 diam the first row has an effectiveness of approximately 0.49 and the second row 0.36 so that with a rate of 10,000 Btu/hr to the first row, the rate to the second row is approximately 7400, or almost three quarters of the rates to the first row. Therefore any ratio of rates between 3:1 and 1.3:1 can be obtained in two sections of a coil by using a two-row bank with the proper spacing.

Even wider variations in heat-input rates can be obtained by a combination of single and double-row banks and different spacings, as shown on the layout of a bank in a circular heater, Fig. 7. Table 4 shows a tabulation of the range of heat-input rates which can be obtained in the different portions of the coil with the arrangement shown in Fig. 7. The numerical values of the heat-input rates in the table are derived from the effectiveness of the tube banks, as shown in Fig. 6, and from the graphs based on the

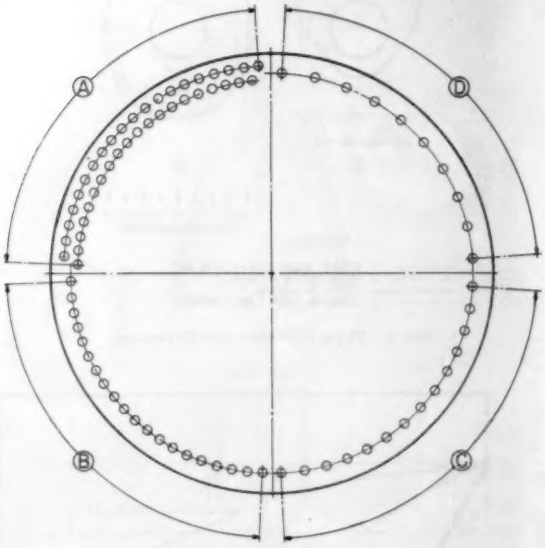

Fig. 7 Schematic Arrangement of Coil With Different Heat-Input Rates

TABLE 4 EFFECT OF TUBE ARRANGEMENT ON RADIANT HEAT-INPUT RATES IN TUBE BANKS

(Over-all effectiveness of heater 0.90. Flame-burst temperature 3400 F. Metal temperature of all portions of coil 800 F.)

Portion of coil	A	B	C	D
Rows of tubes in portion	2	1	1	1
Spacing: diameter	2	2	3	4
(1) Liberation, Btu/hr/sq ft of projected area,[a] Q_1	25000	25000	25000	25000
(2) Effectiveness of tubes				
Total	0.98	0.88	0.72	0.60
First row	0.69			
Second row	0.29			
(3) Over-all effectiveness of banks, (2) × 0.90				
Total	0.88	0.79	0.65	0.54
First row	0.62			
Second row	0.26			
(4) Liberation, Btu/hr/sq ft of effective area, Q_2 (1):(3)	28500	31600	38800	46300
(5) Absorption, Btu/hr/sq ft of effective area, Q_3 (also maximum flux)	18000	19500	23000	26200
(6) Absorption, Btu/hr/sq ft of circumf. surface, Q_4 [(3) × (5) × spacing]:				
Total		9800	14300	18000
First row	7500			
Second row	3000			

[a] Projected area in circular heaters = (tube circle) × (exposed length of tubes)

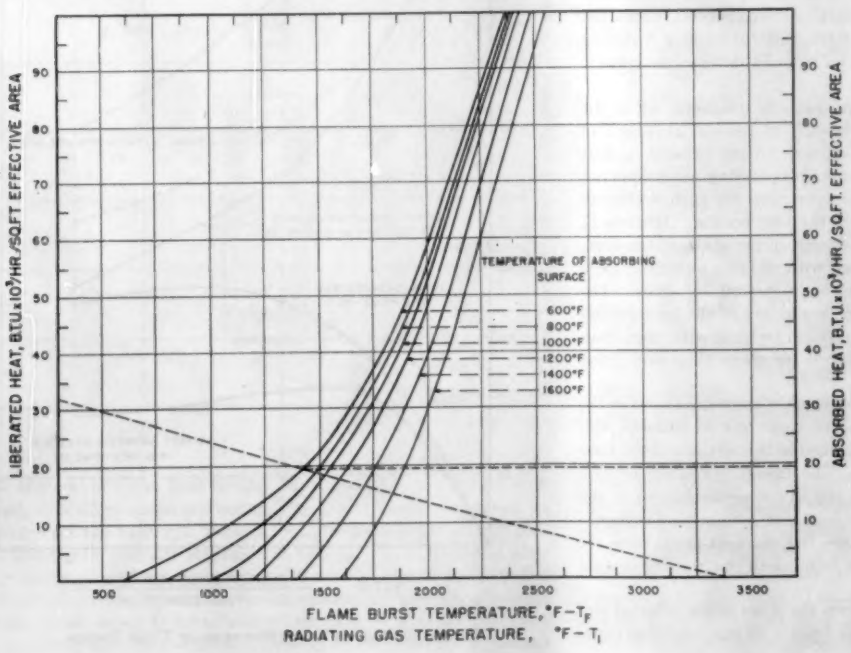

Fig. 8 Curves for Solving Stefan-Boltzmann Equation

Stefan-Boltzmann equation in Fig. 8, which give the relationship between the flame-burst temperature, or the theoretical temperature of combustion with the amount of excess air used, the temperature of the heat-absorbing surface, the heat liberation in the heater, Btu/hr/sq ft of effective area, and radiant-heat absorption per sq ft of the same area. The effective area is the equivalent area of a black body which will absorb the same amount of radiation as the tube bank, and is equal to the projected area of the bank, including the space between the tubes, multiplied by the emissivity of the heater and by the effectiveness of the tube bank as obtained from Fig. 6. The example in Fig. 8 shows the method of determining the radiant heat absorption per sq ft of effective area for portion B of the coil (item 5 of the table).

The rates in item 6 of Table 4 are based on the assumption of uniform emissivity throughout the heater which is true only for circular heaters. In other types of heaters the banks along the different planes of the heater envelope have different emissivities so that the effectiveness of the banks, item 3, and the numerical value of the heat-input rates may be different for each bank. The rates in Table 4 are also based on uniform metal temperature throughout the bank. This will not cause appreciable error with maximum metal temperatures below 1000 F and extreme difference of metal temperatures of less than 300 F. In some processes the charge is heated from 400 F on the inlet to 1500 F on the outlet and the metal temperatures vary from 450 to 1600 F. With this range of temperatures the heat-input rates on the basis of an average metal temperature of, say, 1000 F, will be considerably lower than the actual at the beginning of the coil and much higher than the actual at the end of the coil.

High-Temperature Processes

In high-temperature processes the metal temperature at the point of maximum flux limits the rates which can be used. Wide tube spacing by increasing relative effectiveness of the shielded half of the tube helps to equalize the rates and the metal temperatures along the circumference of the tube and thus permits higher average rates for any given maximum flux. Table 5 shows

TABLE 5 RADIANT HEAT-ABSORPTION RATE IN SINGLE-ROW BANKS

		A for spacing = $2D$;	B for spacing = $4D$	
	Liberation, Btu/hr/sq ft of effective area of bank	30000	30000	25000
2	Flame-burst temperature, deg F	3400	3400	3400
3	Metal temperature, deg F	800	800	800
4	Absorption, Btu/hr/sq ft of effective area of bank	18500	18500	16200
5	Equilibrium (residual) temperature of gases, deg F	1460	1460	1400
6	Effectiveness of tube bank	0.88	0.60	0.60
7	Absorption, Btu/hr/sq ft of projected plane of bank (4) × (6)	16300	11100	9700
	Absorption, Btu/hr/sq ft of circumferential area $\frac{(7) \times (\text{spacing})}{\pi}$	10300	14100	12400
9	Percentage absorbed by exposed half from Fig. 6, $D:(B\text{-}D)$	70	58	58
10	Absorption by exposed half, Btu/hr/sq ft/2, (7) × (9):100	7200	8200	7200
11	Absorption by shielded half, Btu/hr/sq ft/2, 7 × [100 — (9)]:100	3100	5900	5200

the approximate relationship between the average rates and the rates on the exposed and shielded halves of the tube obtained with different spacings. The values in the table are based on the assumption that the rates to the exposed face are equal to the direct radiation to the whole tube and that the rates to the shielded face are equal to the reradiation to the whole tube. The error resulting from this assumption is very small.

A few years ago many thermophysical and thermochemical processes were carried out in batch operation because this was the only way to obtain the exacting requirements of the time-temperature relationships in these processes. At the present stage of the art of designing process tubular heaters, most of these processes can be converted to continuous operation if it is economically justified.

Acknowledgment

The author wishes to express his appreciation to the Petro-Chem Development Company for permission to use some of its design and operating data in preparation of this paper.

Note: The following types of heaters are designed and supplied by:

Heaters C and M—The Lummus Company, New York, N. Y.
Heater D—The M. W. Kellogg Company, New York, N. Y.
Heaters E and G—Universal Oil Products Company, Des Plaines, Ill.
Heaters J and K—Petro-Chem Development Company, Inc., New York, N. Y.
Heater L—Selas Corporation of America, Philadelphia, Pa.

Discussion

D. J. Bergman.[6] This paper gives an insight to the combustion engineer of the calculations which may be involved on the process side of a heater tube. Too often, the combustion engineer stops at the heat-transfer surface and leaves the remaining calculations to the process engineer. The best-designed heater is one in which both sets of calculations are fitted together.

Table 1 of the paper might well bear scrutiny from the standpoint of determining the optimum temperature outside of the specific run points. Plotting the points for conversion efficiency and weight of products decomposed reveals some scattering due to experimental error, but on the basis of reasonably smooth curves through the points it appears that the optimum temperature would be in the neighborhood of 1450 F, instead of 1428 F as found from the four experimental points.

In Table 4 of the paper, projected area is defined as tube circle times exposed length of tubes of a circular heater. It would seem since projected area of a tube has such a specific and well-known definition of diameter of tube times length that it would be better to use another name for the previous quantity, such as plane or wall area of tube bank.

Also in Table 4, the heat-liberation rates are based upon this plane area for each of the four quadrants of the circular heater, as if separated into individual cells by brick walls and fired separately, although this is not shown in Fig. 7. If these are not individual cells, the over-all effective area of the entire tube bank should be used to find the maximum flux rate and the effectiveness of each quadrant used to find the average absorption per square foot of circumferential surface.

This seems like a good opportunity to commend to combustion engineers the use of Fig. 8 for a quick and clear understanding and evaluation of the changes in heat pickup by an absorbing surface which may be caused by variations in the mechanical arrangement of the radiant and receiving surfaces, and particularly the changes in fuel burned, excess air, air preheat, and so on. While more exact calculations are available using emissivity of the gas mass due to water vapor and CO_2 and other properties of the system, they do not portray the effect of changes in design or operation so clearly to the average engineer.

C. K. Mader[7] and R. H. Shoulberg.[8] The author has ably described in a relatively brief paper many of the aspects of the design of tubular process heaters. However, there are a few points which seem to require amplification and modification.

[6] Chief Engineer, Universal Oil Products Company, Des Plaines, Ill. Mem. ASME.

[7] Furnace Division Engineer, The M. W. Kellogg Company, New York, N. Y.

[8] Acting Section Engr., Furnace Division, The M. W. Kellogg Company, New York, N. Y. Assoc. Mem. ASME.

He speaks of the "emissivity" of heaters and the emissivity of different planes of the heater envelope, when he apparently has in mind what Hottel[9] has termed an "over-all exchange factor," relating unit heat-transfer rates in the furnace to the temperatures of the energy source (the hot flue gases) and the energy sink (the tubes). The over-all exchange factor is not a function of the tube and refractory geometry alone, as is apparently implied when the various heaters of Fig. 4 are compared, but depends also upon the gas emissivity (as defined by Hottel) and upon the tube-surface emissivity. The tube emissivity is usually close enough to 0.9 so that it need not be considered as varying between different designs. However, the gas emissivity varies with the flue-gas composition and temperature and with the size and shape of the furnace enclosure, since the latter affect the mean apparent beam length for radiation. Assuming that the author is comparing furnaces operating with similar flue gases, the over-all exchange factors will still depend upon the furnace size. This dependency is not strong but neither is it negligible; doubling the beam length of a heater of given shape without altering the flue-gas and tube characteristics may increase the over-all exchange factor by 25 per cent.

Another point to be made is that a circular vertical-tube furnace is not a heater of "uniform emissivity." It is true that, neglecting variations in tube-metal temperature, each tube has the same total heat transfer to it. However, the heat transfer per ft of tube varies along the tube because (1) the "view" of the furnace enclosure varies at different elevations on the tube, (2) the flue-gas temperature is in general not constant throughout the furnace, and (3) heat transfer by convection is not uniform throughout the enclosure. (These things are also true, of course, for box or "cell" heaters.) Some experimental data in our possession taken on a vertical-tube test furnace using upshot firing with 16-ft 9-in. tubes indicate that the ratio of the maximum heat-transfer rate along the tube length to the average rate along the tube length was about 1.4. (These rates are in each case average circumferential rates.) This ratio will vary from furnace to furnace and will change with different firing conditions in a given furnace, so it is not intended as a representative figure for all vertical furnaces. However, it does demonstrate a rate variation along the tube length. We should be interested in any data which the author may have on rate distribution in other vertical-tube furnaces.

Author's Closure

Dr. Bergman is correct in pointing out that smooth curves drawn through the values of weight per cent decomposed and conversion efficiency for the four runs shown in Table 1 would indicate an optimum temperature intermediate between runs 2 and 3. However, since Table 1 is used only to illustrate the concept of optimum temperature and is a quotation from another publication, which gives no data of temperatures other than those shown, the author had to use the 1428 F value for this temperature. He fully agrees with the thought behind Dr. Bergman's comment that careful analysis of available data may bring out interpolated data which may be of greater significance than the actual data obtained.

Theoretically, in a heater without physical radial partitions between the banks, each quadrant in Fig. 7 of the paper would have a substantial effect on the heat-absorption rates by the other quadrants, particularly if it is assumed that the products of combustion in the heater are fully transparent so that the heat liberated by the burners in one quadrant would be transferred through the gases to the tubes in the other quadrants. Actually, with the relatively luminous flames used to fire large circular heaters, the equalizing effect of one quadrant on the heat absorption by the tubes in the other quadrants is only a fraction of the theoretical. Also, in the actual heater, which is Type J in Fig. 4, the cone is a source of a larger portion of total radiation than the gases. The radiation from a quadrant of the cone is most effectively applied to the quadrant of the tube bank it faces, so that in this type of heater the major portion of radiant-heat absorption in each quadrant is only slightly dependent of each other.

The accurate evaluation of the secondary intereffects between the quadrants of the tube banks in a heater without partitions, or of the effects of reradiation from the partitions, if partitions are used, is beyond the scope of this paper. These effects were not mentioned in connection with Table 4 and Fig. 7 so as not to obscure, by involved explanation, the main point of Tables 4 and

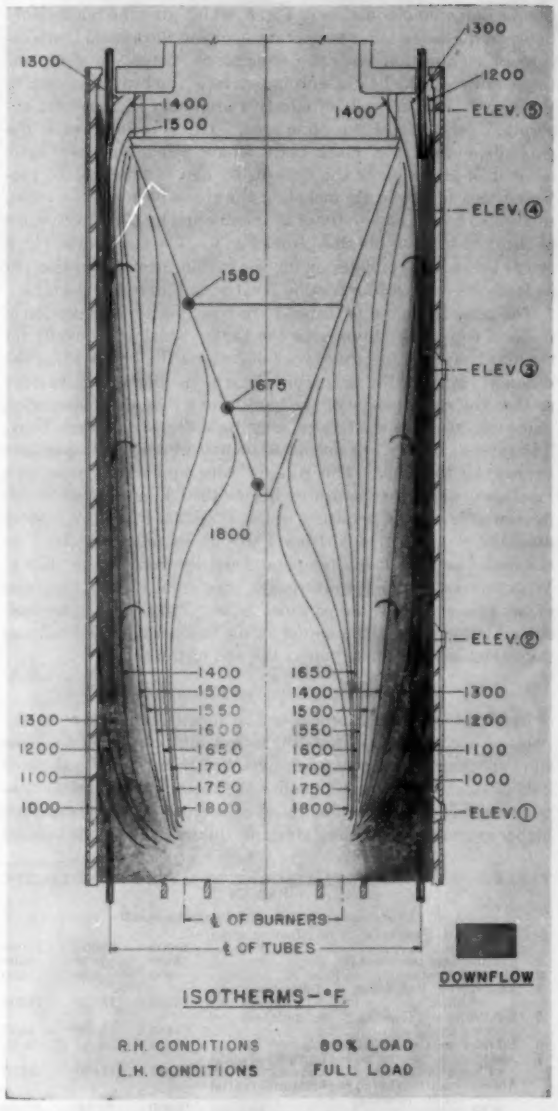

Fig. 9 Isotherms Through Type J Heater With 40-Ft Tubes

[9] "Radiant Heat Transmission," by H. C. Hottel, chapter 4 of "Heat Transmission," by W. H. McAdams, third edition, 1954.

5, that different relative rates for the whole circumference of tubes and for the exposed and shielded halves of the tube circumference can be obtained in the same heater by changing the ratio of spacing to tube diameter.

Referring to the discussion by Messrs. Mader and Shoulberg; the term "emissivity" as used in the paper is synonymous with Hottel's "over-all radiant heat-transfer factor" and corresponds to the term "combined emissivity" used in Table 4 of reference 5 for different types of heaters. In that table the combined emissivity is the sum of the gas emissivity (item 4 of the table) and the emissivity of the bare reradiating refractories (item 5 minus item 4) for the heaters in Fig. 4 of the reference. The gas emissivity was calculated according to the procedures on pages 64–70, McAdams, second edition, using the same gas composition for all heaters, the theoretical equilibrium temperature as the temperature of the gases, and the corresponding mean beam for each heater. The emissivity resulting from reradiation from the refractories was derived by graphic integration of the shape factors of the banks and the bare refractories of each heater and by formulas given in the text of the reference. The author wishes to thank Messrs. Mader and Shoulberg for raising the question since it gives him the opportunity to clarify the matter for those who are not acquainted with reference 5.

The uniformity of emissivity in circular heaters mentioned in connection with item (6) of Table 4 of the paper refers not to the average circumferential heat-transfer rates along the length of the tubes but to multitube sections of the total coil in a heater. Any differences in circumferential rates from top to bottom of individual tubes are theoretically the same in each section so that even with large differences in circumferential rates along the length of the individual tubes, the emissivities of the complete sections in a circular heater are substantially the same.

As to uniformity of circumferential rates along the length of the tubes, in circular heaters with a 35 to 45-deg cone at the top and a ratio of height to diameter of tube circle between 2.5 and 3.0, which are normally used in heaters J and K of Fig. 4 of the paper, the average circumferential rates along the length of the tubes are much more uniform than the rates in the heater used as as example by Messrs. Mader and Shoulberg. The cone absorbs by radiation some of the heat from the normally hotter gases in the lower half of the heater. Since the cone reradiates this heat and the heat absorbed by convection from the gases flowing along the surface of the cone primarily to the upper half of the tubes, reradiation from the cone tends to compensate for the higher radiant heat-absorption rates from the hotter gases and the floor at the bottom. The reradiation from the cone to the upper half of the tubes also tends to be uniform because, while the temperatures of the surface of the cone decrease from the tip to the base, its area per unit length of tube and the effectiveness of the area increase.

Convection heat input to "radiant" tubes by contact with portions of the main stream of high-temperature gases is one of the principal causes of large variation in average circumferential heat-input rates along the length of the tubes. In vertical heaters there is a downflow of cooler gases along the tubes because of the cooling action by the tubes on the gases along the periphery of the main gas stream. The cone, by "nudging" the gases toward the tubes, increases the downflow in heaters with cone to many times that in heaters without a cone, so that, except for a small fraction of the tube length at the top beyond the downflow, the tubes in a circular heater with a cone are subjected to convection not from the main stream of hot gases but from much cooler gases in the downflow.

Fig. 9 of this closure shows the isotherms through a heater, Type J, with 40-ft tubes, obtained by high-speed thermocouple traverses at five levels. The temperatures in the main flow vary from above 1800 F near the floor of the heater to approximately 1400 F near the base of the cone. The temperatures of the gases in the downflow which wash the tubes (the shaded portion of the cross section of the heater) vary through the major portion of the length of the tubes from an average of 1200 F at the bottom to 1300 F at the top. However, the average velocities in the downflow as determined by a Velometer traverse at the same levels increase from approximately 5 fps at the top to approximately 10 fps at the bottom so that the convection heat-input rates from the gases in actual contact with the tubes are more uniform and represent a lower portion of the total heat input, than if the tubes were subjected to convection from the gases in the main stream, as would be the case in a short circular heater without a cone where the velocity and the mass of the downflow are not sufficient to keep the gases in the main stream out of contact with the tubes.

It is hoped the foregoing explanation and the results of tests as shown in Fig. 9 answer the question raised as to the uniformity of emissivity of coils in any multicoil circular heater, and explain why, in a heater with a cone of the general geometry, as used in heaters J and K, the average circumferential rates along the length of the individual tubes are much more uniform than the 1.4:1 ratio of maximum to average rates cited by Messrs. Mader and Shoulberg.

On the Tool-Life and Temperature Relationship in Metal Cutting

By F. F. LING[1] and EDWARD SAIBEL,[2] PITTSBURGH, PA.

The empirical relationship of Schallbroch, Schaumann, and Wallichs (1)[3] between tool life and cutting temperature is examined in the light of recent developments in rupture theory. Cutting-tool failure is viewed essentially as a rupture process and the data relating tool life and cutting temperature are interpreted from a reaction-rate theory point of view. The significance of cutting temperature is examined critically and its limitations are pointed out.

Introduction

In metal machining the method of determining tool life is still an empirical matter. The conventional criterion of tool life is based on tool wear and/or failure (2). A measure for this is set in an American standard (ASA B5.19–1946). Since the advent of the paper of Schallbroch and Schaumann (3) which correlated tool life and cutting temperature in a simple manner, much attention has been given to using cutting temperature as a criterion for determining tool life. Fig. 1 shows a plot of log tool life against cutting temperature. This was obtained by Schallbroch, Schaumann, and Wallichs from their curves, Fig. 2, showing the relationship between log tool life versus cutting velocity for a single tool material and a constant width of cut. Corresponding to a given cutting condition, that is, cutting velocity, depth of cut, etc., there is an average chip-tool interface temperature measurable by the so-called chip-tool thermocouple method. Using this, the data of Fig. 2 are reduced to the single curve shown in Fig. 1. Since the latter is close to a straight line, Schallbroch and Schaumann proposed a relationship of the form

$$L = A\theta^{-B} \quad \ldots\ldots [1]$$

where L is the tool life, θ is the cutting temperature as defined, and A and B are constants. The former depends on the tool material and the latter depends on the tool and workpiece material among other factors. The value of the constant B is approximately 20.

It is the purpose of this analysis to derive a tool life versus temperature relationship from a more fundamental basis and to investigate the feasibility of using cutting temperature as a tool-life criterion.

Proposed Tool-Life Cutting Temperature Relationship for Metal Machining

The reaction-rate theory of Eyring (4, 5) has been found applicable to problems of creep and rupture under certain conditions (6, 7, 8) and we propose to show that it can be used with success in the present problem.

Criteria for tool failure are generally classified as (*a*) a certain amount of wear as for example 0.03 in. for carbide tools, and (*b*) the so-called "burning," a term which is applied to high-speed tool steels. Both of these types may be considered activation-energy processes and without specifying the detailed processes of the mechanism of the failure, energy or thermodynamic methods may be applied to develop useful relationships. This possibility naturally suggests the use of reaction-rate theory.

As a first check on this feasibility we have replotted the curve of Schallbroch, et al., Equation [1], shown in Fig. 3, in the form demanded by reaction-rate theory based on Boltzmann statistics, namely

$$L = Ce^{D/T} \quad \ldots\ldots [2]$$

where C and D are constants which for the present will simply be empirical, selected to give good fit to the curve. Their interpretation and theoretical estimation will be shown later.

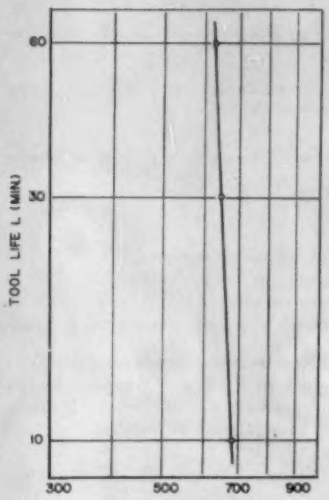

Fig. 1 Tool Life Versus Cutting Temperature Due to Schallbroch and Schaumann

It has been shown theoretically (6) that the time of rupture is given by

$$t_r = \frac{h}{kT} e^{\Delta F^*/RT} \quad \ldots\ldots [3]$$

where

t_r = time of rupture (this is L of Equation [1])
h = Planck's constant
k = Boltzmann constant
T = absolute temperature
ΔF^* = free energy of activation
R = universal gas constant

[1] Assistant Professor of Mechanics, Department of Mathematics, Carnegie Institute of Technology. Assoc. Mem. ASME.

[2] Professor of Mechanics, Department of Mathematics, Carnegie Institute of Technology. Mem. ASME.

[3] Numbers in parentheses refer to the Bibliography at the end of the paper.

Contributed by the Production Engineering Division and presented at a joint session of the Production Engineering Division and the Research Committee on Metal Processing at the Diamond Jubilee Semi-Annual Meeting, Boston, Mass., June 19–23, 1955, of The American Society of Mechanical Engineers.

Note: Statements and opinions advanced in papers are to be understood as individual expressions of their authors and not those of the Society. Manuscript received at ASME Headquarters, February 24, 1955. Paper No. 55—SA–23.

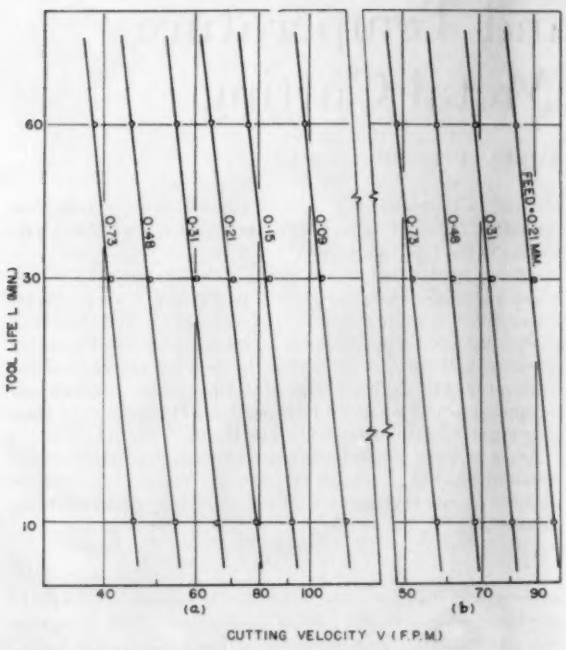

(a) Tool material: Wo—18 per cent, Cr—4 per cent, Mo—1 per cent
Workpiece material: St. 60.11
Width of cut: 10 mm

(b) Tool material: Wo—18 per cent, Cr—4 per cent, Mo—1 per cent
Workpiece material: St. 50.11
Width of cut: 10 mm

FIG. 2 TOOL LIFE VERSUS CUTTING VELOCTY DUE TO SCHALLBROCH AND SCHAUMANN

Now the free energy of activation may be expressed as follows

$$\Delta F^* = \Delta H^* - T\Delta S^* - \alpha s_s \quad \ldots\ldots [4]$$

where

ΔH^* = so-called apparent activation energy
ΔS^* = so-called apparent entropy of activation
s_s = shear stress causing rupture
α = proportionality factor which depends on temperature

It has been shown to be quite satisfactory in processes similar to the present one to consider the term h/kT to be constant; i.e., to treat it as though it were independent of temperature. If this is done, Equation [3] together with [4] may be written

$$t_r = M \exp\left[\frac{\Delta H^* - T\Delta S^* - \alpha s_s}{RT}\right] \quad \ldots\ldots [5]$$

where M is a constant.

Since tool failure is taken as a process of rupture, $L = t_r$. For a particular pair of metals ΔH^* and ΔS^* are constants and Equation [5] reduces to

$$L = N \exp\left[\frac{\Delta H^* - f(T)}{RT}\right] \quad \ldots\ldots [6]$$

where $N = Me^{-\Delta S^*/R}$

and $f(T) = \alpha s_s$

This is so only when one is dealing with a particular physical setup of metal machining where there is a cutting temperature corresponding to an applied stress at the tool causing failure.

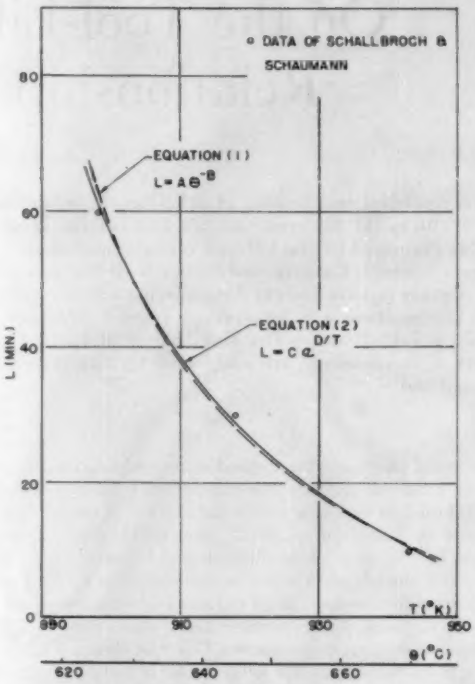

FIG. 3 EQUATIONS [1] AND [2] FITTED TO DATA IN FIG. 1

Actually in the general case s_s should be treated as a function of the depth of cut, width of cut, tool-material properties, and workpiece-material properties as well as a function of cutting temperature.

It is evident that much more about the state of stress in the tool and its relationship to the other parameters must be known before a precise quantitative analysis can be made. Nevertheless, in the following an example is worked out in a particular case solely for illustrative purpose.

EXAMPLE ON A PARTICULAR PROBLEM

Any quantitative check on Equation [6] would require both rupture data of tool steel, i.e., rupture time versus stress at various temperatures, and metal-machining data, i.e., applied stress at the tool, cutting temperature, and tool life. As pointed out previously, Equation [6] holds only for a particular physical setup in which case only cutting velocity varies and s_s is uniquely correlated with T. Unfortunately, no experimental data of the kind sought are available. Therefore, for illustrative purposes, we shall combine data from various sources.

Fig. 4 shows rupture data due to Larson and Miller (7) for rupture of an S-590 alloy. The slopes are $Q'/2.3\ R \times 10^{-4}$ deg Rankine and they find that the equation

$$t_r = \text{const}\ (e^{Q'/RT}) = L \quad \ldots\ldots [7]$$

fits data in Fig. 4. The data have been replotted using constants determined by Kanter (9) from atomic considerations. Fig. 5 is a plot of $Q'/2.3\ R \times 10^{-4}$ deg Rankine versus $\sigma \times 10^{-2}$ psi, where σ is the applied tensile stress causing rupture.

We now refer to metal-machining data of Chao and Trigger (10) which are listed in part in Table 1. A rough calculation of maximum shear stress s_s in the tool is shown in Fig. 6, and the values are listed in column 8 of Table 1. Following a similar

TABLE 1 METAL-MACHINING DATA ACCORDING TO CHAO AND TRIGGER (10)

(1) T(deg R)[a]	(2) Fc(lb)[a]	(3) F(lb)[a]	(4) $A \times 10^{-3}$(in.^{2})[a]	(5) $\sigma_1 \times 10^{-3}$(psi)
1610	384	268	7.32	52.5
1660	371	247	7.02	52.9
1710	358	227	6.75	53.1
1760	347	211	6.5	53.4

(6) $\sigma_2 \times 10^{-3}$ (psi)[b]	(7) $\gamma \times 10^{-3}$ (psi)	(8) $s_s \times 10^{-3}$ (psi)	(9) $\sigma \times 10^{-3}$ (psi)	(10) $\frac{Q'}{2.3R} \times 10^{-4}$ (deg R)
32.7	36.6	38	76	3.028
28.8	35.2	37.1	74.2	3.042
25.15	33.6	36.2	72.4	3.056
23	32.4	35.4	70.8	3.07

[a] Data from reference (10).
[b] Yield strength for Cr-Mo forged steel, reference (11)
Symbols are as defined in Fig. 6 in text.

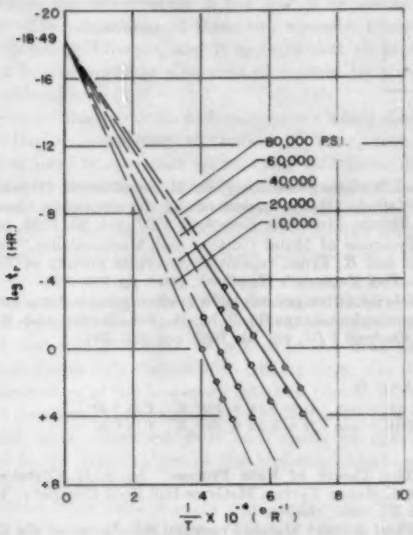

FIG. 4 LOG RUPTURE TIME VERSUS TEMPERATURE FOR S-590 ALLOY DUE TO LARSON AND MILLER

method to that used in the study of the creep and rupture, we assume the simple relationship that $\sigma = 2s_s$. This is listed in column 9, Table 1.

From Fig. 5 the values of $Q'/2.3\ R \times 10^{-4}$ deg Rankine corresponding to σ are found and listed in column 10, Table 1. Fig. 7 shows the plot of $Q'/2.3\ R \times 10^{-4}$ deg Rankine versus T. A comparison of Equations [6] and [7] shows immediately that

$$Q'/R = \Delta H^*/R - f(T)/R \quad [8]$$

For the range of T concerned Q'/R can be expressed as, see Fig. 7

$$Q'/R = Q/R + \epsilon/RT \quad [9]$$

where $$Q/R = \Delta H^*/R - f_0 R$$

and f_0 is the value of $f(T)$ extrapolated to $T = 0$, and ϵ is a constant. Equation [6] now can be written

$$L = ce^{D/T} \quad [10]$$

where $$\dot{C} = \frac{h}{kT} \exp\left[\frac{-\Delta s^* + \epsilon}{R}\right]$$

$$D = Q/R$$

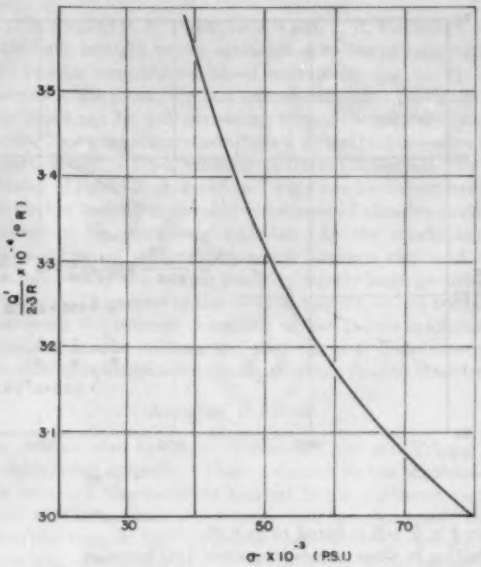

FIG. 5 SLOPE CONSTANT VERSUS APPLIED STRESS FROM FIG. 4

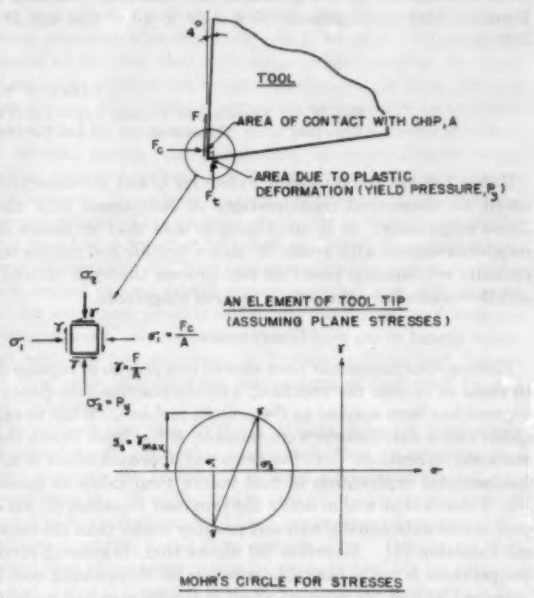

FIG. 6 APPROXIMATE STRESS CONDITIONS ABOUT TOOL FACE

Kanter has determined the value of N for Equation [6] on the basis of atomic vibration frequencies. For an S-590 alloy, $N = 1.93 \times 10^{-17}$ min. From this value $\Delta S^*/R$ is deduced to be 3.8 since the other factors are constants and T is taken as an average over the range of temperature concerned. This value of $\Delta S^*/R$ is not unreasonable when compared with what is known. Also from Kanter's work $\Delta H^*/R$ is calculated to be 3.56×10^4 deg K and it compares favorably with the value of

$$Q/R(\equiv \Delta H^*/R - f_0/R) = 3.28 \times 10^4 \text{ deg K}$$

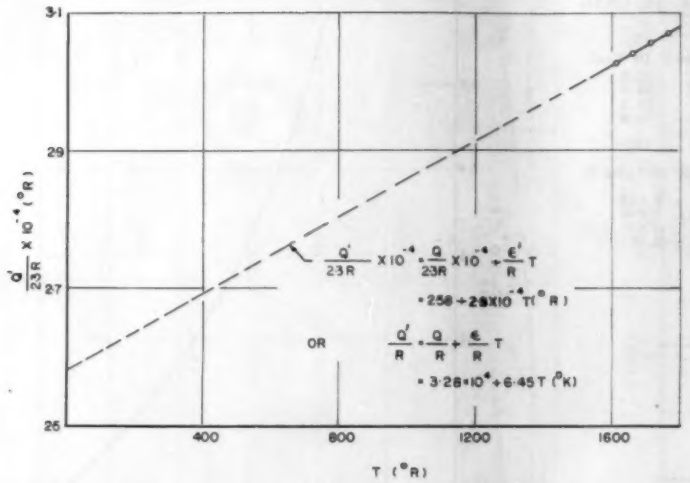

FIG. 7 SLOPE CONSTANT VERSUS CUTTING TEMPERATURE

From Fig. 7 ϵ/R is found to be 6.45.

Putting in these values, Equation [10] becomes

$$L = 1.19 \times 10^{-14} e^{3.28 \times 10^4/T} \text{ min} \quad \ldots\ldots\ldots\ldots [11]$$

As a consequence of the estimate, the following constants for Equation [10] are obtained: $C = 1.19 \times 10^{-14}$ min and $D = 3.28 \times 10^4$.

TABLE 2 VALUES OF C AND D

Equ. [2]	Empirical fit to data	$L = Ce^{D/T}$ min	$C = 3.9 \times 10^{-14}$ min	$D = 3.14 \times 10^4$° K	T in ° K
Equ. [10]	Theoretical	$L = Ce^{D/T}$ min	$C = 1.19 \times 10^{-14}$ min	$D = 3.28 \times 10^4$° K	T in ° K

Table 2 shows the estimated values for C and D, respectively, based on theoretical considerations in comparison with those found empirically. It is interesting to note that by means of a rough calculation with available data a tool-life and cutting temperature relationship based on rate-process theory is arrived at and the results have the correct order of magnitude.

CONCLUSION

Cutting-tool failure has been viewed as a process of rupture due to shear at or near the tool face; and the reaction-rate theory of rupture has been applied to the present problem. While no exact quantitative calculations were possible, it has been shown there are good indications that the proposed approach offers a more fundamental explanation of tool failure than exists at present. Fig. 3 shows that within limits the proposed Equation [3] fits experimental data equally well and possibly better than the empirical Equation [1]. Equation [6] shows that, in general, cutting temperature is not a desirable criterion for determining tool life inasmuch as tool life depends on all of the independent variables. Nevertheless, for a particular physical setup, tool life and cutting temperature are well correlated as shown by Equation [10]. Two constants are involved: C which is seen to be a function of the so-called apparent entropy of activation of the metal, and the parameter ϵ/R which is a function of tool and workpiece material as well as other given dimensions; D is seen to be a function of the so-called apparent activation energy of the material and a parameter f_0/R, which depends on the tool and workpiece material as well as other given dimensions.

BIBLIOGRAPHY

1 "Zerspanbarkeitsprufung durch Messurfahren für Schnittemperatur und Weiksengvershleiss," by H. Schallbroch, H. Schaumann, and R. Wallichs, Hauptversaummlung der deutschen Gesellschaft für Metallkinde, Munchen, *Zeitschrift VDI*, vol. 30, 1938, pp. 34–38.

2 "Principle of Metal Cutting and Machinability," by M. E. Merchant and H. Ernst, reprint of American Society of Tool Engineer, *The Tool Engineer's Handbook*, 1949, pp. 316–323.

3 "Die Schnittemperatur beim Drehvorgang und ihre anwendung als Zerspanbarkeitskennziffer," by H. Schallbroch and H. Schaumann, *Zeitschrift VDI*, vol. 81, 1937, pp. 325–330.

4 "The Theory of Rate Process," by S. G. Glasstone, K. J. Laidler, and Henry Eyring, McGraw-Hill Book Company, Inc., New York, N. Y., 1941, chapter 9.

5 "Flow of Solid Metals From the Standpoint of the Chemical-Rate Theory," by W. Kausman, Trans. AIME, vol. 143, 1941, pp. 57–81.

6 "Stress Rupture of Heat-Resisting Alloys as a Rate Process," by L. S. Machlin and A. S. Nowick, NACA TN No. 1126, September, 1946.

7 "A Time-Temperature Relationship for Rupture and Creep Stresses," by F. R. Larson and J. Miller, Trans. ASME, vol. 74, 1952, pp. 765–771.

8 "Effect of Temperature Variation on the Long-Time Rupture Strength of Steels," by E. L. Robinson, Trans. ASME, vol. 74, 1952, pp. 777–787.

9 Discussion by J. J. Kanter to reference (7).

10 "Cutting Temperature and Metal-Cutting Phenomena," by B. T. Chao and K. J. Trigger, Trans. ASME, vol. 73, 1951, pp. 771–793.

11 "Creep Data," compilation of "Available High-Temperature Creep Characteristics of Metals and Alloys," ASME-ASTM, 1938.

Discussion

B. T. CHAO[4] AND K. J. TRIGGER.[5] The authors have prepared an interesting paper suggesting a new and fundamental approach to the all-important problem of tool life in metal machining. However, there are a few pertinent facts which the writers wish to discuss in connection with the paper.

Schallbroch, Schaumann, and Wallich's cutting-temperature data were based on the "two-tool" method (zweimeissel verfah-

[4] Associate Professor of Mechanical Engineering, University of Illinois, Urbana, Ill.

[5] Professor of Mechanical Engineering, Univeristy of Illinois, Urbana, Ill. Mem. ASME.

ren), the reliability of which has been seriously questioned since its introduction by Gottwein and Reichel. Inasmuch as the frictional behavior between the chip and the tool face for the two different tool-work combinations may not be identical, the cutting geometry and hence the interface temperatures are likewise different. It is for this reason that the two-tool thermocouple method has virtually been abandoned by recent investigators.

The manner in which a cutting tool wears and fails to function depends to a large extent upon the cutting conditions. The top face wear or "cratering" is usually of great significance at relatively high cutting speeds for a given tool-work combination. Recent investigations on the subject have shown that tool failure due to such cause is decisively temperature dependent.[6] On the other hand, flank wear of carbide tools is often excessive at low cutting speeds where the temperature is low and is of secondary importance. The mechanism of these two common types of tool wear is obviously different, and it appears that an attempt to treat tool failure solely as a process of rupture by shear is an over-simplification.

The authors' analysis deals with parameters which also govern the more likely phenomenon of "cratering" wear, namely, the influence of local temperature on tool-chip interfacial diffusion. Trent[7] has demonstrated that diffusion between steel and free tungsten carbide in the cutting-tool material and the subsequent carrying away of the alloy so formed constitutes the major cause of cratering. Solid-state diffusion may be treated as a reaction-rate process.

Temperature values obtained with the tool-work thermocouple technique represent some sort of average temperature along the length of tool-chip contact. As a tool is put into use, such temperature varies only slightly with cutting time. On the other hand, temperature at the tool-work interface (flank) increases as wear land develops.[8] It is, therefore, difficult to see how tool-life data based on a prescribed wear land could be theoretically correlated to the temperature at the tool-chip interface rather than at tool-work interface.

The writers offer the foregoing comments with the hope of enhancing the value of the paper. When a cutting tool fails by cratering due to excessive temperature, the theory of rate process is applicable in view of the fact that rapid interfacial diffusion takes place. To derive a more universal relationship for tool life, one has to look into the mechanism of tool wear under diversified conditions.

[6] "The Mechanism of Crater Wear of Cemented Carbide Tools," by K. J. Trigger and B. T. Chao, ASME Paper No. 55—SA-11.

[7] "Some Factors Affecting Wear on Cemented Carbide Tools," by E. M. Trent, Proceedings of the Institution of Mechanical Engineers, vol. 166, 1952, pp. 64–74.

[8] "Temperature and Heat Flux Distribution at Tool-Chip and Tool-Work Interface in Metal Machining," by B. T. Chao, K. J. Trigger, and Y. H. Lee, ME Tech. Note ORD-1121-1, University of Illinois, May, 1955.

[9] Research Engineer, Charge of Metal Cutting, Kearney & Trecker Corporation, Milwaukee, Wis. Assoc. Mem. ASME.

[10] Kearney & Trecker Corporation, Milwaukee, Wis.

[11] Machine Designer, Research and Development, Kearney & Trecker Corporation, Milwaukee, Wis. Assoc. Mem. ASME.

A. O. Schmidt,[9] B. F. Turkovich,[10] and J. R. Roubik.[11] The authors have brought to our attention a means of relating tool life to tool-tip temperature based on rate-process theory. As mentioned in the paper, life and temperature for a particular set of conditions can be well correlated through empirical determinations. Tool temperature manifests a general influence on tool life, particularly in the machining of ferrous materials. In the machining of light alloys, rapid tool wear can be encountered at relatively low tool-tip temperatures because of abrasive particles embedded in the workpiece material. In the machining of titanium a kind of cold-welding action between chip and tool occurs followed by the tearing out of relatively large particles of tool material. A general relationship of tool life to tool temperature covering the extreme characters of tool-failure mechanisms as mentioned is most welcome and all the more so if the constants in the relating equation are determinable on a fundamental basis.

Authors' Closure

The authors wish to thank Professors Chao and Trigger for their stimulating remarks. Their comment on the obsolescence of the twin-tool thermocouple method is not pertinent to the paper in that refinements which have since been made still show relationships between tool life and temperature of the same character as that of reference (1). It is the object of the paper, not to analyze the data of reference (1), but to use the existence of a relationship of this character between tool life and temperature as a starting point in the analysis of the general problem. Furthermore, as is stated, this is not a detailed theory of the mechanisms of wear processes, whatever their type or location. They may be adhesive or abrasive, they may occur at the crater or the flank, and naturally different mechanisms are involved in these different types of wear, thus different activation energies will be involved. It is felt that by expressing the wear problem in terms of activation energies, among other parameters, the magnitudes of the activation energies involved may furnish clues to the mechanisms which operate. There is no doubt in the authors' minds that they have oversimplified the problem, but prior to this approach (the paper was first submitted in February, 1954) the existing empirical relationships did little to focus attention on the variables which needed control during experimentation and it is thought that the work may provide additional motivation to future experimental work. Nevertheless, the authors are in hearty agreement with the last statement of Professors Chao and Trigger that they must look into the mechanisms of tool wear for the final "solution."

The authors also wish to thank Messrs. Schmidt, Turkovich, and Roubik for their remarks. It is thought that the reaction-rate-theory approach can be used in at least a semiquantitative way in predicting the life of the tool in that, if one knows the type of failure which is going to occur, he can use appropriate values of the necessary constants found from simpler tests. Conversely, it is thought that improvements can be made in tool life by treating the tool material in such a way as to affect advantageously the values of these constants.

The Mechanism of Crater Wear of Cemented Carbide Tools

By K. J. TRIGGER[1] and B. T. CHAO,[2] URBANA, ILL.

This paper presents an analysis of tool-wear data in terms of fundamental variables consistent with the nature of the contact and rubbing of clean metallic surfaces. Wear of cemented-carbide tools on the top surface is examined in the light of the mechanism of frictional wear as proposed originally by Holm and recently as modified by Burwell, Strang, and Archard. It has been found that wear at the top surface is essentially of the transfer type and that the formation of crater wear is strongly temperature-dependent. For a given tool-work combination, the top face wear can be correlated with tool-chip interface temperature in a manner predictable from the simple laws of adhesion wear in combination with the theory of rate process.

Introduction

TOOL life has an important bearing on the economy of production. It is a factor of major concern in ascertaining the machinability of materials. However, in spite of its importance, the meaning of the term, tool life, may have several interpretations. It can be either the useful life of a cutting tool expressed in minutes between grinds or the total time which a tool can withstand before complete destruction. The latter often has been used in connection with high-speed-steel tools. For sintered carbides, tool life is frequently designated as the time to produce a specified amount of flank wear, e.g., 0.030 in.

While tool life expressed in time alone may have merit in computing machining costs, it may not be a fair index of a tool's effectiveness to remove metal by chip formation, since the cuts can be deep or shallow, the feeds heavy or light, and the speeds fast or slow. Hence, in a great majority of the tests recently reported, tool life is expressed in terms of the volume of metal removed. However, it is questionable that wear at the tool flank can, under all circumstances, be the sole gage in prescribing the useful life of a carbide cutting tool. A more logical approach is to examine at all active portions of the tool the nature and development of wear which ultimately will prevent it from functioning properly and economically.

A wealth of data on tool-life tests has been published since Taylor's work at the turn of the century. Among the valuable compilations is the work of the ASME Special Research Committee on Cutting of Metals (1)[3] which co-ordinated the results of investigations carried out in England, Germany, and in this country. Data cover all phases of machinability with respect to single-point tools. The machinability reports of the U. S. Air Force (2) demonstrate the importance of microstructure of steels on tool life and are forward steps in correlating cutting data. However, there has been little information on the nature of the wear process in cutting tools.

After a tool has been in use for some time, wear develops along the tool flank and also on the top surface. The latter is commonly described as cratering. Following a series of investigations on crater wear of cemented-carbide tools, Dawihl (3) concluded that mutual diffusion of materials at the tool-chip contact and the propensity to welding of certain constituents in sintered carbide with steel were of direct concern. The importance of temperature at the tool-chip contact was pointed out. When machining steel, Dawihl attributed the superior performance of tools containing titanium carbides to their greater oxidation resistance and hence higher "welding-on" temperature with the steel chip.

Following a similar line of reasoning, Trent (4) proposed a theory to account for the cratering wear of cemented-carbide tools. He postulated that a fused layer of alloy was formed between the steel and the free tungsten carbide in the cutting-tool material at the tool-chip interface. Wear was the consequence of the carrying away of the fused alloy by the moving chip. The extent of cratering was controlled by the distribution of temperature near the cutting edge. More recently, a method has been developed to evaluate quantitatively the temperature distribution at the tool-chip interface (5). When incorporated with the general relationship between temperature and intermetallic diffusion, it offers a plausible explanation of the formation of the crater. The results shed light on the basic mechanism of tool wear.

A Simplified Theory of Tool Wear

Numerous experiments have been conducted on tool-wear studies during the past decades, and much is still to be done. Many instances of present-day practice in metalworking are based on cut-and-try methods. No general laws of tool wear have been deduced. Since metallic wear is, in general, a complex phenomenon, involving chemical, physical, and mechanical processes, oftentimes interwoven, it is clear that a theoretical treatment of the problem of tool wear at present must be accompanied by simplifications.

Metallic wear may be of many types, such as that occurring in rolling contact, wear due to hammering, corrosion, erosion, fatigue, and so on. The wear which occurs at sliding contacts is known as frictional wear. The admirable work of Ernst and Merchant (6) has shown that when two clean metals are brought together, intermetallic junctions at the surfaces of actual contact will form as a result of solid-state diffusion. These junctions may have to be disrupted if there is relative sliding between members of the mating pair. Furthermore, the surfaces may interlock at an angle and thus create additional resistance to relative sliding. A similar view was held by Bowden and his collaborators (7). One of the many important findings of their systematic investigation is that friction between clean metallic surfaces is not purely a surface property but also is influenced by the bulk properties of the mating metals.

While wear, or the amount of metal removed from the sur-

[1] Professor of Mechanical Engineering, University of Illinois. Mem. ASME.

[2] Associate Professor of Mechanical Engineering, University of Illinois.

[3] Numbers in parentheses refer to the Bibliography at the end of the paper.

Contributed by the Research Committee on Metal Processing and presented at a joint session with the Production Engineering Division at the Diamond Jubilee Semi-Annual Meeting, Boston, Mass., June 19–23, 1955, of The American Society of Mechanical Engineers.

Note: Statements and opinions advanced in papers are to be understood as individual expressions of their authors and not those of the Society. Manuscript received at ASME Headquarters, March 3, 1955. Paper No. 55—SA-11.

faces, in general, will bear little relation to the frictional resistance during sliding, both are the consequence of the separation of contact asperities. If the intermetallic junction possesses a lower shearing strength than either of the original metals, disruption during sliding will be mainly interfacial. A high sliding speed produces not only a high temperature at the rubbing contact but also a steep temperature gradient in a direction normal to sliding. As a consequence of the thermal gradient the shear strength of the interface alloy will be less than that of either of the parent metals. Such a condition favors shearing in the thin layer of material at the interface and the accompanying wear is of the so-called microtransfer type. Under these circumstances, diffusion is the principal cause of metal transfer and the wear process is essentially temperature-dependent. Other possibilities of shearing of the metallic junction at surfaces of actual contact also have been described in the literature (7).

Before applying the foregoing concept of the nature of sliding contacts to an analysis of tool wear, a brief description is presented on the manner of wear development in the neighborhood of the cutting edge. Fig. 1 illustrates the cross section of a carbide tool which has been in use for some time. It is clearly seen that wear occurs in two distinct regions. Rubbing of the hot chip on the top of the tool forms a craterlike wear on this surface and extends for a certain distance behind the cutting edge. Wear

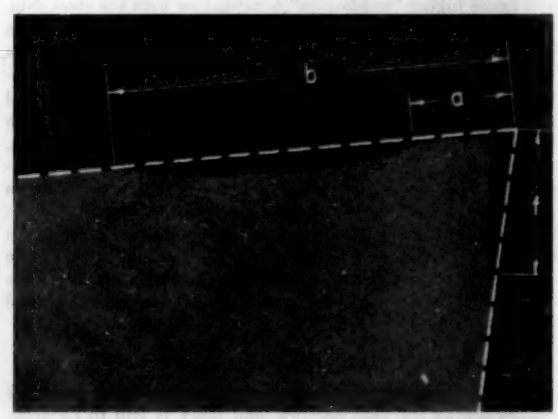

Work material: AISI 4150 (mod) steel, Q & T, 325 Bhn
Tool material: S-grade carbide
Tool shape: 0–6–7–7–10–0–0.0125 in.
Cutting speed: V_c = 367 fpm
Feed: f_1 = 0.00632 ipr
Depth of cut: w_1 = 0.125 in.
Total cutting time: t = 17.78 min

FIG. 1 CROSS-SECTIONAL VIEW OF A WORN TOOL; ×145

is also evident on the clearance face or flank as a result of the rubbing of the relatively cold workpiece, possibly with entrapped hard debris of the built-up edge. A tool also may fail by mechanical damage, such as chipping of the cutting edge as a result of improper handling, grinding, and the like, but this is not the concern of the present work.

By the nature of the action of the heated chip sliding on the top surface of a cutting tool, it appears logical to regard its wear as of the frictional type. There are two possible mechanisms to which this tool wear can be attributed. They are:

(*a*) Adhesion and asperity-transfer wear, in which rupture occurs in a thin layer of tool material adjacent to tool-chip interface as a result of weakening due to diffusion and alloy formation. For a given chemical composition and micro constituents (including impurities) of the workpiece and tool material, temperature and its distribution at the sliding contact are governing factors. Transfer of metal takes place discontinuously, and by lumps.

(*b*) Abrasion or plowing wear. Interlocking of surfaces at the sliding contact produces not only additional resistance to sliding but also wear of mechanical origin. Analogous to the "plowing" component of friction force as designated by Bowden (7) and his co-workers, the term plowing or abrasion wear is adopted in this discussion. Such wear depends primarily upon the relative hardness of the tool and the workpiece under the operating conditions, the amount and distribution of the hard constituents in the work material, its rate of strain hardening, and so on. While it is suggested that the top face wear of a cutting tool be examined in terms of these two distinct mechanisms, some degree of interaction may be expected to exist between them.

In their studies using radioactive tools for rapid tool-life evaluation, Merchant, Ernst, and Krabacher (8) concluded that a major portion of the wear products was transferred to the chips. They reported that when AISI 8650 steel was turned with a sintered-carbide tool, 95.8 per cent of the wear products, both top and flank, adhered to the chips. It appears logical to assume that tool wear is essentially of the adhesion and transfer type with little formation of loose wear particles.

A semiquantitative theory of microtransfer type of wear has been proposed by Holm (9). It makes use of one of the basic concepts in the theory of metallic friction, namely, that plastic deformation at local asperities forms the actual area of contact between two rubbing surfaces. Holm also postulated that during sliding, for every encounter of a surface atom in the real area of contact with an atom in the mating surface, there was a statistically constant probability of either of the two atoms being pulled out of its parent surface. With these hypotheses, Holm showed that the worn volume per unit sliding distance W/s, could be expressed by

$$\frac{W}{s} = Z\frac{P}{H} \quad \text{[1]}$$

in which

Z = probability of material removal, number of atoms worn away per atomic encounter
P = normal load
H = mean pressure hardness of softer material at point of contact (other terms, such as contact hardness, flow pressure, etc. also have been used.)

Burwell and Strang (10) disputed Holm's concept of atomic removal on the basis of evidence revealed by photographs of wear products taken with an electron microscope. They suggested that Holm's atomic encounter should be replaced by asperity encounter and, following the analysis of experimental results, they concluded that adhesion wear could be expressed in a form virtually identical to that of Holm, to wit

$$\frac{W}{s} = K\frac{P}{H} \quad \text{[2]}$$

where K is the fraction of the actual area of contact which results in a wear product. It depends, among other things, upon the composition of the surfaces, condition of lubrication, etc. Recently, Archard (11) refined the Burwell-Strang theory by removing unnecessary assumptions. The general conclusion concerning the relationship between distance of rubbing, normal load, and wear volume remains unaltered. Burwell and Strang's experiment was conducted at a constant rubbing speed of 20 cm/sec (39.4 fpm) with wide range of normal loads. Archard's results were obtained under similar conditions; the one sliding speed used was approximtely 98 fpm. In either investigation, K was regarded as a material constant, being dependent upon the combination of mating surfaces. The influence of temperature

generated by higher rubbing speed and heavy load on the possible variation of K has not been reported.

Following detailed microscopic examination of the roughening of the interface at contacting asperities, Feng (12) proposed an interlock-welding theory. In the presence of surface contamination which may prevent significant diffusion or welding, the formation of loose wear particles is attributed to the mechanical interlocking effect. The application of radioactive isotopes to the study of tool wear reveals that it is essentially of the transfer type. Nevertheless, some modification in the interpretation of the physical quantities involved in Equation [2] is necessary as will be made clear in the following section.

Experimental Procedure, Results, and Discussion

According to Equation [2], if W_i represents the volumetric wear at the tool-chip interface developed during any given time of cutting t, and s_i, the distance which the chip slides over the tool face in the same period of time, then, under a fixed cutting condition, the wear rate, W_i/s_i, is constant.

The force component acting normal to the top surface of the tool is presumably unchanged. Since $s_i = v_f t$, v_f being the chip flow velocity, it is clear that under these circumstances, W_i should vary linearly with respect to cutting time.

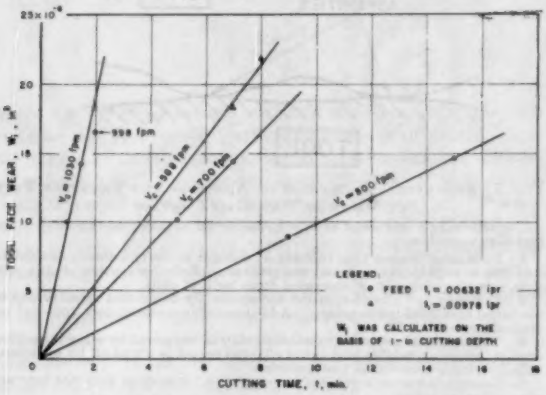

Work material: AISI 4142, annealed, 212 Bhn
Tool shape: 0–6–7–7–10–0–0.015 in.
Tool material: 8-grade carbide
Depth of cut: 0.100 in.

Fig. 2 Relationship Between Tool-Face Wear and Cutting Time

Fig. 2 shows the results of crater measurement obtained during turning an annealed AISI 4142 steel with a steel-cutting-grade carbide tool at several combinations of speeds and feeds. Other cutting conditions are as indicated in the figure. All tests were conducted without cutting fluid on a 16-in. × 54-in. heavy-duty lathe. The carbide tool tips were of the detachable type, triangular in shape, approximately $^5/_8$ in. on a side, $^1/_8$ in. thick, and mechanically attached to $^1/_2$-in-square shanks.

Great care was exercised in the preparation of the tool tip. The top surface was finished by lapping on fine-grain cast-iron wheels charged with diamond dust. This lapping consisted of a roughing operation with 18-micron dust followed by finishing with 4-micron dust. All lapping was done dry since the presence of an oil film makes it difficult to obtain a surface flatness of high precision. Using this procedure a surface flatness of 0.00001 in. or better was easily obtained. A profilometer check indicated a surface roughness of 2 to 3 microinches (rms). The clearance surface was finished after the tip was mounted securely in place in the tool shank. Final lapping on the latter surface was done with a 320-grit diamond wheel.

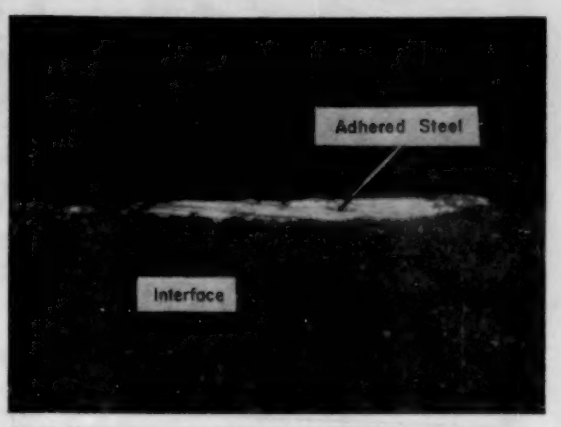

Fig. 3 Polished and Etched Section of a Worn Tool Showing Adherent Steel; ×300

Examination of the worn surface of a carbide cutting tool reveals that thin layers of steel debris adhere sporadically over the tool-chip contact. The adhering material is of irregular thickness as shown in Fig. 3 which depicts a portion of the carbide-steel interface at about ×300. This figure was prepared from a tool tip sectioned perpendicular to the cutting edge. The surface was polished using the same procedure employed for the top surface. It was then etched, at room temperature, for about $2^1/_2$ min with a solution of 10 per cent potassium ferric-cyanide and 10 per cent potassium hydroxide mixed in equal amounts. The microstructure of the carbide tool was thus revealed clearly while the adhered steel was virtually unattacked. This technique made possible the accurate determination of the carbide-steel interface and consequently the volume of the crater wear. Removal of the adhered steel by dissolving in strong acids has the disadvantage of attacking the cobalt in sintered carbides.

For actual crater volume measurement, the micrograph was taken at a magnification of 100 and was then projected on a sheet of graph paper; the contour of the cross section of the crater was traced and its area measured. The total magnification including the enlargement due to projection was about 640 diameters. The section of the worn tool studied in this manner was always taken far enough from the tip so that the influence of the nose radius vanished. Occasionally, it was necessary to prepare more than one section to obtain representative data.

The linear relationship between tool-face wear and cutting time also has been found to exist when a cast-iron cutting-grade carbide was used for machining steel. This is shown in Fig. 4 in which, for comparison, one of the wear curves in Fig. 2 is reproduced. The vast superiority of titanium-bearing carbide tools in resisting crater formation is clearly demonstrated, notwithstanding the fact that the work material employed in the two series of tests was slightly different.

In deducing a more general law of the tool-face wear at different speeds and feeds, reference is made again to Equation [2]. Wear at the tool-chip interface can be expressed as

$$\frac{W_i}{s_i N} = \left(\frac{K}{H}\right)_i \quad \ldots\ldots\ldots\ldots\ldots\ldots\ldots\ldots [3]$$

wherein N is the normal force acting on the top face of the tool. The subscript i refers to the interface, hence H is the asperity hardness at the sliding contact. W_i and s_i have been defined previously.

The exact nature in which this superficial hardness is affected

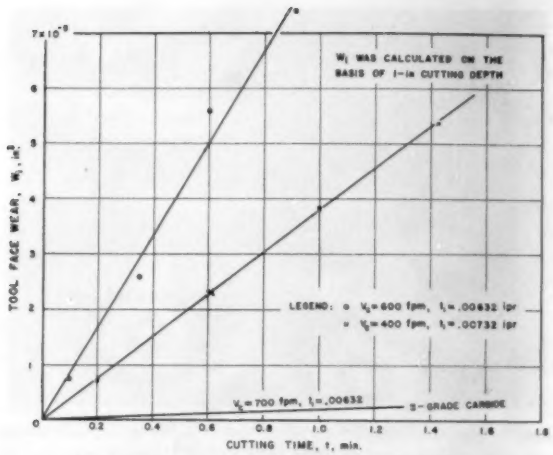

Work material: AISI 4150 (mod), annealed, 197 Bhn
Tool material: C-grade carbide, except as noted
Tool shape: 0-0-7-7-10-0-0.015 in.
Depth of cut: 0.100 in.

FIG. 4 RELATIONSHIP BETWEEN TOOL-FACE WEAR AND CUTTING TIME

by local rate of straining and temperature cannot be ascertained quantitatively at the moment. Following its formation at the shear zone, the severely deformed chip material undergoes further localized plastic straining at the contact asperities. An increase in cutting speed will (*a*) generally reduce plastic strain in the shear zone, (*b*) raise the local asperity temperature, and (*c*) render further asperity deformation more adiabatic. The higher strain rate is the result not only of the higher velocity involved but also is due to the thinner deformed layer as a consequence of the steeper temperature gradient. In so far as the hardness is concerned, the increased adiabaticity of the deformation process will have an effect equivalent to a decrease in temperature and thus compensating tendencies are present. With the relatively high temperature encountered at the interface, it will be presumed that the effect of increase in temperature will predominate.

The dimensionless probability factor K represents the proportion of the contact asperities which results in metal transfer (independent of their size). It also may be interpreted as the fraction of each contact resulting in transfer (independent of their number). In either case, the transfer of metal taking place at the interface arises from atomic movement, the rate of which will be strongly temperature-dependent for the temperature level existing at the tool-chip interface. Metal transferred in this manner can be considered as the direct consequence of a solid-state diffusion process.

The theory of diffusion in solids has been treated extensively in the literature (13). In general, it is a temperature and time-dependent phenomenon. In order to apply the general diffusion theory to the tool-wear process, it is necessary to examine closely how the wear product is being transferred to the chip. An autoradiograph by Merchant, et al. (8) supports the lump-removal concept of tool wear. Fig. 5 suggests schematically how a discontinuous, lump removal wear process is effected at the tool-chip interface.

As the chip slides over the tool surface local adhesion (welding) occurs at some contact asperities. The temperature rise due to local deformation at the asperity is virtually instantaneous ($\sim 10^{-12}$ sec) and adhesion results. The junction fails in the weaker of the pair, which for the time being is the heated chip, and a segment of chip material adheres to the tool. Continued heating by rubbing maintains high local temperature at the tool-chip contact asperity and rapid diffusion and alloy formation[4] ensues. The action is maintained until the tool material adjacent to the adhered layer is weakened to such an extent that the entire affected region (lump) becomes unstable and is then wiped out by an encounter with the oncoming chip. The "life" of the adhered mass is dependent upon its individual size and the temperature level at the alloy zone. A low chip sliding velocity allows more time for localized adhesion at the asperity. The individual adhered area is relatively large. The low interface temperature results in slow diffusion and alloy formation, so that the adhering mass persists relatively longer and may pile on more chip aggregates. Upon removal, a lump of tool material is transferred to the chip.

At high speeds, with higher interface temperature and steeper temperature gradient, the individual contact asperities are thinner, diffusion and alloy formation faster, and the adhering lumps are swept away shortly after formation.

The foregoing postulate suggests that the principal influence of chip velocity is in its effect on interface temperature, size of individual contact asperity, and life of each such contact. The

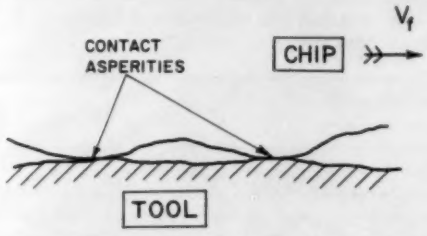

FIG. 5 SUGGESTED MECHANISM OF ADHESION AND TRANSFER TYPE OF WEAR AT TOOL-CHIP CONTACT

The following sequence of events is considered to take place at some of the tool-chip asperities:

1 Portion of heated chip rubbing at contact asperity adheres (welds) to tool due to high local stress and temperature. Relative motion of chip particle becomes zero as it is separated from bulk of chip.
2 Diffusion and alloy formation occurs rapidly at contact asperity due to sustained high local temperature. Additional chip material may "pile up" on original portion.
3 Tool material adjacent to adhered chip is weakened by alloy formation until it becomes unstable and entire affected region is wiped off by oncoming chip, i.e., lump removal of tool material.
4 Lump adheres to surface of moving chip; it may or may not interact with other asperities.

time involved for diffusion and alloy formation between the tool and the adhered chip material is governed by the local temperature.

Following the foregoing argument, it is deduced that for the contact asperities at the tool-chip interface, K would be governed by the energy of activation E of the metal pair and the local temperature T_i (absolute scale) according to a relationship of the form

$$K \propto e^{-\frac{E}{RT_i}} \quad \ldots\ldots [4]$$

where R is the universal gas constant. For a given toolwork combination, E is essentially a fixed quantity.

Assuming that the effect of strain rate on H_i is of secondary importance, the influence of local temperature on the asperity hardness follows a relationship not unlike that of [4], to wit

$$H_i \propto e^{\frac{E'}{RT_i}} \quad \ldots\ldots [5]$$

The formal expression is given by the following equations relating hardness (H) to strain (ϵ)

$$H = H_p(\epsilon)$$

[4] According to Trent, in the case of a carbide tool-cutting steel, the reaction is essentially between ferrite and free-tungsten carbide.

TABLE 1 SUMMARY OF THE QUANTITY $W_i/(s_iN)$

Work material: AISI 4142 steel, annealed, 212 Bhn. Tool shape: 0–6–7–7–10–0–0.015 in.
Tool material: S-grade carbide. Depth of cut: w_1 = 0.100 in. Cutting speed and feed: Variable

Feed, f_1, ipr	0.00632			0.00736		0.00979	
Cutting speed, V_c, fpm	500	700	1030	638	426	588	897
Avg interface temp, θ_i, deg F	1477	1581	1730	1580	1490	1590	1745
Avg interface temp, T_i, deg R	1937	2041	2190	2040	1950	2050	2205
$1/T_i$, $1/°R$	5.16×10^{-4}	4.9×10^{-4}	4.56×10^{-4}	4.9×10^{-4}	5.13×10^{-4}	4.87×10^{-4}	4.54×10^{-4}
Top-face wear, W_i, in.^{3}	$0.98 \times 10^{-6}t$*	$2.07 \times 10^{-6}t$	$9.5 \times 10^{-6}t$	$1.84 \times 10^{-6}t$	$1.96 \times 10^{-6}t$	$2.67 \times 10^{-6}t$	$15.9 \times 10^{-6}t$
Chip-thickness ratio, r_t	0.412	0.436	0.455	0.436	0.421	0.462	0.477
Chip-flow velocity, v_f, ipm	2.47×10^3	3.66×10^3	5.63×10^3	3.34×10^3	2.15×10^3	3.26×10^3	5.05×10^3
Chip sliding distance, s_i, in.	2.47×10^3t	3.66×10^3t	5.63×10^3t	3.34×10^3t	2.15×10^3t	3.26×10^3t	5.05×10^3t
Normal force acting on top face of tool, N, lb	203**	193	184	212	322	280	278
$\frac{W_i}{s_iN}$, in.^{3}/lb	1.95×10^{-13}	2.93×10^{-13}	9.16×10^{-13}	2.59×10^{-13}	2.11×10^{-13}	2.92×10^{-13}	11.3×10^{-13}
$\log_{10} \frac{W_i}{s_iN}$	−11.710	−11.533	−11.038	−11.587	−11.676	−11.535	−10.947

* Term t is cutting time in minutes. The multiplying factor is the slope of the corresponding straight line shown in Fig. 2.

** N is calculated as follows: For instance, at V_c = 500 fpm, F_c = 215 lb, F_t = 101 lb (sharp tool forces) and shear angle ϕ = 23.2°. Thus

$$F = F_t \cos\alpha + F_c \sin\alpha = 122.9 \text{ lb } (\alpha = 6°)$$

$$\mu = \frac{F_t + F_c \tan\alpha}{F_c - F_t \tan\alpha} = 0.604, \qquad \therefore N = \frac{F}{\mu} = 203 \text{ lb}$$

in which the parameter p as given by Zener and Holloman (16) is

$$p = \frac{\frac{E'}{RT}}{\dot{\epsilon} e f_0}$$

where $\dot{\epsilon}$ is the strain rate, E' the heat of activation of the chip material, and f_0 a constant with the dimension of time^{-1}. It is the number of times per second any given atom acquires the heat of activation E'. Ignoring the small effect on H of changing strain as a result of velocity changes, and the secondary influence of strain rate, one obtains Equation [5].

Substituting Equations [4] and [5] into Equation [3] and taking logarithms, one can conclude that, as a first approximation, the logarithm of the quantity $W_i/(s_iN)$ should bear a linear relation to the reciprocal of the interface temperature, $1/T_i$.[5]

Two separate series of tests were conducted to confirm the proposed theory. In the first series, the workpiece material was annealed AISI 4142 steel of 212 Bhn. Cutting was performed dry at various combinations of feeds and speeds as listed in Table 1. In the second series, a quenched and tempered AISI 4150 (modified) steel was used. Its hardness varied from 331 to 352 Bhn at various locations of the test log.

Aside from the top-face wear measurement as described previously, chip thickness, both components of tool force, and cutting temperature also were determined. The general procedures for the measurement of the latter three quantities were, in principle, identical to those reported in earlier papers (14, 15). Tool-force and temperature readings were recorded continuously with photoelectric potentiometers. During the course of prolonged cutting of annealed AISI 4142 steel, variations in chip thickness had been found to be negligible as shown in Fig. 6. Under the cutting conditions employed, both components of tool forces increased gradually with cutting time. Inasmuch as the chip thickness remained virtually unchanged,[6] the shear angle and hence the coefficient of friction at the interface would likewise be unaltered.[7]

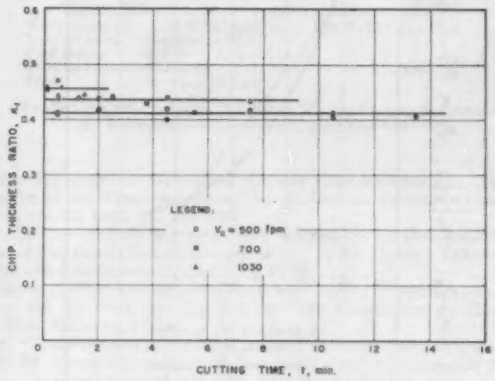

Work material: AISI 4142 steel, annealed, 212 Bhn
Tool shape: 0–6–7–7–10–0–0.015 in.
Feed: f_1 = 0.00632 ipr
Tool material: S-grade carbide
Depth of cut: w_1 = 0.100 in.

FIG. 6 CHIP-THICKNESS RATIO DURING PROLONGED CUTTING

Therefore it was concluded as an approximation that the forces acting on the top surface of the tool remained constant, being unaffected by the development of the crater wear.

Cutting temperatures as determined by the tool-work thermocouple technique at various speeds and feeds are summarized in Fig. 7. Measurements were made in relatively short-time tests (10–15 sec). Clearly, the interface temperature—cutting-speed plots are straight lines on logarithmic co-ordinates—a relationship which has been found to be almost universally true when steel is machined with sintered-carbide tools under cutting conditions which produce type 2 chips (14).

With these experimental data on hand, the quantity $W_i/(s_iN)$ and $1/T_i$ can be computed readily. Table 1 summarizes the results of the various tests on annealed AISI 4142 steel. Fig. 8 shows the relationship between the logarithm of the quantity $W_i/(s_iN)$ and the reciprocal of the average interface temperature (degrees Rankine). As may be expected from the theoretical consideration of the mechanism of tool wear at the top face, the experimentally determined points lie approximately on a straight line.

Cutting temperature as determined by the tool-work thermocouple is some sort of average temperature over the entire tool-

[5] This involves an approximation since temperature distribution over the tool-chip interface is not uniform. Its implications will be pointed out later.

[6] When the quenched and tempered AISI 4150 steel was machined, there was a small, but persistent, increase in chip thickness with time.

[7] Based on Merchant's plasticity equation, assuming α remains constant.

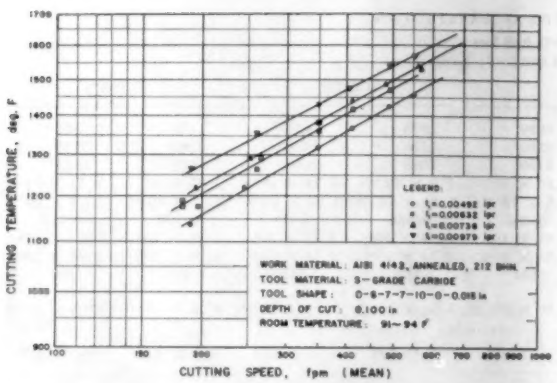

FIG. 7 CUTTING-SPEED CUTTING-TEMPERATURE RELATIONSHIPS AT VARIOUS FEEDS

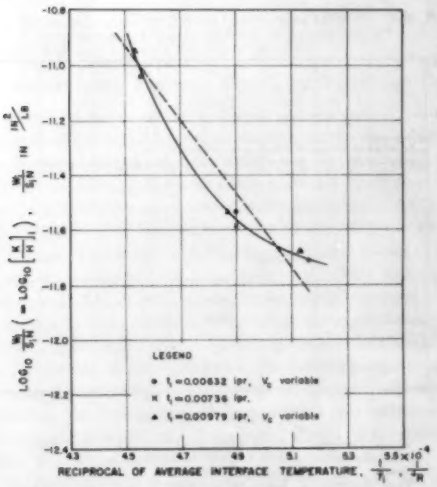

Work material: AISI 4142 steel, annealed, 212 Bhn
Tool shape: 0-6-7-7-10-0-0.015 in.
Tool material: S-grade carbide
Depth of cut: w_1 = 0.100 in.

FIG. 8 RELATIONSHIP BETWEEN $\text{LOG}_{10}\ W_t/(s_tN)$ AND RECIPROCAL OF TOOL-CHIP-INTERFACE TEMPERATURE

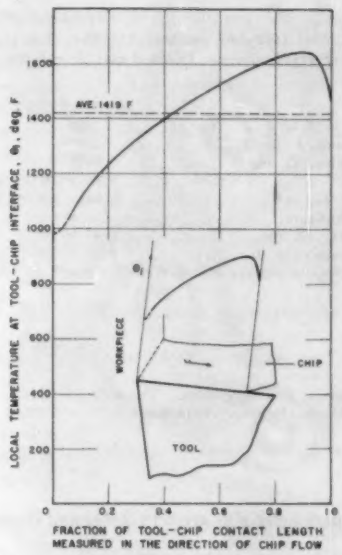

Work material: AISI 4150 (mod), annealed, 197 Bhn
Tool material: S-grade carbide
Tool shape: 0-6-7-7-10-0-0.015 in.
Depth of cut: w_1 = 0.125 in.
Feed: t_1 = 0.00632 ipr
Cutting speed: V_c = 456 fpm
Room temperature: θ_0 = 78 F
Average interface temp: θ_t = 1385 F (as determined by tool-work thermocouple)

FIG. 9 TOOL-CHIP-INTERFACE TEMPERATURE DISTRIBUTION (5)

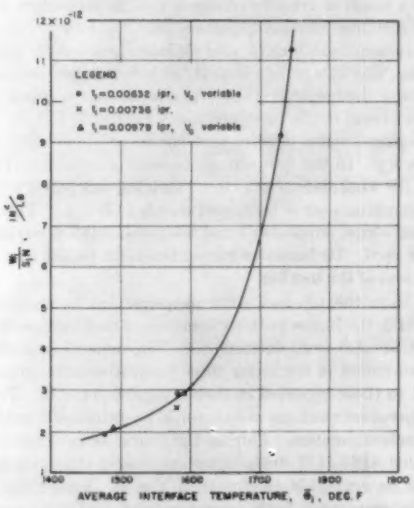

FIG. 10 RELATIONSHIP BETWEEN $W_t/(s_tN)$ AND AVERAGE INTERFACE TEMPERATURE (CUTTING CONDITIONS SAME AS IN FIG. 8)

work contact. The local temperature at the interface is not distributed uniformly but has a maximum which shifts toward the separating edge of the chip. The general trend is shown in Fig. 9. Because of the exponential relationship which exists between diffusion rate and temperature, it is obvious that the use of an average interface temperature in correlating wear at the top surface of a cutting tool actually would yield a curve slightly concave upward on the log $W_t/(s_tN)$ versus $1/T_t$ plot. This viewpoint is borne out in Fig. 8 by the solid line drawn through the experimental data.

Fig. 10 illustrates the relationship between $W_t/(s_tN)$ and interface temperature when plotted on rectangular co-ordinates. Referring to this figure, it is significant that the quantity $W_t/(s_tN)$ calculated for the same interface temperature but three totally different combinations of speed and feed (V_c = 700 fpm, t_1 = 0.00632 ipr; V_c = 638, t_1 = 0.00736 ipr, V_c = 588, t_1 = 0.00979 ipr) is virtually identical.

Results obtained from cutting quenched and tempered AISI 4150 (modified) steel of hardness ranging from 331 to 352 Bhn are summarized in Table 2. A graphical representation of the relation between logarithm of $W_t/(s_tN)$ and the reciprocal of the interface temperature is shown in Fig. 11. It will be noted that the relationship is similar to that shown for the annealed steel.

It is significant to point out that these findings concerning the influence of interface temperature on the rate of tool wear at the tool-chip contact are in harmony with an earlier paper on temperature distribution at the interface (5). The rate of top wear is

TABLE 2 SUMMARY OF QUANTITY $W_i/(s_iN)$

Work material: AISI 4150 (mod) steel, quenched and tempered, 331–352 Bhn
Tool material: S-grade carbide
Tool shape: 0–6–7–7–10–0–0.015 in.
Depth of cut: w_i = 0.100 in.
Feed: f_i = 0.00632 ipr
Cutting speed: Variable

Cutting speed, V_c, fpm	285	390	475
Avg interface temp, θ_i, deg F	1380	1470	1530
Avg interface temp, T_i, deg R	1840	1930	1990
$\frac{1}{T_i}, \frac{1}{°R}$	5.44×10^{-4}	5.18×10^{-4}	5.02×10^{-4}
Total cutting time, min	12.0	7.05	8.0
Top-face wear, W_i, in.^{3}	$0.262 \times 10^{-4}t$*	$0.817 \times 10^{-4}t$*	$2.24 \times 10^{-4}t$*
Chip-thickness ratio, r_i**	0.562	0.594	0.570
Chip-flow velocity, v_f, ipm	1.02×10^3	2.78×10^3	3.25×10^3
Chip sliding distance, s_i, in.	1.02×10^4	2.78×10^4	3.25×10^4
Normal force acting on top face of tool, N, lb	225	217	211
$\frac{W_i}{s_iN}$, in.^{3}/lb	6.06×10^{-18}	13.54×10^{-18}	32.62×10^{-18}
$\log_{10} \frac{W_i}{s_iN}$	−12.218	−11.868	−11.487

* Term t is cutting time in minutes.
** Since, in this series of tests, chip thickness changes during prolonged cutting, the values listed represent the average over the total time of cutting.

related to the average interface temperature while the temperature distribution governs the geometrical shape of the wear crater.

Conclusions

1 A simplified adhesion and transfer type of wear mechanism for the top surface of a cutting tool has been presented. The theory is consistent with observations on the role of cutting speed or feed upon the surface condition of the chip when steel is machined with carbide tools.

2 For a given cutting condition, the volumetric wear rate on the top surface of a cemented-carbide tool is substantially constant.

3 For a fixed tool-work pair the interface temperature is the governing factor influencing the rate of tool crater expressed in terms of $W_i/(s_iN)$.

Acknowledgment

This investigation was conducted at the University of Illinois and sponsored by the Office of Ordnance Research, U. S. Army, under Contract No. DA-11-022-ORD-1121. The authors hereby express their sincere appreciation to that Office for the support of the program. Acknowledgment is made to Kennametal, Inc., Latrobe, Pa., and to Mr. W. L. Kennicott, for the carbide-tool materials used in the investigation; to Prof. D. E. McFeron, Mr. D. L. Mykkanen, and Mr. Y. H. Lee, all of the Department of Mechanical Engineering, University of Illinois, for their help in collecting data, preparation of drawings, and their helpful discussion during the preparation of the manuscript. Acknowledgment is also made to Mr. B. F. Turkovich of Kearney and Trecker Corporation, Milwaukee, Wis., for his contribution during an early portion of the project, and to Miss Irene Cunningham for the typing of the manuscript.

BIBLIOGRAPHY

1 "Manual on Cutting of Metals," by ASME Research Committee on Metal Cutting Data and Bibliography, The American Society of Mechanical Engineers, second edition, 1952.

2 "United States Air Force Machinability Report," prepared by Curtiss-Wright Corporation, vol. 1, 1950; vol. 2, 1951; vol. 3, 1954.

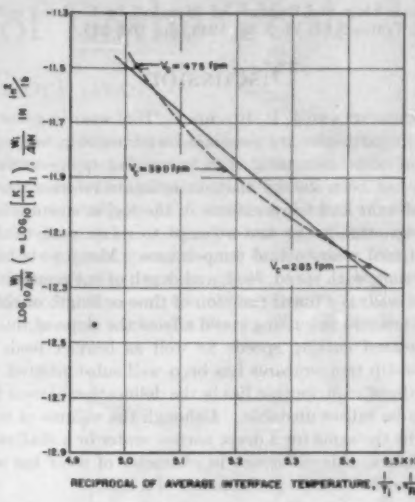

Work material: AISI 4150 (mod) steel, Q & T, 331–352 Bhn
Tool material: S-grade carbide
Tool shape: 0–6–7–7–10–0–0.015 in.
Cutting speed: Variable
Feed: f_i = 0.00632 ipr

FIG. 11 RELATIONSHIP BETWEEN $\log_{10} W_i/(s_iN)$ AND RECIPROCAL OF TOOL-CHIP-INTERFACE TEMPERATURE

3 "Properties of Cemented Carbide Compositions and Their Relation to the Wear Resistance," by W. Dawihl, *Zeitschrift Metallkunde*, vol. 32, 1940, pp. 320–325.

"Influence of Diffusion and Alloy Formation on Resistance to Wear of Cemented Carbide Compositions," by W. Dawihl, *Zeitschrift Technische Physik*, vol. 21, 1940, pp. 44–48.

"Study of Wear of Cemented Carbides," by W. Dawihl, *Stahl und Eisen*, vol. 61, 1941, pp. 210–213. All are translations by Henry Bruchter, Altadena, Calif.

4 "Some Factors Affecting Wear on Cemented Carbide Tools," by E. M. Trent, Proceedings of The Institution of Mechanical Engineers, London, England, vol. 166, 1952, pp. 64–74.

5 "Temperature Distribution at the Tool-Chip Interface in Metal Cutting," by B. T. Chao and K. J. Trigger, ASME Paper No. 54—A-115.

6 "Surface Friction of Clean Metals—A Basic Factor in the Metal Cutting Process," by Hans Ernst and M. E. Merchant, Proceedings of the Special Summer Conferences on Friction and Surface Finish, Massachusetts Institute of Technology, Cambridge, Mass., 1940.

7 "The Friction and Lubrication of Solids," by F. P. Bowden and D. Tabor, Clarendon Press, Oxford, England, 1950.

8 "Radioactive Cutting Tools for Rapid Tool-Life Testing," by M. E. Merchant, Hans Ernst, and E. J. Krabacher, Trans. ASME, vol. 75, 1953, pp. 549–559.

9 "Electric Contacts," by R. Holm, Hugo Gebers Förlag, Stockholm, Sweden, 1946, p. 214; "Mechanical Wear," edited by J. T. Burwell, Jr., American Society for Metals, 1950, chapter 14.

10 "On the Empirical Laws of Adhesive Wear," by J. T. Burwell and C. D. Strang, *Journal of Applied Physics*, vol. 23, 1952, pp. 18–28.

11 "Contact and Rubbing of Flat Surfaces," by J. F. Archard, *Journal of Applied Physics*, vol. 24, 1953, pp. 981–988.

12 "Metal Transfer and Wear," by I-Ming Feng, *Journal of Applied Physics*, vol. 23, 1952, pp. 1011–1019.

"A New Theory of Metal Transfer and Wear," by I-Ming Feng, *Lubrication Engineering*, vol. 10, 1954, pp. 34–38.

13 "Diffusion," by W. Jost, Academic Press, Inc., New York, N. Y., 1952, chapters III and V.

14 "Progress Report No. 1 on Tool-Chip Interface Temperatures," by K. J. Trigger, Trans. ASME, vol. 70, 1948, pp. 91–98.

"Progress Report No. 2 on Tool-Chip Interface Temperatures," by K. J. Trigger, Trans. ASME, vol. 71, 1949, pp. 163–174.

15 "An Analytical Evaluation of Metal-Cutting Temperatures," by K. J. Trigger and B. T. Chao, Trans. ASME, vol. 73, 1951, pp. 57–68.

16 "Plastic Flow and Rupture of Metals," by C. Zener and J. H. Holloman, Trans. ASM, vol. 33, 1944, pp. 163–235.

Discussion

A. O. Schmidt[8] and J. R. Roubik.[9] Tool wear in general and cratering in particular are associated with tool-tip temperature, the rate of wear increasing with increasing temperature. Although it has been known that an intimate relation exists between tool wear and temperatures in the region surrounding the cutting edge, this is the first attempt to relate analytically the volume of tool wear to tool temperature. Many tests have established that, with speed, feed, and depth of cut remaining constant, tool wear is a linear function of time or length of chip produced Variation in cutting speed affects the slope of the curve. That increased cutting speeds as well as heavier feeds entail higher tool-tip temperatures has been well substantiated.

The authors' contribution lies in the delineation of wear factors which can be rather unstable. Although the volume of tool top wear can be the same for a deep, narrow crater or a shallow, wide abrasion mark, this difference in character of wear has a great influence on the over-all performance of a tool.

Authors' Closure

The authors appreciate the remarks by Dr. Schmidt and Mr. Roubik. The tool crater wear measured after a cut represents the total due to (1) adhesion and transfer, (2) abrasion, and (3) chemical wear (if any). If abrasive wear for a given tool-work pair can be considered to be influenced by chip asperity hardness, it is evident that both this type of wear and that due to adhesion are dependent upon temperature in the same manner. Removal of material due to a chemical reaction would similarly depend upon temperature as an exponential function.

The degree of crater wear for the several tool-work combinations depends upon such factors as initial hardness, degree of strain hardening, presence of abrasive constituents, tendency toward adhesion (welding), and so on. Whether abrasion or adhesion wear predominates would depend upon the characteristics of a particular pair.

The authors agree that the geometrical shape of the crater has an important bearing on tool performance. For the same volume a deep narrow crater would endanger the cutting edge more than a shallow broad crater. Numerous factors affect the geometrical shape of the crater. Included are the tool-work pair, the cutting conditions, and adhesion temperature.

It is pertinent to point out that the numerical values of $W_i/(s_i N)$ tabulated in Tables 1 and 2 were calculated on the basis of a 1-in. depth of cut whereas the normal forces were determined for a 0.1-in. depth. Accordingly, the values of $W_i/(s_i N)$ are too large by a factor of 10.

Confirmation of the proposed theory of crater wear has been obtained for Type T1 (18-4-1) high-speed-steel tools turning annealed AISI 4142 steel under diversified cutting conditions. Details can be found elsewhere.[10]

[8] Research Engineer, Charge of Metal Cutting, Kearney & Trecker Corporation, Milwaukee, Wis. Mem. ASME.

[9] Machine Designer, Research and Development, Kearney & Trecker Corporation, Milwaukee, Wis. Assoc. Mem. ASME.

[10] Final Report, Contract DA-11-022-1121, August, 1955, by K. J. Trigger and B. T. Chao, Office of Ordnance Research, U. S. Army, Durham, N. C.

Chatter Vibration of Lathe Tools

By S. DOI[1] and S. KATO,[2] NAGOYA, JAPAN

This paper deals with a chatter vibration which occurs frequently when metals are being machined. It has been ascertained experimentally that the chatter is a self-excited vibration caused by the lag in fluctuation taking place in the horizontal cutting force behind the horizontal vibration of the work. Because of this delay in cutting force, it has been proved that the chatter may be expressed in terms of a difference-differential equation.

Introduction

CHATTER is the vibration of cutting tool or workpiece occurring frequently in machining metals. These vibrations are of two kinds, i.e., forced and self-excited. Those occurring in lathe work are classified into four types: (*a*) Self-excited vibrations due to flexible cutting tools; (*b*) self-excited vibrations due to deflection of main spindle or workpiece supported between both centers; (*c*) forced vibrations due to headstock gears of insufficient accuracies; and (*d*) forced vibrations due to the out-of-balance of any one of three things, the machine, the workpiece, or the dog. The authors (1)[3] investigated the chatter of type (*c*) in 1952.

Arnold (2) and Chisholm (3) investigated the chatter of type (*a*) and reported that it is self-excited vibration caused by the falling characteristic of cutting force depending upon the cutting speed. According to our experiment (4, 5) in 1953, it is ascertained that this chatter resembles in character that of frictional vibration. However, this chatter is not caused by the effect of cutting speed on cutting force. We considered that this chatter and the chatter due to the deflection of the workpiece or of the main spindle have the same cause. In 1953 Hahn (6) also reported that tool chatter is not influenced or caused by the falling characteristic of cutting force depending upon the cutting speed.

The chatter vibrations of type (*b*) are the most likely to occur and are the most troublesome for the lathe turner because they have a large amplitude of workpiece and of cutting tool. The purpose of this paper is to examine experimentally and theoretically the cause.

Experimental Research

Method of Experiment. To ascertain the causes of type (*b*) chatter, the lateral vibration of rotating workpiece and the cutting force must be measured simultaneously. When the cutting force acts on the cutting edge of a tool, the tool is slightly deflected. The deflection angle of the tool end is approximately proportional to the cutting force. If we can measure this small deflection angle of the tool end during a cutting operation, the vibration of the tool end and the cutting force can be ascertained. To insure purely elastic deflection of the tool, we employed a special tool post without upper slide, and to hold the tool rigid the upper and lower surfaces of the tool were ground down.

The chuck of a lathe held a mild-steel bar, 5 in. diam, 11.6 in. long. To simplify the cutting process an orthogonal cutting of a side lathe tool was operated on a flange taken from the work. The tool was fed by the cross spindle of the lathe so as to obtain the desired thickness of the chip. The method of our experimental apparatus is given in Fig. 1. No. 1 is the lens, No. 2 the

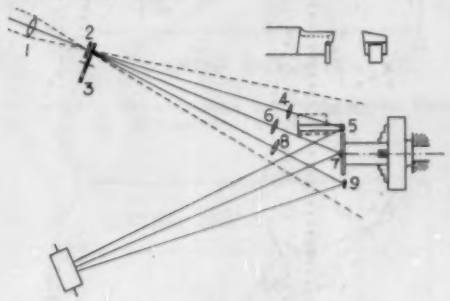

Fig. 1 Method of Experiment

small circular hole, No. 3 the time marker. Through these the light passes and is projected toward the lathe. A beam of that light passes through lens 4, is reflected by the mirror 5, pasted on the lower end of the tool, and this reflected light is recorded on a rotating film. Lens 4 is adjusted so as to bring the focus of the small hole on the rotating film. To measure the deflection angle of the tool end accurately the distance between the mirror and the rotating film must be enlarged. In this experiment it was set at 10.5 ft. The tool was 2.4 in. in length and its cross section was 0.41 in. square with a natural frequency of about 2900/sec.

To measure the lateral vibration of rotating work, another beam of the light passing through lens 6 is reflected by the mirror 7 and recorded on the same film. Mirror 7 is so centered on the work end, and the surface of the mirror is so exactly perpendicular to the rotating axis of the work, that the beam is deflected only because of the lateral vibration of the work and is not affected in any way by the rotation of the work. To increase displacement of the reflected light, the distance between the mirror and the film is lengthened. A third beam of light, passing through lens 8, is reflected by mirror 9 which is stationary, and is recorded on the same film, becoming the measuring basis of the light beams reflected by the mirrors 5 and 7.

To find the relation between the cutting force and the vibration of work in each phase, the light is interrupted by the time marker 3 at interval of 0.001 sec. To record these three lights at the same instant, thick marks are made at intervals of 0.02 sec. The cutting force and the vibration of work in each phase are noted at each period of 0.001 sec.

Preliminary measurements of relation between the deflection angles of mirrors 5 and 7 and the deflections of the cutting edge and the work were made when the statical loads were applied on the cutting edge of the tool and where the workpiece was cut. We found that there exists nearly linear relations between the load and the deflection angle as well as the deflection.

Results of Experiment. In Fig. 2 we have three parallel records

[1] Professor-Doctor, Department of Engineering, Nagoya University, Furo-cho, Chigusa-ku.

[2] Assistant Professor, Department of Engineering, Nagoya University, Furo-cho, Chigusa-ku.

[3] Numbers in parentheses refer to Bibliography at end of paper.

Contributed by the Production Engineering Division and presented at a joint session with the Research Committee on Metal Processing at the Diamond Jubilee Semi-Annual Meeting, Boston, Mass., June 19–23, 1955, of The American Society of Mechanical Engineers.

Note: Statements and opinions advanced in papers are to be understood as individual expressions of their authors and not those of the Society. Manuscript received at ASME Headquarters, June 3, 1954. Paper No. 55—SA-22.

obtained simultaneously in the cutting operation with a cutting speed of 123 fpm, a feed of 0.002 in., and a cutting angle of 85 deg. The thickness of the flange of the work was 0.24 in. The three records (*a*), (*b*), (*c*) represent the vibration of work, the fluctuation of the cutting force, and the stationary position, respectively. The heavy dots spaced every 20 dots in all of the records indicate the same instant and are connected by lines introduced to make them quickly identified in the figure. The positions of each dot in records (*a*) and (*b*) were compared with the position of the corresponding instant in record (*c*) and thus the velocity of

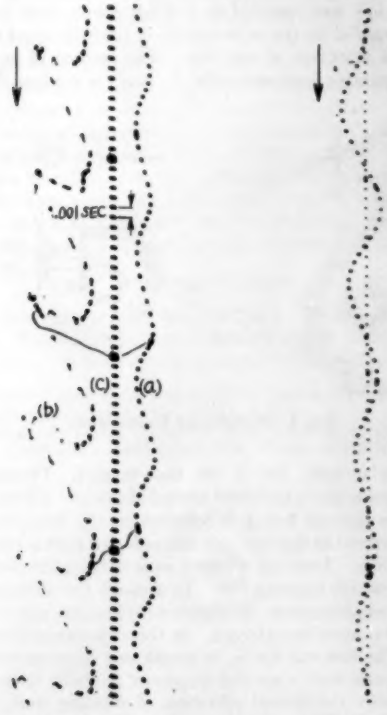

FIG. 2 EXPERIMENTAL RECORDS

FIG. 4 EXPERIMENTAL RECORDS

the measuring film need not be considered. Fig. 3 is obtained from Fig. 2 by this process. The right-hand curves in the figure represent the vibration of work and the curves on the left represent the fluctuation of cutting force. The full-line curve shows the previous cycle of vibration and the broken line, the following cycle. The frequency of this vibration is about 77/sec and this is almost equal to that obtained from the natural vibration shown in Fig. 4. This frequency depended on the size of the work or of the chuck, and was not affected by either the cutting speed, the feed, or the cutting angle of the tool. Therefore this chatter must be considered as a self-excited vibration.

In Fig. 3 the work vibrates in a somewhat elliptical orbit and its rotational direction is reverse to work rotation. This vibrating manner varied according to the cutting condition. The vibration of the work and the fluctuation of the cutting force, Fig. 3, are illustrated as observed from the recording film looking toward the lathe. As shown in this figure, the tool deflects in almost the same direction as the work deflects, and it also deflects in an elliptical orbit. The horizontal cutting force then fluctuates in a phase slightly faster than the vertical cutting force. The dots indicated

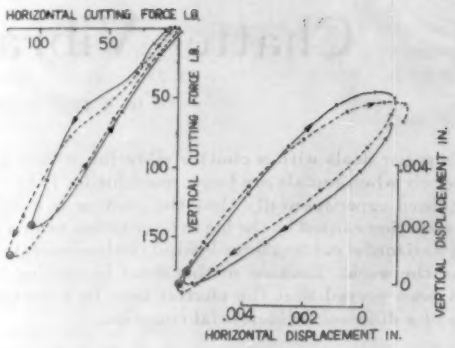

FIG. 3 CUTTING FORCE AND VIBRATION OF WORK

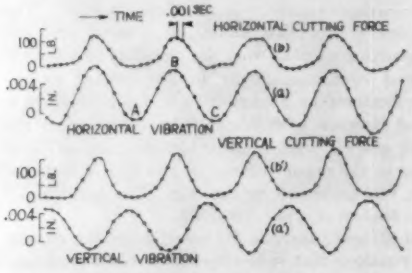

FIG. 5 HORIZONTAL AND VERTICAL COMPONENTS OF CUTTING FORCE AND VIBRATION OF WORK

by the mark ⊙ in the curve of vibration and in that of the cutting force are at the same instant.

The horizontal and vertical components of vibration and cutting force are now considered. Fig. 5 is obtained from Fig. 3. Curve (*b*) is the horizontal component of the cutting force; (*a*) the horizontal component of the vibration of the work; (*b'*) the vertical component of the cutting force; and (*a'*) the vertical component of the work. The vertically corresponding dots are at the same instant. All upper displacements in curve (*a*) correspond to the approach of the work to the cutting edge. In each cycle of curves (*b*) and (*a*), the horizontal cutting force becomes maximum at about 0.0005 sec after the instant at which the work deflects nearest to the cutting edge. Subsequently this cutting force sustains itself at a comparatively high value during the period of the work movement away from the cutting edge. The fluctuation in horizontal cutting force lags about 0.0005 sec behind the horizontal vibration of work. Further, the time in which the horizontal cutting force increases from zero to maximum in each cycle is usually shorter than that in which the force decreases from maximum to zero. These results completely coincide with that of a previous experiment (7) in which the lateral vibration of a rotating work was measured by a microscope.

The curves (*a*)(*b'*) show that the fluctuation in vertical cutting force depends on the horizontal vibration of the work and that it lags about 0.001 sec behind the horizontal vibration of the work. In curves (*b'*)(*a'*) the phase of vertical vibration lags about 140 deg behind that of the fluctuation in vertical force. The degree of this lag in phase differs widely according to the cutting conditions.

As shown in Fig. 5, the horizontal cutting force remains constant during a brief instant of each cycle of vibration; consequently, the work must be free from the cutting edge. The work

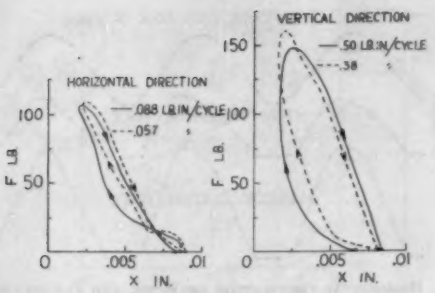

FIG. 6 FORCE-DISPLACEMENT CURVES

in this period is considered to be completely apart from the cutting edge and the horizontal cutting force is zero. In the horizontal displacement AB in Fig. 5 the work moves toward the cutting edge against the horizontal cutting force, dissipating the energy of vibration. In displacement BC in which the work moves away from the cutting edge, the horizontal cutting force acts in the same direction as the displacement of the work so that the vibration system gains the energy necessary to maintain vibration.

Fig. 6 is obtained by plotting F lb (cutting force) in the ordinate and X in. (displacement measured from a base line) in the abcissa at each cycle of the vibration. The full line in this figure shows a previous cycle of vibration and the broken line shows the following cycle. The closed area within these lines covers the amount of energy relating to the amplitude. These energies estimated diagrammatically are 0.088, 0.057 lb-in. in a horizontal direction and 0.50, 0.38 lb-in. in the vertical direction. Without exception, in 17 experimental records similar to Fig. 2 in which the cutting speed or thickness of chip was changed, certain available energies were ascertained.

The energy which is dissipated in one cycle of vibration can be estimated from the natural vibration shown in Fig. 4. In this estimate is used an equivalent mass of chuck and work which are supposed to be concentrated at the cutting position.

Figs. 7 and 8 show the balance of these energies in both horizontal and vertical directions. In those figures the available energies are a little larger than those estimated for dissipation, but on the whole both energies coincide almost completely. Therefore chatter is the self-excited vibration caused by the lag of fluctuation in the horizontal cutting force behind the horizontal vibration of the work.

The following experiments were carried out to ascertain whether, during the cutting without chatter, the fluctuation in horizontal cutting force does or does not lag behind the variation of undeformed chip thickness caused by the horizontal deflection of the work.

Method of Experiment. Work with a diameter of 2.8 in., length 20 in., was held by the chuck of a lathe. The end of this work is held by a bearing supported only in a vertical position by means of a steady rest as shown in Fig. 9. The bearing together with the work was deflected periodically by means of the eccentric roller 1, driven by the shaft 2, as shown in this figure, and thus the chip thickness was changed periodically.

To measure precisely the horizontal oscillation of the work which is rotating, a ring of mild steel was fitted on the workpiece near the place at which the work was cut. On that ring, mirror (A) was glued and its surface was sooted. Rotating the work by hand, the soot was scratched with a sharp razor blade so as to draw in a fine line a precise circle. A vertical bright line in the black matrix can be observed when a small segment of the circle

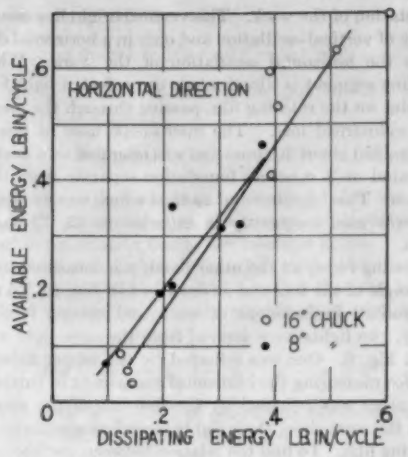

FIG. 7 BALANCE OF AVAILABLE AND DISSIPATING ENERGIES—HORIZONTAL DIRECTION

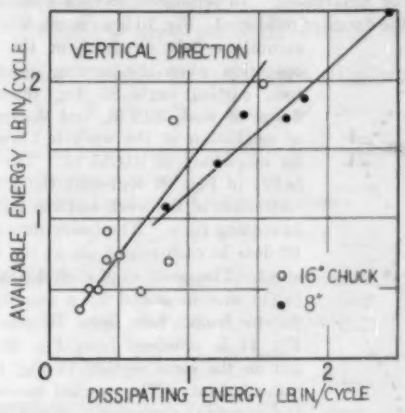

FIG. 8 BALANCE OF AVAILABLE AND DISSIPATING ENERGIES—VERTICAL DIRECTION

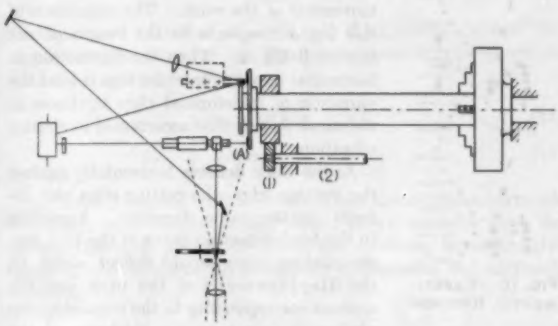

FIG. 9 METHOD OF EXPERIMENT

at the outermost position is lighted by a vertical illuminator of a microscope. The center of the circle drawn on the mirror coincides exactly with the axis of rotation of the work, so that the vertical-line segment is stationary and is not affected in any way

by the rotation of the work. This vertical bright line moves independently of vertical oscillation and only in a horizontal direction owing to the horizontal oscillation of the work. When this vertical-line segment is illuminated, the reflected light forms an image point on the rotating film passing through the microscope and the cylindrical lens. The microscope used in this experiment magnified about 20 times and was mounted on a heavy angle plate located on a concrete foundation separate from the lathe foundation. This experimental method which was devised by the authors was used frequently in experiments (5, 7) on chatter vibration.

The cutting force, on the other hand, was measured by the deflection angle of the tool end as described in Fig. 1. To measure the horizontal displacement of work and cutting force simultaneously, two lights were derived from the same light source as shown in Fig. 9. One was reflected by the mirror fitted to the tool end for measuring the horizontal component of cutting force, and the other was reflected by the fine line of the ring mirror fitted on the workpiece, these lights recording simultaneously on the rotating film. To find the relation between the fluctuation in cutting force and the deflection of work in each phase, the light source is interrupted by the time-marker at interval of 0.04 sec and thick marks are made at every interval of 0.4 sec.

Results of Experiment. An orthogonal cutting operation was made on the flange of mild steel. Fig. 10 is an example of experimental records obtained in the cutting operation when the cutting speed is 3.4 fpm, cutting angle 80 deg, thickness of flange of work 0.12 in., and the frequency of oscillation of the work is 1.5/sec with an amplitude of 0.0055 in. The records (*a*)(*b*) in Fig. 10 represent the horizontal oscillation of the work and the fluctuation in cutting force. The heavy dots at every 10 dots in each record are at the same instant. The position of each dot in records (*a*)(*b*) was measured by a sensitive comparator from a base line. By this process, Fig. 11 is obtained from Fig. 10. Each dot on the same vertical in Fig. 11 is the same instant. The upward movement in the curve (*a*) corresponds to the approaching movement of the work to the cutting edge. In each cycle the fluctuation in cutting force lags about 0.04 sec behind the movement of the work. The magnitude of this lag corresponds to the length of cut surface 0.028 in. Then the fluctuation in horizontal cutting force also lags behind the variation of undeformed chip thickness in the same way as that ascertained in chatter vibration.

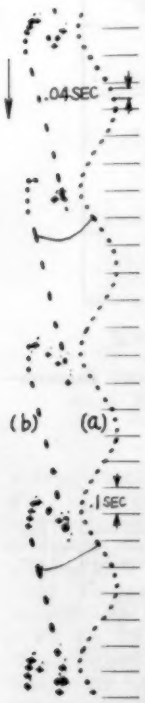

Fig. 10 Experimental Records

As the work deflects horizontally against the cutting edge, the cutting edge also deflects in the same direction. According to the load-deflection curve of the tool end, the cutting edge should deflect about 1/2 the displacement of the work and the amount corresponding to the remaining displacement is cut to the thickness of the chip. In Fig. 11 the maximum thickness of the chip is estimated to be about 0.0044 in. As shown in this figure, the cutting force remains constant during the brief instant of each cycle when the work is moving away from the cutting edge. The work in this period is thus considered to be completely apart from the cutting edge.

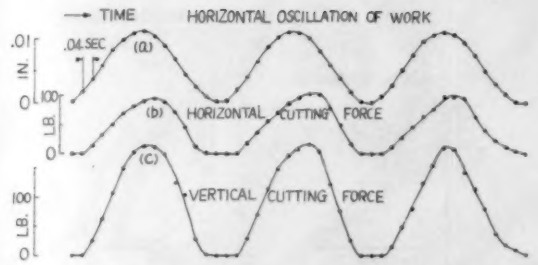

Fig. 11 Horizontal Oscillation of Work and Fluctuation of Cutting Force

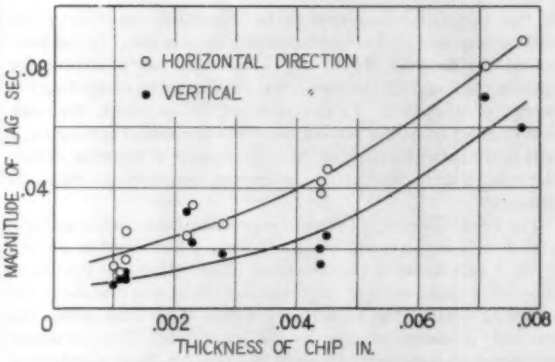

Fig. 12 Relation Between Thickness of Chip and Time Lag

The magnitude of lag in cutting force is considered to depend upon the thickness of chip. Therefore experiments were made on various chip thicknesses. In Fig. 12 results are shown of an experiment obtained from records similar to that shown in Fig. 10. In Fig. 12 the magnitude of lag increases as the chip thickness increases. This is considered to be a reasonable result.

It is considered that when the work does not leave the cutting edge at all periods of each cycle, notwithstanding the periodic deflection of work, the magnitude of time lag is much smaller than that shown in Figs. 11 and 12.

Fig. 13 shows the effects of cutting angle on the lag of cutting force. The magnitude of time lag of cutting force increases when the cutting angle is larger. The lag in cutting force is presumed to be related to the degree of chip failure.

Finally, experiments were made on various cutting speeds. As the cutting speed increases, the magnitude of time lag decreases and the length of cut surface corresponding to this time lag increases slightly.

The results of these experiments, even in a cutting operation without chatter, show that the horizontal cutting force does not reach a maximum value when the work moves horizontally nearest to the cutting edge. When the work rotates a few times after that instant, the horizontal cutting force becomes maximum and subsequently sustains itself at a comparative high value during the period of movement of work away from the cutting edge. The cause of this lag in cutting force is considered to be as follows: In the cutting producing a flow-type chip, the shear strength of chip formation depends upon the compressive stress perpendicular to the plane of shear, as indicated in Merchant's analysis of cutting. The magnitude of the compressive stress depends on the frictional resistance of the chip which slides over the tool face. Then the presence of after-effect or lag of cutting

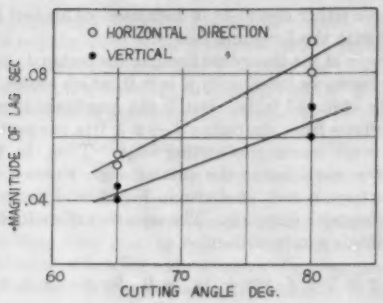

FIG. 13 RELATION BETWEEN CUTTING ANGLE AND TIME LAG

force can be explained. This is considered as a special character of cutting metals.

THEORETICAL RESEARCH

The following research introduces an equation of the chatter based on the foregoing experimental results and discusses to what extent the character of the chatter can be explained by the theoretical equation. Because chatter is caused by the horizontal vibration of work (as described), we treat the problem based upon that direction only.

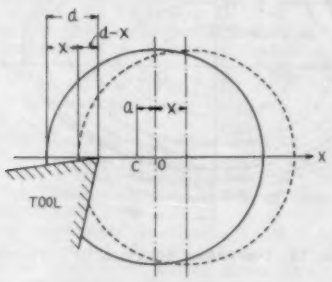

FIG. 14 WORK AND CUTTING EDGE

In Fig. 14 let C denote the center of the work before cutting. If a cut is operated on the work the center C displaces to the point O and this displacement is denoted by a. Taking O as the point of origin and indicating displacement of work by x, when the movement is in the direction away from the cutting edge, it is considered positive. Assuming, for the sake of simplicity, that the system has one degree of freedom, the expression for the chatter becomes

$$m\ddot{x} + c\dot{x} + k(x + a) = F[d - x(t - h)] \quad \ldots\ldots [1]$$

where m, c, and k are well-known physical constants, $k(x + a)$ is the spring force, and $F[d - x(t - h)]$ is the horizontal cutting force which is represented as the function of the depth of cut having the constant time lag h, where the deflection of tool is neglected.

Setting

$$\frac{c}{m} = 2n, \quad \frac{k}{m} = p^2, \quad x(t - h) = x_h$$

and

$$\frac{1}{m} F(d - x_h) - \frac{k}{m} a = f(d - x_h)$$

the preceding equation becomes

$$\ddot{x} + 2n\dot{x} + p^2 x - f(d - x_h) = 0 \quad \ldots\ldots [2]$$

N. Minorsky (8), in 1948, derived an equation for the antirolling stabilization of ships as

$$\ddot{\theta} + p\dot{\theta} + q(\lambda)\dot{\theta}_h + \omega_0^2\theta = 0 \quad \ldots\ldots [3]$$

where $\dot{\theta}_h = \dot{\theta}(t - h)$ is the retarded velocity, h being the constant time lag. He concluded that the system of Equation [3] is capable of self-excitation due to the retarded action.

We can deal with Equation [2] by a method similar to that used by Minorsky. Now, we will consider that the horizontal cutting force is proportional to the magnitude of depth of cut, so that

$$F(d - x_h) = K \cdot (d - x_h), \quad d - x \geqq 0$$

in which K is the coefficient of proportion depending upon the cutting conditions. So that we obtain

$$f(d - x_h) = -\lambda x_h$$

where $\lambda = K/m$. Replacing the last expression in Equation [2], we have the following equation

$$\ddot{x} + 2n\dot{x} + p^2 x + \lambda x_h = 0 \quad \ldots\ldots [4]$$

We try to satisfy Equation [4] by a solution of the form

$$x = x_0 e^{zt}, \quad z = \alpha + j\omega \quad \ldots\ldots [5]$$

where α is either a decrement (if $\alpha < 0$) or an increment (if $\alpha > 0$) and ω is the frequency, where $j = \sqrt{-1}$.

On substituting Equation [5] for [4] we obtain

$$z^2 + 2nz + p^2 + \lambda e^{-zh} = 0 \quad \ldots\ldots [6]$$

The real and the imaginary parts of this expression yield

$$\begin{cases} p^2 - \omega^2 + \alpha^2 + 2n\alpha + \lambda e^{-h\alpha}\cos\omega h = 0 \quad \ldots\ldots [7] \\ 2(\alpha + n)\omega - \lambda e^{-h\alpha}\sin\omega h = 0 \quad \ldots\ldots [8] \end{cases}$$

For a harmonic vibration ($\alpha = 0$), we have

$$\begin{cases} p^2 - \omega^2 + \lambda\cos\omega h = 0 \quad \ldots\ldots [9] \\ 2n\omega - \lambda\sin\omega h = 0 \quad \ldots\ldots [10] \end{cases}$$

A harmonic vibration can exist only if Equations [9] and [10] are fulfilled simultaneously. Combining these equations, we obtain the following expressions

$$\begin{cases} \omega_1 = \omega(\lambda, n, h, p) \quad \ldots\ldots [11] \\ \varphi(\lambda, n, h, p) = 0 \quad \ldots\ldots [12] \end{cases}$$

Only when Equation [12] is satisfied, can there exist a harmonic vibration with frequency ω_1. First, if we consider that the parameters n, h, and p, except λ, are constant, Equation [12] gives a certain value of parameter λ, so-called the harmonic value λ_1, i.e.

$$\lambda_1 = \frac{2n\omega_1}{\sin\omega_1 h} \quad \ldots\ldots [12a]$$

and the frequency of the harmonic vibration is

$$\frac{\omega_1^2 - p^2}{2n\omega_1} = \cot\omega_1 h \quad \ldots\ldots [11a]$$

The value of ω_1 can be obtained graphically.

Now, let us consider a small change $\Delta\lambda$ of the parameter λ from its harmonic value λ_1 for which $\alpha = 0$, $z = j\omega_1$. For $\lambda_1 + \Delta\lambda$, the corresponding value of z will be

$$z = j\omega_1 + \Delta z, \quad \Delta z = \Delta\alpha + j\Delta\omega$$

Substituting this value in Equation [6], separating the real and the imaginary parts, and carrying out calculations to the first order of small quantities $\Delta\lambda$, $\Delta\alpha$, and $\Delta\omega$, we have

$$\left\{\begin{array}{l} \dfrac{\Delta\alpha}{\Delta\lambda} \\ \qquad = \dfrac{\lambda_1{}^2 h + 2n(p^2 + \omega_1{}^2)}{\lambda_1[(2n - \lambda_1 h\cos\omega_1 h)^2 + (2\omega_1 + \lambda_1 h\sin\omega_1 h)^2]} \quad \ldots [13] \\ \dfrac{\Delta\omega}{\Delta\lambda} \\ \qquad = \dfrac{2\omega_1(2n^2 + \omega_1{}^2 - p^2)}{\lambda_1[(2n - \lambda_1 h\cos\omega_1 h)^2 + (2\omega_1 + \lambda_1 h\sin\omega_1 h)^2]} \quad \ldots [14] \end{array}\right.$$

The right-hand side of Equation [13] is always positive; hence $\Delta\alpha \gtrless 0$ for $\Delta\lambda \gtrless 0$, but since $\alpha = 0$ for $\Delta\lambda = 0$, this means $\alpha \gtrless 0$ for $\Delta\lambda \gtrless 0$. Therefore, if $\Delta\lambda > 0$(that is, $\lambda > \lambda_1$) the motion occurs with increments, and if $\Delta\lambda < 0(\lambda < \lambda_1)$ the vibration dies out, and only for $\Delta\lambda = 0$ (that is, $\lambda = \lambda_1$) the harmonic vibration exists.

For the parameters n, h, and p, the same expressions as Equation [13] can be led as [15] $\sim$ [17]

$$\left.\begin{array}{l} n_1 = \dfrac{\lambda\sin\omega_1 h}{2\omega_1} \\ \dfrac{\Delta\alpha}{\Delta n} = \dfrac{-2\omega_1(2\omega_1 + \lambda h\sin\omega_1 h)}{[(2n_1 - \lambda h\cos\omega_1 h)^2 + (2\omega_1 + \lambda h\sin\omega_1 h)^2]} \end{array}\right\} \ldots [15]$$

Since $\sin\omega_1 h > 0$ from Equation [10], $\Delta\alpha/\Delta n < 0$, so that $\alpha \gtrless 0$ for $\Delta n \lessgtr 0$

$$\left.\begin{array}{l} h_1 = \dfrac{1}{\omega_1}\sin^{-1}\dfrac{2n\omega_1}{\lambda} \\ \dfrac{\Delta\alpha}{\Delta h} = \dfrac{2\omega_1(2n^2 + \omega_1{}^2 - p^2)}{[(2n - \lambda h_1\cos\omega_1 h_1)^2 + (2\omega_1 + \lambda h_1\sin\omega_1 h_1)^2]} \end{array}\right\} \ldots [16]$$

If $(2n^2 + \omega_1{}^2 - p^2) > 0$, $\Delta\alpha/\Delta h > 0$, hence $\alpha \gtrless 0$ for $\Delta h \gtrless 0$, and if $(2n^2 + \omega_1{}^2 - p^2) < 0$, vice versa

$$\left.\begin{array}{l} p_1{}^2 = \omega_1{}^2 - \lambda\cos\omega_1 h \\ \dfrac{\Delta\alpha}{\Delta p} = \dfrac{-2p_1(2n - \lambda h\cos\omega_1 h)}{[(2n - \lambda h\cos\omega_1 h)^2 + (2\omega_1 + \lambda h\sin\omega_1 h)^2]} \end{array}\right\} \ldots [17]$$

If

$$(2n - \lambda h\cos\omega_1 h) > 0, \quad \Delta\alpha/\Delta p < 0$$

then $\alpha \gtrless 0$ for $\Delta p \lessgtr 0$, and if

$$(2n - \lambda h\cos\omega_1 h) < 0$$

vice versa.

From the foregoing, the systems given by Equation [2] are capable of self-excited vibration due to the time lag h.

Previously we have dealt with this problem in the region where $d - x \gtrless 0$. In this region it is evident that there can scarcely exist the stable vibration ($\alpha = 0$); in most cases the vibration dies out ($\alpha < 0$) or the amplitude increases indefinitely ($\alpha > 0$). According to the foregoing experimental researches, the chatter in the region $d - x \gtrless 0$ is unstable in general and in most cases its amplitude either decreases or increases. This fact is in good agreement with the foregoing theory.

On the basis of the theory outlined, in the region $d - x \gtrless 0$ the amplitude increases indefinitely if $\alpha > 0$, which seems to be contrary to the observed facts. But, if the amplitude increases, the motion deviates from the region $d - x \gtrless 0$ in one part of a cycle when the work leaves the cutting edge. Thus, in the region in which the work leaves the cutting edge, where $d - x < 0$, the cutting force is zero, as shown in Fig. 5, and the motion is a free vibration with damping. The equation of such vibration of large amplitude can be written

$$\left.\begin{array}{ll} \ddot{x} + 2n\dot{x} + p^2 x + \lambda x_k = 0 & \text{for } d - x \gtrless 0 \\ \ddot{x} + 2n\dot{x} + p^2(x + a) = 0 & \text{for } d - x < 0 \end{array}\right\} \ldots [4a]$$

This equation is solved graphically by Jacobsen's "phase-plane-delta" method (9). Fig. 15 shows an example of graphical solution using the cutting conditions of Fig. 2; viz, $d = 0.002$ in., $p = 2\pi f = 377$/sec ($f = 60$/sec), $n = 40$/sec, $h = 0.0005$ sec, and $K = k_s b = 172{,}000 \times 0.24$ lb/in. (k_s is the specific horizontal cutting force and b is the thickness of flange) and $\lambda = 2.45 \times 10^5$/sec.^{2} The harmonic value of the parameter λ in this case is

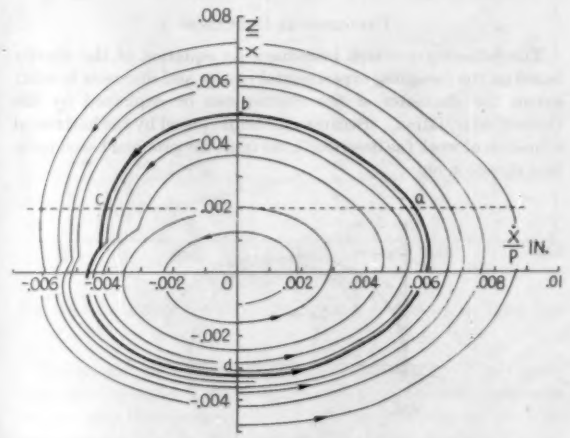

Fig. 15 Graphical Solution of Vibration

$$\lambda_1 = 1.62 \times 10^5/\text{sec}^2$$

so that $\alpha > 0$.

As shown in Fig. 15, the curves starting near the origin spiral away from it, while those starting far from the origin spiral toward it, and there exists a limit cycle a-b-c-d-a. In the segment a-b-c of the limit cycle, in which $d - x < 0$, the work leaves the cutting edge. Thus it is evident that the amplitude cannot increase indefinitely even if $\alpha > 0$, but there exists a stable limit cycle with such a sufficient amplitude to cause the work to leave the cutting edge in one part of the cycle. In practice this type of chatter vibration is most common. The amplitude of the limit cycle is in good agreement with that of Fig. 2.

Further, the stability or instability of the system can be drawn by Equations [13], [15], [16], and [17]; viz, (a) the vibrations are liable to occur when the magnitude of cutting angle of tool is large and the length of the cutting edge engaged in cutting and the wear of the edge are large, corresponding to the large value of the parameter λ; (b) the vibrations cannot occur when the value of n is beyond a certain limit; (c) since the magnitude of the time

lag seems to depend on the cutting speed, the chatter cannot occur when the cutting speed is higher than a certain value.

Finally, the authors believe that if further investigations are made of the foregoing time lag in cutting without chatter the occurrence of chatter in practice will be better explained.

Conclusions

The fundamental cause of chatter vibration and the presence of vibrational energy have been ascertained. The chatter vibration is a type of self-excited vibration caused by a lag in fluctuation of horizontal cutting force existing behind the horizontal vibration of work. Because of this lag some amount of energy per cycle is available for maintaining or increasing the vibration of the workpiece. It is ascertained also in some cases of cutting without chatter that the fluctuation in horizontal cutting force lags behind the variation of undeformed chip thickness. Next, because of this delay in cutting force, it has been proved that the chatter vibration is expressible in terms of a difference-differential equation and many characters of chatter vibration can be explained theoretically.

BIBLIOGRAPHY

1 "On Chatter Vibration Caused by the Headstock Gears of Lathe," by S. Doi and S. Kato, Transactions of the Society of Mechanical Engineers, Japan, No. 74, 1952, p. 1.

2 "Mechanism of Tool Vibration in Cutting of Steel," by R. N. Arnold, Proceedings of The Institution of Mechanical Engineers, London, England, vol. 154, 1946, p. 261.

3 "The Causes of Chatter Vibrations," by A. J. Chisholm, *Machinery*, London, England, vol. 75, 1949, p. 51.

4 "On Chatter Vibration Due to Flexible Lathe Tool," by S. Doi and S. Kato, Transactions of the Society of Mechanical Engineers, Japan, No. 86, 1953, p. 26.

5 "On Chatter Vibrations of Lathe Tools," by S. Doi, Memoirs of Department of Engineering, Nagoya University, Japan, vol. 5, 1953, p. 179.

6 "Metal-Cutting Chatter and Its Elimination," by R. S. Hahn, Trans. ASME, vol. 75, 1953, p. 1073.

7 "On the Chatter of Lathe Tool (1st report). On the Cause of Chatter," by S. Doi, Transactions of the Society of Mechanical Engineers, Japan, No. 10, 1937, p. 94.

8 "Self-Excited Mechanical Oscillations," by N. Minorsky, *Journal of Applied Physics*, vol. 19, 1948, p. 332.

9 "On a General Method of Solving Second-Order Ordinary Differential Equations by Phase-Plane Displacements," by L. S. Jacobsen, *Journal of Applied Mechanics*, Trans. ASME, vol. 74, 1952, p. 543.

Discussion

N. H. Cook.[4] The authors are to be commended on their use of optical measurements as applied to machine-tool vibrations. They have been employing these methods skillfully for many years and have been able to obtain accurate phase relationships. Their general experimental excellence can be verified by the amazingly close match of available and dissipating energies as shown in Figs. 7 and 8 of the paper. However, it is not at all clear why the authors feel that the vibration is caused solely by the force lag in the horizontal direction. Indeed, the magnitude of available energy in the vertical direction is larger by an order of magnitude than that in the horizontal direction. The particular vibration investigated by the authors has two degrees of freedom and the problem must be considered in its entirety as there is very strong cross-coupling between motion in the horizontal and vertical direction. It is readily shown[5,6] that if a linear two-degree-of-freedom system is considered there are several possible types of instability. Of these only two generally develop in practice. One is basically due to variation of force with velocity. This is the same general type as investigated by Arnold and Chisholm on a single-degree-of-freedom system. The other type of vibration is due primarily to the strong cross-coupling between the horizontal and vertical directions. It is this type that the authors have investigated. A theoretical investigation of the two-degree system[6] shows that the time lag observed by the authors is an effect rather than a cause. However, there are no critical experimental data to show whether this lag is a cause or an effect.

Based upon the disputable assumption that the vertical motion is unimportant, the authors have obtained a solution for the single-degree-of-freedom nonlinear case involving horizontal vibrations which are larger than the undeformed chip thickness. The authors feel that vibrations of amplitude less than the chip thickness will not be self-sustaining. It is the experience of the writer and of others that the horizontal vibrations can be of any size up to the chip thickness but seldom become appreciably greater than this amount (as indicated by the authors' limit cycle).

It would be of interest to obtain a solution for the two-degree-of-freedom system based upon the horizontal time-lag theory. The writer also would like to hear the authors' comments on vibration of tools which are extremely stiff in the horizontal direction compared to the vertical direction. Such tools (as investigated by Arnold, Chisholm, Saljé, and Doi) do vibrate with large vertical amplitude and insignificant horizontal amplitude.

R. S. Hahn.[7] The authors have presented some very interesting data derived through the use of an ingenious method for measuring lathe vibrations.

There are some interesting questions to consider in connection with these tests.

In studying the stability of a system it is usually best to confine oneself to small oscillations about the equilibrium position, thereby avoiding nonlinearities. The data of Fig. 5 show the chatter after it has attained considerable magnitude. It is not purely sinusoidal. Have the authors similar data pertaining to small oscillations that do not allow the tool and work to separate?

According to Fig. 5 of the paper there is a very slight and hardly discernible phase lag between the vibration and the force. To the casual glance they would seem in phase. In reality the displacement of the tool is being measured and it is tacitly assumed that the force on the tool is in phase with the motion of the tool. Actually one is dealing with a two-degree vibrational system in which one oscillator (a mass on a spring), the workpiece system is coupled by a spring (the tool-work contact) to another oscillator the tool system. The workpiece oscillator has an uncoupled natural frequency of 77 cps. The tool oscillator has a natural uncoupled frequency of 2900 cps. When the two systems are coupled together it is possible for the 77-cps system to "drive" the 2900-cps system and to do so with a very small phase lag. In other words can one be sure that the phase lag observed is entirely due to cutting phenomena and not partially due to the vibratory system?

The writer, on the other hand, is inclined to agree with the authors that some sort of lag takes place. For example, the writer has evidence[8] which indicates that appreciable time is required for the establishment of stress-thermal-strength conditions on and in the vicinity of the shear plane as evidenced by

[4] Assistant Professor of Mechanical Engineering, Massachusetts Institute of Technology, Cambridge, Mass.

[5] "Beitrag zur Theorie der Selbsterregten Schwingungen," by Hans Stefaniak, *der Maschinenmarkt*, June, 1954.

[6] "Self-Excited Vibrations in Metal Cutting," by N. H. Cook, ScD thesis, Massachusetts Institute of Technology, Cambridge, Mass., 1955.

[7] Research Engineer, Heald Machine Company, Worcester, Mass. Mem. ASME.

[8] "Some Observations on Chip Curl in the Metal-Cutting Process Under Orthogonal Cutting Conditions," by R. S. Hahn, Trans. ASME, vol. 75, 1953, pp. 581–590.

the time required for the chip curvature to reach equilibrium.

It should be pointed out that the data of Fig. 5 deal with conditions where "feedback" is occurring whereas those of Fig. 11 apparently deal with very low speed and are not subject to feedback.

The authors' Equation [1] is essentially identical to the writer's equation for feedback in grinding chatter.[9] The Nyquist stability criteria could equally well be applied to this equation also.

A. O. Schmidt,[10] B. F. Turkovich,[11] and J. R. Roubik.[12] An interesting extension of the authors' previous investigations is presented. This report is certainly based on painstaking and well-devised experiments. If these tests were extended or repeated with higher cutting speeds it would be most helpful to those concerned with practical metal-cutting applications. Some of the results of the reported experiments serve to confirm certain conceptions of metal cutting at low speeds. The explanation as given for the horizontal deflection of tool and workpiece can aid us in understanding how, at slow cutting speeds, a cutting fluid has a chance to exert a lubricating effect between the chip and tool face.

We look forward to another report from these investigators and hope they can direct their attention to conditions more closely resembling those encountered in production shops.

E. Saljé.[13] Doi and Kato's work in the field of self-excited vibration is evidently significant. It is likely to result in drastic innovations in the treatment of self-excited vibrations attendant on machining operations. The authors are to be congratulated on their distinguished contribution.

Optical measurement of forces and deflections, while simple, is reliable and precise. The authors may be assumed to have made sure that the work and the tool were the only elements capable of motion in the system. Had this not been the case, it would be uncertain whether it was possible to measure a static cutting force—but one varying with time—by the deflection of the cutting tool. The actual magnitude of the force would have been distorted owing to inertia and damping forces. There could also have been phase displacement. Specifically, however, the phase of the force relative to the deflection is to be ascertained with great precision. Indeed, the chief developments that follow are based essentially on this quantity h.

Another point: The ratio of observed tool displacements to work deflections must be small; otherwise the results will again be falsified.

Finally, it may be noted that sources of error may arise in reproduction of diagrams, as when graphs are constructed from oscillograms. The writer is thinking particularly of Figs. 2, 3, 5, and 6.

A salient point is the authors' simultaneous measurement of deflections and forces, the energies being determined from the result. This technique opens up new possibilities in the study of self-excited oscillations. Tendencies in the same direction are to be found in the Russian literature. All of the data indicates that Arnold's declining force-speed characteristic does not afford a complete explanation of self-excited oscillation.

The lag h measured by the authors between the peaks for deflection and force may be regarded as the most important feature of the article. The lag h makes possible an unstable condition such as the authors have demonstrated for one degree of freedom. Besides, the lag is dependent on cutting conditions (chip breakers, cutting angle) and we can at last anticipate exact explanations for certain vibration phenomena.

In future work, the relationship between lag and external cutting conditions is particularly in need of clarification. In this connection, special importance would seem to attach to the range of higher cutting speeds from 80 to 120 m/min, or about 240 to 360 fpm, and greater chip thicknesses (with continuous chip).

Authors' Closure

The authors greatly appreciate the most interesting discussions of Dr. Cook, Dr. Hahn, Dr. Schmidt, Dr. Turkovich, Dr. Roubik, and Dr. Saljé.

(1) Dr. Hahn and Dr. Saljé, in connection with the measuring method of cutting force, remark that the displacement of cutting edge lags behind the cutting force due to the inertia of cutting tool and the damping force. It is indeed a fact that the lag of cutting force shown in Fig. 5 is partially due to the tool inertia. But the amount of the lag is considered to be less than $^1/_{1800}$ sec, because the natural frequency of tool is 2900 cps.

(2) Dr. Hahn's remark as to small oscillations that do not allow the tool and work to separate is most interesting. One record of such vibrations has been reported in (5), figs. 70 and 72. The authors intend to carry out further investigations on this problem.

In connection with "feedback," the experimental result of chatter not subject to feedback was reported in (5), fig. 79. According to that report, the lag of horizontal cutting force was ascertained similarly to that of Fig. 5 of this paper; but the variation mode of the horizontal cutting force in fig. 79 differed somewhat from that of Fig. 5, and the amount of available energy was less than that of Fig. 6 of the paper.

(3) Dr. Cook asks why the authors feel that the chatter is caused solely by the force lag in the horizontal direction. The authors consider that the cause of chatter is due to the horizontal vibration of work. If the horizontal vibration is initially started in workpiece at its own natural frequency, the area of cut, and thus the vertical cutting force, will fluctuate with that frequency setting up the vertical vibration of work. According to the authors' experiments, it was ascertained that when the chatter was excited the horizontal amplitude of work was enlarged faster than that of vertical; on the other hand, when the chatter died out the horizontal amplitude was decreased faster than that of vertical. According to the experiments on prevention of chatter, chatter can be effectively avoided by preventing both the horizontal vibration of work and of cutting edge. It was observed that when the natural frequency of work differed in vertical and horizontal directions, the vertical vibration of work having its horizontal natural frequency was caused.

Dr. Cook remarks that two types of chatter develop in practice, one due to variation of cutting force with velocity, the other the same as studied in the paper. However, the authors believe that in practical cutting operation there is no self-excited chatter caused solely by the variation of vertical cutting force with velocity. In other words, there is no chatter which is not accompanied by variation of area of cut and which does not produce chatter marks on cut surface.

---

[9] "On the Theory of Regenerative Chatter in Precision-Grinding Operations," by R. S. Hahn, Trans. ASME, vol. 76, 1954, pp. 593–597.

[10] Research Engineer, Charge of Metal Cutting, Kearney & Trecker Corporation, Milwaukee, Wis. Mem. ASME.

[11] Kearney & Trecker Corporation.

[12] Machine Designer, Research and Development, Kearney & Trecker Corporation. Assoc. Mem. ASME.

[13] Dr. of Engineering, Lehrstuhl für Werkzeugmaschinen und Betribslehre, Technischen Hochschule, Aachen, Germany.

Study of Die Wear by Means of Radioactivated Surfaces

By B. J. JAOUL,[1] PARIS, FRANCE

The recent development of the production of radioactive isotopes has given rise to a number of new techniques which may be applied in several fields of science, especially medicine, biology, chemistry, and mechanics. The study of wear by friction is a very good field for applying radioactivation techniques. Several investigations have been made on gear wear, ram wear, and so on. In these studies, one of the abrading members is radioactive and the products of its wear may be located in the lubricant. In the study of dry friction, e.g, in cylinders, automobile tires, tools, etc., the radioactive particles may be found on the unactivated member. In this paper a particular application is explained—namely, the wear of a die face during the hot extrusion of steels.

Introduction

A SUBSTANCE that is put into the path of neutrons flowing in an atomic generator becomes radioactive. Such an unstable radioactive isotope yields α, β, or γ rays by disintegration of its atoms. These α, β, or γ rays are, respectively, helium ions, electrons, or photons. The number of the atoms that disintegrate per unit of time is proportionate to the number of radioactive atoms. Thus the development of radiation intensity in time is

$$N = N_0 e^{-\lambda t}$$

Here N is the number of rays at time t, N_0 at the start, and λ is the probability of destruction of an atom per unit of time, which is a characteristic of a given material. The half life is the specific time required for the activity to be reduced to one half

$$T = \frac{Ln2}{\lambda}$$

The half lives of the radioactive isotopes vary from a fraction of a second to millions of years.

The radiation energies, as well as the ability to penetrate matter, are subject to wide variations. α rays are stopped by an aluminum sheet of a few thousandths of a centimeter in thickness, β rays by an aluminum shield a few millimeters thick, γ rays are much more penetrating and can overcome a few centimeters of lead.

There are numerous methods for the detection and study of radiations. Quantitative measurements are based on the ionization of the gases in which the rays travel; thus the detection apparatus consists of ionization chambers with two electrodes. The Geiger-Müller tubes permit the detection of the rays, i.e., they count the number of disintegrating atoms, and thereby deduce the number of radioactive atoms that are in front of the tube. Also, the sensitivity is a very important factor; it is theoretically possible to observe the disintegration of even only one atom. Therefore it would be possible to use an infinitely small amount of radioactive product. Furthermore, since the radiation affects photographic film, it is possible to photograph radioactive elements, taking an "autoradiograph." This method is less precise and quantitative than the former, but locates the emitting atoms, permitting a different type of determination.

Wear Study Related to Homogeneous Radioactivated Mass

Radioactive techniques show up the movement of atoms in materials, in parts or even in a machine.

We have used this method for a particular application, namely, the wear of the die face during the hot extrusion of steels. During the Sejournet extrusion process of the "Comptoir Industriel d'Etirage et Profilage des Metaux" such dies are subject to very severe service conditions. The temperature of the billets may range up to 1300 C and the pressures are about 100 kg per sq mm.

The die, made of a 10 per cent tungsten tool steel, was exposed for about 2 days to the neutron stream of the atomic pile at Chatillon. The tungsten became radioactive to the extent of about 1.5 mc per gram.

A curie, i.e., the radiation emitted by 1 gram of radium, is equivalent to 3.7×10^{10} rays per sec. It is thus possible to determine the weight of steel of the die which corresponds to a certain level of impulses. All factors being known, 1 mg of die steel had to produce 1500 impulses per min immediately after irradiation. But this value varies with time; while the half life (24.1 hr) of tungsten is known, other elements may interfere, so that it is better to keep a standard for comparison. This control was provided by chips of the same metal which were placed in the atomic pile together with the die and provided a standard for the decreases in radioactivity.

It is thus possible to observe and weigh very small particles of the die metal with an accuracy of about 10^{-6} grams.

Determinations of radioactivity were made on several sides of the extruded bars, giving average wear under normal conditions. In some cases a certain die shape wore by a definite amount per meter, while other shapes wore to an extent that was hardly measurable. The influence of temperature, ingot surface, rate of extrusion, die surface, and lubricant, etc., on die wear was evaluated.

This radioactivation method of the determination of die wear has several disadvantages:

1 The dimensions of the experimental die are limited by the compartments of the atomic pile. Thus only the wear in the extrusion of small round bars, but not the extrusion of shapes, could be studied.

2 Readings must be taken quickly, the half life of tungsten being only 1 day. The degree of accuracy decreases by half each day, and this method permits the activation only of the atoms in the metal.

3 The part of the extruded bar that wears the die can be determined, but there is no indication of the points where this wear has been substantial.

[1] Doctor of Physical Sciences, École Nationale Supérieure des Mines de Paris.

Contributed by the Production Engineering Division and presented at the Diamond Jubilee Semi-Annual Meeting, Boston, Mass., June 19–23, 1955, of The American Society of Mechanical Engineers.

Note: Statements and opinions advanced in papers are to be understood as individual expressions of their authors and not those of the Society. Manuscript received at ASME Headquarters, June 30, 1954. Paper No. 55—SA-24.

Thus another method had to be developed to study wear distribution on the die.

Surface Activation

The surface of a sample can be immersed in a radioactive bath for a period of time sufficient to insure a penetration of the radioactive atoms into the metal, either by exchange or by diffusion. The surface radioactivation of the metal decreases very rapidly as the metal is analyzed in depth at a given point. The concentration of radioactive elements may be stated as a function of distance from the surface. When these conditions are known, a curve can be developed to show radioactivity versus depth, and the determination of the radioactivity at a given point of the die will show the amount of metal that has been worn away.

In the series of experiments, the selection of a suitable radioactive element for the penetration test was the first problem. The die being tool steel, an exchange of the atoms of the die with those of a radioactive ferrous salt was tried first.

Surface Activation With Fe 59. Experiments were conducted with die-steel samples whose surface was 20 × 20 mm, thickness 6 mm, and weight about 25 grams.

The radioactive bath used was a solution of ferrous chloride, the atomic weight of the iron atoms being 55 and 59 (50 per cent of each). The radioactive solution, provided by the Atomic Energy Research Establishment of Harwell, England, had a total activity of 10 microcuries. Iron 55 decomposes, giving x rays (5 kw) that are not detectable by the Geiger tube. Iron 59, whose period is 47 days, gives out γ rays and β rays. As a result of the experimental conditions (shields employed, efficiency of the Geiger tube), the instrument recorded the same number of γ rays and of β rays.

The contact of the specimen with the radioactive solution has been maintained for a definite time, the surface having previously been polished. After cleaning the surface, the Geiger tube records 2400 impulses per min. To determine the penetration of the radio elements, the sample is weighed with a precision of $^1/_{100}$ mg, then lightly polished (taking care of possibilities of contamination of the lower layers), and weighed again. It is thus possible to determine the amount of metal removed by polishing.

Experiments were run with two solutions: 20 hr with a 20 per cent solution, and 4 days with a 5 per cent solution.

It is thus possible to relate radioactivity to depth of penetration, as shown in Fig. 1.

This method has the advantage of permitting the measurement of wear at a given point of a surface. In so far as dies are concerned, it should be interesting to study the entire contact area, sq mm by sq mm. For that purpose, a shield is required which passes only rays from the surface section under review. This condition is difficult to meet; indeed, the γ rays of Fe 59 can only be stopped to the extent of 90 per cent by a lead shield of 5 mm thickness. On the one hand, the method of study of the die surface limits the shield thickness; on the other hand, there will always be a certain amount of parasitic radiation emanating from the whole surface. To get a complete picture, the die actually should be cut up, but then the advantage of a nondestructive testing method would be lost.

To avoid these difficulties, a radioactive element should be selected which gives out only β rays. The radioactivity of this element should have a rather extended half life, and should be easily available with large specific activities. These conditions are best met by Phosphorus 32.

Surface Activation With P 32. Phosphorus 32, which has a half life of 14.3 days, becomes stable phosphorus 31 under emission of a β ray. The "Commissariat a l'Energie Atomique," French organization for atomic research, was able to supply us with large amounts of phosphorus 32 in the form of a solution of phosphoric acid. However, two problems arise in the use of this element:

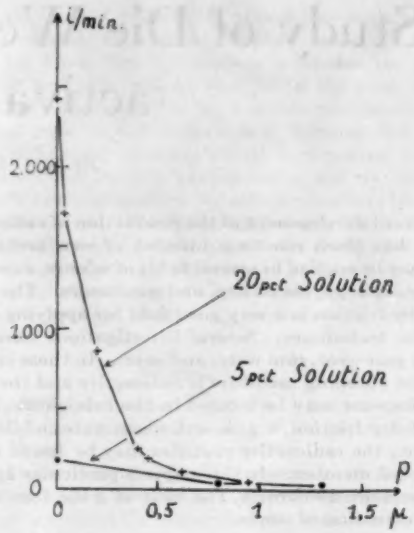

Fig. 1 Activity Versus Depth After Immersion in Solutions With 5 Per Cent and 20 Per Cent of Fe 59

1 Penetration in depth of the metal. It is no longer possible to assume that merely an exchange of radioactive and nonradioactive elements takes place. The mechanism of penetration can only be a case of etching or diffusion. But it is known that the diffusion coefficient of phosphorus in steel is very low.

2 Although phosphorus causes brittleness in steel, and phosphorus atoms entering the metal must be considered to have a deleterious effect, only small amounts are used in this experiment. The largest radioactivities were developed during preliminary tests with an atomic P-concentration in the metal of much less than 10^{-4} per cent, a figure which is negligible compared with the amount of phosphorus that is present in the steel. The mere immersion of the tool steel in a very dilute solution of phosphoric acid does not change the mechanical properties of the metal.

Furthermore, if the phosphorus can be induced to penetrate to a sufficient depth below the surface of the metal, conditions will be excellent for studying wear. Preliminary tests were repeated under the same conditions as with the radioactive iron. The solution had an activity of 1 millicurie per cu cm, corresponding to a very large dilution, and the tool was activated by immersion for different lengths of time at several temperatures.

Very high radioactivities were obtained on the surface before cleaning; up to 2,000,000 impulses per min on a 4 sq cm area. But the specimen was covered with a pulverulent layer that is removed by washing in water, and the first measurements were made after a light polishing.

The curves in Fig. 2 show the number of rays per minute as a function of the polishing depth at different temperatures and periods of immersion. The first value corresponds to 0.1 micron, and is measured after the first light polishing following the washing of the specimen.

The absolute values of radioactivity cannot be considered, because the concentration of the radioactive solution has not always been the same.

Plotted against logarithmic co-ordinates, the curves are fairly

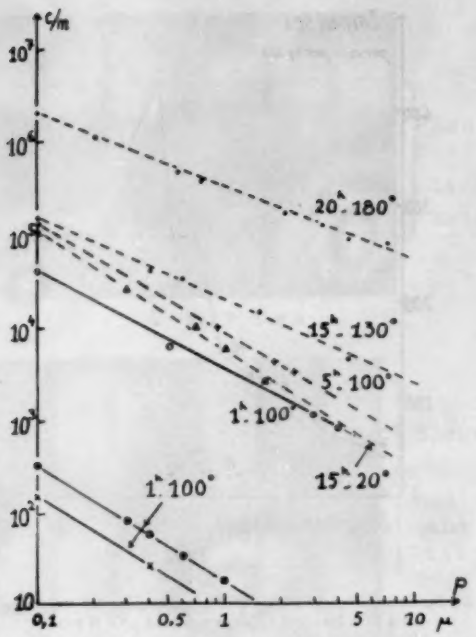

FIG. 2 ACTIVITY VERSUS DEPTH AFTER IMMERSIONS OF SEVERAL TIMES AND AT SEVERAL TEMPERATURES IN THE P_{32} SOLUTION

straight lines, and correspond to the simple relation

$$\log N = A + m \log p$$

in which m is the slope. This relationship has of course no physical meaning, but gives a good approximation of the results. Also

$$p = p_0 \left(\frac{A}{A_0}\right)^n$$

where p is the depth in microns, p_0 the 0.1 depth, corresponding to A_0. Following are the values obtained for n:

After 15 hr, 20 C: $n = 0.75$
After 1 hr, 100 C
After 5 hr, 100 C
: $n = 1.0, 0.80, 0.85, 0.85$
After 15 hr, 130 C: $n = 1.10$
After 20 hr, 180 C: $n = 1.25$

The variation of the exponential n is small and seems to depend not on the time, but only on the temperature of the radioactive bath.

These curious results need an explanation, as to how the phosphorus diffuses so far into the steel.

It is possible to assume that the penetration is only apparent, and that the radioactive atoms might have been forced into the metal during polishing. It is difficult to make a precise balance of radioactivity, including the determination of radioactivity removed by the polishing papers. But there is a point that permits the rejection of a packing hypothesis, namely, the variations of penetration while the polishing conditions are always the same. Moreover, in the course of the experiments with extrusion it can be shown that penetration did actually take place.

Another hypothesis might be that the surface of the specimen being not perfectly polished before activation, a coating of radioactive solution might merely have penetrated to the base of the surface scratches; thus radioactive elements would only be found when the lowest level is reached. But the pitch of the surface irregularities is smaller than the depth of penetration.

In attempting to arrive at a determination of the kind of penetration that took place, readings were taken on other steels. A low-carbon stainless steel showed no penetration of radioactivity after an immersion of 1 hr at 100 C in the irradiated P-solution. But in a molybdenum stainless steel with some corrosive susceptibility, there may be an appreciable penetration.

The variations of penetration in a steel subject to temper embrittlement also were studied.[2] In a nickel-chromium steel with an impact resistance after heat-treatment of 13 kgm/cm², phosphorus had a slight penetration after micrographic surface polishing, but at a 1-micron depth no more activity was observed. If this steel is embrittled (impact strength of 2 kgm/cm²), the penetration of phosphoric-acid solution becomes very substantial. Then at a depth of 1 micron the radioactivity had only decreased by one half and the specimen kept its micrographic polish. Perhaps it may be concluded that the penetration is related to an intergranular corrosion or to the etching of some constituent that is preferentially located in the grain boundaries or sub-boundaries.

In tool steels the penetration may also be due to microscopic cracks in the metal.

It is difficult at this time to arrive at a final conclusion. Experiments are being conducted to determine why phosphoric acid enters the metal. At present it can merely be said that the radioactive solution diffuses into the metal, that the gradient of activity permits measurements in depth, and that this can be done without adversely affecting mechanical properties of the die close to the surface.

STUDY OF DIE WEAR

Dies of relatively large dimensions (outside diameter, 11 cm) were used in the tests. Since the quantity of radioactive solution available was limited, a setup as shown in Fig. 3 was used. Here

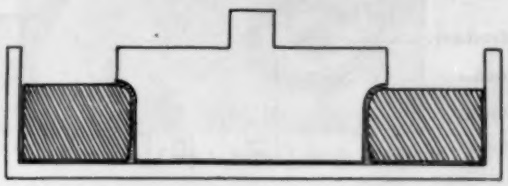

FIG. 3 APPARATUS FOR THE ACTIVATION OF THE DIES

the die was placed in a tight-fitting stainless-steel vessel, and a stainless-steel plug filled out the center with a tolerance of about 0.05 cm. The radioactive solution was introduced into this small space. Thus, for studying one die, about 1 millicurie was used in a volume of 2.5 cu cm. After insuring that no air bubbles would adhere to the tool, the entire assembly was placed in an oven for 1 hr at a temperature of 95 C (to limit evaporation of water) and the radioactive solution was reintroduced two or three times between the die shape and the plug.

Geiger-Tube Measurements. At the extremity of the steel sheath protecting the Geiger-Müller tube, was placed a conical shield, Fig. 4, 4 mm thick with a 1-mm-diam hole in the end that admitted only the rays from the die zone being explored. The conical shape was chosen so that the entire die face could be examined, and for this reason a 4-mm thickness was a limit.

However, the activated surface was about 400 sq mm and the conical shield did not stop all the rays. Therefore a second cone was used which was identical to the first but without a hole. The difference between the two readings was a measure of the number of rays issuing from the explored zone. (Under prevailing

[2] "Nouvelle méthode pour déceler la fragilité de revenu des aciers," by B. Jaoul and P. Lacombe, Comptes Rendus de l'Academie des Sciences, vol. 238, February 15, 1954, pp. 817–819.

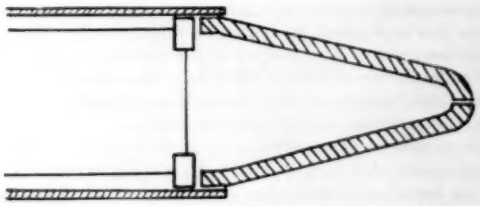

FIG. 4 CONICAL LEAD SHIELD WITH A 1-SQ-MM HOLE

geometrical conditions, only about 0.2 per cent of the rays coming from the small surface entered the cone.)

Fig. 5 gives the number of impulses (N_0) that were counted at a number of points of the die (the average of measurements on four points distant by 90 deg around the die). It is evident that the first radioactivation was not homogeneous. This was attributed to water evaporating during the heating. (Phosphoric acid is stable up to 255 C.)

After activation, the die was used for hot-extruding a stainless-steel tube of 47 mm ID and 52 mm OD, length about 10 meters. The extrusion temperature was 1250 C. Radioactive measurements were repeated over the die face and the average values are represented (dotted line) in Fig. 5. An important drop in radioactivity was observed at the radius and a minimum of wear at the beginning of the land.

As the slope of the curve of radioactivity as a function of depth is known, wear may be determined by the relation

$$p = 0.1 \left(\frac{N_0}{N} \right)^{1.2}$$

	N_0	N	N_0/N	p (microns)
Front face	48	54	1	0
	67	59	1.1	0.1
Radius	115	89	1.3	0.15
	125	27	4.7	0.65
	150	21	7.3	1.1
Land	270	47	5.8	0.8
	270	25	11.1	1.8
Relief	430	180	2.4	0.3
	360	350	1	0

The total amount of metal that has been removed, approximated from these results, is about the same as that determined in the experiments with the completely radioactivated die.

The radioactive particles lost by the die can be found again on the extruded bars. The activity measured on these bars is much more considerable than on those extruded with dies activated in their bulk. This feature made for speedier and more precise measurements. Unfortunately, it is impossible to get quantitative results, because of the nonhomogeneous radioactivation of the die.

Autoradiographs. Since radioactivity varies as a function of the distance from the surface, the application of a photographic film, with an appropriate sensitivity, to the surface-activated die, maps the wear. In the photograph, wear corresponds to the degree of obscurity.

The apparatus shown in Fig. 3 was used again, placing the photographic film between the die and the stainless-steel plug that did not become activated, as discussed previously. During an exposure, four strips (of about 1 cm width) were placed at four points 90 deg distant from each other.

Fig. 6 shows the result obtained after the extrusion of one tube. The curve corresponds to the wear depth calculated in the foregoing and the black areas of the autoradiograph represent the worn zones.

The two methods are in good agreement, minimum wear at the beginning of the land, maximum at the end. On the other hand, in the two cases, wear may be appreciable only behind a point on the radius where the slope is about 30 deg.

This autoradiographic method shows local abnormalities under continuous wear.

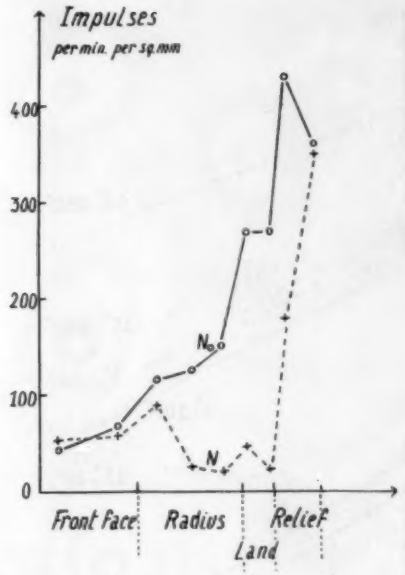

FIG. 5 IMPULSES GIVEN OUT BY A SQUARE MM OF THE SURFACE OF A DIE BEFORE (N_0) AND AFTER (N) WEAR

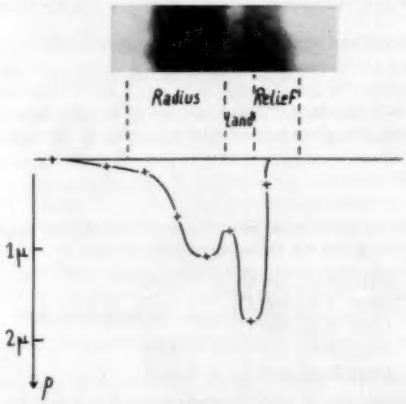

FIG. 6 COMPARISON OF MEASUREMENT WITH A COUNTER AND AUTORADIOGRAPHY

While in the foregoing results, N_0 and N represent the difference in activity of the die before and after one extrusion, a much more pronounced difference in radioactivity will result after a number of passes. As the range of exposure time of the film is relatively narrow, exposure must be extended to several times that required after a single pass.

DIE WEAR WITH REGARD TO SHAPE

This method of radioactivity measurements also has been used for determining wear as a function of the die shape.

FIG. 7 DIE A

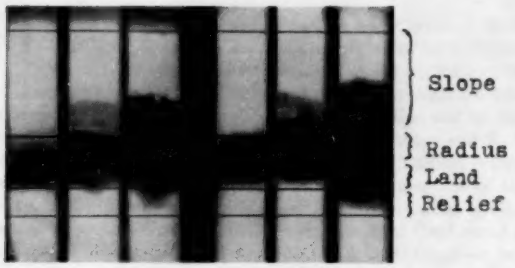

FIG. 9 DIE C

Four dies have been investigated simultaneously. The surface activation was developed by contact for 1 hr at 95 C with a radioactive solution with an activity of 0.5 mc/cm³.

Autoradiographs made immediately after exposure show a regular activation without local abnormalities.

Determinations by Geiger counter and autoradiographs were made after the extrusion of one tube, several tubes, and of a sufficient number of tubes leading to the scrapping of the die as a result of wear.

Results are shown in Figs. 7 to 10. Each figure shows the autoradiographs made with two strips of film placed on the upper and lower parts of the die generatrix of the shape, in three stages of wear. On the same photograph the exposure time has been the same, taking into account the decrease of phosphorus activity.

Fig. 11 corresponds to a long exposure, 20 hr instead of 2 hr. The photographs of the four dies in the two last stages made it possible to determine the zone of the greatest wear and the displacement of this zone during the working of the dies.

The method just described reveals the mechanism of die wear and the best shape for minimum die wear and increased die life.

CONCLUSION

The method of surface radioactivation is a further development of radioactive-wear studies. It permits the precise determination of the location of wear. The autoradiographic method maps the relief of the die which can then be calibrated against Geiger-Müller tube measurements.

FIG. 8 DIE B

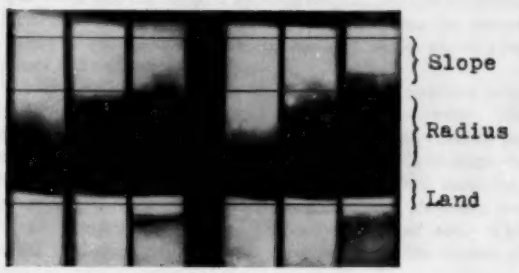

FIG. 10 DIE D

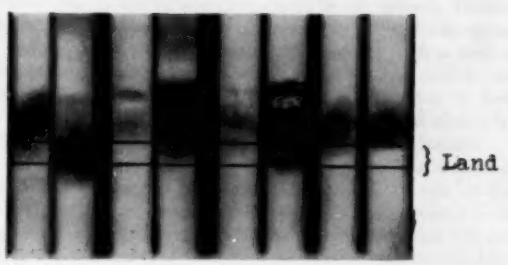

FIG. 11 DIES A, B, C, D—LONG EXPOSURE

This technique is particularly interesting where wear is a function of time, because it can follow such wear with a nondestructive testing method that can be considered full-safe. Weak points and the concentrations of friction forces can also be determined after a very slight amount of wear.

Finally, nothing prevents the application of this method to the study of wear on very large members that cannot be activated throughout their mass, and where wear cannot be determined by the classical methods.

ACKNOWLEDGMENT

The author is grateful to the "Comptoir Industriel d'Etirage et Profilage des Metaux" and its General Manager, M. J. Sejournet, who provided the facilities for studying and applying this method.

Hydraulic-Turbine Runner Vibration

By R. M. DONALDSON,[1] NEWPORT NEWS, VA.

This paper describes an investigation of the vibration characteristics of Francis-turbine runners and some experiments to determine the influence of different shapes of runner-bucket discharge edges on the excitation forces. Modifications suggested by the experiments were made to field runners and were successful in eliminating some objectionable vibration.

Introduction

HYDRAULIC turbines are subject to many types of vibration, but the most common appears to be a runner vibration excited by the shedding of the vortexes of the von Karman trail from the trailing edges of the runner buckets. An investigation of one case of this type of vibration and its cure were described in a paper by Messrs. John Parmakian and R. S. Jacobson entitled, "Measurement of Hydraulic Turbine Vibration," and presented at the November, 1951, meeting of the ASME. The discussions of this paper listed many other similar cases of vibration. In June, 1952, at the National Conference of the Applied Mechanics Division, ASME, Mr. C. A. Gongwer presented a paper, "A Study of Vanes Singing in Water," which included formulas for calculating the frequency at which vortexes are shed from a trailing edge and for calculating the alternating forces associated with this phenomenon. The formulas show that for a wide range of Reynolds numbers the frequency of the applied forces varies directly with the velocity and inversely with the thickness of the discharge edges. Mr. Gongwer also described experiments in which vanes with different edge thicknesses were towed at speeds up to 50 knots in a model tank and in which vibrations as predicted were observed.

Prediction of Vibration

The publication of these two papers served to crystallize the concept of the character of this predominant type of turbine vibration. A study of the papers also suggested a method for predicting cases where there was a likelihood of vibration and for making the necessary alterations to the runners to avoid this condition. The procedure was to strike the trailing edges of the buckets of the finished runner with a rubber mallet and determine their natural frequency. The exciting frequencies for the expected range of turbine operation could be calculated, using the formulas from Gongwer's paper and estimating the velocity of the water past the discharge edges of the buckets. If the natural frequency of the blades fell within the range of exciting frequencies, vibration could be expected. In such a case the bucket-discharge edges could be thinned down until the range of exciting frequencies was above the natural frequency. This procedure was adopted for several installations and it was found that thinning the bucket edges and fairing back well into the buckets had a negligible effect on the natural frequency.

A Typical Case

One of the installations investigated in this fashion was for the Bureau of Reclamation at Canyon Ferry. This installation contained three identical Francis turbines, each rated 23,500 hp at 150 rpm and 125 ft net head. When the discharge edges of the runner buckets were struck, a predominant frequency of about 210 cycles per second (cps) was noted. The discharge edges were $^{11}/_{16}$ in. thick and the range of exciting frequencies was calculated to be from 60 cps to 176 cps. It was considered that the natural frequency of 210 cps was sufficiently higher than the exciting frequencies to avoid resonance.

The first of these three units to go into service operated satisfactorily from zero to full load with no evidence of vibration. The second unit, however, developed a strong vibration from 60 per cent gate to full gate. The vibration could be felt through the floor plates and heard as a loud singing noise. Tape recordings were made in the powerhouse and, when analyzed, showed a predominant frequency of about 180 vibrations per sec. This checked with the measured natural frequency of the runner allowing for the damping effect of the water.

Units 1 and 2 were carefully compared and no significant differences in any of the turbine parts could be discovered. In order to ascertain that the vibration originated in the turbine runner, the trailing edges of Unit 2 were tied together with a hoop of round concrete reinforcing rod which was welded to each bucket at about the middle of the trailing edge. This ring or hoop effectively removed the vibration for a short time, but after a few hours of operation the reinforcing rod broke at each bucket.

Since the natural frequency was higher than the maximum estimated frequency of the von Karman trail, it was at first thought that the exciting forces came from another source in the turbine. No such force could be found, however, and the conclusion was reached that the forces associated with the shedding vortexes were providing the exciting forces. This could be explained either by regions of higher-than-average velocity of flow through the runner, or by excitations of $^1/_2$ natural frequency. In either event the usual method of changing the exciting frequencies by thinning the discharge edges did not seem attractive, since they would have to be thinned excessively to raise the exciting frequencies above the natural frequency.

Laboratory Tests

A laboratory investigation was then instituted to determine if any changes to the shape of the discharge edges would be effective in changing the frequency at which the vortexes were shed or in reducing the amplitude of the associated alternating forces. Some impetus was given to this program when the third unit in the plant was started and developed a vibration very similar to Unit 2.

The procedure in general was to fix an aluminum plate in a water channel and to measure the frequency and amplitude of the plate vibrations as the water velocity was varied. Aluminum plates $^1/_4$ in. thick and with a length which would place the natural frequency somewhere within the available exciting frequency range were used. Strain gages were used to measure vibrations and the outputs were recorded by means of a Brush analyzer and tape recorder up to a frequency of 100 cps. Measurements above this range were taken by cathode-ray oscilloscope. All trailing-edge conditions shown in Fig. 1 were precisely machined by milling machine. Fig. 2 shows a sketch of one of the test plates. Electrical leads from the strain gages were brought

[1] Hydraulic Engineer, Newport News Shipbuilding and Dry Dock Company. Mem. ASME.

Contributed by the Hydraulic Division and presented at the Diamond Jubilee Annual Meeting, Chicago, Ill., November 13–18, 1955, of The American Society of Mechanical Engineers.

Note: Statements and opinions advanced in papers are to be understood as individual expressions of their authors and not those of the Society. Manuscript received at ASME Headquarters, August 22, 1955. Paper No. 55—A-130.

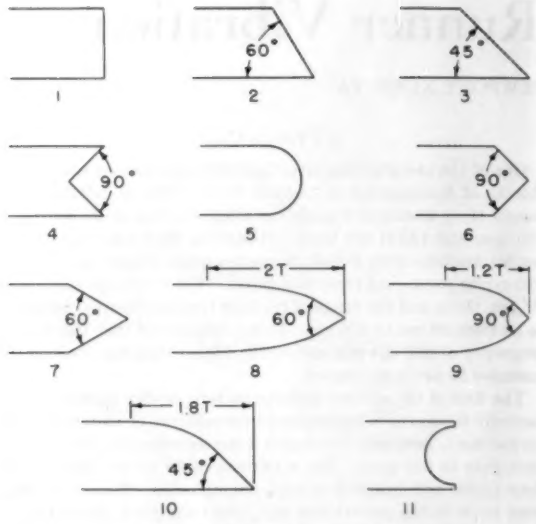

FIG. 1 TRAILING-EDGE SHAPES

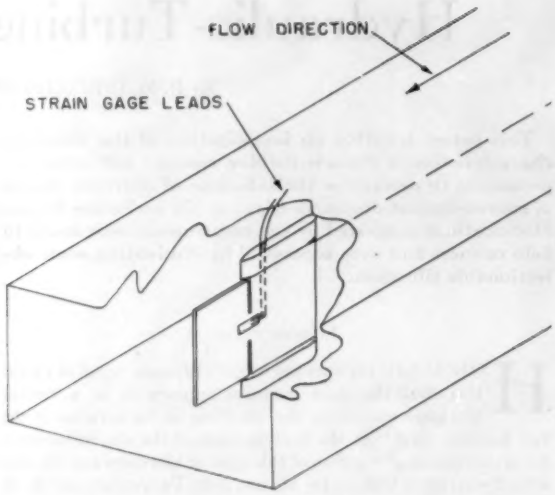

FIG. 2 SKETCH OF TEST PLATE IN WATER CHANNEL

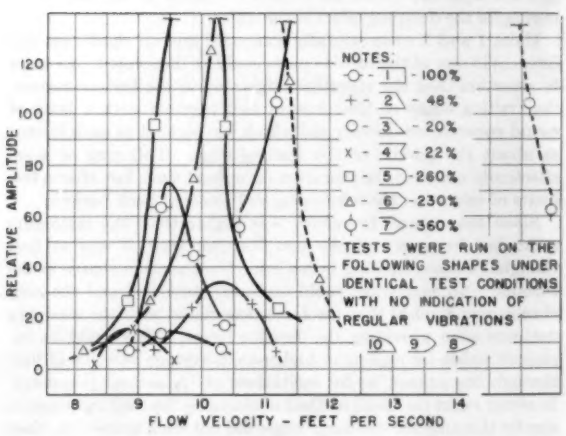

FIG. 3 VIBRATION AMPLITUDES OF VARIOUS TRAILING-EDGE SHAPES

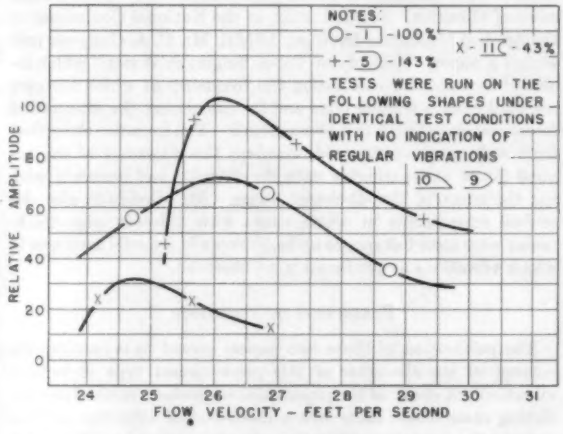

FIG. 4 VIBRATION AMPLITUDES OF TRAILING-EDGE SHAPES AT HIGHER FLOW VELOCITIES

out through the plate in order not to affect the fluid flow past the plate. Saw cuts were made from either side of the plate to lessen the supporting area and thereby increase the output of the strain gages.

It was found that none of the changes to the shape of the discharge edges appreciably changed the frequency of the exciting forces.

Graphs of fluid velocity versus vibration amplitude are shown for some of the edge conditions tested, Fig. 3. It can be seen that in most cases the amplitude peaked quite sharply and it is the measure of this peak amplitude which shows the relative effectiveness of the trailing-edge configurations. The table in Fig. 3 shows the percentage amplitude in relation to the square-edge condition. Peak amplitudes for different edge variations occur at various fluid velocities because the plates were being continuously shortened with each new test, thereby raising the natural frequency of the plate. As the natural frequency of the plate increases, the exciting frequency at resonance must also increase. The higher exciting frequencies coincide with the higher fluid velocities and thereby support the relationship that the frequency of the vortexes varies directly as fluid velocity.

Several of the most promising designs were tested at considerably higher fluid velocities with shorter plates and consequent higher natural frequencies in order to ascertain that the improvement shown at low velocities was also true at higher velocities. Fig. 4 shows the results of this part of the test.

MODES OF VIBRATION

While the foregoing tests to determine the effect of edge configuration were being made, another series of tests was conducted to investigate the modes of vibration of the Francis runners installed at Canyon Ferry. One of the objects of these tests was to find out if the natural frequency picked up by striking the bucket-discharge edges with a rubber mallet was the most likely frequency to be excited in service, or if there were other frequencies that could cause trouble. Another object was to determine whether or not the natural frequencies of a prototype runner could be predicted from tests on a scale model.

The model of the Canyon Ferry runner that was used for testing was made of cast bronze and had an inlet diameter of 15 in. The prototype runners were made of cast steel with an inlet diameter of 107 in. No duplicate of these runners was available for shop testing, but there was a large prototype of the same model in the shops. This runner was made of steel and had an inlet diameter of 178 in.

The following formula was developed to show the relationship between the natural frequencies of model and prototype

$$f_p = \frac{f_m}{K\sqrt{\frac{d_p}{d_m}\,\frac{E_m}{E_p}}}$$

where

f_p = frequency of prototype, cps
f_m = frequency of model, cps
K = ratio of prototype diameter to model diameter
E_m = 15×10^6, Young's modulus for bronze
E_p = 30×10^6, Young's modulus for cast steel
d_p = density of prototype = 0.284
d_m = density of model = 0.303

The model was vibrated by means of a small magnetostrictive vibrator which was driven by a 5-watt Hewlett-Packard oscillator through a 40-watt amplifier which operates down to 200 cps. Below 200 cps the model was vibrated by a small induction coil driven directly by the 5-watt oscillator. Small steel adapters screwed into $^3/_{16}$-in-diam holes tapped into the model served as the attachment for the vibrator. In this way it was possible to apply the exciting force either tangentially, radially, or axially to the band and crown and either tangentially or radially at the center of the inlet edge of a blade. This versatile arrangement made it comparatively easy to excite the whole range of frequencies in the runner.

For most of the tests the runner was securely fastened to a 5-in. × 24-in. × 30-in. steel block by bolting a circular steel plate $^3/_4$ in. thick to the crown and placing the runner crown down on the block and bolting the plate to the block. Tests were also made with the crown up and the band resting on four wooden blocks to simulate tests made on the prototype in the turret shop.

The total weight of the vibrator and adapter was less than 1 lb, and it was found that this mass did not appreciably alter the natural frequencies.

Modes of vibration were determined by sense of touch and by use of a crystal pickup, with phase shifts being determined by means of an oscilloscope. A shift in phase of 180 deg between any two points indicates a node between the points. Strain gages attached to the inlet and discharge edges of six blades were very helpful in determining blade frequencies.

The effect of immersion in water on frequency and amplitude was determined by submerging the model in a steel paint drum about 1 in. larger in diameter than the model.

The prototype runner was vibrated at several of the higher frequencies in the turret shop using a larger magnetostrictive vibrator. This equipment is not suitable for low frequencies because of its low force output in this range. The 4-node pattern (2 nodal diameters) which occurs at 34 cps in the prototype was excited very strongly with 50 lb force using a little pipe-shaker motor.

The most easily excited mode of vibration is the 4-node pattern with the crown vibrating as a disk with two nodal diameters and the band vibrating as a hoop with 4 nodes directly under the nodes in the crown. This mode can be excited by applying the exciting force in any direction. Other modes which are fairly easy to excite are the 2-node and 6-node patterns and the "umbrella" mode in which the band and blades vibrate in unison, with the crown vibrating with one nodal circle. Several other modes were found, but these were a combination of two frequencies acting to cancel out in certain places and reinforce in others. This phenomenon resulted in several blades vibrating with a large amplitude while others were either vibrating very little or none at all. A tabulation of the main frequencies is given in Table 1.

TABLE 1 PRINCIPAL FREQUENCIES, CPS

No. of nodes	Model	—Prototype— Est.	Actual	Canyon Ferry est.
0	615	75	63	105
2 (1 nodal diam.)	220	27	23	38
4 (2 nodal diam.)	330	40	34	57
6 (3 nodal diam.)	590	72	61	101
Blades	950	117	98	163
Blades	1260	155	130	216

The variation between the estimated and actual values of the natural frequencies of the prototype can probably be accounted for by variations from true similarity between model and prototype.

When the prototype was vibrating at the 4-node frequency of 34 cps, it was possible to see the direction of motion with a strobe light and the direction and amplitude at any point could be easily measured with a 25-power microscope. A total amplitude of 0.009 in. was noted on the crown of the runner during the test. The amplitude of vibration was considerably less for the 2-node frequency, but the phase was easily determined with two MB pickups. Frequencies above the 4-node pattern could not be excited with the motor-drive shaker because of the limit on motor speed.

Immersing the model in water lowered the frequency 15 per cent and attenuated the vibration intensity appreciably. The amount of attenuation was determined from the reduction in vibration intensity indicated on the sound-level meter from the Brush crystal pickup.

These tests indicated that the vibration encountered at Canyon Ferry was runner-bucket vibration of the type that could be excited by striking the buckets with a mallet. They also indicated that there were other modes of vibration of lower frequencies that could be excited quite easily. It would appear that in the design stages of a turbine installation these frequencies could be predicted from model tests and that numbers of bucket and wicket gates could be selected to avoid resonances.

Field Results

To alleviate the vibration in the Canyon Ferry units it was decided to leave Unit 1 as installed, to apply edge configuration No. 11, Fig. 1, to the discharge edges of Unit 2 runner, and to apply edge configuration No. 10, Fig. 1, to the discharge edges of Unit 3. On Unit 3 the necessary chipping was done on the back side of the buckets in order to leave the vent openings undisturbed. The alterations were made to the full length of the discharge edges, from crown to band. This program was undertaken with the consent of the Bureau of Reclamation in order to determine as quickly as possible the relative merits of two edge configurations both as to effectiveness in eliminating vibration and as to susceptibility to cavitation.

The following quotation is taken from an inspection report prepared by the Bureau of Reclamation after these units had been in continuous service for approximately one year:

"The attached runner inspection reports indicate the following concerning the discharge edges of the runner vanes.

"Unit 1. The Unit 1 discharge edges were not modified in the field. The back corner of the discharge edge is chipped in a manner indicating possibly that pieces of the metal were thrown

out. There is no indication of cavitation on these discharge edges as ordinarily characterized by pitting. The area affected and depth of the chipping are indicated on the Unit 1 runner inspection report.

"Unit 2. The Unit 2 discharge edges were modified in the field by chipping and grinding a groove in them. There is some cavitation in this groove in small patches. These patches were on the side of the groove next to the back of the vane as indicated on the runner inspection report. The amount of cavitated area in the groove was a small part of the total area of the groove and appeared to be caused by irregular surfaces resulting from the chipping operations.

"Unit 3. The Unit 3 discharge edge was modified in the field by chipping and grinding to a bullet shape. At the time of this inspection the Unit 3 discharge edges were in very good condition. The edges had been painted with red priming paint after they were modified. Some of the paint has come off but the edges are still very smooth, showing no indication of cavitation pitting.

"As a result of the observations made during these runner inspections we would summarize this report as follows:

"The three units are all fairly smooth running with Unit 1 being a little rougher than the others.

"The discharge edges of the Unit 3 runner indicate at this time that it is giving the least trouble, with Unit 2 showing a little cavitation in the grooves in the discharge edges and Unit 1 definitely showing some raveling of the discharge edge."

Edge configuration No. 10, Fig. 1, was also applied to two runners at Whitney Dam, Texas. These units when they were first started had a vibration at the point of best efficiency. All traces of this vibration were removed by the alterations to the edges.

The investigations described in this paper did not extend to a determination of how the various edge configurations act on the von Karman trail to affect the exciting forces associated with it. Such a study would be very interesting and might lead to other equally effective edge shapes.

Discussion

D. C. Hazen[2] and C. P. Kittredge.[3] Vibrations of turbine runners which are induced by von Karman vortex trails behind the discharge edges of the buckets can be eliminated if the vortex trail can be reduced sufficiently or removed altogether. The vortex trail will be eliminated if a vortex can be stabilized along the discharge edge of the bucket.

The Department of Aeronautical Engineering, Princeton University, has undertaken preliminary investigation of the flow phenomena around a cusp-shaped profile tentatively designed as the "suction vortex airfoil." Fig. 5 shows a typical profile. A

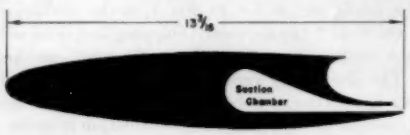

Fig. 5 Suction Vortex Wing

vortex is stabilized in the cusp by means of suction applied through a slot along the lower trailing edge. No vortex trail appears behind the profile as long as the vortex is stabilized within the cusp. Fig. 6 shows the profile in a wind tunnel with streamlines made visible by smoke. The suction is slightly less than that required

[2] Assistant Professor of Aeronautical Engineering, Princeton University, Princeton, N. J.

[3] Associate Professor of Mechanical Engineering, Princeton University, Princeton, N. J. Mem. ASME.

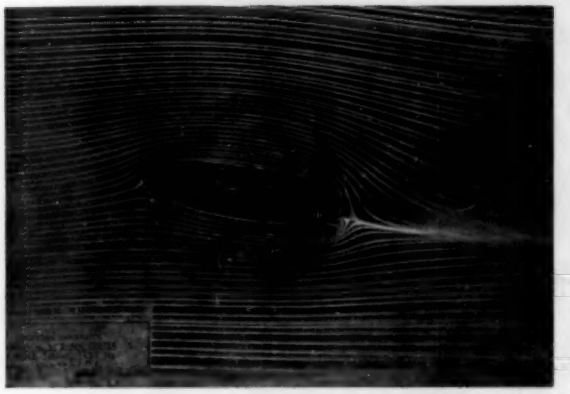

Fig. 6 Flow Around Suction Vortex Wing

to stabilize a strong vortex in the cusp. Experiments have indicated that the vortex can be stabilized under some circumstances by a component of the fluid velocity parallel to the trailing edge in which case suction is not required. It is emphasized that the research has not progressed far enough to permit statements regarding possible size effects or the magnitude of the velocity parallel to the trailing edge which would be required to stabilize a vortex.

The relative flow through a mixed-flow runner is of a type that might provide adequate velocity components parallel to the discharge edges of the buckets to stabilize a vortex along all or most of each discharge edge. A suitable cusp along the back of each bucket at the discharge edge would be required. Stabilization of a vortex along the discharge edge of each bucket should improve the exit flow conditions and eliminate one source of vibration.

F. E. Jaski.[4] This paper is an interesting description of a new method of correcting bucket vibration in Francis-turbine runners. The type of sharpening of the discharge edge on the back side of the bucket as shown by item 10, Fig. 1 of the paper, which was the most effective in stopping the vibration, appears to have an influence on the exciting forces causing the buckets to vibrate. As shown in the figure, the sharpening and rounding is carried back from the discharge edge along the bucket a distance of 1.8 times the thickness of the edge. If the vortexes in the von Karman trail coming off the face and back of the vane are in staggered formation it is possible that this starts them off on the back side a little ahead of those on the face of the bucket. By starting the sharpening on the back side at the most effective distance it may be possible that the two sets of vortexes quench each other with a result that there is no side force left to excite the bucket into vibration. The bucket vibration is influenced by its natural frequency and its relation to the frequency of the exciting forces. If the two are in resonance critical vibration may occur. Thus a possible remedy would be to separate them sufficiently so they will not be in resonance, or destroy the exciting forces such as perhaps occurs in the remedy used by the author.

This type of vibration is not limited to Francis-type runners, but also may occur in propeller runners. The writer had experience in correcting blade vibration on both Francis and propeller-type runners while he was employed by the author's company and believes it may be of interest to relate the remedy used to correct vibration in those applications. The first experience was with the 66,000-hp 165-ft-head units at Norris Dam of the Tennessee Valley Authority. In the original design the discharge

[4] Engineer-in-Charge, Pump Turbines, Allis-Chalmers Manufacturing Company, Milwaukee, Wis. Mem. ASME.

edge of these buckets was rounded with about a 3/8-in. radius and the back side was tapered off at the edge for about 5–6 in. These runners had a singing note that could be heard in the turbine pit. On these runners permanent steel struts about 3 in. wide and tapered from 1 1/2 to 3/4 in. in thickness were welded between all the buckets to correct the vibration. They were located on the mean flow line and about midway between entrance and discharge of the bucket. These struts did not affect the output of the units. A duplicate of this runner was later used at the Hiwassee Power Plant for a rating of 80,000 hp under 190 ft head. In order to correct the vibration, the buckets for Hiwassee were made about 1/2 in. thicker across the entire back side at the top and tapered off to the original thickness about at the center line of the distributor. The discharge edge was made square about 3/4 in. thick and gradually tapered on the back side for a long faired surface. No vibration occurred in this runner. The specific speed is about 48.

At Claytor Dam of the Appalachian Electric Power Company vibration occurred in two Francis turbines rated about 26,000 hp under 110 ft head. The bucket vibration occurred at about 62 per cent gate opening. The specific speed is about 68. These units have 16 buckets and 16 wicket gates. However, the vibration was not caused by this combination of wicket gates to runner buckets but was caused by the von Karman trail at the discharge edge. The vibration could be felt in the generator floor. In this case the original design had a square edge about 1 3/8–1 1/4 in. thick. This thickness of the edge was reduced to about 11/16 in. by chipping off metal on the face or pressure side and the surface was then faired to a long taper. This eliminated the vibration and increased the output of the units. While the chipping was in progress on the first runner it was necessary to put the unit in service because of a flood on the New River in the summer of 1940. Only 12 of the 16 buckets had been chipped and were still rough before they were ground smooth, but when the unit was put on load there was no vibration at any gate opening.

At Drop 4 Power Plant of the Imperial Irrigation District, about 1942, vibration occurred in a fixed-blade-propeller turbine rated 13,300 hp at 51 ft head. This is a 5-bladed propeller with a specific speed of about 127. This unit had vibration periods at 28, 42, and 63 per cent gate opening. It was so severe that it caused the railings to rattle outside the powerhouse. The remedy used here was to reduce the thickness of the discharge edge from about 1 1/4 to 3/4 in. for about 2/3 of the length from the outer circumference toward the hub. The chipping was done on the face of the blade and then faired to a long gradual taper. After the blades were ground smooth the unit was put back in service and there was no vibration.

At Grand Coulee Dam the first three units L1, L2, and L3, developed vibration at about 60–65 per cent gate opening. These units are rated 150,000 hp at 330 ft head with a specific speed of about 34. The vibration could be felt on the top cover plate and railings in the turbine pit. The remedy used here was to reduce the thickness of the discharge edge from 1 1/4 in. down to about 11/16 in. The chipping was done on the face of the bucket and the surface was faired to a long gradual taper and ground smooth. The vibration was eliminated and the output increased about 5000 kw. The increase in output at Grand Coulee and Claytor Dam occurred because the discharge openings of the buckets were slightly increased by the chipping of the face.

The Bureau of Reclamation also experienced vibration on the units at Parker Dam which resulted in cracks in some of the runner blades as described in a paper by John Parmakian.[5] These units are rated 40,000 hp at 80 ft head. Here the final remedy was obtained by chipping the discharge edge to about 3/4 in. and a gradual taper on the face of the bucket. The output of the unit was also increased about 6 1/2 per cent.

In the units in which vibration was corrected by the writer the thickness at the discharge edge was reduced to about 55 per cent of the original thickness. At the same time the openings between the buckets were slightly increased. If the frequency of the exciting forces caused by vortexes at the discharge edge varies with velocity divided by thickness V/T, then by reducing T to about 55 per cent and increasing V about 5 per cent, the exciting frequency would be almost doubled. It is possible that in each of these cases this carried the exciting forces out of resonance with the natural frequency of the buckets and thus reduced the vibration so it was no longer critical.

The method of sharpening the discharge edge of the bucket proposed in the paper is a rather simple process and suggests that the bucket edges could be finished in this manner in the shop before the runner is shipped to the job.

G. D. JOHNSON.[6] Naturally, this subject is of interest to all manufacturers and users of hydraulic turbines. A paper[5] by Messrs. Parmakian and Jacobson dealt primarily with runners furnished to the U. S. Bureau of Reclamation by the writer's company. Consequently, we are particularly interested in this further discussion of the problem.

Theoretically, the bucket-discharge edge should have zero thickness (i.e., a knife-edge), but a fairly thick edge is required to obtain a satisfactory casting. Gratifying results were obtained at the Parker and Keswick Plants of the U. S. Bureau of Reclamation by thinning the discharge edges of the turbine-runner buckets to approximately 3/4 in. (0.004 × runner discharge diameter). The only disadvantage of this obvious solution is the expense of chipping and grinding to fair the thinned edge shape gradually into the upstream bucket contours.

Presumably, the main attraction of the various edge shapes shown in the author's Fig. 1 is the small amount of metal that must be removed from the bucket edges as cast. It is difficult to explain the relative vibration amplitudes shown by Figs. 3 and 4, especially in the case of configuration No. 11 with no thinning and just a groove along the discharge edge, as was employed on Unit 2 at Canyon Ferry. The fact that it proved to be satisfactory in that particular case is not too significant, since Unit 1 required no modification at all. Referring again to Figs. 3 and 4, it is extremely difficult to explain the high vibration amplitude of configuration No. 5 relative to No. 1, although it seems plausible that configuration No. 8 (as well as Nos. 9 and 10) would have a smaller amplitude.

At the Denison Dam Plant (in Texas) of the U. S. Army Corps of Engineers, audible bucket vibration was satisfactorily eliminated at minimum cost on the 192-in. discharge diameter runner of Unit 2 by welding a hoop of 1 1/2-in-diam stainless-steel bar stock to each bucket near the middle of the trailing edge. Struts were used between all of the buckets of Unit 1, but the ring in Unit 2 has proved to be just as durable and effective.

It is also interesting to note that, although vibration pickups and analyzers give more complete information, the existence of definite runner-bucket vibration is evident to the human ear as a loud and disturbing hum, so that elimination of the noise may be construed as satisfactory treatment of the problem. In this connection it is also worth mentioning that a small amount of compressed air released upstream of the runner buckets effectively eliminated the noise and the measured vibration amplitude on all three runners at Keswick, before thinning the discharge edges. The beneficial effect of compressed air has also been demonstrated

[5] "Measurement of Hydraulic Turbine Vibration," by J. Parmakian and R. S. Jacobson, Trans. ASME, vol. 74, 1952, pp. 733–741.

[6] Chief Hydraulic Engineer, S. Morgan Smith Company, York, Pa. Mem. ASME.

in the case of vane vibration resulting from high velocities in a large 90 deg vaned elbow.

Another significant observation is that we have not been able to establish definitely any connection between runner-bucket vibration and cracking of the runner buckets where the trailing edges join the runner crown or band. At Denison, there was definite bucket vibration without any evidence of cracking whatsoever; at Parker and Keswick, there was definite bucket vibration as well as fairly extensive cracking where the bucket-discharge edges join the runner crown. At several other plants there was no observed bucket vibration but cracking of the discharge edges near the crown was rather extensive.

Comments on these points would be appreciated.

W. J. Rheingans.[7] The runner-blade vibrations described by the author are not a recent development, although probably due to a trend in recent years to larger physical-size runners, vibration problems of this type have been on the increase. While blade vibration is usually associated with low-head units of large size, such vibrations have occurred on large-size units under heads as high as 330 ft.

The writer's first experience with runner-blade vibration was in 1930 on a 6500-hp, 48-ft-head, 125-rpm Francis turbine at the Upper Notch Power Plant, Canada. Loud singing noises were present for narrow gate ranges at several different gate positions. After locating the source of the vibrations, they were completely eliminated by placing streamlined struts between the runner blades. These struts have been in place for 25 years and have shown no cavitation or other detrimental effects. The vibration was eliminated before the runner had been in operation long enough to produce cracks, and no cracks have developed in the 25 years of operation with the struts installed.

The writer had no further experience with this type of vibration until quite recently. In 1930 six Francis units were installed at the Osage Power Plant, rated 35,400 hp, 90 ft head, 112.5 rpm. There was no evidence at that time, nor during subsequent 25 years of operation of any serious vibration. In 1953 two additional units of exactly the same design were installed. One unit was equipped with the spare runner which had been furnished with the original six units in 1930, and which had never been used. This unit with the spare runner showed no evidence of blade vibration. The runner for the second unit, installed in 1953, was made from the same pattern that had been used for the original runners. However, the pattern required some repair work, and it is possible that the discharge edges of the runner blades were somewhat thicker. This last unit showed considerable vibration. The vibration was not serious enough to prevent operation, but was quite annoying to the operating personnel in certain locations in the powerhouse. An inspection of the runner showed no blade cracks, but it was decided to groove the discharge edges of the runner blades similar to shape 11, Fig. 1 of the author's paper.

This modification showed a remarkable improvement in the operation of the unit, which was evident as soon as it was placed in operation. The high-frequency vibration had disappeared completely. The experience at this plant shows how sensitive runner-blade vibration apparently is to small variations in runner castings.

Runner-blade vibration is not always accompanied by unusually loud singing noises, and the physical evidence of the vibration may be slight. This is probably due to the absence of any other parts of the unit or powerhouse structure with a resonant vibration frequency to pick up the blade vibration. However, the actual blade vibration can be serious enough to eventually cause runner-blade cracking.

[7] Manager, Hydraulic Department, Allis-Chalmers Manufacturing Company, Milwaukee, Wis. Mem. ASME.

A situation of this type occurred at the Wilson Power Plant of the T.V.A. Four units rated 35,000 hp, 92 ft head, 100 rpm were installed in 1942, two in 1943, one in 1949, and three in 1950.

The six units installed in 1942 and 1943 showed some slight cavitation and were repaired by welding in 1948. Shortly thereafter, cracks appeared in the runner blades. These were repaired by welding in 1950, but kept on reappearing. The units had never produced any loud singing noises, nor any unusual vibrations. However, a careful investigation showed that there was a slight high-frequency vibration at full gate which could be produced by runner-blade vibration. Accordingly, struts were inserted between the runner blades. This eliminated the vibration at full load and stopped any further cracking of the runner blades.

Thus, as stated, runner-blade vibration is not a recent problem. However, up to the time of the investigations described by the author, the remedy has been either the installation of struts between the runner blades, or trimming down the thickness of the discharge edges. Therefore the results obtained by the author with varying shapes of trailing edges are a decided contribution to the art. His investigations comprise the first published data for this type of approach to the problem.

Further research along these lines is indicated, to determine exactly how the von Karman trails perform and how they produce the forces to cause blade vibration.

G. J. Vencill.[8] This type of paper is of great value to an operating organization in need of a solution to a problem. There is sometimes a tendency to pass over reports of trouble as subjects for technical papers, and while such matters are often freely discussed, they may not be made available for general reference.

When our organization was faced with a turbine-vibration problem recently, we found the literature on the subject exceedingly sparse. At the Osage Plant vibration developed in two new units when they were placed in service in 1953. Six original units which had been operating since 1931 had given no trouble. Unlike the case described in the paper no "loud singing noise" was observed, but vibration was felt and the noise was a loud grinding noise with a pulsating characteristic corresponding to each revolution of the shaft. The noise occurred in two ranges of gate opening between 0.65 and full gate with a relatively quiet spot between. It is doubtful that an analysis of the noise would have shown any predominant frequency. The noise was not noticeable with low tailwater levels, but increased with rising tailwater and reached a maximum when the level approached the bottom of the turbine runner. The same characteristic was observed at Keswick Power Plant mentioned in the discussion of the paper by Parmakian and Jacobson.[6]

Shaping the trailing edges of the runner buckets similar to configuration No. 11 in Fig. 1 of the paper eliminated the noise and vibration.

It was observed while the work was being done that a corner of the trailing edge was being pitted and that in places it had been beveled as much as $^1/_4$ in. If this action continued, the shape of the edge would approach that of configuration No. 10, and might have eliminated the vibration without assistance in due course.

Studies of this kind are carried out much more readily in the laboratory and in the shop than after a turbine has been placed in operation. It is to be hoped that a full understanding of vibration can be reached which will enable these troublesome cases to be eliminated in the design stage, and not become problems in operating units. This paper is evidence of progress being made.

[8] Union Electric Company of Missouri, St. Louis, Mo.

Author's Closure

One explanation that has been advanced for the effectiveness of configuration No. 11 is that a vortex was stabilized in the cusp formed in the discharge edge. The experiments described by Professors Hazen and Kittredge lend credibility to this theory.

As suggested by Mr. Rheingans, many cases of runner-blade vibration may exist that are not evidenced by noise or vibration of the accessible parts of the units. Such cases may or may not be severe enough to cause eventual cracking of the runner blades. Conversely, it is possible that some of the noisiest cases of blade vibration are quite harmless.

Several of the discussions mentioned the successful use of struts and hoops to suppress runner-blade vibration. Such cures, which are often effective, do not remove or reduce the periodic exciting forces, but merely limit the amplitude of blade vibration. One objection to this type of cure is that there may be significant drag forces associated with a fully developed von Karman trail. These drag forces could cause an appreciable power loss which would be unaffected by the use of struts or hoops, but which might be eliminated by a change in edge shape. The author concurs with Mr. Rheingans that further research on trailing-edge phenomena is desirable.